frontiers | Research Topics

Neuroimaging of brain structure-function coupling mechanism in neuropsychiatric disorders

Edited by
Junghun Cho, Han Lv, Lingfei Guo, Hongwei Wen and Jing Li

Coordinated by
Mengmeng Feng

Published in
Frontiers in Neuroscience
Frontiers in Aging Neuroscience

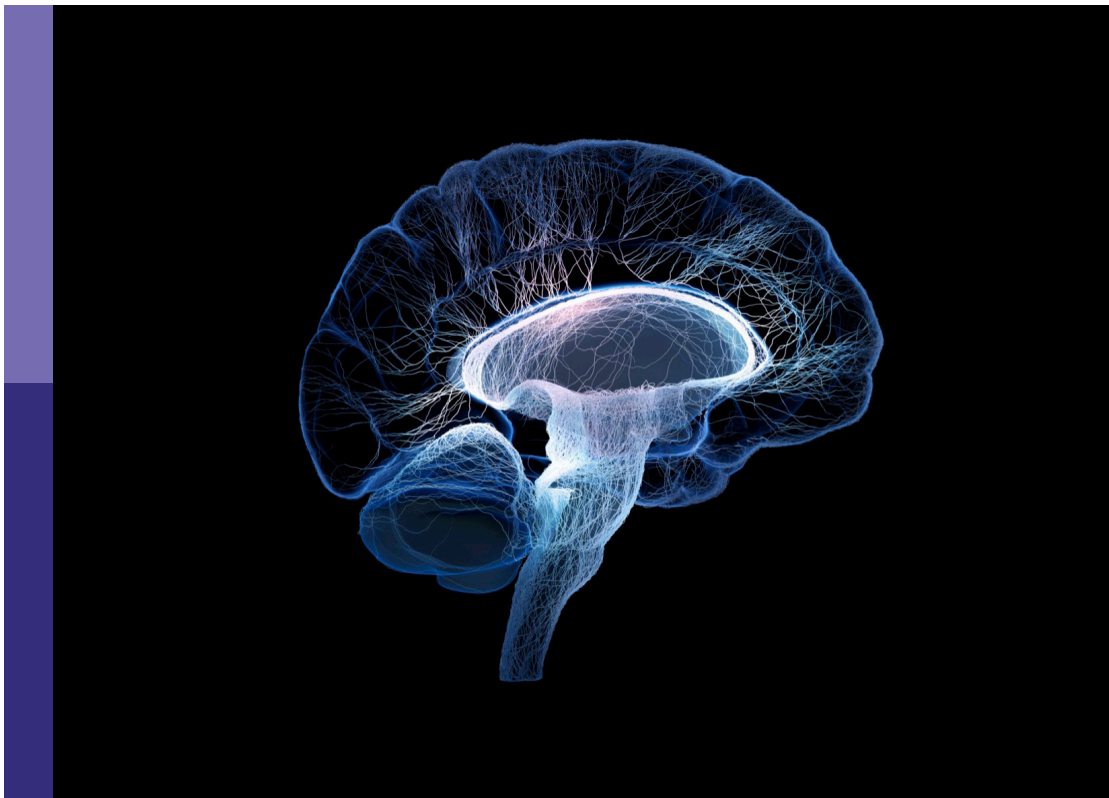

ISSN 1664-8714
ISBN 978-2-8325-3332-1
DOI 10.3389/978-2-8325-3332-1

About Frontiers

Frontiers is more than just an open access publisher of scholarly articles: it is a pioneering approach to the world of academia, radically improving the way scholarly research is managed. The grand vision of Frontiers is a world where all people have an equal opportunity to seek, share and generate knowledge. Frontiers provides immediate and permanent online open access to all its publications, but this alone is not enough to realize our grand goals.

Frontiers journal series

The Frontiers journal series is a multi-tier and interdisciplinary set of open-access, online journals, promising a paradigm shift from the current review, selection and dissemination processes in academic publishing. All Frontiers journals are driven by researchers for researchers; therefore, they constitute a service to the scholarly community. At the same time, the *Frontiers journal series* operates on a revolutionary invention, the tiered publishing system, initially addressing specific communities of scholars, and gradually climbing up to broader public understanding, thus serving the interests of the lay society, too.

Dedication to quality

Each Frontiers article is a landmark of the highest quality, thanks to genuinely collaborative interactions between authors and review editors, who include some of the world's best academicians. Research must be certified by peers before entering a stream of knowledge that may eventually reach the public - and shape society; therefore, Frontiers only applies the most rigorous and unbiased reviews. Frontiers revolutionizes research publishing by freely delivering the most outstanding research, evaluated with no bias from both the academic and social point of view. By applying the most advanced information technologies, Frontiers is catapulting scholarly publishing into a new generation.

What are Frontiers Research Topics?

Frontiers Research Topics are very popular trademarks of the *Frontiers journals series*: they are collections of at least ten articles, all centered on a particular subject. With their unique mix of varied contributions from Original Research to Review Articles, Frontiers Research Topics unify the most influential researchers, the latest key findings and historical advances in a hot research area.

Find out more on how to host your own Frontiers Research Topic or contribute to one as an author by contacting the Frontiers editorial office: frontiersin.org/about/contact

Neuroimaging of brain structure-function coupling mechanism in neuropsychiatric disorders

Topic editors

Junghun Cho — University at Buffalo, United States
Han Lv — Capital Medical University, China
Lingfei Guo — Shandong Provincial Hospital, China
Hongwei Wen — Southwest University, China
Jing Li — Capital Medical University, China

Topic Coordinator

Mengmeng Feng — Shandong University, China

Citation

Cho, J., Lv, H., Guo, L., Wen, H., Li, J., Feng, M., eds. (2023). *Neuroimaging of brain structure-function coupling mechanism in neuropsychiatric disorders*. Lausanne: Frontiers Media SA. doi: 10.3389/978-2-8325-3332-1

Table of contents

frontiers | Frontiers in Neuroscience

TYPE Editorial
PUBLISHED 14 August 2023
DOI 10.3389/fnins.2023.1270645

OPEN ACCESS

EDITED AND REVIEWED BY
Vince D. Calhoun,
Georgia State University, United States

*CORRESPONDENCE
Lingfei Guo
✉ glfsci@163.com

RECEIVED 01 August 2023
ACCEPTED 02 August 2023
PUBLISHED 14 August 2023

CITATION
Feng M, Wen H, Li J, Lv H, Cho J and Guo L (2023) Editorial: Neuroimaging of brain structure-function coupling mechanism in neuropsychiatric disorders.
Front. Neurosci. 17:1270645.
doi: 10.3389/fnins.2023.1270645

Editorial: Neuroimaging of brain structure-function coupling mechanism in neuropsychiatric disorders

Mengmeng Feng[1], Hongwei Wen[2], Jing Li[3], Han Lv[3], Junghun Cho[4] and Lingfei Guo[5,6]*

[1]Department of Radiology, Shandong Provincial Hospital, Shandong University, Jinan, Shandong, China, [2]Key Laboratory of Cognition and Personality (Ministry of Education), Faculty of Psychology, Southwest University, Chongqing, China, [3]Department of Radiology, Beijing Friendship Hospital, Capital Medical University, Beijing, China, [4]Department of Biomedical Engineering, University at Buffalo, The State University of New York, New York, NY, United States, [5]Key Laboratory of Endocrine Glucose and Lipids Metabolism and Brain Aging, Ministry of Education, Jinan, Shandong, China, [6]Department of Radiology, Shandong Provincial Hospital Affiliated to Shandong First Medical University, Jinan, Shandong, China

KEYWORDS

neuropsychiatric disorders, multimodal MRI, structure-function coupling, neurovascular coupling, function impairment

Editorial on the Research Topic
Neuroimaging of brain structure-function coupling mechanism in neuropsychiatric disorders

Neuropsychiatric disorders are diseases with alterations in the nervous system or mental activity disorders, with cognitive and motor disorders and behavioral changes as the core, mainly including Parkinson's disease (PD), Alzheimer's disease, Huntington's disease, narcolepsy, schizophrenia, Tourette syndrome and autism spectrum disorders (ASD) (Dugger and Dickson, 2017). With the development of multimodal magnetic resonance imaging (MRI) neuroimaging methods, the underlying neurobiological mechanisms of neuropsychiatric disorders have been increasingly investigated, and the brain structure-function coupling approach has received more focused attention in recent years because it can enhance sensitivity to detect brain pathophysiological abnormalities compared to single functional or structural indicators (Sarwar et al., 2021). In addition, neurovascular coupling (NVC), as an important mechanism for neurogenic regulation of cerebral blood flow (CBF), also plays an important role in neuropsychiatric diseases, and alterations in NVC can also cause structure-function coupling changes, which can lead to neurocognitive aging and behavioral disorders (Kisler et al., 2017). The purpose of this Research Topic is to investigate the structural and functional changes, especially coupling changes, in patients with neuropsychiatric disorders, and their correlation mechanisms with cognitive/motor/other functional parameters, in conjunction with multimodal MRI techniques and thus provide the theoretical basis for clinical diagnosis and treatment. The authors focused not only on the common neuropsychiatric disorders mentioned above, but also on other neuropsychiatric disorders that affect the quality of life and survival of pregnant women, children, and adults, and explored the mechanisms involved in the disorders from multiple perspectives, including structure, function, and metabolic, using multimodal MRI.

Many parameters can describe structure-function coupling in neuroimaging. Wang N. et al. systematically summarized the current multimodal MRI-based analysis techniques and coupling parameters from the perspectives of voxel-wise structure-function coupling, structural connectivity-functional connectivity coupling, and NVC in patients with cerebral small vessel disease (CSVD), providing an imaging perspective for studying the pathogenesis and early diagnosis of the disease. Some studies in this Research Topic obtain parameters such as amplitude of low-frequency fluctuation (ALFF), fractional amplitude of low-frequency fluctuation (fALFF), regional homogeneity (ReHo), degree centrality (DC), and functional connectivity strength (FCS) based on resting-state functional MRI (rs-fMRI), and obtain CBF maps based on 3D pseudo-continuous arterial spin labeling (3D pCASL). And they characterize NVC with the correlation between rs-fMRI parameters and CBF maps. Li X. et al. focused on medication-overuse headache (MOH) and revealed a significantly decreased NVC in the left orbit part of the superior frontal gyrus, the bilateral gyrus rectus, and the olfactory cortex, and a negative correlation between neuronal activity and CBF at the voxel level in MOH, implying a disturbance of normal physiological conditions. Yang et al. studied whole gray matter CBF-FCS coupling in Meige syndrome (MS) patients. They found the CBF-FCS coupling was increased, and the CBF values of the middle frontal gyrus and the bilateral precentral gyrus were significantly increased in MS patients, which indicates a compensated blood perfusion in motor-related brain regions and reorganized the balance between neuronal activity and brain blood supply. Ruan et al. found that NVC was significantly reduced at both whole-brain and brain region levels in small vessel disease cognitive impairment (SVCI) and post-stroke cognitive impairment (PSCI) patients. They also used mediation analysis to reveal the mediating role of NVC between white matter (WM) lesion burden and cognitive impairment. The potential of NVC in accurately measuring cognitive impairment cannot be underestimated, and it may guide targeted therapies aimed at improving cognitive function in this patient population in the future. Zhang, Liang et al. used ALFF and voxel-based morphometry (VBM) to define NVC and found that structure-function decoupling in the bilateral caudate nucleus has advantages in identifying patients with severe CSVD burden, which is helpful for early prediction and diagnosis in the development of CSVD. Understanding the regulatory mechanism of NVC in diseases is of great significance in preventing further disease development and guiding treatment.

The characteristically unilateral pattern of symptoms in PD at onset and early stages is considered an important diagnostic feature. To compare the differences in brain structure and function in PD patients with different onset sides, Zhang, Li et al. obtained the topology of functional and structural connectome based on rs-fMRI and diffusion weighted imaging (DTI) by graph theory. Ultimately, no difference was evident from the rs-fMRI- or DTI-derived network alone among patients with different sides of onset and HCs, but there were significant differences in network metrics of resting-state-informed structural connectome. Topological properties of motor-related brain networks could distinguish LPD and RPD, which provides neurobiological insights into the lateralization of PD onset. Lin et al. used the microstructural and functional neuroimaging from the Adolescents Behavior Cognitive Development (ABCD) database to comprehensively assess the underlying neural mechanisms of Attention-Deficit Hyperactivity Disorder (ADHD) in children. The results indicate a pervasive reduced microstructural integrity in WM in ADHD children, which may lead to impaired connectivity of attention and default mode functional networks. In addition, the authors used a machine learning approach to combine multiple structural and functional imaging metrics to validate different combinations of classification models to aid in the diagnosis of ADHD in clinical children. Bian et al. used machine learning to combine functional and structural connectivity parameters to predict motor impairment after stroke, which provides a theoretical basis for personalized treatment and effective rehabilitation. In addition, they also found that models utilizing functional connectivity tended to have better performance than those utilizing structural connectivity, in which the dorsal and ventral attention networks are important features. In general, these studies fit into our Research Topic theme of interpreting neural mechanisms from a structure-function perspective and have important implications for both mechanistic studies and clinical diagnosis, treatment, and prognostic assessment.

Although structure-function coupling is a more comprehensive approach to studying the mechanisms of neuropsychiatric disorders, independent analysis of structural or functional MRI methods can also facilitate in-depth exploration of disease mechanisms. Wang H. et al. studied the WM structural networks of High myopia (HM) patients based on diffusion kurtosis imaging (DKI) and topography. They found the local efficiency and clustering coefficient decreased significantly, the hub distributions were partially reorganized, and the node betweenness centrality also changed significantly in HM patients. The changes in the networks provided a new perspective for people to explore the mechanism. Guo et al. introduced Mendelian randomization study into the correlation analysis of brain structure and migraine to further explore whether there is a causal relationship. The results showed that the decreased cerebral cortical surface area and hippocampal volume are associated with higher migraine risk. It will be more helpful to elucidate the underlying mechanisms of migraine and will also provide new ideas for the subsequent treatment of migraine. A review of cobalamin C (cblC) defects in infants found ventricular dilation, cerebral atrophy, and corpus callosum thinning are the main MRI abnormalities of cblC defects, and these manifestations are significantly correlated with delayed development in children. MRI findings can be considered an important tool for determining the severity of cblC defects. Gao et al. proposed that gray matter volume (GMV) could be used as a potential biological indicator of type 2 diabetes mellitus (T2DM), and revealed the correlation between the GMV and serum P-tau-181 in T2DM patients. In future research, the role of P-tau-181 in diabetes encephalopathy cannot be ignored. At the same time, early detection and early intervention should be carried out for T2DM patients to prevent the disease from further worsening and causing more serious complications.

Li, Du et al. used rs-fMRI to assess altered spontaneous brain activity of overseas college students during the coronavirus

2019 pandemic. The MRI data showed altered ALFF and ReHo values in the superior medial frontal gyrus, precentral gyrus, and paracentral lobule in the overseas students and the spontaneous brain activity correlated with anxiety and depression. Focusing on patients with major depressive disorder (MDD), Liu et al. showed that short-term repeated treatment with ketamine altered resting-state functional connectivity (RSFC) of amygdala-related networks, suggesting that the baseline RSFC between bilateral amygdala and right putamen may be a predictor of the response of ketamine's antidepressant and antisuicidal, facilitating the clinical assessment of MDD. In addition, the ASL technique allows quantitative measurement of brain perfusion and is currently the most popular imaging technique for responding to tissue metabolism. Ye et al. used PCASL to compare regional CBF in ASD individuals with their age-matched typically developing (TD) children using pCASL perfusion imaging and to explore the relationship between CBF and clinical characteristics/developmental profile of ASD. The results indicated that CBF values are a potential MRI-based biomarker of disease severity in ASD patients. The above-mentioned articles explore the structural, functional, or perfusion alterations in specific brain regions of patients with neuropsychiatric disorders through different imaging methods and how these alterations lead to clinical symptoms, as well as providing a basis for future precise treatment of patients.

Several authors in this Research Topic focused on preeclampsia (PE), a condition specific to pregnant women. Zhang N. et al. reviewed PE-related reversible posterior leukoencephalopathy syndrome (RPLS), which is a serious threat to the health of pregnant women. The advantages and characteristic imaging manifestations of different current imaging methods, especially multimodal MRI, for the detection of PE-RPLS were summarized. Because the syndrome can lead to brain injury and has high morbidity and mortality rates, early detection, early diagnosis and prognostic assessment of RPLS can be achieved through ever-advancing imaging techniques. In addition, Wang Y. et al. investigated the changes in cognitive function and serum indicators (P-tau181 protein and T-tau protein) of PE patients during pregnancy. The results showed that PE patients had a certain degree of cognitive impairment, as the cognitive test scores of PE patients were lower than those of the pregnant healthy controls and non-pregnant healthy controls. At the same time, the concentration of serum P-tau181 had a great correlation with the cognitive test scores. Thus, serum P-tau181 protein concentration has potential value in the diagnosis of cognitive impairment in PE patients, which can serve as a simple, accessible, and scalable marker for the screening and diagnosis of cognitive functional impairment in PE. Sui et al. found the local GMV in the right middle temporal gyrus will be significantly reduced, which affected the language motor function and cognitive flexibility in PE superimposed on chronic hypertension patients. These studies highlight the importance of brain damage and cognitive decline in pregnant women with PE, and multimodal MRI methods and serology can be used for early diagnosis and treatment of the disease.

The Research Topic also includes two review reports. Li, Bao et al. reviewed the neuroimaging mechanisms of heart failure (HF)-induced cognitive impairment from MRI perspective and summarized the key roles of decreased cerebral perfusion pressure, an inflammatory response, oxidative stress, and BBB breakdown in the development of cognitive impairment and changes in the structural, functional, and metabolic status of the brain in HF patients. Emerging MRI techniques allow non-invasive detection of functional and structural changes in the brain, which can help further investigate early pathophysiological changes in HF patients with CI. Another review focused on methylmalonic acidemia (MMA), which affects the survival rate and quality of life of newborns or infants, and summarized the neuroimaging features of MMA. The accumulation of methylmalonic acid and other metabolites in the body of patients causes brain tissue damage, which can manifest as various degrees of intellectual disability and severe neurological dysfunction. MRI functional brain imaging can assess the development of the brain and the degree of brain damage, and derive a qualitative diagnosis, which provides an objective basis for early clinical diagnosis and also helps to determine the prognosis and improve the quality of life of patients.

In summary, multimodal MRI plays an increasingly important role in the study of the mechanisms of neuropsychiatric diseases. Obtaining structure-function coupling parameters through multimodal MRI has become a new tool for exploring disease mechanisms, early diagnosis, guiding treatment, and evaluating prognosis. In addition, a single structural or functional study cannot be ignored, and the development of any single technology will drive the development of coupling. The papers in this Research Topic also demonstrated the potential for structure-function coupling in the future.

Author contributions

MF: Writing—original draft, Writing—review and editing. HW: Writing—original draft, Writing—review and editing. JL: Writing—original draft, Writing—review and editing. HL: Writing—original draft, Writing—review and editing. JC: Writing—original draft, Writing—review and editing. LG: Writing—original draft, Writing—review and editing.

Conflict of interest

The authors declare that the research was conducted in the absence of any commercial or financial relationships that could be construed as a potential conflict of interest.

Publisher's note

References

Dugger, B. N., and Dickson, D. W. (2017). Pathology of neurodegenerative diseases. *Cold Spring Harb. Perspect. Biol.* 9:a028035. doi: 10.1101/cshperspect.a028035

Kisler, K., Nelson, A. R., Montagne, A., and Zlokovic, B. V. (2017). Cerebral blood flow regulation and neurovascular dysfunction in Alzheimer disease. *Nat. Rev. Neurosci.* 18, 419–434. doi: 10.1038/nrn.2017.48

Sarwar, T., Tian, Y., Yeo, B. T. T., Ramamohanarao, K., and Zalesky, A. (2021). Structure-function coupling in the human connectome: a machine learning approach. *Neuroimage* 226, 117609. doi: 10.1016/j.neuroimage.2020.117609

frontiers | Frontiers in Aging Neuroscience

TYPE Original Research
PUBLISHED 26 October 2022
DOI 10.3389/fnagi.2022.1041744

OPEN ACCESS

EDITED BY
Lingfei Guo,
Shandong Provincial Hospital Affiliated to Shandong First Medical University, China

REVIEWED BY
Yuanqiang Zhu,
Fourth Military Medical University, China
Weimin Zheng,
Capital Medical University, China

*CORRESPONDENCE
Chao Zhang
chaozhang0328@hotmail.com
Kai Xu
xukai@xzhmu.edu.cn

†These authors have contributed equally to this work

SPECIALTY SECTION
This article was submitted to Neurocognitive Aging and Behavior, a section of the journal Frontiers in Aging Neuroscience

RECEIVED 11 September 2022
ACCEPTED 12 October 2022
PUBLISHED 26 October 2022

CITATION
Zhang X, Li R, Xia Y, Zhao H, Cai L, Sha J, Xiao Q, Xiang J, Zhang C and Xu K (2022) Topological patterns of motor networks in Parkinson's disease with different sides of onset: A resting-state-informed structural connectome study.
Front. Aging Neurosci. 14:1041744.
doi: 10.3389/fnagi.2022.1041744

Topological patterns of motor networks in Parkinson's disease with different sides of onset: A resting-state-informed structural connectome study

Xiuli Zhang[1,2†], Ruohan Li[1,2†], Yingying Xia[1,2], Houliang Zhao[2], Lulu Cai[2], Jingyun Sha[1,2], Qihua Xiao[3], Jie Xiang[4], Chao Zhang[1,2*] and Kai Xu[1,2*]

[1]Department of Radiology, Affiliated Hospital of Xuzhou Medical University, Xuzhou, Jiangsu, China, [2]School of Medical Imaging, Xuzhou Medical University, Xuzhou, Jiangsu, China, [3]Department of Neurology, Affiliated Hospital of Xuzhou Medical University, Xuzhou, Jiangsu, China, [4]Department of Rehabilitation, Affiliated Hospital of Xuzhou Medical University, Xuzhou, Jiangsu, China

Parkinson's disease (PD) has a characteristically unilateral pattern of symptoms at onset and in the early stages; this lateralization is considered a diagnostically important diagnosis feature. We aimed to compare the graph-theoretical properties of whole-brain networks generated by using resting-state functional MRI (rs-fMRI), diffusion tensor imaging (DTI), and the resting-state-informed structural connectome (rsSC) in patients with left-onset PD (LPD), right-onset PD (RPD), and healthy controls (HCs). We recruited 26 patients with PD (13 with LPD and 13 with RPD) as well as 13 age- and sex-matched HCs. Rs-fMRI and DTI were performed in all subjects. Graph-theoretical analysis was used to calculate the local and global efficiency of a whole-brain network generated by rs-fMRI, DTI, and rsSC. Two-sample *t*-tests and Pearson correlation analysis were conducted. Significantly decreased global and local efficiency were revealed specifically in LPD patients compared with HCs when the rsSC network was used; no significant intergroup difference was found by using rs-fMRI or DTI alone. For rsSC network analysis, multiple network metrics were found to be abnormal in LPD. The degree centrality of the left precuneus was significantly correlated with the Unified Parkinson's Disease Rating Scale (UPDRS) score and disease duration ($p = 0.030$, $r = 0.599$; $p = 0.037$, $r = 0.582$). The topological properties of motor-related brain networks can differentiate LPD and RPD. Nodal metrics may serve as important structural features for PD diagnosis and monitoring of disease progression. Collectively, these findings may provide neurobiological insights into the lateralization of PD onset.

KEYWORDS

Parkinson's disease, graph theory, fMRI, diffusion tensor imaging, resting state

Introduction

Parkinson's disease (PD) has a characteristically asymmetrical pattern of onset, manifesting as unilateral motor abnormalities, and the symptoms can remain lateralized throughout the disease course (Djaldetti et al., 2006; Verreyt et al., 2011; Elkurd et al., 2021). Unilateral motor symptoms can help differentiate PD from atypical PD syndrome (Hughes et al., 1992). Left-onset PD (LPD) and right-onset PD (RPD) differ in their progression and risk of complications (Baumann et al., 2014). In particular, a recent study has concluded that patients with LPD may have greater motor and non-motor symptoms but a better quality of life than those with RPD (Cubo et al., 2020). Patients with LPD and RPD respond differently to levodopa and rehabilitation treatments in some cognitive domains (Hanna-Pladdy et al., 2015; Ortelli et al., 2018). An improved understanding of the onset of asymmetric symptoms could aid in the early diagnosis of PD and the monitoring of disease progression, which may enable personalized treatment of PD in the future (Feis et al., 2015). However, it is worth noting that the mechanism that causes the asymmetry of motor symptoms in PD has not yet been elucidated.

Numerous studies have found that PD is a brain network disorder (Canu et al., 2015; Wang et al., 2016; Ji et al., 2018). In the early stages of PD, the accumulation and dissemination of α-synuclein aggregates in the brain are associated with alterations in resting-state functional connectivity (FC) in the basal ganglia and intercortical and intracortical networks (Tessitore et al., 2019). Resting-state functional MRI (rs-fMRI) studies have also provided evidence that motor and non-motor symptoms of PD are closely related to the disruption of brain structural and FC (Yang et al., 2021). The current perspective suggests that the asymmetric motor symptoms of PD may be the result of unequal degeneration of midbrain dopaminergic neurons (Li et al., 2020a); however, it remains difficult to explain the relationship between PD-related brain network alterations and clinical manifestations.

The brain is a complex network with functional integration and separation (Shirer et al., 2012). Rs-fMRI is an established tool to non-invasively and effectively explore intrinsic brain activity, and it has been widely used to investigate neurological diseases (Yagi et al., 2010; Li et al., 2020b). Recently, various approaches based on rs-fMRI have been employed to explore the mechanism of PD; such approaches include spontaneous local brain activity, amplitude of low-frequency fluctuation, regional homogeneity (Li et al., 2020a,b), FC between remote brain regions, and graph-theory-based approaches to clarify the properties of the brain connectome (Kim et al., 2017; Tang et al., 2018). PD patients have been demonstrated to have FC changes in multiple brain regions, such as decreased FC between the premotor cortex and the putamen, increased FC between the primary motor cortex and the cerebellum (Wu et al., 2010), decreased cortico-striatal-thalamic FC (Hacker et al., 2012) and increased FC between the primary motor cortex and the subthalamic nucleus (Baudrexel et al., 2011). Decreased FC indicates disease progression, and increased FC may suggest compensation or remodeling of brain function (Agosta et al., 2014; Ji et al., 2018). Few previous fMRI-based studies have separated LPD from RPD when exploring abnormal brain network connectivity.

Graph-theory-based approaches are a new method of brain network analysis that can quantitatively describe the characteristics of brain connectivity (Sporns, 2018). A previous study using a graph-theory-based approach found that the topological properties of brain networks were disrupted in PD patients; the ability to identify these disruptions can be helpful in diagnosing PD (Kim et al., 2017), evaluating disease progression and monitoring the effects of treatment (Suo et al., 2017; Huang et al., 2020). By investigating the network topological properties of patients with different degrees of cognitive impairment in PD, researchers found that the topological organization of the networks was gradually destroyed; this degradation is a diagnostically useful sign of prodromal PD dementia (Lopes et al., 2017). Comparing the topology of the brain functional connectome between PD patients and healthy controls (HCs) may provide new insight into the pathophysiological mechanisms of PD (Prajapati and Emerson, 2021). However, previous graph-theoretical analysis of PD combined patients with LPD and RPD into a single group to compare them with HCs, whereas little extant research has focused on differences in network properties between PD patients with different sides of onset and HCs.

Functional-by-structural hierarchical (FSH) mapping is a novel method that integrates rs-fMRI and diffusion tensor imaging (DTI) data into a single functional-structural network; this method can improve sensitivity for detecting network-level vulnerabilities in people with subtle age-related cognitive decline before the onset of overt cognitive impairment (Korthauer et al., 2018). It remains unknown whether FSH mapping is sensitive enough to detect brain network differences among LPD patients, RPD patients and HCs. Therefore, the purpose of the present investigation was to compare the graph-theoretical properties of a whole-brain network generated by using rs-fMRI, DTI, and the resting-state-informed structural connectome (rsSC) in patients with LPD, patients with RPD, and HCs. This study is motivated by an interest in discovering how these connectivity measures can help clarify the underlying pathogenesis of LPD and RPD.

Materials and methods

Subjects

This study was approved by the local ethical committee of Xuzhou Affiliated Hospital, Xuzhou Medical University. In compliance with the Declaration of Helsinki, written informed consent was obtained from all subjects before participation.

The project used a convenience sample of 32 right-handed hospitalized PD patients (17 with LPD and 15 with RPD) who met the diagnostic criteria for PD as set forth by the UK Parkinson's Disease Society Brain Bank (Hughes et al., 1992). All patients underwent a comprehensive clinical assessment, including the Unified Parkinson's Disease Rating Scale (UPDRS), Hoehn and Yahr (H-Y) staging, the Montreal Cognitive Assessment (MoCA), and the Mini-Mental State Examination (MMSE). All the patients underwent routine medical treatment, and none of them received any other relevant interventions. Additionally, all patients were free of cognitive impairment. The exclusion criteria for the participants included MRI-confirmed brain abnormalities (trauma, stroke, tumor, and infection) and MRI contraindications (claustrophobia and implanted metal parts). In addition, subjects with a history of drug abuse, alcohol abuse, or syncope were excluded. Fifteen right-handed age- and sex-matched healthy volunteers were included as HCs. All the patients underwent neuropsychological tests and fMRI scans in their off-medication state, and HCs were examined according to the same protocol.

Magnetic resonance imaging data acquisition

All participants were scanned in a 3.0-tesla MRI scanner (GE Medical Systems, Signa HD, Waukesha, WI, USA) with an eight-channel head coil. During MRI scanning, comfortable foam pads were used to stabilize the head of each subject to minimize head motion, and all the subjects wore earplugs to reduce noise from the MRI machine. A 3D-T1 brain volume (BRAVO) sequence was used to acquire high-resolution T1-weighted images, providing isotropic voxels that measured 1 mm × 1 mm × 1 mm. Then, an echo-planar imaging sequence was employed to acquire resting blood oxygen level-dependent images. The parameters of the protocol were as follows: repetition time (TR) = 2,000 ms; echo time (TE) = 30 ms; field of view = 220 mm × 220 mm; slice thickness = 3 mm; slice gap = 1 mm; voxel size = 3.4 mm × 3.4 mm × 4.0 mm; 36 slices; flip angle = 90°; total number of volumes per subject, 185. DTI data were obtained using the following parameters: TR/TE = 9,000/90 ms, matrix = 128 mm × 128 mm, field of view = 256 mm × 256 mm, number of diffusion gradient directions = 64, b value = 1,000, voxel size 3 mm × 2 mm × 2 mm.

Preprocessing of resting-state functional MRI and diffusion tensor imaging data

A graph-theoretical network analysis toolbox for imaging connectomics (GRETNA)[1] was used to perform data preprocessing (Wang et al., 2015). The main steps were as follows: (1) the first 10 time points from each subject were removed; (2) slice-timing correction was used to correct time differences on the remaining 175 volumes; and (3) realignment was used to correct individual-level head motion through Friston's 24-parameter model, and any subject with maximum head displacement >2 mm, maximum rotation >2.0°, or mean framewise displacement (FD) > 0.3 was excluded from the study (Yan et al., 2013; Zhang et al., 2020). To further minimize the potential influence of head motion, mean FD was set as a covariate for further group-level statistics (Satterthwaite et al., 2012; Zeng et al., 2014). Subsequently, individual structural images were coregistered to the mean functional image, and then the transformed structural images were segmented into gray matter, white matter (WM) and cerebrospinal fluid. Diffeomorphic anatomical registration through exponentiated Lie algebra (DARTEL) was performed to estimate the normalization parameters from individual native space to Montreal Neurological Institute (MNI) space (Ashburner, 2007). After spatial normalization, functional images were resampled at a voxel size of 2 mm × 2 mm × 2 mm. The functional volumes were spatially smoothed with a 6-mm full-width-at-half-maximum Gaussian kernel.

Diffusion tensor imaging data in the Digital Imaging and Communications in Medicine (DICOM) format were processed on a Linux workstation. The software Pipeline for Analyzing braiN Diffusion imAges (PANDA) was employed for fully automated processing of brain diffusion images (Cui et al., 2013). The main steps of the process were as follows: (1) converting DICOM data to the NIFTI format; (2) eddy current correction; (3) estimating brain masks; (4) cropping images; and (5) averaging acquisitions and calculating DTI metrics. The resultant warping transformations were then used to resample the images of the diffusion metric of interest (fractional anisotropy, FA) into the MNI space with a customized spatial resolution of 2 mm × 2 mm × 2 mm. Network nodes were defined according to the AAL90 atlas (Ham et al., 2015). Finally, deterministic tractography was performed to obtain the FA matrix, with the following parameters: FA threshold = 0.2–1, angle threshold = 45°.

1 https://www.nitrc.org/projects/gretna/

Network construction of the brain

Edges and nodes are the basic elements of a brain network, where each node represents a brain region and each edge describes the connectivity between two brain regions. We employed GRETNA software to determine the FC, structural connectivity, and functional-structural matrices on the basis of brain images (Chung et al., 2019). For the construction of the FC network, each node was defined using the AAL90 brain atlas template, and each region was considered a node to create the connectivity matrix. The edges were calculated using Pearson correlation coefficients of the mean time series obtained from each node. Finally, the 90 × 90 FC matrix was determined for each subject. The definition of each node of the structural network was also using the AAL90 brain atlas template, and the edges of the structural network were defined as WM fiber between each node, which were constructed utilizing deterministic fiber tracing technology. Similarly, the 90 × 90 WM matrix was determined for each subject.

The sparsity threshold was applied to create the binary matrix (adjacency matrix). The sparsity threshold denotes the ratio of the number of actual edges to the total number of possible edges in the fMRI matrix. We used threshold values ranging from 0.05 to 0.5 within 0.05 intervals to remove the possible false edges of the fMRI matrix. We chose an FA threshold of 0, leaving the DTI matrix unchanged. Next, the fMRI and DTI matrices were z-transformed before being input into the FSH mapping pipeline.

Functional-by-structural hierarchical mapping

The FSH mapping pipeline has been described in detail in previous works in the literature (Leow et al., 2012; Ajilore et al., 2014; Korthauer et al., 2018). Briefly, FSH mapping employs simulated annealing to find the optimal utilization matrix to maximize the observed goodness-of-fit between rs-fMRI and rsSC. Using a randomly chosen starting seed, calculate the probability distribution to create the optimal solution U for each group. A Weighted rsSCs were then created by multiplying each participant's structural connectivity matrix S by the binarized group U matrix. In the current study, FSH mapping was used to integrate the functional data (in the form of FC) and structural data (in the form of FA) into a single graph and generate rsSC. WM fiber connectivity and resting-state brain FC are not intended to be equivalent; resting-state FC can correspond to either direct or indirect neuroanatomical WM connections between two brain regions. FSH mapping assumes that higher levels of rs-fMRI correlation reflect stronger structural interactions, and FC data may be used to infer the underlying pattern of WM engagement that occurs during this particular resting state. The resulting rsSC in this study reflects the FA network underlying the observed functional connectome.

Statistical analysis

A chi-square test was employed to test for significant differences in gender distribution, and a one-way ANOVA test was used to observe the age difference among the three groups. For the LPD and RPD groups, a two-sample t-test was performed to analyze intergroup differences in disease duration, UPDRS scores, H-Y stages, MoCA scores, and MMSE scores. The statistical analysis described above was performed in SPSS version 28.0 (SPSS Inc., Chicago, IL, USA). These group differences in global and nodal metrics were compared through a two-sample t-test by using the GRETNA toolbox, and the results were corrected for multiple comparisons using the false discovery rate (FDR) correction with a threshold of $p < 0.05$. To further observe the relationship between brain network changes and clinical symptoms, Pearson correlation analysis was conducted between network metrics and clinical scale scores, including UPDRS scores, H-Y stages, MoCA scores, and MMSE scores.

Results

Demographics of the participants

Six patients and four healthy volunteers were excluded due to obvious head movement or failure to complete the scored evaluations. Ultimately, 13 LPD patients (7 males and 6 females, 60.62 ± 6.39 years old), 13 RPD patients (8 males and 5 females, 59.15 ± 6.26 years old), and 13 healthy volunteers (5 males and 8 females, 61.42 ± 7.42 years old) were included in the present study. No significant difference was found in age ($p = 0.72$) or gender ($p = 0.45$) among the LPD, RPD, and HC groups. There was also no difference in PD duration, UPDRS scores, H-Y stages, MoCA scores, or MMSE scores between the LPD and RPD groups ($p > 0.05$) (**Table 1**).

Group analysis of global network metrics

All three groups of subjects (LPD patients, RPD patients, and HCs) showed small-world properties (**Supplementary Figure 1**). In the comparison fMRI and DTI network metrics, no significant difference was found in global or local efficiency

TABLE 1 Demographics and clinical data.

Variable	HCs (N = 13)	LPD (N = 13)	RPD (N = 13)	p
Gender (M/F)	5/8	7/6	8/5	0.45[#]
Age (years)	61.42 ± 7.42	60.62 ± 6.39	59.15 ± 6.26	0.72*
Duration of PD (years)	N/A	3.92 ± 1.85	3.6 ± 1.76	0.67[&]
UPDRS-III score	N/A	24.08 ± 6.76	24.53 ± 6.31	0.28[&]
H-Y stage	N/A	1.65 ± 0.80	1.84 ± 0.66	0.27[&]
MoCA score	N/A	25.15 ± 2.15	24.04 ± 2.81	0.86[&]
MMSE score	N/A	27.9 ± 1.12	27.38 ± 1.33	0.51[&]

PD, Parkinson's disease; HCs, healthy controls; M, male; F, female; UPDRS-III, Unified Parkinson's Disease Rating Scale; H-Y, Hoehn and Yahr; MoCA, Montreal Cognitive Assessment; MMSE, Mini-Mental State Examination.
Data are presented as range and mean ± SD.
[#]The p-value was obtained using a chi-square test.
*The p-value was obtained using a one-way ANOVA test.
[&]The p-value was obtained using a two-sample t-test.

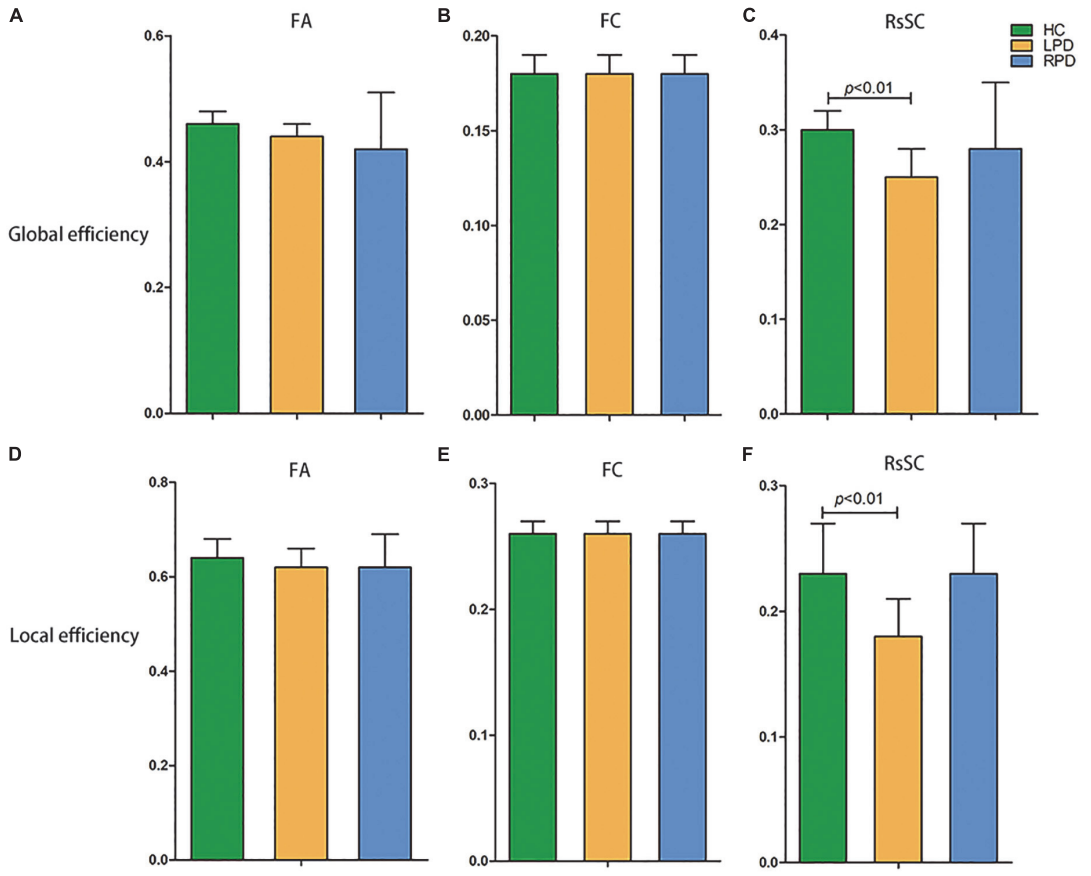

FIGURE 1
Decreased global efficiency **(C)** and local efficiency **(F)** were revealed in left-onset PD (LPD) patients compared with healthy controls (HCs) when the resting-state-informed structural connectome (rsSC) network was used, but no difference in global or local efficiency was revealed between LPD and right-onset PD (RPD) or between RPD and HCs. In the comparison fMRI (FC) and DTI (FA) network metrics, no significant difference was found in global or local efficiency among the LPD, RPD and HC groups **(A,B,D,E)**. FA, fractional anisotropy; FC, functional connectivity.

between the LPD and HC groups or between the RPD and HC groups. However, the rsSC network revealed significantly decreased global and local efficiency in LPD patients compared with HCs, while no difference in global or local efficiency was revealed between the LPD and RPD groups or between the RPD and HC groups (Figure 1).

TABLE 2 Coordinates and abbreviations for the network nodes of the automated anatomical labeling (AAL) atlas.

Nodal metrics	Regions	Abbreviation	MNI coordinates			Brodmann area (BA)
			X	*Y*	*Z*	
Betweenness centrality	Superior occipital gyrus	SOG.L	−16	−84	28	BA7
		SOG.R	24	81	30	BA7
	Middle occipital gyrus	MOG.L	−32	−81	16	BA7
		MOG.R	37	−80	19	BA7
Degree centrality	Superior occipital gyrus	SOG.L	−16	−84	28	BA7
	Rolandic operculum	ROL.R	53	−6	14	BA6
	Supplementary motor area	SMA.R	8	0	62	BA4/6/8
	Precentral gyrus	PreCG.L	−5	−43	25	BA4/6
	Rolandic operculum	ROL.R	53	−6	14	BA6
	Precuneus	PCUN.L	−7	−56	48	BA4/5/7
	Precuneus	PCUN.R	10	−56	44	BA4/5/7
Nodal efficiency	Median cingulate and paracingulate gyri	DCG.L	−5	−15	42	BA6
	Precentral gyrus	PreCG.L	−5	−43	25	BA4/6
	Paracentral lobule	PCL.L	−7	−25	71	BA4/6
	Precuneus	PCUN.L	−7	−56	48	BA5/7
	Supplementary motor area	SMA.R	8	0.2	62	BA4/6/8
	Paracentral lobule	PCL.R	7	−31	68	BA4
	Superior occipital gyrus	SOG.L	−16	−84	28	BA7

Group analysis of nodal network metrics in motor-related brain regions

The purpose of this study was to investigate the topological pattern of the motor-related networks on the side of PD onset; therefore, we chose the motion-related network for further analysis based on the Brodmann area (BA) template as well as the AAL template (Table 2).

Upon fMRI and DTI network analysis, we found no significant difference in the nodal network metrics when LPD and RPD patients were compared with HCs. Upon rsSC network analysis, we found significant intergroup differences in multiple network metrics (Table 2). Upon BC analysis, LPD patients showed increased BC in the bilateral superior occipital gyrus (SOG) and bilateral middle occipital gyrus (MOG) and decreased BC in the right Rolandic operculum (ROL.R) (Figure 2). In the DC comparison, LPD patients showed decreased DC in the left median cingulate and paracingulate gyri (DCG.L), right supplementary motor area (SMA.R), left precentral gyrus (PreCG.L), ROL.R, and bilateral precuneus (PCUN) as well as increased DC in the left SOG (SOG.L) (Figure 3). In the NE study, LPD patients showed decreased NE in the DCG.L, left PreCG (PreCG.L), bilateral paracentral lobule (PCL), and SMA.R as well as increased NE in the SOG.L (Figure 4). However, RPD patients did not show obvious differences in nodal network metrics compared with HCs.

Upon correlation analysis, we found that the NE of the PCL.L and the DC of the PCUN.L were significantly correlated with UPDRS scores ($p = 0.031$, $r = 0.599$; $p = 0.030$, $r = 0.599$). In addition, the DC of the PCUN.L was found to be significantly associated with disease duration ($p = 0.037$, $r = 0.582$) (Figure 5). No other significant correlation was revealed between network metrics and clinical scores.

Discussion

We investigated the topological properties of the functional and structural connectomes of PD patients with different sides of onset. The property of small-worldness was present in PD. The current study found the following on the basis of the rsSC network: (1) significant differences in brain network metrics were detectable among patients with different sides of onset and HCs when graph-theoretical measures were used to characterize the properties of rsSC, even though no difference was evident from the rs-fMRI- or DTI-derived network alone; (2) significantly decreased global efficiency and local efficiency were evident in LPD patients; (3) compared with HCs, patients with LPD showed obvious abnormalities at the nodal level, such as decreased DC/NE and increased BC in multiple motor-related networks; and (4) certain brain regions were significantly associated with clinical conditions, including disease duration and UPDRS scores. These findings may provide neurobiological insights into the lateralization of the onset of PD.

Graph-theoretical indices have been considered to be more sensitive than traditional region of interest (ROI)–based analysis for detecting early-stage brain aberrations

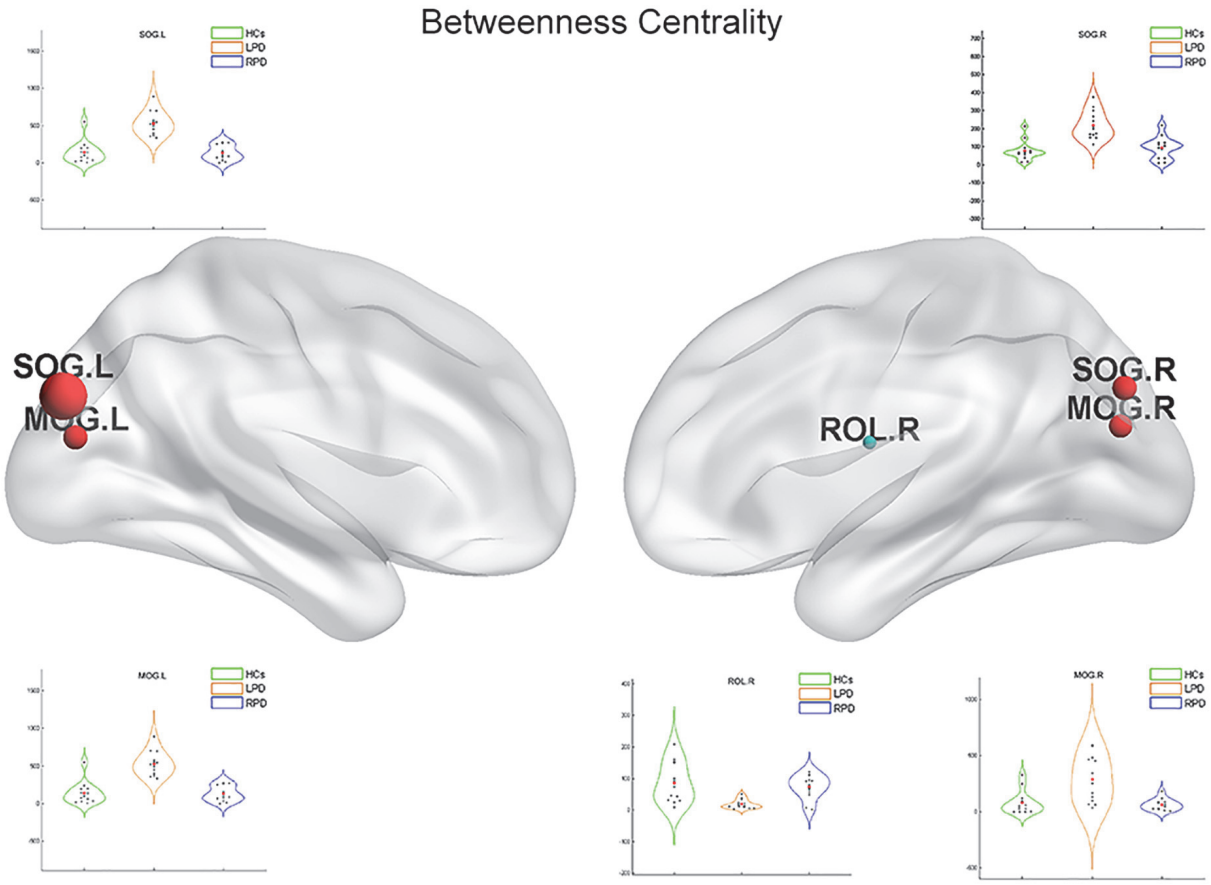

FIGURE 2
Left-onset PD (LPD) patients showed increased betweenness centrality (BC) in the bilateral superior occipital gyrus and bilateral middle occipital gyrus as well as decreased BC in the right Rolandic operculum.

(Bullmore and Sporns, 2009). The brain has properties of functional separation and integration. Brain network integration can be measured using global efficiency, which is the average inverse shortest path length in the network. Local efficiency is defined by evaluating which of a node's neighbors are neighbors of each other and is a measure of network segregation. The accumulation and dissemination of α-synuclein aggregates in the brain in the early stages of PD has been demonstrated to be associated with alterations in resting-state FC in the basal ganglia, intercortical, and intracortical networks (Stanziano et al., 2021). It has also been demonstrated that brain structural and functional connections are damaged in the early stages of PD. A previous rs-fMRI study of 54 PD patients found that the global efficiency of the motor network was decreased in PD patients compared with tremor patients and HCs (Novaes et al., 2021). Another rs-fMRI study showed that the global and local efficiency of the sensorimotor network and the visual network were disrupted in PD (Fang et al., 2017). In addition, a study of 23 early-stage PD patients showed that these patients had reduced global efficiency and segregation of structural brain network information processing compared with HCs (Vriend et al., 2018). In our study, rsSC networks showed that global and local efficiency were significantly reduced in patients with LPD; this finding is consistent with previous studies. On the other hand, we found no group difference in global or local efficiency generated through the rs-fMRI or DTI network alone, which may be because the sample size was too small to provide sufficient statistical power; however, this also demonstrates that rsSC is more sensitive than either rs-fMRI or DTI alone in identifying abnormal brain network properties in patients with PD (Korthauer et al., 2018). Furthermore, unlike previous studies, our study delineated the brain networks of LPD and RPD separately, and only patients with LPD were revealed to have abnormal network topology.

To observe local separation of brain function, three nodal metrics of the motor-related networks, namely, the DC, BC, and NE, were compared between groups by using rsSC. The nodal metrics for all rs-fMRI and DTI connectomes were calculated over the sparsity threshold. DC and BC can measure how important a node is within a network, that

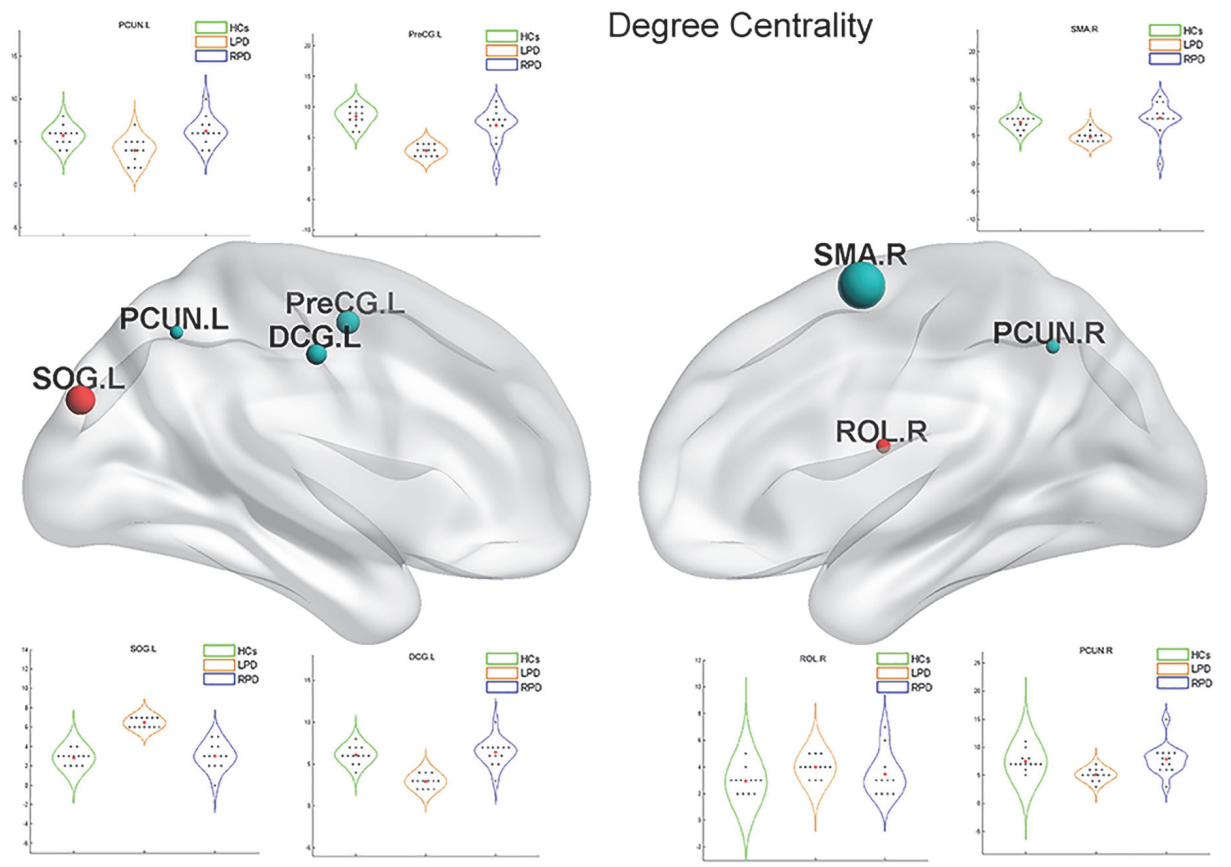

FIGURE 3
Left-onset PD (LPD) patients showed decreased degree centrality (DC) in the left median cingulate and paracingulate gyri, right supplementary motor area, left precentral gyrus, right Rolandic operculum, and bilateral precuneus as well as increased DC in the left superior occipital gyrus.

is, the centrality of a node, while NE is mainly related to short-range connections, which represent the capacity for local integration and transmission of information. Compared with HCs, LPD patients showed rsSC abnormalities in the motor-related networks, including the primary motor cortex (bilateral PCL), somatosensory association cortex (PreCG.L and DCG.L), and SMA. The most significant reductions in BC and DC were found in the primary motor cortex, SMA, PreCG, and bilateral PCUN, which are closely related to various motor functions (Ugur et al., 2005; Ikeda, 2007; Thibes et al., 2017; Bhattacharjee et al., 2021). Previous studies have demonstrated that stimulation of the primary motor cortex can significantly reduce the slowing and loss of motor function in patients with PD (Qiu et al., 2019). The current study found the BC and DC of the PCL.L simultaneously decreased in patients with LPD; additionally, the NE of the PCL.L was revealed to be closely correlated with the UPDRS score. The current findings indicated that the NE of the PCL.L can quantify motor dysfunction in patients with PD, which may provide theoretical support for future targeted therapy.

The PreCG.L is an important cortical projection region in the striato-thalamo-cortical (STC) loop and is responsible for the planning, initiation, and execution of exercise. The STC forms the neural network basis of PD bradykinesia, myotonia, and resting tremor (DeLong et al., 1984; Alexander et al., 1986; Lewis et al., 2007) as part of its involvement in PD (Stankovic et al., 2014). In addition, the SMA, one of the major components of the sensorimotor STC loop, rapidly evaluates successful and erroneous actions and thus mediates action monitoring (Bonini et al., 2014). In the present study, the LPD group exhibited nodal property alterations in the regions of the STC loop. Decreased nodal centrality and local information processing efficiency in these motor-related areas indicated their reduced roles in the motor-related networks of patients with PD. In addition, we found that the NE of the PreCG.L decreased, which means that there were fewer short-range connections in the PreCG.L and that the capacity for local integration of information was disrupted. The PreCG is an important portion of the cerebello-thalamo-cortical (CTC) loop. This circuit connects regions of the cerebellar cortex with the cerebral cortex. Lateral portions of the cerebellar cortex send projections

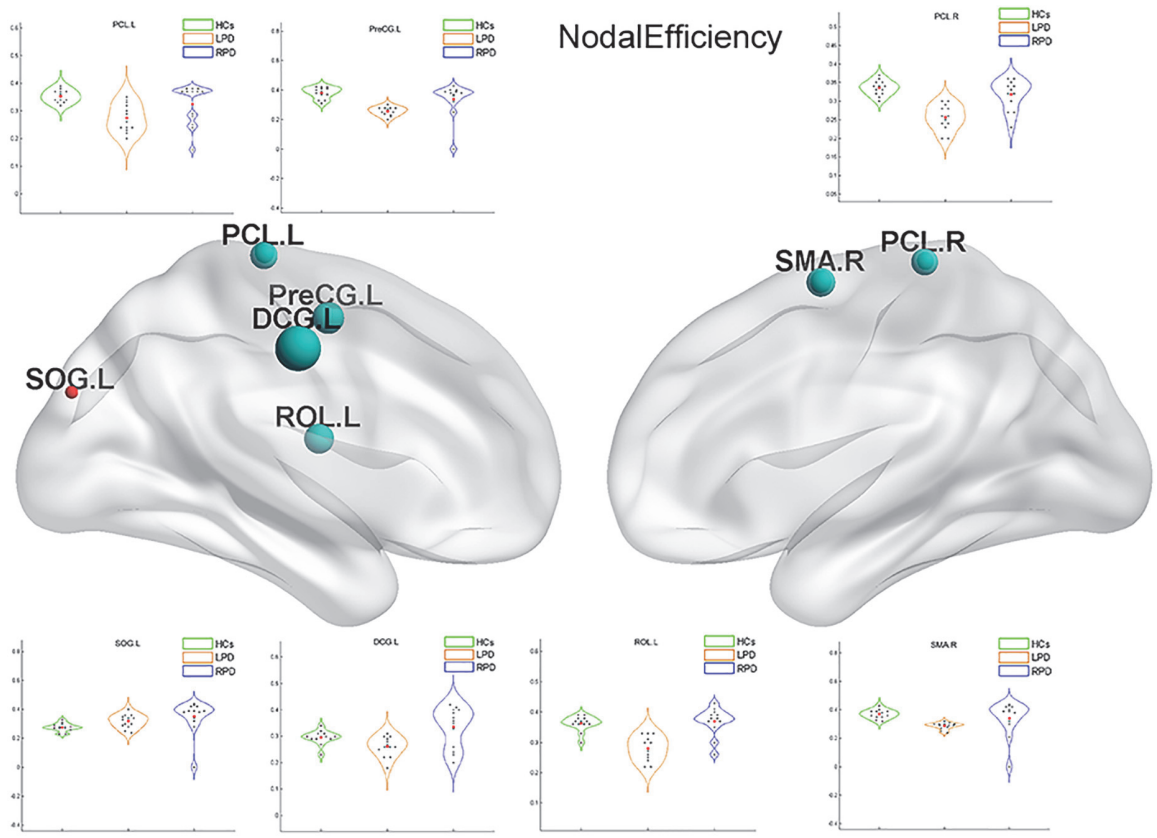

FIGURE 4
Left-onset PD (LPD) patients showed decreased nodal efficiency (NE) in the left median cingulate and paracingulate gyri, left precentral gyrus, bilateral paracentral lobule, and right supplementary motor area as well as increased NE in the left superior occipital gyrus.

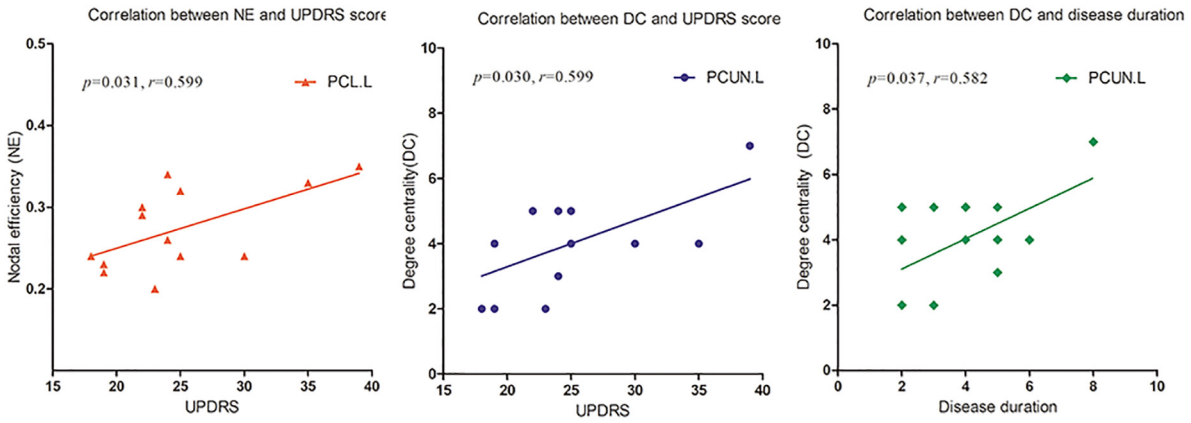

FIGURE 5
The nodal efficiency (NE) of left paracentral lobule (PCL.L) and degree centrality (DC) of the left precuneus (PCUN.L) were significantly correlated with Unified Parkinson's Disease Rating Scale (UPDRS) scores (p = 0.031, r = 0.599; p = 0.030, r = 0.599). The DC of PCUN.L was also found to be significantly associated with disease duration (p = 0.037, r = 0.582).

via the dentate nucleus to the thalamus, which, in turn, projects to specific cortical areas. The CTC loop is generally considered a compensatory network, capable of offsetting the ill effects of STC degradation on motor regulation (Martinu and Monchi, 2013). The disrupted efficiency of the PreCG may be the result of this effect.

The DC of the bilateral PCUN in patients with LPD was decreased. The PCUN located mainly in the medial and posterior parietal lobe, consumes 35% more glucose than other brain regions in the resting state (Gusnard et al., 2001). According to previously published reports by our group and others, the PCUN.L is a vulnerable area, and it is closely associated with motor and non-motor symptoms of PD (Thibes et al., 2017; Jia et al., 2018; Zhang et al., 2019). Furthermore, we found that the DC of the PCUN.L was significantly related to the UPDRS score and disease duration. Thus, DC can not only directly reflect disruption of the PCUN.L but also quantify the degree of motor function impairment. Our study once again proved the importance of the PCUN.L in PD, and this region may be useful as a potential imaging feature to diagnose PD and monitor its progression.

Interestingly, we found that LPD patients showed increased BC in several regions of the occipital lobe, such as the bilateral SOG and MOG. The occipital lobe is the visual information processing center, which contains most of the visual cortex–related areas and participates in the transmission and reception of most visual information. The occipital lobe was demonstrated to be a vulnerable structure in studies of spontaneous brain activity and brain morphology (Uribe et al., 2016; Chen et al., 2022). The regional brain activity and volume of the occipital lobe were found to decrease in PD patients. However, other studies showed that the SOG and MOG had greater activity and volume in PD patients than in HCs (Choe et al., 2013; Li et al., 2016), which might reflect compensation for the disruption of visuospatial ability in PD. Increased nodal centrality in these brain regions in the current study indicates improved visual information integration in LPD patients and may further confirm its compensatory role in maintaining normal brain function, even normal motor function.

In our study, there were no evident differences in these regional metrics between RPD patients and HCs. Some researchers have proposed that RPD patients have better neural reserve and greater neural plasticity than LPD patients, and previous research has shown that patients with dominant-side onset exhibit a greater ability to cope with PD-related pathological changes than those with non-dominant-side onset (Ham et al., 2015; Chung et al., 2019). In the current study, all the subjects were right-handed. This may explain why patients with RPD did not markedly differ from HCs. The small sample size may be another potential factor underlying the lack of significant difference.

This study had some limitations. First, some patients with PD received dopamine treatment; although the treatment was terminated before MRI scanning, a possible effect of the drug cannot be completely ruled out. Second, the current analysis was not performed on different motor subtypes; it would have been more informative to do so. Finally, the current findings are based on a small sample; future studies should use larger sample sizes for in-depth exploration.

Conclusion

In this study, we used rs-fMRI, DTI and FSH approaches to investigate the topological organization of the brain functional and structural connectome in PD with different sides of onset. The topological properties of the brain network differed between LPD and RPD. The nodal metrics may serve as potential imaging features to diagnose PD and monitor its progression. Collectively, these findings may provide neurobiological insights into the lateralization of the onset of PD.

Data availability statement

The original contributions presented in this study are included in the article/**Supplementary material**, further inquiries can be directed to the corresponding authors.

Ethics statement

The studies involving human participants were reviewed and approved by Xuzhou Affiliated Hospital. The patients/participants provided their written informed consent to participate in this study.

Author contributions

XZ, CZ, and KX: research project conception. XZ, YX, and JX: research project organization and execution. HZ, RL, JS, QX, and CZ: statistical analysis design and execution. QX, RL, JX, and KX: statistical analysis review. XZ, YX, and LC: writing of the first draft. RL and KX: manuscript review. CZ and KX: take responsibility for the data. All authors contributed to the article and approved the submitted version.

Funding

This research was supported by a project of the Affiliated Hospital of Xuzhou Medical University (2020KA013).

Acknowledgments

We thank the study participants and the staff of the Department of Radiology.

Conflict of interest

The authors declare that the research was conducted in the absence of any commercial or financial relationships that could be construed as a potential conflict of interest.

Publisher's note

All claims expressed in this article are solely those of the authors and do not necessarily represent those of their affiliated organizations, or those of the publisher, the editors and the reviewers. Any product that may be evaluated in this article, or claim that may be made by its manufacturer, is not guaranteed or endorsed by the publisher.

Supplementary material

The Supplementary Material for this article can be found online at: https://www.frontiersin.org/articles/10.3389/fnagi.2022.1041744/full#supplementary-material

References

Agosta, F., Caso, F., Stankovic, I., Inuggi, A., Petrovic, I., Svetel, M., et al. (2014). Cortico-striatal-thalamic network functional connectivity in hemiparkinsonism. *Neurobiol. Aging* 35, 2592–2602. doi: 10.1016/j.neurobiolaging.2014.05.032

Ajilore, O., Lamar, M., Leow, A., Zhang, A., Yang, S., and Kumar, A. (2014). Graph theory analysis of cortical-subcortical networks in late-life depression. *Am. J. Geriatr. Psychiatry* 22, 195–206. doi: 10.1016/j.jagp.2013.03.005

Alexander, G. E., Delong, M. R., and Strick, P. L. (1986). Parallel organization of functionally segregated circuits linking basal ganglia and cortex. *Annu. Rev. Neurosci.* 9, 357–381. doi: 10.1146/annurev.ne.09.030186.002041

Ashburner, J. (2007). A fast diffeomorphic image registration algorithm. *Neuroimage* 38, 95–113. doi: 10.1016/j.neuroimage.2007.07.007

Baudrexel, S., Witte, T., Seifried, C., Von Wegner, F., Beissner, F., Klein, J. C., et al. (2011). Resting state fMRI reveals increased subthalamic nucleus-motor cortex connectivity in Parkinson's disease. *Neuroimage* 55, 1728–1738. doi: 10.1016/j.neuroimage.2011.01.017

Baumann, C. R., Held, U., Valko, P. O., Wienecke, M., and Waldvogel, D. (2014). Body side and predominant motor features at the onset of Parkinson's disease are linked to motor and nonmotor progression. *Mov. Disord.* 29, 207–213. doi: 10.1002/mds.25650

Bhattacharjee, S., Kashyap, R., Abualait, T., Chen, S. H. A., Yoo, W. K., and Bashir, S. (2021). The role of primary motor cortex: More than movement execution. *J. Motor Behav.* 53, 258–274. doi: 10.1080/00222895.2020.1738992

Bonini, F., Burle, B., Liegeois-Chauvel, C., Regis, J., Chauvel, P., and Vidal, F. (2014). Action monitoring and medial frontal cortex: Leading role of supplementary motor area. *Science* 343, 888–891. doi: 10.1126/science.1247412

Bullmore, E., and Sporns, O. (2009). Complex brain networks: Graph theoretical analysis of structural and functional systems. *Nat. Rev. Neurosci.* 10, 186–198. doi: 10.1038/nrn2575

Canu, E., Agosta, F., Sarasso, E., Volontè, M. A., Basaia, S., Stojkovic, T., et al. (2015). Brain structural and functional connectivity in Parkinson's disease with freezing of gait. *Hum. Brain Mapp.* 36, 5064–5078. doi: 10.1002/hbm.22994

Chen, M., Li, Y., Chen, J., Gao, L., Sun, J., Gu, Z., et al. (2022). Structural and functional brain alterations in patients with idiopathic rapid eye movement sleep behavior disorder. *J. Neuroradiol.* 49, 66–72. doi: 10.1016/j.neurad.2020.04.007

Choe, I. H., Yeo, S., Chung, K. C., Kim, S. H., and Lim, S. (2013). Decreased and increased cerebral regional homogeneity in early Parkinson's disease. *Brain Res.* 1527, 230–237. doi: 10.1016/j.brainres.2013.06.027

Chung, S. J., Yoo, H. S., Lee, H. S., Lee, P. H., and Sohn, Y. H. (2019). Does the side onset of Parkinson's disease influence the time to develop levodopa-induced dyskinesia? *J. Parkinsons Dis.* 9, 241–247. doi: 10.3233/JPD-181512

Cubo, E., Martínez-Martín, P., González-Bernal, J., Casas, E., Arnaiz, S., Miranda, J., et al. (2020). Effects of motor symptom laterality on clinical manifestations and quality of life in Parkinson's disease. *J. Parkinsons Dis.* 10, 1611–1620. doi: 10.3233/JPD-202067

Cui, Z., Zhong, S., Xu, P., He, Y., and Gong, G. (2013). PANDA: A pipeline toolbox for analyzing brain diffusion images. *Front. Hum. Neurosci.* 7:42. doi: 10.3389/fnhum.2013.00042

DeLong, M. R., Alexander, G. E., Georgopoulos, A. P., Crutcher, M. D., Mitchell, S. J., and Richardson, R. T. (1984). Role of basal ganglia in limb movements. *Hum. Neurobiol.* 2, 235–244.

Djaldetti, R., Ziv, I., and Melamed, E. (2006). The mystery of motor asymmetry in Parkinson's disease. *Lancet Neurol.* 5, 796–802. doi: 10.1016/S1474-4422(06)70549-X

Elkurd, M., Wang, J., and Dewey, R. B. (2021). Lateralization of motor signs affects symptom progression in Parkinson disease. *Front. Neurol.* 12:711045. doi: 10.3389/fneur.2021.711045

Fang, J., Chen, H., Cao, Z., Jiang, Y., Ma, L., Ma, H., et al. (2017). Impaired brain network architecture in newly diagnosed Parkinson's disease based on graph theoretical analysis. *Neurosci. Lett.* 657, 151–158. doi: 10.1016/j.neulet.2017.08.002

Feis, D. L., Pelzer, E. A., Timmermann, L., and Tittgemeyer, M. (2015). Classification of symptom-side predominance in idiopathic Parkinson's disease. *NPJ Parkinsons Dis.* 1:15018. doi: 10.1038/npjparkd.2015.18

Gusnard, D. A., Akbudak, E., Shulman, G. L., and Raichle, M. E. (2001). Medial prefrontal cortex and self-referential mental activity: Relation to a default mode of brain function. *Proc. Natl. Acad. Sci. U.S.A.* 98, 4259–4264. doi: 10.1073/pnas.071043098

Hacker, C. D., Perlmutter, J. S., Criswell, S. R., Ances, B. M., and Snyder, A. Z. (2012). Resting state functional connectivity of the striatum in Parkinson's disease. *Brain* 135, 3699–3711. doi: 10.1093/brain/aws281

Ham, J. H., Lee, J. J., Kim, J. S., Lee, P. H., and Sohn, Y. H. (2015). Is dominant-side onset associated with a better motor compensation in Parkinson's disease? *Mov. Disord.* 30, 1921–1925. doi: 10.1002/mds.26418

Hanna-Pladdy, B., Pahwa, R., and Lyons, K. E. (2015). Paradoxical effect of dopamine medication on cognition in Parkinson's disease: Relationship to side of motor onset. *J. Int. Neuropsychol. Soc.* 21, 259–270. doi: 10.1017/S1355617715000181

Huang, L. C., Wang, H. Z., Chu, Y. C., Ng, K. F., and Chuang, C. K. (2020). Clinicopathological presentation and management of penile Schwannoma. *Sex Med. Rev.* 8, 615–621. doi: 10.1016/j.sxmr.2019.12.001

Hughes, A. J., Daniel, S. E., Kilford, L., and Lees, A. J. (1992). Accuracy of clinical diagnosis of idiopathic Parkinson's disease: A clinico-pathological study of 100 cases. *J. Neurol. Neurosurg. Psychiatry* 55, 181–184. doi: 10.1136/jnnp.55.3.181

Ikeda, A. (2007). [Human supplementary motor area: A role in voluntary movements and its clinical significance]. *Rinsho Shinkeigaku* 47, 723–726.

Ji, G. J., Hu, P., Liu, T. T., Li, Y., Chen, X., Zhu, C., et al. (2018). Functional connectivity of the corticobasal ganglia-thalamocortical network in Parkinson disease: A systematic review and meta-analysis with cross-validation. *Radiology* 287, 973–982. doi: 10.1148/radiol.2018172183

Jia, X., Li, Y., Li, K., Liang, P., and Fu, X. (2018). Precuneus dysfunction in Parkinson's disease with mild cognitive impairment. *Front. Aging Neurosci.* 10:427. doi: 10.3389/fnagi.2018.00427

Kim, J., Criaud, M., Cho, S. S., Díez-Cirarda, M., Mihaescu, A., Coakeley, S., et al. (2017). Abnormal intrinsic brain functional network dynamics in Parkinson's disease. *Brain* 140, 2955–2967. doi: 10.1093/brain/awx233

Korthauer, L. E., Zhan, L., Ajilore, O., Leow, A., and Driscoll, I. (2018). Disrupted topology of the resting state structural connectome in middle-aged APOE epsilon4 carriers. *Neuroimage* 178, 295–305. doi: 10.1016/j.neuroimage.2018.05.052

Leow, A. D., Zhan, L., Arienzo, D., Gadelkarim, J. J., Zhang, A. F., Ajilore, O., et al. (2012). Hierarchical structural mapping for globally optimized estimation of functional networks. *Med. Image Comput. Comput. Assist. Interv.* 15, 228–236. doi: 10.1007/978-3-642-33418-4_29

Lewis, M. M., Slagle, C. G., Smith, A. B., Truong, Y., Bai, P., Mckeown, M. J., et al. (2007). Task specific influences of Parkinson's disease on the striato-thalamo-cortical and cerebello-thalamo-cortical motor circuitries. *Neuroscience* 147, 224–235. doi: 10.1016/j.neuroscience.2007.04.006

Li, K., Su, W., Chen, M., Li, C. M., Ma, X. X., Wang, R., et al. (2020a). Abnormal spontaneous brain activity in left-onset Parkinson disease: A resting-state functional MRI study. *Front. Neurol.* 11:727. doi: 10.3389/fneur.2020.00727

Li, K., Zhao, H., Li, C. M., Ma, X. X., Chen, M., Li, S. H., et al. (2020b). The relationship between side of onset and cerebral regional homogeneity in Parkinson's disease: A resting-state fMRI study. *Parkinsons Dis.* 2020:5146253. doi: 10.1155/2020/5146253

Li, Y., Liang, P., Jia, X., and Li, K. (2016). Abnormal regional homogeneity in Parkinson's disease: A resting state fMRI study. *Clin. Radiol.* 71, e28–e34. doi: 10.1016/j.crad.2015.10.006

Lopes, R., Delmaire, C., Defebvre, L., Moonen, A. J., Duits, A. A., Hofman, P., et al. (2017). Cognitive phenotypes in parkinson's disease differ in terms of brain-network organization and connectivity. *Hum. Brain Mapp.* 38, 1604–1621. doi: 10.1002/hbm.23474

Martinu, K., and Monchi, O. (2013). Cortico-basal ganglia and cortico-cerebellar circuits in Parkinson's disease: Pathophysiology or compensation? *Behav. Neurosci.* 127, 222–236. doi: 10.1037/a0031226

Novaes, N. P., Balardin, J. B., Hirata, F. C., Melo, L., Amaro, E. Jr., Barbosa, E. R., et al. (2021). Global efficiency of the motor network is decreased in Parkinson's disease in comparison with essential tremor and healthy controls. *Brain Behav.* 11, e02178. doi: 10.1002/brb3.2178

Ortelli, P., Ferrazzoli, D., Zarucchi, M., Maestri, R., and Frazzitta, G. (2018). Asymmetric dopaminergic degeneration and attentional resources in Parkinson's disease. *Front. Neurosci.* 12:972. doi: 10.3389/fnins.2018.00972

Prajapati, R., and Emerson, I. A. (2021). Global and regional connectivity analysis of resting-state function MRI brain images using graph theory in Parkinson's disease. *Int. J. Neurosci.* 131, 105–115. doi: 10.1080/00207454.2020.1733559

Qiu, T., Zhang, Y., Tang, X., Liu, X., Wang, Y., Zhou, C., et al. (2019). Precentral degeneration and cerebellar compensation in amyotrophic lateral sclerosis: A multimodal MRI analysis. *Hum. Brain Mapp.* 40, 3464–3474. doi: 10.1002/hbm.24609

Satterthwaite, T. D., Wolf, D. H., Loughead, J., Ruparel, K., Elliott, M. A., Hakonarson, H., et al. (2012). Impact of in-scanner head motion on multiple measures of functional connectivity: Relevance for studies of neurodevelopment in youth. *Neuroimage* 60, 623–632. doi: 10.1016/j.neuroimage.2011.12.063

Shirer, W. R., Ryali, S., Rykhlevskaia, E., Menon, V., and Greicius, M. D. (2012). Decoding subject-driven cognitive states with whole-brain connectivity patterns. *Cereb. Cortex* 22, 158–165. doi: 10.1093/cercor/bhr099

Sporns, O. (2018). Graph theory methods: Applications in brain networks. *Dialogues Clin. Neurosci.* 20, 111–121. doi: 10.31887/DCNS.2018.20.2/osporns

Stankovic, I., Krismer, F., Jesic, A., Antonini, A., Benke, T., Brown, R. G., et al. (2014). Cognitive impairment in multiple system atrophy: A position statement by the Neuropsychology Task Force of the MDS Multiple System Atrophy (MODIMSA) study group. *Mov. Disord.* 29, 857–867. doi: 10.1002/mds.25880

Stanziano, M., Golfre Andreasi, N., Messina, G., Rinaldo, S., Palermo, S., Verri, M., et al. (2021). Resting state functional connectivity signatures of MRgFUS vim thalamotomy in Parkinson's disease: A preliminary study. *Front. Neurol.* 12:786734. doi: 10.3389/fneur.2021.786734

Suo, X., Lei, D., Li, N., Cheng, L., Chen, F., Wang, M., et al. (2017). Functional brain connectome and its relation to hoehn and yahr stage in Parkinson disease. *Radiology* 285, 904–913. doi: 10.1148/radiol.2017162929

Tang, Y., Liu, B., Yang, Y., Wang, C. M., Meng, L., Tang, B. S., et al. (2018). Identifying mild-moderate Parkinson's disease using whole-brain functional connectivity. *Clin. Neurophysiol.* 129, 2507–2516. doi: 10.1016/j.clinph.2018.09.006

Tessitore, A., Cirillo, M., and De Micco, R. (2019). Functional connectivity signatures of Parkinson's disease. *J. Parkinsons Dis.* 9, 637–652. doi: 10.3233/JPD-191592

Thibes, R. B., Novaes, N. P., Lucato, L. T., Campanholo, K. R., Melo, L. M., Leite, C. C., et al. (2017). Altered functional connectivity between precuneus and motor systems in Parkinson's disease patients. *Brain Connect.* 7, 643–647. doi: 10.1089/brain.2017.0534

Ugur, H. C., Kahilogullari, G., Coscarella, E., Unlu, A., Tekdemir, I., Morcos, J. J., et al. (2005). Arterial vascularization of primary motor cortex (precentral gyrus). *Surg. Neurol.* 64(Suppl. 2), S48–S52. doi: 10.1016/j.surneu.2005.07.049

Uribe, C., Segura, B., Baggio, H. C., Abos, A., Marti, M. J., Valldeoriola, F., et al. (2016). Patterns of cortical thinning in nondemented Parkinson's disease patients. *Mov. Disord.* 31, 699–708. doi: 10.1002/mds.26590

Verreyt, N., Nys, G. M., Santens, P., and Vingerhoets, G. (2011). Cognitive differences between patients with left-sided and right-sided Parkinso's disease A review. *Neuropsychol. Rev.* 21, 405–424. doi: 10.1007/s11065-011-9182-x

Vriend, C., Van Den Heuvel, O. A., Berendse, H. W., Van Der Werf, Y. D., and Douw, L. (2018). Global and subnetwork changes of the structural connectome in *de novo* Parkinson's disease. *Neuroscience* 386, 295–308. doi: 10.1016/j.neuroscience.2018.06.050

Wang, J., Wang, X., Xia, M., Liao, X., Evans, A., and He, Y. (2015). GRETNA: A graph theoretical network analysis toolbox for imaging connectomics. *Front. Hum. Neurosci.* 9:386. doi: 10.3389/fnhum.2015.00386

Wang, M., Jiang, S., Yuan, Y., Zhang, L., Ding, J., Wang, J., et al. (2016). Alterations of functional and structural connectivity of freezing of gait in Parkinson's disease. *J. Neurol.* 263, 1583–1592. doi: 10.1007/s00415-016-8174-4

Wu, T., Chan, P., and Hallett, M. (2010). Effective connectivity of neural networks in automatic movements in Parkinson's disease. *Neuroimage* 49, 2581–2587. doi: 10.1016/j.neuroimage.2009.10.051

Yagi, S., Yoshikawa, E., Futatsubashi, M., Yokokura, M., Yoshihara, Y., Torizuka, T., et al. (2010). Progression from unilateral to bilateral parkinsonism in early Parkinson disease: Implication of mesocortical dopamine dysfunction by PET. *J. Nucl. Med.* 51, 1250–1257. doi: 10.2967/jnumed.110.076802

Yan, C. G., Cheung, B., Kelly, C., Colcombe, S., Craddock, R. C., Di Martino, A., et al. (2013). A comprehensive assessment of regional variation in the impact of head micromovements on functional connectomics. *Neuroimage* 76, 183–201. doi: 10.1016/j.neuroimage.2013.03.004

Yang, Y., Ye, C., Sun, J., Liang, L., Lv, H., Gao, L., et al. (2021). Alteration of brain structural connectivity in progression of Parkinson's disease: A connectome-wide network analysis. *Neuroimage Clin.* 31:102715. doi: 10.1016/j.nicl.2021.102715

Zeng, L. L., Wang, D., Fox, M. D., Sabuncu, M., Hu, D., Ge, M., et al. (2014). Neurobiological basis of head motion in brain imaging. *Proc. Natl. Acad. Sci. U.S.A.* 111, 6058–6062. doi: 10.1073/pnas.1317424111

Zhang, C., Dou, B., Wang, J., Xu, K., Zhang, H., Sami, M. U., et al. (2019). Dynamic alterations of spontaneous neural activity in Parkinson's Disease: A resting-State fMRI study. *Front. Neurol.* 10:1052. doi: 10.3389/fneur.2019.01052

Zhang, C., Wu, C., Zhang, H., Dou, W., Li, W., Sami, M. U., et al. (2020). Disrupted resting-state functional connectivity of the nucleus basalis of meynert in Parkinson's disease with mild cognitive impairment. *Neuroscience* 442, 228–236. doi: 10.1016/j.neuroscience.2020.07.008

frontiers | Frontiers in Neuroscience

TYPE Original Research
PUBLISHED 08 November 2022
DOI 10.3389/fnins.2022.1045585

OPEN ACCESS

EDITED BY
Han Lv,
Beijing Friendship Hospital, Capital Medical University, China

REVIEWED BY
Ruiwang Huang,
South China Normal University, China
Kristen Willeumier,
Independent Researcher, Beverly Hills, CA, United States
Zhiqiang Zhang,
Nanjing University School of Medicine, China

*CORRESPONDENCE
Guolin Ma
maguolin1007@qq.com
Qi Zhang
zhangqi0355@sina.com

†These authors have contributed equally to this work

SPECIALTY SECTION
This article was submitted to Brain Imaging Methods, a section of the journal Frontiers in Neuroscience

RECEIVED 15 September 2022
ACCEPTED 17 October 2022
PUBLISHED 08 November 2022

CITATION
Ye F, Du L, Liu B, Gao X, Yang A, Liu D, Chen Y, Lv K, Xu P, Chen Y, Liu J, Zhang L, Li S, Shmuel A, Zhang Q and Ma G (2022) Application of pseudocontinuous arterial spin labeling perfusion imaging in children with autism spectrum disorders. *Front. Neurosci.* 16:1045585. doi: 10.3389/fnins.2022.1045585

Application of pseudocontinuous arterial spin labeling perfusion imaging in children with autism spectrum disorders

Fang Ye[1†], Lei Du[2,3†], Bing Liu[2,4†], Xinying Gao[1], Aocai Yang[2,4], Die Liu[1], Yue Chen[2,5], Kuan Lv[2,5], Pengfei Xu[1], Yuanmei Chen[1], Jing Liu[1,4], Lipeng Zhang[1,4], Shijun Li[6], Amir Shmuel[7,8], Qi Zhang[1]* and Guolin Ma[2]*

[1]Department of Pediatrics, China-Japan Friendship Hospital, Beijing, China, [2]Department of Radiology, China-Japan Friendship Hospital, Beijing, China, [3]Key Laboratory of Carcinogenesis and Translational Research, Ministry of Education, Department of Radiology, Peking University, Cancer Hospital and Institute, Beijing, China, [4]Graduate School of Peking Union Medical College, Chinese Academy of Medical Sciences, Beijing, China, [5]Peking University China-Japan Friendship School of Clinical Medicine, Beijing, China, [6]Department of Radiology, First Medical Center of Chinese PLA General Hospital, Beijing, China, [7]McConnell Brain Imaging Centre, Montreal Neurological Institute, McGill University, Montreal, QC, Canada, [8]Department of Neurology and Neurosurgery, McGill University, Montreal, QC, Canada

Introduction: Pseudocontinuous Arterial Spin Labeling (pCASL) perfusion imaging allows non-invasive quantification of regional cerebral blood flow (CBF) as part of a multimodal magnetic resonance imaging (MRI) protocol. This study aimed to compare regional CBF in autism spectrum disorders (ASD) individuals with their age-matched typically developing (TD) children using pCASL perfusion imaging.

Materials and methods: This cross-sectional study enrolled 17 individuals with ASD and 13 TD children. All participants underwent pCASL examination on a 3.0 T MRI scanner. Children in two groups were assessed for clinical characteristics and developmental profiles using Autism Behavior Checklist (ABC) and Gesell development diagnosis scale (GDDS), respectively. We compared CBF in different cerebral regions of ASD and TD children. We also assessed the association between CBF and clinical characteristics/developmental profile.

Results: Compared with TD children, individuals with ASD demonstrated a reduction in CBF in the left frontal lobe, the bilateral parietal lobes, and the bilateral temporal lobes. Within the ASD group, CBF was significantly higher in the right parietal lobe than in the left side. Correlation analysis of behavior characteristics and CBF in different regions showed a positive correlation between body and object domain scores on the ABC and CBF of the bilateral occipital lobes, and separately, between language domain scores and CBF of the left frontal lobe. The score of the social and self-help domain was

negatively correlated with the CBF of the left frontal lobe, the left parietal lobe, and the left temporal lobe.

Conclusion: Cerebral blood flow was found to be negatively correlated with scores in the social and self-help domain, and positively correlated with those in the body and object domain, indicating that CBF values are a potential MRI-based biomarker of disease severity in ASD patients. The findings may provide novel insight into the pathophysiological mechanisms of ASD.

KEYWORDS

cerebral blood flow, arterial spin labeling, autism spectrum disorders, magnetic resonance imaging, children

Introduction

Autism spectrum disorders (ASD) is a group of disabilities characterized by impairments in social interaction and communication, as well as restricted, repetitive, and stereotyped patterns of behavior, activities, or interests (Pardo and Eberhart, 2007; Sztainberg and Zoghbi, 2016). In recent decades, ASD has become one of the most relevant neurodevelopmental disorders in children and, therefore, an urgent public health problem. This group of disorders is considered a large unmet medical need and a heavy burden on individuals with ASD, their families, and society worldwide (Buescher et al., 2014). To date, the prevalence of ASD is one in 44 children in the United States (Kogan et al., 2018).

As a behavioral disease, ASD is considered to be highly correlated with brain dysfunction. At present, the pathology and etiology of ASD remain uncertain, and its clinical diagnosis is mainly based on medical observation and clinical symptom evaluation of the patient by a certified specialist. Disorders that are characterized by atypical social functioning, such as ASD, are known to correlate with impaired neural network function. The establishment of quantitative objective biomarkers (e.g., cerebral perfusion and cerebral function) for ASD would aid in the auxiliary diagnosis of ASD. In recent decades, neuroimaging studies have provided new insights into the neurobiological underpinnings of behavioral impairments associated with ASD (Ecker et al., 2015; Mori et al., 2015; Walsh et al., 2021).

Among the above-mentioned neuroimaging studies, multimodal magnetic resonance imaging (MRI) techniques have been used to understand the pathophysiological characteristics of ASD in recent years, including structural MRI (sMRI), functional MRI (fMRI), ASL, etc. sMRI examination has been widely used to investigate brain morphology. Two major types of sMRI have been used in studies: geometric features and volumetric features (Ozgen et al., 2013). However, sMRI cannot determine how brain regions communicate and how information is integrated across networks (Chen et al., 2011). To further identify metabolic disorders of the brain instead of structural abnormalities, fMRI has been used in several ASD studies (Chen et al., 2016; Abraham et al., 2017; Sherkatghanad et al., 2019). This technique estimates neuronal activity based on the blood oxygen level dependent (BOLD) signal (Yin et al., 2021) that reflects fluctuations in brain blood oxygenation levels. However, the BOLD signal is an indirect measure of neuronal activity. BOLD signal results from the combination of cerebral blood flow (CBF), cerebral blood volume, and cerebral metabolic rate of oxygen consumption (Chen et al., 2015). To overcome this limitation and utilize a more direct and quantitative measure of brain metabolism, ASL has been increasingly adopted as a novel functional technique.

Arterial Spin Labeling is based on magnetically labeled endogenous water in the blood and using it as a tracer (Ohnishi et al., 2000; Zheng et al., 2019; Wang et al., 2022). This approach enables the quantification of CBF without radiation exposure (Hernandez-Garcia et al., 2019). The ASL method offers several advantages: it is safe, non-invasive, non-radioactive, easy to acquire, and reproducible. Its high spatial resolution, accuracy, and capacity to quantitatively demonstrate perfusion abnormalities make ASL a reliable physiological marker of neural activity (Chen et al., 2015; Ivanov et al., 2017; Li et al., 2020). It has been widely used in areas of neurodevelopmental disorders such as periventricular leukomalacia, ischemic stroke, and sickle-cell-related cerebral ischemia (Smith et al., 2019). It also has the potential to become a good biomarker for ASD studies (Mori et al., 2015).

Arterial Spin Labeling can be divided into three types according to different labeling methods: pulsed ASL (PASL), continuous ASL (CASL), and pseudocontinuous ASL (pCASL). pCASL is a hybrid approach that simulates CASL using many short pulses to achieve continuous labeling for better compensation of adverse magnetization transfer effects (Boudes et al., 2014). It could improve the sensitivity and temporal signal-to-noise ratio (SNR) of ASL. This technique allows both reliable CBF measurement and functional connectivity analysis

of perfusion image series because the potential contributions of the blood oxygenation level-dependent are minimized (Jann et al., 2015; Zhao et al., 2022).

In recent years, several studies have focused on CBF changes in ASD individuals. These studies indicated decreased blood flow (hypoperfusion) in the cerebrum regions of ASD individuals compared with neurotypical children (Hashimoto et al., 2000; Ohnishi et al., 2000; Yerys et al., 2018). Hashimoto et al. (2000) identified a decrease in CBF in both the frontal and temporal lobes in autistic brains using the CBF single-photon emission computed tomography (SPECT) method. Ohnishi et al. (2000) found hypoperfusion in the insula, superior temporal gyrus (STG), and prefrontal area in young individuals with ASD. Yerys et al. (2018) demonstrated a reduction in CBF in regions critical to social perception and cognition in children with ASD.

Previous studies have primarily focused on the comparison of CBF between ASD and typically developed individuals. To the best of our knowledge, the relationship between changes in CBF and the clinical characteristics and developmental profile of ASD remains unknown. The present study was designed to detect regional CBF changes in ASD individuals using the three-dimensional pCASL (3D–pCASL) technique and to further explore the correlation between ASD characteristics and CBF changes. Our results provide novel insight to support the investigation of the pathophysiological mechanisms of ASD.

Materials and methods

Participants

Thirty-two children [19 in ASD; 13 in typically developing (TD)] between the ages of 3 and 8 were invited to participate in this study. The inclusion criteria for the children in the ASD group are as follows: (1) 3–8 years old; (2) meet the diagnostic criteria of the Diagnostic and Statistical Manual of Mental Disorders–the 5th edition (DSM-V) checklist for autism (Ben-Ari et al., 2022); (3) have an Autism Behavior Checklist (ABC) score $\geq$53; (4) right-handedness; (5) no other diseases that may affect brain function and structure, with no abnormalities on routine head MRI; and (6) no history of medical treatment or intervention. To be enrolled in the ASD group, the child was first screened by a pediatrician using the ABC. Then, the diagnosis of the child was performed by a pediatric expert according to DSM-V (Ben-Ari et al., 2022). Subsequently, their intellectual functioning was evaluated by an experienced developmental-behavioral pediatrician based on the Gesell development diagnosis scale (GDDS).

The inclusion criteria for children in the control group are as follows: (1) 3–8 years old; (2) normally developed; (3) have an ABC score $\leq$ 53, have a DQ $\geq$ 75 or IQ $\geq$ 70; (4) right-handedness; and (5) no other diseases that may affect brain function and structure, with no abnormalities on routine head MRI. To be enrolled in the TD group, participants were first screened by a pediatrician using the ABC and then the GDDS (for children 3–6 years old) or Raven's Standard Progressive Matrices (RPM) (for children over 6 years old). And the exclusion criteria for both groups are as follows: (1) have abnormal brain lesions; (2) do not cooperate with sedation; (3) suffer from epilepsy; (4) without informed consent obtained from the parents; and (5) parents reported any known genetic, neurological, or psychiatric disorder. Two eligible children withdrew from the study prior to the MRI examination. Ultimately, there were 17 individuals with ASD and 13 TD children enrolled in this study.

Assessment tool

Autism behavior checklist

The ABC is a 57-item questionnaire used to assess behavioral problems in ASD children (Volkmar et al., 1988). Previous domestic studies have shown that the ABC has good reliability and validity and is one of the most commonly used autism symptom assessment tools in China (Zhu et al., 2017). In this study, we used the ABC as a tool to assess the severity of autism symptoms. The total score directly correlated with the severity of behavioral symptoms. The ABC is divided into five subscales, including problems related to sensory (sensation and perception; 10 items), relating (relation and connection; 14 items), body and object use (physical activity and rigid use of objects; 9 items), language (communication and interaction; 13 items), and social and self-help (adaptability and self-care; 11 items) domains. All items were rated as "yes" (scored from 1 to 4 with different symptoms) or "no" (scored as 0 without symptom) for each question during the assessment. The score ranges from 0 to 158, with score greater than 53 indicating ASD. In this study, we utilized this test for participant screening and assessing autistic symptoms.

Gesell development diagnosis scale

The GDDS is one of the gold standards for neurodevelopment assessment and one of the most commonly used tools for assessing neurodevelopment in children (Wei et al., 2021). The GDDS can comprehensively and continuously reflect individual neurodevelopment and is widely used in clinical and scientific research in China. It uses direct observation to evaluate a child's cognitive, language, motor, and social-emotional responses in the domains of gross motor, fine motor, adaptive behavior, language and social behavior. The development quotient (DQ) of each domain was calculated for each participant. The DQ less than 75 indicates developmental retardation. In this study, we utilized this test for participant screening if the child was younger than 6.

Raven's standard progressive matrices

The RPM is a commonly used test of intelligence quotient (IQ) that contains multiple choice questions pertaining to abstract reasoning (David and Skilbeck, 1984). In each test question in the RPM, the child is asked to identify the missing item that completes a pattern. The IQ less than 70 indicates mental retardation. In this study, we utilized this test for participant screening if the child was over 6 years old.

Study procedures

All participants completed three data collection sessions. The first session was an evaluation to confirm that individuals had ASD or were neurotypical. Then, the GDDS was conducted on the ASD individuals for DQ evaluation. All participants then completed an MRI scan. The study was approved by the Institutional Review Board of China–Japan Friendship Hospital. Informed consent was obtained from the caregivers of all the participants after the purpose and risks of the study had been fully explained. As all the participants could not cooperate with the MRI examination, they were administered with chloral hydrate 50 mg/kg orally, with maximum dose of 1 g.

Magnetic resonance imaging scanning

A 3-Tesla MRI with 8-channel head coils was used for scanning (Discovery MR 750 scanner, GE Medical Systems, USA). pCASL with one post-labeling delay (PLD) was performed in the study. All perfusion and reference images were obtained with a 3-dimensional stack-of spirals rapid acquisition with refocused echoes imaging sequence (Stivaros et al., 2018). The imaging parameters were as follows: repetition time, 4,632 ms; PLD, 1,500 ms; echo time, 10.5 ms; flip angle, 90 degrees; field of view, 240 mm × 240 mm; bandwidth = 6250 Hz/pixel; slice thickness, 4 mm; number of slices, 36; and total scan time, 3 min 24 s.

Data processing

Arterial Spin Labeling data were processed using the CereFlow software (An–Image Technology Co, China). The procedures were as follows:

(1) The 3-dimensional ASL perfusion-weighted images and proton density images (generated from the GE MR scanner) were converted into the CBF map of cerebral perfusion for each participant based on the simplified one compartment model (St Lawrence and Wang, 2005).
(2) The CBF map was normalized to the Montreal Neurological Institute (MNI) space by using intensity-based image registration. In this image registration method, each participant's CBF map served as the motion image and would be transformed to match the MNI152 brain template that acted as the fixed image.
(3) Then, the Automated anatomical labeling (AAL) atlas was overlaid onto the normalized CBF map.
(4) The average CBF value of different regions was obtained (**Figure 1**).

Statistical analysis

Analyses were performed using the SPSS 22.0 software (Chicago, IL, United States). The Shapiro–Wilk test and Levene's test were used to assess data normality and homogeneity, respectively. Student's *t*-test was used for variables with a normal distribution and equal variance, while the Kolmogorov–Smirnov test was used for those with a skewed distribution or unequal variance. CBF within the bilateral hemispheres was compared using a paired *t*-test. Pearson and Spearman correlation analyses were conducted between CBF and scores of the GDDS and ABC assessment tools for normally or skewed distributed variables, respectively. Partial correlation analysis was utilized to control for the effect of possible confounders of sex and age. Sensitivity analysis was conducted to evaluate whether the outliers affect the outcomes by comparing the results before and after eliminating the outliers. To control for multiple comparisons (Breznik et al., 2020), the Benjamini-Hochberg false discovery rate (FDR) procedure was used, and corrected *q*-values less than 0.05 were designated as statistically significant.

Results

Characteristics of participants

The demographic profile and clinical characteristics of all 17 ASD individuals and 13 TD children are summarized in **Table 1**. The two groups were balanced in age, but the percentage of male participants was higher in the ASD group. However, we performed a subgroup analysis to further compare CBF between male and female participants, and no significant difference was observed (**Supplementary Table 1**).

Comparison of cerebral blood flow in different regions between the two groups

Compared with TD individuals, ASD individuals exhibited significant reductions in CBF in the left frontal lobe

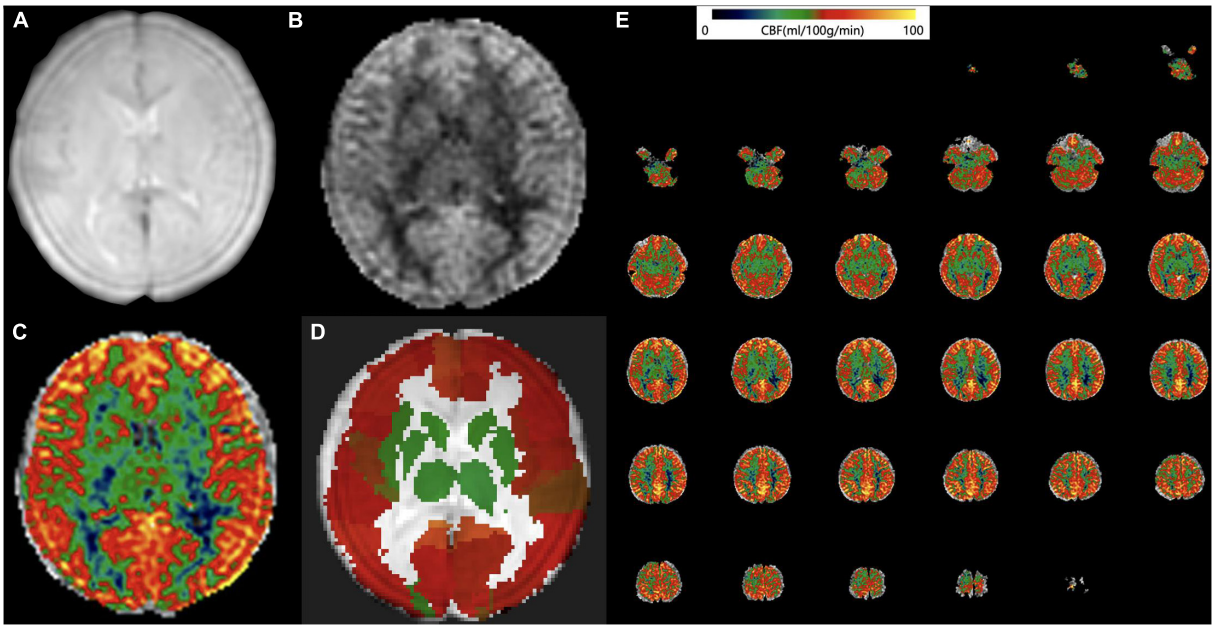

FIGURE 1
Arterial spin labeling (ASL) data processing workflow. Convert the **(A)** 3D ASL proton density images and **(B)** perfusion weighted images into the cerebral blood flow (CBF) map of cerebral perfusion for each participant. **(C)** The CBF map was normalized to the Montreal Neurological Institute (MNI) space and then the Automated anatomical labelling (AAL) atlas was overlaid. **(D)** The average CBF value of each brain region from AAL atlas was obtained. **(E)** An example CBF map of a four-year old male ASD patient calculated by Cereflow software.

(q-value = 0.045), bilateral parietal lobes (both q-values = 0.045), and bilateral temporal lobes (both q-values = 0.045) (Figure 2).

Comparison of cerebral blood flow in different regions between bilateral hemispheres

Within each group, we compared the CBF between homologous regions in the two hemispheres (Table 2). In the ASD group, the CBF in the parietal lobe of the left hemisphere was lower than that in the right hemisphere (p = 0.032). No significant difference was observed in the TD group.

Correlation analysis between clinical characteristics and cerebral blood flow of different regions within the two groups

Within the ASD group, the body and object domain score on the ABC was positively correlated with the CBF of the bilateral occipital lobes (Figures 3A,B). The language domain score on the ABC was positively correlated with the CBF of the left frontal lobe (Figure 3C). In addition, the social and self-help domain score was negatively correlated with the CBF of the left frontal lobe (Figure 3D), left parietal lobe (Figure 3E), and left temporal lobe (Figure 3F).

However, after correcting for multiple comparisons, all the correlations were not statistically significant. Besides, no statistically significant correlation was observed in the TD group (Supplementary Table 2).

Correlation analysis between developmental indicators and cerebral blood flow of different regions within the two groups

The correlation between the DQ of GDDS and the CBF of different regions was analyzed, but no statistically significant correlation was observed (Supplementary Table 3).

Sensitivity analysis of outliers within autism spectrum disorders group

Figure 4 presents the distributions of all the variables obtained from the ASD group. Outliers were detected in three variables, including the sensation domain score on the ABC, the social and self-help domain score on the ABC, and the language domain DQ on the GDDS. The results of the sensitivity analysis

indicated that all statistically significant findings prevailed after the exclusion of outliers (**Supplementary Tables 4**, **5**).

Discussion

Using the 3D-pCASL technique, the current study investigated the patterns of CBF changes in ASD individuals. To the best of our knowledge, this study is the first to explore CBF changes and their relationships with clinical characteristics. ASD pathogenesis is not yet completely understood. The present study moves us closer to identifying biologically based marker that relates ASD to a basic social perception deficit. This study also highlights the value of ASL neuroimaging in the field of ASD.

One of the major findings is the different CBF characteristics in individuals with ASD compared with typically developed controls. In line with previous findings, we identified CBF decreases in the left frontal lobe (Hashimoto et al., 2000), the bilateral parietal lobes (Yerys et al., 2018), and the bilateral temporal lobes (Yerys et al., 2018; Tang et al., 2022).

TABLE 1 Demographic and clinical characteristics of participants.

Characteristic	ASD ($n = 17$)		TD ($n = 13$)		Z-value[c]	P-value
	Median	IQR	Median	IQR		
Demographic profile						
Male sex	15[a]	88.2[b]	5[a]	38.5[b]	6.126[d]	**0.013**
Age (years)	4.0	2.0	4.5	4.0	1.093	0.183
Clinical characteristic						
Scores on ABC subscales						
Total	68.0	17.0	10.0	9.5	4.627	<**0.001**
Sensory	10.0	3.5	2.0	3.0	4.656	<**0.001**
Relating	15.0	10.5	2.0	3.5	4.558	<**0.001**
Body and object use	5.0	9.5	0.0	1.5	3.130	**0.002**
Language	21.0	6.5	1.0	3.0	4.641	<**0.001**
Social and self-help skills	14.0	5.5	3.0	2.5	4.280	<**0.001**
Developmental profile[e]						
DQ of GDDS subscales						
Total	68.6	16.0	100.0	4.3	3.961	<**0.001**
Cognition	69.0	20.0	100.0	10.8	3.965	<**0.001**
Gross motor	84.0	21.5	105.5	16.5	3.971	<**0.001**
Minor motor	73.0	14.5	99.0	7.8	3.822	<**0.001**
Language	53.0	12.5	100.0	11.3	3.967	<**0.001**
Personal-Social behavior	68.0	20.0	101.5	5.3	3.908	<**0.001**

ASD, autism spectrum disorders; TD, typically developing; ABC, autism behavior checklist; GDDS, Gesell development diagnosis scale; DQ, development quotient; IQ, intelligence quotient; IQR, interquartile range. [a]n of male participants. [b]% of male participants. [c]Z-value of Wilcoxon rank sum test. [d]Continuity correction value of Chi-Square. [e]5 children in TD group were tested for IQ, the median of which was 99.0, and IQR was 5.0. Bold values mean statistically significant.

First, CBF, which is a variable that reflects neurovascular coupling, is regulated by local neuronal activity and metabolism (Iadecola, 2004). Local CBF reductions affect ATP synthesis, diminishing (Na^+-K^+) ATPase activity and the capacity of neurons to generate action potentials (Kalaria, 2010). The decreased activity of (Na^+-K^+) ATPase further contributes to the accumulation of glutamate (Zlokovic, 2011). Glutamate is the most prevalent excitatory neurotransmitter. Based on data from human patients and animal models, excess glutamate leads to an elevation in cortical excitability, which has been proposed to be a fundamental neurobiological characteristic of ASD (Bozzi et al., 2018; Horder et al., 2018; Antoine et al., 2019; Sohal and Rubenstein, 2019). Local circuit hyperexcitability could contribute to aberrations in brain connectivity in autism. Alternatively, excess glutamate activates glutamate receptors, leading to the production of nitric oxide (NO) (Reynell and Harris, 2013; Raju et al., 2015). As a signaling molecule in the central nervous system (CNS), NO is one of the most essential messenger molecules (Son et al., 1996; Raju et al., 2015). NO-mediated signaling contributes to cerebrovascular and synaptic transmission coupling in the CNS (Son et al., 1996). Studies have confirmed that NO leads to the S-nitrosylation (SNO) of many proteins and receptors through various pathways (Amal et al., 2020). SNO targets a wide range of prominent intracellular proteins, which leads to alterations in specific signaling pathways. These alterations may cause deficits in synapses, neurons, and behavior (Tripathi et al., 2020).

Second, the abnormal patterns of CBF in essential regions of the cerebrum would affect corresponding functions. The frontal lobes support high-level cognition; they are extremely important for the development of social behavior. Recent studies have implied that the medial prefrontal cortex (mPFC), the so-called "social brain" (Hiser and Koenigs, 2018), is involved in social behaviors (Hazlett et al., 2017). The "social brain" region is involved in computing and associating reward value with various types of stimulation. This association is relevant to "decreased social motivation," an explanatory theory of autism (Chevallier et al., 2012). In addition, studies have found that the orbitofrontal cortex, another region of the frontal lobes, computes individual preferences and social hierarchies (Azzi et al., 2012). A deficit in this cortical region was considered to underlie social function disorders, which is a typical defect in ASD (Jonker et al., 2015). Moreover, the posterior cingulate gyrus located in the frontal lobe is an important part of emotional circuits (Miao et al., 2011). Two studies (Lee et al., 2013; Sophia et al., 2013) have reported dysfunction in this area in ASD patients.

Joint attention is an early indicator and a key deficit in autism (Osterling and Dawson, 1994). This deficit was proven to be associated with executive function, which was described as a set of cognitive processes including planning, working memory, impulse control, inhibition, and shifting set, as well as the initiation and monitoring of action (Gallagher and Frith, 2003).

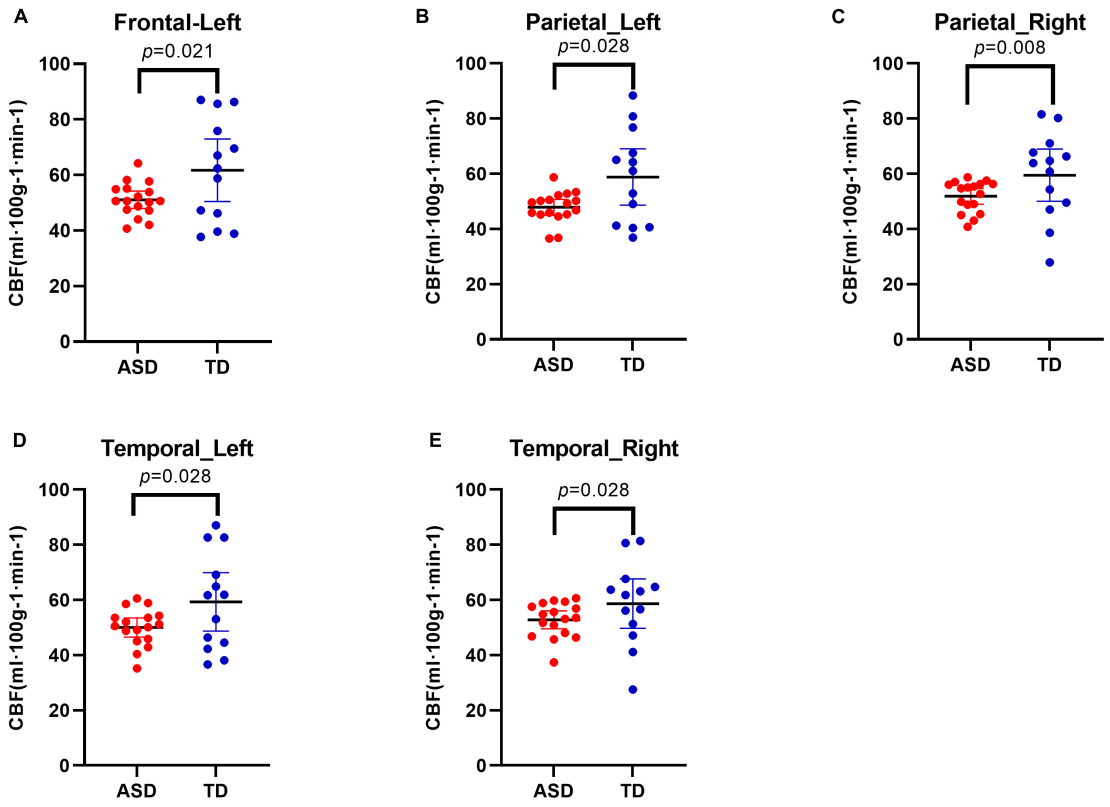

FIGURE 2
Decreased cerebral blood flow (CBF) in different regions in Autism Spectrum Disorders (ASD) group compared with typically developing (TD) group. Results showed decreased CBF in the left frontal lobe **(A)**, in the bilateral parietal lobes **(B,C)**, and in the bilateral temporal lobes **(D,E)**.

Structural studies of the autistic brain identified delayed postnatal maturation of the frontal lobes (Zilbovicius et al., 1995) and structural abnormalities in the orbitofrontal cortex (Salmond et al., 2003). In line with previous results, we found hypoperfusion in the left frontal lobe, and a negative correlation between CBF and scores in the social and self-help domains in our study. The results indicated functional abnormalities or abnormal social overture in this region. Further studies should explore executive function and characteristics in neuroimaging studies in ASD.

Interestingly, the current study showed that the ABC scores of social and self-help skills were negatively correlated with CBF in the left frontal lobe. Social and self-help skills were thought to be based on executive functions, which are defined as a set of interrelated cognitive processes required for complex goal-directed activity. The frontal lobe is highly evolved and regulate complex behaviors, which include complex cognitive functions such as planning complex cognitive behaviors, personality expression, decision-making, and regulating social behavior. Thus, hypofrontality may contribute to the clinical symptoms in ASD (Diedrichsen et al., 2019). In addition, distinct cognitive and behavioral processes are mediated by different regions of the frontal lobe. Further studies should focus on the correlation between symptoms in ASD individuals and CBF changes within subregions of the cerebrum, particularly in the frontal lobe. Different CBF patterns in this region may be one of the characteristics of ASD individuals.

TABLE 2 Comparison of CBF between homologous regions in the two hemispheres.

	Left hemisphere	Right hemisphere	*t*-value	*q*-value[a]
ASD (*n* = 17)				
Frontal lobe	51.1 ± 6.0	51.7 ± 6.2	0.502	0.787
Parietal lobe	47.9 ± 5.6	51.9 ± 5.6	3.371	**0.032**
Temporal lobe	50.0 ± 6.7	52.8 ± 6.3	2.433	0.080
Occipital lobe	54.2 ± 7.7	56.0 ± 7.2	2.382	0.080
TD (*n* = 13)				
Frontal lobe	61.7 ± 18.6	59.7 ± 15.8	0.892	0.780
Parietal lobe	58.8 ± 16.9	59.5 ± 15.6	0.309	0.787
Temporal lobe	59.3 ± 17.5	58.7 ± 14.9	0.276	0.787
Occipital lobe	59.2 ± 14.9	59.6 ± 14.4	0.601	0.787

CBF, cerebral blood flow; ASD, autism spectrum disorders; TD, typically developing. [a]Benjamini-Hochberg FDR procedure for multiple comparison correction was used and *q*-values were reported, *q*-value < 0.05 were considered significant. Bold values mean statistically significant.

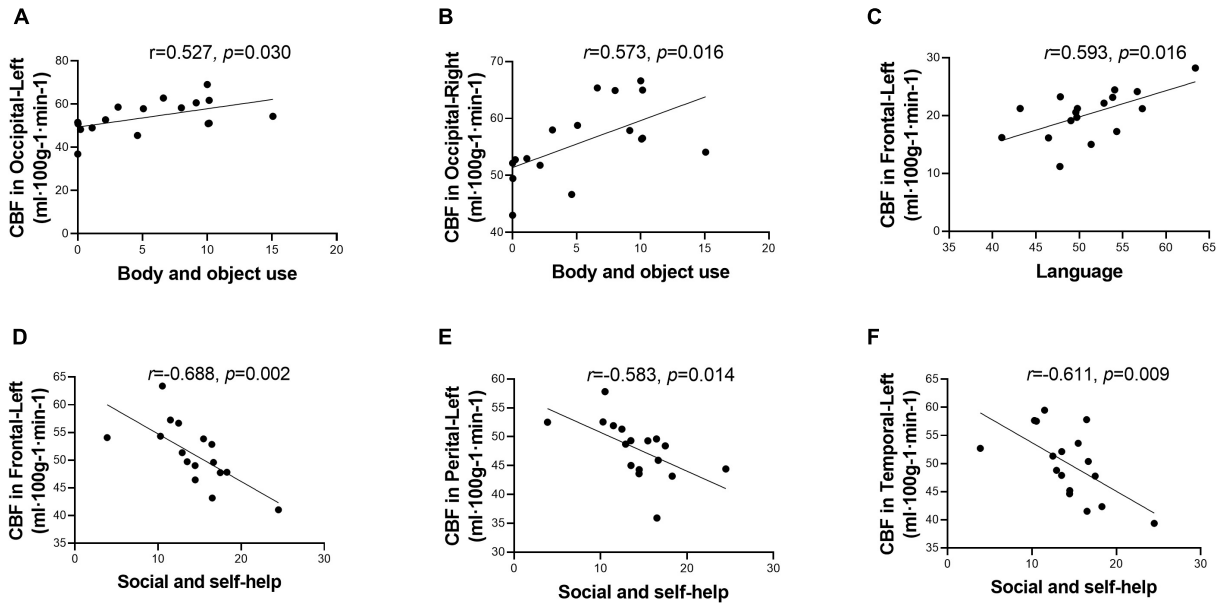

FIGURE 3
Score of Autism Behavior Checklist (ABC) domains correlated with cerebral blood flow (CBF) in different regions. Score of body and object use was positively correlated with CBF in the bilateral occipital lobes **(A,B)**. Score of language was positively correlated with CBF in the left frontal lobe **(C)**. Score of social and self-help was negatively correlated with CBF in the left hemisphere, including frontal lobe, perietal lobe, and temporal lobe **(D–F)**. While after multiple comparisons correction, the correlation was not statistically signicant.

Within the temporal lobes, we identified hypoperfusion and a negative association with social and self-help domain scores. This finding was consistent with significantly reduced activation in the left STG and the superior temporal sulcus (STS) in autistic children with Fragile X Syndrome (Philip et al., 2012). In addition, one of the hypotheses of ASD indicates a primary factor of abnormal processing of the information conveyed by behavior (Kaiser et al., 2012). This hypothesis suggests that understanding and using gaze or emotional expressions requires specific neural mechanisms, and the STG, STS, and the temporal–parietal junction have been selectively associated with the processing of body and face movement (Annaz et al., 2010). The atypical processing of bodily movement and gaze might be a vital factor in ASD.

Within the bilateral parietal lobes, our study revealed lower perfusion in ASD individuals and a negative correlation between CBF and the ABC score of the social and self-help domains. This finding is consistent with the consensus from numerous studies: patients with lesions in the parietal lobe exhibit difficulty with self-care, such as dressing and washing (Glasser et al., 2016). This difficulty may be related to the sensory and linguistic functions and specific structures in the parietal lobes. The parietal lobes are related to sensory and linguistic functions (Johnson et al., 2011). Located in the parietal lobes, the angular gyrus is one of the most important centers of visual language. Through the function of the angular gyrus, various forms of information generate integrated language activities, since the left angular gyrus connects the auditory, visual, and somatosensory cortices (Hofmann et al., 2008). Liang et al. (2021) found that the number of functional connectivity neural circuits in the left angular gyrus was abnormally decreased in the ASD group. This decrease may be related to lower perfusion in this area, as shown in our study. Both decreased functional connectivity and lower perfusion indicate cognitive dysfunction in ASD patients and the disconnection between what they see and what they hear (Liang et al., 2021).

The lack of correlation between the developmental performance and reduction of CBF suggests that the difficulty experienced by ASD individuals in daily life is not necessarily correlated with their DQ, which was in line with a previous study (Mori et al., 2015).

Different reviews noted that the language-relevant cortex includes Broca's area in the inferior frontal gyrus, Wernicke's area in the STG, parts of the middle temporal gyrus, and the inferior parietal and angular gyrus in the parietal lobe (Friederici, 2002; Hickok and Poeppel, 2007). This finding is in accordance with our results that the ABC language scores were positively correlated with CBF in the left frontal lobe, where Broca's area is located.

Our results showed that body and object use scores were positively correlated with CBF in the bilateral occipital lobes. The key function of the occipital lobe, where the visual cortex is located, is processing visual information (Van Essen et al., 2018). Visuospatial processing and distance perception, which are also

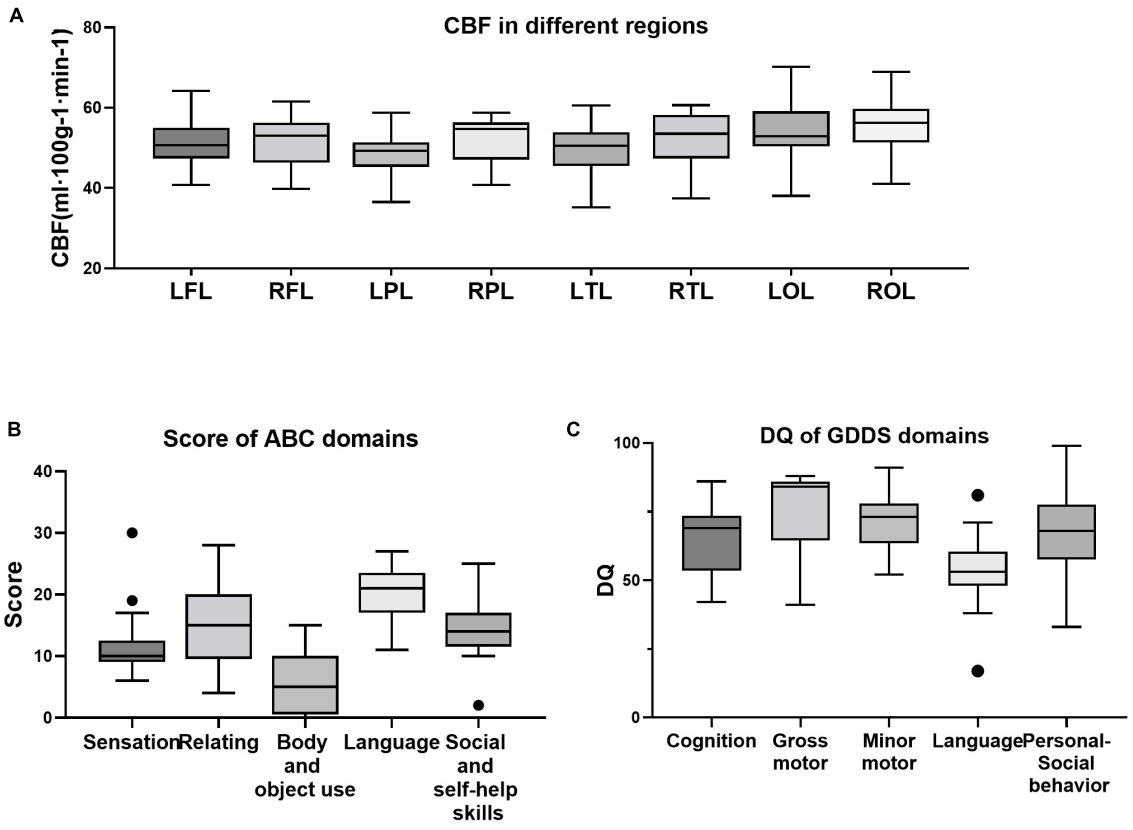

FIGURE 4
Distribution of all variables of cerebral blood flow (CBF) **(A)**, clinical characteristics **(B)**, and developmental indicators **(C)**. Within ASD group, outliers were detected in the sensation domain score on the Autism Behavior Checklist (ABC) **(B)**, the social and self-help domain score on the ABC **(B)**, and the language domain DQ on the Gesell development diagnosis scale (GDDS) **(C)**.

related to the function of the occipital lobe, may play a key part in the process of "body and object use." These results suggested the involvement of the occipital lobe in the performance of ASD individuals.

Derived from MRI using ASL, CBF changes are thought to reflect regional changes in neural activity over time (Detre et al., 2012). Furthermore, CBF provides quantitative absolute measures associated with regional brain function. Therefore, it may provide a more reliable marker of trait-like effects than measures obtained through contrasting conditions, such as BOLD fMRI which is typically used in task-based studies. The advantages of ASL position it as an optimal non-invasive biological marker of ASD.

Several limitations of our study should be acknowledged. First, we enrolled a relatively small sample due to the strict inclusion and exclusion criteria, which may affect the statistical reliability of our results. Further studies should focus on establishing the diagnostic value of CBF in ASD individuals with larger sample sizes among different populations. Second, the sex ratio was skewed in this study. We compared male and female participants in subgroup analyses. The results showed no difference in any CBF or behavioral data. Moreover, partial correlation analysis was conducted to control for the effect of possible confounders of gender and age. In a future study, we will enroll more female ASD individuals to minimize the effect of sex, and subgroup analysis will be conducted to explore the difference in CBF between male and female ASD individuals. Third, the CBF data analyzed in the current study were collected from each lobe of the cerebrum, and further studies should focus on more specific cortical regions in ASD individuals.

Data availability statement

The raw data supporting the conclusions of this article will be made available by the authors, without undue reservation.

Ethics statement

The studies involving human participants were reviewed and approved by the Ethics Committee of China–Japan Friendship Hospital. Written informed consent to participate

in this study was provided by the participants' legal guardian/next of kin.

Author contributions

FY, LD, and BL acquired and analyzed the ASL data and drafted the manuscript. DL, XYG, JL, YMC, and LPZ searched and managed the literature. KL, YC, and ACY did the MRI scanning. PFX, SJL, and AS revised the manuscript. GLM and QZ designed the study and revised the manuscript. All authors contributed to the article and approved the submitted version.

Funding

This study was supported by the National Natural Science Foundation of China (NSFC) (Nos. 81971585 and 82271953), the National Key Research and Development Program of China (No. 2020YFC2003903), the Guangzhou Science and Technology Plan Project (Grant No. 202103010001), the Capital's Funds for Health Improvement and Research (2020-2-4061), and the Scientific Research Foundation of China-Japan Friendship Hospital (2019-RC-3).

Conflict of interest

The authors declare that the research was conducted in the absence of any commercial or financial relationships that could be construed as a potential conflict of interest.

The handling editor HL shares an affiliation with the author LPZ outside of the time of review.

Publisher's note

All claims expressed in this article are solely those of the authors and do not necessarily represent those of their affiliated organizations, or those of the publisher, the editors and the reviewers. Any product that may be evaluated in this article, or claim that may be made by its manufacturer, is not guaranteed or endorsed by the publisher.

Supplementary material

The Supplementary Material for this article can be found online at: https://www.frontiersin.org/articles/10.3389/fnins.2022.1045585/full#supplementary-material

References

Abraham, A., Milham, M. P., Di Martino, A., Craddock, R. C., Samaras, D., Thirion, B., et al. (2017). 'Deriving reproducible biomarkers from multi-site resting-state data: An Autism-based example'. *Neuroimage* 147, 736–745. doi: 10.1016/j.neuroimage.2016.10.045

Amal, H., Barak, B., Bhat, V., Gong, G., Joughin, B. A., Wang, X., et al. (2020). 'Shank3 mutation in a mouse model of autism leads to changes in the S-nitroso-proteome and affects key proteins involved in vesicle release and synaptic function'. *Mol. Psychiatry* 25, 1835–1848. doi: 10.1038/s41380-018-0113-6

Annaz, D., Remington, A., Milne, E., Coleman, M., Campbell, R., Thomas, M. S., et al. (2010). 'Development of motion processing in children with autism'. *Dev. Sci.* 13, 826–838. doi: 10.1111/j.1467-7687.2009.00939.x

Antoine, M. W., Langberg, T., Schnepel, P., and Feldman, D. E. (2019). 'Increased excitation-inhibition ratio stabilizes synapse and circuit excitability in four autism mouse models'. *Neuron* 101, 648–661.e4.

Azzi, J. C., Sirigu, A., and Duhamel, J. R. (2012). 'Modulation of value representation by social context in the primate orbitofrontal cortex'. *Proc. Natl. Acad. Sci. U.S.A.* 109, 2126–2131. doi: 10.1073/pnas.1111715109

Ben-Ari, Y., Caly, H., Rabiei, H., and Lemonnier, É (2022). 'Early prognostic of ASD: A challenge'. *Med. Sci.* 38, 431–437. doi: 10.1051/medsci/2022054

Boudes, E., Gilbert, G., Leppert, I. R., Tan, X., Pike, G. B., Saint-Martin, C., et al. (2014). 'Measurement of brain perfusion in newborns: Pulsed arterial spin labeling (PASL) versus pseudo-continuous arterial spin labeling (pCASL)'. *Neuroimage Clin.* 6, 126–133. doi: 10.1016/j.nicl.2014.08.010

Bozzi, Y., Provenzano, G., and Casarosa, S. (2018). 'Neurobiological bases of autism-epilepsy comorbidity: A focus on excitation/inhibition imbalance'. *Eur. J. Neurosci.* 47, 534–548. doi: 10.1111/ejn.13595

Breznik, E., Malmberg, F., Kullberg, J., Ahlström, H., and Strand, R. (2020). 'Multiple comparison correction methods for whole-body magnetic resonance imaging'. *J. Med. Imaging* 7:014005. doi: 10.1117/1.Jmi.7.1.014005

Buescher, A. V., Cidav, Z., Knapp, M., and Mandell, D. S. (2014). 'Costs of autism spectrum disorders in the United Kingdom and the United States'. *JAMA Pediatr.* 168, 721–728. doi: 10.1001/jamapediatrics.2014.210

Chen, H., Duan, X., Liu, F., Lu, F., Ma, X., Zhang, Y., et al. (2016). 'Multivariate classification of autism spectrum disorder using frequency-specific resting-state functional connectivity–a multi-center study'. *Prog. Neuropsychopharmacol. Biol. Psychiatry* 64, 1–9. doi: 10.1016/j.pnpbp.2015.06.014

Chen, J. J., Jann, K., and Wang, D. J. (2015). 'Characterizing resting-state brain function using arterial spin labeling'. *Brain Connect.* 5, 527–542. doi: 10.1089/brain.2015.0344

Chen, R., Jiao, Y., and Herskovits, E. H. (2011). 'Structural MRI in autism spectrum disorder'. *Pediatr. Res.* 69:63R–8R. doi: 10.1203/PDR.0b013e318212c2b3

Chevallier, C., Kohls, G., Troiani, V., Brodkin, E. S., and Schultz, R. T. (2012). 'The social motivation theory of autism'. *Trends Cogn. Sci.* 16, 231–239. doi: 10.1016/j.tics.2012.02.007

David, R. M., and Skilbeck, C. E. (1984). 'Raven IQ and language recovery following stroke'. *J. Clin. Neuropsychol.* 6, 302–308. doi: 10.1080/01688638408401220

Detre, J. A., Rao, H., Wang, D. J., Chen, Y. F., and Wang, Z. (2012). 'Applications of arterial spin labeled MRI in the brain'. *J. Magn. Reson. Imaging* 35, 1026–1037. doi: 10.1002/jmri.23581

Diedrichsen, J., King, M., Hernandez-Castillo, C., Sereno, M., and Ivry, R. B. (2019). 'Universal transform or multiple functionality? understanding the contribution of the human cerebellum across task domains'. *Neuron* 102, 918–928. doi: 10.1016/j.neuron.2019.04.021

Ecker, C., Bookheimer, S. Y., and Murphy, D. G. (2015). 'Neuroimaging in autism spectrum disorder: Brain structure and function across the lifespan'. *Lancet Neurol.* 14, 1121–1134. doi: 10.1016/s1474-4422(15)00050-2

Friederici, A. D. (2002). 'Towards a neural basis of auditory sentence processing'. *Trends Cogn. Sci.* 6, 78–84. doi: 10.1016/s1364-6613(00)01839-8

Gallagher, H. L., and Frith, C. D. (2003). 'Functional imaging of 'theory of mind''. *Trends Cogn. Sci.* 7, 77–83. doi: 10.1016/s1364-6613(02)00025-6

Glasser, M. F., Coalson, T. S., Robinson, E. C., Hacker, C. D., Harwell, J., Yacoub, E., et al. (2016). 'A multi-modal parcellation of human cerebral cortex'. *Nature* 536, 171–178. doi: 10.1038/nature18933

Hashimoto, T., Sasaki, M., Fukumizu, M., Hanaoka, S., Sugai, K., and Matsuda, H. (2000). 'Single-photon emission computed tomography of the brain in autism: Effect of the developmental level'. *Pediatr. Neurol.* 23, 416–420. doi: 10.1016/s0887-8994(00)00224-1

Hazlett, H. C., Gu, H., Munsell, B. C., Kim, S. H., Styner, M., Wolff, J. J., et al. (2017). 'Early brain development in infants at high risk for autism spectrum disorder'. *Nature* 542, 348–351. doi: 10.1038/nature21369

Hernandez-Garcia, L., Lahiri, A., and Schollenberger, J. (2019). 'Recent progress in ASL'. *Neuroimage* 187, 3–16. doi: 10.1016/j.neuroimage.2017.12.095

Hickok, G., and Poeppel, D. (2007). 'The cortical organization of speech processing'. *Nat. Rev. Neurosci.* 8, 393–402. doi: 10.1038/nrn2113

Hiser, J., and Koenigs, M. (2018). 'The multifaceted role of the ventromedial prefrontal cortex in emotion, decision making, social cognition, and psychopathology'. *Biol. Psychiatry* 83, 638–647. doi: 10.1016/j.biopsych.2017.10.030

Hofmann, M. J., Herrmann, M. J., Dan, I., Obrig, H., Conrad, M., Kuchinke, L., et al. (2008). Differential activation of frontal and parietal regions during visual word recognition: An optical topography study. *NeuroImage* 40, 1340–1349. doi: 10.1016/j.neuroimage.2007.12.037

Horder, J., Petrinovic, M. M., Mendez, M. A., Bruns, A., Takumi, T., Spooren, W., et al. (2018). 'Glutamate and GABA in autism spectrum disorder-a translational magnetic resonance spectroscopy study in man and rodent models'. *Transl. Psychiatry* 8:106. doi: 10.1038/s41398-018-0155-1

Iadecola, C. (2004). 'Neurovascular regulation in the normal brain and in Alzheimer's disease'. *Nat. Rev. Neurosci.* 5, 347–360. doi: 10.1038/nrn1387

Ivanov, D., Gardumi, A., Haast, R. A. M., Pfeuffer, J., Poser, B. A., and Uludağ, K. (2017). 'Comparison of 3T and 7T ASL techniques for concurrent functional perfusion and BOLD studies'. *Neuroimage* 156, 363–376. doi: 10.1016/j.neuroimage.2017.05.038

Jann, K., Gee, D. G., Kilroy, E., Schwab, S., Smith, R. X., Cannon, T. D., et al. (2015). 'Functional connectivity in BOLD and CBF data: Similarity and reliability of resting brain networks'. *Neuroimage* 106, 111–122. doi: 10.1016/j.neuroimage.2014.11.028

Johnson, R., Simon, E. J., Henkell, H., and Zhu, J. (2011). The role of episodic memory in controlled evaluative judgments about attitudes: An event-related potential study. *Neuropsychologia* 49, 945–960. doi: 10.1016/j.neuropsychologia.2011.01.028

Jonker, F. A., Jonker, C., Scheltens, P., and Scherder, E. J. (2015). 'The role of the orbitofrontal cortex in cognition and behavior'. *Rev. Neurosci.* 26, 1–11. doi: 10.1515/revneuro-2014-0043

Kaiser, M. D., Shiffrar, M., and Pelphrey, K. A. (2012). 'Socially tuned: Brain responses differentiating human and animal motion'. *Soc. Neurosci.* 7, 301–310. doi: 10.1080/17470919.2011.614003

Kalaria, R. N. (2010). 'Vascular basis for brain degeneration: Faltering controls and risk factors for dementia'. *Nutr. Rev.* 68:S74–S87. doi: 10.1111/j.1753-4887.2010.00352.x

Kogan, M. D., Vladutiu, C. J., Schieve, L. A., Ghandour, R. M., Blumberg, S. J., Zablotsky, B., et al. (2018). 'The prevalence of parent-reported autism spectrum disorder among US children'. *Pediatrics* 142:e20174161. doi: 10.1542/peds.2017-4161

Lee, M. H., Smyser, C. D., and Shimony, J. S. (2013). 'Resting-state fMRI: A review of methods and clinical applications'. *AJNR Am. J. Neuroradiol.* 34, 1866–1872. doi: 10.3174/ajnr.A3263

Li, X., Zhao, P., Qiu, X., Ding, H., Lv, H., Yang, Z., et al. (2020). 'Lateralization effects on cerebral blood flow in patients with unilateral pulsatile tinnitus measured with arterial spin labeling'. *Front. Hum. Neurosci.* 14:591260. doi: 10.3389/fnhum.2020.591260

Liang, D., Xia, S., Zhang, X., and Zhang, W. (2021). 'Analysis of brain functional connectivity neural circuits in children with autism based on persistent homology'. *Front. Hum. Neurosci.* 15:745671. doi: 10.3389/fnhum.2021.745671

Miao, X., Wu, X., Li, R., Chen, K., and Yao, L. (2011). 'Altered connectivity pattern of hubs in default-mode network with Alzheimer's disease: An granger causality modeling approach'. *PLoS One* 6:e25546. doi: 10.1371/journal.pone.0025546

Mori, K., Toda, Y., Ito, H., Mori, T., Mori, K., Goji, A., et al. (2015). 'Neuroimaging in autism spectrum disorders: 1H-MRS and NIRS study'. *J. Med. Investig.* 62, 29–36. doi: 10.2152/jmi.62.29

Ohnishi, T., Matsuda, H., Hashimoto, T., Kunihiro, T., Nishikawa, M., Uema, T., et al. (2000). 'Abnormal regional cerebral blood flow in childhood autism'. *Brain* 123, 1838–1844. doi: 10.1093/brain/123.9.1838

Osterling, J., and Dawson, G. (1994). 'Early recognition of children with autism: A study of first birthday home videotapes'. *J. Autism Dev. Disord.* 24, 247–257. doi: 10.1007/bf02172225

Ozgen, H., Hellemann, G. S., de Jonge, M. V., Beemer, F. A., and van Engeland, H. (2013). 'Predictive value of morphological features in patients with autism versus normal controls'. *J. Autism Dev. Disord.* 43, 147–155. doi: 10.1007/s10803-012-1554-4

Pardo, C. A., and Eberhart, C. G. (2007). 'The neurobiology of autism'. *Brain Pathol.* 17, 434–447. doi: 10.1111/j.1750-3639.2007.00102.x

Philip, R. C., Dauvermann, M. R., Whalley, H. C., Baynham, K., Lawrie, S. M., and Stanfield, A. C. (2012). 'A systematic review and meta-analysis of the fMRI investigation of autism spectrum disorders'. *Neurosci. Biobehav. Rev.* 36, 901–942. doi: 10.1016/j.neubiorev.2011.10.008

Raju, K., Doulias, P. T., Evans, P., Krizman, E. N., Jackson, J. G., Horyn, O., et al. (2015). 'Regulation of brain glutamate metabolism by nitric oxide and S-nitrosylation'. *Sci. Signal.* 8:ra68. doi: 10.1126/scisignal.aaa4312

Reynell, C., and Harris, J. J. (2013). 'The BOLD signal and neurovascular coupling in autism'. *Dev. Cogn. Neurosci.* 6, 72–79. doi: 10.1016/j.dcn.2013.07.003

Salmond, C. H., de Haan, M., Friston, K. J., Gadian, D. G., and Vargha-Khadem, F. (2003). 'Investigating individual differences in brain abnormalities in autism'. *Philos. Trans. R. Soc. Lond. B Biol. Sci.* 358, 405–413. doi: 10.1098/rstb.2002.1210

Sherkatghanad, Z., Akhondzadeh, M., Salari, S., Zomorodi-Moghadam, M., Abdar, M., Acharya, U. R., et al. (2019). 'Automated detection of autism spectrum disorder using a convolutional neural network'. *Front. Neurosci.* 13:1325. doi: 10.3389/fnins.2019.01325

Smith, L. G. F., Milliron, E., Ho, M. L., Hu, H. H., Rusin, J., Leonard, J., et al. (2019). 'Advanced neuroimaging in traumatic brain injury: An overview'. *Neurosurg. Focus* 47:E17. doi: 10.3171/2019.9.Focus19652

Sohal, V. S., and Rubenstein, J. L. R. (2019). 'Excitation-inhibition balance as a framework for investigating mechanisms in neuropsychiatric disorders'. *Mol. Psychiatry* 24, 1248–1257. doi: 10.1038/s41380-019-0426-0

Son, H., Hawkins, R. D., Martin, K., Kiebler, M., Huang, P. L., Fishman, M. C., et al. (1996). 'Long-term potentiation is reduced in mice that are doubly mutant in endothelial and neuronal nitric oxide synthase'. *Cell* 87, 1015–1023. doi: 10.1016/s0092-8674(00)81796-1

Sophia, M., Daniel, K., Samson, A. C., Valerie, K., Janusch, B., Michel, G., et al. (2013). Convergent findings of altered functional and structural brain connectivity in individuals with high functioning autism: a multimodal MRI study. *PLoS One* 8:e67329. doi: 10.1371/journal.pone.0067329

St Lawrence, K. S., and Wang, J. (2005). Effects of the apparent transverse relaxation time on cerebral blood flow measurements obtained by arterial spin labeling. *Magn. Reson. Med.* 53, 425–433. doi: 10.1002/mrm.20364

Stivaros, S., Garg, S., Tziraki, M., Cai, Y., Thomas, O., Mellor, J., et al. (2018). 'Randomised controlled trial of simvastatin treatment for autism in young children with neurofibromatosis type 1 (SANTA)'. *Mol. Autism* 9:12. doi: 10.1186/s13229-018-0190-z

Sztainberg, Y., and Zoghbi, H. Y. (2016). 'Lessons learned from studying syndromic autism spectrum disorders'. *Nat. Neurosci.* 19, 1408–1417. doi: 10.1038/nn.4420

Tang, S., Liu, X., Ran, Q., Nie, L., Wu, L., Pan, Z., et al. (2022). 'Application of three-dimensional pseudocontinuous arterial spin labeling perfusion imaging in the brains of children with autism'. *Front. Neurol.* 13:851430. doi: 10.3389/fneur.2022.851430

Tripathi, M. K., Kartawy, M., and Amal, H. (2020). 'The role of nitric oxide in brain disorders: Autism spectrum disorder and other psychiatric, neurological, and neurodegenerative disorders'. *Redox Biol.* 34:101567. doi: 10.1016/j.redox.2020.101567

Van Essen, D. C., Donahue, C. J., and Glasser, M. F. (2018). 'Development and evolution of cerebral and cerebellar cortex'. *Brain Behav. Evol.* 91, 158–169. doi: 10.1159/000489943

Volkmar, F. R., Cicchetti, D. V., Dykens, E., Sparrow, S. S., Leckman, J. F., and Cohen, D. J. (1988). 'An evaluation of the autism behavior checklist'. *J. Autism Dev. Disord.* 18, 81–97. doi: 10.1007/bf02211820

Walsh, M. J. M., Wallace, G. L., Gallegos, S. M., and Braden, B. B. (2021). 'Brain-based sex differences in autism spectrum disorder across the lifespan: A systematic review of structural MRI, fMRI, and DTI findings'. *Neuroimage Clin.* 31:102719. doi: 10.1016/j.nicl.2021.102719

Wang, X. H., Liu, X. F., Ao, M., Wang, T., He, J., Gu, Y. W., et al. (2022). 'Cerebral perfusion patterns of anxiety state in patients with pulmonary nodules: A study of cerebral blood flow based on arterial spin labeling'. *Front. Neurosci.* 16:912665. doi: 10.3389/fnins.2022.912665

Wei, X., Hu, J., Yang, L., Gao, M., Li, L., Ding, N., et al. (2021). 'Bidirectional association of neurodevelopment with growth: A prospective cohort study'. *BMC Pediatr.* 21:203. doi: 10.1186/s12887-021-02655-7

Yerys, B. E., Herrington, J. D., Bartley, G. K., Liu, H. S., Detre, J. A., and Schultz, R. T. (2018). 'Arterial spin labeling provides a reliable neurobiological marker of autism spectrum disorder'. *J. Neurodev. Disord.* 10:32. doi: 10.1186/s11689-018-9250-0

Yin, W., Mostafa, S., and Wu, F. X. (2021). 'Diagnosis of Autism Spectrum Disorder Based on Functional Brain Networks with Deep Learning'. *J. Comput. Biol.* 28, 146–165. doi: 10.1089/cmb.2020.0252

Zhao, M. Y., Woodward, A., Fan, A. P., Chen, K. T., Yu, Y., Chen, D. Y., et al. (2022). 'Reproducibility of cerebrovascular reactivity measurements: A systematic review of neuroimaging techniques()'. *J. Cereb. Blood Flow Metab.* 42, 700–717.

Zheng, W., Ren, S., Zhang, H., Liu, M., Zhang, Q., Chen, Z., et al. (2019). 'Spatial Patterns of Decreased Cerebral Blood Flow and Functional Connectivity in Multiple System Atrophy (Cerebellar-Type): A Combined Arterial Spin Labeling Perfusion and Resting State Functional Magnetic Resonance Imaging Study'. *Front. Neurosci.* 13:777. doi: 10.3389/fnins.2019.00777

Zhu, J., Guo, M., Yang, T., Lai, X., Lei, Y., He, M., et al. (2017). 'Association between behavioral problems and gastrointestinal disorders among children with autism spectrum disorder'. *Chin. J. Pediatr.* 55, 905–910. doi: 10.3760/cma.j.issn.0578-1310.2017.12.007

Zilbovicius, M., Garreau, B., Samson, Y., Remy, P., Barthélémy, C., Syrota, A., et al. (1995). 'Delayed maturation of the frontal cortex in childhood autism'. *Am. J. Psychiatry* 152, 248–252. doi: 10.1176/ajp.152.2.248

Zlokovic, B. V. (2011). 'Neurovascular pathways to neurodegeneration in Alzheimer's disease and other disorders'. *Nat. Rev. Neurosci.* 12, 723–738. doi: 10.1038/nrn3114

frontiers | Frontiers in Neuroscience

TYPE Original Research
PUBLISHED 14 December 2022
DOI 10.3389/fnins.2022.1093850

OPEN ACCESS

EDITED BY
Han Lv,
Beijing Friendship Hospital, Capital Medical University, China

REVIEWED BY
Xiaoyan Yang,
Affiliated Hospital of Guizhou Medical University, China
Runsong Hao,
Fourth People's Hospital of Jinan, China

*CORRESPONDENCE
Linfeng Yang
ylf19860928@126.com

†These authors have contributed equally to this work and share first authorship

SPECIALTY SECTION
This article was submitted to Brain Imaging Methods, a section of the journal Frontiers in Neuroscience

RECEIVED 09 November 2022
ACCEPTED 28 November 2022
PUBLISHED 14 December 2022

CITATION
Chen T, Sui C, Lin S, Guo B, Wang Y and Yang L (2022) Follow-up study of neuropsychological scores of infant patients with cobalamin C defects and influencing factors of cerebral magnetic resonance imaging characteristics.
Front. Neurosci. 16:1093850.
doi: 10.3389/fnins.2022.1093850

Follow-up study of neuropsychological scores of infant patients with cobalamin C defects and influencing factors of cerebral magnetic resonance imaging characteristics

Tao Chen [1†], Chaofan Sui [2†], Suna Lin [3], Bin Guo [4], Yuanyuan Wang [5] and Linfeng Yang [4*]

[1]Department of Clinical Laboratory, Jinan Maternity and Child Care Hospital Affiliated to Shandong First Medical University, Jinan, Shandong, China, [2]Department of Radiology, Shandong Provincial Hospital Affiliated to Shandong First Medical University, Jinan, Shandong, China, [3]Department of Scientific Research and Foreign Affairs, Jinan Maternity and Child Care Hospital Affiliated to Shandong First Medical University, Jinan, Shandong, China, [4]Department of Radiology, Jinan Maternity and Child Care Hospital Affiliated to Shandong First Medical University, Jinan, Shandong, China, [5]Department of Radiology, Binzhou Medical University, Yantai, Shandong, China

Purpose: The purpose of this study was to investigate whether baseline cerebral magnetic resonance imaging (MRI) characteristics could predict therapeutic responsiveness in patients with cobalamin C (cblC) defects.

Materials and methods: The cerebral MRI results of 40 patients with cblC defects were evaluated by a neuroradiologist. Neuropsychological scores and imaging data were collected. Neuropsychological tests were performed before and after standardized treatment.

Results: Thirty-eight patients initially underwent neuropsychological testing [developmental quotient (DQ)]. CblC defects with cerebellar atrophy, corpus callosum thinning and ventricular dilation had significantly lower DQs than those without ($P < 0.05$). Through a multivariate linear stepwise regression equation after univariate analysis, ventricular dilation was the most valuable predictor of lower DQs. Thirty-six patients (94.7%) underwent follow-up neuropsychological testing. The pre- and post-treatment DQ values were not significantly different ($Z = -1.611$, $P = 0.107$). The post-treatment DQ classification (normal, moderately low, or extremely low) showed nearly no change compared to the pretreatment DQ classification ($k = 0.790$, $P < 0.001$).

Conclusion: Ventricular dilation, cerebral atrophy and corpus callosum thinning are the main MRI abnormalities of cblC defects,

and these manifestations are significantly correlated with delayed development in children. MRI findings can be considered an important tool for determining the severity of cblC defects.

KEYWORDS

cblC defect, inborn error of metabolism, magnetic resonance imaging, neuropsychological test, follow-up study

Introduction

Cobalamin C (cblC) defects, also called combined methylmalonic aciduria and homocystinuria cblC type, are the most common inherited disorders of cobalamin metabolism, with an incidence of approximately 1/100,000 live births (Weisfeld-Adams et al., 2010). It causes impaired conversion of dietary vitamin B12 into two metabolically active forms, methylcobalamin and adenosylcobalamin. The impaired activity of these two enzymes results in the accumulation of homocysteine and methylmalonic acid as well as in the reduced synthesis of methionine (Martinelli et al., 2011). Enhanced oxidative stress due to a disturbance of glutathione metabolism has been shown in patients with cblC defects and may contribute to the underlying pathophysiology (Pastore et al., 2014). In mainland China, cblC defects are the main type of combined methylmalonic aciduria (MMA) and homocystinuria (Cui et al., 2018). Studies have found that the prevalence of cb1C deficiency in Shandong province of China was 1/3,920 from 2011 to 2014 (Han et al., 2016), however, the nationwide prevalence of cblC deficiency is unclear (Chen et al., 2022). In the case of combined defects (cblC, cblD, and cblF), both MMA and homocysteine accumulate, and these defects are vital characteristics of patients with MMA. Patients with cblC, cblD, and cblF defects are classified as having MMA combined with homocysteinemia (Fowler et al., 2008; Wang et al., 2010) accounting for 60–80% of cases in China (Wu et al., 2019), and cblC defects are the most common subtype (Carrillo-Carrasco et al., 2012).

Cobalamin C defects often cause damage to multiple body systems, especially to the central nervous system (Li et al., 2015). Although the incidence of the disease is low, the mortality and disability rates are very high (Thompson et al., 1989). This disease has diverse and non-specific clinical manifestations, such as feeding difficulties, intellectual disabilities, ataxia, abnormal muscle tone, convulsions, epilepsy, and lethargy (Fraser and Venditti, 2016; Han et al., 2016). The presence of cognitive and neurological deficits has been observed in patients with cblC defects, and these deficits include developmental delays and hyperkinetic movement disorders secondary to striatum injury (Guo et al., 2020). Patients with cblC defects usually have symptoms of neurological damage; hence, brain imaging is necessary to rule out congenital or acquired brain abnormalities, and magnetic resonance imaging (MRI) is the most valuable method for obtaining brain images because of the lack of radiation damage and its suitability for use in pediatric brain examinations (Yesildag et al., 2005). Because of the development of genetic diagnostic technologies, the diagnostic efficiency of cblC defects has greatly improved. Standardized treatment regimens for different clinical types have been established (Fraser and Venditti, 2016), and their prognosis has become a matter of widespread interest. Some previous studies have attempted to retrospectively analyze neurocognitive prognosis in patients with MMA, relying on surveys of clinical data collected across medical institutions and/or using various testing protocols to measure cognition (Baumgarter and Viardot, 1995; Hörster et al., 2009; Carrillo-Carrasco et al., 2012; Han et al., 2015).

At present, there have been many reports involving cerebral MRI characteristics of combined MMA and homocystinuria patients (Radmanesh et al., 2008; Yang et al., 2020), including detection using many functional MRI sequences (Cheng et al., 2019). However, the definite correlation between conventional MRI features and neurocognitive impairments in infant patients with cblC defects remains unclear. Follow-up studies of neurocognitive function after standardized treatment are lacking. It is unknown which MRI characteristics could predict a better recovery of neurocognitive function in patients with cblC defects. The purpose of this study was to investigate relationships between cerebral MRI characteristics and neuropsychological scores, compare changes in neuropsychological scores before and after treatment, and identify which cerebral MRI characteristics could predict a better prognosis in patients with cblC defects.

Materials and methods

Patient diagnosis and clinical data acquisition

Forty patients diagnosed with cblC defects were enrolled in the present study from March 2017 to December 2019. Informed consent was obtained from their guardians. This study was

Abbreviations: MMA, methylmalonic acidemia; MCM, methylmalonyl-CoA mutase; MRI, magnetic resonance imaging; GC/MS, gas chromatography–mass spectrometry; C3, propionyl carnitine; C2, acetylcarnitine; tHcy, total plasma homocysteine; AMM, blood ammonia; LAC, blood lactic acid; PCR, polymerase chain reaction; OHCbl, hydroxocobalamin; DQ, developmental quotient; IQ, integrated intelligence; WISC, Wechsler intelligence scale.

approved by the Ethical Committee of the Institutional Review Board (IRB) of Jinan Maternal and Child Care Hospital (201811). All experiments were performed in accordance with relevant guidelines and regulations. The diagnosis of cblC defects was made when increased plasma methylmalonyl carnitine levels or increased urine methylmalonic acid levels were detected using gas chromatography–mass spectrometry (GC/MS) and the propionate incorporation test, respectively (Radmanesh et al., 2008). The levels of propionyl carnitine (C3) and C3/acetylcarnitine (C2) were measured by tandem mass spectrometry methionine in dried blood spots. The levels of organic acids in urine were measured using GC/MS in patients with suspected cblC defects. In addition, the concentrations of total plasma homocysteine (tHcy) and blood ammonia were measured (Weisfeld-Adams et al., 2010). Genomic DNA was extracted from the peripheral blood leukocytes of patients using the phenol–chloroform method. The entire coding sequence of MMACHC was amplified by polymerase chain reaction (PCR), and the PCR products were sequenced. Variant analysis was performed using the normal MMACHC complementary DNA (NM_015506.2) sequence (Lerner-Ellis et al., 2006). Detailed genetic data and experimental data are provided in **Supplementary material 1**.

Magnetic resonance imaging examination and neuropsychological tests were performed before treatment. The laboratory test results, gene type, age at the time of MRI and symptoms of each patient were collected. CblC defect patients were treated with standardized treatment regimens on the basis of their different clinical types. If patients had motor system damage, sensory and motor function rehabilitation training and language cognitive ability training were carried out to facilitate the growth and development of patients. Details of the standardized treatment regimens are provided in **Supplementary material 2**.

Neuropsychological assessment

The neuropsychological test used a pediatric neuropsychological development examination scale for 0- to 6-year-old patients [China neuropsychological and Behavior Scale-Revision 2016 (CNBS-R2016) scale, Capital Medical University]. This scale mainly tests the physical abilities and intelligence of infants and children in five aspects: Gross movements, fine movements, adaptability, language, and social behavior. Gross movements mainly involve the movements of the head, neck, torso, and limbs with large amplitudes; fine movements mainly refer to the movements of the hand and the hand-eye coordination ability that follows; adaptability is mainly the ability of infants and young children to analyze and synthesize external stimuli; language ability involves unique psychological activities of human beings; and social behavior is the child's personal reaction to the real social culture.

This scale calculates the intellectual age and developmental quotient (DQ) based on age in months. Intellectual age = sum of scores in five areas/5; DQ = (intellectual age/actual age in months) × 100. The neuropsychological tests resulted in the assignment of DQs, which were classified into normal, lower and low subgroups. The classification criteria were as follows: ≥130, excellent; 115–129, intelligent; 85–114, normal; 70–84, moderately low; and ≤69, extremely low (Guo et al., 2020). Scores ≥84 were considered normal, and scores ≤84 were considered low. Follow-up tests were conducted after 6 to 12 months of treatment, and the neuropsychological scores were recorded and compared.

Magnetic resonance imaging parameters and image interpretation

Imaging data were obtained using a 1.5-T MR scanner (Achieva, Philips Healthcare, Best, Netherlands) and a 16-channel phased-array head coil. The following sequences were performed: axial and sagittal T2-weighted imaging (T2WI) (repetition time, 2100 ms; echo time, 90–100 ms), axial T1-weighted imaging (T1WI) (TR, 568 ms; TE, 15 ms), axial T2-weighted fluid-attenuated inversion recovery (T2-FLAIR) (TR, 700 ms; TE, 115 ms), and axial diffusion-weighted imaging (DWI) (TR, 3,090 ms; TE, 99 ms; b = 0 to 1,000). The scanning parameters were field of view (FOV) = 230 mm × 190 mm, slice thickness = 5 mm, and slice gap = 0.5 mm. The scan time was approximately 10 min.

Images were evaluated by an experienced pediatric radiologist. The assessment of the severity of cortical atrophy and ventricular dilation was performed using the semiquantitative scale devised by Yue et al. (1997). Age-related white matter changes were assessed using the rating scale established by Wahlund et al. (2001). Then, the imaging features were defined in a binary fashion (i.e., presence or absence). Thinning of the corpus callosum was subjectively evaluated as present or absent by an experienced pediatric radiologist. To verify the accuracy of the evaluation, we measured the corpus callosum and lateral ventricle and compared the differences among healthy controls and patients with and without corresponding features. The results proved that our subjective evaluation was accurate. The specific results are presented in **Supplementary material 2**.

Statistical analysis

Statistical analysis was performed using the Statistical Package for the Social Sciences (Version 21.0 for Windows; SPSS, Chicago, IL, USA). P-values of < 0.05 were considered

to be statistically significant. First, a descriptive analysis of the 40 patients was performed. The measurement data are expressed as the median (interquartile range), and the count data are expressed as n (%). Considering that the sample size was relatively small, the Mann–Whitney *U*-test was used to compare the basic neuropsychological scores between the two groups divided by different imaging features in the baseline MRI. Then, the features that significantly influenced the DQ were selected to perform the multiple linear stepwise regression analysis. The Wilcoxon paired rank-sum test was used to compare the neuropsychological scores (DQ and five subscales), tHcy levels, blood ammonia (AMM) levels, and blood lactic acid (LAC) levels of the patients with cblC defects before and after treatment, and Bonferroni's correction was used to avoid type I errors. Weighted *k*-values were used to assess whether the post-treatment DQ classifications were altered compared with the pretreatment DQ classifications. *K*-values of $\leq$ 0.4, 0.41–0.6, 0.61–0.8, and $\geq$0.81 indicated poor, moderate, good, and excellent agreement, respectively. To determine which image feature could potentially predict prognosis, the change value of the pre- and post-treatment DQ scores was considered a marker for evaluating prognosis, and the Mann–Whitney *U*-test was used to compare the difference in the change values between the two groups into which patients were divided based on baseline MRI image features.

Results

Of the 40 patients (29 males and 11 females), 19 patients were diagnosed by genetic screening shortly after birth, and 21 patients were diagnosed by blood and genetic tests after exhibiting suspicious symptoms. In these 40 patients, the age at which they began to exhibit symptoms was 7.05 (3.00, 20.50) months. The presenting symptom age of patients who were diagnosed by genetic screening was 18.00 (3.00, 30.0) months, while the presenting symptom age of patients who were diagnosed by blood and genetic tests after exhibiting suspicious symptoms was 5.00 (2.05, 11.00) months. The difference in onset age was not statistically significant between these two groups (Z = 1.939, p = 0.052). In these 40 patients, the age at which the baseline MRI scan was conducted was 9.00 (3.25, 23.75) months, usually several weeks after symptom onset. The first neuropsychological test and MRI examination usually occurred on the same day or within 2 days. When the pediatrician received the results within 2 days, the treatment started immediately; therefore, neuropsychological test time, MRI examination time and treatment initiation time could be considered approximately one time point. Neuropsychological evaluations were performed at intervals of 6 to 12 months before and after treatment, and the age at follow-up DQ evaluation was 18.50 (13.12, 30.75) months. These patients' symptoms included seizures, developmental regression, hypotonia, psychomotor delay, recurrent vomiting, respiratory distress, agitation, coma, lethargy, growth retardation, and poor feeding. Thirty-eight cblC defect patients received neuropsychological testing, and 2 patients (5.3%) were not successfully tested due to non-compliance. Thirty-six patients (94.7%) were followed up and received a second neuropsychological test after 6 to 12 months of standardized treatment.

All patients included in this study underwent routine MRI examinations. The main MRI feature details are shown in Table 1. The patients with cblC defects were divided into two groups based on the presence or absence of a particular MRI feature, and differences in DQ scores were compared. Because the number of samples in some groups was small and the data were not normally distributed, the rank-sum test of two independent samples was used. The comparison results are shown in Table 1. The cblC defect patients with characteristics of cerebellar atrophy, corpus callosum thinning and ventricular dilation had significantly lower DQs than the patients without these characteristics ($P < 0.05$). Using Spearman bivariate correlation analysis, we found that the DQ value negatively correlated with tHcy ($r = -0.333$, $p = 0.041$). However, AMM and LAC had no relationships with the DQ values ($r = 0.123$, $p = 0.464$; $r = 0.218$, $p = 0.189$). After univariate analyses, the factors cerebellar atrophy, corpus callosum thinning, ventricular dilation and tHcy were entered into the multivariate linear stepwise regression equation. Only the parameter of ventricular dilation was included in the final equation. The results showed that the patients with ventricular dilation had a lower DQ, as shown in Table 2. In addition to the change in DQ scores before and after treatment between the two groups (divided by the presence or absence of a particular MRI feature in the baseline scan), the results showed that there were no significant differences in the DQ value changes between these two groups ($P > 0.05$).

In this study, 38 patients received neuropsychological testing before treatment [DQ, 74.85 (49.68, 86.45)], and of these patients, 36 were followed up after 6–12 months of treatment [DQ, 78.00 (62.40, 85.75)]. There were no significant differences in DQs before and after treatment. Using the DQ subscales, all the subscores from the follow-up evaluation were higher than those before the treatment. To avoid type I error, Bonferroni's correction was used, and finally, no difference between these subscores reached the level of statistical significance (see Table 3 for details). Weighted *k*-values were used to compare the changes in DQ classification pre- and post-treatment (*k*-values = 0.790, $P < 0.001$; Table 4). After treatment, the classification of 31 patients remained unchanged; the classification of 5 patients increased to a higher rank, and the classification of only one patient decreased to a lower rank.

In this study, the tHCy, AMM and LAC values of 40 cblC defect patients after treatment were significantly lower than those before treatment (see Table 5 for details).

TABLE 1 Cerebral MRI characteristics in patients with cblC defects and comparison of DQ among different groups.

MRI characteristics	Descriptive MRI image feature analysis of 40 patients			Basic DQ comparison between two group based different MRI image features				Comparison of the difference of two time-point DQ values based different MRI image features			
		N (40)	%	*N* (38)	Median (interquartile range)	*Z*	*P*	*N* (36)	Median (interquartile range)	*Z*	*P*
Cerebral sulcus widened	No	24	60.0	22	76.90 (46.67, 87.63)	−0.325	0.759	20	0.40 (−2.5, 6.58)	−0.653	0.519
	Yes	16	40.0	16	71.40 (50.00, 85.70)			16	0.95 (−2.35,11.85)		
Cerebellar atrophy	No	32	80.0	30	78.95 (60.90, 87.63)	−2.166	0.028	28	0.55 (−2.5, 9.38)	−0.133	0.896
	Yes	8	20.0	8	44.5 (32.15, 73.95)			8	0.90 (−2.35, 2.25)		
Brainstem thinning	No	36	90.0	34	76.95 (60.90, 86.25)	−2.759	0.051	32	0.30 (−3.0, 7.73)	−1.435	0.157
	Yes	4	10.0	4	33.70 (20.55, 38.45)			4	2.10 (1.50,31.35)		
Corpus callosum thinning	No	21	52.5	20	85.50 (70.48, 88.95)	−3.070	0.002	19	0.10 (−3.0, 3.80)	−1.363	0.175
	Yes	19	47.5	18	56.95 (35.25, 76.28)			17	1.80 (−1.90, 19.95)		
Cortical atrophy (sulcal widening)	No	25	62.5	23	79.60 (63.90, 88.00)	−1.643	0.101	22	0.4 (−2.5, 6.58)	−0.114	0.911
	Yes	15	37.5	15	69.00 (36.80, 83.30)			14	0.95 (−2.35, 11.85)		
Subcortical/periventricular white matter change	No	12	30.0	10	66.95 (42.10, 80.20)	−1.293	0.196	8	3.20 (0.25, 16.85)	−1.389	0.165
	Yes	28	70.0	28	77.55 (50.00, 87.88)			28	0.35 (−4.28, 6.58)		
Ventricular dilation	No	28	70.0	26	82.50 (69.43, 88.20)	−3.360	0.000	24	0.15 (−2.5, 5.38)	−1.695	0.090
	Yes	12	30.0	12	44.50 (24.38, 69.75)			12	2.1 (−2.15, 26.78)		
Myelination abnormality	No	17	42.5	15	75.60 (51.90, 85.90)	−0.164	0.883	14	1.15 (−0.03, 15.30)	−1.347	0.180
	Yes	23	57.5	23	74.20 (48.70, 87.50)			22	0.35 (−3.43, 4.73)		
Internal capsule change	No	36	90.0	34	74.85 (49.68, 86.83)	−0.428	0.697	32	0.70 (−2.5, 7.73)	−0.201	0.865
	Yes	4	10.0	4	75.60 (40.20, 82.65)			4	−0.35 (−2.45, 30.78)		
Signal change consistent with focal infarct	No	37	92.5	35	75.50 (50.00, 86.40)	−0.217	0.839	33	0.50 (−2.0, 7.65)	−0.344	0.746
	Yes	3	7.5	3	39 (50, 92)*			3	−4.70 (1.40, 28.5*		
Abnormal signal in basal ganglia	No	39	97.5	37	75.50 (49.35, 86.50)	−0.821	0.526	35	0.50 (−3.0, 7.50)	−1.493	0.167
	Yes	1	2.5	1	50♦			1	28.50♦		

*There were only three patients in this group, and no interquartile range is shown. All values are shown in the table. ♦There was only one patient in this group, and no interquartile range is shown. The values are shown in the table.

10.3389/fnins.2022.1093850

TABLE 2 Multiple linear stepwise regression equation.

Variable	Non-normalized B	Standard error	Normalized B	*t*	*p*
C	75.72	3.960		19.121	0.000
Ventricular dilation	−28.890	7.047	−0.564	−4.100	0.000

TABLE 3 Comparative analysis of DQ before and after treatment in patients with cblC defects.

DQ scale and subscales	DQ-first (n = 38) median (interquartile range)	DQ follow-up (n = 36) median (interquartile range)	Statistics	
			Z	*P**
DQ	74.85 (49.68, 86.45)	78.00 (62.40, 85.75)	−1.611	0.107
Gross movements	73.75 (41.80, 85.60)	79.85 (59.35, 90.55)	−2.211	0.027
Fine movements	72.50 (46.05, 86.18)	71.50 (59.95, 84.83)	−0.744	0.457
Adaptability	74.60 (42.73, 87.35)	79.40 (60.00, 89.93)	−2.453	0.014
Language	73.75 (50.73, 88.50)	74.45 (61.50, 81.18)	−0.368	0.713
Social behavior	76.90 (50.98, 87.95)	76.40 (61.00, 88.00)	−0.838	0.402

DQ-first, DQ obtained before treatment; DQ-follow up, DQ obtained after 6 months of treatment. The Wilcoxon paired rank sum test was used to compare the neuropsychological scores (DQ and five subscales) of the cblC defects before and after treatment, and the Bonferroni's method was used for correction to avoid type-I error. *Statistical test level, $P < 0.05/6 = 0.008$ (Bonferroni's correction).

TABLE 4 Kappa test of DQ classification reproducibility before and after treatment in patients with cblC defects.

DQ-first	DQ-follow up			Total
	Low	Lower	Normal	
Low	10	3	0	13
Lower	0	12	2	14
Normal	0	1	9	9
Total	10	15	11	36

DQ: 84–114, normal; 70–84, moderately low; ≤69, extremely low. Kappa = 0.790, $P < 0.001$.

TABLE 5 Comparative analysis of blood examination before and after treatment in patients with cblC defects.

Variables	Before treatment	After treatment	Statistics	
			Z	*P*
tHcy (μmol/L)	61.95 (51.05, 93.53)	30.85 (21.50, 37.10)	−5.511	0.000
AMM (μmol/L)	49.50 (36.13, 65.66)	26.55 (22.83, 30.63)	−5.511	0.000
LAC (mmol/L)	4.08 (3.04, 6.04)	2.68 (2.37, 2.99)	−4.967	0.000

Discussion

This study demonstrated that the DQs of cblC defects with cerebellar atrophy, thinned corpus callosum, and ventricular dilation were significantly lower than those without these features; the results of multiple stepwise linear regression indicated that the occurrence of ventricular dilation had the greatest effect on the DQ scores. By comparing the changes in DQ before and after treatment, we found that the DQ of the cblC defect did not significantly decrease. After standardized treatment, the DQ of most patients increased. However, among the abnormal features detected by routine MRI, no features could predict better prognosis.

Magnetic resonance imaging has become the preferred imaging method for examining newborns or infants because it does not involve radiation and is characterized by high tissue contrast and high spatial resolution. In this study, forty cblC defects underwent routine MRI examinations. The most common imaging findings in the patients in this study were corpus callosum thinning (47.5%), cerebral sulcus widening (40%), cortical atrophy (37.5%), subcortical/periventricular white matter changes (35%), and ventricular dilation 30%) (**Figures 1A–F**). These findings are similar to previous studies (Gebarski et al., 1983; Korf et al., 1986; Heidenreich et al., 1988; Desousa et al., 1989; Brismar and Ozand, 1994; Enns et al., 1999; Biancheri et al., 2001; Pui and Ahmad, 2002; Takeuchi et al., 2003; Yesildag et al., 2005; Radmanesh et al., 2008).

Furthermore, we found that the DQ of cblC defect patients with cerebellar atrophy, thinned corpus callosum, and ventricular dilation was significantly decreased. The results of multivariate linear stepwise regression analysis showed that the occurrence of ventricular dilation had the largest impact on the brain development of patients with cblC defects. Ventricular dilation, cerebral sulcal widening and cerebellar atrophy are vital MRI signs reflecting neuropsychological developmental disorders in cblC defects. Some researchers have also considered that screening for inherited metabolic diseases should be immediately conducted when pediatric patients with cblC defects develop progressive and refractory hydrocephalus (Zhang et al., 2019). Previous studies have reported that ventricular dilation might be related to intracerebral vascular

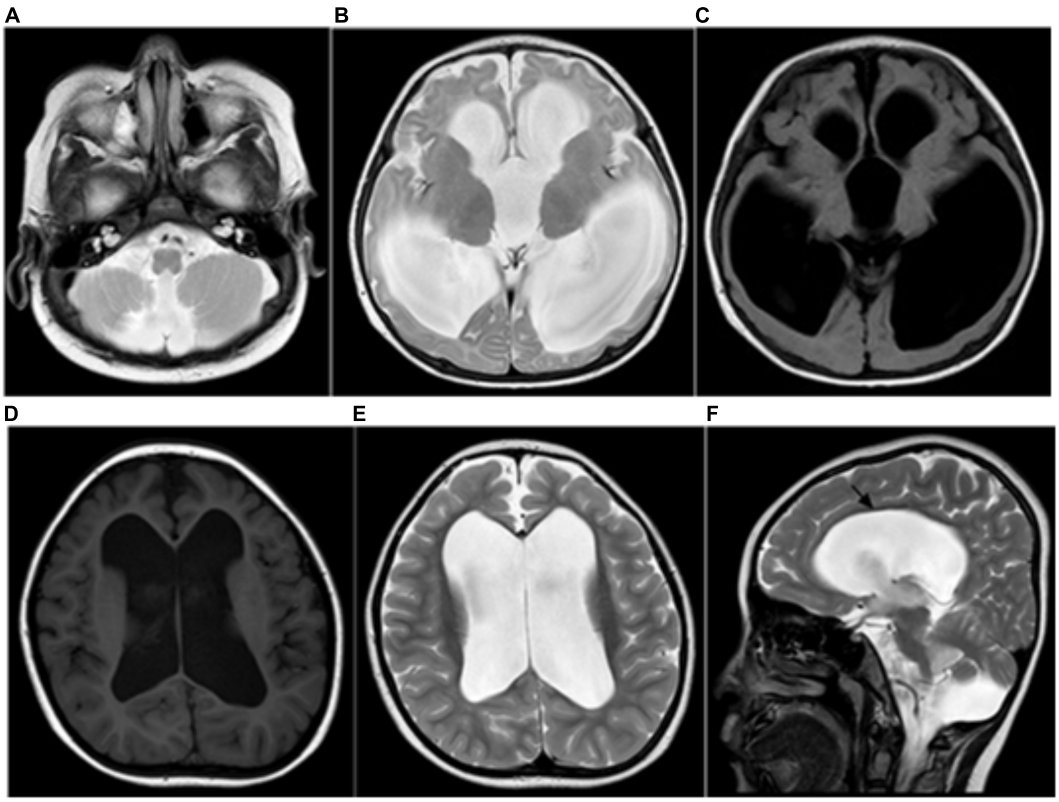

FIGURE 1
(A–C) Ventricular dilation and a small cerebellar vermis, consistent with the Dandy–Walker variant. **(D–F)** MRI showing severe ventricular dilation and corpus callosal thinning (black arrow, sagittal T2WI).

stiffness (Greitz et al., 2010). The toxic effects of high concentrations of cysteine metabolites on the vascular wall are the main cause of vascular endothelial damage (Herrmann and Knapp, 2002), which could lead to a decrease in the ploidy of arteries. The cause of cerebral atrophy is a reduction in white matter volume, which is known to stunt growth. Cerebral atrophy can directly affect the development of the cerebral nervous system in newborns or infants (Radmanesh et al., 2008). However, follow-up images of cblC defects after treatment were lacking, and we could not explain whether the severity of these signs would decrease after treatment. Longitudinal research is needed, and we will further study this question.

Currently, the most widely used intelligence test assessment method worldwide is the Wechsler Intelligence Scale (WISC); this scale can measure the general level of integrated intelligence (IQ) and different aspects of IQ, namely, language IQ and operational IQ, and this scale can be used to assess children (aged 6–16 years old) (Na and Burns, 2016). This testing method has been widely used to assess the brain development of children. Many studies have explored correlations between scale scores and related MRI indicators (Nestor et al., 2015; Xia et al., 2016). However, the children in this study were approximately 0–6 years old, and the WISC was not suitable for patients with cblC defects in our study. In our study, we used a scale suitable for use with 0- to 6-year-old patients [(CNBS-R2016) scale] to assess the neuropsychological development of pediatric patients when MRI examinations were performed. The DQ was calculated to evaluate the neuropsychological development status of the cblC defect patients. This scale not only used the DQ to evaluate the rate of development of the child's intelligence but also used intellectual age to indicate the child's development level, which provides a reliable early diagnostic basis for abnormal intelligence or developmental delay. This scale is currently widely used in China and is more suitable for evaluating the developmental characteristics of Chinese children. The scale was also applied to our recent assessment of brain development in cblC defects (Guo et al., 2020). Abnormal MRI findings provide a visual basis for understanding morphological changes associated with the impaired neuropsychological development of cblC defects. Our results suggested that damage to the central nervous system and delay of neuropsychological development in children with cblC defects can be reflected by MRI findings.

We used MRI images to analyze the abnormal brain structure of patients with cblC defects and attempted to identify specific features that were closely related to the

prognosis of patients, which has not been done in previous related research. Our research team is part of the national diagnosis and treatment center for genetic and metabolic diseases. After the onset of cblC defects, MRI examination and neuropsychological evaluation were performed in a timely manner (see **Table 1** for details). After receiving clinical and laboratory examinations, patients with cblC defects were treated in a timely manner according to their genotypes and received a periodic follow-up evaluation after 6 to 12 months of treatment. Neuropsychological scores can objectively reflect the changes in the conditions of patients with cblC defects before and after treatment, which makes it possible for us to identify specific MRI features that could predict the prognosis of patients with cblC defects.

In this study, 36 patients underwent neuropsychological testing after standardized treatment. It was found that the DQ obtained from the two tests did not show significant changes. We further conducted evaluations using DQ subscales and found that the scores for gross movement, fine movement, adaptability, language, and social behavior all increased after a 6–12 months standardized treatment. To ensure the accuracy of the multiple comparisons and to avoid type I errors, Bonferroni's correction was adopted. Although the increases in these scores did not reach the level of significance, the results were still encouraging. The kappa value indicated that the DQ classification of 31 patients was stable; the classification of 5 patients improved to a higher rank, and the classification of only one patient decreased to a lower rank. Such follow-up results suggest that standardized treatment in patients with cblC defects can maintain stable DQ levels with a tendency to improve. If patients continue to receive standardized treatment, the DQ may significantly improve. However, long-term follow-up tests and MRI examinations are needed to understand subsequent changes in DQs in cblC defects. From another perspective, it was also suggested that regardless of what abnormal MRI manifestations were observed, patients would improve after standardized treatment; this would stabilize the patient's condition, and the DQ could be improved to a certain extent. We are optimistic that with the extension of the treatment time, patients will show a significant improvement. Therefore, pediatricians and parents can have increased confidence in continuing treatment, which is necessary in our clinical practice.

The short follow-up period is a limitation of this study. However, clinicians and parents are eager to know whether the patients have improved, which is important for them to establish confidence in the next treatment. In future studies, we should continue to follow up with the patients included in this study and obtain neuropsychological scores and MRI data at multiple time points to better explore the prognosis of cblC defects and their influencing factors. No comparisons were made across the different genetic subgroups regarding the imaging manifestations. Furthermore, we will continue to expand the sample size to observe the different genetic subgroups of MMA and homocystinuria patients. Various functional imaging sequences, such as magnetic resonance spectroscopy, have been applied to the study of patients with combined MMA and homocystinuria (Cheng et al., 2019). We will also apply multimodal MRI in these studies to obtain additional morphological and functional data.

Conclusion

Ventricular dilation, cerebral atrophy and corpus callosal thinning are the main MRI abnormalities of cblC defects, and these manifestations are significantly correlated with delayed development in children. However, in routine MRI findings, no abnormal features were found to have the ability to predict the prognosis of cblC defects. After standardized treatment, the DQ and subscale scores increased in most of the patients, although these differences did not reach significance. MRI findings can be considered an important tool for evaluating the neuropsychological development of cblC defects.

Data availability statement

The original contributions presented in this study are included in the article/**Supplementary material**, further inquiries can be directed to the corresponding author.

Ethics statement

The studies involving human participants were reviewed and approved by the Ethical Committee of the Institutional Review Board (IRB) of Jinan Maternal and Child Care Hospital (201811). Written informed consent to participate in this study was provided by the participants' legal guardian/next of kin.

Author contributions

TC and CS wrote the main manuscript text. CS prepared the figure. SL did the statistical analysis. BG and YW prepared the clinical data and imaging data. LY revised the main manuscript text. All authors reviewed the manuscript.

Funding

This work was supported by grants from the Technology Development Plan of Jinan (202134072 and 202225035), Science and Technology Project of Jinan Municipal Health Commission (2021-2-89 and 2021-2-93), and Special Fund for Scientific

and Technological Innovation of Shandong Maternal and Child Health Care Commission (Lu Fu You Xie Fa 2021-19).

Acknowledgments

We thank all of the volunteers and patients for their participation in our study. This manuscript was edited and proofread by the American Journal Experts.

Conflict of interest

The authors declare that the research was conducted in the absence of any commercial or financial relationships that could be construed as a potential conflict of interest.

Publisher's note

Supplementary material

The Supplementary Material for this article can be found online at: https://www.frontiersin.org/articles/10.3389/fnins.2022.1093850/full#supplementary-material

References

Baumgarter, E. R., and Viardot, C. (1995). Long-term follow-up of 77 patients with isolated methylmalonic acidaemia. *J. Inherit. Metab. Dis.* 18, 138–142. doi: 10.1007/BF00711749

Biancheri, R., Cerone, R., Schiaffino, M. C., Caruso, U., Veneselli, E., Perrone, M. V., et al. (2001). Cobalamin (Cbl) C/D deficiency: Clinical, neurophysiological and neuroradiologic findings in 14 cases. *Neuropediatrics* 32, 14–22. doi: 10.1055/s-2001-12217

Brismar, J., and Ozand, P. T. (1994). CT and NR of the brain in disorders of the propionate and methylmalonate metabolism. *Am. J. Neuroradiol.* 15, 1459–1473.

Carrillo-Carrasco, N., Chandler, R. J., and Venditti, C. P. (2012). Combined methylmalonic acidemia and homocystinuria, cblC type. I. Clinical presentations, diagnosis and management. *J. Inherit. Metab. Dis.* 35, 91–102.

Chen, Z., Dong, H., Liu, Y., He, R., Song, J., Jin, Y., et al. (2022). Late-onset cblC deficiency around puberty: A retrospective study of the clinical characteristics, diagnosis, and treatment. *Orphanet J. Rare Dis.* 17:330. doi: 10.1186/s13023-022-02471-x

Cheng, A. L., Yao, R., Cao, W. J., and Yu, H. (2019). The value of 1H-MRS and MRI in combined methylmalonic aciduria and homocystinuria. *J. Comput. Assist. Tomogr.* 43, 559–562. doi: 10.1097/RCT.0000000000000854

Cui, Y. Z., Han, J. X., Zhou, X., Cui, Y., and Han, J. (2018). Methylmalonic acidemia: Current status and research priorities. *Intract. Rare Dis. Res.* 7, 73–78.

Desousa, C., Piesowicz, A. T., Brett, E. M., and Leonard, J. V. (1989). Focal changes in the globi-pallidi associated with neurological dysfunction in methylmalonic acidemia. *Neuropediatrics* 20, 199–201. doi: 10.1055/s-2008-1071292

Enns, G. M., Barkovich, A. J., Rosenblatt, D. S., Fredrick, D. R., Weisiger, K., Ohnstad, C., et al. (1999). Progressive neurological deterioration and MRI changes in cblC methylmalonic acidaemia treated with hydroxocobalamin. *J. Inherit. Metab. Dis.* 22, 599–607. doi: 10.1023/a:1005517727451

Fowler, B., Leonard, J. V., and Baumgartner, M. R. (2008). Causes of and diagnostic approach to methylmalonic acidurias. *J. Inherit. Metab. Dis.* 31, 350–360.

Fraser, J. L., and Venditti, C. P. (2016). Methylmalonic and propionic acidemias: Clinical management update. *Curr. Opin. Pediatr.* 28, 682–693.

Gebarski, S. S., Gabrielsen, T. O., Knake, J. E., and Latack, J. T. (1983). Cerebral CT findings in methylmalonic and propionic acidemias. *Am. J. Neuroradiol.* 4, 955–957.

Greitz, D., Greitz, T., and Hindmarsh, T. (2010). A new view on the CSF-circulation with the potential for pharmacological treatment of childhood hydrocephalus. *Acta Paediatr.* 86, 125–132. doi: 10.1111/j.1651-2227.1997.tb08850.x

Guo, B., Yang, L., Li, X., Liu, X., Wei, X., and Guo, L. (2020). The correlation between the evolution of bilateral basal ganglia hemorrhage using MR imaging and neurological damage recovery in an infant with methylmalonic aciduria. *Brain Dev.* 42, 357–362. doi: 10.1016/j.braindev.2019.12.011

Han, B., Cao, Z., Tian, L., Zou, H., Yang, L., Zhu, W., et al. (2016). Clinical presentation, gene analysis and outcomes in young patients with early-treated combined methylmalonic acidemia and homocysteinemia (cblC type) in Shandong province. China. *Brain Dev.* 38, 491–497. doi: 10.1016/j.braindev.2015.10.016

Han, L. S., Huang, Z., Han, F., Ye, J., Qiu, W. J., Zhang, H. W., et al. (2015). Clinical features and MUT gene mutation spectrum in Chinese patients with isolated methylmalonic acidemia: Identification of ten novel allelic variants. *World J. Pediatr.* 11, 358–365. doi: 10.1007/s12519-015-0043-1

Heidenreich, R., Natowicz, M., Hainline, B. E., Berman, P., Kelley, R. I., Hillman, R. E., et al. (1988). Acute extrapyramidal syndrome in methylmalonic acidemia - metabolic stroke involving the globus pallidus. *J. Pediatr.* 113, 1022–1027. doi: 10.1016/s0022-3476(88)80574-2

Herrmann, W., and Knapp, J. P. (2002). Hyperhomocysteinemia: A new risk factor for degenerative diseases. *Clin. Lab.* 48, 471–481.

Hörster, F., Garbade, S. F., Zwickler, T., Aydin, H. I., Bodamer, O. A., Burlina, A. B., et al. (2009). Prediction of outcome in isolated methylmalonic acidurias: Combined use of clinical and biochemical parameters. *J. Inheri. Metab. Dis.* 32:630. doi: 10.1007/s10545-009-1189-6

Korf, B., Wallman, J. K., and Levy, H. L. (1986). Bilateral lucency of the globus-pallidus complicating methylmalonic acidemia. *Ann. Neurol.* 20, 364–366. doi: 10.1002/ana.410200317

Lerner-Ellis, J. P., Tirone, J. C., Pawelek, P. D., Dore, C., Atkinson, J. L., Watkins, D., et al. (2006). Identification of the gene responsible for methylmalonic aciduria and homocystinuria, cblC type. *Nat. Genet.* 38, 93–100.

Li, Q. L., Song, W. Q., Wang, Q., Yang, X. Y., Li, J. W., Sun, Q., et al. (2015). Predictors of Survival in children with methymalonic acidemia with homocystinuria in Beijing. China: A prospective cohort study. *Indian Pediatr.* 52, 119–124. doi: 10.1007/s13312-015-0584-3

Martinelli, D., Deodato, F., and Dionisi-Vici, C. (2011). Cobalamin C defect: Natural history, pathophysiology, and treatment. *J. Inherit. Metab. Dis.* 34, 127–135.

Na, S. D., and Burns, T. G. (2016). Wechsler intelligence scale for children-V: Test review. *Appl. Neuropsychol. Child* 5, 156–160. doi: 10.1080/21622965.2015.1015337

Nestor, P. G., Nakamura, M., Niznikiewicz, M., Levitt, J. J., Newell, D. T., Shenton, M. E., et al. (2015). Attentional control and intelligence: MRI

orbital frontal gray matter and neuropsychological correlates. *Behav. Neurol.* 2015:354186. doi: 10.1155/2015/354186

Pastore, A., Martinelli, D., Piemonte, F., Tozzi, G., Boenzi, S., Di Giovamberardino, G., et al. (2014). Glutathione metabolism in cobalamin deficiency type C (cblC). *J. Inherit. Metab. Dis.* 37, 125–129.

Pui, M., and Ahmad, M. J. N. (2002). Magnetization transfer imaging diagnosis of intracranial tuberculomas. *Neuroradiology* 44, 210–215.

Radmanesh, A., Zaman, T., Ghanaati, H., Molaei, S., Robertson, R. L., and Zamani, A. A. (2008). Methylmalonic acidemia: Brain imaging findings in 52 children and a review of the literature. *Pediatr. Radiol.* 38, 1054–1061. doi: 10.1007/s00247-008-0940-8

Takeuchi, M., Harada, M., Matsuzaki, K., Hisaoka, S., Nishitani, H., and Mori, K. (2003). Magnetic resonance imaging and spectroscopy in a patient with treated methylmalonic acidemia. *J. Comput. Assist. Tomogr.* 27, 547–551. doi: 10.1097/00004728-200307000-00018

Thompson, G. N., Christodoulou, J., and Danks, D. M. (1989). Metabolic stroke in methylmalonic acidemia. *J. Pediatr.* 115, 499–500.

Wahlund, L. O., Barkhof, F., Fazekas, F., Bronge, L., Augustin, M., Sjogren, M., et al. (2001). A new rating scale for age-related white matter changes applicable to MRI and CT. *Stroke* 32, 1318–1322. doi: 10.1161/01.str.32.6.1318

Wang, F., Han, L. S., Yang, Y. L., Gu, X. F., Ye, J., Qiu, W. J., et al. (2010). Clinical, biochemical, and molecular analysis of combined methylmalonic acidemia and hyperhomocysteinemia (cblC type) in China. *J. Inherit. Metab. Dis.* 33, S435–S442. doi: 10.1007/s10545-010-9217-0

Weisfeld-Adams, J. D., Morrissey, M. A., Kirmse, B. M., Salveson, B. R., Wasserstein, M. P., Mcguire, P. J., et al. (2010). Newborn screening and early biochemical follow-up in combined methylmalonic aciduria and homocystinuria, cblC type, and utility of methionine as a secondary screening analyte. *Mol. Genet. Metab.* 99, 116–123. doi: 10.1016/j.ymgme.2009.09.008

Wu, J., Lu, A. D., Zhang, L. P., Zuo, Y. X., and Jia, Y. P. (2019). [Study of clinical outcome and prognosis in pediatric core binding factor-acute myeloid leukemia]. *Zhonghua Xue Ye Xue Za Zhi* 40, 52–57.

Xia, B., Wang, J. H., Xiao, Y. M., Liu, K. Y., Yang, X. D., and Ge, L. H. (2016). Children's intelligence quotient following general anesthesia for dental care: A clinical observation by Chinese Wechsler young children scale of intelligence. *J. Peking Univers.* 48, 336–340.

Yang, L., Guo, B., Li, X., Liu, X., Wei, X., and Guo, L. (2020). Brain MRI features of methylmalonic acidemia in children: The relationship between neuropsychological scores and MRI findings. *Sci. Rep.* 10:13099. doi: 10.1038/s41598-020-70113-y

Yesildag, A., Ayata, A., Baykal, B., Koroglu, M., Yildiz, H., Oral, B., et al. (2005). Magnetic resonance imaging and diffusion-weighted imaging in methylmalonic acidemia. *Acta Radiol.* 46, 101–103.

Yue, N. C., Arnold, A. M., Longstreth, W. T., Elster, A. D., Jungreis, C. A., Oleary, D. H., et al. (1997). Sulcal, ventricular, and white matter changes at MR imaging in the aging brain: Data from the cardiovascular health study. *Radiology* 202, 33–39. doi: 10.1148/radiology.202.1.8988189

Zhang, K. H., Gao, M., Wang, G. Y., Shi, Y. Y., Li, X. Y., Lv, Y. Q., et al. (2019). Hydrocephalus in cblC type methylmalonic acidemia. *Metab. Dis.* 34, 451–458.

frontiers | Frontiers in Neuroscience

TYPE Mini Review
PUBLISHED 26 January 2023
DOI 10.3389/fnins.2023.1110942

OPEN ACCESS

EDITED BY
Jing Li,
Capital Medical University, China

REVIEWED BY
Xiaofei Hu,
Army Medical University, China
Cheng Liu,
Shandong University, China

*CORRESPONDENCE
Linfeng Yang
ylf19860928@126.com

†These authors have contributed equally to this work and share first authorship

SPECIALTY SECTION
This article was submitted to Brain Imaging Methods, a section of the journal Frontiers in Neuroscience

RECEIVED 29 November 2022
ACCEPTED 12 January 2023
PUBLISHED 26 January 2023

CITATION
Chen T, Gao Y, Zhang S, Wang Y, Sui C and Yang L (2023) Methylmalonic acidemia: Neurodevelopment and neuroimaging. *Front. Neurosci.* 17:1110942. doi: 10.3389/fnins.2023.1110942

Methylmalonic acidemia: Neurodevelopment and neuroimaging

Tao Chen[1†], Yian Gao[2†], Shengdong Zhang[3], Yuanyuan Wang[4], Chaofan Sui[2] and Linfeng Yang[5*]

[1]Department of Clinical Laboratory, Jinan Maternity and Child Care Hospital Affiliated to Shandong First Medical University, Jinan, Shandong, China, [2]Department of Radiology, Shandong Provincial Hospital Affiliated to Shandong First Medical University, Jinan, Shandong, China, [3]Department of Radiology, Shandong Yinan People's Hospital, Linyi, Shandong, China, [4]Department of Radiology, Binzhou Medical University, Yantai, Shandong, China, [5]Department of Radiology, Jinan Maternity and Child Care Hospital Affiliated to Shandong First Medical University, Jinan, Shandong, China

Methylmalonic acidemia (MMA) is a genetic disease of abnormal organic acid metabolism, which is one of the important factors affecting the survival rate and quality of life of newborns or infants. Early detection and diagnosis are particularly important. The diagnosis of MMA mainly depends on clinical symptoms, newborn screening, biochemical detection, gene sequencing and neuroimaging diagnosis. The accumulation of methylmalonic acid and other metabolites in the body of patients causes brain tissue damage, which can manifest as various degrees of intellectual disability and severe neurological dysfunction. Neuroimaging examination has important clinical significance in the diagnosis and prognosis of MMA. This review mainly reviews the etiology, pathogenesis, and nervous system development, especially the neuroimaging features of MMA.

KEYWORDS

methylmalonic acidemia, diagnosis, nervous system injury, neurodevelopmental characteristics, neuroimaging

1. Introduction

Methylmalonic acidemia (MMA), also known as methylmalonic aciduria, is a congenital organic acidemia with multifactorial autosomal recessive inheritance. The disease often causes multisystem injury, especially to the central nervous system (Han et al., 2015). Although the incidence of this disease is low, the mortality rate is very high (Thompson et al., 1989). Estimates of incidence in Western populations range from 1:48,000 to 1:61,000 births for MMA (Manoli et al., 1993). In mainland of China, the morbidity of MMA is about 1:4,000 to 1:26,000 (Zhou et al., 2018). Patients with MMA experience significant mortality, and the prognosis for long term survival is poor. The mortality of mut MMA was 60-88% in the first reports in the 1980s and 1990s and has improved somewhat to ∼40% by the first decade in the 2000s (Zhou et al., 2018). In a study of 88 cblC defects, the mortality rate was 11.4%, and early standard treatment was found to improve biochemical abnormalities, non-neurological signs, and mortality (Fischer et al., 2014). Onset of the manifestations of MMA ranges from the neonatal period to adulthood. If the disease cannot be diagnosed and treated promptly, the financial and psychological burdens on patients, families, and society will be heavy. This study mainly reviews the etiology and pathogenesis of MMA, especially its diagnosis by central neuroimaging, and provides the basis for early diagnosis, early intervention, and improvement of the prognosis.

2. Etiology and pathogenesis of MMA

Methylmalonic acidemia (MMA) is the most common type of congenital organic acidemia (Lee and Kim, 2022). It is mainly caused by the deficiency of methylmalonyl-coenzyme A mutase (MCM) or abnormal metabolism of adenosylcobalamin. Under normal circumstances, methylmalonyl-CoA generates succinyl-CoA under the action of MCM and adenosylcobalamin and participates in the tricarboxylic acid cycle. As a result, the conversion of methylmalonyl-coenzyme A to succinyl-CoA is blocked, causing an increase in methylmalonic acid and its associated organic acids, which leads to the abnormal accumulation of intermediate metabolites such as methylmalonic acids, methylmalonyl-CoA, methylmalonyl carnitine, propanoic acid, methylcitric acid, and β- hydroxybutyric acid. The abnormal accumulation of intermediate metabolites causes mitochondrial dysfunction, resulting in multisystem injuries, mainly of the central nervous system (Longo et al., 2005; Obeid and Herrmann, 2006). Brain injuries are the most obvious central nervous system injuries. They mainly manifest as impairments in brain development, brain structure, brain networks, and brain function.

The etiology of MMA is essentially clear. According to the type of enzyme deficiency, MMA can be divided into two categories, MCM deficiency and coenzyme cobalamin metabolism disorder, i.e., mutant type and cobalamin type (Zhou et al., 2018). The mutant type is caused by MCM gene mutations that change the activity of allosteric enzymes. According to the degree of MCM activity reduction, there are two types: mut- and mut0. MCM activity was partially absent in patients with mut- type and completely absent in patients with mut0 type. The degree of MCM activity loss is not only related to the type of MUT gene mutation, but also related to the transcription, translation, protein expression and modification of MUT gene mutation between individuals. The cobalamin type is due to congenital defects in the synthesis, activation or transport of cobalamin (coenzyme of allosteric enzymes), which hinder the synthesis of an effective coenzyme, deoxyadenosylcobalamin, thereby impairing the function of MCM, eventually causing MMA. The cobalamin type can be subdivided into six subtypes (cblA, cblB, cblC, cblD, cblF, and cblH). The mut, cblA, cblB, and cblH types show only MMA and are therefore called isolated MMA; cblC, cblD, and cblF deficiencies are usually associated with homocystinuria, and the resulting condition is called combined methylmalonic aciduria and homocystinuria (MMA-HC). MMA-HC is the main biochemical type of MMA in China, and 60-80% of MMA patients found in China are complicated with homocystinuria (Zhang et al., 2007). Among MMA-HC cases, the cblC type is the most common one (Carrillo-Carrasco et al., 2012).

According to the onset age of MMA patients, MMA can be divided into early-onset MMA (≤ 1 year) and late-onset MMA (>1 year), and early-onset MMA is more common. Different types of MMA patients have symptoms onset at different ages. Most pediatric patients with early-onset MMA develop disease within 1 year and have rapid disease progression, extremely high mortality and morbidity, and poor prognosis; 80% of children with early-onset MMA (those with complete deficiency in allosteric enzyme activity) develop the disease within 1 week of birth, and 90% show clinical symptoms within 1 month of birth; most patients with adenosylcobalamin deficiency or partial deficiency in allosteric enzyme activity show clinical symptoms after 1 month of birth (Matsui et al., 1983). Late-onset MMA patients mostly develop disease between 1 and 3 years of age, with limited symptoms and good prognosis.

3. Diagnosis of MMA

3.1. Clinical presentation

The clinical manifestations of MMA are diverse and lack specificity, which is related to the type of the disease and the degree of enzyme deficiency. The main clinical manifestations of MMA include feeding difficulty, intellectual disability, psychomotor retardation, ataxia, abnormal muscle tone, seizures, epilepsy, and lethargy (Brismar and Ozand, 1994; Jin et al., 2004). MMA clinical presentations reveal no specific obvious signs and symptoms but rather demonstrate that these conditions affect multiple systems, with the disease often appearing as a fairly multifaceted syndrome, and are age-related (**Table 1**). In the neonatal period, patients can develop encephalopathy with symptoms such as lethargy, apnea, feeding difficulty, hypotonia, seizures and nystagmus, as well as non-neurological symptoms such as hematological abnormalities, hydrocephalus, and pulmonary hypertension. In infancy, symptoms include vomiting, weight loss, hypoglycemia, visual inattention, neurological deterioration with hypotonia, irritability, and lethargy eventually leading to coma in cases with an acute early-onset neonatal presentation (Forny et al., 2021). Late-onset patients exhibit a wider range of presentations, which can include failure to thrive, various neurological symptoms (encephalopathy, developmental delay, cognitive impairment, epilepsy, ataxia, and pyramidal and peripheral nerve symptoms), and cardiac and kidney manifestations (Grangé et al., 2015; Forny et al., 2021). For patients with MMA, neurological symptoms may be the first symptoms, creating a challenge for physicians in terms of identifying clinical manifestations suggestive of MMA.

3.2. Newborn screening and biochemical detection

Expanded newborn screening for inborn errors of metabolism (IEMs) by tandem mass spectrometry (MS/MS) has enabled simultaneous analyses of more than 40 metabolites and the identification of approximately 50 IEMs during the neonatal period using dry blood spots (Therrell et al., 2015). The levels of propionylcarnitine (C3), C3/acetylcarnitine (C2), and methionine in dry blood spots were measured by MS/MS. When MS/MS screening results exceed the cutoff value and exclude suspected organic acidemia, MMA can be diagnosed by measuring organic acids via gas chromatography (GC)/MS in urine. Increases in methylmalonic acid together with 3-hydroxypropionate and the presence of 2-methylcitrate confirm the diagnosis of MMA (Forny et al., 2021). In China, detection of C3 by MS/MS and detection of organic acids in urine and blood by GC/MS are the preferred methods for the diagnosis of MMA. Newborn screening has been shown to increase the likelihood of early diagnosis of MMA, especially in late-onset cases (Heringer et al., 2016). A follow-up study confirmed significant differences in the incidence rates of intellectual impairment, movement disorders, ocular complication, hydrocephalus, and death when comparing patients with clinical

TABLE 1 Clinical presentation of MMA patients of different ages.

Ages	System	Clinical presentation
Neonates (0–28 days)	Nervous system	Lethargy, apnoea Muscular hypotonia Seizures, neurocognitive impairment Visual inattention or nystagmus Hydrocephalus
	Digestive system	Poor feeding, vomiting
	Blood circulation system	Anemia/thrombocytopenia or pancytopenia Megaloblastosis Cardiomyopathy Pulmonary hypertension
	Urinary system	Hemolytic uremic syndrome
Infants (1–12 months)	Nervous system	Developmental delay (learning disabilities, intellectual disability) Acute encephalopathy Visual and cognitive impairment Microcephaly Muscular hypotonia Seizures Visual inattention or nystagmus
	Digestive system	Anorexia Failure to thrive
	Blood circulation system	Anemia/thrombocytopenia or pancytopenia Megaloblastosis Pulmonary hypertension
	Urinary system	Hemolytic uremic syndrome
Children (1–12 years)	Nervous system	Acute or chronic behavioral or psychiatric abnormalities Acute encephalopathy Movement disorders, dystonia, ataxia, limb weakness Seizures, lethargy Neuropsychiatric disturbance, personality changes Visual impairment (maculopathy, optic atrophy, Peripheral retinopathy) Sensory disturbance
	Blood circulation System	Pulmonary hypertension Venous thrombosis, pulmonary thromboembolism Hypertensive encephalopathy
	Urinary system	Hemolytic uremic syndrome Kidney failure
Adolescence and adulthood (>12years)	Nervous system	Cognitive decline Neuropsychiatric disturbance, personality changes, social withdrawal, depression Decreased ability to study or work Sensory disturbance, ataxia, limb weakness Visual impairment or blindness
	Blood circulation system	Pulmonary hypertension Venous thrombosis, pulmonary thromboembolism Hypertensive encephalopathy
	Urinary system	Hemolytic uremic syndrome Thrombotic microangiopathy Kidney failure

signs before treatment to asymptomatic patients (Ling et al., 2022). When children or adults have atypical manifestations of nervous system damage, MS/MS screening and urinary organic acid examination should be performed promptly to diagnose MMA (Heringer et al., 2016).

Biochemical examination may indicate hyperammonemia, hyperlactemia, metabolic acidosis, hypoglycemia, anemia, urine protein or occult blood positive (Baumgartner et al., 2014). In addition, plasma total homocysteine (tHcy) (rather than free homocysteine) and vitamin B12 were tested to determine whether each case was isolated or combined MMA. We strongly recommend secondary testing using tHcy and MMA to improve specificity and distinguish MMA from other diseases (Huemer et al., 2017).

3.3. Molecular genetic analysis

MMA is inherited in an autosomal recessive fashion. To confirm the biochemical diagnosis, guide management, and provide genetic counseling to families, the underlying genetic defect must be identified (Forny et al., 2021). MMA is highly genetically heterogeneous, and at least 10 disease-related genes have been identified; among them, mutations in MUT (mut type), MMAA (cblA type), MMAB (cblB type), MMACHC (cblC type), MMADHC (cblD type), LMBRD1 (cblF type), ABCD4 (cblJ type), and HCFC1 (cblX type) are the most common (Hwang et al., 2021).

Patients of different races or from different regions have varying hotspot mutations. Among combined methylmalonic acidemia cases in China, MMACHC gene mutation is the most common, accounting for approximately 99% of cases, and the most common mutant subtype is c.609G>A (p.W203X), followed by c.80A>G (p.Q27R) and c.658-660delAAG (p.K220del) (Liu et al., 2010; Yu et al., 2021). c.609G>A (p.W203X) and c.567dupT (p.I190fs) are independently associated with poor outcomes, especially for neurodevelopmental deterioration (Ling et al., 2022). In Canada, the most common mutation site in the MMACHC gene is c.271dupA (p.R91KfsX14), where a frameshift mutation accounts for at least 40% of the pathogenic alleles (Morel et al., 2006). However, in isolated MMA, mutation of the MUT gene is the most common, and the most common mutation in China is c.729_730insTT (p.D244LfsX39), accounting for 16.5% of cases (Han et al., 2015). The most common mutations in Brazil and Spain are c.655A>T (p.N219Y) and 322C>T (p.R108C), respectively (Worgan et al., 2006; Randon et al., 2020).

3.4. Neuroimaging examination

Neuroimaging in patients with MMA is not routinely performed and often takes place in an emergency situation, especially for those diagnosed by newborn screening who are doing well clinically (Harting et al., 2008). In addition, neuroimaging does not significantly affect clinical decision making in MMA. However, imaging can objectively reflect brain injury conditions, guide diagnosis and treatment, improve the understanding of the disease, and provide an objective basis for early diagnosis and intervention.

Because ultrasound has the characteristics of non-ionizing radiation and low costs, it can also evaluate brain development, degree of brain injury, and neurodevelopmental prognosis. Ultrasound has become a commonly used screening tool for brain

examinations of newborns and infants. However, because of the restrictions of imaging technology, the scope of these examinations is limited. Only the brain tissue below the fontanelle can be clearly displayed using ultrasound, and it is significantly less effective than magnetic resonance imaging (MRI) at evaluating the development and extent of the damage to the surrounding brain tissue (Yang et al., 2017). Moreover, ultrasound examination cannot be performed after the fontanelle is completely closed.

The resolution of computed tomography (CT) is relatively high, allowing it to clearly reveal the structure of the brain. However, the brain water content of newborns is relatively high, and the contrast between gray and white matter is not obvious, a situation that is difficult to distinguish from the low density caused by cerebral edema. CT also uses ionizing radiation, which greatly limits the application of CT in the assessment of brain development and brain injury.

Single-photon-emission computed tomography and positron-emission tomography have relatively high sensitivity and can be used to assess brain function and metabolism. However, these two types of examination require the application of radiopharmaceuticals, which can harm newborns and infants, thus limiting their application.

Because of its characteristics of non-ionizing radiation, high tissue contrast, and high spatial resolution, MRI has become the preferred imaging method for newborn or infant brains. The routine brain MRI examination sequences of MMA patients includes T1-weighted imaging (T1WI), T2WI, T2-weighted fluid-attenuated inversion recovery, and diffusion-weighted imaging (DWI). T1WI is mainly used to observe the myelin sheath formation in nerve fibers, giving a high signal. T2WI is mainly used to observe myelin sheath maturation in nerve fibers, giving a low signal. T1WI is mainly done before 6 months of age, and T2WI is mainly done after 6 month of age. Therefore, MRI can be used to observe the formation of a normal myelination process, delayed myelination, or myelination hypoplasia and to evaluate brain development. In particular, MRI functional brain imaging and other technologies can comprehensively evaluate the brain development and brain injury degree of MMA patients, and make qualitative diagnosis, provide objective basis for clinical diagnosis, help to judge prognosis and improve the quality of life of patients.

4. Mechanism of nervous system injury and neurodevelopmental characteristics

4.1. Mechanism of nervous system injury

Nervous system injury is the main injury caused by MMA (Cudré-Cung et al., 2016). The pathophysiological mechanism of nervous system injury involves inhibition of succinate dehydrogenase by high concentrations of methylmalonic acid, which is necessary for aerobic oxidation of mitochondrial glucose. High concentration of organic acid metabolites such as methylmalonic acid, propionic acid and 2-methylcitric acid lead to mitochondrial dysfunction and further lead to neuronal cell apoptosis (Jafari et al., 2013). The globus pallidus is the most sensitive to mitochondrial dysfunction and is often the first site of injury. In MMA-HC, methionine synthase is obstructed, resulting in blocked methylation, homocysteine accumulation, and S-adenosinemethionine reduction, the deficiency of which is associated with dysmyelination (Rossi et al., 2001). The role of myelin sheath is to protect neurons and transmit the nerve impulse to the neuron, therefore, the dysmyelination can affect the conduction of nerve impulse, triggering a series of nerve damage. Furthermore, children with congenital succinate dehydrogenase dysfunction often present with globular lesions, and an increased lactate content compensates for mitochondrial energy metabolism disorders (Okun et al., 2002). In addition, brain development, including ganglioside-mediated regulation of synaptic plasticity, is also impaired, and cognitive and behavioral changes will occur (Kölker et al., 2003). Current studies mainly focus on the enhancement of oxidative stress and mitochondrial dysfunction caused by MMA, and most of these theories are involved in the nervous system injury of MMA through neuronal apoptosis. This has also been confirmed in animal studies, high concentrations of methylmalonic acid could significantly alter the morphology of rat cortical neurons, attenuate cell viability and aggravate cell apoptosis. Enrichment analysis of the apoptosis-related genes revealed that the MAPK and p53 signaling pathways may be involved in the pathogenesis of MMA (Han et al., 2015). Unfortunately, even if the majority of MMA patients are treated promptly, there will be some degree of neurological damage, residual mental retardation, motor and language delays and other complications (Shea et al., 2012).

4.2. Neurodevelopmental characteristics

4.2.1. Cognitive impairments

Many MMA patients suffer from cognitive impairments (Molema et al., 2021). Cognitive impairment occurs through neuroinflammatory and stress-induced damage pathways during the process of neuroinflammation and oxidative stress injury caused by MMA (Gabbi et al., 2017; Li et al., 2021). O'Shea et al. adopted the age-appropriate Wechsler Intelligence Scale to evaluate the neuropsychological results of 43 patients with simple MMA (including the mut type, cblA type, and cblB type) and reported significant differences in neurocognitive outcomes among patients (Shea et al., 2012). Intelligence is affected by the MMA subtype and onset age, and patients with early-onset MMA exhibit the most severe neurocognitive impairment, with even greater impairment in patients with a history of hyperammonemia and seizures at diagnosis. Children with this disorder are at risk for developmental delays, cognitive difficulties, and progressive declines in function. With the exception of patients with the enzyme-deficient cblA subtype, the mean IQ of the patient population including all types is rarely above 85, while the mean IQ of the patient population with the mut0 enzyme subtype is considerably lower (Waisbren, 2022). A clinical cohort study reported that 12 children with cblC defects diagnosed by newborn screening were found to have developmental delays, most of whom presented with hypotonia and nystagmus, while neurodevelopmental assessments suggested that impaired motor development was the most prominent deficiency (Weisfeld-Adams et al., 2013). Late-onset patients may have atypical symptoms such as mental symptoms and cognitive decline (Hwang et al., 2021).

4.2.2. Intellectual and motor developmental disorders

The clinical symptoms of early onset MMA are mainly neuropsychiatric injury, common developmental lag, abnormal mental behavior, hydrocephalus, epilepsy and so on. Neurological

impairment most commonly manifests as movement disorders, such as involuntary tremor, gait instability, dystonia, hypotonia, muscular rigidity and chorea (Mink, 2003). For the developmental follow-up of MMA patients, the developmental quotient (DQ) can be evaluated from five aspects: adaptive behavior, gross motor, fine motor, language, and personal social behavior. Intelligence quotient (IQ) can also be used to evaluate intelligence. It has also been demonstrated that serum methylmalonic acid, cytokines, reactive oxygen species (ROS) and reactive nitrogen species (RNS) cross the blood-brain barrier, cause cognitive impairment, and are positively correlated with DQ and IQ scores (Li et al., 2021). MMA can lead to nervous system injury, resulting in varying degrees of intellectual and motor retardation, seriously affecting the quality of life of children. A follow-up study in China used a pediatric neuropsychological development examination scale for 0- to 6-year-old patients [China neuropsychological and Behavior Scale-Revision 2016 (CNBS-R2016) scale, Capital Medical University] (Fischer et al., 2014). This scale mainly tests the physical abilities and intelligence of infants and children in five aspects: gross movements, fine movements, adaptability, language, and social behavior. After standardized treatment, the DQ and subscale scores increased in most of the patients, although these differences did not reach significance.

4.2.3. Visual damage

Long-term neurological damage may be present in the visual system. In particular, optic atrophy is an increasingly recognized late presentation of MMA, resulting in acute or chronic vision loss (Alvarez et al., 2016). In patients with MMA, it can also show macular disease, peripheral retinopathy, nystagmus, strabismus, optic atrophy, etc. (Gizicki et al., 2014).

4.2.4. Seizures

Seizures are also a recognized symptom of MMA and may occur at the time of onset or later (Kölker et al., 2015). Seizures may present tonic-clonic seizures, tonic seizures, clonic seizures and partial motor seizures. The electroencephalo-graph and seizure patterns are non-specific. Severely affected patients may be difficult to treat and may have recurrent status epilepticus.

5. Imaging findings of the central nervous system in MMA patients

Some new functional MRI technologies have gradually emerged, including susceptibility-weighted imaging, high-resolution 3D-T1WI, magnetic resonance spectroscopy (MRS), Positron Emission Tomography/Magnetic Resonance (PET/MR) and diffusion tensor imaging (DTI), diffusion kurtosis imaging, neurite orientation dispersion and density imaging, and resting-state functional connectivity MRI. Some studies have shown that the lesion area is characterized by decreased acetylaspartate (NAA) level and increased lactate (Lac) level in MRS, while the creatine (Cr) and choline (Cho) levels in other brain areas are normal, after treatment, the levels of Lac and Cr decreased, the level of NAA decreased, and the clinical symptoms gradually improved, so it can be used for non-invasive detection of treatment effect (Takeuchi et al., 2003). Lac was not detected in normal brain parenchyma and cerebrospinal fluid, and elevated Lac levels were detected in some cerebrospinal fluids. PET/MR brain scanning showed that the uptake of 18F-FDG in bilateral caudate nucleus and putamen increased, the uptake of 18F-FDG in frontal lobe decreased, and the extracerebral space widened in the early stage. The decreased uptake of 18F-FDG in frontal lobe reflected the atrophy and volume reduction of frontal lobe. The uptake of 18F-FDG in the caudate nucleus and putamen decreased in the late stage (al-Essa et al., 1999). Studies have shown that DTI has the potential to quantify nerve fibers and is more sensitive than conventional MRI in evaluating brain development and brain injury. However, these new technologies have not been widely used in routine MRI examinations for patients, only part of functional imaging has been gradually applied to the research of MMA. MRS has a relatively large number of cases in the study of MMA, but the number of cases in different literatures (Takeuchi et al., 2003; Michel et al., 2004) is small, and large-sample literature support is needed. Some studies have found that functional changes confirmed by PET/MR are greater than morphological abnormalities shown by MRI, and have better correlation with the clinical course of the disease; There is great potential in the assessment of neurodegenerative diseases in children; However, caution should be exercised when extrapolating data from individual case reports and further detailed studies are therefore required. There is also evidence that DTI is a more sensitive technique for evaluating nerve fibers (Gao et al., 2009). DTI has great potential for brain evaluation in children with MMA, but one of the challenges is to determine the size and shape of the scan field. However, at present, the number of cases involved in various functional imaging is relatively small, and its representativeness needs further research. With the continuous improvement of the above techniques, we believe that these new technologies can be gradually applied in the imaging diagnosis of MMA in the near future.

Patients with early-onset MMA are characterized by brain retardation or dysplasia and brain tissue damage. The main manifestations include decreased white matter volume, widened extracerebral space, cortical atrophy, delayed myelination or myelination hypoplasia, thin corpus callosum, widened ventricular system, and symmetrical abnormal signals of the basal ganglia (especially the globus pallidus) (Michel et al., 2004; Radmanesh et al., 2008). Myelination retardation or dysplasia showed white matter isointensity and hypointensity on T1WI and white matter hyperintensity on T2WI and T2 FLAIR, which distributed around the lateral ventricle, partially confined to the lateral ventricle triangle or the posterior part of the semioval center, and distributed symmetrically on both sides. The corpus callosum was thin and hyperintense on T2WI. In acute phase, globus pallidus showed symmetrical hypointensity on T1WI, hyperintensity on T2WI and T2FLAIR, hyperintensity on DWI and hypointensity on ADC. The result showed that that globus pallidus increase in early stage, decreased in late stage, and finally showed hypointensity on T1WI, hyperintensity on T2WI and hypointensity on T2FLAIR (Trinh et al., 2001; Burlina et al., 2003). The imaging findings in patients with late-onset MMA also include anomalies such as spinal cord atrophy (Martinelli et al., 2011). The pathological changes associated with late-onset MMA are mainly characterized by multifocal demyelination in the brain and spinal cord. The lesions were isointense or hypointense on T1WI and hyperintense on T2WI and T2 FLAIR (Bodamer et al., 2001; Smith et al., 2006; Tsai et al., 2007; Thauvin-Robinet et al., 2008) (**Table 2**).

The most common imaging manifestation in the brain of MMA patients is brain atrophy (Chen, 2008; Radmanesh et al., 2008),

TABLE 2 Imaging manifestations of MMA.

Early-onset MMA	From a whole point of view	The volume of white matter decreased, the sulci of cerebrum and cerebellum deepened, and the cortex atrophied		
	From a local point of view	Myelination retardation or dysplasia	The white matter was isointense or hypointense on T 1WI and hyperintense on T 2WI and T 2 FLAIR. The white matter was distributed around the lateral ventricle, partly confined to the lateral ventricle triangle or the posterior part of the semioval center, and distributed symmetrically on both sides	
		Corpus callosum	In addition to thinning, hyperintensity was also observed on T 2WI	
		Globus pallidus	Acute phase	Symmetrical hypointensity on T1WI, hyperintensity on T2WI and T2FLAIR, hyperintensity on DWI and ADC were observed
			Dynamic follow-up	The volume of globus pallidus increased in the early stage and decreased in the late stage, and finally showed cerebrospinal fluid signal intensity, which was hypointensity on T1WI, hyperintensity on T2WI and hypointensity on T2FLAIR
Late-onset MMA	In addition to that above manifestation, late onset MMA also includes spinal cord atrophy and other abnormal change. Its pathological changes are mainly characterized by multifocal demyelination in the brain and spinal cord, which is isointense or hypointense on T1WI and hyperintense on T2WI and T2 FLAIR			

manifested as varying degrees of deepening cerebral and cerebellar sulci, cortical atrophy, and enlargement of the extracerebral space. The cause of brain atrophy is the decrease in the cerebral white matter volume, that is, the developmental delay of the white matter or white matter hypoplasia. Brain atrophy can directly affect the development of the brain and nervous system in newborns or infants.

Diffuse supratentorial white matter swelling in MMA-HC patients is common, and white matter swelling can cause white matter damage that involves U-shaped fibers (Weisfeld-Adams et al., 2013). The abnormal MRI signals in white matter may be related to edema, developmental delay, and hypoplasia of myelin. Some scholars believe that the pathophysiological changes of white matter are mainly vascular injury, which may be related to poor methylation and accumulation of non-physiological fatty acids (Rossi et al., 2001).

The brain myelination hypoplasia of MMA patients is usually located in the anterior and posterior horns of bilateral lateral ventricles and the periventricular white matter and semioval center, showing a symmetric distribution, which are different from demyelinating lesions. Brain myelination hypoplasia is associated with deficiency of S-adenosylmethionine in the brain caused by metabolic abnormalities (Weisfeld-Adams et al., 2013). If the dysplastic myelin sheath cannot be diagnosed and effectively treated at an early stage, it will result in low white matter volume, leading to a poor prognosis. A thin corpus callosum is common in children with low white matter volume and is a response to the decrease in white matter volume. It may be congenital or acquired. The abnormal MR signals of the bilateral lateral paraventricular nucleus and semioval center white matter and the thin corpus callosum may all be associated with delayed myelination or myelination hypoplasia (Yeşilda et al., 2005).

Hydrocephalus is also common in MMA patients. Some scholars have suggested that its formation mechanism may be related to increased cerebrovascular stiffness, which results in decreased arterial compliance, increased arterial pressure, no decay of arterial pressure, and increased intracranial pressure, eventually causing hydrocephalus (Greitz et al., 2010). High concentrations of cysteine metabolites have toxic effects on the vascular wall, which is the main cause of vascular endothelial damage (Herrmann and Knapp, 2002).

The basal ganglia (especially the globus pallidus) are the most frequently involved sites in MMA patients. The mechanism of basal ganglia involvement may be related to the reduced activity of cytochrome C oxidase and succinate dehydrogenase, resulting in the accumulation of toxic organic acid metabolites, leading to damage to the basal ganglia, especially the globus pallidus, which has a relatively high energy demand (Michel et al., 2004; Baker et al., 2015; Fraser and Venditti, 2016). During the acute exacerbation of MMA patients, the globus pallidus shows low density on plain CT images; MRI manifests as a low T1WI signal, high T2WI signal, high DWI signal, and apparent diffusion coefficient graphs with a low signal with symmetrical distribution; MRS shows an increase in the lactate peak and a decrease in the N-acetylaspartic acid (NAA) peak. During metabolic decompensation, there is an abnormally high signal on DWI, suggesting infarction, which Trinh et al., 2001 believed is related to cell membrane rupture caused by mitochondrial dysfunction with accumulation of lactic acid. After a reasonable drug treatment, the abnormally high signal on DWI can gradually disappear and return to normal, the blocked diffusion subsides, and the lactate peak decreases. Therefore, many scholars believe that an abnormally high DWI signal reflects some cytotoxic edema. The persistently abnormally high signal intensity of DWI suggests nervous system injury and poor prognosis. Although the abnormal signal in the basal ganglia (especially globus pallidus) is a relatively specific manifestation in MMA patients, the incidence of this sign is not very high (Krishna et al., 2008).

DWI has been used to investigate the apparent diffusion coefficient (ADC) in MMA, which has been reported to be associated with restricted water diffusion in the globus pallidus that may resolve after clinical intervention, including carnitine supplementation.

Findings from 12 MMA patients demonstrated significant reductions in fractional anisotropy (FA) in the globus pallidus and frontal, temporal, and occipital white matter on diffusion tensor imaging (DTI), which were not observed on conventional T1/T2 images (Gao et al., 2009), suggesting that in addition to restricted water diffusion in the globus pallidus, MMA is associated with more widespread disturbances in white matter integrity. The referenced study serves as an example of how DTI has been demonstrated to be superior to routine imaging in identifying these diffuse lesions. Neurocognitive lesions in MMA have yet to be investigated with fMRI (Gropman and Anderson, 2020).

In summary, with the rapid development and innovation of gene technology, MMA patients have received increasing attention in clinical practice. Early detection and early diagnosis using imaging examinations are particularly important. In particular, brain functional imaging by MRI and other technologies can comprehensively assess the brain development and the degree of brain damage in MMA patients and lead to a qualitative diagnosis. Because MRI evaluation and qualitative diagnosis can provide an objective basis for the clinical diagnosis, it can help determine the prognosis and improve the quality of life of patients.

6. Conclusion

This paper reviews the etiology, pathogenesis, diagnosis, neurodevelopmental features, and recent advances in neuroimaging studies of MMA. MMA is a serious disease with a complex clinical phenotype and genotype and is difficult to identify from signs and symptoms, thus necessitating biochemical tests. Newborn screening is of marked significance and is the key to early detection and treatment. Accurate diagnosis is the basis of accurate treatment. Given the various forms of the disease, misdiagnosis and missed diagnosis are not uncommon. For children with low intelligence, abnormal behavior, general convulsions, hypertonia or hypotonia, symmetrical limb paralysis, or polyneuropathy as the main symptom in combination with imaging characteristics, the possibility of MMA should be considered regardless of whether a positive family history has been identified. Early diagnosis and treatment of MMA are essential for improving the prognosis and quality of life of patients.

Author contributions

TC and YG drafted the manuscript for publication. SZ prepared the tables. YW participated in writing chapter etiology and pathogenesis and diagnosis of MMA. CS participated in writing chapter neuropsychology and neuroimaging of MMA. LY reviewed and revised the manuscript. All authors contributed to the article and approved the submitted version.

Funding

This work was supported by grants from the Technology Development Plan of Jinan (202134072 and 202225035), Science and Technology Project of Jinan Municipal Health Commission (2021-2-89 and 2021-2-93), and Special Fund for Scientific and Technological Innovation of Shandong Maternal and Child Health Care Commission (Lu Fu You Xie Fa 2021-19).

Conflict of interest

The authors declare that the research was conducted in the absence of any commercial or financial relationships that could be construed as a potential conflict of interest.

Publisher's note

References

al-Essa, M. A., al-Shamsan, L. A., and Ozand, P. T. (1999). Clinical and brain 18fluoro-2-deoxyglucose positron emission tomographic findings in ethylmalonic aciduria, a progressive neurometabolic disease. *Eur. J. Paediatr. Neurol.* 3, 125–127. doi: 10.1016/s1090-3798(99)90100-9

Alvarez, L. M., Jameson, E., Parry, N. R., Lloyd, C., and Ashworth, J. L. (2016). Optic neuropathy in methylmalonic acidemia and propionic acidemia. *Br. J. Ophthalmol.* 100, 98–104.

Baker, E. H., Sloan, J. L., Hauser, N. S., Gropman, A. L., Adams, D. R., Toro, C., et al. (2015). MRI characteristics of globus pallidus infarcts in isolated methylmalonic acidemia. *AJNR Am. J. Neuroradiol.* 36, 194–201. doi: 10.3174/ajnr.A4087

Baumgartner, M. R., Hörster, F., Dionisi-Vici, C., Haliloglu, G., Karall, D., Chapman, K. A., et al. (2014). Proposed guidelines for the diagnosis and management of methylmalonic and propionic acidemia. *Orphanet J. Rare Dis.* 9:130. doi: 10.1186/s13023-014-0130-8

Bodamer, O. A., Rosenblatt, D., Appel, S., and Beaudet, A. (2001). Adult-onset combined methylmalonic aciduria and homocystinuria (cblC). *Neurology* 56:1113.

Brismar, J., and Ozand, P. T. (1994). CT and MR of the brain in disorders of the propionate and methylmalonate metabolism. *AJNR Am. J. Neuroradiol.* 15, 1459–1473.

Burlina, A. P., Manara, R., Calderone, M., Catuogno, S., and Burlina, A. B. (2003). Diffusion-weighted imaging in the assessment of neurological damage in patients with methylmalonic aciduria. *J. Inherit. Metab. Dis.* 26, 417–422. doi: 10.1023/a:1025106909213

Carrillo-Carrasco, N., Chandler, R. J., and Venditti, C. P. (2012). Combined methylmalonic acidemia and homocystinuria, cblC type. I. Clinical presentations, diagnosis and management. *J. Inherit. Metab. Dis.* 35, 91–102.

Chen, J. (2008). MR imaging of the brain in methylmalonic aciduria and propionic aciduria. *Radiol. Pract.* 23, 595–597. doi: 10.3969/j.issn.1000-0313.2008.06.005

Cudré-Cung, H., Zavadakova, P., Vale-Pereira, S d, Remacle, N., Henry, H., Ivanisevic, J., et al. (2016). Ammonium accumulation is a primary effect of 2-methylcitrate exposure in an in vitro model for brain damage in methylmalonic aciduria. *Mol. Genet. Metab.* 119, 57–67. doi: 10.1016/j.ymgme.2016.07.013

Fischer, S., Huemer, M., Baumgartner, M., Deodato, F., Ballhausen, D., Boneh, A., et al. (2014). Clinical presentation and outcome in a series of 88 patients with the cblC defect. *J. Inherit Metab. Dis.* 37, 831–840. doi: 10.1007/s10545-014-9687-6

Forny, P., Hörster, F., Ballhausen, D., Chakrapani, A., Chapman, K., Dionisi-Vici, C., et al. (2021). Guidelines for the diagnosis and management of methylmalonic acidaemia

and propionic acidaemia: First revision. *J. Inherit. Metab. Dis.* 44, 566–592. doi: 10.1002/jimd.12370

Fraser, J. L., and Venditti, C. P. (2016). Methylmalonic and propionic acidemias: Clinical management update. *Curr. Opin. Pediatr.* 28, 682–693.

Gabbi, P., Ribeiro, L. R., Martins, G. J., Cardoso, A. S., Haupental, F., Rodrigues, F. S., et al. (2017). Methylmalonate induces inflammatory and apoptotic potential: A link to glial activation and neurological dysfunction. *J. Neuropathol. Exp. Neurol.* 76, 160–178. doi: 10.1093/jnen/nlw121

Gao, Y., Guan, W., Wang, J., Zhang, Y., Li, Y., and Han, L. (2009). Fractional anisotropy for assessment of white matter tracts injury in methylmalonic acidemia. *Chin. Med. J. (Engl)* 122, 945–949.

Gizicki, R., Robert, M., Gómez-López, L., Orquin, J., Decarie, J., Mitchell, G. A., et al. (2014). Long-term visual outcome of methylmalonic aciduria and homocystinuria, cobalamin C type. *Ophthalmology* 121, 381–386. doi: 10.1016/j.ophtha.2013.08.034

Grangé, S., Grangé, S., Bekri, S., Artaud-Macari, E., Francois, A., Girault, C., et al. (2015). Adult-onset renal thrombotic microangiopathy and pulmonary arterial hypertension in cobalamin C deficiency. *Lancet* 386, 1011–1012. doi: 10.1016/S0140-6736(15)00076-8

Greitz, D., Greitz, T., and Hindmarsh, T. (2010). A new view on the CSF-circulation with the potential for pharmacological treatment of childhood hydrocephalus. *Acta Paediatrica* 86, 125–132. doi: 10.1111/j.1651-2227.1997.tb08850.x

Gropman, A. L., and Anderson, A. (2020). Novel imaging technologies for genetic diagnoses in the inborn errors of metabolism. *J. Transl. Genet. Genom.* 4, 429–445.

Han, L., Huang, Z., Han, F., Ye, J., Qiu, W., Zhang, H., et al. (2015). Clinical features and MUT gene mutation spectrum in Chinese patients with isolated methylmalonic acidemia: Identification of ten novel allelic variants. *World J. Pediatr.* 11, 358–365. doi: 10.1007/s12519-015-0043-1

Han, L., Wu, S., Han, F., and Gu, X. (2015). Insights into the molecular mechanisms of methylmalonic acidemia using microarray technology. *Int. J. Clin. Exp. Med.* 8, 8866–8879.

Harting, I., Seitz, A., Geb, S., Zwickler, T., Porto, L., Lindner, M., et al. (2008). Looking beyond the basal ganglia: The spectrum of MRI changes in methylmalonic acidaemia. *J. Inherit. Metab. Dis.* 31, 368–378. doi: 10.1007/s10545-008-0801-5

Heringer, J., Valayannopoulos, V., Lund, A. M., Wijburg, F. A., Freisinger, P., Bari, I., et al. (2016). Impact of age at onset and newborn screening on outcome in organic acidurias. *J. Inherit. Metab. Dis.* 39, 341–353.

Herrmann, W., and Knapp, J. P. (2002). Hyperhomocysteinemia: A new risk factor for degenerative diseases. *Clin. Lab.* 48, 471–481.

Huemer, M., Diodato, D., Schwahn, B., Schiff, M., Bandeira, A., Benoist, J., et al. (2017). Guidelines for diagnosis and management of the cobalamin-related remethylation disorders cblC, cblD, cblE, cblF, cblG, cblJ and MTHFR deficiency. *J. Inherit. Metab. Dis.* 40, 21–48. doi: 10.1007/s10545-016-9991-4

Hwang, N., Jang, J., Cho, E., Choi, R., Choi, S., and Park, H. (2021). Prenatal diagnosis of combined methylmalonic acidemia and homocystinuria cobalamin C type using clinical exome sequencing and targeted gene analysis. *Mol. Genet. Genomic Med.* 9:e1838. doi: 10.1002/mgg3.1838

Jafari, P., Braissant, O., Zavadakova, P., Henry, H., Bonaf, L., and Ballhausen, D. (2013). Brain damage in methylmalonic aciduria: 2-Methylcitrate induces cerebral ammonium accumulation and apoptosis in 3D organotypic brain cell cultures. *Orphanet J. Rare Dis.* 8:4.

Jin, H., Zou, L., Zhang, C., Fang, F., Xiao, J., Wu, H., et al. (2004). Diagnosis and treatment of methylmalonic acidemia in 14 cases. *Zhonghua Er Ke Za Zhi* 42, 581–584.

Kölker, S., Schwab, M., Hörster, F., Sauer, S., Hinz, A., Wolf, N. I., et al. (2003). Methylmalonic acid, a biochemical hallmark of methylmalonic acidurias but no inhibitor of mitochondrial respiratory chain. *J. Biol. Chem.* 278, 47388–47393. doi: 10.1074/jbc.M308861200

Kölker, S., Valayannopoulos, V., Burlina, A. B., Sykut-Cegielska, J., Wijburg, F. A., Teles, E. L., et al. (2015). The phenotypic spectrum of organic acidurias and urea cycle disorders. Part 2: The evolving clinical phenotype. *J. Inherit. Metab. Dis.* 38, 1059–1074. doi: 10.1007/s10545-015-9840-x

Krishna, S. H., McKinney, A. M., and Lucato, L. T. (2008). MR appearance in pediatric patients with methylmalonic aciduria. *Chin. J. Med. Imaging Technol.* 24, 1192–1194.

Lee, N., and Kim, D. (2022). Toxic metabolites and inborn errors of amino acid metabolism: What one informs about the other. *Metabolites* 12:527. doi: 10.3390/metabo12060527

Li, Q., Jin, H., Liu, Y., Rong, Y., Yang, T., Nie, X., et al. (2021). Determination of cytokines and oxidative stress biomarkers in cognitive impairment induced by methylmalonic acidemia. *Neuroimmunomodulation* 28, 178–186. doi: 10.1159/000511590

Ling, S., Wu, S., Shuai, R., Yu, Y., Qiu, W., Wei, H., et al. (2022). The follow-up of chinese patients in cblC type methylmalonic acidemia identified through expanded newborn screening. *Front. Genet.* 13:805599. doi: 10.3389/fgene.2022.805599

Liu, M., Yang, Y., Chang, Y., Chiang, S., Lin, S., Han, L., et al. (2010). Mutation spectrum of MMACHC in Chinese patients with combined methylmalonic aciduria and homocystinuria. *J. Hum. Genet.* 55, 621–626. doi: 10.1038/jhg.2010.81

Longo, D., Fariello, G., Dionisi-Vici, C., Cannatà, V., Boenzi, S., Genovese, E., et al. (2005). MRI and 1H-MRS findings in early-onset cobalamin C/D defect. *Neuropediatrics* 36, 366–372. doi: 10.1055/s-2005-873057

Manoli, I., Sloan, J. L., and Venditti, C. P. (1993). *Isolated methylmalonic acidemia, in genereviews*. Seattle, WA: University of Washington.

Martinelli, D., Deodato, F., and Dionisi-Vici, C. (2011). Cobalamin C defect: Natural history, pathophysiology, and treatment. *J. Inherit. Metab. Dis.* 34, 127–135. doi: 10.1007/s10545-010-9161-z

Matsui, S. M., Mahoney, M. J., and Rosenberg, L. E. (1983). The natural history of the inherited methylmalonic acidemias. *N. Engl. J. Med.* 308, 857–861.doi: 10.1056/NEJM198304143081501

Michel, S. J., Given, C. A. II, and Robertson, W. C. Jr. (2004). Imaging of the brain, including diffusion-weighted imaging in methylmalonic acidemia. *Pediatr. Radiol.* 34, 580–582. doi: 10.1007/s00247-004-1155-2

Mink, J. W. (2003). The Basal Ganglia and involuntary movements: Impaired inhibition of competing motor patterns. *Arch. Neurol.* 60, 1365–1368. doi: 10.1001/archneur.60.10.1365

Molema, F., Haijes, H. A., Janssen, M. C., Bosch, A. M., Spronsen, F. J., Mulder, M. F., et al. (2021). High protein prescription in methylmalonic and propionic acidemia patients and its negative association with long-term outcome. *Clin. Nutr.* 40, 3622–3630. doi: 10.1016/j.clnu.2020.12.027

Morel, C. F., Lerner-Ellis, J. P., and Rosenblatt, D. S. (2006). Combined methylmalonic aciduria and homocystinuria (cblC): Phenotype-genotype correlations and ethnic-specific observations. *Mol. Genet. Metab.* 88, 315–321. doi: 10.1016/j.ymgme.2006.04.001

Obeid, R., and Herrmann, W. (2006). Mechanisms of homocysteine neurotoxicity in neurodegenerative diseases with special reference to dementia. *Febs. Letters* 580, 2994–3005. doi: 10.1016/j.febslet.2006.04.088

Okun, J. G., Hörster, F., Farkas, L. M., Feyh, P., Hinz, A., Sauer, S., et al. (2002). Neurodegeneration in methylmalonic aciduria involves inhibition of complex II and the tricarboxylic Acid cycle, and synergistically acting excitotoxicity. *J. Biol. Chem.* 277, 14674–14680. doi: 10.1074/jbc.M200997200

Radmanesh, A., Zaman, T., Ghanaati, H., Molaei, S., Robertson, R. L., and Zamani, A. A. (2008). Methylmalonic acidemia: Brain imaging findings in 52 children and a review of the literature. *Pediatr. Radiol.* 38, 1054–1061. doi: 10.1007/s00247-008-0940-8

Randon, D. N., Sperb-Ludwig, F., Vianna, F. S., Becker, A. P., Vargas, C. R., Sitta, A., et al. (2020). Prevalence of the most common pathogenic variants in three genes for inborn errors of metabolism associated with sudden unexpected death in infancy: A population-based study in south Brazil. *Genet. Mol. Biol.* 43:20190298. doi: 10.1590/1678-4685-GMB-2019-0298

Rossi, A., Cerone, R., Biancheri, R., Gatti, R., Schiaffino, M. C., Fonda, C., et al. (2001). Early-onset combined methylmalonic aciduria and homocystinuria: Neuroradiologic findings. *AJNR Am. J. Neuroradiol.* 22, 554–563.

Shea, C. J., Sloan, J. L., Wiggs, E. A., Pao, M., Gropman, A., Baker, E. H., et al. (2012). Neurocognitive phenotype of isolated methylmalonic acidemia. *Pediatrics* 129, e1541–e1551. doi: 10.1542/peds.2011-1715

Smith, S. E., Kinney, H. C., Swoboda, K. J., and Levy, H. L. (2006). Subacute combined degeneration of the spinal cord in cblC disorder despite treatment with B12. *Mol. Genet. Metab.* 88, 138–145. doi: 10.1016/j.ymgme.2006.02.007

Takeuchi, M., Harada, M., Matsuzaki, K., Hisaoka, S., Nishitani, H., and Mori, K. (2003). Magnetic resonance imaging and spectroscopy in a patient with treated methylmalonic acidemia. *J. Comput. Assist. Tomogr.* 27, 547–551. doi: 10.1097/00004728-200307000-00018

Thauvin-Robinet, C., Roze, E., Couvreur, G., Horellou, M., Sedel, F., Grabli, D., et al. (2008). The adolescent and adult form of cobalamin C disease: Clinical and molecular spectrum. *J. Neurol. Neurosurg. Psychiatry* 79, 725–728. doi: 10.1136/jnnp.2007.133025

Therrell, B. L., Padilla, C. D., Loeber, J. G., Kneisser, I., Saadallah, A., Borrajo, G. J., et al. (2015). Current status of newborn screening worldwide: 2015. *Semin. Perinatol.* 39, 171–187. doi: 10.1053/j.semperi.2015.03.002

Thompson, G. N., Christodoulou, J., and Danks, D. M. (1989). Metabolic stroke in methylmalonic acidemia. *J. Pediatr.* 115, 499–500. doi: 10.1016/S0022-3476(89)80867-4

Trinh, B. C., Melhem, E. R., and Barker, P. B. (2001). Multi-slice proton MR spectroscopy and diffusion-weighted imaging in methylmalonic acidemia: Report of two cases and review of the literature. *AJNR Am. J. Neuroradiol.* 22, 831–833.

Tsai, A. C., Morel, C. F., Scharer, G., Yang, M., Lerner-Ellis, J. P., Rosenblatt, D. S., et al. (2007). Late-onset combined homocystinuria and methylmalonic aciduria (cblC) and neuropsychiatric disturbance. *Am. J. Med. Genet. A* 143a, 2430–2434. doi: 10.1002/ajmg.a.31932

Waisbren, S. E. (2022). Review of neuropsychological outcomes in isolated methylmalonic acidemia: Recommendations for assessing impact of treatments. *Metab. Brain Dis.* 37, 1317–1335. doi: 10.1007/s11011-022-00954-1

Weisfeld-Adams, J. D., Bender, H. A., Miley-Åkerstedt, A., Frempong, T., Schrager, N. L., and Patel, K. (2013). Neurologic and neurodevelopmental phenotypes in young children with early-treated combined methylmalonic acidemia and homocystinuria,

cobalamin C type. *Mol. Genet. Metab.* 110, 241–247. doi: 10.1016/j.ymgme.2013.07.018

Worgan, L. C., Niles, K., Tirone, J. C., Hofmann, A., Verner, A., Sammak, A., et al. (2006). Spectrum of mutations in mut methylmalonic acidemia and identification of a common Hispanic mutation and haplotype. *Hum. Mutat.* 27, 31–43. doi: 10.1002/humu.20258

Yang, J., Wang, M. M., Liu, H., Liu, C. C., Jiang, H. X., Ning, N., et al. (2017). Imaging assessment of brain development of preterm and young infants. *China J. Pract. Pediatr.* 32, 825–830. doi: 10.19538/j.ek2017110607

Yeşilda, A., Ayata, A., Baykal, B., Koroglu, M., Yildiz, H., Oral, B., et al. (2005). Magnetic resonance imaging and diffusion-weighted imaging in methylmalonic acidemia. *Acta Radiol.* 46, 101–103. doi: 10.1080/02841850510020888

Yu, Y., Ling, S., Shuai, R., Qiu, W., Zhang, H., Liang, L., et al. (2021). Clinical features and outcomes of patients with cblC type methylmalonic acidemia carrying gene c.609G>A mutation. *Zhejiang Da Xue Xue Bao Yi Xue Ban* 50, 436–443. doi: 10.3724/zdxbyxb-2021-0276

Zhang, Y., Song, J., Liu, P., Yan, R., Dong, J., Yang, Y., et al. (2007). [Clinical studies on fifty-seven Chinese patients with combined methylmalonic aciduria and homocysteinemia]. *Zhonghua Er Ke Za Zhi* 45, 513–517.

Zhou, X., Cui, Y., and Han, J. (2018). Methylmalonic acidemia: Current status and research priorities. *Intractable Rare Dis. Res.* 7, 73–78. doi: 10.5582/irdr.2018.01026

frontiers | Frontiers in Neuroscience

TYPE Clinical Trial
PUBLISHED 02 February 2023
DOI 10.3389/fnins.2023.1123797

OPEN ACCESS

EDITED BY
Lingfei Guo,
Shandong Provincial Hospital Affiliated to Shandong First Medical University, China

REVIEWED BY
Haotian Xin,
Shandong University, China
Yimeng Zhao,
China Medical University, China

*CORRESPONDENCE
Yuping Ning
✉ ningjeny@126.com
Yanling Zhou
✉ zhouylivy@aliyun.com

SPECIALTY SECTION
This article was submitted to Brain Imaging Methods, a section of the journal Frontiers in Neuroscience

RECEIVED 14 December 2022
ACCEPTED 11 January 2023
PUBLISHED 02 February 2023

CITATION
Liu H, Wang C, Lan X, Li W, Zhang F, Fu L, Ye Y, Ning Y and Zhou Y (2023) Functional connectivity of the amygdala and the antidepressant and antisuicidal effects of repeated ketamine infusions in major depressive disorder.
Front. Neurosci. 17:1123797.
doi: 10.3389/fnins.2023.1123797

Functional connectivity of the amygdala and the antidepressant and antisuicidal effects of repeated ketamine infusions in major depressive disorder

Haiyan Liu[1,2,3], Chengyu Wang[1,2,3], Xiaofeng Lan[1,2,3], Weicheng Li[1,2,3,4], Fan Zhang[1,2,3,4], Ling Fu[1,2,3,4], Yanxiang Ye[1,2,3], Yuping Ning[1,2,3,4]* and Yanling Zhou[1,2,3]*

[1]Department of Child and Adolescent Psychiatry, Affiliated Brain Hospital of Guangzhou Medical University, Guangzhou, China, [2]Key Laboratory of Neurogenetics and Channelopathies of Guangdong Province and the Ministry of Education of China, The Second Affiliated Hospital of Guangzhou Medical University, Guangzhou, China, [3]Guangdong Engineering Technology Research Center for Translational Medicine of Mental Disorders, Guangzhou, China, [4]Department of Psychology, The First School of Clinical Medicine, Southern Medical University, Guangzhou, China

Background: Dysfunction of the amygdala is the core pathogenesis of major depressive disorder (MDD). However, it remains unclear whether ketamine treatment could modulate characteristics of amygdala-related networks. We aimed to explore the relationship between changes in the resting-state functional connectivity (RSFC) of the amygdala and the treatment of ketamine in MDD patients and to identify important neuroimaging predictors of treatment outcome.

Methods: Thirty-nine MDD patients received six subanesthetic dose infusions of ketamine. Depressive and suicidal symptoms were assessed and magnetic resonance imaging (MRI) scans were performed before and after six ketamine infusions. Forty-five healthy controls also underwent once MRI scans. Seed-based RSFC analyses were performed, focusing on the bilateral amygdala.

Results: After ketamine treatment, the RSFC between the left amygdala (LA) and the left medial superior frontal gyrus (mSFG) of MDD patients enhanced significantly, and this change was positively correlated with the reduction in depressive symptoms (r = 0.40, p = 0.012). The combination baseline RSFC of LA – right putamen and right amygdala (RA) – right putamen was related to the antidepressant and antisuicidal effects of ketamine. The combination baseline RSFC of LA – right putamen and RA – right putamen could predict the ineffective antidepressant (AUC = 0.739, p = 0.011) and antisuicidal effects of ketamine (AUC = 0.827, p = 0.001).

Conclusion: Ketamine can regulate the relevant circuits of amygdala and mSFG, and the baseline RSFC between bilateral amygdala and right putamen may be a predictor of the response of ketamine's antidepressant and antisuicidal treatment.

Clinical trial registration: https://www.chictr.org.cn/showproj.aspx?proj=20875, identifier ChiCTR-OOC-17012239.

KEYWORDS

major depressive disorder, ketamine, amygdala, functional connectivity, antidepressant

1. Introduction

Major depressive disorder (MDD) is a major contributor to the global burden of disease, due to its high incidence of disability and suicide (Ferrari et al., 2013). However, a high proportion of patients have poor outcomes after receiving the current evidence-based treatments: less than half recover within the first 3 months of treatment (Trivedi et al., 2006), and nearly one-third do not respond to two or more traditional antidepressant medications (McGrath et al., 2006; Mrazek et al., 2014).

Ketamine, a novel antidepressant, is an N-methyl-D-aspartate (NMDA) receptor antagonist that has attracted widespread attention for its rapid antidepressant effects. Evidence has demonstrated that subanesthetic doses of ketamine could rapidly and effectively improve depressive symptoms and suicidal ideation in MDD patients (Wilkinson et al., 2018; Zheng et al., 2018; Marcantoni et al., 2020). Repeated use of ketamine over 2–4 weeks may be more effective and longer lasting than a single dose (Aan et al., 2010; Murrough et al., 2013; Zheng et al., 2018, 2019). However, some patients still failed to respond to ketamine treatment. For example, our previous study reported nearly 40% did not respond to six infusions of ketamine (Zheng et al., 2019). Therefore, using neuroimaging to determine predictor of response to ketamine treatment and the neural mechanism of its antidepressant and antisuicidal effects is crucially important.

Our previous study found that the volume of the left amygdala (LA) increased after six ketamine treatments, corresponding to an improvement in depressive symptoms (Zhou et al., 2020). As the amygdala is the main area responsible for emotion perception and generation (Davis and Whalen, 2001; Phelps and LeDoux, 2005), further analysis of the amygdala using functional imaging, is needed to determine whether its resting-state functional connectivity (RSFC) would be involved in ketamine's antidepressant action.

The amygdala is involved in key symptoms of MDD, not only related to the regulation of emotions and sensory processing but also to the processing of visceral information related to emotional stimuli (Price, 2003). A large sample study found that amygdala voxels had decreased RSFC with the orbitofrontal cortex, temporal lobe areas, including the temporal pole, inferior temporal gyrus and the parahippocampal gyrus in MDD patients compared to healthy controls (Cheng et al., 2018). Another meta-analysis showed that in MDD patients, abnormal RSFC of the amygdala occurred mainly in the affective network, including strengthened RSFC with the right hippocampus/parahippocampus and bilateral ventromedial orbitofrontal cortex and weakened RSFC with the bilateral insula and left caudate (Tang et al., 2018). The alteration in the RSFC of the amygdala is also associated with the risk of suicide. Emotional disorder patients with suicidal ideation or those who have attempted suicide exhibited abnormal RSFC between the amygdala and regions such as the parahippocampal area, paracentral lobule/precuneus, insula, middle temporal gyrus, and superior orbitofrontal area compared to those without suicidal ideation/suicide attempts (Kang et al., 2017; Zhang et al., 2020).

In addition, antidepressant treatment was found to associate with changes in the RSFC of the amygdala. Fluoxetine treatment was associated with significantly strengthened RSFC between the amygdala and right frontal and cingulate cortex, striatum, and thalamus in MDD patients (Chen et al., 2008). Transcutaneous vagus nerve stimulation could reduce depressive symptoms, accompanied by strengthened RSFC in the right amygdala (RA) and left dorsolateral prefrontal cortex (PFC) (Liu et al., 2016). However, up to now it is not clear whether the amygdala RSFC play a role in modulating ketamine's antidepressant and antisuicide effects.

Herein, we set the amygdala as a region of interest (ROI) and applied a voxel-based RSFC analysis to investigate alterations in RSFC between the mentioned above seed point and the whole brain after six infusions of ketamine treatment in MDD patients. Then we investigated the relationship between these changes and reductions in depressive symptoms and suicidal ideation after ketamine treatment. Additionally, the receiver operating characteristic (ROC) curve analysis was used to examine the baseline amygdala RSFC could predict the antidepressant and antisuicidal effects of ketamine.

2. Methods

2.1. Participants

The data came from a clinical trial that explored the antidepressant effect of repeated ketamine infusions on MDD patients (clinical trial No. ChiCTR-OOC-17012239). Patients who met the following criteria (regardless of sex) were included in the study: (1) 18–65 years old; (2) diagnosed with MDD without psychotic features according to the structured clinical interview for Diagnostic and Statistical Manual of Mental Diseases-5 (DSM-5); (3) failed to respond to at least two suitable antidepressant agents with adequate dosage or exhibited suicidal ideation [confirmed by the Beck Scale for Suicidal Ideation (SSI) – Part I, with a score $\geq$2 at screening]; (4) total score of 17 items of Hamilton Depression Rating Scale (HAMD-17) $\geq$17; (5) no current pregnancy or lactation; (6) without serious medical or nervous system diseases and substance dependence; (7) no metal implants or other magnetic resonance imaging (MRI) contraindications; and (8) underwent resting-state functional MRI (rs-fMRI) scans at baseline and follow-up.

Forty-five healthy controls (HCs) were recruited from the community. All HCs were in a healthy state without any previous or current mental illness or drug abuse or dependence. At the same time, there were no contraindications to MRI.

All research procedures were conducted in accordance with the Declaration of Helsinki ethical principles and approved by the Review Committee of the Brain Hospital Affiliated to Guangzhou Medical University. All subjects had provided written informed consent before participation.

2.2. Procedures

All MDD patients received a 40-min open-label infusion of ketamine (0.5 mg/kg) three times a week for 2 weeks. The details of our methods have been described in our previous studies (Zheng et al., 2018; Zhou et al., 2018a,b). Hemodynamics and clinical status were monitored during this period. The MDD patients were not restricted from using psychiatric drugs throughout the study, but were only eligible to use if they took a stable dosage of antidepressants for at least 4 weeks before entering the study and continuing to receive the same regimen and dose throughout the study.

MDD patients were assessed for clinical symptoms and underwent rs-fMRI scans 24 h prior to ketamine infusion (T0) and 24 h after the sixth ketamine infusion (T1). HCs underwent only one rs-fMRI scan.

2.3. Rating scales

The severity of depressive symptoms was assessed with the HAMD-17; the higher their score on this scale, the more severe the depressive symptoms were. The SSI scale was used to assess suicidal ideation and which was consisted of 19 items administered by a clinician. We utilized the first five items of the SSI (SSI-5), which included hope to live, hope to die, reasons for living or dying, desire to actively attempt suicide, and passive suicidal thoughts. The higher score of SSI-5 indicated a higher risk of suicide. The interrater reliability of the clinicians who administered the HAMD-17 was assessed; the intraclass correlation coefficients were >0.9.

The reduction rate (ΔHAMD-17% and ΔSSI-5%) was used to index the antidepressant and antisuicide effect of ketamine. The reduction rate was calculated with the following equation: pre-treatment score minus post-treatment score, then divided by the pre-treatment score, and finally multiplied by 100%. Responders were defined as having a reduction rate in HAMD-17 score or SSI-5 score $\geq$50%.

2.4. MRI acquisition

All imaging data were acquired by the Philips Achieva X-series 3T scanner with an eight-channel phased-array head coils. The gradient-echo echo-planar imaging (GRE-EPI) sequence was used to acquire blood oxygen level dependent (BOLD) images with an echo time of 30 ms, repetition time of 2,000 ms, flip angle of 90°, filed of view of 220 mm $\times$ 220 mm^2, matrix of 64 $\times$ 64, slice thickness of 4 mm, slice gap of 0.6 mm. The functional run lasted 8 min and 240 volumes acquired. Total of 33 transverse interleaved slices covered the whole brain. During the scan, the subjects were instructed to remain still with their eyes closed, avoid systematic thinking and remain awake.

2.5. Image preprocessing

All rsfMRI data was preprocessed using the Data Processing and Analysis of Brain Imaging (DPABI, version 5.0)[1]. The main steps were as follows: (1) removing the first 10 volumes; (2) slice timing; (3)realigning (subjects who had excessive head motion >2.0 mm translation and/or $>2.0°$ rotation during the scan were excluded); (3) spatially normalizing by using EPI templates; (4) smoothing using a 4-mm full width at half maxima (FWHM) isotropic Gaussian kernel; (5) removing linear and quadratic trends; (6) regressing out head motion effects using the Friston 24-parameter model, the white matter and cerebrospinal fluid. Moreover, the global signal was regressed in the whole brain analysis at the same time (Fox et al., 2009; Engman et al., 2016); (7) temporal band-pass filtering (0.01–0.1 Hz); and (8) "scrubbed" one time points before and one time points after bad images, whose frame displacement (FD) >0.5.

2.6. Definition of ROI and RSFC analyses

The bilateral amygdala was defined as seed-based two ROI according to the automated anatomical labels (Tzourio-Mazoyer et al., 2002). Then, whole-brain voxel-level RSFC of each amygdala was mapped for all subjects. The main steps were as follows: (1) calculating the mean time series of each amygdala; (2) calculating the Pearson correlation coefficients between the mean time series of each amygdala and that of each voxel in the rest of the brain; and (3) converting each correlation coefficient z values using Fisher's z transformation to improve normality.

3. Statistical analysis

3.1. Baseline demographic characteristics

Independent-sample t-tests and χ^2 tests were conducted to determine whether the MDD and HC groups differed in age and sex with the Statistical Package for Social Sciences (SPSS 25.0). All significance levels were set at $p < 0.05$.

3.2. Imaging analysis

The DPABI (version 5.0) toolbox was used to obtain the RSFC from the bilateral amygdala to the whole-brain of HCs, pre-treatment and post-treatment MDD patients. The difference in the mean time course of the rs-fMRI scans before and after ketamine treatment was defined as the change in the RSFC of the amygdala.

First, the statistical parametric mapping version 12 (SPM12),[2] was used to apply two sample t-test comparing the RSFC images between the HCs and pre-treatment MDD groups, controlling for age, sex, and head motion. If aberrant RSFC was found in MDD patients, the RSFC of the amygdala in this region was extracted for correlation analysis with the HAMD-17 score, SSI-5 score.

Second, to investigate the relationship between the changes in abnormal RSFC of amygdala and the improvements in clinical symptoms after ketamine treatment, paired t-test was applied with SPM12 to compare the RSFC of pre-treatment and pro-treatment MDD patients, with head motion as a covariate. If the change in the RSFC of the amygdala was found in post-treatment patients, we would extract the above RSFC for correlation analysis with the reduction rate of HAMD-17 and SSI-5 scores.

Third, the correlation analysis between abnormal amygdala RSFC at baseline and the reduction rate of depressive symptoms and suicidal symptoms after ketamine treatment were conducted, and ROC curves were performed to determine whether the abnormal RSFC of the amygdala at baseline could predict the treatment effect of ketamine.

All resulting group-level analyses had a threshold of $p < 0.05$ [cluster-corrected using the familywise error rate (FWE) with a height threshold of $p < 0.001$]. All Images were displayed through the DPABI Viewer.

1 http://rfmri.org/DPARSF

2 https://www.fil.ion.ucl.ac.uk/spm/

4. Results

4.1. Baseline characteristics

A total of 45 MDD patients were enrolled in the study. Of these, one exhibited serious artifacts in the rs-fMRI scan, and another five were excluded due to head movement during the scans. Therefore, 39 MDD patients were included in the final analysis.

The two groups (HCs and MDD) exhibited a significant difference in age; specifically, the mean age of the MDD group was higher than that of the HC group (36.5 ± 12.1 vs. 31.4 ± 8.0, $p = 0.031$). The baseline characteristics were shown in Table 1.

4.2. Abnormal amygdala RSFCs in MDD patients

For each of the two *a priori*-defined amygdala seeds, we assessed and compared its whole-brain RSFCs in MDD patients and HCs. Compared to HCs, MDD patients displayed hypoconnectivity between LA and bilateral putamen, right MCC and left insula. In addition, MDD patients showed hyperconnectivity between the LA and the bilateral posterior central gyrus (PCG) (Table 2 and Figure 1A).

Compared to HCs, the hypoconnectivity was showed between the RA and left cerebellum_6 as well as the RA and the right putamen in MDD patients. Moreover, MDD patients displayed hyperconnectivity between RA and left calcarine gyrus, left lingual, the left middle occipital gyrus (MOG) and left paracentral lobule (Table 2 and Figure 1B).

TABLE 1 Baseline characteristics of participants.

Characteristic	MDD (n = 39)	HCs (n = 45)	t/χ^2	*P*-value
Age (years)	36.5 ± 12.1	31.4 ± 8.0	−2.206	0.031
Gender (% female)[a]	24 (61.5%)	27 (60.0%)		0.886
Education (years)	11.8 ± 3.3			
BMI (kg/m^2)	23.0 ± 3.2			
Duration of illness (months)	84.1 ± 80.0			
Age of onset (years)	29.0 ± 11.4			
First episode (yes)	15 (38.5%)			
Psychiatric comorbidity	6 (15.4%)			
Current smoking (yes)	5 (12.8%)			
Current drinking (yes)[b]	1 (2.6%)			
Baseline HAMD-17 score	23.2 ± 4.6			
Baseline SSI-5 score	9.0 ± 3.5			
Use of drugs				
Antidepressant dose (mg/day)	44.4 ± 24.1			
Benzodiazepines	21 (53.8%)			
Antipsychotics	25 (64.1%)			

MDD, major depressive disorder; HCs, healthy controls; BMI, body mass index; HAMD-17, 17-item Hamilton Depression Rating Scale; SSI-5, the first five items of Baker Suicide Scale. [a]χ^2 test of continuity correction. [b]Drinking behavior without alcohol abuse or alcohol dependence.

4.3. Correlation of abnormal amygdala RSFC with depressive symptoms and suicidal ideation in MDD patients at baseline

At baseline, showed as Figure 2, HAMD-17 score was negatively correlated with RSFC in the LA and left insula ($r = -0.44$, $p = 0.005$). SSI-5 score was positively correlated with the abnormal RSFCs of LA and left PCG ($r = 0.47$, $p = 0.002$) as well as LA and right PCG ($r = 0.35$, $p = 0.030$). SSI-5 score was also negatively correlated with abnormal RSFC in the LA and right MCC ($r = -0.41$, $p = 0.010$), the LA and the right putamen ($r = -0.35$, $p = 0.030$).

No abnormal RSFC was found in the RA associated with HAMD-17 and SSI-5 score.

4.4. Changes in the amygdala RSFC after treatment and their relationship with the improvements in depressive symptoms and suicidal ideation

After ketamine treatment, the HAMD-17 score significantly decreased by 11.0 points (23.2 ± 4.6 vs. 12.2 ± 7.4, $p < 0.001$), and the SSI-5 score significantly decreased by 3.3 points (9.0 ± 3.5 vs. 6.0 ± 2.3, $p < 0.001$).

After ketamine treatment, the RSFC between the LA and the left medial superior frontal gyrus (mSFG) was strengthened (Figure 3A). The altered RSFC between the LA and the left mSFG [cluster size = 43; Montreal Neurological Institute (MNI) coordinates: $x = -9$, $y = 60$, $z = 15$; pFWE-corr = 0.020), a brain region that exhibited significant changes after ketamine treatment, was positively correlated with the HAMD-17 reduction rate ($r = 0.40$, $p = 0.012$, Figure 3B). But the altered RSFC between the LA and the left mSFG was not correlated with the SSI-5 reduction rate. There was no significant difference in RSFC of left LA - left mSFG between the pre-treatment MDD patients and HCs and between post-treatment MDD patients and HCs (Figure 3C). The RSFC of the RA did not exhibit significant changes after treatment.

4.5. Baseline amygdala RSFC predicted ketamine's antidepressant and antisuicidal effects

At baseline, the RSFC between the LA and the right putamen ($r = -0.37$, $p = 0.021$, Figure 4A) and the RSFC between the RA and the right putamen ($r = -0.40$, $p = 0.011$, Figure 4B) were negatively correlated with the reduction rate of HAMD-17 score, respectively. The RSFC between the LA and the right putamen ($r = -0.53$, $p = 0.001$, Figure 4D), the RSFC between the RA and the right putamen ($r = -0.38$, $p = 0.017$, Figure 4E) and the LA and right MCC ($r = -0.38$, $p = 0.017$, Figure 4F), were negatively correlated with the reduction rate of SSI-5, respectively.

For antidepressant response, ROC curves analysis was showed that the baseline amygdala RSFC was significant predictor, with the AUC of the LA – right putamen connectivity was 0.689 [95% confidence interval (CI), 0.504–0.875; $p = 0.043$], the AUC of the RA – right putamen connectivity was 0.726 (95% CI, 0.561–0.892;

TABLE 2 Abnormal amygdala RSFCs in pre-treatment MDD patients compared to HCs.

ROI	Brain regions (AAL)	Side	Cluster size	MNI coordinates (peak)[a]			*t*-Value	pFWE-corr
				x	*y*	*z*		
LA	MDD_{T0} > HCs							
	PCG	L	95	−42	−36	63	4.84	0.001
	PCG	R	62	48	−30	57	5.18	0.006
	MDD_{T0} < HCs							
	MCC	R	162	6	15	42	5.13	<0.001
	Putamen	R	162	30	−9	9	4.69	<0.001
	Putamen	L	65	−30	−15	0	5.31	0.005
	Insula	L	83	−33	−15	3	4.82	0.001
RA	MDD_{T0} > HCs							
	Calcarine gyrus	L	48	0	−90	−6	4.15	0.023
	Lingual gyrus	L	241	−6	−66	−3	5.37	<0.001
	MOG	L	58	−21	−93	0	3.88	0.009
	Paracentral lobule	L	44	−15	−24	75	3.92	0.034
	MDD_{T0} < HCs							
	Cerebellum_6	L	179	−12	−66	−24	5.43	<0.001
	Putamen	R	88	30	0	0	4.81	0.001
	Undefined*	L	132	−18	3	12	4.66	<0.001

RSFC, resting-state functional connectivity; MDD, major depressive disorder; HCs, healthy controls; ROI, region of interest; AAL, anatomical automatic labeling; FWE, family-wise error rate; LA, left amygdala; RA, right amygdala; PCG, posterior central gyrus; MCC, mid-cingulate cortex; MOG, middle occipital gyrus; L, left; R, right.

[a]*x*, *y*, *z* = MNI (Montreal Neurological Institute) coordinates of significant effects.

*The peak point of the cluster did not fall in the AAL division area, which contains part of the putamen.

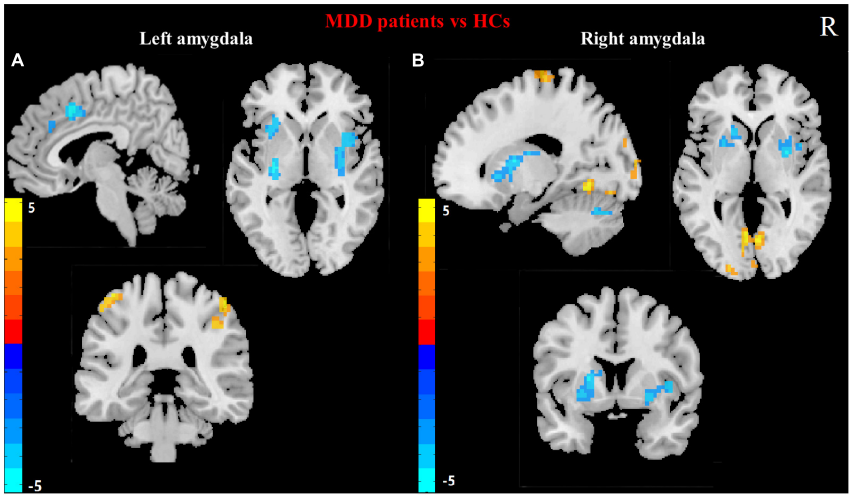

FIGURE 1
Differences in left **(A)** and right **(B)** amygdala RSFC between MDD patients and HCs. (Two sample *t*-test, voxel- level $p < 0.001$, corrected by FWE). Color bar represents *t*-values. R: right.

$p = 0.016$) and the AUC of combination of LA – right putamen connectivity and RA – right putamen connectivity was 0.739 (95% CI, 0.578–0.901; $p = 0.011$). See Figure 4C and Table 3 for details.

For antisuicidal response, the AUC of the LA - right putamen connectivity was 0.799 (95% CI, 0.641 to 0.958; $p = 0.003$), and the AUC of the RA- right putamen connectivity was 0.787 (95% CI, 0.628 to 0.946; $p = 0.005$) and the AUC of combination of LA - right putamen connectivity and RA-right putamen connectivity was 0.827 (95% CI, 0.676 to 0.978; $p = 0.001$). See Figure 4G and Table 3 for details.

5. Discussion

In this study, we found that after ketamine treatment, the RSFC between the LA and the left mSFG of MDD patients enhanced

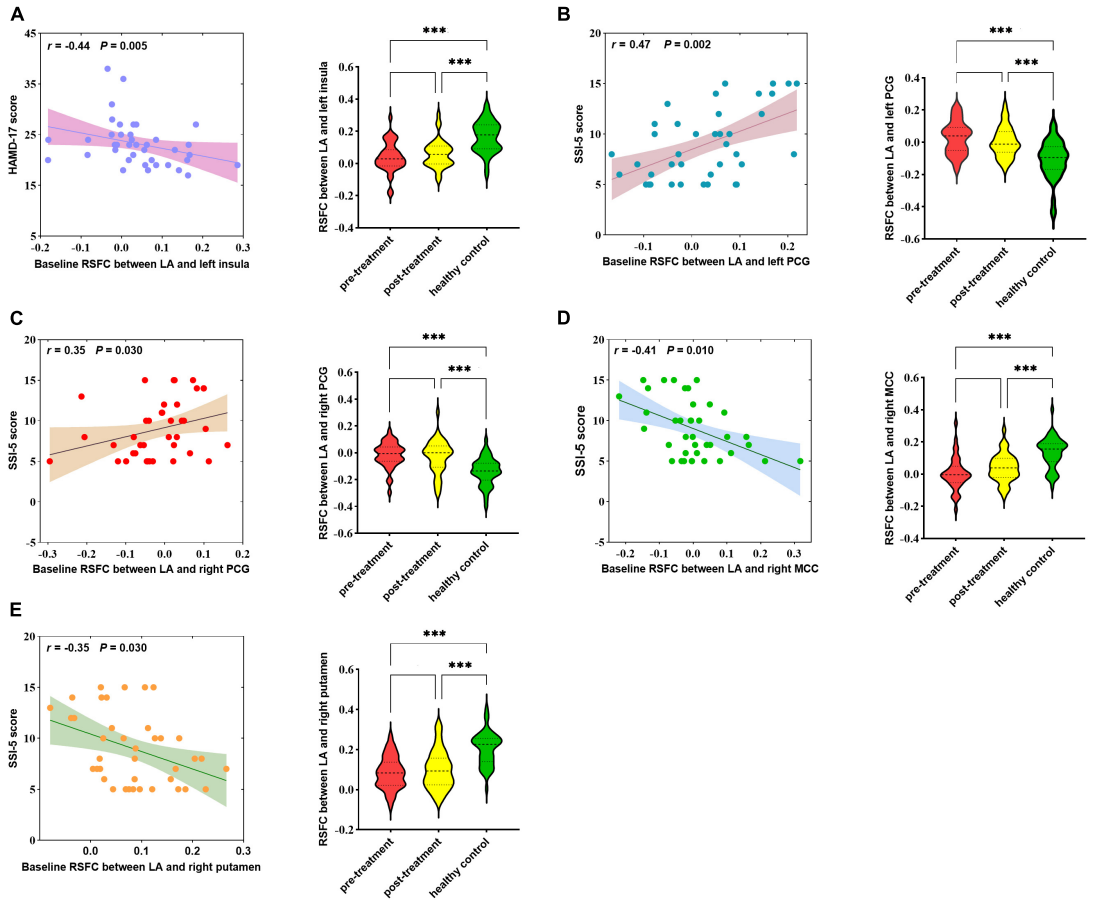

FIGURE 2
Correlation between abnormal RSFCs of bilateral amygdala and HAMD-17 score **(A)** or SSI-5 score **(B–E)** in MDD patients at baseline. RSFC, resting-state functional connectivity; MDD, Major depressive disorder; HCs, healthy controls; LA, left amygdala; PCG, posterior central gyrus; MCC, mid-cingulate cortex; MOG, middle occipital gyrus. ***$P < 0.001$.

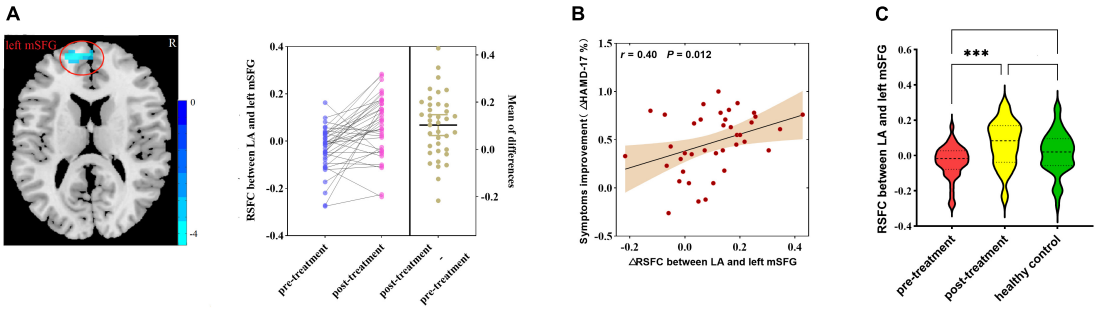

FIGURE 3
(A) Differences in RSFC between pre-treatment and post-treatment MDD patients (paired samples *t*-test, voxel-level $p < 0.001$, corrected by FWE; left amygdala cluster size threshold $k \geq 40$). Color bar represents *t*-values. **(B)** Correlation analysis of changes in RSFC of the amygdala with the rate of reduction in HAMD-17 in MDD patients after ketamine treatment. **(C)** Differences in RSFC among pre-treatment, post-treatment MDD patients, and HCs (analysis of variance). RSFC, resting-state functional connectivity; MDD, major depressive disorder; HAMD-17, 17-item of Hamilton Depression Rating Scale; LA, left amygdala; mSFG, medial superior frontal gyrus; ΔHAMD-17%, HAMD-17 reduction rate. ***$p < 0.001$.

significantly, and this change was positively correlated with the improvements in depressive symptoms. The baseline RSFC of the LA and right putamen, and the baseline RSFC of the RA and right putamen could predict antidepressant and the antisuicidal effects of ketamine.

Previous studies reported that the RSFC of the amygdala in MDD patients differ from that of HCs (Cheng et al., 2018; Tang et al., 2018), and our findings further validate this conclusion. Our study found that the strength of the RSFC between the amygdala and insula was associated with the severity of depression; the weaker the RSFC was, the more severe the depressive symptoms, consistent with previous study (Bebko et al., 2015). In addition, we found that the strength of the RSFC between amygdala and putamen, MCC and PCG were related to suicide, and these regions associated with mood and the

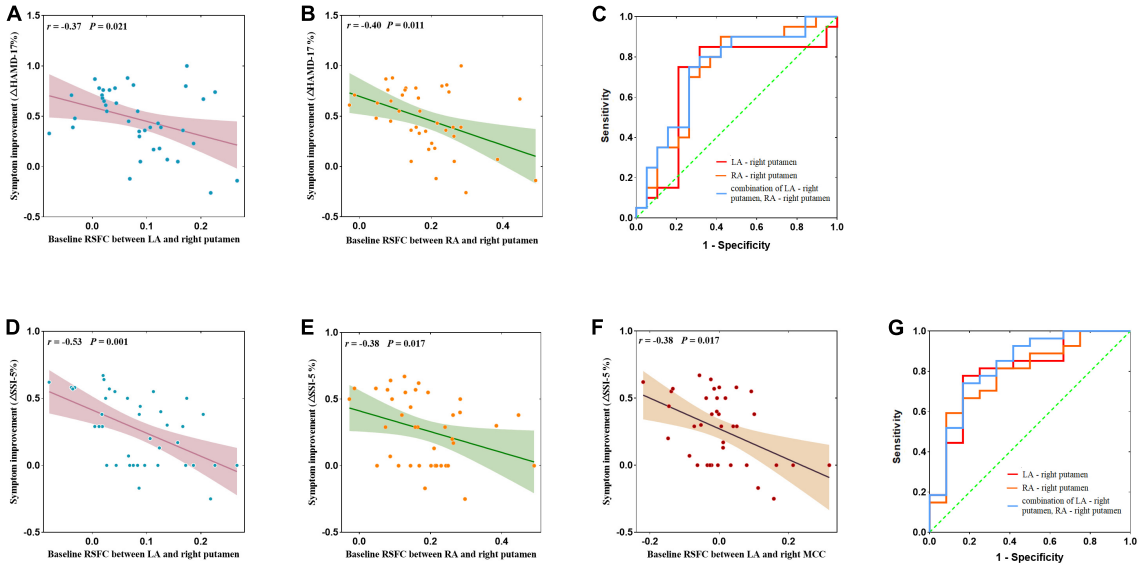

FIGURE 4

(A,B,D–F) Correlation between abnormal amygdala RSFC at baseline and the remission rate of depressive symptoms and suicidal symptoms after ketamine treatment and ROC curve analysis. **(C)** Neuroimaging predictors of treatment non-response, with the non-responders defined with <50% improvements in HAMD-17 obtained after the ketamine infusions. The area under the ROC curve was 0.689 (p = 0.043) for the RSFC of the LA – right putamen, with a sensitivity of 91.4%, and specificity of 59.1%; the area under the ROC curve was 0.726 (p = 0.016) for RA – right putamen connectivity, with a sensitivity of 82.4%, and specificity of 68.2%; and the area under the ROC curve was 0.739 (p = 0.011) for LA – right putamen connectivity and RA-right putamen connectivity, with a sensitivity of 75.0%, and specificity of 73.7%. **(G)** Non-responders defined with <50% improvements SSI-5 score obtained after the ketamine infusions. The area under the ROC curve was 0.799 (p = 0.003) for the RSFC of the LA – right putamen, with a sensitivity of 77.8%, and specificity of 83.3%; the area under the ROC curve was 0.787 (p = 0.005) for the RA – right putamen connectivity, with a sensitivity of 59.3%, and specificity of 91.7%; and the area under the ROC curve was 0.827 (p = 0.001) for LA – right putamen connectivity and RA – right putamen connectivity, with a sensitivity of 74.1%, and specificity of 83.3%. AUC, area under curve; LA, left amygdala; RA, right amygdala.

TABLE 3 Results of ROC curve analysis of antidepressant and antisuicidal response at 24 h after six ketamine infusions.

Independent variables	AUC	Cut-off	Sensibility	Specificity	Youden index
Antidepressant response					
LA – right putamen	0.689	0.085	0.750	0.789	0.539
RA – right putamen	0.726	0.136	0.900	0.579	0.479
Combination of LA – right putamen, RA – right putamen	0.739	0.513	0.750	0.737	0.487
Antisuicidal response					
LA – right putamen	0.799	0.066	0.778	0.833	0.611
RA – right putamen	0.787	0.197	0.593	0.917	0.510
Combination of LA – right putamen, RA – right putamen	0.827	0.664	0.741	0.833	0.574

AUC, area under curve; LA, left amygdala; RA, right amygdala.

risk of suicide (Straube and Miltner, 2011; van Heeringen et al., 2014; Gifuni et al., 2021). However, few studies have explored the relationship between the RSFC of the amygdala and suicidal ideation in MDD patients. One study reported that suicide was associated with the RSFC between the amygdala and the insula, middle temporal gyrus, and supraorbital frontal regions (Kang et al., 2017). Possible explanations for the lack of consistent findings were differences in the methods used to analyze the RSFC and the heterogeneity of subjects. In addition, the sample sizes of our study and the above studies was small; further investigations should increase the sample size.

In the present study, we found strengthened RSFC between the LA and left mSFG after ketamine treatment; these changes were positively correlated with the improvements in depressive symptoms. The mSFG is part of the medial PFC (mPFC), which is normally extensively associated with the amygdala and exerts top-down inhibitory control over its activity, thereby regulating emotional expression (Likhtik et al., 2014; Bukalo et al., 2015). Hyperactivity of the amygdala in MDD patients has been suggested to result from reduced inhibitory input. Although our study did not find a significant difference in the RSFC between the amygdala and mPFC between MDD patients and HCs, previous studies of MDD patients have found weakened RSFC in the amygdala and PFC (Dannlowski et al., 2009; Tang et al., 2013; Connolly et al., 2017). A previous study found that the RSFC between the amygdala and PFC was strengthened after treatment with conventional antidepressants and that the RSFC of the LA was more significantly strengthened than

that of the RA (Chen et al., 2008). The effect of ketamine may be related to mPFC activity. One study reported that the concentration of glutamate and glutamine complex in mPFC of ketamine responder began to rise rapidly when ketamine was injected (Milak et al., 2016). Another study showed that subanesthetic doses of ketamine cause a glutamatergic burst in the mPFC and enhanced mPFC activity, whereas silencing the mPFC blocks the effects of ketamine (Fuchikami et al., 2015). Additionally, MDD patients exhibited reduced PFC volume, decreased neurotrophic factor release, and neuronal atrophy (Botteron et al., 2002; Duman and Monteggia, 2006; Duman and Li, 2012). Ketamine could promote the production and release of neurotrophic factors within the mPFC and restores its function (Li et al., 2010, 2011). Therefore, the strengthened RSFC between the LA and left mSFG after ketamine treatment further indicated that the antidepressant effect of ketamine may be related to enhanced PFC activity to regulate amygdala function.

Our study found that the RSFC between the amygdala and the right putamen may be a predictor of clinical response to ketamine treatment. MDD patients with greater decoupling of amygdala and right putamen may be the target population for ketamine treatment. The putamen is an important part of the striatum, a system that increases responses to negative emotions and is a core region of the reward network (Keren et al., 2018). Previous studies have demonstrated that loss of pleasure in MDD patients was associated with abnormal reward circuits. One study showed that glycolysis in the putamen of bipolar depressive patients with treatment-resistant was associated with reduced anhedonia and the anti-anhedonic effects of ketamine was due to ketamine-induced increases in glucose metabolism in the putamen and MCC (Lally et al., 2014). Moreover, Yang et al. (2017) found that female MDD patients had reduced amygdala and putamen volume and decreased RSFC between amygdala and putamen, which was similar to our results. In our study, we also found that the lower RSFC between amygdala and putamen was associated with stronger suicidal ideation, which may suggest that functional decoupling between amygdala and putamen may be related to the occurrence of suicidal ideation. Previous studies suggest that the putamen was also involved in suicidal ideation. Putamen volume was decreased in MDD patients with suicidal ideation (Dombrovski et al., 2012), and that lower putamen activation during motor tasks was associated with higher suicidal ideation in adult BD patients (Marchand et al., 2011). After ketamine treatment, putamen gray matter volume increased, and activity in brain regions such as the putamen and caudate nucleus increased (Rao et al., 2017; Gallay et al., 2021). Our findings may further confirm that the antidepressant and antisuicide effects of ketamine may be related to the functional changes of reward related brain regions.

In addition, our study found that RSFC between the amygdala and MCC was associated with improvement in suicidal ideation. MCC is also thought to be part of the reward circuit, involved in action reinforcement association and selection based on the rewarding or aversive nature of the underlying movement (Bracht et al., 2015). Animal studies have found that this amygdala – MCC pathway is associated with the influence of the amygdala's facial processing subsystem on the perception of emotional facial expressions, such as fearful, sad, and happy expressions (Morecraft et al., 2007; Rolls, 2007; Grabenhorst and Rolls, 2011). Previous study has suggested that the sustained antidepressant effect of a low-dose ketamine infusion was mediated by increased activation of the supplementary motor area (SMA) and MCC; a single optimal dose of ketamine facilitated glutamatergic neurotransmission in the SMA and MCC, activating both regions, whereas a greater increase in the activation of MCC was associated with a reduction in depressive symptoms (Chen et al., 2018). Except for ketamine, other drug also seem to target the RSFC between the amygdala and MCC. One study showed that after 8-weeks of quetiapine treatment, decreased HAMD scores in anxiety depressive patients were associated with increased RSFC in the amygdala-MCC and amygdala-precuneus (Altinay et al., 2016). Our results reveal a connection between the amygdala and MCC that may also be a target for ketamine treatment.

This study had several limitations. First, the sample size was small. Since MDD patients commonly experience symptoms of anxiety, they are prone to irritability during scans, causing excessive head movement, which affects the acquisition of high-quality data. Second, due to the open-label design and the lack of placebo-treated controls, the influence of temporal effects on functional changes in the brain cannot be excluded. Third, RSFC describes the temporal correlation of blood signals between brain regions, that is, the synchronization of functional activity in related brain regions; it cannot determine anatomical directionality or causal relationships. Fourth, as all MDD patients were not restricted in terms of the use of psychiatric drugs throughout the study, we cannot rule out a group effect due to medication. Fifth, we focused on the amygdala and explored its RSFC with the whole brain, but the results indicated that the amygdala is not a single homogeneous structure and exhibits structural and functional subdivisions; thus, further exploration of the subregions of the amygdala is needed.

6. Conclusion

Short-term repeated use of ketamine may modulate the RSFC of the amygdala in MDD patients. The mechanism of improving depressive symptoms by ketamine may be related to it is regulation of the RSFC of amygdala. The combination baseline RSFC of bilateral amygdala and right putamen may be a predictor of the response of ketamine's antidepressant and antisuicidal treatment.

Data availability statement

The raw data supporting the conclusions of this article will be made available by the authors, without undue reservation.

Ethics statement

The studies involving human participants were reviewed and approved by the Ethics Committee of Guangzhou Hui'ai Hospital. The patients/participants provided their written informed consent to participate in this study.

Author contributions

HL: investigation, formal analysis, writing—original drafting, and visualization. CW, XL, and WL: validation and investigation. FZ, LF, and YY: investigation. YN and YZ: conceptualization, supervision,

and writing—review and editing. All authors contributed to the article and approved the submitted version.

Funding

This work was supported by the National Natural Science Foundation of China (grant number 81801343), the Guangdong Basic and Applied Basic Research Foundation (grant number 2019A1515011366), Science and Technology Plan Project of Guangdong Province (No. 2019B030316001), Guangzhou Municipal Key Discipline in Medicine (2017-2019), and Science and Technology Plan Project of Guangzhou (202102020557). The funding source had no role in the study design, analysis or interpretation of data or in the preparation of the report or decision to publish.

Acknowledgments

The authors would like to acknowledge the participants in this study and the clinicians for their hard work and significant contribution.

Conflict of interest

The authors declare that the research was conducted in the absence of any commercial or financial relationships that could be construed as a potential conflict of interest.

Publisher's note

All claims expressed in this article are solely those of the authors and do not necessarily represent those of their affiliated organizations, or those of the publisher, the editors and the reviewers. Any product that may be evaluated in this article, or claim that may be made by its manufacturer, is not guaranteed or endorsed by the publisher.

Author disclaimer

The views expressed in this article are those of the authors and do not necessarily reflect the position or policy of the funders.

References

Aan, H. R. M., Collins, K. A., Murrough, J. W., Perez, A. M., Reich, D. L., Charney, D. S., et al. (2010). Safety and efficacy of repeated-dose intravenous ketamine for treatment-resistant depression. *Biol. Psychiatry* 67, 139–145. doi: 10.1016/j.biopsych.2009.08.038

Altinay, M., Karne, H., Beall, E., and Anand, A. (2016). Quetiapine extended release open-label treatment associated changes in amygdala activation and connectivity in anxious depression: An fMRI study. *J. Clin. Psychopharmacol.* 36, 562–571. doi: 10.1097/JCP.0000000000000600

Bebko, G., Bertocci, M., Chase, H., Dwojak, A., Bonar, L., Almeida, J., et al. (2015). Decreased amygdala-insula resting state connectivity in behaviorally and emotionally dysregulated youth. *Psychiatry Res.* 231, 77–86. doi: 10.1016/j.pscychresns.2014.10.015

Botteron, K. N., Raichle, M. E., Drevets, W. C., Heath, A. C., and Todd, R. D. (2002). Volumetric reduction in left subgenual prefrontal cortex in early onset depression. *Biol. Psychiatry* 51, 342–344. doi: 10.1016/S0006-3223(01)01280-X

Bracht, T., Linden, D., and Keedwell, P. (2015). A review of white matter microstructure alterations of pathways of the reward circuit in depression. *J. Affect. Disord.* 187, 45–53. doi: 10.1016/j.jad.2015.06.041

Bukalo, O., Pinard, C. R., Silverstein, S., Brehm, C., Hartley, N., Whittle, N., et al. (2015). Prefrontal inputs to the amygdala instruct fear extinction memory formation. *Sci. Adv.* 1:e1500251. doi: 10.1126/sciadv.1500251

Chen, C., Suckling, J., Ooi, C., Fu, C. H., Williams, S. C., Walsh, N. D., et al. (2008). Functional coupling of the amygdala in depressed patients treated with antidepressant medication. *Neuropsychopharmacology* 33, 1909–1918. doi: 10.1038/sj.npp.1301593

Chen, M., Li, C., Lin, W., Hong, C., Tu, P., Bai, Y., et al. (2018). Persistent antidepressant effect of low-dose ketamine and activation in the supplementary motor area and anterior cingulate cortex in treatment-resistant depression: A randomized control study. *J. Affect. Disord.* 225, 709–714. doi: 10.1016/j.jad.2017.09.008

Cheng, W., Rolls, E. T., Qiu, J., Xie, X., Lyu, W., Li, Y., et al. (2018). Functional connectivity of the human amygdala in health and in depression. *Soc. Cogn. Affect. Neurosci.* 13, 557–568. doi: 10.1093/scan/nsy032

Connolly, C. G., Ho, T. C., Blom, E. H., LeWinn, K. Z., Sacchet, M. D., Tymofiyeva, O., et al. (2017). Resting-state functional connectivity of the amygdala and longitudinal changes in depression severity in adolescent depression. *J. Affect. Disord.* 207, 86–94. doi: 10.1016/j.jad.2016.09.026

Dannlowski, U., Ohrmann, P., Konrad, C., Domschke, K., Bauer, J., Kugel, H., et al. (2009). Reduced amygdala-prefrontal coupling in major depression: Association with MAOA genotype and illness severity. *Int. J. Neuropsychopharmacol.* 12, 11–22. doi: 10.1017/S1461145708008973

Davis, M., and Whalen, P. J. (2001). The amygdala: Vigilance and emotion. *Mol. Psychiatry* 6, 13–34. doi: 10.1038/sj.mp.4000812

Dombrovski, A. Y., Siegle, G. J., Szanto, K., Clark, L., Reynolds, C. F., and Aizenstein, H. (2012). The temptation of suicide: Striatal gray matter, discounting of delayed rewards, and suicide attempts in late-life depression. *Psychol. Med.* 42, 1203–1215. doi: 10.1017/S0033291711002133

Duman, R. S., and Li, N. (2012). A neurotrophic hypothesis of depression: Role of synaptogenesis in the actions of NMDA receptor antagonists. *Philos. Trans. R. Soc. Lond. B Biol. Sci.* 367, 2475–2484. doi: 10.1098/rstb.2011.0357

Duman, R. S., and Monteggia, L. M. (2006). A neurotrophic model for stress-related mood disorders. *Biol. Psychiatry* 59, 1116–1127. doi: 10.1016/j.biopsych.2006.02.013

Engman, J., Linnman, C., Dijk, K. R., and Milad, M. R. (2016). Amygdala subnuclei resting-state functional connectivity sex and estrogen differences. *Psychoneuroendocrinology* 63, 34–42. doi: 10.1016/j.psyneuen.2015.09.012

Ferrari, A. J., Charlson, F. J., Norman, R. E., Patten, S. B., Freedman, G., Murray, C. J., et al. (2013). Burden of depressive disorders by country, sex, age, and year: Findings from the global burden of disease study 2010. *PLoS Med.* 10:e1001547. doi: 10.1371/journal.pmed.1001547

Fox, M. D., Zhang, D., Snyder, A. Z., and Raichle, M. E. (2009). The global signal and observed anticorrelated resting state brain networks. *J. Neurophysiol.* 101, 3270–3283. doi: 10.1152/jn.90777.2008

Fuchikami, M., Thomas, A., Liu, R., Wohleb, E. S., Land, B. B., DiLeone, R. J., et al. (2015). Optogenetic stimulation of infralimbic PFC reproduces ketamine's rapid and sustained antidepressant actions. *Proc. Natl. Acad. Sci. U.S.A.* 112, 8106–8111. doi: 10.1073/pnas.1414728112

Gallay, C. C., Forsyth, G., Can, A. T., Dutton, M., Jamieson, D., Jensen, E., et al. (2021). Six-week oral ketamine treatment for chronic suicidality is associated with increased grey matter volume. *Psychiatry Res. Neuroimaging* 317:111369. doi: 10.1016/j.pscychresns.2021.111369

Gifuni, A. J., Chakravarty, M. M., Lepage, M., Ho, T. C., Geoffroy, M., Lacourse, E., et al. (2021). Brain cortical and subcortical morphology in adolescents with depression and a history of suicide attempt. *J. Psychiatry Neurosci.* 46, E347–E357. doi: 10.1503/jpn.200198

Grabenhorst, F., and Rolls, E. T. (2011). Value, pleasure and choice in the ventral prefrontal cortex. *Trends Cogn. Sci.* 15, 56–67. doi: 10.1016/j.tics.2010.12.004

Kang, S., Na, K., Choi, J., Kim, J., Son, Y., and Lee, Y. J. (2017). Resting-state functional connectivity of the amygdala in suicide attempters with major depressive disorder. *Prog. Neuropsychopharmacol. Biol. Psychiatry* 77, 222–227. doi: 10.1016/j.pnpbp.2017.04.029

Keren, H., O'Callaghan, G., Vidal-Ribas, P., Buzzell, G. A., Brotman, M. A., Leibenluft, E., et al. (2018). Reward processing in depression: A conceptual and meta-analytic review across fMRI and EEG studies. *Am. J. Psychiatry* 175, 1111–1120. doi: 10.1176/appi.ajp.2018.17101124

Lally, N., Nugent, A. C., Luckenbaugh, D. A., Ameli, R., Roiser, J. P., and Zarate, C. A. (2014). Anti-anhedonic effect of ketamine and its neural correlates in treatment-resistant bipolar depression. *Transl. Psychiatry* 4:e469. doi: 10.1038/tp.2014.105

Li, N., Lee, B., Liu, R., Banasr, M., Dwyer, J. M., Iwata, M., et al. (2010). mTOR-dependent synapse formation underlies the rapid antidepressant effects of NMDA antagonists. *Science* 329, 959–964. doi: 10.1126/science.1190287

Li, N., Liu, R., Dwyer, J. M., Banasr, M., Lee, B., Son, H., et al. (2011). Glutamate N-methyl-D-aspartate receptor antagonists rapidly reverse behavioral and synaptic deficits caused by chronic stress exposure. *Biol. Psychiatry* 69, 754–761. doi: 10.1016/j.biopsych.2010.12.015

Likhtik, E., Stujenske, J. M., Topiwala, M. A., Harris, A. Z., and Gordon, J. A. (2014). Prefrontal entrainment of amygdala activity signals safety in learned fear and innate anxiety. *Nat. Neurosci.* 17, 106–113. doi: 10.1038/nn.3582

Liu, J., Fang, J., Wang, Z., Rong, P., Hong, Y., Fan, Y., et al. (2016). Transcutaneous vagus nerve stimulation modulates amygdala functional connectivity in patients with depression. *J. Affect. Disord.* 205, 319–326. doi: 10.1016/j.jad.2016.08.003

Marcantoni, W. S., Akoumba, B. S., Wassef, M., Mayrand, J., Lai, H., Richard-Devantoy, S., et al. (2020). A systematic review and meta-analysis of the efficacy of intravenous ketamine infusion for treatment resistant depression: January 2009–January 2019. *J. Affect. Disord.* 277, 831–841. doi: 10.1016/j.jad.2020.09.007

Marchand, W. R., Lee, J. N., Garn, C., Thatcher, J., Gale, P., Kreitschitz, S., et al. (2011). Striatal and cortical midline activation and connectivity associated with suicidal ideation and depression in bipolar II disorder. *J. Affect. Disord.* 133, 638–645. doi: 10.1016/j.jad.2011.04.039

McGrath, P. J., Stewart, J. W., Fava, M., Trivedi, M., Wisniewski, S., Nierenberg, A., et al. (2006). Tranylcypromine versus venlafaxine plus mirtazapine following three failed antidepressant medication trials for depression: A STAR*D report. *Am. J. Psychiatry* 163, 1531–1541. doi: 10.1176/ajp.2006.163.9.1531

Milak, M. S., Proper, C. J., Mulhern, S. T., Parter, A. L., Kegeles, L. S., Ogden, R. T., et al. (2016). A pilot in vivo proton magnetic resonance spectroscopy study of amino acid neurotransmitter response to ketamine treatment of major depressive disorder. *Mol. Psychiatry* 21, 320–327. doi: 10.1038/mp.2015.83

Morecraft, R. J., McNeal, D. W., Stilwell-Morecraft, K. S., Gedney, M., Ge, J., Schroeder, C. M., et al. (2007). Amygdala interconnections with the cingulate motor cortex in the rhesus monkey. *J. Comp. Neurol.* 500, 134–165. doi: 10.1002/cne.21165

Mrazek, D. A., Hornberger, J. C., Altar, C. A., and Degtiar, I. (2014). A review of the clinical, economic, and societal burden of treatment-resistant depression: 1996-2013. *Psychiatr. Serv.* 65, 977–987. doi: 10.1176/appi.ps.201300059

Murrough, J. W., Perez, A. M., Pillemer, S., Stern, J., Parides, M. K., Rot, M a, et al. (2013). Rapid and longer-term antidepressant effects of repeated ketamine infusions in treatment-resistant major depression. *Biol. Psychiatry* 74, 250–256. doi: 10.1016/j.biopsych.2012.06.022

Phelps, E. A., and LeDoux, J. E. (2005). Contributions of the amygdala to emotion processing: From animal models to human behavior. *Neuron* 48, 175–187. doi: 10.1016/j.neuron.2005.09.025

Price, J. L. (2003). Comparative aspects of amygdala connectivity. *Ann. N. Y. Acad. Sci.* 985, 50–58. doi: 10.1111/j.1749-6632.2003.tb07070.x

Rao, J., Liu, Z., Zhao, C., Wei, R., Zhao, W., Tian, P., et al. (2017). Ketamine changes the local resting-state functional properties of anesthetized-monkey brain. *Magn. Reson. Imaging* 43, 144–150. doi: 10.1016/j.mri.2017.07.025

Rolls, E. T. (2007). The representation of information about faces in the temporal and frontal lobes. *Neuropsychologia* 45, 124–143. doi: 10.1016/j.neuropsychologia.2006.04.019

Straube, T., and Miltner, W. H. (2011). Attention to aversive emotion and specific activation of the right insula and right somatosensory cortex. *Neuroimage* 54, 2534–2538. doi: 10.1016/j.neuroimage.2010.10.010

Tang, S., Lu, L., Zhang, L., Hu, X., Bu, X., Li, H., et al. (2018). Abnormal amygdala resting-state functional connectivity in adults and adolescents with major depressive disorder: A comparative meta-analysis. *EBioMedicine* 36, 436–445. doi: 10.1016/j.ebiom.2018.09.010

Tang, Y., Kong, L., Wu, F., Womer, F., Jiang, W., Cao, Y., et al. (2013). Decreased functional connectivity between the amygdala and the left ventral prefrontal cortex in treatment-naive patients with major depressive disorder: A resting-state functional magnetic resonance imaging study. *Psychol. Med.* 43, 1921–1927. doi: 10.1017/S0033291712002759

Trivedi, M. H., Rush, A. J., Wisniewski, S. R., Nierenberg, A. A., Warden, D., Ritz, L., et al. (2006). Evaluation of outcomes with citalopram for depression using measurement-based care in STAR*D: Implications for clinical practice. *Am. J. Psychiatry* 163, 28–40. doi: 10.1176/appi.ajp.163.1.28

Tzourio-Mazoyer, N., Landeau, B., Papathanassiou, D., Crivello, F., Etard, O., Delcroix, N., et al. (2002). Automated anatomical labeling of activations in SPM using a macroscopic anatomical parcellation of the MNI MRI single-subject brain. *Neuroimage* 15, 273–289. doi: 10.1006/nimg.2001.0978

van Heeringen, K., Bijttebier, S., Desmyter, S., Vervaet, M., and Baeken, C. (2014). Is there a neuroanatomical basis of the vulnerability to suicidal behavior? A coordinate-based meta-analysis of structural and functional MRI studies. *Front. Hum. Neurosci.* 8:824. doi: 10.3389/fnhum.2014.00824

Wilkinson, S. T., Ballard, E. D., Bloch, M. H., Mathew, S. J., Murrough, J. W., Feder, A., et al. (2018). The effect of a single dose of intravenous ketamine on suicidal ideation: A systematic review and individual participant data meta-analysis. *Am. J. Psychiatry* 175, 150–158. doi: 10.1176/appi.ajp.2017.17040472

Yang, J., Yin, Y., Svob, C., Long, J., He, X., Zhang, Y., et al. (2017). Amygdala atrophy and its functional disconnection with the cortico-striatal-pallidal-thalamic circuit in major depressive disorder in females. *PLoS One* 12:e0168239. doi: 10.1371/journal.pone.0168239

Zhang, R., Zhang, L., Wei, S., Wang, P., Jiang, X., Tang, Y., et al. (2020). Increased amygdala-paracentral lobule/precuneus functional connectivity associated with patients with mood disorder and suicidal behavior. *Front. Hum. Neurosci.* 14:585664. doi: 10.3389/fnhum.2020.585664

Zheng, W., Zhou, Y., Liu, W., Wang, C., Zhan, Y., Li, H., et al. (2018). Rapid and longer-term antidepressant effects of repeated-dose intravenous ketamine for patients with unipolar and bipolar depression. *J. Psychiatr. Res.* 106, 61–68. doi: 10.1016/j.jpsychires.2018.09.013

Zheng, W., Zhou, Y., Liu, W., Wang, C., Zhan, Y., Li, H., et al. (2019). Investigation of medical effect of multiple ketamine infusions on patients with major depressive disorder. *J. Psychopharmacol.* 33, 494–501. doi: 10.1177/0269881119827811

Zhou, Y., Wu, F., Liu, W., Zheng, W., Wang, C., Zhan, Y., et al. (2020). Volumetric changes in subcortical structures following repeated ketamine treatment in patients with major depressive disorder: A longitudinal analysis. *Transl. Psychiatry* 10:264. doi: 10.1038/s41398-020-00945-9

Zhou, Y., Zheng, W., Liu, W., Wang, C., Zhan, Y., Li, H., et al. (2018a). Antidepressant effect of repeated ketamine administration on kynurenine pathway metabolites in patients with unipolar and bipolar depression. *Brain Behav. Immun.* 74, 205–212. doi: 10.1016/j.bbi.2018.09.007

Zhou, Y., Zheng, W., Liu, W., Wang, C., Zhan, Y., Li, H., et al. (2018b). Neurocognitive effects of six ketamine infusions and the association with antidepressant response in patients with unipolar and bipolar depression. *J. Psychopharmacol.* 32, 1118–1126.

frontiers | Frontiers in Neuroscience

TYPE Original Research
PUBLISHED 03 February 2023
DOI 10.3389/fnins.2023.1078119

OPEN ACCESS

EDITED BY
Han Lv,
Department of Radiology, Beijing Friendship Hospital, Capital Medical University, China

REVIEWED BY
Chao Zhang,
The Affiliated Hospital of Xuzhou Medical University, China
Feng Liu,
Tianjin Medical University General Hospital, China
Kaizhong Xue,
Tianjin Medical University General Hospital, China

*CORRESPONDENCE
Ximing Wang
✉ wxming369@163.com

SPECIALTY SECTION
This article was submitted to Brain Imaging Methods, a section of the journal Frontiers in Neuroscience

RECEIVED 24 October 2022
ACCEPTED 17 January 2023
PUBLISHED 03 February 2023

CITATION
Li T, Du X, Zhang X, Dong A, Yuan X, Yu T, Diao R, Duan S, Shen Z, Yuan L and Wang X (2023) From study abroad to study at home: Spontaneous neuronal activity predicts depressive symptoms in overseas students during the COVID-19 pandemic. *Front. Neurosci.* 17:1078119. doi: 10.3389/fnins.2023.1078119

From study abroad to study at home: Spontaneous neuronal activity predicts depressive symptoms in overseas students during the COVID-19 pandemic

Tong Li[1], Xiaoyu Du[2], Xiang Zhang[3], Aiping Dong[4], Xianshun Yuan[1], Tianyi Yu[1], Ruiyuan Diao[1], Shuai Duan[1], Zijian Shen[1], Letian Yuan[1] and Ximing Wang[1]*

[1]Department of Radiology, Shandong Provincial Hospital Affiliated to Shandong First Medical University, Jinan, Shandong, China, [2]Faculty of Medicine, Dentistry and Health Sciences, The University of Melbourne, Melbourne, VIC, Australia, [3]College of Sports Medicine and Rehabilitation, Shandong Provincial Hospital Affiliated to Shandong First Medical University, Jinan, Shandong, China, [4]Department of Radiology, The Second Affiliated Hospital of Shandong University of Traditional Chinese Medicine, Jinan, China

The objective of this study was to evaluate symptoms of depression and anxiety as well as changes in spontaneous neuronal activity in college students studying abroad during the coronavirus 2019 (COVID-19) pandemic. We examined functional brain changes using resting-state functional magnetic resonance imaging (fMRI), the amplitude of low-frequency fluctuations (ALFF), and regional homogeneity (ReHo) in overseas students with enforced isolation due to the COVID-19 pandemic. Additionally, emotional assessments were administered to determine the severity of depression and anxiety. The questionnaire results showed that anxiety and depressive symptoms differed between overseas students (i.e., those attending an overseas college virtually) and local students (i.e., those attending a local college in person). The fMRI data revealed higher ALFF values in the bilateral superior medial frontal gyrus, bilateral pre-central gyrus, left insula, and left superior temporal gyrus as well as lower ALFF values in the bilateral paracentral lobule (supplementary motor area) in overseas students. Moreover, ReHo analysis also revealed significant differences between overseas students and local students. Compared with local students, overseas students showed significantly increased ReHo in the right inferior frontal and superior temporal gyri and decreased ReHo in the bilateral paracentral lobule, bilateral superior medial frontal gyrus (supplementary motor area), and bilateral pre-central gyrus. In addition, in overseas students, altered ReHo in the cluster including the left superior and medial frontal gyri, pre-central gyrus, and paracentral lobule was significantly positively correlated with Self-Rating Depression Scale scores. Thus, spontaneous brain activity in overseas students changed during the COVID-19 pandemic. This change in brain function might be related to depression and anxiety symptoms. These results suggest that mental health services are needed to decrease the risk of anxiety and depression among college students studying abroad during the COVID-19 pandemic.

KEYWORDS

COVID-19 pandemic, fMRI, overseas college students, spontaneous neuronal activity, depression

1. Introduction

Coronavirus disease 2019 (COVID-19) has swept across the world, leading to a global pandemic (Wang C. et al., 2020) and unprecedented changes in daily routines and social life. The impacts of this pandemic on people have been multifaceted, including short-term changes to physical, psychological, and emotional wellbeing as well as long-term changes in specific populations such as study-abroad students or older people. Students previously studying abroad had to stay in their home country because of the global lockdown initiated by various countries due to the COVID-19 pandemic, attending classes online. However, the pandemic and subsequent lockdowns imposed a variety of unprecedented challenges among study-abroad students. For example, these students had to receive online instruction in their university curricula and limit their daily activities to indoor areas (Shah et al., 2020); this lockdown stage limited interaction with peers and reduced sports activity. However, humans are inherently social, and the formation of social bonds is fundamental to survival as well as healthy cognitive, emotional, hormonal, and immune functions (Smith, 2012). Indeed, universities are one of the most important social environments. Unfortunately, during the COVID-19 pandemic, many college students have been unable to attend school, which has limited their interactions with peers, in addition to the gap imposed by social distancing measures. Lee et al. found that school routines played a positive role in coping specifically for young people with mental health issues (Lee, 2020). Moreover, social touch is essential for the healthy development of cognitive function, emotions, attachments, and relationships (Cascio et al., 2019). Wang et al. reported that periods without school are associated with increased screen time, irregular sleep patterns, and decreased physical activity (Wang G. et al., 2020). Therefore, school life is important for college students.

Students, especially overseas students, experienced enforced isolation during the lockdowns; their mental health might have been altered due to the COVID-19 pandemic. Recent studies have also indicated possible short-term effects of exposure to COVID-related stressors at this stage of life, including distress and hopelessness as well as irregular food intake, and possible long-term consequences, including altered brain circuitry, lack of emotional processing, psychiatric disorders, and suicidal thoughts (de Figueiredo et al., 2021). Evidence has suggested that the COVID-19 pandemic has generally increased levels of stress and depression among college students (Lee, 2020); moreover, the proportion of individuals reporting depression, anxiety, and/or suicidal thoughts is alarming (Wang G. et al., 2020; Wang C. et al., 2020; de Figueiredo et al., 2021). An online questionnaire revealed that pandemic-related factors might be associated with a higher risk of depressive symptoms among college students in China (Cascio et al., 2019). Therefore, the current study focused on the impact of the COVID-19 pandemic on the mental health of overseas college students, especially students who planned to continue studying abroad but were prevented by the closure of educational activities at universities in other countries.

Structural alteration of the brain is usually considered a long-term result of neural plasticity. Resting-state functional magnetic resonance imaging (rs-fMRI) is generally recognized as a non-invasive neuroimaging technique and is widely utilized to investigate resting-state brain activity *via* blood oxygen level-dependent signals (Fox and Raichle, 2007). Hence, resting-state brain activity serves as a baseline, reflecting spontaneous neural activity, and rs-fMRI data provide a more feasible method of assessing the brain's functional response to instantaneous extrinsic behaviors. The amplitude of low-frequency fluctuations (ALFF) and regional homogeneity (ReHo) are common measures used to describe regional properties of brain activity in rs-fMRI studies (Zang et al., 2004; Yu-Feng et al., 2007). ALFF values are used to indicate the intensity of neural activity at the single-voxel level (Yu-Feng et al., 2007), while ReHo values are used to characterize the synchronization of fluctuations of a voxel with its neighboring voxels (Zang et al., 2004). These two metrics are two data-driven approaches widely established as having high reliability. ReHo may be more sensitive to regional changes than ALFF. However, ALFF and ReHo complement each other in terms of detecting global spontaneous activity (An et al., 2013). Therefore, the ALFF and ReHo methods might be jointly applied to collect more data in the field of cognitive neuroscience.

Here, we identified differences in spontaneous whole-brain activity between college students who planned to continue to study abroad but were prevented by the closure of educational activities in foreign universities (overseas students) and those who did not originally plan to study abroad and attended school in China (local students). We collected rs-fMRI data from these two groups to analyze ALFF and ReHo values. Furthermore, the relationship between brain regions with significant differences in these values and behavioral data was analyzed. We specifically hypothesized that the activity of neural circuits would be differentially altered in the two groups. We hypothesized that college students may have experienced not only short-term but also long-term consequences of COVID-19 stressors. In the context of COVID-19 lockdowns, we predicted that the stress of social isolation and other pandemic-related adversities affected the brains of these students. However, the precise changes in the brains of college students, especially in key regions associated with emotion regulation, empathy, and decision-making skills, remain unclear.

2. Materials and methods

2.1. Subjects

We recruited 51 subjects by posting physical and digital (social media) advertizements. One group was comprised of 25 overseas students who had studied abroad for over 1 year (age, mean ± standard deviation: 22.68 ± 3.38 years). If there was no COVID-19 pandemic, they would have continued to study abroad. However, because international flights were halted to prevent imported cases of COVID-19, these students had to stay in China and take online classes. In addition, we recruited 26 local college students (age, mean ± standard deviation: 21.69 ± 1.78 years) attending universities in China, matched by age and sex. No subjects had a history of neurological, medical, or psychiatric conditions or a history of severe head trauma according to screening; all subjects were screened for MRI contraindications after providing written consent to participate. The Chinese Hand Preference Questionnaire, adapted from the Edinburgh Handedness Inventory, was used to screen participants for handedness; only right-handed individuals were included. Clinical and demographic data for the two groups are shown in **Table 1**. **Figure 1** shows the participant recruitment and data collection procedures.

All procedures were approved by the Ethics Committee of Shandong Provincial Hospital Affiliated to Shandong First Medical University. Each volunteer signed an informed consent form, which was approved by the committee. All methods in our study were carried out in accordance with the principles outlined in the Declaration of Helsinki.

2.2. Questionnaire analysis

The Beck Depression Inventory (BDI) (Beck et al., 1988b) was originally developed by Beck et al. (1961). This questionnaire was designed to assess the severity of depressive symptoms. Participants rate each item on a four-point scale. Evidence indicates that the reliability and validity of the Chinese version of the BDI scale are acceptable (Sun et al., 2017). The Beck Anxiety Inventory (BAI) (Beck et al., 1988a) is a scale measuring the severity of self-reported anxiety symptoms. Participants are asked to rate symptoms of anxiety (e.g., "fear of losing control" and "racing or pounding heart") using a four-point scale. The Chinese version of the BAI was demonstrated to provide satisfactory reliability and convergent validity on psychometric indices (Liang et al., 2018). In addition, Zung's Self-Rating Depression Scale (SDS) (Zung, 1965) and Self-Rating Anxiety Scale (SAS) (Zung, 1971) are two widely used self-report scales that assess depression and anxiety. The two scales cover both affective and somatic symptoms. Participants are asked to answer the questions based on their experiences and feelings using a four-point Likert scale ranging from 1 to 4. The SAS and SDS have good internal consistency and can be used to measure depression and anxiety. Moreover, previous studies have used the SAS (Wang Z. H. et al., 2020), SDS (Tong Li et al., 2021), BAI and BDI (Ganji et al., 2022) to assess the impact of the COVID-19 pandemic on the mental health of college students. Hence, in the current study, all participants completed these scales to assess the severity of symptoms of depression and anxiety. For all measures, descriptive statistics were performed. Subsequently, we conducted independent-sample t tests to compare overseas students and local students. Significant results were reported at $P < 0.05$.

2.3. MRI image acquisition

Magnetic resonance imaging scans were performed on a Siemens 3.0 T Prisma MR system at the Shandong Provincial Hospital Affiliated to Shandong First Medical University (Jinan, Shandong, China). We used a 64-channel head coil for whole-brain scanning. Anatomical images were collected using a high-resolution T1-weighted 3-dimensional magnetization-prepared rapid-acquisition gradient-echo pulse sequence with the following acquisition parameters: repetition time (TR) = 2,530 ms, echo time (TE) = 2.98 ms, inversion time (TI) = 1,100 ms, field of view (FOV) = 256 mm, acquisition matrix = 256 × 256 mm^2, flip angle = 7°, and slice number = 192 slices. During the rs-fMRI scan, a T2*-weighted gradient-echo echo-planar-imaging (GRE-EPI) sequence, which is sensitive to blood oxygen level-dependent (BOLD) signals, with the following parameters was utilized: TR = 2,000 ms, TE = 30 ms, FOV = 220 × 220 mm^2, matrix size = 64 × 64, slice thickness = 3.5 mm, flip angle = 90°, slices = 33, transverse orientation, and 25% distance factor. A total of 210 whole-brain volumes were acquired. All participants were instructed to relax with their eyes closed and not think of anything in particular during the entire scan session.

2.4. MRI data analysis

2.4.1. Data pre-processing

MRI data were analyzed using a toolbox for Data Processing and Analysis for Brain Imaging (DPABI[1]) (Yan et al., 2016) and Statistical Parametric Mapping software (SPM12[2]) based on MATLAB 2021a. Data analysis included pre-processing and statistical analysis. Pre-processing involved the following steps. First, the DICOM MRI data format was converted to NIFTI images. The initial 10 time points were discarded to allow for steady-state magnetization, and the remaining volumes underwent slice-timing correction and spatial realignment to correct for head motion using a six-parameter (rigid body) linear transformation; participants with head movement > 2 mm or head rotation > 2° were excluded. Next, the mean functional images were coregistered to the high-resolution T1-weighted images, and the high-resolution T1-weighted images were segmented into gray matter, white matter and cerebrospinal fluid (Ashburner and Friston, 2005). These individual images were spatially normalized to the Montreal Neurological Institute template with diffeomorphic anatomical registration through the exponentiated lie algebra (DARTEL) (Ashburner, 2007) tool (resolution: 3 mm × 3 mm × 3 mm). This step was followed by regressing nuisance variables, including the time series of six head motion parameters, the white matter signal and the cerebral spinal fluid signal, using a general linear model.

2.4.2. ALFF analysis

ALFF analysis was performed with DPABI (Yan et al., 2016). For ALFF values, the generated images were processed using spatial smoothing with a 6 mm FWHM Gaussian kernel. Then, we transformed each voxel of the filtered time series into the frequency domain with a fast Fourier transform, and the power spectrum was calculated. After calculating the square root of the signal across 0.01–0.1 Hz for each voxel, subtracting the average value, and dividing by the whole-brain voxel deviation, the ALFF values for all participants were converted to an m-distribution to achieve standardization. Finally, standardized whole-brain ALFF maps were obtained for each participant (Zang et al., 2007).

2.4.3. ReHo analysis

After a 0.01–0.1 Hz bandpass filter was applied, the unsmoothed pre-processed data were used for ReHo calculations. Kendall's coefficient of concordance (KCC) was applied to calculate the synchronicity of the time series of the fMRI signal of this voxel and those of its adjacent 26 voxels. Each individual ReHo map was generated by calculating the KCC using a voxel wise method. Each individual's ReHo map was converted into a standard z score map by subtracting the global mean and dividing by the standard deviation within the whole-brain ReHo map. Then, a 6 mm FWHM Gaussian kernel was used to complete the smoothing process to reduce noise.

1 http://rfmri.org/dpabi

2 http://www.fil.ion.ucl.ac.uk/spm/software/spm12

Finally, the ReHo value of each participant was divided by the average ReHo value of all participants in each group.

2.4.4. Statistical analysis

After pre-processing, statistical analysis was performed using SPM12. The two-sample *t* test was used to determine brain regions that significantly differed in ALFF and ReHo. Note that age, sex, education level, mean frame displacement (FD), and physical activity were regressed in the between-group comparison. An initial threshold of $P < 0.001$ (uncorrected) was applied, and results that survived family wise error (FWE) correction at a cluster-level threshold of $P < 0.05$ were reported.

TABLE 1 Demographic and questionnaire data of college students in the overseas and local groups.

Dimensions	Overseas	Local	*T* value	*P* value (two-tailed)
N	*n* = 25	*n* = 26	–	–
Age	22.47 ± 3.38	21.69 ± 1.78	1.034	0.306
Education (years)	14.12 ± 1.48	14.73 ± 0.53	1.89	0.069
Parental companionship (hours)	5.10 ± 6.89	7.44 ± 7.54	−1.13	0.264
Sports activity (hours)	1.07 ± 1.33	1.00 ± 0.69	0.224	0.824
Online classes (hours)	2.83 ± 1.13	4.08 ± 0.97	−4.194	**0.001**
Sleep (hours)	7.67 ± 1.42	7.74 ± 0.69	−0.231	0.818
BDI score	7.13 ± 5.17	1.62 ± 2.16	4.988	**0.001**
SDS score	0.22 ± 0.12	0.16 ± 0.10	1.927	**0.030**
BAI score	30.63 ± 9.65	26.08 ± 4.26	2.186	**0.017**
SAS score	33.29 ± 7.01	29.81 ± 4.98	2.038	**0.023**

Data are presented as the mean ± standard deviation (SD). Comparisons were calculated using independent sample *t* tests, and the significance threshold was set at $P < 0.05$. BDI, Beck Depression Inventory; BAI, Beck Anxiety Inventory; SDS, Self-Rating Depression Scale; SAS, Self-Rating Anxiety Scale. Bold values indicate the $P < 0.05$.

TABLE 2 Brain regions with significant alterations in ALFF and ReHo values between overseas students and local students.

Group	*N*	Regions	BA	Voxels	*X*	*Y*	*Z*	*T*	P_{FWE}
ALFF									
	1	Left insula Left superior temporal gyrus	13	70	−42	9	−9	5.70	0.011
Overseas > Local (increases)	2	Left inferior frontal gyrus Left superior temporal gyrus	45/47	126	−57	18	−9	5.45	0.001
	3	Right medial frontal gyrus Right superior frontal gyrus	10	60	6	63	15	5.15	0.024
	4	Right superior temporal gyrus Right inferior frontal gyrus	38/47	62	57	24	−9	4.05	0.020
Overseas < Local (decreases)	1	Left and right medial frontal gyrus Left and right paracentral lobule Left and right pre-central gyrus Left and right post-central gyrus (supplementary motor area)	6/4	158	0	−21	69	4.94	0.001
	2	Right cerebellum posterior lobe		92	42	−78	−54	4.13	0.002
ReHo									
Overseas < Local (increases)	1	Right inferior frontal gyrus Right superior temporal gyrus	47	124	57	30	−24	5.59	0.001
Overseas > Local (decreases)	1	Left pre-central gyrus Left middle frontal gyrus Left paracentral lobule Left medial frontal gyrus (supplementary motor area) Left superior frontal gyrus	4/3/6	111	−12	−12	69	6.06	0.001
	2	Right pre-central gyrus Right medial frontal gyrus (supplementary motor area) Right superior frontal gyrus	6	121	27	−21	69	4.76	0.001

This table indicates the changes in ALFF and ReHo for the two groups. X, Y, Z = MNI coordinates. The results reported are significant at the peak level with $P < 0.001$ (uncorrected) and at the cluster level with $P < 0.05$ (FWE-corrected).

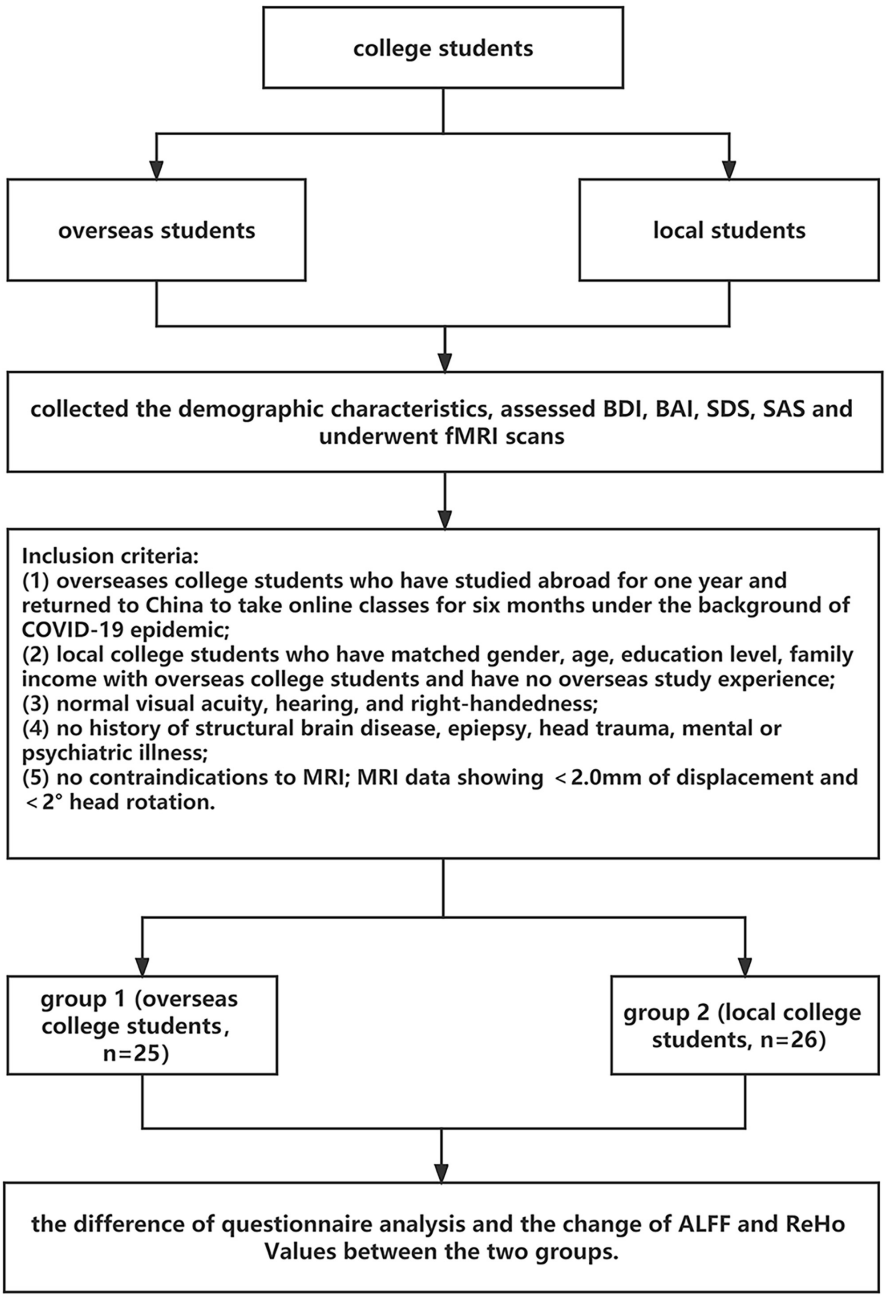

FIGURE 1
Flowchart of participant recruitment and data collection.

To investigate the relationship of differences in ALFF and ReHo values with behavioral scores, partial correlation analysis was performed using SPSS 24.0 (SPSS, Inc., Chicago, IL, USA). Age, years of education, sleep duration, duration of online classes, and duration of sports activity were regressed out. First, the mean ALFF and ReHo values of brain regions with significant differences were individually extracted. Then, partial correlation analyses were applied to examine possible associations of these ALFF and ReHo values with behavioral scores. The statistical threshold was set at $P < 0.05$ using a Benjamini-Hochberg false discovery rate (FDR) correction with MATLAB to explore the most significant correlations.

3. Results

3.1. Demographic and questionnaire data

The demographic characteristics of overseas students and local students are listed in Table 1, including the means and standard deviation for age, years of education, duration of parental accompaniment, duration of physical activity, duration of online classes, duration of sleep and scores on each questionnaire. As shown in Table 1, significant group differences were found in the online class duration, BDI score, SDS score, BAI score, and SAS score ($P < 0.05$).

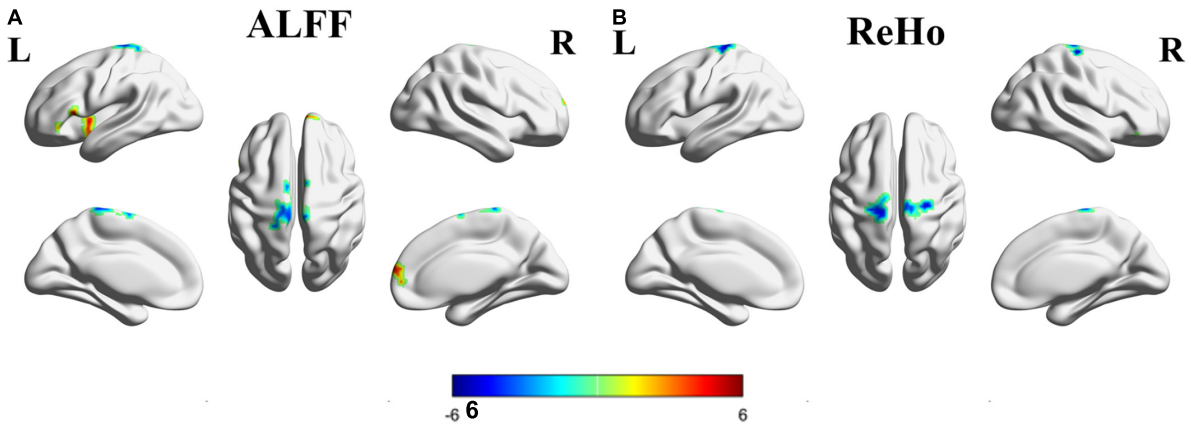

FIGURE 2
Brain regions with significantly different ALFF and ReHo values between the overseas group and the local group. Colors (blue-red) represent decreased and increased ALFF or ReHo values. L, left; R, right; **(A)** ALFF; **(B)** ReHo.

Compared with local students, overseas students had significantly higher BDI, SDS, and BAI scores.

3.2. ALFF and ReHo results

Differences in ALFF and ReHo values (FWE corrected $P < 0.05$) between overseas students and local students are shown in Table 2 and Figure 1. The following brain regions had significantly higher ALFF values in overseas students than in local students: the bilateral superior frontal gyrus, bilateral superior temporal gyrus, bilateral inferior frontal gyrus, left insula, right superior frontal gyrus, and right medial frontal gyrus. In contrast, the ALFF values of the bilateral paracentral lobule (in the supplementary motor area), bilateral pre-central gyrus, bilateral post-central gyrus, and right cerebellum posterior lobe were lower in overseas students.

Compared to local students, overseas students showed significantly lower ReHo values in the bilateral frontal lobules, including the superior frontal gyrus, medial frontal gyrus (in the supplementary motor area), pre-central gyrus, paracentral lobule, and middle frontal gyrus. However, overseas students showed significantly higher ReHo values in right inferior frontal gyrus and superior temporal gyrus (Figure 2 and Table 2). In summary, compared to local students, overseas students had significantly altered ALFF and ReHo values around the frontal pole. The surviving clusters represent a significant difference at a peak level of $P < 0.001$ and cluster level of $P < 0.05$ with FWE corrections.

3.3. Correlations of MRI data and questionnaire data

Partial correlation analysis was applied to investigate correlations of anxiety and depressive symptoms with spontaneous brain activity. In overseas students, the decreased ReHo values in the cluster ($x = -18$, y $= -27$, $z = 57$, $r = 0.582$, $P = 0.036$) including the left superior and medial frontal gyri, pre-central gyrus, and paracentral lobule were significantly positively correlated with SDS scores (Figure 3). However, in local students, no significant relationships were found between ALFF or ReHo values and depression or anxiety scores.

4. Discussion

To the best of our knowledge, this is the first rs-fMRI study to investigate differences in spontaneous brain activity between overseas students and local students against the background of the COVID-19 pandemic. Our main findings are as follows. (a) Compared with local students, overseas students had altered ALFF and ReHo values in the following regions: the bilateral frontal lobule, including the medial frontal gyrus, middle frontal gyrus, superior frontal gyrus, pre-central gyrus, and paracentral lobule. (b) In overseas students, the altered ReHo values in the cluster including the left superior and medial frontal gyri, pre-central gyrus, and paracentral lobule were significantly positively correlated with SDS scores.

Compared to local students, overseas students had notably altered ALFF and ReHo values in the bilateral frontal lobule. Abnormalities in this region, which includes the prefrontal cortex (Ye et al., 2012), middle frontal gyrus (Zhang et al., 2011), and insula (Avery et al., 2014), have been frequently reported in fMRI studies of major depressive disorder. Previous studies have indicated that the middle frontal gyrus is involved in regulating the strength of reactions to emotional stimuli and that the superior frontal gyrus is a core brain region related to emotion regulation processes, especially regarding feelings of amusement (Frank et al., 2014; Zhang et al., 2021). According to these findings, alterations to these regions might influence the development of depressive symptoms. In addition, these regions are crucial areas of the dorsolateral prefrontal cortex, which has been closely linked to depression. For example, Kaiser et al. suggested that higher functional activity in the dorsolateral prefrontal cortex is frequently observed in major depressive disorder (Kaiser et al., 2015). Furthermore, the prefrontal cortex is a critical region for attention regulation and emotional judgment. The prefrontal cortex is the primary region targeted by repetitive transcranial magnetic stimulation to treat young patients with treatment-resistant depression (Zheng et al., 2010). These results demonstrate that dysfunction in the prefrontal cortex might appear during the early stage of depression. In the current study, we

10.3389/fnins.2023.1078119

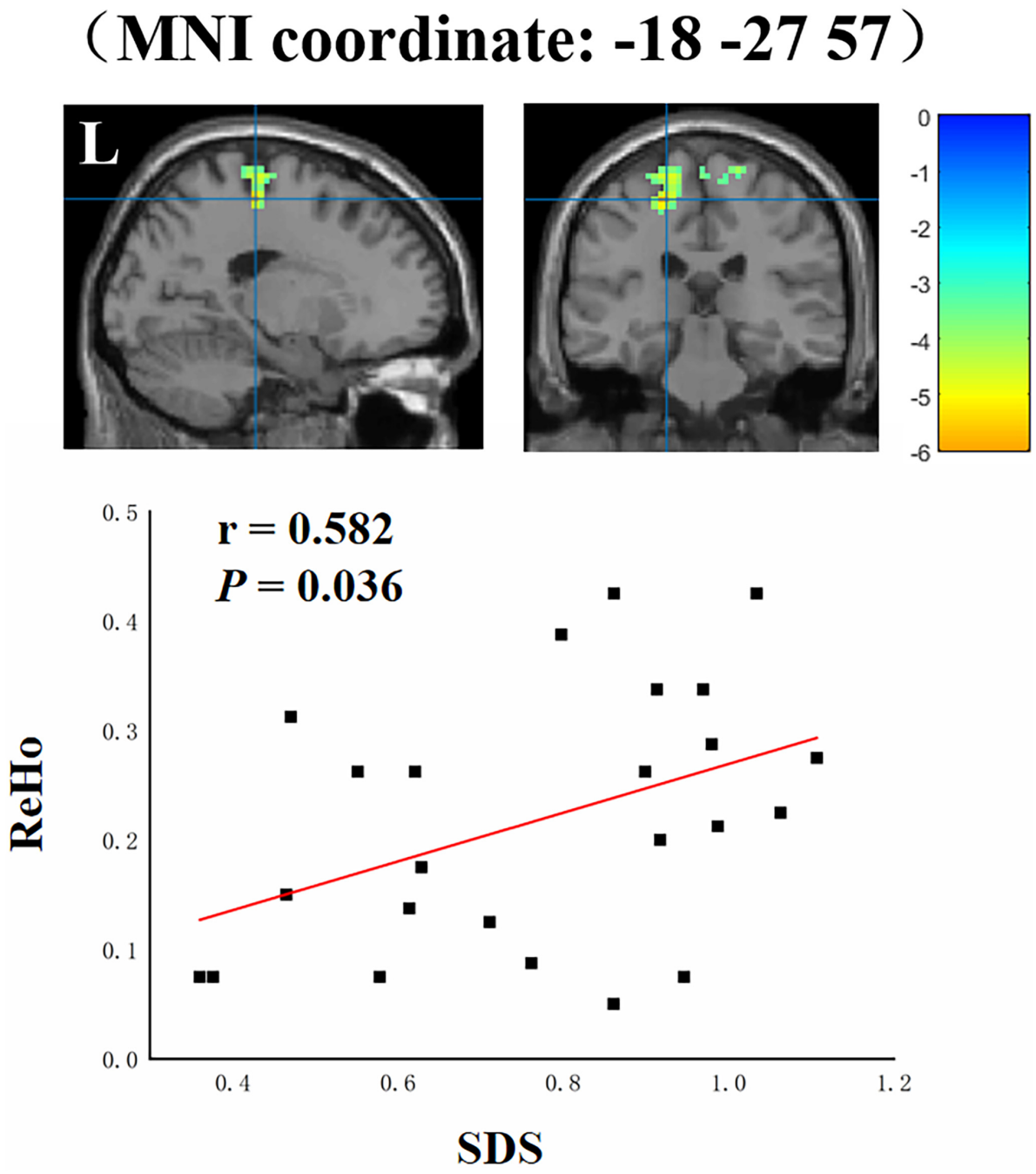

FIGURE 3
Correlations between ReHo values and SDS scores in overseas students. L, left.

found that the superior and medial frontal gyri and pre-central gyrus (including the inferior frontal junction) displayed altered spontaneous neural activity in overseas students during the COVID-19 pandemic, suggesting abnormal brain function in these areas. We compared these results to those of previous studies on depression or anxiety and found that similar brain changes as those in individuals with depression or anxiety occurred in overseas students. Thus, the COVID-19 pandemic potentially imposed additional stressors on college students during this challenging time, leading to depression or anxiety. These findings can enhance the understanding of regions initially impaired in anxiety disorders and depression. The altered ALFF and ReHo values further suggest dysfunction in emotion-related regions in overseas students; functional impairments in these regions might directly influence the inappropriate responses to emotional events observed in overseas students.

In the current study, anxiety and depression scores were significantly higher in overseas students than in local students. These scales measure symptoms of depression and anxiety. The group differences in questionnaire scores suggest that overseas students might have a higher prevalence of anxiety and depressive symptoms than local students. These results suggest that overseas students tended to experience depression due to the COVID-19 pandemic. This finding is consistent with studies that also found poor mental

health among college students during the COVID-19 pandemic (Son et al., 2020; Copeland et al., 2021).

In addition, we also found a significant positive correlation between depression severity and alterations in activity in the cluster including the left superior and medial frontal gyri, pre-central gyrus, and paracentral lobule. These regions are associated with emotion regulation (Rive et al., 2013). Increased spontaneous neural activity in these regions and a positive correlation between this activity and depression severity were found in overseas students compared to local students. These results further imply that dysfunction of the prefrontal-cortical circuit is a key factor that leads to depression.

Although our research revealed that spontaneous brain activity in overseas students changed during the COVID-19 pandemic, this study had several limitations. First, the sample size was relatively small, and more subjects and observations are needed to verify the current results. Second, this study had a cross-sectional design. In future studies, we will verify these changes using a longitudinal design. Third, future experiments should control for confounding factors (e.g., college student majors) to confirm that differences in spontaneous brain activity between overseas students and local students are linked to COVID-19 pandemic.

In summary, we observed altered patterns of brain activity in overseas students according to rs-fMRI data, with increased ALFF mainly in the PFC and decreased ALFF in the paracentral lobule. The vulnerability of overseas students to depression and anxiety is potentially related to a concerted mechanism that involves distinct regional alterations in resting-state activity in the mPFC and dlPFC. Our findings of abnormal resting-state activity in a unique frontoposterior pattern may enhance the current understanding of the neurobiological underpinnings of mental disorders in overseas students during the COVID-19 pandemic. Overall, this study of local spontaneous brain activity provided evidence of differences between overseas students and local students. In future work, we will use connectivity measures to explore the interactions among brain regions.

Data availability statement

The original contributions presented in this study are included in the article/supplementary material, further inquiries can be directed to the corresponding author.

Ethics statement

The studies involving human participants were reviewed and approved by Shandong Provincial Hospital Affiliated to Shandong First Medical University. The patients/participants provided their written informed consent to participate in this study.

Author contributions

TL, XD, and XW contributed to the study conception, design, material preparation, data analysis, and writing draft. XD and XZ contributed to revising and writing manuscript. AD, XY, TY, RD, SD, ZS, and LY were performed data collection. All authors read and approved the final manuscript.

Funding

This work was financially supported by the National Natural Science Foundation of China (Grant Nos. 81871354, 81571672, and 81901740), the Taishan Scholars Project of Shandong province, and the Academic Promotion Program of Shandong First Medical University.

Acknowledgments

We thank all participants involved in this research.

Conflict of interest

The authors declare that the research was conducted in the absence of any commercial or financial relationships that could be construed as a potential conflict of interest.

Publisher's note

References

An, L., Cao, Q. J., Sui, M. Q., Sun, L., Zou, Q. H., Zang, Y. F., et al. (2013). Local synchronization and amplitude of the fluctuation of spontaneous brain activity in attention-deficit/hyperactivity disorder: A resting-state fMRI study. *Neurosci. Bull.* 29, 603–613. doi: 10.1007/s12264-013-1353-8

Ashburner, J. (2007). A fast diffeomorphic image registration algorithm. *Neuroimage* 38, 95–113. doi: 10.1016/j.neuroimage.2007.07.007

Ashburner, J., and Friston, K. J. (2005). Unified segmentation. *Neuroimage* 26, 839–851. doi: 10.1016/j.neuroimage.2005.02.018

Avery, J. A., Drevets, W. C., Moseman, S. E., Bodurka, J., Barcalow, J. C., and Simmons, W. K. (2014). Major depressive disorder is associated with abnormal interoceptive activity and functional connectivity in the insula. *Biol. Psychiatry* 76, 258–266.

Beck, A. T., Steer, R. A., and Carbin, M. G. (1988b). Psychometric properties of the beck depression inventory: Twenty-five years of evaluation. *Clin. Psychol. Rev.* 8, 77–100.

Beck, A. T., Epstein, N., Brown, G., and Steer, R. A. (1988a). An inventory for measuring clinical anxiety: Psychometric properties. *J. Consult. Clin. Psychol.* 56, 893–897. doi: 10.1037//0022-006x.56.6.893

Beck, A. T., Ward, C., and Mendelson, M. (1961). Beck depression inventory (BDI). *Arch. Gen. Psychiatry* 4, 561–571.

Cascio, C. J., Moore, D., and McGlone, F. (2019). Social touch and human development. *Dev. Cogn. Neurosci.* 35, 5–11. doi: 10.1016/j.dcn.2018.04.009

Copeland, W. E., McGinnis, E., Bai, Y., Adams, Z., Nardone, H., Devadanam, V., et al. (2021). Impact of COVID-19 pandemic on college student mental health and wellness. *J. Am. Acad. Child Adolesc. Psychiatry* 60, 134–141.e2. doi: 10.1016/j.jaac.2020.08.466

de Figueiredo, C. S., Sandre, P. C., Portugal, L. C. L., Mazala-de-Oliveira, T., da Silva Chagas, L., Raony, I., et al. (2021). COVID-19 pandemic impact on children and adolescents' mental health: Biological, environmental, and social factors. *Prog. Neuropsychopharmacol. Biol. Psychiatry* 106:110171. doi: 10.1016/j.pnpbp.2020.110171

Fox, M. D., and Raichle, M. E. (2007). Spontaneous fluctuations in brain activity observed with functional magnetic resonance imaging. *Nat. Rev. Neurosci.* 8, 700–711. doi: 10.1038/nrn2201

Frank, D. W., Dewitt, M., Hudgens-Haney, M., Schaeffer, D. J., Ball, B. H., Schwarz, N. F., et al. (2014). Emotion regulation: Quantitative meta-analysis of functional activation and deactivation. *Neurosci. Biobehav. Rev.* 45, 202–211. doi: 10.1016/j.neubiorev.2014.06.010

Ganji, K. K., Alam, M. K., Siddiqui, A. A., Munisekhar, M. S., and Alduraywish, A. (2022). COVID-19 and stress: An evaluation using Beck's depression and anxiety inventory among college students and faculty members of Jouf University. *Work* 72, 399–407. doi: 10.3233/wor-210346

Kaiser, R. H., Andrews-Hanna, J. R., Wager, T. D., and Pizzagalli, D. A. (2015). Large-scale network dysfunction in major depressive disorder: A meta-analysis of resting-state functional connectivity. *JAMA Psychiatry* 72, 603–611.

Lee, J. (2020). Mental health effects of school closures during COVID-19. *Lancet Child Adolesc. Health* 4:421. doi: 10.1016/s2352-4642(20)30109-7

Li, Y., Wang, A., Wu, Y., Han, N., and Huang, H. (2021). Impact of the COVID-19 Pandemic on the mental health of college students: A systematic review and meta-analysis. *Front. Psychol.* 12:669119. doi: 10.3389/fpsyg.2021.669119

Liang, Y., Wang, L., and Zhu, J. (2018). Factor structure and psychometric properties of Chinese version of Beck anxiety inventory in Chinese doctors. *J. Health Psychol.* 23, 657–666. doi: 10.1177/1359105316658971

Rive, M. M., van Rooijen, G., Veltman, D. J., Phillips, M. L., Schene, A. H., and Ruhe, H. G. (2013). Neural correlates of dysfunctional emotion regulation in major depressive disorder. A systematic review of neuroimaging studies. *Neurosci. Biobehav. Rev.* 37, 2529–2553. doi: 10.1016/j.neubiorev.2013.07.018

Shah, K., Kamrai, D., Mekala, H., Mann, B., Desai, K., and Patel, R. S. (2020). Focus on mental health during the coronavirus (COVID-19) pandemic: Applying learnings from the past outbreaks. *Cureus* 12:e7405. doi: 10.7759/cureus.7405

Smith, K. (2012). Brain imaging: fMRI 2.0. *Nature* 484, 24–26. doi: 10.1038/484024a

Son, C., Hegde, S., Smith, A., Wang, X., and Sasangohar, F. (2020). Effects of COVID-19 on college students' mental health in the United States: Interview survey study. *J. Med. Internet Res.* 22:e21279. doi: 10.2196/21279

Sun, X. Y., Li, Y. X., Yu, C. Q., and Li, L. M. (2017). [Reliability and validity of depression scales of Chinese version: A systematic review]. *Zhonghua Liu Xing Bing Xue Za Zhi* 38, 110–116. doi: 10.3760/cma.j.issn.0254-6450.2017.01.021

Wang, C., Horby, P. W., Hayden, F. G., and Gao, G. F. (2020). A novel coronavirus outbreak of global health concern. *Lancet* 395, 470–473. doi: 10.1016/S0140-6736(20)30185-9

Wang, G., Zhang, Y., Zhao, J., Zhang, J., and Jiang, F. (2020). Mitigate the effects of home confinement on children during the COVID-19 outbreak. *Lancet* 395, 945–947. doi: 10.1016/s0140-6736(20)30547-x

Wang, X., Hegde, S., Son, C., Keller, B., Smith, A., and Sasangohar, F. (2020). Investigating mental health of US college students during the COVID-19 pandemic: Cross-sectional survey study. *J. Med. Internet Res.* 22:e22817. doi: 10.2196/22817

Wang, Z. H., Yang, H. L., Yang, Y. Q., Liu, D., Li, Z. H., Zhang, X. R., et al. (2020). Prevalence of anxiety and depression symptom, and the demands for psychological knowledge and interventions in college students during COVID-19 epidemic: A large cross-sectional study. *J. Affect. Disord.* 275, 188–193. doi: 10.1016/j.jad.2020.06.034

Yan, C. G., Wang, X. D., Zuo, X. N., and Zang, Y. F. (2016). DPABI: Data processing & analysis for (Resting-State) brain imaging. *Neuroinformatics* 14, 339–351. doi: 10.1007/s12021-016-9299-4

Ye, T., Peng, J., Nie, B., Gao, J., Liu, J., Li, Y., et al. (2012). Altered functional connectivity of the dorsolateral prefrontal cortex in first-episode patients with major depressive disorder. *Eur. J. Radiol.* 81, 4035–4040. doi: 10.1016/j.ejrad.2011.04.058

Yu-Feng, Z., Yong, H., Chao-Zhe, Z., Qing-Jiu, C., Man-Qiu, S., Meng, L., et al. (2007). Altered baseline brain activity in children with ADHD revealed by resting-state functional MRI. *Brain Dev.* 29, 83–91.

Zang, Y. F., He, Y., Zhu, C. Z., Cao, Q. J., Sui, M. Q., Liang, M., et al. (2007). Altered baseline brain activity in children with ADHD revealed by resting-state functional MRI. *Brain Dev.* 29, 83–91.

Zang, Y. F., Jiang, T. Z., Lu, Y. L., He, Y., and Tian, L. X. (2004). Regional homogeneity approach to fMRI data analysis. *Neuroimage* 22, 394–400. doi: 10.1016/j.neuroimage.2003.12.030

Zhang, B., Qi, S., Liu, S., Liu, X., Wei, X., and Ming, D. (2021). Altered spontaneous neural activity in the precuneus, middle and superior frontal gyri, and *Hippocampus* in college students with subclinical depression. *BMC Psychiatry* 21:280. doi: 10.1186/s12888-021-03292-1

Zhang, J., Wang, J., Wu, Q., Kuang, W., Huang, X., He, Y., et al. (2011). Disrupted brain connectivity networks in drug-naive, first-episode major depressive disorder. *Biol. Psychiatry* 70, 334–342. doi: 10.1016/j.biopsych.2011.05.018

Zheng, H., Zhang, L., Li, L., Liu, P., Gao, J., Liu, X., et al. (2010). High-frequency rTMS treatment increases left prefrontal myo-inositol in young patients with treatment-resistant depression. *Prog. Neuropsychopharmacol. Biol. Psychiatry* 34, 1189–1195. doi: 10.1016/j.pnpbp.2010.06.009

Zung, W. W. K. (1965). A self-rating depression scale. *Arch. Gen. Psychiatry* 12, 63–70. doi: 10.1001/archpsyc.1965.01720310065008

Zung, W. W. K. (1971). A rating instrument for anxiety disorders. *Psychosomatics* 12, 371–379. doi: 10.1016/S0033-3182(71)71479-0

frontiers | Frontiers in Aging Neuroscience

TYPE Original Research
PUBLISHED 15 February 2023
DOI 10.3389/fnagi.2023.1131415

OPEN ACCESS

EDITED BY
Han Lv,
Beijing Friendship Hospital, Capital Medical University, China

REVIEWED BY
Chunlei Shan,
Shanghai University of Traditional Chinese Medicine, China
Chun-Ming Chen,
China Medical University Hospital, Taiwan
Zaira Romeo,
University of Padua, Italy

*CORRESPONDENCE
Li Liu
liulicao1976@163.com
Michael E. Sughrue
sughruevs@gmail.com

†These authors have contributed equally to this work and share first authorship

SPECIALTY SECTION
This article was submitted to Neurocognitive Aging and Behavior, a section of the journal Frontiers in Aging Neuroscience

RECEIVED 25 December 2022
ACCEPTED 30 January 2023
PUBLISHED 15 February 2023

CITATION
Bian R, Huo M, Liu W, Mansouri N, Tanglay O, Young I, Osipowicz K, Hu X, Zhang X, Doyen S, Sughrue ME and Liu L (2023) Connectomics underlying motor functional outcomes in the acute period following stroke.
Front. Aging Neurosci. 15:1131415.
doi: 10.3389/fnagi.2023.1131415

Connectomics underlying motor functional outcomes in the acute period following stroke

Rong Bian[1†], Ming Huo[2†], Wan Liu[3], Negar Mansouri[4], Onur Tanglay[4], Isabella Young[4], Karol Osipowicz[4], Xiaorong Hu[5], Xia Zhang[5,6], Stephane Doyen[4], Michael E. Sughrue[4,6*] and Li Liu[3*]

[1]Department of Rehabilitation, The First Affiliated Hospital of Nanjing Medical University, Nanjing, Jiangsu, China, [2]University of Health and Rehabilitation Sciences, Qingdao, China, [3]Department of Rehabilitation, The Affiliated Brain Hospital of Nanjing Medical University, Nanjing, Jiangsu, China, [4]Omniscient Neurotechnology, Sydney, NSW, Australia, [5]Xijia Medical Technology Company Limited, Shenzhen, China, [6]International Joint Research Center on Precision Brain Medicine, Xidian Group Hospital, Xi'an, China

Objective: Stroke remains the number one cause of morbidity in many developing countries, and while effective neurorehabilitation strategies exist, it remains difficult to predict the individual trajectories of patients in the acute period, making personalized therapies difficult. Sophisticated and data-driven methods are necessary to identify markers of functional outcomes.

Methods: Baseline anatomical T1 magnetic resonance imaging (MRI), resting-state functional MRI (rsfMRI), and diffusion weighted scans were obtained from 79 patients following stroke. Sixteen models were constructed to predict performance across six tests of motor impairment, spasticity, and activities of daily living, using either whole-brain structural or functional connectivity. Feature importance analysis was also performed to identify brain regions and networks associated with performance in each test.

Results: The area under the receiver operating characteristic curve ranged from 0.650 to 0.868. Models utilizing functional connectivity tended to have better performance than those utilizing structural connectivity. The Dorsal and Ventral Attention Networks were among the top three features in several structural and functional models, while the Language and Accessory Language Networks were most commonly implicated in structural models.

Conclusions: Our study highlights the potential of machine learning methods combined with connectivity analysis in predicting outcomes in neurorehabilitation and disentangling the neural correlates of functional impairments, though further longitudinal studies are necessary.

KEYWORDS

stroke, machine learning, connectomic analysis, functional prediction, structural and functional connectivity, motor functional outcome, language networks, attention networks

1. Introduction

Stroke is among the leading causes of long-term functional impairment worldwide (Karahan et al., 2014). Survivors often suffer residual motor, sensory, and cognitive deficits, all contributing to a deterioration in quality of life (Dobkin, 2005; Meyer et al., 2015). Beyond acute revascularization therapies, rehabilitation interventions remain paramount to aiding patients to regain function. However, one of the challenges in rehabilitation medicine is the heterogeneity in patient recovery trajectories after stroke. It remains difficult to predict whether or not patients will benefit from a given therapy, and it is clear that information beyond the observed deficits on

assessment are necessary to prognosticate patients and prescribe individualized therapies which will improve quality of life. Machine learning methods may have a key role in traversing this gap and be a tool for prescribing precise treatments.

Several studies have already utilized machine learning algorithms to predict functional outcomes in the acute/subacute stroke period. Lin et al. compared the performance of several machine learning methods in predicting the Barthel Index (Lin W.-Y. et al., 2018). Other studies have assessed the ability of machine learning models in predicting cognitive, motor and sensory outcomes, many achieving high accuracy in classifying participants (Fang et al., 2021; Campagnini et al., 2022; Kim et al., 2022; Liao et al., 2022). Some of these studies have also examined the important features contributing to the model's classification. For example, Thakkar et al. found that the time since stroke, baseline functional independence, and baseline motor ability were the most predictive factors of motor function improvement in chronic stroke patients (Thakkar et al., 2020). It is unclear which set of features is most optimal to include in a predictive model, though it is likely that the input of these models must reflect the heterogeneity among patients. Moreover, it is unclear if there are any specific connectomic features that are predictive of outcome.

Magnetic resonance imaging (MRI)-based functional and structural connectivity may be potential candidates in prognosticating stroke outcomes, as they could provide personalized brain information at the individual level. Several studies have demonstrated an association between disruptions in structural and functional connectivity and stroke outcomes (Carter et al., 2010; Ding et al., 2014; Lin L. Y. et al., 2018; Puig et al., 2018; Lee et al., 2020). However, there has been limited attention on combining machine learning with connectivity analysis to predict functional outcomes; to-date, there have not been any exploratory analyses of whole brain connectomics predictive of post-stroke motor functional outcome in machine learning models. Here, we analyze functional connectivity (FC) and structural connectivity (SC) in a clinical sample, in order to (1) predict several stroke related motor functional outcomes, and (2) describe the connectomic correlates contributing to those predictions.

2. Methods

2.1. Patient cohort

A total of 79 first-time stroke patients with hemiplegia who were hospitalized in the Rehabilitation Medicine Department of The Affiliated Brain Hospital of Nanjing Medical University from April 2018 to December 2021 were prospectively included in this study. The study protocol was approved by the Ethics Committee of The Affiliated Brain Hospital of Nanjing Medical University, and written informed consent was obtained from all patients or their family members.

The inclusion criteria of the study included: (1) diagnosis of first-ever subcortical ischemic or hemorrhagic stroke by computed tomography or magnetic resonance; (2) patients were within 2–12 months after stroke; (3) patients only had unilateral limb hemiplegia (Modified Brunnstrom classification as grade I–IV); (4) patients did not have severe cognitive impairment; (5) patients did not have other acute diseases or serious complications; (6) right-handedness. The exclusion criteria were: (1) disturbance of consciousness, severe hearing and visual impairment; (2) significant pain in the affected side (Ten-point Visual Analog Scale $>$ 4); (3) severe primary heart, lung, liver, kidney or hematopoietic system diseases; (4) after craniectomy or cranioplasty. (5) MRI contraindications.

2.2. Outcome assessment

The hospital records of the 79 patients were retrospectively reviewed for data collection. The following data on demographics and relevant past medical history were collected: age, sex, (hospitalization time, date of stroke onset and lesion location). Information on motor functional outcomes were also collected, using the following the assessment tools: Brunnstrom recovery stage (BRS) (Brunnstrom, 1966), modified Ashworth scale (MAS) (Bohannon and Smith, 1987), Barthel Index (Mahoney and Barthel, 1965), Fugl-Meyer Assessment (FMA) (Fugl-Meyer et al., 1975), functional ambulation category (FAC) (Holden et al., 1984), and Semans balance scale (Wang, 2018).

The functional classification of stroke patients was based on the BRS scale, which includes three parts: upper limb, lower limb and hand, with each part having six levels (0–6). The higher the level, the stronger the motor ability (Brunnstrom, 1966). The scale has good internal consistency in stroke patients. The MAS scale was used to evaluate spasticity in the biceps brachii and triceps surae muscles, which was graded out of six levels (0, 1, 1+, 2, 3, 4) (Bohannon and Smith, 1987). The higher the level, the more severe the spasm. The Barthel Index was used for the ability of daily living, with a total score of 100. The higher the score, the better the quality of life (Mahoney and Barthel, 1965). FMA was used to evaluate motor function, with a total score of 100, including 66 for upper limbs and 34 for lower limbs. The higher the score, the better the motor ability (Fugl-Meyer et al., 1975). FAC was used for assessing walking ability, and was divided into six levels—the higher the level, the better the walking function (Holden et al., 1984). The Semans balance scale was used to assess balance. It is an observational assessment method mainly used in the balance assessment of pediatric cerebral palsy and hemiplegic patients after stroke (Wang, 2018). It classifies balance into eight levels, with higher levels corresponding to better balance.

2.3. Imaging protocol

Image scanning was performed on the same day as functional assessment, on a 3.0-T MRI scanner (Siemens, Verio, Germany) in the Affiliated Brain Hospital of Nanjing Medical University. All patients lay supine with their head fixed by foam pads with a standard birdcage head coil to minimize head movement. Participants were instructed to remain as still as possible, open their eyes, remain awake, and not think of anything. High-resolution T1-weighted images were acquired by 3D magnetization-prepared rapid gradient-echo (MPRAGE) sequence [repetition time (TR) = 2,300 ms; echo time (TE) = 2.85 ms; flip angle (FA) = 9 degrees; matrix = 256 × 256; field of view (FOV) = 256 × 256 mm^2; slice thickness/gap = 1/0.5 mm; 176 slices covered the whole brain] for image registration and functional localization. The imaging took ∼260 s. The resting-state of functional MRI (rsfMRI) were subsequently collected in the same slice orientation with a gradient-recalled echo-planar imaging pulse sequence (TR = 2,000 ms; TE = 30 ms; FA = 90 degrees; matrix

= 64 × 64, FOV = 240 × 240 mm^2; thickness/gap = 4.0/0 mm; voxel size = 3.8 × 3.8 × 4 mm^3; slice numbers = 30). A total of 251 volumes were obtained in this acquisition sequence and each functional resting-state session lasted ~500 s.

Diffusion-weighted imaging was performed with the SE-EPI sequence scanning. Using iPAT technology, axial scanning, TR = 11,000 ms, TE = 90 ms, slice number = 67, slice thickness = 2 mm, slice spacing 0 mm, FOV = 256 mm × 256 mm, matrix: 128 × 128, voxel size = 2 × 2 × 2 mm^3, diffusion weighted scan b = 1,000 s/mm^2 in 30 gradient directions, and another non-diffusion weighted image with b = 0. Excitation times (NEX) = 2. Scan time = 11 min and 57 s.

2.4. Diffusion weighted imaging pre-processing

Diffusion weighted imaging (DWI) was processed using the Infinitome software (Omniscient Neurotechnology, 2020). Infinitome relies on standard processing steps using Python (Garyfallidis et al., 2014). The diffusion image was resliced to obtain isotropic voxels. A rigid body alignment was used for motion correction, and slices with excess motion, defined as DVARS >2 sigma from the mean slice were eliminated. The T1 image was then skull stripped using a convolution neural net, described elsewhere (Isensee et al., 2019). This was then inverted and aligned to the DWI image using a rigid alignment, which was then used as a mask to skull strip the DWI image. A diffeomorphic warping method was then used to correct for gradient distortion to similarize the DWI and T1 images, and eddy current correction was performed. Finally, the fiber response function was estimated and constrained spherical deconvolution was used calculate the diffusion tensors. Deterministic tractography was then performed, with random seeding, manifesting in around 300,000 streamlines per brain (Doyen et al., 2022).

2.5. Structural-connectivity based parcellation

A parcellation scheme is necessary for measuring FC changes at an anatomical level. Most available atlasing methods to parcellate the brain into functional regions however are derived from healthy subjects. These atlases also are based on a group average of these healthy cohorts, and are therefore unable to account for individual morphological differences such as gyral variation. This is especially problematic when applying these atlases to brains altered by pathology, such as in stroke. In order to account for any morphological deficits caused by stroke, we utilized a machine learning based method to individually parcellate each brain based on the Human Connectome Project Multimodal Parcellation (HCP-MMP1) atlas (Glasser et al., 2016), creating a subject-specific atlas. While we have described this method in detail elsewhere (Doyen et al., 2022), briefly, a machine learning model was trained using DWI data from 178 healthy controls from the Schiz Connect database, which were pre-processed as above. The model consequently learnt the structural connectivity pattern between each voxel. The unalted HCP-MMP1 was then warped to each brain in the current study's cohort, and the machine learning model was applied to each brain to re-appoint voxels to their most likely parcellation based on structural connectivity features. This method manifested in "reparcellation" of voxels, creating a subject-specific version of the HCP-MMP1 atlas with 180 cortical regions, 9 subcortical regions, and the brainstem.

Each brain region was then automatically mapped to a known large-scale brain network by the Infinitome software, which itself relies upon previous meta-analyses mapping each large-scale brain network. The network template described by Yeo et al. (2011) was utilized, including the core networks: the Central Executive Network (CEN), Default Mode Network (DMN), Dorsal Attention Network (DAN), Limbic Network (LN), Salience Network (SN), Sensorimotor Network (SMN), and the Visual Network (VN), along with several networks which are either part of the extended versions of the core networks, or additional networks described in the literature, including the Accessory Language and Language Networks (part of the extended DMN), Auditory System (part of the SMN), Multiple demand network, and Ventral Attention Network (VAN).

2.6. Resting-state fMRI pre-processing steps

rsfMRI images were pre-processed prior to analysis according to standard pre-processing steps. A rigid body alignment was used to perform motion correction on the T1 and blood-oxygen-level-dependent (BOLD) images. Slices with excess movement (defined as DVARS > 2 sigma from the mean slice) were eliminated. A CNN was used to skull strip the T1 image (Isensee et al., 2019). In order to then skull strip the rsfMRI image, the T1 image was inverted and aligned to the BOLD image using a rigid alignment, and then used as a mask. Slice timing correction, global intensity normalization, and gradient distortion correction were performed, the latter using a diffeomorphic warping method to register the rsfMRI and T1 images. The CompCor methodwas used to calculate high variance confounds (Behzadi et al., 2007), which were regressed out of the rsfMRI image along with the motion confounds. The linear and quadratic signals were detrended (note this method does not perform global signal regression). A 4 mm FWHM Gaussian kernel was used to perform spatial smoothing. The subject-specific brain atlas created in the previous steps were then registered to the T1 image, and the regions were aligned with the regions in each subject's scan. A visual check was then performed by two neuroanatomists, independently, to ensure the methodology accounted for the morphological changes caused by the lesion. The atlas was therefore ideally positioned to extract a BOLD time series, averaged over all the voxels within a region, from 379 brain regions (180 cortical regions from two hemispheres, along with 19 subcortical structures). A Pearson correlation coefficient was then calculated between the BOLD signals of each unique pair of regions, yielding. Thus, it is ideally positioned for extracting a BOLD time series, averaged over all voxels within a region, from all 379 regions (180 parcels from two hemispheres, plus 19 subcortical structures). The Pearson correlation coefficient is calculated between the BOLD signals of each unique area pair (self to self-inclusive), which yields 71,631 unique correlations.

2.7. Machine learning classification and feature extraction

Machine learning was used to model the test performance of each participant based on the pairwise functional correlation or structural connectivity between the 379 regions of each individual's

TABLE 1 Cutoffs for each functional outcome scale utilized in the machine learning models.

Functional outcome scale	Scoring cutoffs	
Brunnstrom Stage Recovery (BRS)—upper extremity	Stages 1–3	Worse
	Stages 4–6	Better
Fugl-Meyer Assessment (FMA)—lower extremity	<21	Worse capacity
	≥21	Better capacity
Fugl-Meyer Assessment (FMA)—upper extremity	≤31	Worse capacity
	≥32	Better capacity
Modified Ashworth Scale (MAS)—upper extremity	0	No muscle tone
	>0	Some muscle tone
Modified Ashworth Scale (MAS)—lower extremity	0	No muscle tone
	>0	Some muscle tone
Barthel index	≤40	Very or totally dependent
	41–100	Partially to fully independent
Semans balance	0–1	Severe
	>1	Moderate to none
Functional ambulation category	0	Non-ambulatory
	1–5	Ambulatory

brain atlas. XGBoost Classifier (Chen and Guestrin, 2016), a boosted trees approach was used to fit each model. All models included age and sex as nuisance predictors. A total of 16 models were trained—one utilizing structural connectivity (SC), and another functional connectivity (FC)—to predict performance on the BRS on upper extremity, FMA on upper and lower extremities, MAS on upper and lower limbs, Barthel Index, FAC, and Semans balance scale. The scores for each of these tests were binarized for the models to classify subjects into either category, as detailed in Table 1.

Five-fold cross-validation was used for each model, with different training and test data splits to ensure the hyperparameters were not being optimized just for the given training and test data splits. The models were evaluated with the mean area under the receiver operating characteristic curve (AUC-ROC) ± standard deviation. Given the small sample size, several strategies were utilized to minimize the impact of class imbalances on the performance of each model. Five-fold cross-validation ensured that each fold had an equal ratio of both classes; a stopping criterion was applied to stop training if the model performance did not improve over consecutive iterations of hyperparameter tuning—an attempt to prevent overfitting; and, feature importance analysis only relied upon the correctly predicted cases, therefore being independent of whether one class was predicted slightly better than the other. These strategies aimed to approximate a balanced class AUC even in cases of class imbalance. Our predominant aim in each model was also feature importance analysis, with a focus on identifying what resulted in the classifications. Consequently, while AUC is inherently affected by class imbalances, the guardrails applied, along with the significantly higher than chance performance of each model counteract any AUC bias, and make it largely irrelevant to the aim of our analysis.

The feature importance analysis for each model was visualized using a SHAP plot of the top 20 features, either functional or structural connectivity between two regions of the HCP-MMP1 atlas, contributing to the model. The SHAP method, based on cooperative game theory, calculates Shapley values for each feature, which estimate the marginal contribution of each feature to the outcome of models relying on every possible permutation of features (Lundberg and Lee, 2017). Each SHAP plot shows a list of features in descending order of importance, quantifying the impact on the model along the x-axis, with the color of each point representing a single observation, indicating whether a high (red), or low (blue) value of that feature is associated with the model. A network-based summary plot is also produced, aggregating the contribution of each parcel by their network affiliation. This gives an indication of which brain networks are most influential in each model's classification.

3. Results

3.1. Subject demographics

Subject demographics are detailed in Table 2. The median age (±IQR) of our sample was 62 ± 18. There were 22 females (27.8%) and 57 males (72.2%). The median time (±IQR) from initial stroke to scanning was 35 days (33). There was a small difference in the stroke side, with 55.7% of patients having a left-sided stroke; however, speech deficits were only seen in 21.5% of patients, and most patients had a subcortical stroke. Motor deficits were present in 96.2% of patients.

3.2. Models classifying tests of limb function and spasticity

Machine learning was applied to classify subjects into binarized categories as outlined in Table 1. For each test, two models were constructed to separately evaluate functional and structural connectivity. Both models included age and sex as covariates.

3.2.1. Brunnstrom stage of recovery (BRS)—Upper extremity

The model utilizing subjects' FC to classify the upper limb BRS achieved a mean (±SD) AUC of 0.81 ± 0.12. Utilizing the SHAP method for feature extraction revealed that at the individual brain region level, a low FC between the left area posterior 24 prime (p24pr) and left area posterior insular 1 (PoI1), a high FC between the right primary motor cortex (area 4) and right area 9 posterior (9p), and a high FC between left area anterior 24 (a24) and left area intraparietal 0 (IP0) contributed most to the model's classification (Figure 1A). The rest of the features did not demonstrate as significant an impact on the output. At the network level, the DAN, limbic/paralimbic system, and VAN had the largest contribution to the model's output, followed by the DMN (Figures 1B, E).

The model employing SC to classify the upper limb BRS achieved a mean (±SD) AUC of 0.66 ± 0.13. At the individual brain region level, the structural connectivity between the left Thalamus and right

TABLE 2 Subject demographics.

Demographics	$N = 79$
Age *years (median ± IQR)*	62.0 ± 18.0
Sex F/M *n (%)*	22 (27.8)/57 (72.2)
Years of education *(median ± IQR)*	9.0 ± 6.0
Hand dominance L/R *n (%)*	79 (100)/0 (0)
Time from first admission to fMRI *days (median ± IQR)*	35 (33)
Stroke side* L/R *n (%)*	44 (55.7)/34 (43.0)
Stroke location *n (%)*	
Cortical	12 (15.2)
Subcortical	52 (65.8)
Both	15 (19.0)
Deficits on admission *n (%)*	
Motor	76 (96.2)
Cognition	21 (26.6)
Speech	17 (21.5)
Dysarthria	21 (26.6)
Dysphagia	25 (31.6)
Ataxia	2 (2.5)
Brunnstrom stage of recovery *(median ± IQR)*	
Upper limb	3 (3)
Lower limb	4 (3)
Fugl-Meyer assessment *(median ± IQR)*	
Total motor	39 (53.5)
Upper limb motor	20 (37.5)
Lower limb motor	18 (22)
Modified Ashworth scale *(median ± IQR)*	
Upper limb	0 (1)
Lower limb	0 (0.25)
Barthel index *(median ± IQR)*	50 (42.5)
Semans balance scale *(median ± IQR)*	3 (2)

*One subject had an infarct of the corpus callosum.

area TE2 anterior (TE2a) (though the direction of this connectivity was unclear), and a high connectivity between left parabelt complex (Pbelt) and right V3CD were the top two features (Figure 1C). However, there was significant variability and overlap among the feature contribution values, and this model therefore requires caution while interpreting. At the network level, the accessory language network demonstrated the greatest contribution to the model's classification (Figures 1D, F).

3.2.2. Fugl-Meyer Assessment

The model classifying the FMA lower extremity score using FC achieved a mean AUC of 0.797 ± 0.052. A high FC between the left hippocampus and left V3A had the greatest impact on the model's output, while the rest of the features demonstrated a mixed pattern of FC, with great overlap (Figure 2A). At the network level, the accessory language network demonstrated the greatest contribution, followed by the VAN and medial temporal regions (Figures 2B, E). When utilizing SC, the model achieved a mean AUC of 0.650 ± 0.117. The model performance and the low level of variance among the subjects limited further interpretation of this model, especially at the individual region level (Figure 2C), though the SN and language network demonstrated the greatest contribution at the network level (Figures 2D, F).

Classification of the upper extremity FMA scores using FC yielded a mean AUC of 0.677 ± 0.080. At the individual region level, a high FC between the right IFSp and left orbital frontal complex (OFC), right PBelt and left temporoparietooccipital junction (TPOJ2), left dorsal area 8A (8Ad) and left area posterior 10p (p10p), right supplementary and cingulate eye field (SCEF) and left rostral area 10 (10r), right lateral belt complex (LBelt) and right superior temporal visual area (STV) were the top five features contributing to the model's output (Figure 3A). At the network level, the auditory system, followed by the limbic/paralimbic system had the greatest contribution (Figures 3B, E). When utilizing structural connectivity to classify upper extremity FMA scores, the model demonstrated a mean AUC of 0.788 ± 0.045. A high connectivity between the right hippocampus and left area 8B lateral (8BL) was the top feature contributing to the model's output, while the rest of the features generally were associated with low connectivity, though there was too much overlap to highlight a single feature and these features did not show as a significant contribution to the model (Figure 3C). At the network level, the medial temporal regions and VAN, followed by the auditory system demonstrated the greatest contribution to the output (Figures 3D, F).

3.2.3. Modified Ashworth scale

The model classifying the MAS lower extremity score into no change in muscle tone and some change in muscle tone achieved a mean AUC of 0.753 ± 0.140. Due to the relative class imbalance of this model, the SHAP output was difficult to interpret at the individual brain region level, and while a high FC between the right medial belt complex (Mbelt) and right posterior operculum 2-3 (OP2-3) had the highest contribution to the output, it should be interpreted with caution (Figure 4A). At the network level however, the medial temporal regions and CEN, followed by the auditory system and VN demonstrated the greatest contribution to the model's output (Figures 4B, E). When utilizing SC to classify MAS lower extremity scores, the model achieved a mean AUC of 0.802 ± 0.108. A low connectivity between the left thalamus and left area 9 posterior (9p) had the greatest contribution to the model's output, and the top 10 features generally pointed to low connectivity (Figure 4C). There was however significant overlap among the features, making it difficult to ascertain the relative importance of features. At the network level, the auditory system and CEN were once again among the top four networks contributing to the model's output, and were followed by the language system and SN (Figures 4D, F).

Classification of the upper extremity scores using FC yielded a mean AUC of 0.815 ± 0.080. At the individual region level, a high FC between the left cerebellum and right area 31p ventral (31pv) had the greatest contribution to the model's output, followed by a high FC between left area anterior 47r (a47r) and right area p32 prime (p32pr) (Figure 5A); while at the network level, the DMN contributed most

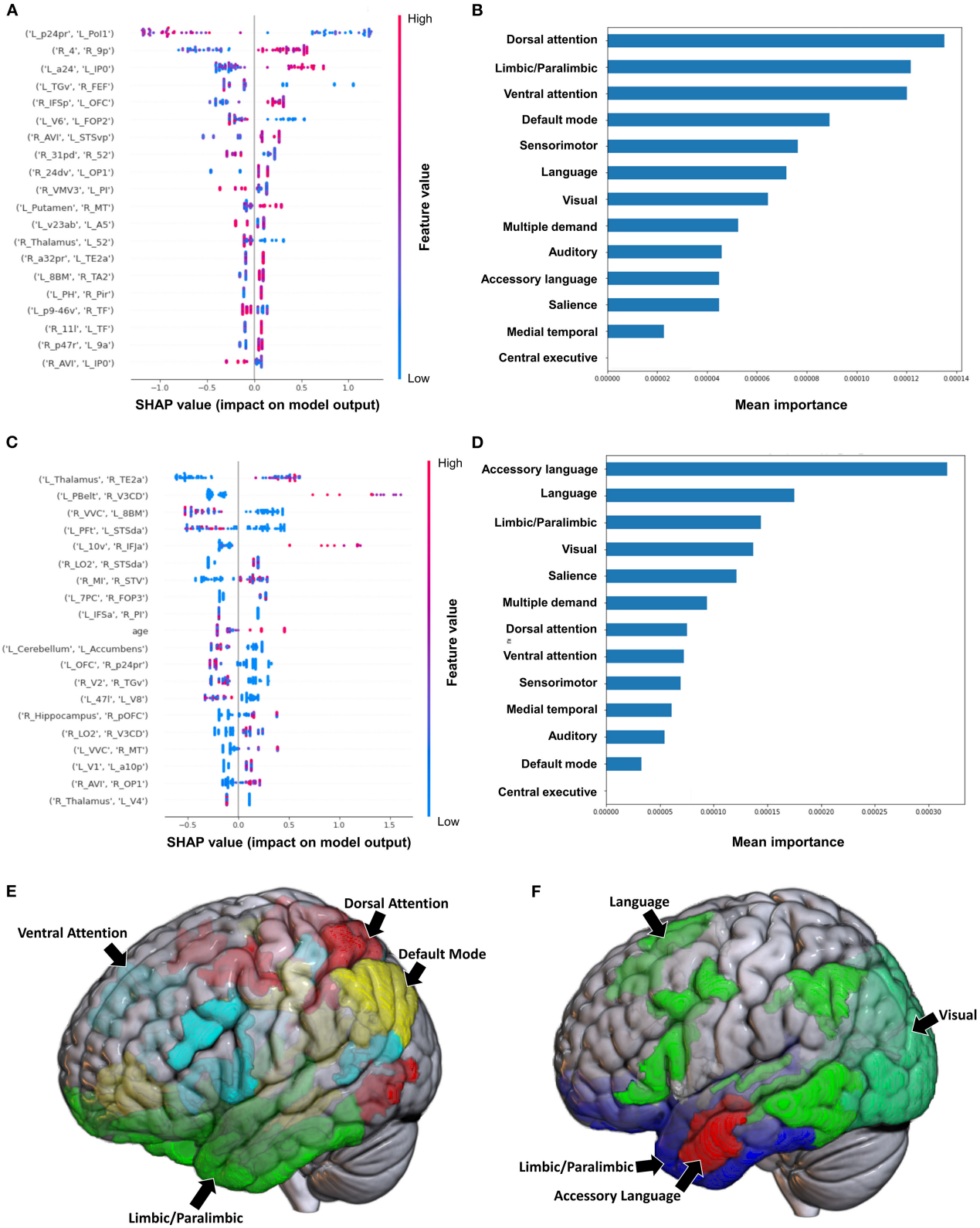

FIGURE 1
Feature importance analysis of the models classifying the Brunnstrom stage of recovery—upper extremity based on functional connectivity at the **(A)** individual brain region level, and **(B)** the network level; and based on structural connectivity at the **(C)** the individual brain region level, and **(D)** the network level. The networks contributing most to the models' classifications, based on **(E)** functional connectivity, and **(F)** structural connectivity, have also been visualized on brain models.

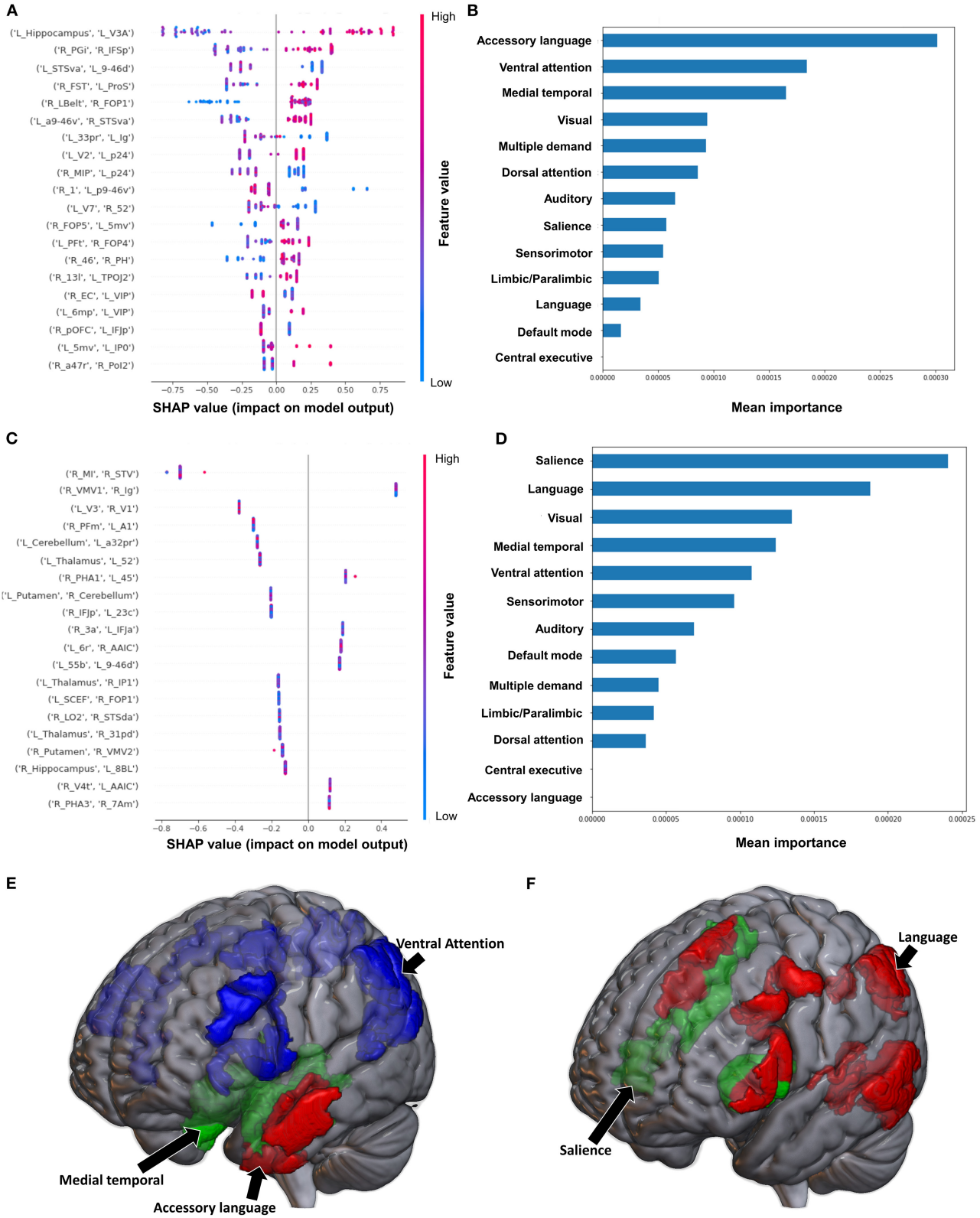

FIGURE 2
Feature Importance Analysis of the models classifying the Fugl Meyer assessment—lower extremity based on functional connectivity at the **(A)** individual brain region level, and **(B)** the network level; and based on structural connectivity at the **(C)** the individual brain region level, and **(D)** the network level. The networks contributing most to the models' classifications, based on **(E)** functional connectivity, and **(F)** structural connectivity, have also been visualized on brain models.

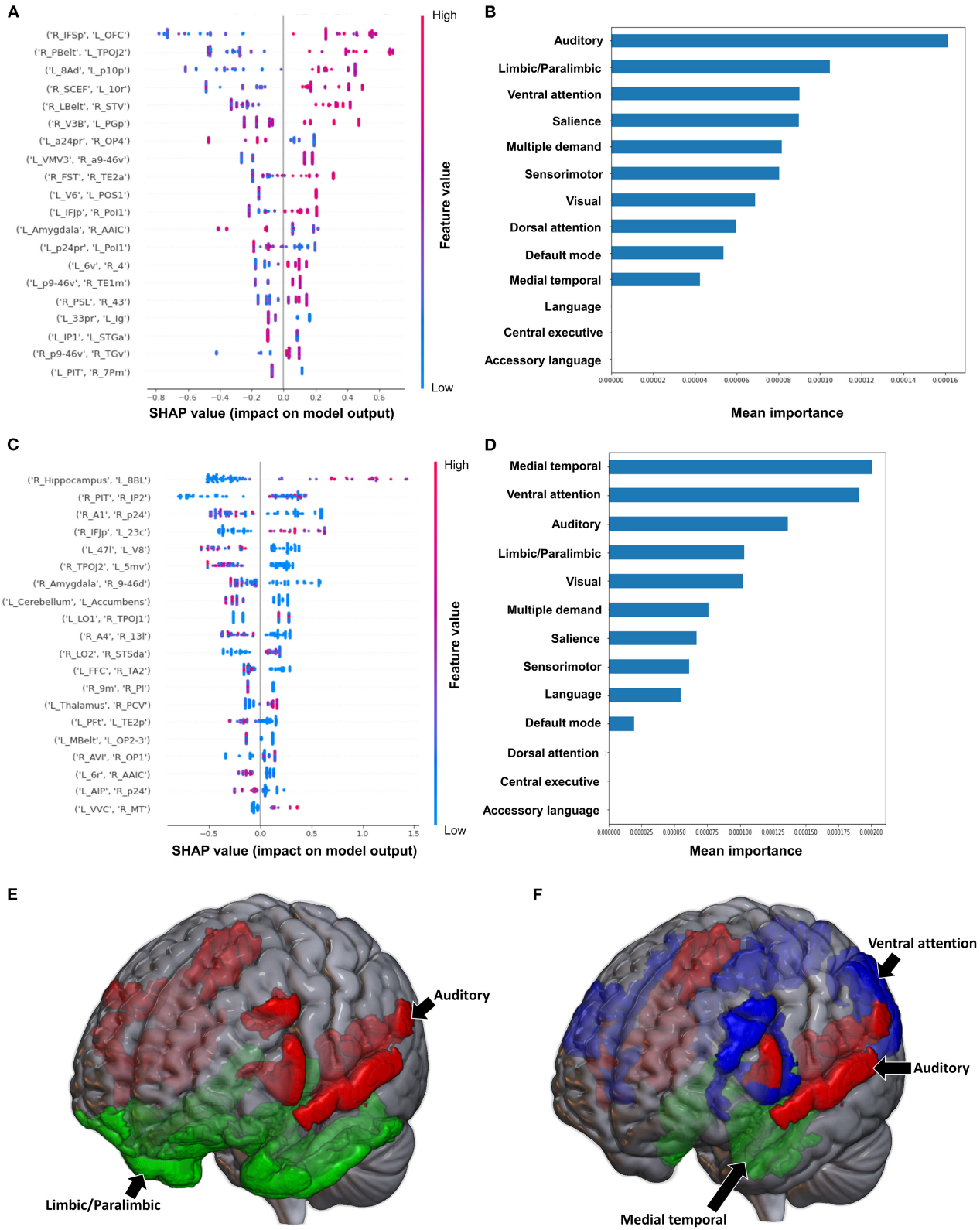

FIGURE 3
Feature Importance Analysis of the models classifying the Fugl Meyer assessment—upper extremity based on functional connectivity at the **(A)** individual brain region level, and **(B)** the network level; and based on structural connectivity at the **(C)** the individual brain region level, and **(D)** the network level. The networks contributing most to the models' classifications, based on **(E)** functional connectivity, and **(F)** structural connectivity, have also been visualized on brain models.

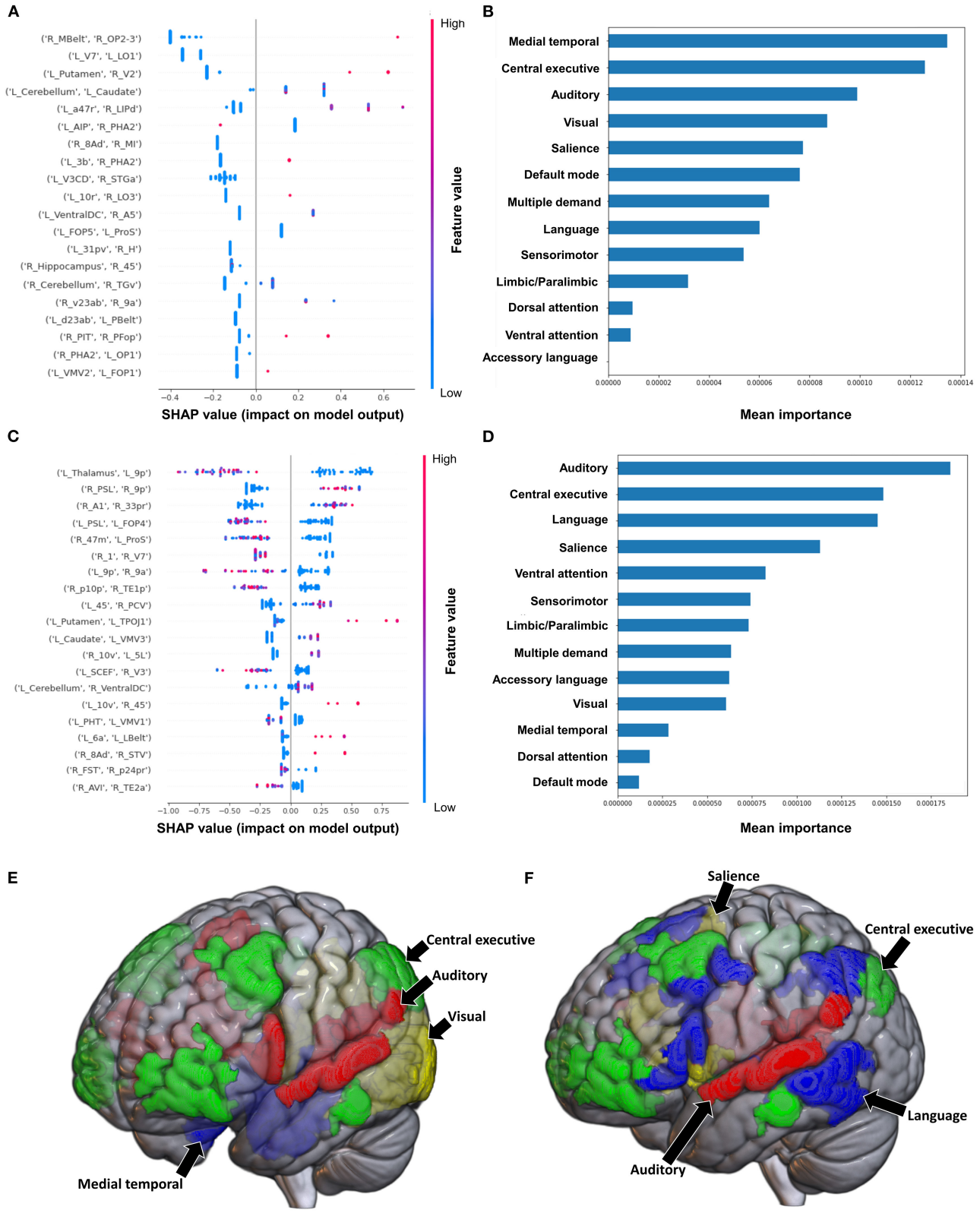

FIGURE 4
Feature Importance Analysis of the models classifying the modified Ashworth scale—lower extremity based on functional connectivity at the **(A)** individual brain region level, and **(B)** the network level; and based on structural connectivity at the **(C)** the individual brain region level, and **(D)** the network level. The networks contributing most to the models' classifications, based on **(E)** functional connectivity, and **(F)** structural connectivity, have also been visualized on brain models.

to the output, followed by medial temporal regions (Figures 5B, E). When utilizing structural connectivity to classify upper extremity scores, the model demonstrated a mean AUC of 0.737 ± 0.150. A low SC between the right area 6mp and left area 52, right area 47m and left prostriate area (ProS), and right posterior inferotemporal complex (PIT) and right area 45 were the top three features contributing to the model's classification (Figure 5C). At the network level, the DAN, VAN, and SN demonstrated the greatest contribution (Figures 5D, F).

3.3. Models classifying tests of general functional performance activities of daily living

3.3.1. Barthel Index

When using FC to classify subjects based on the Barthel Index, the model achieved a mean AUC of 0.808 ± 0.094. A low FC between the brainstem and right medial area 7P (7Pm), and right para-insular area (PI) and right area TE2 posterior (TE2p) were the top 2 features contributing to the model's classification, while the rest of the features demonstrated great overlap in contribution (Figure 6A). The VAN had the greatest contribution at the network level (Figures 6B, E).

The model utilizing SC achieved a mean AUC of 0.742 ± 0.175. Low connectivity between the left area superior temporal sulcus ventral-anterior (STSva) and left area V4t, and left area temporoparietooccipital junction 1 (TPOJ1) and right premotor eye field (PEF) had the greatest impact on the model's output, though there was once again significant overlap in contribution values (Figure 6C). At the network level, the accessory language network had the greatest contribution to the model's classification (Figures 6D, F).

3.3.2. Semans balance scale

The model utilizing FC to classify balance performance yielded a mean AUC of 0.868 ± 0.155. A low FC between the right area intraparietal 1 (IP1) and left area 44 had the greatest contribution to the model's output (Figure 7A), while at the network level, the language system was the top network (Figures 7B, E). The model utilizing structural connectivity had a mean AUC of 0.685 ± 0.069. A low level of structural connectivity between the left area 6 medial-anterior (6ma) and the right area superior temporal sulcus dorsal anterior (STSda) had the greatest impact on this model's output, while the rest of the features demonstrated a mix of low and high levels of connectivity, with great overlap (Figure 7C). At the network level, the language system had the greatest contribution to the model, followed by the SN, SMN, multiple demand network, and the VAN (Figures 7D, F).

3.3.3. Functional ambulation category

The model utilizing FC to predict FAC achieved a mean AUC of 0.75 ± 0.10 following hyperparameter tuning. At the individual brain region level, a high FC between the right area 33 prime (33pr) and right area 9 posterior (9p), and a low FC between the left area anterior 9-46v (a9-46v) and right STSva were the top two features contributing to the model (Figure 8A). The CEN demonstrated the greatest contribution to the model at the network level (Figures 8B, E).

When utilizing FC, the model achieved a mean AUC of 0.804 ± 0.115. A low connectivity between the left superior frontal language area (SFL) and left area 9 anterior (9a), left area temporal gyrus ventral (TGv) and right PI, and left p32pr and left parahippocampal area 3 (PHA3) were the top three features contributing to the model's output, though there was overlap among the top 20 features' contributions (Figure 8C). At the network level, the language system and the SMN demonstrated the greatest contribution, followed by the SN and the VN (Figures 8D, F).

4. Discussion

In this study, we utilized machine learning models to predict functional impairment after stroke using functional and structural connectivity and analyzed important features to identify the neuroanatomical basis of this impairment. Notably, our models achieved a high performance when classifying standardized tests of functional impairment. Our data also revealed broad disruptions across multiple brain networks in functional and structural connectivity, especially within the DAN and VAN. Together, our findings demonstrate the utility of our methodology to explore and discover the connectomic disturbances underlying stroke, and how networks respond to insults. While our study was the first comprehensive analysis utilizing both functional and structural connectivity to classify standardized tests of functional impairment using machine learning, the generalizability of our findings is limited by a relatively small and heterogeneous sample. The following discussion will therefore examine whether our findings may be explained by the existing literature, though we acknowledge that our hypotheses are speculative in nature and further studies are necessary to validate these claims.

4.1. Attention and language networks in stroke

Although our models pointed to several large-scale networks which are known to be important in functional recovery after stroke, such as the DMN, CEN, and SMN (Tuladhar et al., 2013; Larivière et al., 2018; Wu et al., 2020; Olafson et al., 2021; Vicentini et al., 2021), the attention networks, the DAN and VAN were among the top contributors in several of our models. Classically, The DAN is considered to be crucial for sustaining attention on a given task (Ptak and Schnider, 2010), while the VAN is thought to act as a circuit breaker by redirecting attention in response to salient events (Corbetta and Shulman, 2002; Corbetta et al., 2008). Generally, impairment in the DAN following stroke has been associated with neglect (Corbetta and Shulman, 2011; Barrett et al., 2019) and the severity of motor impairment (Siegel et al., 2016), however, the exact nature of changes within the attention networks in stroke patients remains unknown. Some studies have reported increased connectivity (Rehme et al., 2012; Wang et al., 2014; Siegel et al., 2016; Lee et al., 2018), contextualized by the greater need for patients to direct attention to movements following stroke. While others have demonstrated lower FC within the VAN and DAN in both task-free and task-based settings (He et al., 2007; Baldassarre

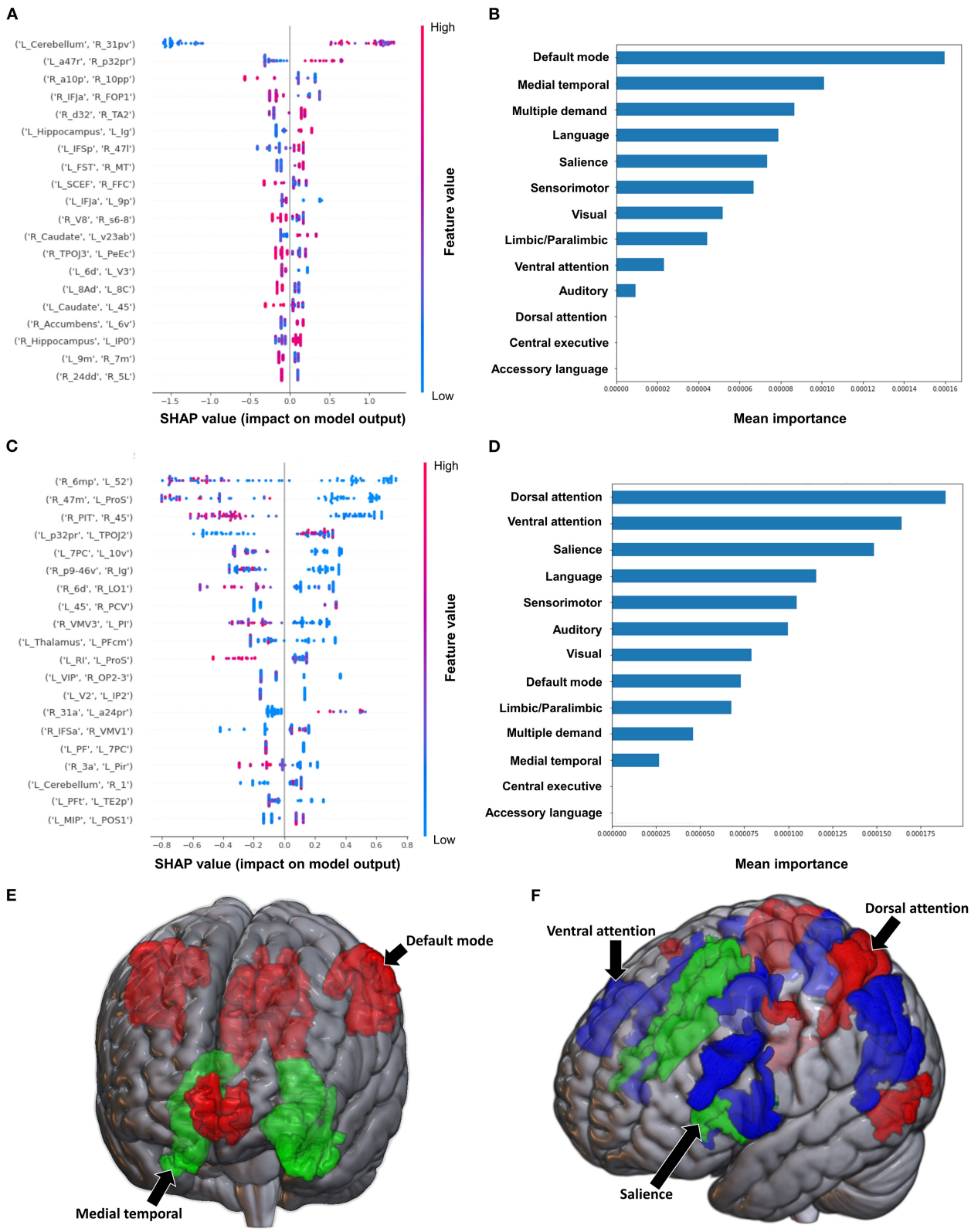

FIGURE 5
Feature Importance Analysis of the models classifying the modified Ashworth scale—upper extremity based on functional connectivity at the **(A)** individual brain region level, and **(B)** the network level; and based on structural connectivity at the **(C)** the individual brain region level, and **(D)** the network level. The networks contributing most to the models' classifications, based on **(E)** functional connectivity, and **(F)** structural connectivity, have also been visualized on brain models.

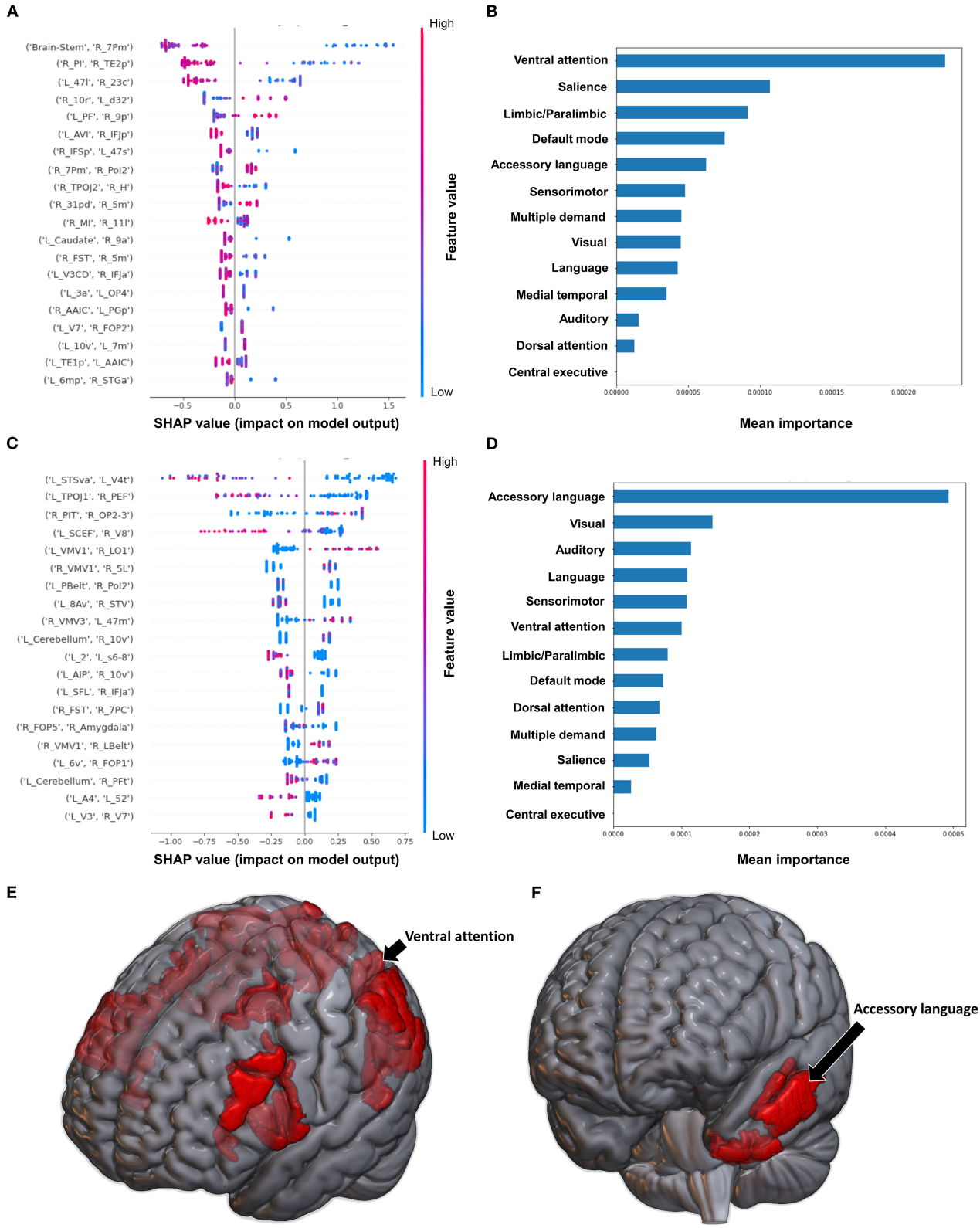

FIGURE 6
Feature Importance Analysis of the models classifying the Barthel index based on functional connectivity at the **(A)** individual brain region level, and **(B)** the network level; and based on structural connectivity at the **(C)** the individual brain region level, and **(D)** the network level. The networks contributing most to the models' classifications, based on **(E)** functional connectivity, and **(F)** structural connectivity, have also been visualized on brain models.

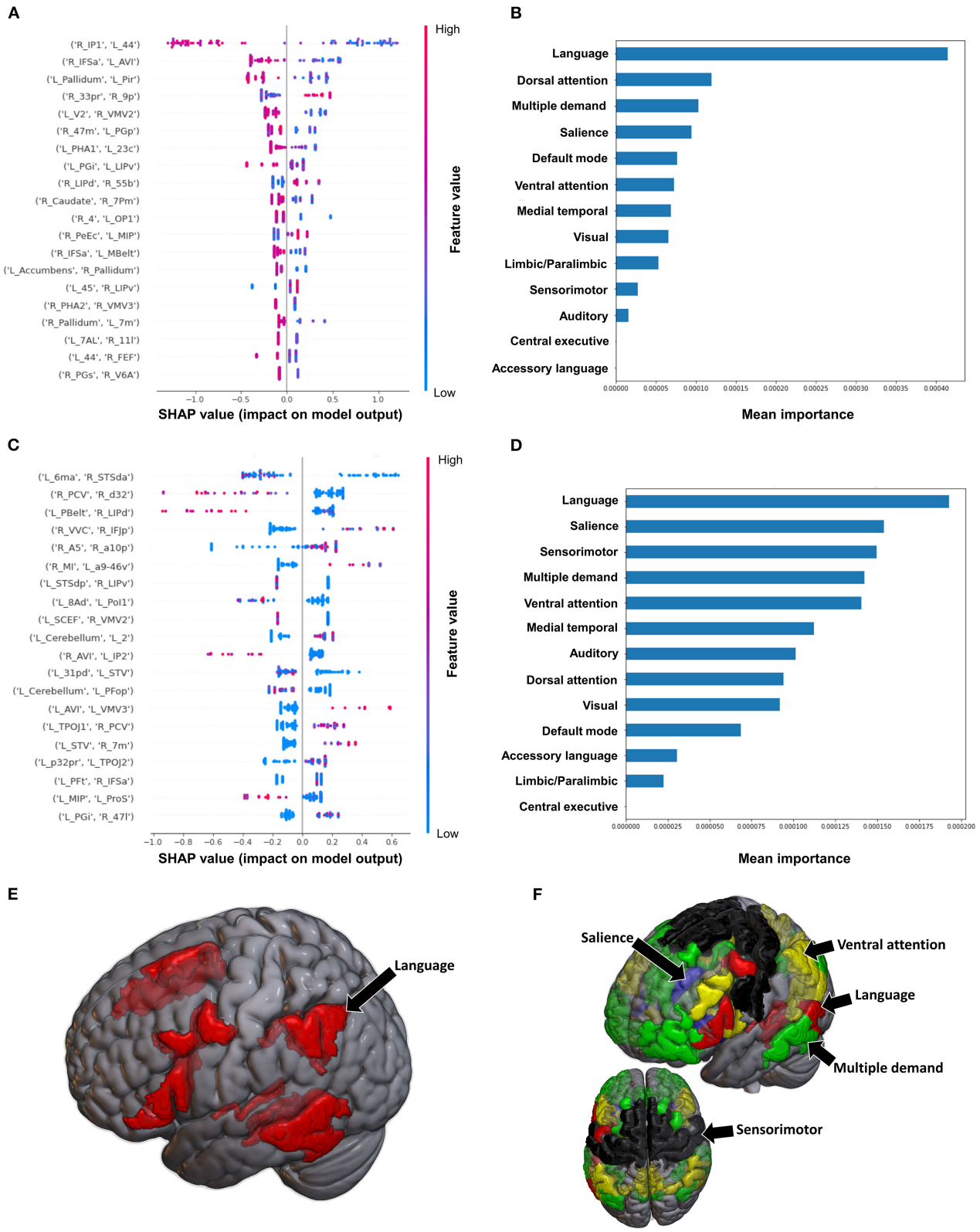

FIGURE 7
Feature Importance Analysis of the models classifying the Semans balance scale based on functional connectivity at the **(A)** individual brain region level, and **(B)** the network level; and based on structural connectivity at the **(C)** the individual brain region level, and **(D)** the network level. The networks contributing most to the models' classifications, based on **(E)** functional connectivity, and **(F)** structural connectivity, have also been visualized on brain models.

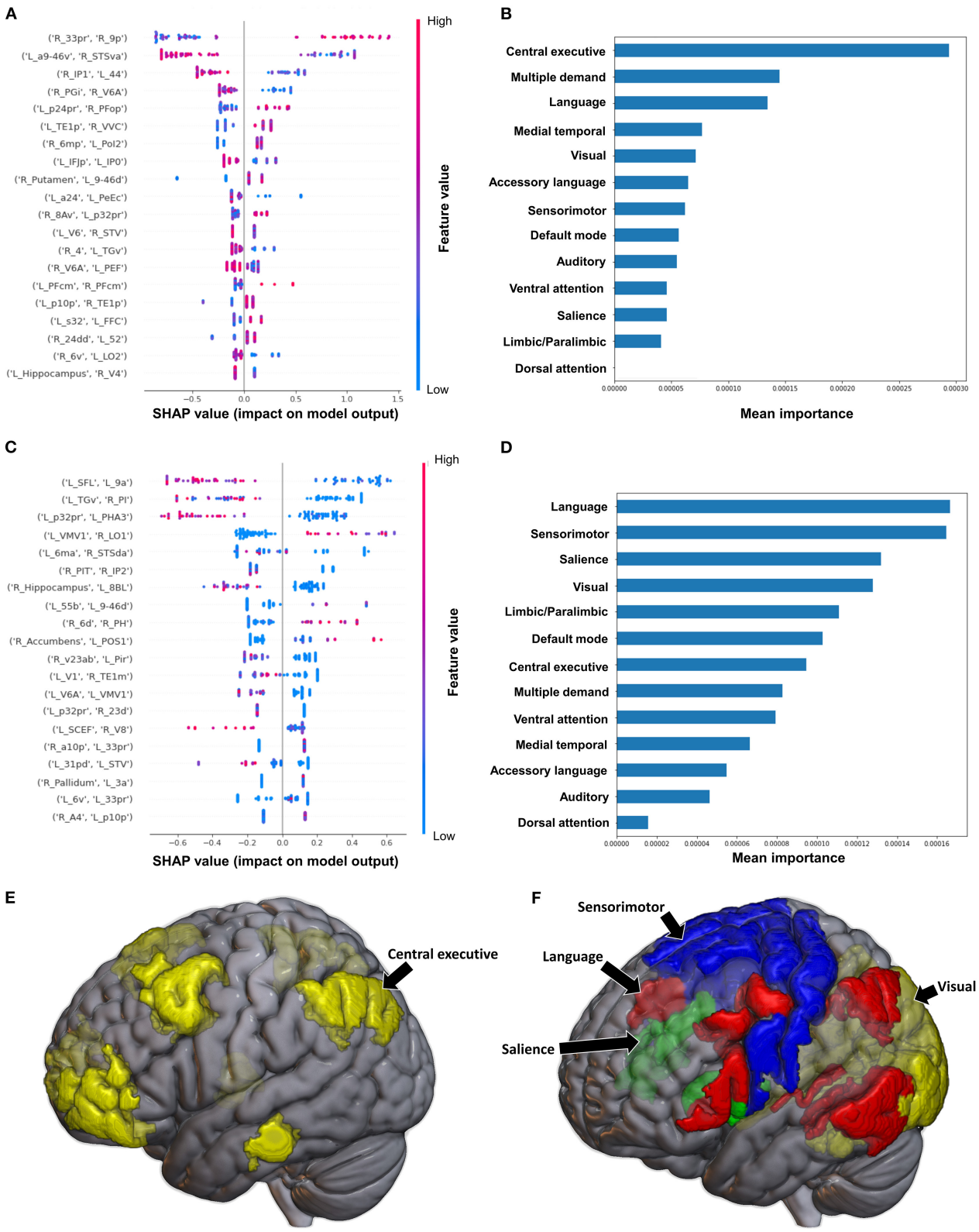

FIGURE 8
Feature Importance Analysis of the models classifying the functional ambulation category based on functional connectivity at the **(A)** individual brain region level, and **(B)** the network level; and based on structural connectivity at the **(C)** the individual brain region level, and **(D)** the network level. The networks contributing most to the models' classifications, based on **(E)** functional connectivity, and **(F)** structural connectivity, have also been visualized on brain models.

et al., 2016; Adhikari et al., 2017; Barrett et al., 2019). This may be pointing to increased inter-network connectivity and decreased intra-network connectivity, representing the loss of network segregation and specialization following stroke (Caliandro et al., 2017; Marebwa et al., 2017; Guo et al., 2019). Interestingly, congruent to our findings, Romeo et al. recently demonstrated a positive correlation between decreased connectivity of the DAN and the motor component of the Functional Independence Measure (FIM) in the sub-acute to chronic period following stroke (Romeo et al., 2021). Furthermore, several studies have shown that the outcome of motor rehabilitation may be associated with preserved FC within the ipsilesional DAN (Cheng et al., 2021; D'Imperio et al., 2021). Therefore, patients with preserved connectivity within the DAN and VAN may be performing better across the tests in our models. We however cannot validate this given the task-free nature of our study. Nonetheless, it is evident that the attention networks play a role in mediating functional performance, though further studies on large, homogeneous samples are necessary to elucidate the mechanism behind this, which may provide further therapeutic avenues.

Interestingly, the language and accessory language networks were highlighted in our models classifying the BRS, FMA, Barthel Index, Semans balance scale and FAC. This may be due to impairments in the language system typically accompanying strokes with worse motor and functional impairment, and indeed those with expressive aphasia tend to have an 80% chance of also suffering hemiplegia (Romeo et al., 2021). Due to our small sample size, we were unable to perform separate analyses on patients reporting a brain lesion in the left compared to the right hemisphere. However, given most of the strokes within our cohort were subcortical, only nine out of 17 strokes affecting speech were left-sided cortical strokes, and most patients with motor deficits did not have speech deficits, we speculate that there may be alternative reasons for why the language network contributed to our classifications. This finding may instead be pointing to the functional symbiosis between language and motor function (recently reviewed by Anderlini et al., 2019). Recently, several studies have demonstrated that not only do deficits in these domains co-occur, but they also interact in their treatment. For example, Romeo et al. also demonstrated an association between the FIM motor score and the language network, specifically a higher integration within the region of the precentral gyrus, pointing to a possible role of the language network in motor sequence planning (Romeo et al., 2021). Indeed, Maitra et al. have reported an improvement in motor function through self-vocalization (Maitra et al., 2006), while Arya et al. demonstrated inadvertent improvement in language following upper limb therapy (Arya and Pandian, 2014). A similar effect was also found following transcranial direct current stimulation over the motor cortex, which led to improved language outcomes (Meinzer et al., 2016). More recently, Hybbinette et al. also demonstrated that similar mechanism of recovery may be involved in language and motor recovery post-stroke, further contributing to the so-termed "shared recovery hypothesis" (Hybbinette et al., 2021). While well-controlled studies examining this phenomenon are lacking, our findings may suggest either: functional compensation by the language system associated with better performance, or impaired connectivity within the language system manifesting in poor sensorimotor outcomes. Since our models are unable to point to which is the case, further studies are necessary to elucidate the interaction of the language and motor networks following stroke. Nonetheless, both our findings, and the literature highlight the possible need to simultaneously target the language and motor systems for effective neurorehabilitation.

4.2. The role of the limbic system in motor recovery

Our models classifying the BRS Upper Limb and FMA Upper Limb both suggested that the limbic/paralimbic system may be playing an important role in motor function following stroke. A similar finding was reported recently by Li et al., who found that the connectivity between the limbic network and DAN was predictive of the FMA (Nishimura et al., 2011). It is therefore possible that the limbic system may be contributing to motor learning after stroke. The limbic system in the Infinitome atlas comprises the orbitofrontal cortex, amygdala, hippocampus, along with other medial temporal regions. Previous studies have established that motor sequence learning relies on the interaction between the prefrontal cortex and hippocampal and striatal networks, along with cortico-cerebellar networks (Albouy et al., 2008; Fernández-Seara et al., 2009; Rose et al., 2011; Burman, 2019; Schapiro et al., 2019; Gann et al., 2021). The activity within the fronto-hippocampal networks decrease as learning progresses (Albouy et al., 2013). As motor learning and re-learning is a key part of neurorehabilitation in the post-stroke period, the limbic system may be key to this process. Alternatively, as the limbic system is also associated with reward and motivation, this finding may be implicating motivation as a key factor in performance. Although one study has examined the role of the motivation in motor recovery following spinal-cord injury in macaques, demonstrating increased functional connectivity between the primary motor cortex and the ventral striatum, orbitofrontal cortex, and anterior cingulate (Nishimura et al., 2011), the role of the limbic network in motor recovery in humans has not garnered much attention. However, it is widely assumed that motivation is a significant component of neurorehabilitation (Widmer et al., 2017; Oyake et al., 2020). Consequently, the limbic system may potentially be a target to improve motor recovery in the post-stroke period, though this remains conjectural and further studies are required to substantiate it.

4.3. Machine learning prediction of stroke outcomes

The prediction performance of our models was comparable to those reported in previous studies examining acute/subacute stroke patients. Wang et al. achieved an AUC of 0.899 using random forest models in acute stroke patients (Wang et al., 2019), while Thakkar et al. had an AUC of 0.77 (Thakkar et al., 2020). It should be noted that direct comparisons of performance are not possible, as most other studies have not combined both DWI based structural and rsfMRI-based FC metrics in machine learning models. Riahi et al. utilized EEG-based FC to estimate the FMA scores in chronic stroke, achieving an R^2 of 0.97 in their regression model (Riahi et al., 2020). Tozlu et al. compared the performance of several types of models in predicting FMA scores based on a combination of demographic, clinical, neurophysiological, and structural connectivity based metrics, achieving an R^2 between 0.70 and 0.91 (Tozlu et al., 2020). In order to compare and generalize

the performance of our models, future research should incorporate functional and structural connectivity measures into holistic brain connectivity models.

Interestingly, our models utilizing FC tended to have better performance than those utilizing structural connectivity. While this needs to be further investigated and validated in independent cohorts, we speculate that this may be reflective of the rapidity of functional compensation, compared to the structural changes which may occur over a longer time span. This is in line with several studies suggesting that functional reorganization is observed within the first 4–5 weeks following stroke (Golestani et al., 2013; Nijboer et al., 2017; Xia et al., 2021), while structural changes occur from 3 to 12 months (Lin L. Y. et al., 2018); though these timings are contentious. For example, a recent study found no changes in the connectivity of motor areas over a year, despite motor improvement (Branscheidt et al., 2022). This may suggest that functional connectivity changes occur distributively to promote recovery, or that some reported connectivity changes are lesion-related, and not a form of compensation. These discrepancies must be addressed through much larger studies utilizing longitudinal data looking at whole-brain functional connectivity. Though there are a number of outstanding questions, our findings make clear that structural and functional connectome changes are related to functional outcomes, and that machine learning models may be necessary to elucidate the complex patterns of neural change occurring in response to stroke.

4.4. Future directions

Overall, our analysis highlighted several networks which may be playing key roles in motor recovery post-stroke, including the DAN, VAN, the language network, and the limbic system. It is possible that enhancing these networks through non-invasive stimulation techniques, such as repetitive transcranial magnetic stimulation, may improve functional outcomes post-stroke. This is however entirely speculative, and clinical trials are necessary to test these targets. rTMS has already demonstrated benefit for motor recovery the post-acute period, however, treatment often targets the primary motor cortex (Dionísio et al., 2018; Fisicaro et al., 2019). It is therefore necessary to investigate whether a more individualized network-based approach to target selection would improve outcomes. While some of our group has demonstrated that this may be a promising and efficacious technique in a case study (Yeung et al., 2021), larger, controlled trials are needed.

Our study also reveals the need to adopt a global-approach when examining deficits in stroke, and therefore looking beyond classically defined motor-regions when investigating motor deficits. This may consequently allow for the development of deficit-specific brain network—networks of functionally connected regions which may be associated with upper limb or lower limb function, or even a spasticity network. These may then enable for further identification of specific targets for treatment.

4.5. Limitations

Our study is limited by a small, heterogeneous sample, and our findings require larger scale prospective studies for validation. Owing to this, we cannot assume that our results are not biased by overfitting to our sample and class imbalances, though our methodology employs several approaches to mitigate this risk, including 5-fold cross-validation and early stopping criteria. Furthermore, future studies should attempt to replicate functional and structural connectivity-based models in a longitudinal cohort study to investigate whether connectivity changes may reveal pathological and compensatory mechanisms in the acute and chronic stages. Finally, models may further benefit from multimodal inputs, considering baseline information beyond connectomic data as we have done. This may enable the establishment of more individualized diagnostic trajectories for patients.

5. Conclusion

The brain connectivity changes that occur as a consequence of stroke are still poorly understood. Analyses of structural and functional changes associated with behavioral outcomes may begin to disentangle the deleterious effects of injury and the facilitatory effects of compensation and recovery; however, explainable machine learning methods are necessary to model and decode the complexity of brain response. Our study highlights the potential of machine learning methods combined with connectivity analysis in predicting outcomes in neurorehabilitation and disentangling the neural correlates of functional impairments, though further longitudinal studies are necessary.

Data availability statement

The raw data supporting the conclusions of this article will be made available by the authors, without undue reservation.

Ethics statement

The studies involving human participants were reviewed and approved by the Ethical Committee of the Affiliated Brain Hospital of Nanjing Medical University. The patients/participants provided their written informed consent to participate in this study.

Author contributions

RB conceived and designed the study. LL and WL performed the study and collect materials. NM wrote the code. NM and KO analyzed the results. OT and KO visualized the results. OT, KO, and XH wrote the manuscript. IY, XZ, MS, SD, RB, MH, and LL helped coordinate the study and reviewed the manuscript. All authors contributed to the article and approved the submitted version.

Funding

The project was supported by the Key Project of Medical Research in Jiangsu Province (No. ZD2022030).

Acknowledgments

Authors thank Yan Zheng and Xinliang Li who are employees of Omniscient Neurotechnology, and they provided technical assistance with the machine learning aspects of the project.

Conflict of interest

NM, KO, OT, IY, SD, and MS are employees of Omniscient Neurotechnology. IY, SD, and MS are also stakeholders of Omniscient Neurotechnology. XH and XZ are the employees of Xijia Medical Technology Company.

The remaining authors declare that the research was conducted in the absence of any commercial or financial relationships that could be construed as a potential conflict of interest.

Publisher's note

All claims expressed in this article are solely those of the authors and do not necessarily represent those of their affiliated organizations, or those of the publisher, the editors and the reviewers. Any product that may be evaluated in this article, or claim that may be made by its manufacturer, is not guaranteed or endorsed by the publisher.

References

Adhikari, M. H., Hacker, C. D., Siegel, J. S., Griffa, A., Hagmann, P., Deco, G., et al. (2017). Decreased integration and information capacity in stroke measured by whole brain models of resting state activity. *Brain* 140, 1068–1085. doi: 10.1093/brain/awx021

Albouy, G., King, B. R., Maquet, P., and Doyon, J. (2013). Hippocampus and striatum: dynamics and interaction during acquisition and sleep-related motor sequence memory consolidation. *Hippocampus* 23, 985–1004. doi: 10.1002/hipo.22183

Albouy, G., Sterpenich, V., Balteau, E., Vandewalle, G., Desseilles, M., Dang-Vu, T., et al. (2008). Both the hippocampus and striatum are involved in consolidation of motor sequence memory. *Neuron* 58, 261–272. doi: 10.1016/j.neuron.2008.02.008

Anderlini, D., Wallis, G., and Marinovic, W. (2019). Language as a predictor of motor recovery: the case for a more global approach to stroke rehabilitation. *Neurorehabil. Neural Repair*. 33, 167–178. doi: 10.1177/1545968319829454

Arya, K. N., and Pandian, S. (2014). Inadvertent recovery in communication deficits following the upper limb mirror therapy in stroke: a case report. *J. Bodyw. Mov. Ther.* 18, 566–568. doi: 10.1016/j.jbmt.2014.02.005

Baldassarre, A., Ramsey, L. E., Siegel, J. S., Shulman, G. L., and Corbetta, M. (2016). Brain connectivity and neurological disorders after stroke. *Curr. Opin. Neurol.* 29, 706–713. doi: 10.1097/WCO.0000000000000396

Barrett, A. M., Boukrina, O., and Saleh, S. (2019). Ventral attention and motor network connectivity is relevant to functional impairment in spatial neglect after right brain stroke. *Brain Cogn.*, 129, 16–24. doi: 10.1016/j.bandc.2018.11.013

Behzadi, Y., Restom, K., Liau, J., and Liu, T. T. (2007). A component based noise correction method (CompCor) for BOLD and perfusion based fMRI. *Neuroimage* 37, 90–101. doi: 10.1016/j.neuroimage.2007.04.042

Bohannon, R. W., and Smith, M. B. (1987). Interrater reliability of a modified Ashworth scale of muscle spasticity. *Phys. Ther.* 67, 206–207. doi: 10.1093/ptj/67.2.206

Branscheidt, M., Ejaz, N., Xu, J., Widmer, M., Harran, M. D., Cortés, J. C., et al. (2022). No evidence for motor-recovery-related cortical connectivity changes after stroke using resting-state fMRI. *J. Neurophysiol.* 127, 637–650. doi: 10.1152/jn.00148.2021

Brunnstrom, S. (1966). Motor testing procedures in hemiplegia: based on sequential recovery stages. *Phys. Ther.* 46, 357–375. doi: 10.1093/ptj/46.4.357

Burman, D. D. (2019). Hippocampal connectivity with sensorimotor cortex during volitional finger movements: laterality and relationship to motor learning. *PLoS ONE* 14, e0222064–e0222064. doi: 10.1371/journal.pone.0222064

Caliandro, P., Vecchio, F., Miraglia, F., Reale, G., Marca, G. D., Torre, G. L., et al. (2017). Small-world characteristics of cortical connectivity changes in acute stroke. *Neurorehabil. Neural Repair*. 31, 81–94. doi: 10.1177/1545968316662525

Campagnini, S., Arienti, C., Patrini, M., Liuzzi, P., Mannini, A., and Carrozza, M. C. (2022). Machine learning methods for functional recovery prediction and prognosis in post-stroke rehabilitation: a systematic review. *J. Neuroeng. Rehabil.* 19, 54. doi: 10.1186/s12984-022-01032-4

Carter, A. R., Astafiev, S. V., Lang, C. E., Connor, L. T., Rengachary, J., Strube, M. J., et al. (2010). Resting interhemispheric functional magnetic resonance imaging connectivity predicts performance after stroke. *Ann. Neurol.* 67, 365–375. doi: 10.1002/ana.21905

Chen, T., and Guestrin, C. (2016). XGBoost: a scalable tree boosting system. *arXiv:1603* 02754. doi: 10.1145/2939672.2939785

Cheng, H.-J., Ng, K. K., Qian, X., Ji, F., Lu, Z. K., Teo, W. P., et al. (2021). Task-related brain functional network reconfigurations relate to motor recovery in chronic subcortical stroke. *Sci. Rep.* 11, 8442–8442. doi: 10.1038/s41598-021-87789-5

Corbetta, M., Patel, G., and Shulman, G. L. (2008). The reorienting system of the human brain: from environment to theory of mind. *Neuron* 58, 306–324. doi: 10.1016/j.neuron.2008.04.017

Corbetta, M., and Shulman, G. L. (2002). Control of goal-directed and stimulus-driven attention in the brain. *Nat. Rev. Neurosci.* 3, 201–215. doi: 10.1038/nrn755

Corbetta, M., and Shulman, G. L. (2011). Spatial neglect and attention networks. *Annu. Rev. Neurosci.* 34, 569–599. doi: 10.1146/annurev-neuro-061010-113731

D'Imperio, D., Romeo, Z., Maistrello, L., Durgoni, E., Pietà, C. D., De Grazia, M. D., et al. (2021). Sensorimotor, attentional, and neuroanatomical predictors of upper limb motor deficits and rehabilitation outcome after stroke. *Neural Plast.* 2021, 8845685. doi: 10.1155/2021/8845685

Ding, X., Li, C.-Y., Wang, Q.-S., Du, F.-Z., Ke, Z.-W., Peng, F., et al. (2014). Patterns in default-mode network connectivity for determining outcomes in cognitive function in acute stroke patients. *Neuroscience* 277, 637–646. doi: 10.1016/j.neuroscience.2014.07.060

Dionísio, A., Duarte, I. C., Patrício, M., Castelo-Branco, M. (2018). The use of repetitive transcranial magnetic stimulation for stroke rehabilitation: a systematic review. *J. Stroke Cerebrovasc. Dis.* 27, 1–31. doi: 10.1016/j.jstrokecerebrovasdis.2017.09.008

Dobkin, B. H. (2005). Clinical practice. Rehabilitation after stroke. *N. Engl. J. Med*. 352, 1677–1684. doi: 10.1056/NEJMcp043511

Doyen, S., Nicholas, P., Poologaindran, A., Crawford, L., Young, I. M., Romero-Garcia, R., et al. (2022). Connectivity-based parcellation of normal and anatomically distorted human cerebral cortex. *Hum. Brain Mapp.* 43, 1358–1369. doi: 10.1002/hbm.25728

Fang, G., Huang, Z., and Wang, Z. (2021). Predicting ischemic stroke outcome using deep learning approaches. *Front. Genet.* 12, 827522. doi: 10.3389/fgene.2021.827522

Fernández-Seara, M. A., Aznárez-Sanado, M., Mengual, E., Loayza, F. R., and Pastor, M. A. (2009). Continuous performance of a novel motor sequence leads to highly correlated striatal and hippocampal perfusion increases. *Neuroimage* 47, 1797–1808. doi: 10.1016/j.neuroimage.2009.05.061

Fisicaro, F., Lanza, G., Grasso, A. A., Pennisi, G., Bella, R., Paulus, W., et al. (2019). Repetitive transcranial magnetic stimulation in stroke rehabilitation: review of the current evidence and pitfalls. *Ther. Adv. Neurol. Disord.* 12, 1756286419878317. doi: 10.1177/1756286419878317

Fugl-Meyer, A. R., Jääskö, L., Leyman, I., Olsson, S., and Steglind, S. (1975). The post-stroke hemiplegic patient. 1.A method for evaluation of physical performance. *Scand. J. Rehabil. Med.* 7, 13–31.

Gann, M. A., King, B. R., Dolfen, N., Veldman, M. P., Chan, K. L., Puts, N. A. J., et al. (2021). Hippocampal and striatal responses during motor learning are modulated by prefrontal cortex stimulation. *Neuroimage* 237, 118158. doi: 10.1016/j.neuroimage.2021.118158

Garyfallidis, E., Brett, M., Amirbekian, B., Rokem, A., van der Walt, S., Descoteaux, M., et al. (2014). Dipy, a library for the analysis of diffusion MRI data. *Front. Neuroinform.* 8, 8. doi: 10.3389/fninf.2014.00008

Glasser, M. F., Coalson, T. S., Robinson, E. C., Hacker, C. D., Harwell, J., Yacoub, E., et al. (2016). A multi-modal parcellation of human cerebral cortex. *Nature* 536, 171–178. doi: 10.1038/nature18933

Golestani, A.-M., Tymchuk, S., Demchuk, A., Goodyear, B. G., and VISION-2 Study Group. (2013). Longitudinal evaluation of resting-state FMRI after acute stroke with hemiparesis. *Neurorehabil. Neural Repair*. 27, 153–163. doi: 10.1177/1545968312457827

Guo, J., Biswal, B. B., Han, S., Li, J., Yang, S., Yang, M., et al. (2019). Altered dynamics of brain segregation and integration in poststroke aphasia. *Hum. Brain Mapp.* 40, 3398–3409. doi: 10.1002/hbm.24605

He, B. J., Snyder, A. Z., Vincent, J. L., Epstein, A., Shulman, G. L., and Corbetta, M. (2007). Breakdown of functional connectivity in frontoparietal networks underlies behavioral deficits in spatial neglect. *Neuron* 53, 905–918. doi: 10.1016/j.neuron.2007.02.013

Holden, M. K., Gill, K. M., Magliozzi, M. R., Nathan, J., and Piehl-Baker, L. (1984). Clinical gait assessment in the neurologically impaired. Reliability and meaningfulness. *Phys. Ther.* 64, 35–40. doi: 10.1093/ptj/64.1.35

Hybbinette, H., Schalling, E., Plantin, J., Nygren-Deboussard, C., and Schütz, M., Östberg, P, et al. (2021). Recovery of apraxia of speech and aphasia in patients with hand motor impairment after stroke. *Front. Neurol.* 12, 634065. doi: 10.3389/fneur.2021.634065

Isensee, F., Schell, M., Pflueger, I., Brugnara, G., Bonekamp, D., Neuberger, U., et al. (2019). Automated brain extraction of multisequence MRI using artificial neural networks. *Hum. Brain Mapp.* 40, 4952–4964. doi: 10.1002/hbm.24750

Karahan, A. Y., Kucuksen, S., Yilmaz, H., Salli, A., Gungor, T., and Sahin, M. (2014). Effects of rehabilitation services on anxiety, depression, care-giving burden and perceived social support of stroke caregivers. *Acta Med.* 57, 68–72. doi: 10.14712/18059694.2014.42

Kim, J. K., Lv, Z., Park, D., and Chang, M. C. (2022). Practical machine learning model to predict the recovery of motor function in patients with stroke. *Eur. Neurol.* 85, 273–279. doi: 10.1159/000522254

Larivière, S., Ward, N. S., and Boudrias, M.-H. (2018). Disrupted functional network integrity and flexibility after stroke: relation to motor impairments. *Neuroimage Clin.* 19, 883–891. doi: 10.1016/j.nicl.2018.06.010

Lee, J., Park, E., Lee, A., Chang, W. H., Kim, D.-S., and Kim, Y.-H. (2018). Alteration and role of interhemispheric and intrahemispheric connectivity in motor network after stroke. *Brain Topogr.* 31, 708–719. doi: 10.1007/s10548-018-0644-9

Lee, J., Park, E., Lee, A., Chang, W. H., Kim, D.-S., and Kim, Y.-H. (2020). Prediction of motor recovery using indirect connectivity in a lesion network after ischemic stroke. *Ther. Adv. Neurol. Disord.* 13, 1756286420925679. doi: 10.1177/1756286420925679

Liao, W.-W., Hsieh, Y.-W., Lee, T.-H., Chen, C.-L., and Wu, C.-Y. (2022). Machine learning predicts clinically significant health related quality of life improvement after sensorimotor rehabilitation interventions in chronic stroke. *Sci. Rep.* 12, 11235. doi: 10.1038/s41598-022-14986-1

Lin, L. Y., Ramsey, L., Metcalf, N. V., Rengachary, J., Shulman, G. L., Shimony, J. S., et al. (2018). Stronger prediction of motor recovery and outcome post-stroke by cortico-spinal tract integrity than functional connectivity. *PLoS ONE* 13, e0202504. doi: 10.1371/journal.pone.0202504

Lin, W.-Y., Chen, C.-H., Tseng, Y.-J., Tsai, Y.-T., Chang, C.-Y., Wang, H.-Y., et al. (2018). Predicting post-stroke activities of daily living through a machine learning-based approach on initiating rehabilitation. *Int. J. Med. Inform.* 111, 159–164. doi: 10.1016/j.ijmedinf.2018.01.002

Lundberg, S., and Lee, S.-I. (2017). A unified approach to interpreting model predictions. *arXiv:1705.07874*. doi: 10.48550/arXiv.1705.07874

Mahoney, F. I., and Barthel, D. W. (1965). Functional evaluation: the barthel index. *Md. State Med. J.* 14, 61–65. doi: 10.1037/t02366-000

Maitra, K. K., Telage, K. M., and Rice, M. S. (2006). Self-speech-induced facilitation of simple reaching movements in persons with stroke. *Am. J. Occup. Ther.* 60, 146–154. doi: 10.5014/ajot.60.2.146

Marebwa, B. K., Fridriksson, J., Yourganov, G., Feenaughty, L., Rorden, C., and Bonilha, L. (2017). Chronic post-stroke aphasia severity is determined by fragmentation of residual white matter networks. *Sci. Rep.* 7, 8188. doi: 10.1038/s41598-017-07607-9

Meinzer, M., Darkow, R., Lindenberg, R., and Flöel, A. (2016). Electrical stimulation of the motor cortex enhances treatment outcome in post-stroke aphasia. *Brain* 139(Pt 4), 1152–1163. doi: 10.1093/brain/aww002

Meyer, S., Verheyden, G., Brinkmann, N., Dejaeger, E., De Weerdt, W., Feys, H., et al. (2015). Functional and motor outcome 5 years after stroke is equivalent to outcome at 2 months: follow-up of the collaborative evaluation of rehabilitation in stroke across Europe. *Stroke* 46, 1613–1619. doi: 10.1161/STROKEAHA.115.009421

Nijboer, T. C. W., Buma, F. E., Winters, C., Vansteensel, M. J., Kwakkel, G., Ramsey, N. F., et al. (2017). No changes in functional connectivity during motor recovery beyond 5 weeks after stroke; a longitudinal resting-state fMRI study. *PLoS ONE* 12, e0178017. doi: 10.1371/journal.pone.0178017

Nishimura, Y., Onoe, H., Onoe, K., Morichika, Y., Tsukada, H., and Isa, T. (2011). Neural substrates for the motivational regulation of motor recovery after spinal-cord injury. *PLoS ONE*. 6, e24854. doi: 10.1371/journal.pone.0024854

Olafson, E. R., Jamison, K. W., Sweeney, E. M., Liu, H., Wang, D., Bruss, J. E., et al. (2021). Functional connectome reorganization relates to post-stroke motor recovery and structural and functional disconnection. *Neuroimage* 245, 118642. doi: 10.1016/j.neuroimage.2021.118642

Omniscient Neurotechnology (2020). Infinitome. Available from: https://o8t.com

Oyake, K., Suzuki, M., Otaka, Y., and Tanaka, S. (2020). Motivational strategies for stroke rehabilitation: a descriptive cross-sectional study. *Front. Neurol.* 11, 553. doi: 10.3389/fneur.2020.00553

Ptak, R., and Schnider, A. (2010). The dorsal attention network mediates orienting toward behaviorally relevant stimuli in spatial neglect. *J. Neurosci.* 30, 12557–12565. doi: 10.1523/JNEUROSCI.2722-10.2010

Puig, J., Blasco, G., Alberich-Bayarri, A., Schlaug, G., Deco, G., Biarnes, C., et al. (2018). Resting-state functional connectivity magnetic resonance imaging and outcome after acute stroke. *Stroke* 49, 2353–2360. doi: 10.1161/STROKEAHA.118.021319

Rehme, A. K., Eickhoff, S. B., Rottschy, C., Fink, G. R., and Grefkes, C. (2012). Activation likelihood estimation meta-analysis of motor-related neural activity after stroke. *Neuroimage* 59, 2771–2782. doi: 10.1016/j.neuroimage.2011.10.023

Riahi, N., Vakorin, V. A., and Menon, C. (2020). Estimating fugl-meyer upper extremity motor score from functional-connectivity measures. *IEEE Trans. Neural Syst. Rehabil. Eng.* 28, 860–868. doi: 10.1109/TNSRE.2020.2978381

Romeo, Z., Mantini, D., Durgoni, E., Passarini, L., Meneghello, F., and Zorzi, M. (2021). Electrophysiological signatures of resting state networks predict cognitive deficits in stroke. *Cortex* 138, 59–71. doi: 10.1016/j.cortex.2021.01.019

Rose, M., Haider, H., Salari, N., and Büchel, C. (2011). Functional dissociation of hippocampal mechanism during implicit learning based on the domain of associations. *J. Neurosci.* 31, 13739–13745. doi: 10.1523/JNEUROSCI.3020-11.2011

Schapiro, A. C., Reid, A. G., Morgan, A., Manoach, D. S., Verfaellie, M., and Stickgold, R. (2019). The hippocampus is necessary for the consolidation of a task that does not require the hippocampus for initial learning. *Hippocampus* 29, 1091–1100. doi: 10.1002/hipo.23101

Siegel, J. S., Ramsey, L. E., Snyder, A. Z., Metcalf, N. V., Chacko, R. V., Weinberger, K., et al. (2016). Disruptions of network connectivity predict impairment in multiple behavioral domains after stroke. *Proc. Natl. Acad. Sci. U. S. A.* 113, E4367–E4376. doi: 10.1073/pnas.1521083113

Thakkar, H. K., Liao, W.-W., Wu, C.-Y., Hsieh, Y.-W., and Lee, T.-H. (2020). Predicting clinically significant motor function improvement after contemporary task-oriented interventions using machine learning approaches. *J. Neuroeng. Rehabil.* 17, 131. doi: 10.1186/s12984-020-00758-3

Tozlu, C., Edwards, D., Boes, A., Labar, D., Tsagaris, K. Z., Silverstein, J., et al. (2020). Machine learning methods predict individual upper-limb motor impairment following therapy in chronic stroke. *Neurorehabil. Neural Repair.* 34, 428–439. doi: 10.1177/1545968320909796

Tuladhar, A. M., Snaphaan, L., Shumskaya, E., Rijpkema, M., Fernandez, G., Norris, D. G., et al. (2013). Default mode network connectivity in stroke patients. *PLoS ONE* 8, e66556–e66556. doi: 10.1371/journal.pone.0066556

Vicentini, J. E., Weiler, M., Casseb, R. F., Almeida, S. R., Valler, L., de Campos, B. M., et al. (2021). Subacute functional connectivity correlates with cognitive recovery six months after stroke. *Neuroimage Clin.* 29, 102538. doi: 10.1016/j.nicl.2020.102538

Wang, C., Qin, W., Zhang, J., Tian, T., Li, Y., Meng, L., et al. (2014). Altered functional organization within and between resting-state networks in chronic subcortical infarction. *J. Cereb. Blood Flow Metab.* 34, 597–605. doi: 10.1038/jcbfm.2013.238

Wang, H.-L., Hsu, W.-Y., Lee, M.-H., Weng, H.-H., Chang, S.-W., Yang, J.-T., et al. (2019). Automatic machine-learning-based outcome prediction in patients with primary intracerebral hemorrhage. *Front. Neurol.* 10, 910. doi: 10.3389/fneur.2019.00910

Wang, Y. L. (2018). *Functional Assessment of Rehabilitation, 3rd Edn*. Beijing: People's Medical Publishing House.

Widmer, M., Held, J. P., Wittmann, F., Lambercy, O., Lutz, K., and Luft, A. R. (2017). Does motivation matter in upper-limb rehabilitation after stroke? ArmeoSenso-Reward: study protocol for a randomized controlled trial. *Trials* 18, 580. doi: 10.1186/s13063-017-2328-2

Wu, C. W., Lin, S.-H. N., Hsu, L.-M., Yeh, S.-C., Guu, S.-F., Lee, S.-H., et al. (2020). Synchrony between default-mode and sensorimotor networks facilitates motor function in stroke rehabilitation: a pilot fMRI study. *Front. Neurosci.* 14, 548. doi: 10.3389/fnins.2020.00548

Xia, Y., Huang, G., Quan, X., Qin, Q., Li, H., Xu, C., et al. (2021). Dynamic structural and functional reorganizations following motor stroke. *Med. Sci. Monit.* 27, e929092. doi: 10.12659/MSM.929092

Yeo, B. T. T., Krienen, F. M., Sepulcre, J., Sabuncu, M. R., Lashkari, D., Hollinshead, M., et al. (2011). The organization of the human cerebral cortex estimated by intrinsic functional connectivity. *J. Neurophysiol.* 106, 1125–1165. doi: 10.1152/jn.00338.2011

Yeung, J. T., Young, I. M., Doyen, S., Teo, C., and Sughrue, M. E. (2021). Changes in the brain connectome following repetitive transcranial magnetic stimulation for stroke rehabilitation. *Cureus* 13, e19105. doi: 10.7759/cureus.19105

frontiers | Frontiers in Neuroscience

TYPE Original Research
PUBLISHED 22 February 2023
DOI 10.3389/fnins.2023.1138670

OPEN ACCESS

EDITED BY
Lingfei Guo,
Shandong Provincial Hospital Affiliated to Shandong First Medical University, China

REVIEWED BY
Shengpei Wang,
Institute of Automation (CAS), China
Xuan Bu,
Beijing Normal University, China

*CORRESPONDENCE
Seyedmehdi Payabvash
✉ sam.payabvash@yale.edu

SPECIALTY SECTION
This article was submitted to Brain Imaging Methods, a section of the journal Frontiers in Neuroscience

RECEIVED 06 January 2023
ACCEPTED 07 February 2023
PUBLISHED 22 February 2023

CITATION
Lin H, Haider SP, Kaltenhauser S, Mozayan A, Malhotra A, Constable RT, Scheinost D, Ment LR, Konrad K and Payabvash S (2023) Population level multimodal neuroimaging correlates of attention-deficit hyperactivity disorder among children.
Front. Neurosci. 17:1138670.
doi: 10.3389/fnins.2023.1138670

Population level multimodal neuroimaging correlates of attention-deficit hyperactivity disorder among children

Huang Lin[1,2], Stefan P. Haider[1], Simone Kaltenhauser[1], Ali Mozayan[1], Ajay Malhotra[1], R. Todd Constable[1], Dustin Scheinost[1], Laura R. Ment[3,4], Kerstin Konrad[2,5] and Seyedmehdi Payabvash[1]*

[1]Department of Radiology and Biomedical Imaging, Yale School of Medicine, New Haven, CT, United States, [2]Child Neuropsychology Section, Department of Child and Adolescent Psychiatry, Psychosomatics and Psychotherapy, University Hospital RWTH Aachen, Aachen, Germany, [3]Department of Pediatrics, Yale School of Medicine, New Haven, CT, United States, [4]Department of Neurology, Yale School of Medicine, New Haven, CT, United States, [5]Jülich Research Centre, JARA Brain Institute II, Molecular Neuroscience and Neuroimaging (INM-11), Jülich, Germany

Objectives: Leveraging a large population-level morphologic, microstructural, and functional neuroimaging dataset, we aimed to elucidate the underlying neurobiology of attention-deficit hyperactivity disorder (ADHD) in children. In addition, we evaluated the applicability of machine learning classifiers to predict ADHD diagnosis based on imaging and clinical information.

Methods: From the Adolescents Behavior Cognitive Development (ABCD) database, we included 1,798 children with ADHD diagnosis and 6,007 without ADHD. In multivariate logistic regression adjusted for age and sex, we examined the association of ADHD with different neuroimaging metrics. The neuroimaging metrics included fractional anisotropy (FA), neurite density (ND), mean-(MD), radial-(RD), and axial diffusivity (AD) of white matter (WM) tracts, cortical region thickness and surface areas from T1-MPRAGE series, and functional network connectivity correlations from resting-state fMRI.

Results: Children with ADHD showed markers of pervasive reduced microstructural integrity in white matter (WM) with diminished neural density and fiber-tracks volumes – most notable in the frontal and parietal lobes. In addition, ADHD diagnosis was associated with reduced cortical volume and surface area, especially in the temporal and frontal regions. In functional MRI studies, ADHD children had reduced connectivity among default-mode network and the central and dorsal attention networks, which are implicated in concentration and attention function. The best performing combination of feature selection and machine learning classifier could achieve a receiver operating characteristics area under curve of 0.613 (95% confidence interval = 0.580–0.645) to predict ADHD diagnosis in independent validation, using a combination of multimodal imaging metrics and clinical variables.

Conclusion: Our study highlights the neurobiological implication of frontal lobe cortex and associate WM tracts in pathogenesis of childhood ADHD. We also demonstrated possible potentials and limitations of machine learning models to

assist with ADHD diagnosis in a general population cohort based on multimodal neuroimaging metrics.

KEYWORDS

attention-deficient hyperactivity disorder, brain connectivity, white matter microstructure, cortex morphology, machine learning

1. Introduction

Attention-deficit/hyperactivity disorder (ADHD) is estimated to affect 6.1% of children in the U.S. (Danielson et al., 2018). Neuroimaging studies can help elucidate the underlying neurobiology of ADHD, suggesting that abnormal brain connectivity plays a central role in pathogenesis of ADHD (Aoki et al., 2018). Children with ADHD also have shown abnormalities in axonal density and volume of multiple white matter (WM) tracts (Wu et al., 2020). In addition, subtle differences in cortical surface area, involvement of the frontal cortex and reduced cortical volume (Kumar et al., 2017) as well as alterations in functional connectivity in the left insula and left inferior frontal gyrus (Chiang et al., 2020) have been reported in children with ADHD. The variable range of reported neuroimaging correlates of ADHD may be due to small sample size and differences in diagnostic criteria of prior studies. Large studies – such as the ABCD (Adolescent Brain and Cognitive Development) – can provide powerful tools to determine neuroimaging correlates of ADHD among the general population children.

In this study, we aimed to determine the imaging metrics of brain microstructure, morphology and functional connectivity associated with ADHD diagnosis in a large cross-sectional cohort of preadolescent American children. While prior large-scale studies focused on one set of neuroimaging characteristics (e.g., cortical thickness) in relation to ADHD diagnosis (Hoogman et al., 2019; Bernanke et al., 2022; Sudre et al., 2022), we examined multimodal imaging metrics among the same children cohort to achieve a comprehensive assessment of brain morphology, microstructure and connectivity changes in associated with ADHD. We also trained, finetuned, compared, and validated different combinations of feature selection and machine learning classifiers to predict ADHD diagnosis in children based on multimodal MRI metrics. Such neuroimaging-based tools may complement the clinical assessment for the diagnosis of ADHD among children, particularly in the presence of cultural, language, or communication barriers.

2. Materials and methods

2.1. The ABCD database and study population

The ABCD Study (RRID: SCR_015769) is the largest longitudinal study of neurodevelopment and child health in the United States. Using a school-based recruitment strategy, data from over ten thousand 9–10-year-olds were collected from 21 sites, which included multimodal neuroimaging, and standardized cognitive and clinical assessments (Casey et al., 2018). The study population is representative of the demographics of the general U.S. population (Garavan et al., 2018). The inclusion criteria were children's age and attending a public or private elementary school in the catchment area; whereas, exclusion criteria were: (1) child not being proficient in English language; (2) having severe limitations in sensory, neurological, medical, or intellectual abilities that would prevent the child from following the study protocol; and (3) not being able to complete a baseline MRI scan. The study adheres to the policies and procedures of the Institutional Review Board at each site, and all participants have given their informed consent (for parents) or assent (for children) to participate.

2.2. Subjects' ascertainment

Figure 1 summarizes the subjects' ascertainment process. We retrieved the tabulated imaging information and clinical information from the third public ABCD data release (Yang and Jernigan, 2020) including baseline and the 2-year follow-up assessments. Following the recommendations of the ABCD Consortium in the Release Notes to the 3.0 release, we removed all patients who had an fMRI scan using Philips scanners due to incorrect post-processing (Yang and Jernigan, 2020). To identify patients with ADHD, we used the ABCD Parent Diagnostic Interview scale for the Kiddie-Schedule for Affective Disorders and Schizophrenia (K-SADS) DSM-5 to label the children as having ADHD or not. For assessment, the computerized version of the KSADS (KSADS-COMP) was used by the ABCD Consortium. We selected the KSADS-COMP categorical diagnosis of ADHD as the primary outcome due to its availability in the ABCD dataset, alignment with DSM-5 criteria, established validity and reliability in both research and clinical settings, including in epidemiological studies (Kaufman et al., 1997). Anyone with a present, past or (partial) remission ADHD diagnosis at baseline or 2-year follow-up assessment was assigned to the ADHD-positive group, and remaining subjects were labeled as "without ADHD." We included following covariates from the ABCD dataset: children's age (months), biological sex (female, male), race (White, Black, Asian, Hispanic, Mixed/Other), highest parental education (no Highschool Degree, Highschool/General Education Degree, College/Associate Degree, Bachelor's Degree, Postgraduate Degree), and handedness (Right, Left, Mixed). Biological sex, race and highest parental education were assessed by parental reported questionnaires at baseline. Handedness was assessed at baseline using the Youth Edinburgh Handedness Inventory Short Form. We excluded those with incomplete K-SADS ADHD diagnosis at

baseline or 2-year-follow-up, history of traumatic brain injury, and failure to pass the image quality control performed manually by the ABCD Consortium (e.g., due to artifacts) (Hagler et al., 2019).

2.3. MRI acquisition and neuroimaging measures

The ABCD image acquisition protocol includes structural (sMRI), diffusion (dMRI), and functional (fMRI) MRI collected using Siemens Prisma, GE 750 and Philips Achieva and Ingenia 3 T scanners. According to the ABCD Consortium, standardized imaging protocols were used to create harmonized scans across all sites and scanner manufactures.[1] Full details on image acquisition and image processing steps can be found in paper provided by the ABCD Consortium (Casey et al., 2018; Hagler et al., 2019). Details about acquisition parameter have been described previously (Casey et al., 2018). The standardized processing pipeline was performed with Freesurfer (version 5.3.0). A list of all cortical, subcortical, and WM regions of interest (ROI) can be found in section "1. List of Atlas Regions (**Supplementary material**)." In the following section we will give a brief overview.

2.3.1. Structural MRI

Morphometric and macrostructural properties of different cortical regions of interest (ROI) based on the Desikan-Killiany atlas (Desikan et al., 2006) were extracted from high resolution T1-weighted images (1 mm isotropic) – including cortical volume, thickness, surface areas, and sulcal depths of 35 ROI. The standardized processing included skull stripping, WM segmentation, topological defect correction, surface optimization, and non-linear registration to a spherical surface-based atlas.

2.3.2. Diffusion MRI

The dMRI data was collected in the axial plane using a resolution of 1.7 mm in all directions, which is the same as the dMRI data acquisition resolution, and a multiband acceleration factor of 3. Images were corrected for eddy current distortion, head motion, spatial, and intensity distortion correction and gradient non-linearity correction. The dMRI data was aligned with T1w structural images using mutual information after a rough initial alignment with atlas brains. To examine WM microstructural integrity, neurite density (ND) and fiber tract (FT) thickness as well as water diffusion metrics – including fractional anisotropy (FA), mean- (MD), longitudinal- (RD), and axial diffusivity (AD) – were calculated for 35 WM tracts and only ND for 12 subcortical structures from dMRI scans. These metrics from major WM tracts were extracted using AtlasTrack implemented (Hagler et al., 2009).

2.3.3. Resting-state fMRI

High resolution resting state fMRI data was acquired in four runs of 5 min each, for a total of 20 min. Other resting-state parameters have been previously described.[2] In the ABCD study, a software package called Multi-Modal Processing Stream (MMPS) is used for pre-processing data and incorporates other software packages such as FreeSurfer, AFNI, and FSL. The pre-processing steps include correcting head motion by aligning each frame with the first one, fixing B0 distortions, and resampling the scans to align with each other. The scans are also registered to T1-weighted structural images using mutual information. Linear regression is used to remove quadratic trends, signals that are correlated with estimated motion time courses, and average time courses for WM, ventricles, and the whole brain. Motion regression includes six parameters and their derivatives and squares, and only frames with framewise displacement (FD) less than 0.3 mm are included. Time points with FD more than 0.2 mm are excluded from variance and correlation calculations. The average FD is 0.25 mm. The time courses are filtered between 0.009 and 0.08 Hz. Motion censoring is applied to reduce remaining effects of head motion that survive the pre-analysis regression. Additional censoring is applied based on detecting time points as outliers with respect to spatial variation across the brain to account for lingering effects of head motion. The average correlation between the baseline functional networks according to Gordon parcel atlas (Gordon et al., 2016), were calculated and transformed to *z*-scores, representing the functional connectivity.

2.4. Multivariate models

In separate multivariate logistic regression models, we tested the association of different neuroimaging metrics with presence versus absence of ADHD. In each model, we tested the association of one neuroimaging variable with ADHD presence after correction for children's age, biological sex, race, highest parental education and handedness as covariates. Biological sex, race and highest parental education were assessed by parental reported questionnaires. Handedness was assessed by the Youth Edinburgh Handedness Inventory Short Form. All variables were treated as unordered factors, except of age. The neuroimaging metrics included the averaged FA, ND, MD, RD, FT, and AD of 35 WM tracts and ND of 12 subcortical regions, thickness, and surface areas of 68 cortical regions, the inter- and intra-network correlations of 13 functional networks. To correct for multiple comparisons, we applied false discovery rate separately for each neuroimaging metrics to generate adjusted *p*-values. *p*-Values < 0.05 were considered as significant. All analyses were performed using R software (version 4.1.2) using the *stats*-package (version 3.6.2).

2.5. Feature selection and machine learning

We trained, finetuned, and compared combinations of six different machine learning classifiers and five feature selection methods to predict the presence versus absence of ADHD. The input included all multimodal MRI metrics with and without the clinical information (i.e., sex, age, race, highest parental education, and handedness). Detailed description of the different machine

1 https://abcdstudy.org/wp-content/uploads/2021/05/ABCD_Website_MRI_Acq.pdf

2 https://abcdstudy.org/images/Protocol_Imaging_Sequences.pdf

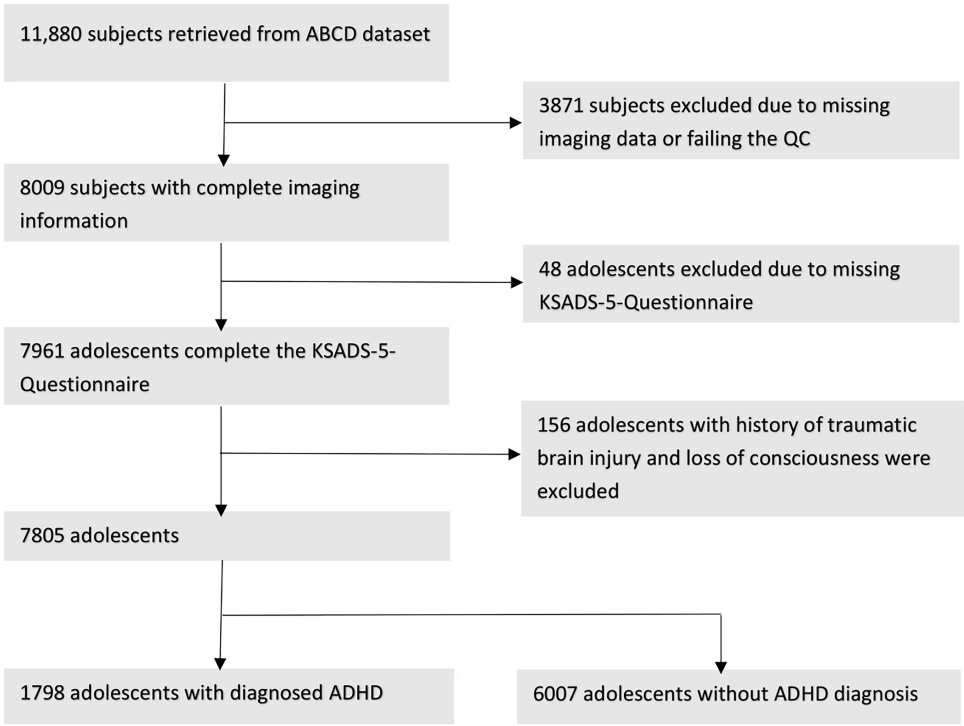

FIGURE 1
Workflow after we proceed to extract our cohorts regarding to the exclusion criteria and showing the remain subjects.

learning algorithms and featured selection methods are in section "2. Machine learning (**Supplementary material**)" and reported previously (Haider et al., 2020). The dataset was randomly split into training/cross-validation and independent validation cohorts in a 4-to-1 ratio. Selection of features were done on the training folds before training the machine-learning classifier to prevent information leakage and reduce overfitting. In every iteration of the cross-validation process, the training data was standardized and certain features were selected, and then a machine learning model was trained using that data. This method ensures accurate estimates of the model's performance on independent validation sets. For each combination we created a framework of five repeats of 10-fold cross-validation for finetuning of feature selection and machine learning hyperparameters using the Bayesian optimization within the training/cross-validation cohort. For every hyperparameter and the number of selected features, an upper and lower bond was set as described previously (see section "2.3. Hyperparameter bounds for Bayesian optimization (**Supplementary material**)"; Haider et al., 2020). The optimized parameters were then adopted in the machine-learning/feature-selection framework followed by five repeats of 10-fold cross-validation. In each fold of cross-validation, we calculated the area under curve (AUC) of receiver operating characteristics (ROC) for prediction of ADHD presence in validation fold. The averaged AUC across all validation folds was used to identify the best combination. Finally, we trained the best performing model with optimized parameters on all training/cross-validation cohort, and tested the model in independent validation set, which was isolated from the training, optimization, and cross-validation process. The trained model was applied to the independent test set and the performance was evaluate by AUC (95% CI).

3. Results

3.1. Subjects' demographics

Figure 1 depicts the inclusion flowchart of children for our analysis. After excluding those with incomplete clinical information, history of traumatic brain injury, and failure to pass image quality control, a total of 7,805 participants (average age of 119.33 months) were included in our analysis – 1,798 with and 6,007 without ADHD. **Table 1** summarizes demographic characteristics of each subcohort. In multivariate analysis, there was a significant difference in racial/ethnicity distribution between those with and without ADHD (**Table 1**), with ratio of black children slightly higher while Asian children lower among those with ADHD. In addition, the rate of handedness and parental education were different between children with and without ADHD (**Table 1**).

3.2. ADHD and cortical morphology

Children with ADHD had reduced cortical surface area and volume compared to those without – especially in frontal and temporal lobes (**Figure 2**). The presence of ADHD was associated with lower cortical surface area with most pronounced differences in the right middle-temporal gyrus

TABLE 1 Characteristics of children with and without ADHD diagnosis.

Demographics description				
	With ADHD	Without ADHD	Total	*p*-value
	1,798	6,007	7,805	
Age (in months)				0.83
Mean (SD)	119.5 (7.5)	119.3 (7.6)	119.3 (7.55)	
Min–max	107–132	107–133	107–133	
Median (IQR)	120	119	119	
Sex, *n* (%)				$<2.2 \times 10^{-16}$
Female	654 (36.4%)	3,224 (53.7%)	3,878 (49.7%)	
Male	1,144 (63.6%)	2,783 (46.3%)	3,927 (50.3%)	
Race, *n* (%)				$<6.53 \times 10^{-4}$
White	997 (55.5%)	3,324 (55.3%)	4,321 (55.4%)	
Black	293 (16.35%)	818 (13.6%)	111 (14.2%)	
Asian	21 (1.2%)	136 (2.3%)	157 (2.0%)	
Hispanic	325 (18.1%)	1,244 (20.7%)	1,569 (20.1%)	
Undetermined	6 (0.3%)	17 (0.3%)	23 (0.3%)	
Mixed/Others	156 (8.7%)	468 (7.8%)	624 (8.0%)	
Handedness, *n* (%)				3.46×10^{-5}
Right	1,388 (77.2%)	4,912 (81.8%)	6,300 (80.7%)	
Left	137 (7.6%)	406 (6.8%)	543 (7.0%)	
Both	273 (15.2%)	689 (11.5%)	962 (12.3%)	
Highest parental education, *n* (%)				1.91×10^{-3}
No highschool degree	96 (5.3%)	345 (5.7%)	441 (5.7%)	
Highschool/General educational development	139 (7.7%)	482 (8.0%)	621 (8.0%)	
Some college/Associate degree	534 (29.7%)	1,439 (24.0%)	1,973 (25.3%)	
Bachelor's degree	483 (26.9%)	1,559 (26.0%)	2,042 (26.2%)	
Postgraduate	543 (30.2%)	2,177 (36.2%)	2,720 (34.8%)	
Undetermined	3 (0.2%)	5 (0.1%)	8 (0.1%)	

(adjusted *p*-value = 1.574×10^{-9}), left rostral-middle-frontal gyrus (adjusted *p*-value = 1.475×10^{-8}), left superior frontal gyrus (adjusted *p*-value = 1.475×10^{-8}), and right inferior/superior temporal gyrus (both adjusted *p*-value = 1.475×10^{-8}). An ADHD diagnosis was also associated with reduced cortical volumes (Figure 2B), most pronounced in the left rostral middle-frontal gyrus (adjusted *p*-value = 8.044×10^{-8}), left superior frontal gyrus (adjusted *p*-value = 5.107×10^{-7}), right middle-temporal gyrus (adjusted *p*-value = 6.347×10^{-7}), and the right inferior-temporal gyrus (adjusted *p*-value = 6.347×10^{-7}) regions. No differences in sulcal depths and cortical thickness remained significant after FDR correction [see section "3.1. Structural MRI (Supplementary material)"].

3.3. ADHD and WM microstructure

Children with ADHD had a significantly lower FA and ND, but higher MD and RD compared to children without ADHD – especially in frontal and parietal WM [see section "3.2. Diffusion MRI (Supplementary material)"]. In addition, ADHD was associated with lower FT. The highly significant changes ($p < 0.001$) in DTI metrics and FT were most notable in the corticostriatal tract which connects the superior frontal and parietal cortex with the striatum; WM tract connecting inferior frontal cortex and superior frontal cortex; and superior longitudinal fasciculus connecting parietal and frontal lobe (Figure 3). There were no differences in WM AD between children with and without ADHD diagnosis.

3.4. ADHD and functional connectivity

Children with ADHD showed increased connectivity between the default network and the dorsal attention network (adjusted *p*-value = 3.721×10^{-6}) and the cingulo-opercular network (adjusted *p*-value = 3.981×10^{-4}) (Figure 4). Moreover, the correlation between the dorsal and the ventral attention networks (adjusted *p*-value = 5.324×10^{-4}) was also higher among those with ADHD. In contrast, ADHD was associated with decreased

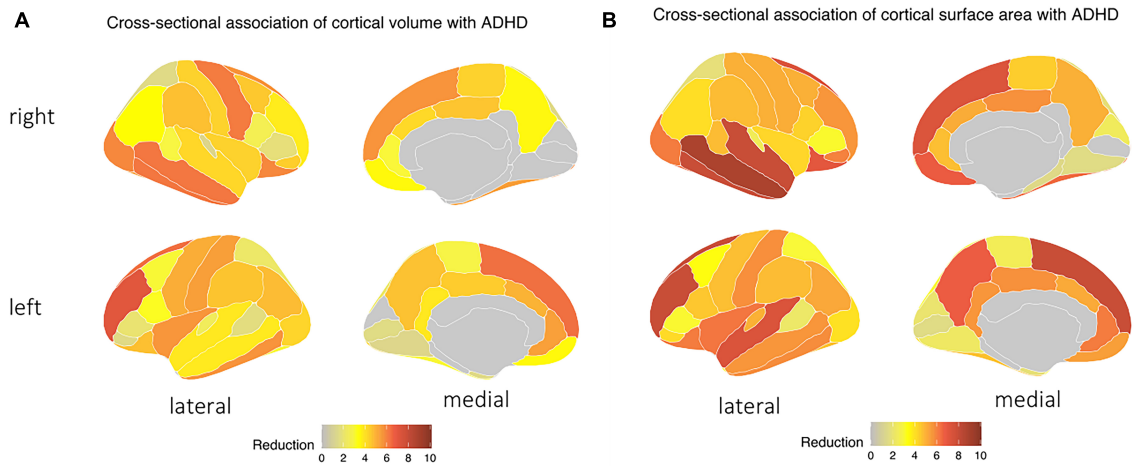

FIGURE 2
Children with ADHD tend to have a decrease in both in **(A)** cortical surface area and **(B)** cortical volume, particularly in the temporal and frontal lobes, as indicated by the blue area – independent of age, biological sex, race, handedness, and highest parental education as a marker of socioeconomic status, and after correction for multiple comparisons.

intra-network connectivity of the dorsal attention (adjusted p-value = 2.169×10^{-4}), default mode (adjusted p-value = 0.020), and retrosplenial temporal (adjusted p-value = 2.169×10^{-4}) networks [see section "3.3. Rest-state fMRI (**Supplementary material**)"].

3.5. Machine learning classifiers for predicting ADHD

The rate of ADHD diagnosis in both training/cross-validation (1,420 out of 6,244, 22.8%) and independent validation test (378 out of 1,561, 24.2%) sets were similar (p = 0.229). **Table 2** summarize the demographics of subjects in training and independent validation sets. The **Figure 5A** heatmap depicts the mean AUCs across validation folds from five repeats of 10-fold cross-validations with neuroimaging variables alone (without any clinical information) as input. The combination of eXtreme Gradient Boosting (XGB) and RIDGE regularized logistic regression (RIDGE) for feature selection had the highest averaged AUC of 0.58. For combined input of clinical and neuroimaging variables, the best performance was achieved by the combination of Support Vector machine with radial kernel (SVM_rad) in combination with Hierarchical Clustering (HClust) feature selection with mean AUC of 0.627 (**Figure 5B**). In this model all clinical features (i.e., sex, age, race, highest parental education, and handedness) were selected by HClust. Selected feature with the feature importance can be found in section "2.4. Selected feature in final model (**Supplementary material**)." In the independent validation test set, the best performing model using neuroimaging variables achieved an AUC of 0.576 (95% CI = 0.546–0.610) with sensitivity of 56.61% and specificity of 64.86% compared to a model using clinical and neuroimaging variables which achieved AUC of 0.613 (95% CI = 0.580–0.645), with sensitivity of 60.05% and specificity of 56.47%. However, the difference between models using neuroimaging versus combined variables for prediction of ADHD diagnosis in the independent validation test cohort was not statistically significant (p = 0.0851).

4. Discussion

Leveraging a large population dataset, we identified the multimodal neuroimaging correlates of ADHD in 9–10-year-old children. While many prior studies have examined smaller selective cohorts of ADHD children versus typically developing controls, we adopted more inclusive criteria comparing multimodal neuroimaging correlates of those with and without ADHD diagnosis in a large demographically representative population of American children. By having a large sample size, our study approach highlights the neuroimaging correlates of ADHD in demographically representative cohort. Our study population are more representative of all-comers children presenting to clinical practices, when ADHD is often accompanied by other comorbidities. We found that children with ADHD had WM microstructural disintegrity and reduced neural density (particularly in frontal and parietal lobes), decreased cortical volume and surface area (most striking in the frontal and temporal lobes); and altered connectivity of attention functional networks compared to those without – after correction for children's age, sex, race/ethnicity, handedness, and highest parental education (as a marker of socioeconomic status). Our findings highlight the neurobiological and connectome mechanism of ADHD among preadolescent children at demographically representative population-level. In addition, we showed the potentials and limitations of machine learning classifiers in combining neuroimaging metrics (and clinical variables) to predict ADHD diagnosis. In addition, multimodal framework of our study further highlights the role of frontal lobe cortical regions and associated WM tracts in neurobiology of childhood ADHD (Bernanke et al., 2022).

Children with ADHD have been found to have morphological differences in brain structure compared to typically developing

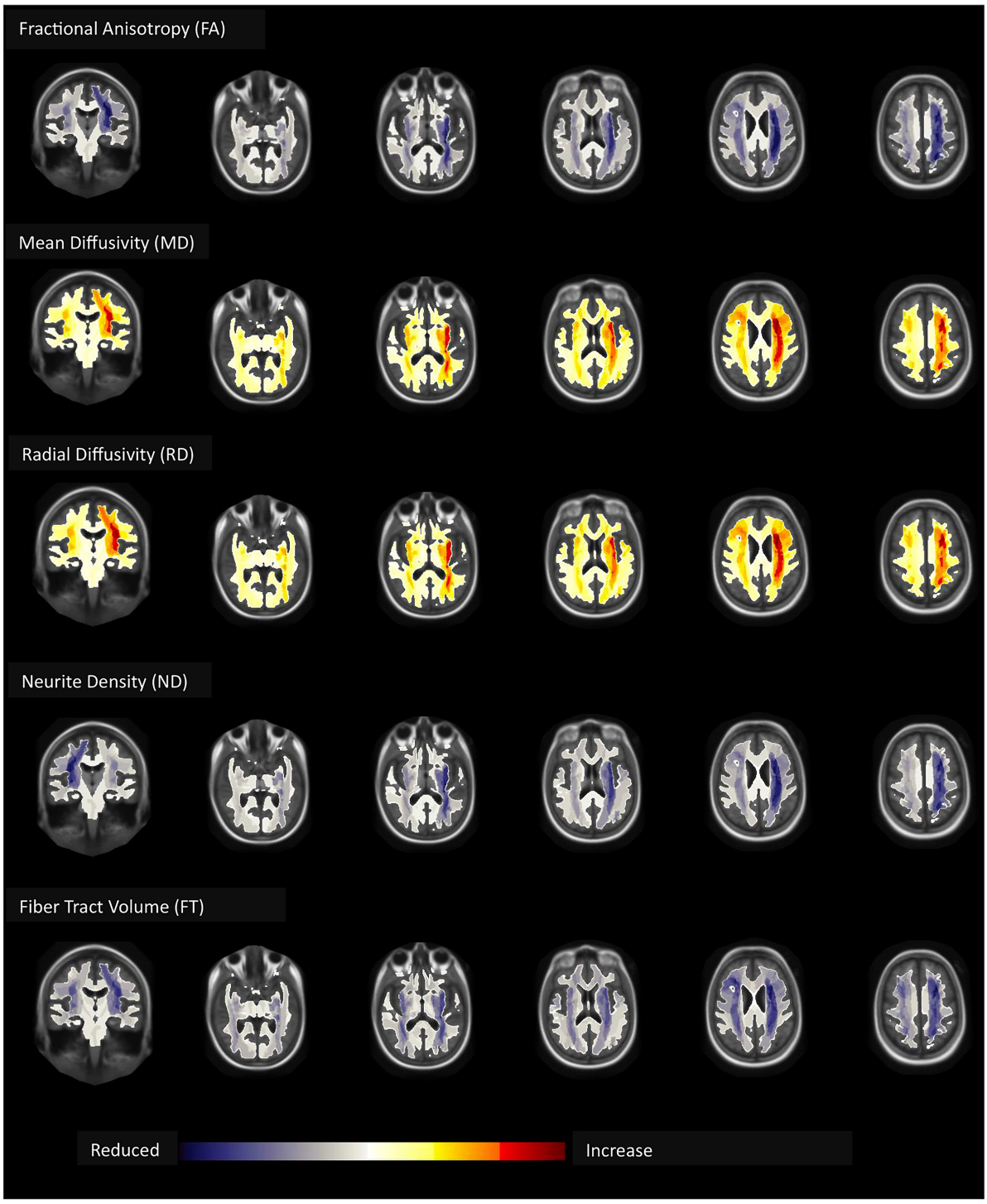

FIGURE 3
Children with ADHD compared to those without had lower fractional anisotropy (FA), neurite density (ND), and fiber tract (FT) volume but higher mean (MD) and radial (RD) diffusivity – most pronounced in the frontal and parietal white matter – independent of age, biological sex, race, handedness, and highest parental education as a marker of socioeconomic status, and after correction for multiple comparisons.

children. Our study shows that childhood ADHD is associated with reduced cortical volumes and surface areas in the frontal lobe, cingulate, and temporal lobe. These areas are known to be associated with complex cognitive behaviors such as decision-making, reasoning, personality expression, and maintaining social appropriateness (El-Baba and Schury, 2022) and visuo-attentional processes (Zarka et al., 2021). Prior studies have proposed an association between smaller prefrontal cortex volume in ADHD children and their ability to suppress their responses to salient but otherwise irrelevant events (Casey et al., 1997). Diffusion MRI results complement our morphological findings as children with ADHD also had lower FA, FT, and ND but higher MD and RD

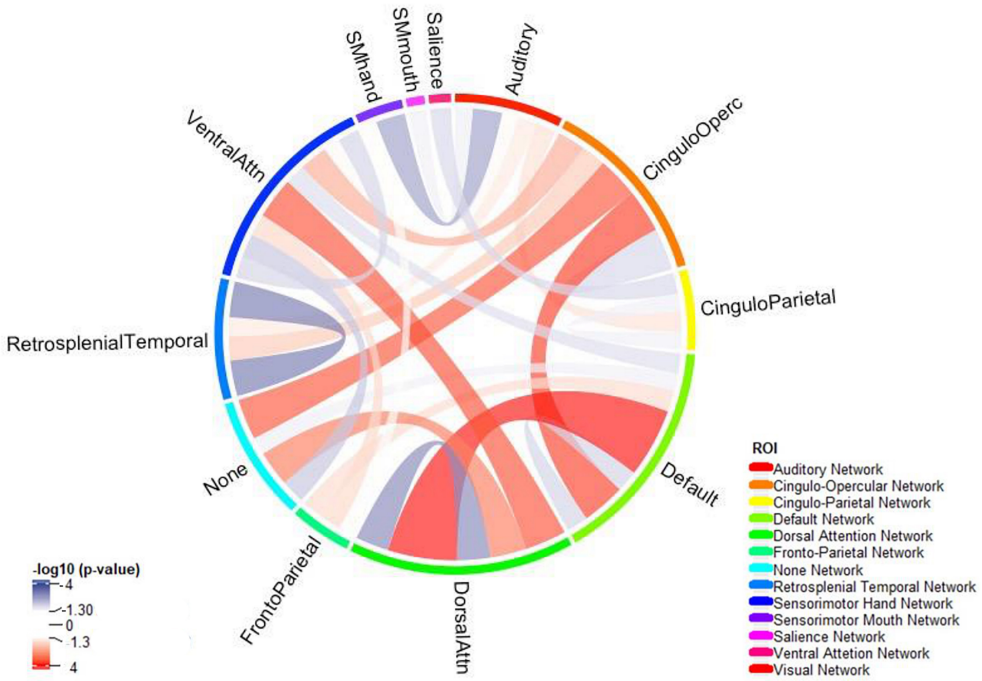

FIGURE 4
The connectogram summarizes reduced (blue) and increased (red) network connectivity between functional areas among children with ADHD compared to those without – independent of age, biological sex, race, handedness, and highest parental education as a marker of socioeconomic status, and after correction for multiple comparisons. Functional network was split using Gordon Parcellation.

in WM tracts originating from the frontal cortex compatible with reduced microstructural integrity and neuronal density, which can affect attention, school function, and non-verbal intelligence (De Zeeuw et al., 2012; Tung et al., 2021).

Furthermore, functional connectivity is also perturbed in individuals with ADHD (Cortese et al., 2018; Gao et al., 2019; Sutcubasi et al., 2020). In our study, children with ADHD had reduced intra-connectivity in the dorsal attention network, the default-mode network and the retrosplenial network. The dorsal attention network as part of task positive network is active while focusing on a particular task and it is important for processing of relevant information and filter out irrelevant information (Rohr et al., 2017). Of note, parts of the dorsal attention network are within the middle temporal region which we prior identify as a region with reduced cortical volume and sulcal depths. On the other hand, default mode network is active while the patient is engaging in internally focused tasks (Buckner, 2013). According to the default-mode network hypothesis, lapses in attention, among ADHD children, are caused by spontaneous intrusions of this network (Sonuga-Barke and Castellanos, 2007). Recent neuroanatomical models localize parts of the default-mode network to prefrontal region and cingulum (Alves et al., 2019). We found that although the intra-connectivity of both dorsal attention and default-mode networks decreases, their network interconnectivity increase implying an overstimulation between these two networks (**Figure 4**). A recent study confirms these findings reporting hyperconnectivity of the default-mode with task-relevant networks (Duffy et al., 2021). Association of ADHD with default mode network dysconnectivity was also reported in a meta-analysis of 21 studies with 700 ADHD patients and 580 controls (Gao et al., 2019), and a meta-analysis of 20 studies with 944 ADHD patients and 1,121 controls (Sutcubasi et al., 2020). Of note, our morphological and microstructural findings in frontal and temporal lobes may – at least partially – explain aberrations of functional connectivity among ADHD children, especially in dorsal attention and default-mode networks.

In contrast to several other studies, we found no significant association between ADHD diagnosis and cortical thickness (unlike cortical volume). Possible explanation could be: both surface area and cortical thickness play a significant mediating role in determining diagnostic differences in volume, with regional brain variation, the contribution of surface area might be bigger than thickness and by using multiple testing correcting the effect of thickness was not statistically significant. Of note, Shaw et al. (2007) reported a maturation delay in reaching peak cortical thickness in children with ADHD. Different cortical and subcortical regions have been implicated in pathogenesis of ADHD: the left parahippocampal gyrus (Carmona et al., 2005), occipital associated cortices (Narr et al., 2009), amygdala and nuclei accumbens (Hoogman et al., 2017; Boedhoe et al., 2020). The difference between our study and priors may be due to selection bias, age-related differences, or sociodemographic variations (Hoogman et al., 2019).

Neuroimaging studies may also facilitate ADHD diagnosis in children. Currently, clinical interviews with children, parents, and caregivers are mainstays of ADHD diagnosis in children (Wolraich et al., 2019). However, the collected questionnaires are subjective and sometimes inconsistent (Gualtieri and Johnson, 2005). Thus, quantitative objective methodologies can potentially supplement clinical examination to achieve a more reliable

TABLE 2 Demographic characteristics of train/Cross-validation versus independent test cohorts.

Patients' characteristic in training/Cross-validation cohort and independent validation cohort			
	Training/Cross-validation cohort	Independent validation cohort	*p*-valuetraining vs. independent
	6,244	1,561	
Patients with ADHD diagnosis	1,420 (22.7)	378 (24.2)	0.229
Age			0.930
Mean (SD)	119.2 (7.5)	119.6 (7.6)	
Min–max	107–133	107–132	
Median (IQR)	119	120	
Sex, *n* (%)			
Female	3,118(49.9)	760 (48.7)	0.292
Male	3,126 (50.0)	801 (51.3)	0.393
Race, *n* (%)			
White	3,470 (55.6)	851 (54.3)	0.470
Black	901 (14.4)	210 (13.5)	0.343
Asian	130 (2.0)	27 (1.3)	0.422
Hispanic	1,241 (19.9)	328 (21.0)	0.333
Undetermined	17 (0.3)	6 (0.4)	0.639
Mixed/Others	485 (7.8)	139 (8.9)	0.153
Handedness, *n* (%)			
Right	5,048 (80.8)	1,252 (80.2)	0.591
Left	440 (7.1)	103 (6.6)	0.477
Both	756 (12.1)	206 (13.2)	0.260
Highest parental education, *n* (%)			
No highschool degree	338 (5.4)	103 (6.6)	0.080
Highschool/General educational development	503 (8.1)	118 (7.6)	0.551
Some college/Associate degree	1,596 (25.6)	377 (24.2)	0.266
Bachelor's degree	1,619 (25.9)	423 (27.1)	0.364
Postgraduate	2,182 (34.9)	538 (34.5)	0.744
Undetermined	6 (0.1)	2 (0.1)	1.000

diagnosis particularly in presence of cultural, language, or communication barriers. This is particularly important since delayed diagnosis of ADHD is associated with higher risk of developing mood and anxiety disorders, substance abuse, and/or personality disorders (Katzman et al., 2017). In our study, we evaluated the applicability of machine learning classifiers in prediction of ADHD diagnosis using multimodal neuroimaging metrics. By exploiting the multimodal data more information for individual subject can be gathered and provide the chance of finding missing links in complex mental illness and giving a comprehensive overview of the same cohort.

Using a rigorous cross-validation framework we could minimize the risk of overfitting and ensure the stability of the model. The stability of our best performed model was proofed with our independent validation set, which was isolated from training and optimization process. A machine-learning model using neuroimaging metrics alone could achieve an AUC of 0.576 (95% CI = 0.546–0.610), which was increased to 0.613 (95% CI = 0.580–0.645) by adding clinical variables, although not statistically different (p = 0.0851). To mitigate the issue of class imbalance in our study (with a 1:3 ratio of children with and without ADHD), we employed the AUC of ROC as the primary measure of performance, as it is not affected by class imbalance, unlike classification accuracy. Prior studies have reported higher accuracy of machine-learning models for prediction of ADHD; however, they have used highly selective ADHD versus control subjects (Ghiassian et al., 2016; Sen et al., 2018), or lacked true independent validation cohort (Deshpande et al., 2015; Qureshi et al., 2017). While our results show that prediction is possible in a diverse group, it still needs to be optimized, e.g., inclusion of clinical features. We demonstrate both the potentials and limitations of machine-learning classifiers for prediction of ADHD diagnosis in general population using multimodal neuroimaging metrics.

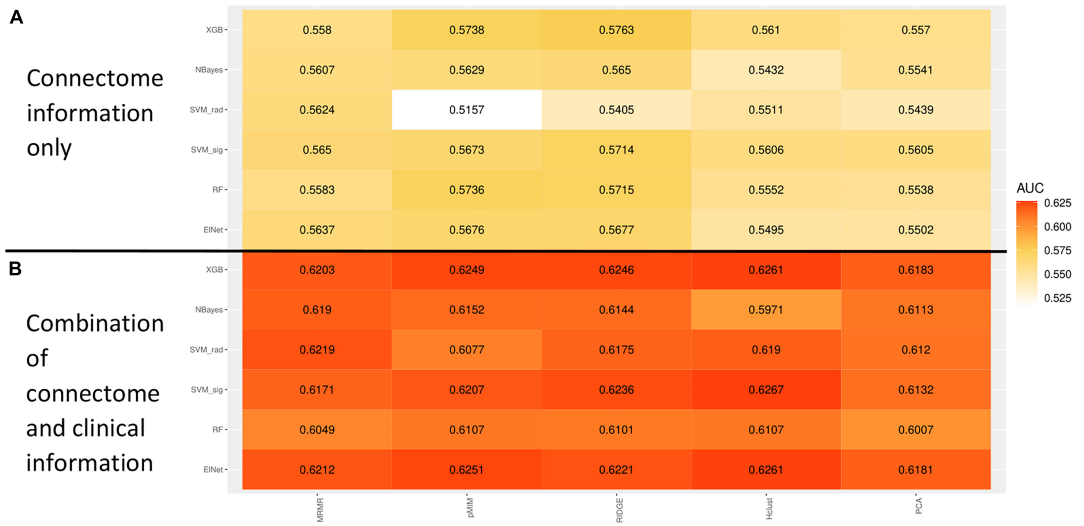

FIGURE 5
Heatmap showing the mean receiver operating characteristics (ROC) area under curve (AUC) across 100 validation folds from combination of different machine-learning classifiers and feature selection methods using imaging variables alone **(A)** or combination of clinical and imaging variables **(B)**.

The main strength of our study is large cohort of children from a narrow age-group, who are reflective of demographically diverse U.S. population. Indeed, one of the objectives of ABCD study is to elucidate factors that influence the course of mental illness (Jernigan and Brown, 2018), which also reflects our aim to investigate microstructural, morphological, and functional connectivity correlates of ADHD in preadolescent children. At the same time, our analysis was limited by using processed imaging metrics from ABCD Consortium. Although a standardized protocol was used for harmonized image acquisition, site differences might still influence our analysis. In addition, different brain atlases were used for sMRI (Desikan-Killiany atlas), dMRI (Atlas Track atlas), and fMRI (Gordon Network Parcellation). It is important to note that these atlases may have variations in the number and location of ROI partitions, which complicates the understanding of the connecting between structure and function. Our present study focused on cortical volume with a few subcortical regions due to the natural noisiness of subcortical measurements. In addition, WM tracts thickness and microstructure provided complementary information for evaluation of whole brain. Nevertheless, some studies suggested that subcortical regions also show ADHD-dependent variations (Hoogman et al., 2017; Boedhoe et al., 2020). The inclusion of this information contains the potential to better understand the pathological mechanisms. Additionally, the linear regression method we employed may not be able to detect more intricate relationships. Further limitations of our study were the absence of cognitive parameters associated with ADHD and separation of patients into subtypes. The diagnosis was generated by K-SADS questionnaires at different sites with various levels of expertise and there is no diagnostic validation study nested with the ABCD study. Finally, we were not able to analyze the effects ADHD subtypes, duration of diagnosis, or any treatment.

5. Conclusion

We could identify the neurostructural and -functional correlates of ADHD in demographically representative cohort of American children. The comprehensive and convergent results implicated brain regions and networks involved in impulse control, executive function, and concentration in pathogenesis of childhood ADHD. Specifically, our results showed the association of childhood ADHD with frontal lobe cortical volume reduction and lower WM integrity and neuronal density. These morphological and microstructural findings may also explain the observed aberrations of functional connectivity in dorsal attention and default-mode networks among children with ADHD. We also showed limited potentials of machine-learning classifiers in prediction of ADHD diagnosis at general population level. Nevertheless, these neuroimaging correlates can potentially help with diagnosis, treatment monitoring, and response prediction.

Data availability statement

Publicly available datasets were analyzed in this study. This data can be found here: the datasets Adolescent Brain Cognitive Development Study: https://nda.nih.gov/abcd/.

Ethics statement

The studies involving human participants were reviewed and approved by the Ethics Committee of ABCD. Written informed consent to participate in this study was provided by the participants' legal guardian/next of kin.

Author contributions

HL implemented the analysis, interpreted the findings, and wrote and revised the manuscript. SP designed the study, interpreted the findings, and supported the writing and revision of the manuscript. SH assisted in data analysis. AMo, SK, AMa, RC, DS, LM, and KK assisted in interpretation the findings and reviewed the manuscript. All authors contributed to the article and approved the submitted version.

Funding

HL received grant support from the Biomedical Education Program. AMo received grant support form Radiological Society of North America (RR2141). SP received grant support from National Institutes of Health (K23NS118056), Doris Duke Charitable Foundation (2020097), and Foundation of American Society of Neuroradiology. The ABCD Study® was supported by the National Institutes of Health and additional federal partners under award numbers U01DA041048, U01DA050989, U01DA051016, U01DA041022, U01DA051018, U01DA051037, U01DA050987, U01DA041174, U01DA041106, U01DA041117, U01DA041028, U01DA041134, U01DA050988, U01DA051039, U01DA041156, U01DA041025, U01DA041120, U01DA051038, U01DA041148, U01DA041093, U01DA041089, U24DA041123, and U24DA041147. A full list of supporters is available at https://abcdstudy.org/federal-partners.html. A listing of participating sites and a complete listing of the study investigators can be found at https://abcdstudy.org/consortium_members/.

Acknowledgments

Data used in the preparation of this article were obtained from the Adolescent Brain Cognitive DevelopmentSM (ABCD) Study (https://abcdstudy.org), held in the NIMH Data Archive (NDA). This is a multisite, longitudinal study designed to recruit more than 10,000 children age 9–10 and follow them over 10 years into early adulthood. ABCD consortium investigators designed and implemented the study and/or provided data but did not necessarily participate in the analysis or writing of this report. This manuscript reflects the views of the authors and may not reflect the opinions or views of the NIH or ABCD consortium investigators.

Conflict of interest

The authors declare that the research was conducted in the absence of any commercial or financial relationships that could be construed as a potential conflict of interest.

Publisher's note

Supplementary material

The Supplementary Material for this article can be found online at: https://www.frontiersin.org/articles/10.3389/fnins.2023.1138670/full#supplementary-material

References

Alves, P. N., Foulon, C., Karolis, V., Bzdok, D., Margulies, D. S., Volle, E., et al. (2019). An improved neuroanatomical model of the default-mode network reconciles previous neuroimaging and neuropathological findings. *Commun. Biol.* 2:370. doi: 10.1038/s42003-019-0611-3

Aoki, Y., Cortese, S., and Castellanos, F. X. (2018). Research review: Diffusion tensor imaging studies of attention-deficit/hyperactivity disorder: Meta-analyses and reflections on head motion. *J. Child Psychol. Psychiatry* 59, 193–202. doi: 10.1111/jcpp.12778

Bernanke, J., Luna, A., Chang, L., Bruno, E., Dworkin, J., and Posner, J. (2022). Structural brain measures among children with and without ADHD in the adolescent brain and cognitive development study cohort: A cross-sectional US population-based study. *Lancet Psychiatry* 9, 222–231. doi: 10.1016/S2215-0366(21)00505-8

Boedhoe, P. S. W., Van Rooij, D., Hoogman, M., Twisk, J. W. R., Schmaal, L., Abe, Y., et al. (2020). Subcortical brain volume, regional cortical thickness, and cortical surface area across disorders: Findings from the ENIGMA ADHD, ASD, and OCD working groups. *Am. J. Psychiatry* 177, 834–843. doi: 10.1176/appi.ajp.2020.19030331

Buckner, R. L. (2013). The brain's default network: Origins and implications for the study of psychosis. *Dialogues Clin. Neurosci.* 15, 351–358. doi: 10.31887/DCNS.2013.15.3/rbuckner

Carmona, S., Vilarroya, O., Bielsa, A., Tremols, V., Soliva, J. C., Rovira, M., et al. (2005). Global and regional gray matter reductions in ADHD: A voxel-based morphometric study. *Neurosci. Lett.* 389, 88–93. doi: 10.1016/j.neulet.2005.07.020

Casey, B. J., Cannonier, T., Conley, M. I., Cohen, A. O., Barch, D. M., Heitzeg, M. M., et al. (2018). The adolescent brain cognitive development (ABCD) study: Imaging acquisition across 21 sites. *Dev. Cogn. Neurosci.* 32, 43–54. doi: 10.1016/j.dcn.2018.03.001

Casey, B. J., Castellanos, F. X., Giedd, J. N., Marsh, W. L., Hamburger, S. D., Schubert, A. B., et al. (1997). Implication of right frontostriatal circuitry in response inhibition and attention-deficit/hyperactivity disorder. *J. Am. Acad. Child Adolesc. Psychiatry* 36, 374–383. doi: 10.1097/00004583-199703000-00016

Chiang, H.-L., Tseng, W.-Y. I., Wey, H.-Y., and Gau, S. S.-F. (2020). Shared intrinsic functional connectivity alterations as a familial risk marker for ADHD: A resting-state functional magnetic resonance imaging study with sibling design. *Psychol. Med.* 52, 1736–1745. doi: 10.1017/s0033291720003529

Cortese, S., Adamo, N., Del Giovane, C., Mohr-Jensen, C., Hayes, A. J., Carucci, S., et al. (2018). Comparative efficacy and tolerability of medications for attention-deficit hyperactivity disorder in children, adolescents, and adults: A systematic review and network meta-analysis. *Lancet Psychiatry* 5, 727–738. doi: 10.1016/S2215-0366(18)30269-4

Danielson, M. L., Bitsko, R. H., Ghandour, R. M., Holbrook, J. R., Kogan, M. D., and Blumberg, S. J. (2018). Prevalence of parent-reported ADHD diagnosis and associated treatment among U.S. children and adolescents, 2016. *J. Clin. Child Adolesc. Psychol.* 47, 199–212. doi: 10.1080/15374416.2017.1417860

De Zeeuw, P., Weusten, J., Van Dijk, S., Van Belle, J., and Durston, S. (2012). Deficits in cognitive control, timing and reward sensitivity appear to be dissociable in ADHD. *PLoS One* 7:e51416. doi: 10.1371/journal.pone.0051416

Deshpande, G., Wang, P., Rangaprakash, D., and Wilamowski, B. (2015). Fully connected cascade artificial neural network architecture for attention deficit hyperactivity disorder classification from functional magnetic resonance imaging data. *IEEE Trans. Cybern.* 45, 2668–2679. doi: 10.1109/TCYB.2014.2379621

Desikan, R. S., Ségonne, F., Fischl, B., Quinn, B. T., Dickerson, B. C., Blacker, D., et al. (2006). An automated labeling system for subdividing the human cerebral cortex on MRI scans into gyral based regions of interest. *NeuroImage* 31, 968–980. doi: 10.1016/j.neuroimage.2006.01.021

Duffy, K. A., Rosch, K. S., Nebel, M. B., Seymour, K. E., Lindquist, M. A., Pekar, J. J., et al. (2021). Increased integration between default mode and task-relevant networks in children with ADHD is associated with impaired response control. *Dev. Cogn. Neurosci.* 50:100980. doi: 10.1016/j.dcn.2021.100980

El-Baba, R. M., and Schury, M. P. (2022). *Neuroanatomy, frontal cortex*. Treasure Island, FL: StatPearls.

Gao, Y., Shuai, D., Bu, X., Hu, X., Tang, S., Zhang, L., et al. (2019). Impairments of large-scale functional networks in attention-deficit/hyperactivity disorder: A meta-analysis of resting-state functional connectivity. *Psychol. Med.* 49, 2475–2485. doi: 10.1017/S003329171900237X

Garavan, H., Bartsch, H., Conway, K., Decastro, A., Goldstein, R. Z., Heeringa, S., et al. (2018). Recruiting the ABCD sample: Design considerations and procedures. *Dev. Cogn. Neurosci.* 32, 16–22. doi: 10.1016/j.dcn.2018.04.004

Ghiassian, S., Greiner, R., Jin, P., and Brown, M. R. (2016). Using functional or structural magnetic resonance images and personal characteristic data to identify ADHD and Autism. *PLoS One* 11:e0166934. doi: 10.1371/journal.pone.0166934

Gordon, E. M., Laumann, T. O., Adeyemo, B., Huckins, J. F., Kelley, W. M., and Petersen, S. E. (2016). Generation and evaluation of a cortical area parcellation from resting-state correlations. *Cereb. Cortex* 26, 288–303. doi: 10.1093/cercor/bhu239

Gualtieri, C. T., and Johnson, L. G. (2005). ADHD: Is objective diagnosis possible? *Psychiatry* 2, 44–53.

Hagler, D. J., Ahmadi, M. E., Kuperman, J., Holland, D., Mcdonald, C. R., Halgren, E., et al. (2009). Automated white-matter tractography using a probabilistic diffusion tensor atlas: Application to temporal lobe epilepsy. *Hum. Brain Mapp.* 30, 1535–1547. doi: 10.1002/hbm.20619

Hagler, D. J., Hatton, S., Cornejo, M. D., Makowski, C., Fair, D. A., Dick, A. S., et al. (2019). Image processing and analysis methods for the adolescent brain cognitive development study. *NeuroImage* 202:116091. doi: 10.1016/j.neuroimage.2019.116091

Haider, S. P., Mahajan, A., Zeevi, T., Baumeister, P., Reichel, C., Sharaf, K., et al. (2020). PET/CT radiomics signature of human papilloma virus association in oropharyngeal squamous cell carcinoma. *Eur. J. Nucl. Med. Mol. Imaging* 47, 2978–2991. doi: 10.1007/s00259-020-04839-2

Hoogman, M., Bralten, J., Hibar, D. P., Mennes, M., Zwiers, M. P., Schweren, L. S. J., et al. (2017). Subcortical brain volume differences in participants with attention deficit hyperactivity disorder in children and adults: A cross-sectional mega-analysis. *Lancet Psychiatry* 4, 310–319. doi: 10.1016/S2215-0366(17)30049-4

Hoogman, M., Muetzel, R., Guimaraes, J. P., Shumskaya, E., Mennes, M., Zwiers, M. P., et al. (2019). Brain imaging of the cortex in ADHD: A coordinated analysis of large-scale clinical and population-based samples. *Am. J. Psychiatry* 176, 531–542. doi: 10.1176/appi.ajp.2019.18091033

Jernigan, T. L., and Brown, S. A. (2018). Introduction. *Dev. Cogn. Neurosci.* 32, 1–3. doi: 10.1016/j.dcn.2018.02.002

Katzman, M. A., Bilkey, T. S., Chokka, P. R., Fallu, A., and Klassen, L. J. (2017). Adult ADHD and comorbid disorders: Clinical implications of a dimensional approach. *BMC Psychiatry* 17:302. doi: 10.1186/s12888-017-1463-3

Kaufman, J., Birmaher, B., Brent, D., Rao, U., Flynn, C., Moreci, P., et al. (1997). Schedule for affective disorders and schizophrenia for school-age children-present and lifetime version (K-SADS-PL): Initial reliability and validity data. *J. Am. Acad. Child Adolesc. Psychiatry* 36, 980–988. doi: 10.1097/00004583-199707000-00021

Kumar, U., Arya, A., and Agarwal, V. (2017). Neural alterations in ADHD children as indicated by voxel-based cortical thickness and morphometry analysis. *Brain Dev.* 39, 403–410. doi: 10.1016/j.braindev.2016.12.002

Narr, K. L., Woods, R. P., Lin, J., Kim, J., Phillips, O. R., Del'homme, M., et al. (2009). Widespread cortical thinning is a robust anatomical marker for attention-deficit/hyperactivity disorder. *J. Am. Acad. Child Adolesc. Psychiatry* 48, 1014–1022. doi: 10.1097/CHI.0b013e3181b395c0

Qureshi, M. N. I., Oh, J., Min, B., Jo, H. J., and Lee, B. (2017). Corrigendum: Multi-modal, multi-measure, and multi-class discrimination of ADHD with hierarchical feature extraction and extreme learning machine using structural and functional brain MRI. *Front. Hum. Neurosci.* 11:292. doi: 10.3389/fnhum.2017.00292

Rohr, C. S., Vinette, S. A., Parsons, K.a.L, Cho, I. Y. K., Dimond, D., Benischek, A., et al. (2017). Functional connectivity of the dorsal attention network predicts selective attention in 4-7 year-old girls. *Cereb. Cortex* 27, 4350–4360.

Sen, B., Borle, N. C., Greiner, R., and Brown, M. R. G. (2018). A general prediction model for the detection of ADHD and Autism using structural and functional MRI. *PLoS One* 13:e0194856. doi: 10.1371/journal.pone.0194856

Shaw, P., Eckstrand, K., Sharp, W., Blumenthal, J., Lerch, J. P., Greenstein, D., et al. (2007). Attention-deficit/hyperactivity disorder is characterized by a delay in cortical maturation. *Proc. Natl. Acad. Sci. U.S.A.* 104, 19649–19654.

Sonuga-Barke, E. J., and Castellanos, F. X. (2007). Spontaneous attentional fluctuations in impaired states and pathological conditions: A neurobiological hypothesis. *Neurosci. Biobehav. Rev.* 31, 977–986. doi: 10.1016/j.neubiorev.2007.02.005

Sudre, G., Gildea, D. E., Shastri, G. G., Sharp, W., Jung, B., Xu, Q., et al. (2022). Mapping the cortico-striatal transcriptome in attention deficit hyperactivity disorder. *Mol. Psychiatry*. 28, 792–800. doi: 10.1038/s41380-022-01844-9

Sutcubasi, B., Metin, B., Kurban, M. K., Metin, Z. E., Beser, B., and Sonuga-Barke, E. (2020). Resting-state network dysconnectivity in ADHD: A system-neuroscience-based meta-analysis. *World J. Biol. Psychiatry* 21, 662–672. doi: 10.1080/15622975.2020.1775889

Tung, Y. H., Lin, H. Y., Chen, C. L., Shang, C. Y., Yang, L. Y., Hsu, Y. C., et al. (2021). Whole brain white matter tract deviation and idiosyncrasy from normative development in Autism and ADHD and unaffected siblings link with dimensions of psychopathology and cognition. *Am. J. Psychiatry* 178, 730–743. doi: 10.1176/appi.ajp.2020.20070999

Wolraich, M. L., Hagan, J. F., Allan, C., Chan, E., Davison, D., Earls, M., et al. (2019). Clinical practice guideline for the diagnosis, evaluation, and treatment of attention-deficit/hyperactivity disorder in children and adolescents. *Pediatrics* 144:e20192528. doi: 10.1542/peds.2019-2528

Wu, W., Mcanulty, G., Hamoda, H. M., Sarill, K., Karmacharya, S., Gagoski, B., et al. (2020). Detecting microstructural white matter abnormalities of frontal pathways in children with ADHD using advanced diffusion models. *Brain Imaging Behav.* 14, 981–997. doi: 10.1007/s11682-019-00108-5

Yang, R., and Jernigan, T. (2020). *Adolescent brain cognitive development study (ABCD) – annual release 3.0*. Available online at: https://nda.nih.gov/study.html?id=1042

Zarka, D., Leroy, A., Cebolla, A. M., Cevallos, C., and Cheron, G. (2021). Neural generators involved in visual cue processing in children with attention-deficit/hyperactivity disorder (ADHD). *Eur. J. Neurosci.* 53, 1207–1224. doi: 10.1111/ejn.15040

frontiers | Frontiers in Neuroscience

TYPE Original Research
PUBLISHED 03 March 2023
DOI 10.3389/fnins.2023.1148458

OPEN ACCESS

EDITED BY
Jing Li,
Capital Medical University, China

REVIEWED BY
Jun Zhou,
Chengdu University of Traditional Chinese Medicine, China
Constantina Aggeli,
National and Kapodistrian University of Athens, Greece

*CORRESPONDENCE
Yuan Hong
✉ hy0904@zju.edu.cn

SPECIALTY SECTION
This article was submitted to Brain Imaging Methods, a section of the journal Frontiers in Neuroscience

RECEIVED 20 January 2023
ACCEPTED 10 February 2023
PUBLISHED 03 March 2023

CITATION
Guo X, Wang D, Ying C and Hong Y (2023) Association between brain structures and migraine: A bidirectional Mendelian randomization study.
Front. Neurosci. 17:1148458.
doi: 10.3389/fnins.2023.1148458

Association between brain structures and migraine: A bidirectional Mendelian randomization study

Xiaoming Guo[1,2], Dingkun Wang[2], Caidi Ying[1] and Yuan Hong[1]*

[1]Department of Neurosurgery, The Second Affiliated Hospital, Zhejiang University School of Medicine, Hangzhou, China, [2]Department of Neurosurgery, Tongde Hospital of Zhejiang Province, Hangzhou, China

Background: Accumulating evidence of clinical and neuroimaging studies indicated that migraine is related to brain structural alterations. However, it is still not clear whether the associations of brain structural alterations with migraine are likely to be causal, or could be explained by reverse causality confounding.

Methods: We carried on a bidirectional Mendelian randomization analysis in order to identify the causal relationship between brain structures and migraine risk. Summary-level data and independent variants used as instruments came from large genome-wide association studies of total surface area and average thickness of cortex (33,992 participants), gray matter volume (8,428 participants), white matter hyperintensities (50,970 participants), hippocampal volume (33,536 participants), and migraine (102,084 cases and 771,257 controls).

Results: We identified suggestive associations of the decreased surface area (OR = 0.85; 95% CI, 0.75–0.96; P = 0.007), and decreased hippocampal volume (OR = 0.74; 95% CI, 0.55–1.00; P = 0.047) with higher migraine risk. We did not find any significant association of gray matter volume, cortical thickness, or white matter hyperintensities with migraine. No evidence supporting the significant association was found in the reverse MR analysis.

Conclusion: We provided suggestive evidence that surface area and hippocampal volume are causally associated with migraine risk.

KEYWORDS

brain structure, NeuroImage, Mendelian randomization, migraine, cortex

Introduction

Migraine is a common and complex neurological disease associated with significant psychosocial impact, and has been a leading burden for global population health (Leonardi et al., 2005; Ashina et al., 2021). This disease is usually diagnosed on the basis of clinical criteria and can be further divided into two subtypes, including with- and without-aura (Charles, 2018; Ashina et al., 2021). In recent years, accumulating evidence of clinical and neuroimaging studies indicated that brain structural alterations played a pivotal role in migraine. These T1-weighted magnetic resonance imaging (MRI) studies used voxel-based morphometry or surface-based morphometry to explore brain morphology differences in

volume, thickness or surface area (SA) between migraine patients and healthy controls (DaSilva et al., 2007; Schmidt-Wilcke et al., 2008; Datta et al., 2011; Messina et al., 2013; Rocca et al., 2014; Coppola et al., 2017; Husøy et al., 2019; Amin et al., 2021; Kim et al., 2021). Currently, migraine has been hypothesized to be a both neuronal and vascular genetic disorder upon the mainstream opinion (Schwedt and Dodick, 2009; MacGregor, 2017). The latest and largest genome-wide association study (GWAS) meta-analysis, including 102,084 migraine cases and 771,257 controls, identified 123 risk loci associated with migraine, which were enriched in both vascular and central nervous system tissue/cell types (Hautakangas et al., 2022). And it supported the concept that migraine is a neurovascular disorder (Hautakangas et al., 2022).

Previous studies have revealed that cortex in migraine patients has peculiar anatomical, functional, and neurochemical properties (Barbanti et al., 2019). And the incidence of white matter hyperintensities obviously increased in migraine patients (Eikermann-Haerter and Huang, 2021). Hippocampus plays an important role in the processing of pain, pain-related attention, and stress response (Liu et al., 2018). Besides, the volume of hippocampus has been found to be related to migraine prognosis (Liu et al., 2018). Although the significant relationships between brain morphology alterations and migraine could be observed in previous studies, it remains unclear whether brain morphology alterations are the cause or consequence of migraine attacks. The relationship between hippocampal volume and migraines remains unclear, with some studies suggesting a positive correlation and others a negative one. Thus, it is necessary to clarify the direction of the association and provide evidence at the genetic level between brain structures and migraine.

Mendelian randomization (MR) is a genetic epidemiologic method by using genetic variants associated with exposures, which can avoid many of the potential methodological limitations of observational studies, such as reverse causation bias and confounding (Smith and Ebrahim, 2003). In view of the basis that both brain morphometry and migraine risk are influenced by genetic factors, using MR analysis to improve the knowledge of the relationship between brain morphometry alterations and migraine is promising. Recently, only one MR study have investigated the association between intracranial volume and migraine (Mitchell et al., 2022). Important brain traits like cortical SA, cortical thickness, and some other traits of interests were not assessed. Here, we carried out an MR study to explore the causal association between these important brain traits and migraine risk using the largest GWAS data.

Materials and methods

Study design

The MR study builds on three predominant assumptions (**Figure 1**). (1) Selected instrumental variables (IVs) are strongly and consistently associated with exposures. (2) There is no association between the IVs and confounders. (3) IVs impact outcomes through exposures directly, but not other pathways. Genetic variants are frequently utilized as IVs, due to their well-defined nature and resistance to alteration by environmental factors, thereby avoiding reverse causation (Burgess et al., 2017b). We conducted this bidirectional MR study to clarify the causal relationship between brain structures and migraine.

Genetic instruments selection and data sources

Genetic variants associated with total cortical SA and average cortical thickness were obtained from a genome-wide meta-analysis, which were based on 51,665 predominantly healthy participants in the Enhancing NeuroImaging Genetics through Meta-Analysis Consortium and the UK Biobank. The total SA and average cortical thickness were measured on MRI (Grasby et al., 2020). A total of 12 SNPs associated with total SA and 2 SNPs associated with average cortical thickness were collected ($P \leq 8.3 \times 10^{-10}$). For gray matter volume (GMV), we drew 8 SNPs ($P \leq 5 \times 10^{-8}$) from a large GWAS of brain imaging-derived phenotypes from an open web server (the Oxford Brain Imaging Genetics),[1] which included 33,224 participants from the UK Biobank (Smith et al., 2021). As for white matter hyperintensities (WMH), we obtained 24 SNPs as IVs of WMH from 50,970 individuals from Cohorts for Heart and Aging Research in Genomic Epidemiology consortium and from the UK Biobank ($P < 5 \times 10^{-8}$) (Sargurupremraj et al., 2020). The aggregated risk variants were then confirmed to be associated with WMH in another cohort of 1,738 young healthy adults ($P = 2.5 \times 10^{-7}$), which provided insight into the lifetime impact of WMH. In addition, we extracted six independent SNPs as IVs significantly associated with hippocampal volume (HV) from a genome-wide meta-analysis with 33,536 individuals ($P \leq 5 \times 10^{-8}$), which accounted for as much as 18.76% of the variance in HV (Hibar et al., 2017). All IVs included were clumped for independence ($r^2 < 0.1$; region size, 3000 kb) according to the Europeans data from the 1,000 Genomes Project. If these included SNPs were not available in the outcome datasets, proxy SNPs ($r^2 > 0.8$) were acquired online as replacements.[2]

The summary-level data of migraine was obtained from the largest available genome-wide meta-analysis, combining five migraine study collections and comprising of 102,084 migraine cases and 771,257 controls of European ancestry (Hautakangas et al., 2022). A total of 123 independent SNPs associated with migraine were utilized as IVs in reverse analysis ($P < 5 \times 10^{-8}$). In this study, migraine phenotype was defined by self-reported information or second edition of international Classification of Headache Disorders. Logistic regression analyses were conducted by adjusting for age, sex, and at least for the four ancestry principal components. We also used a web tool[3] to estimate the bias due to sample overlap and the calculated results were negligible (<1%).

Abbreviations: GMV, gray matter volume; GWAS, genome-wide association study; HV, hippocampal volume; IV, instrumental variable; IVW, inverse-variance weighted; MR, Mendelian randomization; MRI, magnetic resonance imaging; MR-PRESSO, MR pleiotropy residual sum and outlier; OR, odds ratio; SA, surface area; SNP, single nucleotide polymorphism; WMH, white matter hyperintensities.

1 https://open.win.ox.ac.uk/ukbiobank/big40/

2 https://ldlink.nci.nih.gov/

3 https://sb452.shinyapps.io/overlap/

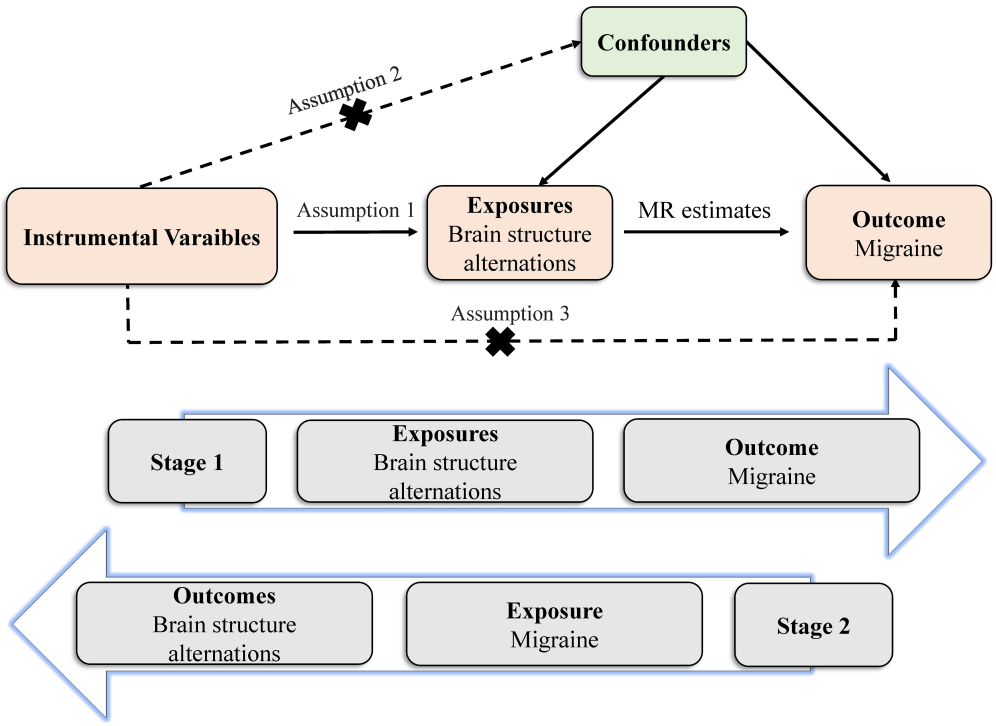

FIGURE 1
Principles of the Mendelian randomization study for brain structural alterations and migraine risks.

All participants gave written informed consent in these studies, and sites involved obtained approval from local research ethics committees or Institutional Review Boards.

Statistical analysis

In the main analyses, we applied the random-effects and fixed-effects inverse-variance weighted (IVW) approach to obtain causal estimates (Burgess et al., 2017a). We conducted several sensitivity analyses to identify potential pleiotropy. Cochran's Q test was used to evaluate the heterogeneity among different instrumental variables (Burgess et al., 2017a). Weighted median method allowed less than 50% of the genetic variants to be invalid instrumental variables (Burgess et al., 2018). MR-Egger method was conducted to detect and adjust pleiotropic bias (Burgess and Thompson, 2017). To further control potential pleiotropy, we used the MR Pleiotropy Residual Sum and Outlier (MR-PRESSO) method to conduct a global test of heterogeneity and identify horizontal pleiotropy (Verbanck et al., 2018). Once the pleiotropic outlier instruments were identified, a repeated IVW analysis after removing these outlier instruments would be performed (Verbanck et al., 2018).

All tests were two sided and the Bonferroni-corrected significance threshold was set to $P < 0.005$ (correcting for 10 outcomes). The *P*-values between 0.005 and 0.05 was defined as suggestive of potential association between exposure and outcome. Odds ratios (ORs) are presented for each 1 standard deviation difference in all exposures. All analyses were conducted by using TwoSampleMR and MR-PRESSO packages in R software (Version 4.1.3).

Results

The main characteristics of datasets adopted in the MR analyses were shown in **Supplementary Table 1**. All F-statistics of these IVs were higher than the threshold of 10, suggesting no weak instrument bias in the present study. The summary information of SNPs on the five traits was shown in **Supplementary Table 2**.

In the random-effect IVW estimates, genetically increased cortical SA was potentially associated with a decreased risk of migraine (OR = 0.850; 95% CI, 0.754–0.957; $P = 0.007$; **Figure 2**). This association was robust in the weighted median and MR-Egger. And MR-PRESSO did not identify any potential SNP outliers and we did not observe evidence of horizontal pleiotropy in MR-Egger (P for intercept = 0.452). The Cochran's Q test indicated significant heterogeneity (Cochran Q-derived $P = 0.032$). There was no significant evidence for association of cortical thickness with migraine (OR = 1.195; 95% CI, 0.958–1.491; $P = 0.115$).

A suggestive association was found between genetically determined HV and migraine (OR = 0.737; 95% CI, 0.546–0.996; $P = 0.047$; **Figure 2**). The Cochran's Q test indicated significant heterogeneity (Cochran Q-derived $P < 0.001$). There was no indication of horizontal pleiotropy in the association of HV with migraine as measured by MR-Egger (P for intercept = 0.959). Three SNPs (rs11979341, rs61921502, and rs7020341) were detected in the MR-PRESSO test, and the result remained suggestive ($P = 0.029$). Genetically determined GMV and WMH were not causally associated with migraine in the IVW method. The lack of causality was also confirmed in the weighted median, MR-Egger estimates, and MR-PRESSO.

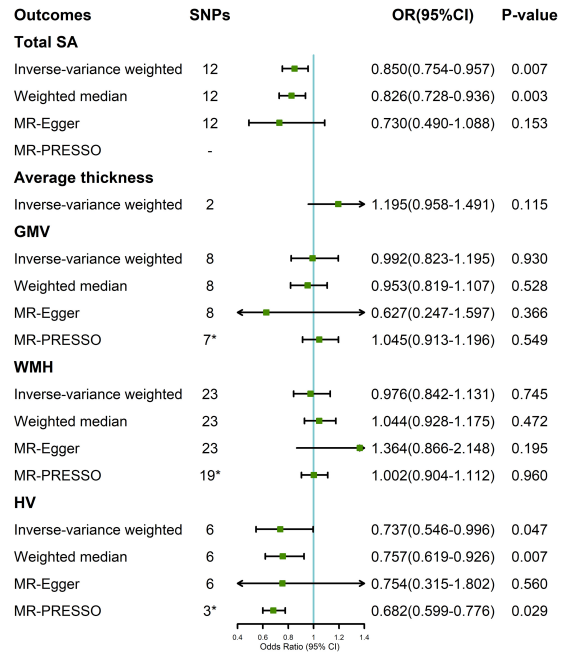

FIGURE 2
Association between genetically determined brain structural alterations and migraine risks. *MR-PRESSO outlier detected (**Supplementary Table 2**). CI, confidence interval; OR, odds ratio; SNP, single nucleotide polymorphism; WMH, white matter hyperintensities.

There were no any significant effects of migraine on brain structural alternation in the reverse estimates (**Supplementary Table 3**).

Discussion

This MR analysis revealed a suggestive causal association of genetically decreased SA and HV with higher risk of migraine. In addition, there was no evidence supporting the association between genetic liability to migraine and brain structural alterations in the reverse MR analysis.

The literatures on the association between brain structural alterations and migraine remained inconclusive. Several observational studies demonstrated that the global or regional SA decreased in migraine cases compared with healthy controls (Messina et al., 2013; Petrusic et al., 2018; Planchuelo-Gómez et al., 2020). And it frequently involved the visual motion processing, pain processing, and executive function regions (Messina et al., 2013; Planchuelo-Gómez et al., 2020). Cortical SA is usually thought to be congenital and is largely independent of environmental or external factors (Kapellou et al., 2006; Frye et al., 2010; Messina et al., 2013). Some authors supposed that cortical SA could be a good biomarker to distinguish migraine patients from healthy controls (Petrusic et al., 2018). Our results of bidirectional MR analysis further supported the causal association between cortical SA and migraine risk. However, the causal relationship was only found in total SA instead of regional SA due to low variance explained by SNPs. Thus, further studies are required to identify the association between migraine and the related regional SA.

Cortical thickness is a marker reflecting gray matter integrity, which can be determined by the number of their neurogenic divisions. In previous literatures, variation in regional or global cortex thickness was controversial (DaSilva et al., 2007; Messina et al., 2013; Husøy et al., 2019; Torres-Ferrus et al., 2021). A possible explanation was that the sample of included subjects was rather small, while the traits to be compared were many, which might lead to false positive results in this way of comparison. Besides, cortical thickness might undergo considerable changes postnatally. For patients with migraine, several factors might affect cortical thickness, such as age, disease duration, frequency of the attacks, and even the scanning timing (attack phase vs. interictal phase). Some authors hypothesized that increased cortical thickness was a compensatory mechanism to meet the requirement for increased sensory processing of migraine attacks. Similar results of increased cortical thickness were found in other neuropsychiatric disorders, including schizophrenia, autism spectrum disorder, early-stage Parkinson's disease and so on (Biundo et al., 2013; Williams et al., 2022). Although the direction of the association in our analysis was in accordance with previous studies, the result was not significant (P = 0.115). In addition, only two available SNPs were applied as IVs in the causal estimate, which might influence the result.

Besides, the decrease in HV was suggestively associated with an increased risk of migraine, which was in lined with most of previous studies (Liu et al., 2013, 2017; Chong et al., 2017). At the same time, observational evidence showed that HV had been negatively associated with the frequency and severity of migraine attacks (Maleki et al., 2013; Liu et al., 2017). Mitchell et al. (2022) suggested that migraine attacks might influence HV in a longitudinal study. However, this reverse relationship was not verified in our study or a recent MR study. WMH and GMV were reported to be associated with migraine. Some studies suggested that a patent foramen ovale might be associated with migraines, accompanied by changes in the gray matter and destruction of the white matter (Signoriello et al., 2018; Cao et al., 2022). Possible mechanisms implicated in the pathophysiology of this phenomenon include microembolus-triggered cortical spreading depression, the vasoactive substance hypothesis, impaired cerebral autoregulation, and a common genetic basis (Signoriello et al., 2018; Cao et al., 2022). However, these association were not discovered in our bidirectional MR analysis. In fact, null findings in our study do not truly reflect lack of associations, since MR analyses are dependent on the power of the original GWAS to a large extent (Pierce and Burgess, 2013).

There are some strengths in our study. Firstly, the use of bidirectional MR design permitted an examination of the reverse causation. Secondly, several sensitivity analyses, including pleiotropy robust methods were applied to ensure the valid estimation of the causal effect size. In addition, we used well-powered GWAS data of migraine, which had more statistical power to detect associations than past smaller study. Finally, our results were in lined with a recent MR study based on voxel-based morphometry, which additionally increased the robustness of our results (Mitchell et al., 2022).

This study also has some limitations. Firstly, we only used total cortical SA and average thickness to explore the causal association between cortical structure and migraine, since the fraction of variance explained by SNPs was low in regional SA and thickness.

Secondly, sample overlapping may occur between exposure and outcomes population, especially for cohort of UK biobank, which may potentially bias the results. But recently, one study showed that two-sample MR can be applied safely and robustly in a single large dataset using large biobanks (Minelli et al., 2021). Thirdly, most of participants in this study were of European descents, which limited our findings to extend to other ancestries.

In conclusion, we provided suggestive evidence that decreased cortical SA, and decreased HV are suggestively associated with higher migraine risk, and we did not find any significant effect of migraine on brain structural alternation in the reverse estimates. Future investigation into the brain regions is recommended, which helps to clarify the underlying mechanisms and point to new therapies against migraine.

Data availability statement

The original contributions presented in this study are included in the article/**Supplementary material**, further inquiries can be directed to the corresponding author.

Ethics statement

Ethical review and approval was not required for the study on human participants in accordance with the local legislation and institutional requirements. Written informed consent for participation was not required for this study in accordance with the national legislation and the institutional requirements.

Author contributions

XG: drafting/revision of the manuscript, study design, and analysis and interpretation of data. DW: analysis and interpretation of data. CY: acquisition of data. YH: revision of the manuscript. All authors contributed to the article and approved the submitted version.

Funding

This study was supported by the National Natural Science Foundation of China (81870964) and Zhejiang Province Traditional Chinese Medicine Science and Technology Project (2023ZR075).

Acknowledgments

The authors thank the IHGC, ENIGMA consortiums, BIG40, and ISGC for providing summary statistics data.

Conflict of interest

The authors declare that the research was conducted in the absence of any commercial or financial relationships that could be construed as a potential conflict of interest.

Publisher's note

Supplementary material

The Supplementary Material for this article can be found online at: https://www.frontiersin.org/articles/10.3389/fnins.2023.1148458/full#supplementary-material

References

Amin, F. M., De Icco, R., Al-Karagholi, M. A., Raghava, J., Wolfram, F., and Larsson, H. B. W. (2021). Investigation of cortical thickness and volume during spontaneous attacks of migraine without aura: A 3-Tesla MRI study. *J. Headache Pain* 22:98. doi: 10.1186/s10194-021-01312-9

Ashina, M., Terwindt, G. M., Al-Karagholi, M. A., de Boer, I., Lee, M. J., Hay, D. L., et al. (2021). Migraine: Disease characterisation, biomarkers, and precision medicine. *Lancet* 397, 1496–1504. doi: 10.1016/S0140-6736(20)32162-0

Barbanti, P., Fofi, L., Aurilia, C., and Egeo, G. (2019). Does the migraine attack start in the cortex and is the cortex critical in the migraine process? *Neurol. Sci.* 40(Suppl. 1), 31–37. doi: 10.1007/s10072-019-03838-y

Biundo, R., Calabrese, M., Weis, L., Facchini, S., Ricchieri, G., and Gallo, P. (2013). Anatomical correlates of cognitive functions in early Parkinson's disease patients. *PLoS One* 8:e64222. doi: 10.1371/journal.pone.0064222

Burgess, S., and Thompson, S. G. (2017). Interpreting findings from Mendelian randomization using the MR-Egger method. *Eur. J. Epidemiol.* 32, 377–389. doi: 10.1007/s10654-017-0255-x

Burgess, S., Small, D. S., and Thompson, S. G. (2017b). A review of instrumental variable estimators for Mendelian randomization. *Stat. Methods Med. Res.* 26, 2333–2355. doi: 10.1177/0962280215597579

Burgess, S., Bowden, J., Fall, T., Ingelsson, E., and Thompson, S. G. (2017a). Sensitivity analyses for robust causal inference from Mendelian randomization analyses with multiple genetic variants. *Epidemiology* 28, 30–42. doi: 10.1097/EDE.0000000000000559

Burgess, S., Zuber, V., Gkatzionis, A., and Foley, C. N. (2018). Modal-based estimation via heterogeneity-penalized weighting: Model averaging for consistent and efficient estimation in Mendelian randomization when a plurality of candidate instruments are valid. *Int. J. Epidemiol.* 47, 1242–1254. doi: 10.1093/ije/dyy080

Cao, W., Shen, Y., Zhong, J., Chen, Z., Wang, N., and Yang, J. (2022). The patent foramen Ovale and migraine: Associated mechanisms and perspectives from MRI Evidence. *Brain Sci.* 12:941. doi: 10.3390/brainsci12070941

Charles, A. (2018). The pathophysiology of migraine: Implications for clinical management. *Lancet Neurol.* 17, 174–182. doi: 10.1016/S1474-4422(17)30435-0

Chong, C. D., Dumkrieger, G. M., and Schwedt, T. J. (2017). Structural co-variance patterns in migraine: A cross-sectional study exploring the role of the hippocampus. *Headache* 57, 1522–1531. doi: 10.1111/head.13193

Coppola, G., Petolicchio, B., Di Renzo, A., Tinelli, E., Di Lorenzo, C., and Parisi, V. (2017). Cerebral gray matter volume in patients with chronic migraine: Correlations with clinical features. *J. Headache Pain* 18:115. doi: 10.1186/s10194-017-0825-z

DaSilva, A. F., Granziera, C., Snyder, J., and Hadjikhani, N. (2007). Thickening in the somatosensory cortex of patients with migraine. *Neurology* 69, 1990–1995. doi: 10.1212/01.wnl.0000291618.32247.2d

Datta, R., Detre, J. A., Aguirre, G. K., and Cucchiara, B. (2011). Absence of changes in cortical thickness in patients with migraine. *Cephalalgia* 31, 1452–1458. doi: 10.1177/033310241142102

Eikermann-Haerter, K., and Huang, S. Y. (2021). White matter lesions in migraine. *Am. J. Pathol.* 191, 1955–1962. doi: 10.1016/j.ajpath.2021.02.007

Frye, R. E., Liederman, J., Malmberg, B., McLean, J., Strickland, D., and Beauchamp, M. S. (2010). Surface area accounts for the relation of gray matter volume to reading-related skills and history of dyslexia. *Cereb. Cortex* 20, 2625–2635. doi: 10.1093/cercor/bhq010

Grasby, K. L., Jahanshad, N., Painter, J. N., Colodro-Conde, L., Bralten, J., and Hibar, D. P. (2020). The genetic architecture of the human cerebral cortex. *Science* 367:eaay6690. doi: 10.1126/science.aay669

Hautakangas, H., Winsvold, B. S., Ruotsalainen, S. E., Bjornsdottir, G., Harder, A. V. E., and Kogelman, L. J. A. (2022). Genome-wide analysis of 102,084 migraine cases identifies 123 risk loci and subtype-specific risk alleles. *Nat. Genet.* 54, 152–160. doi: 10.1038/s41588-021-00990-0

Hibar, D. P., Adams, H. H. H., Jahanshad, N., Chauhan, G., Stein, J. L., and Hofer, E. (2017). Novel genetic loci associated with hippocampal volume. *Nat. Commun.* 8:13624. doi: 10.1038/ncomms13624

Husøy, A. K., Håberg, A. K., Rimol, L. M., Hagen, K., Vangberg, T. R., and Stovner, L. J. (2019). Cerebral cortical dimensions in headache sufferers aged 50 to 66 years: A population-based imaging study in the Nord-Trøndelag health study (HUNT-MRI). *Pain* 160, 1634–1643. doi: 10.1097/j.pain.0000000000001550

Kapellou, O., Counsell, S. J., Kennea, N., Dyet, L., Saeed, N., and Stark, J. (2006). Abnormal cortical development after premature birth shown by altered allometric scaling of brain growth. *PLoS Med.* 3:e265. doi: 10.1371/journal.pmed.0030265

Kim, S. K., Nikolova, S., and Schwedt, T. J. (2021). Structural aberrations of the brain associated with migraine: A narrative review. *Headache* 61, 1159–1179. doi: 10.1111/head.14189

Leonardi, M., Steiner, T. J., Scher, A. T., and Lipton, R. B. (2005). The global burden of migraine: Measuring disability in headache disorders with WHO's classification of functioning, disability and health (ICF). *J. Headache Pain* 6, 429–440. doi: 10.1007/s10194-005-0252-4

Liu, H. Y., Chou, K. H., and Chen, W. T. (2018). Migraine and the hippocampus. *Curr. Pain Headache Rep.* 22:13. doi: 10.1007/s11916-018-0668-6

Liu, H. Y., Chou, K. H., Lee, P. L., Fuh, J. L., Niddam, D. M., and Lai, K. L. (2017). Hippocampus and amygdala volume in relation to migraine frequency and prognosis. *Cephalalgia* 37, 1329–1336. doi: 10.1177/033310241667862

Liu, J., Lan, L., Li, G., Yan, X., Nan, J., and Xiong, S. (2013). Migraine-related gray matter and white matter changes at a 1-year follow-up evaluation. *J. Pain* 14, 1703–1708. doi: 10.1016/j.jpain.2013.08.013

MacGregor, E. A. (2017). Migraine. *Ann. Intern. Med.* 166, ITC49–ITC64. doi: 10.7326/AITC201704040

Maleki, N., Becerra, L., Brawn, J., McEwen, B., Burstein, R., and Borsook, D. (2013). Common hippocampal structural and functional changes in migraine. *Brain Struct. Funct.* 218, 903–912. doi: 10.1007/s00429-012-0437-y

Messina, R., Rocca, M. A., Colombo, B., Valsasina, P., Horsfield, M. A., and Copetti, M. (2013). Cortical abnormalities in patients with migraine: A surface-based analysis. *Radiology* 268, 170–180. doi: 10.1148/radiol.13122004

Minelli, C., Del Greco, M. F., van der Plaat, D. A., Bowden, J., Sheehan, N. A., and Thompson, J. (2021). The use of two-sample methods for Mendelian randomization analyses on single large datasets. *Int. J. Epidemiol.* 50, 1651–1659. doi: 10.1093/ije/dyab084

Mitchell, B. L., Diaz-Torres, S., Bivol, S., Cuellar-Partida, G., International Headache Genetics Consortium, and Gerring, Z. F. (2022). Elucidating the relationship between migraine risk and brain structure using genetic data. *Brain* 145, 3214–3224. doi: 10.1093/brain/awac105

Petrusic, I., Dakovic, M., Kacar, K., and Zidverc-Trajkovic, J. (2018). Migraine with aura: Surface-based analysis of the cerebral cortex with magnetic resonance imaging. *Korean J. Radiol.* 19, 767–776. doi: 10.3348/kjr.2018.19.4.767

Pierce, B. L., and Burgess, S. (2013). Efficient design for Mendelian randomization studies: Subsample and 2-sample instrumental variable estimators. *Am. J. Epidemiol.* 178, 1177–1184. doi: 10.1093/aje/kwt084

Planchuelo-Gómez, Á, García-Azorín, D., Guerrero, ÁL., Rodríguez, M., Aja-Fernández, S., and de Luis-García, R. (2020). Gray matter structural alterations in chronic and episodic migraine: A morphometric magnetic resonance imaging study. *Pain Med.* 21, 2997–3011. doi: 10.1093/pm/pnaa271

Rocca, M. A., Messina, R., Colombo, B., Falini, A., Comi, G., and Filippi, M. (2014). Structural brain MRI abnormalities in pediatric patients with migraine. *J. Neurol.* 261, 350–357. doi: 10.1007/s00415-013-7201-y

Sargurupremraj, M., Suzuki, H., Jian, X., Sarnowski, C., Evans, T. E., and Bis, J. C. (2020). Cerebral small vessel disease genomics and its implications across the lifespan. *Nat. Commun.* 11:6285. doi: 10.1038/s41467-020-19111-2

Schmidt-Wilcke, T., Gänssbauer, S., Neuner, T., Bogdahn, U., and May, A. (2008). Subtle grey matter changes between migraine patients and healthy controls. *Cephalalgia* 28, 1–4. doi: 10.1111/j.1468-2982.2007.01428

Schwedt, T. J., and Dodick, D. W. (2009). Advanced neuroimaging of migraine. *Lancet Neurol.* 8, 560–568. doi: 10.1016/S1474-4422(09)70107-3

Signoriello, E., Cirillo, M., Puoti, G., Signoriello, G., Negro, A., and Koci, E. (2018). Migraine as possible red flag of PFO presence in suspected demyelinating disease. *J. Neurol. Sci.* 390, 222–226. doi: 10.1016/j.jns.2018.04.042

Smith, G. D., and Ebrahim, S. (2003). 'Mendelian randomization': Can genetic epidemiology contribute to understanding environmental determinants of disease? *Int. J. Epidemiol.* 32, 1–22. doi: 10.1093/ije/dyg070

Smith, S. M., Douaud, G., Chen, W., Hanayik, T., Alfaro-Almagro, F., and Sharp, K. (2021). An expanded set of genome-wide association studies of brain imaging phenotypes in UK Biobank. *Nat. Neurosci.* 24, 737–745. doi: 10.1038/s41593-021-00826-4

Torres-Ferrus, M., Pareto, D., Gallardo, V. J., Cuberas-Borrós, G., Alpuente, A., and Caronna, E. (2021). Cortical metabolic and structural differences in patients with chronic migraine. An exploratory 18FDG-PET and MRI study. *J. Headache Pain* 22:75. doi: 10.1186/s10194-021-01289-5

Verbanck, M., Chen, C. Y., Neale, B., and Do, R. (2018). Detection of widespread horizontal pleiotropy in causal relationships inferred from Mendelian randomization between complex traits and diseases. *Nat. Genet.* 50, 693–698. doi: 10.1038/s41588-018-0099-7

Williams, J. A., Burgess, S., Suckling, J., Lalousis, P. A., Batool, F., and Griffiths, S. L. (2022). Inflammation and brain structure in schizophrenia and other neuropsychiatric disorders: A Mendelian randomization study. *JAMA Psychiatry* 79, 498–507. doi: 10.1371/10.1001/jamapsychiatry.2022.0407

frontiers | Frontiers in Neuroscience

TYPE Original Research
PUBLISHED 15 March 2023
DOI 10.3389/fnins.2023.1139086

OPEN ACCESS

EDITED BY
Hongwei Wen,
Southwest University, China

REVIEWED BY
Xiaoshuai Li,
Beijing Friendship Hospital, Capital Medical University, China
Raffaele Ornello,
University of L'Aquila, Italy
Huiguang He,
Institute of Automation (CAS), China
Margarita Sanchez Del Rio,
Clínica Universidad de Navarra, Spain

*CORRESPONDENCE
Zhiye Chen
✉ yyqf@hotmail.com

†These authors have contributed equally to this work

SPECIALTY SECTION
This article was submitted to Brain Imaging Methods, a section of the journal Frontiers in Neuroscience

RECEIVED 06 January 2023
ACCEPTED 16 February 2023
PUBLISHED 15 March 2023

CITATION
Li X, Liu M, Fan W, Xu H and Chen Z (2023) Altered cerebral neurovascular coupling in medication-overuse headache: A study combining multi-modal resting-state fMRI with 3D PCASL. *Front. Neurosci.* 17:1139086. doi: 10.3389/fnins.2023.1139086

Altered cerebral neurovascular coupling in medication-overuse headache: A study combining multi-modal resting-state fMRI with 3D PCASL

Xin Li[1,2†], Mengqi Liu[1†], Wenping Fan[1†], Huan Xu[1] and Zhiye Chen[1,2*]

[1]Department of Radiology, Hainan Hospital of PLA General Hospital, Sanya, China, [2]The Second School of Clinical Medicine, Southern Medical University, Guangzhou, China

Aim: Structural and functional changes in the brain have been identified in individuals with medication-overuse headache (MOH) using MRI. However, it has not been clearly established whether neurovascular dysfunction occurs in MOH, which could be elucidated by examining neurovascular coupling (NVC) from the viewpoints of neuronal activity and cerebral blood flow. The aim of this study was to investigate potential alterations in NVC function of the brain in individuals with MOH using resting-state functional MRI (rs-fMRI) and 3D pseudo-continuous arterial spin labeling (3D PCASL) imaging techniques.

Methods: A total of 40 patients with MOH and 32 normal controls (NCs) were recruited, and rs-fMRI and 3D PCASL data were obtained using a 3.0 T MR scanner. Standard preprocessing of the rs-fMRI data was performed to generate images representing regional homogeneity (ReHo), fractional amplitude of low-frequency fluctuation (fALFF), and degree centrality (DC); cerebral blood flow (CBF) images were generated using 3D PCASL sequence data. These functional maps were all normalized into Montreal Neurological Institute (MNI) space, and NVC was subsequently determined on the basis of Pearson correlation coefficients between the rs-fMRI maps (ReHo, fALFF, and DC) and CBF maps. The statistical significance of differences between the MOH and NC groups in terms of NVC in different brain regions was established *via* Z-test. Further analysis was performed to examine correlations between NVC in the brain regions with NVC dysfunction and clinical variables among patients with MOH.

Results: NVC mainly presented a negative correlation in patients with MOH and NCs. No significant difference between the two groups was detected in terms of average NVC over the entire gray matter area. However, several brain regions with significantly decreased NVC in patients with MOH compared to NCs were identified: the left orbital region of the superior frontal gyrus, the bilateral gyrus rectus, and the olfactory cortex ($P < 0.05$). A correlation analysis revealed that the DC of the brain regions with NVC dysfunction was significantly positively correlated with disease duration ($r = 0.323$, $P = 0.042$), and DC–CBF connectivity was negatively correlated with VAS score ($r = -0.424$, $P = 0.035$).

Conclusion: The current study demonstrated that cerebral NVC dysfunction occurs in patients with MOH, and the NVC technique could function as a new imaging biomarker in headache research.

KEYWORDS

medication-overuse headache, resting-state fMRI, arterial spin labeling, neurovascular coupling, brain, magnetic resonance imaging

Background

Medication-overuse headache (MOH), a consequence of regular overuse of acute or symptomatic headache medication, is defined as a type of secondary headache and most frequently occurs in the context of chronic migraine (CM; 2018; Wakerley, 2019). Although MOH is one of the top 20 causes of disability worldwide, with substantial socioeconomic consequences (Linde et al., 2012; Bendtsen et al., 2014; GBD 2015 Disease Injury Incidence Prevalence Collaborators, 2016), the neuromechanism of this disabling disease remains unknown. Therefore, revealing the possible pathophysiological mechanism might be helpful in developing better monitoring of and treatment for MOH.

Many advanced neuroimaging studies have demonstrated that pain not only causes abnormalities in brain structure but also induces alterations in cerebral function (Xie et al., 2016; Niddam et al., 2017; Shokouhi et al., 2018). These conventional neuroimaging techniques have identified altered gray matter volume, disrupted pain modulatory networks, and abnormal functional connectivity in MOH (Chanraud et al., 2014; Chen et al., 2016; Lai et al., 2016; Torta et al., 2016). However, a new neuroimaging technique that exploits neurovascular coupling (NVC; Fabjan et al., 2015) has also been applied to investigate abnormal brain metabolism in migraine. This technique is based on the coupling of microvascular blood flow and metabolic needs of the brain tissue, and may provide an innovative approach to detection of the pathophysiological mechanism of MOH.

NVC is responsible for ensuring an appropriate supply of blood to the brain and reflects the close temporal and regional linkage between neural activity and cerebral blood flow (CBF; Phillips et al., 2016). The NVC approach can involve assessment of both regional neural activity and regional CBF, thereby obtaining a more precise index for the measurement of microvascular blood flow and the metabolic needs of the surrounding brain tissue; this technique has been used in research on various disorders, such as Alzheimer's disease (AD), amyotrophic lateral sclerosis (ALS), chronic myofascial pain, and CM (Zlokovic, 2011; Osaki et al., 2018; Hu et al., 2019; Song et al., 2021). Therefore, assessment of NVC might be a complementary and comprehensive tool that can be used to observe dysfunction of the cerebral vasculature in MOH.

To date, NVC assessment has mainly employed one of the following techniques: (1) the combination of electroencephalography (EEG) with transcranial doppler (TCD) ultrasound, which had been applied in several previous studies (Rosengarten and Kaps, 2010; Rosengarten et al., 2012), but cannot assess NVC accurately at the same time because of the differences in machine patterns; (2) the combination of resting-state fMRI (rs-fMRI) and CBF analysis, which can provide a more feasible and accurate MRI measurement.

Advanced MRI technologies can help to provide better understanding of both perfusion and neuronal activity in the brain. 3D pseudo-continuous arterial spin labeling (3D PCASL) is an advanced perfusion imaging technique that can measure cerebral blood flow in the brain without an exogenous contrast agent, while rs-fMRI is based on spontaneous fluctuations in the blood oxygen level-dependent (BOLD) signal, which could be used to evaluate neuronal activity (Raimondo et al., 2021). BOLD-based analyses generate various parameters, such as regional homogeneity (ReHo), amplitude of low-frequency (0.01–0.08 Hz) fluctuation (ALFF), fractional ALFF (fALFF), and degree centrality (DC), which can be used to assess neuronal activity from different viewpoints. ReHo is designed to characterize the cohesiveness of resting activity in a given voxel with its neighboring voxels (Zang et al., 2004). The ALFF directly correlates with the intensity of spontaneous neural activity in the resting state, and fALFF further reduces the effects of physiological noise, which could represent the oxygen uptake ability of neurons and neuronal activity (Qiu et al., 2019). DC focuses on the functional relationships between a region and the rest of the brain over the entire connectivity matrix of the brain at the voxel level (Gao et al., 2016). Although all signals in rs-fMRI are derived from blood flow, the related fMRI parameters (ReHo, fALFF, and DC) reflect spontaneous fluctuations in the BOLD signal from a microscopic viewpoint, while CBF reflects true cerebral blood flow from the macroscopic viewpoint. Consequently, we can use the 3D PCASL and rs-fMRI techniques to construct an NVC model in order to assess the correlation between cerebral perfusion and neuronal activity in MOH.

To better explore the underlying brain alterations occurring in MOH, in the current study, we aimed to test the hypothesis that abnormal NVC in the brain occurs in patients with MOH. To address the hypothesis, NVC was determined from the Pearson correlation coefficients between the rs-fMRI map (ReHo, fALFF, and DC) and the CBF map over the whole brain in patients with MOH and normal controls (NCs). Additionally, a correlation analysis was performed to examine the relationship between NVC and clinical variables for the brain regions with NVC dysfunction in patients with MOH.

Methods

Subjects

This study was approved by the ethics committee of the Chinese PLA General Hospital, and written informed consent was obtained from all participants.

In the current study, 40 patients with MOH were recruited from the headache clinic of the Chinese PLA General Hospital. A total of 32 NCs, matched on age and sex, were recruited from among hospital staff members and their relatives. The inclusion criterion for patients with MOH was that they should meet the diagnostic criteria in the International Classification of Headache Disorders, third edition (beta version; ICHD-3 beta; 2018); the inclusion criterion for NCs was that they should never have had any primary headache disorder or other types of headache in the past year. All subjects also needed to meet the following conditions: (1) be right-handed; (2) avoid alcohol, nicotine, caffeine, and other substances for at least 12 h before MRI examinations; (3) be normotensive ($\leq$140/90 mmHg); and (4) for patients with MOH, be in the interictal stage at least 3 days after a migraine attack. The exclusion criteria for all participants were as follows: brain tumor, definite white matter lesion, cerebrovascular disease such as infarction or malacia, psychiatric disorders, and regular use of a psychoactive

or hormone medication. No subjects enrolled in the study had any cardiovascular or metabolic disorders.

All subjects were evaluated on several neuropsychological scales, including the Hamilton Anxiety Scale (HAMA), the Hamilton Depression Scale (HAMD), and the Mini-Mental State Examination (MMSE) for evaluation of cognitive function. Disease duration (DD), Visual Analog Scale (VAS) scores, and Migraine Disability Assessment (MIDAS) questionnaire scores were also used to measure pain intensity and to evaluate level of disability for patients with MOH only.

MRI acquisition

All MR data were obtained using a GE 3.0 T MR system (DISCOVERY MR750, GE Healthcare, Milwaukee, WI, USA). A conventional eight-channel quadrature head coil was used, and foam padding was used to limit head movement. MR sequences were carried out as follows: (1) conventional axial T2WI and diffusion-weighted imaging to exclude subjects with cerebral lesions, such as infarction, malacia, and brain tumor; (2) a three-dimensional T1-weighted fast spoiled gradient recalled echo (3D T1-FSPGR) sequence with voxel size 1*1*1 mm over the whole brain; (3) resting-state fMRI, collected using a gradient echo-planar imaging (EPI) sequence (TR/ TE = 2,000/30 ms, flip angle = 90°, slice thickness = 4 mm, slice gap = 1 mm, FOV = 24 × 24 cm, Matrix = 64 × 64); 180 continuous EPI functional volumes were acquired axially over 6 min, during which subjects were instructed to relax, keep their eyes closed, stay awake, remain still, and clear their heads of all thoughts; (4) cerebral perfusion imaging, obtained using 3D pseudo-continuous arterial spinal labeling (3D PCASL) with the following settings: TR/TE = 5,128/15.9 ms, FOV = 20 ×20 cm, x, y matrix = 1,024 × 8 (spiral acquisition), slice thickness = 3.0 mm, labeling duration = 1.5 s, and post-labeling delay (PLD) time = 1.5 s. The 50

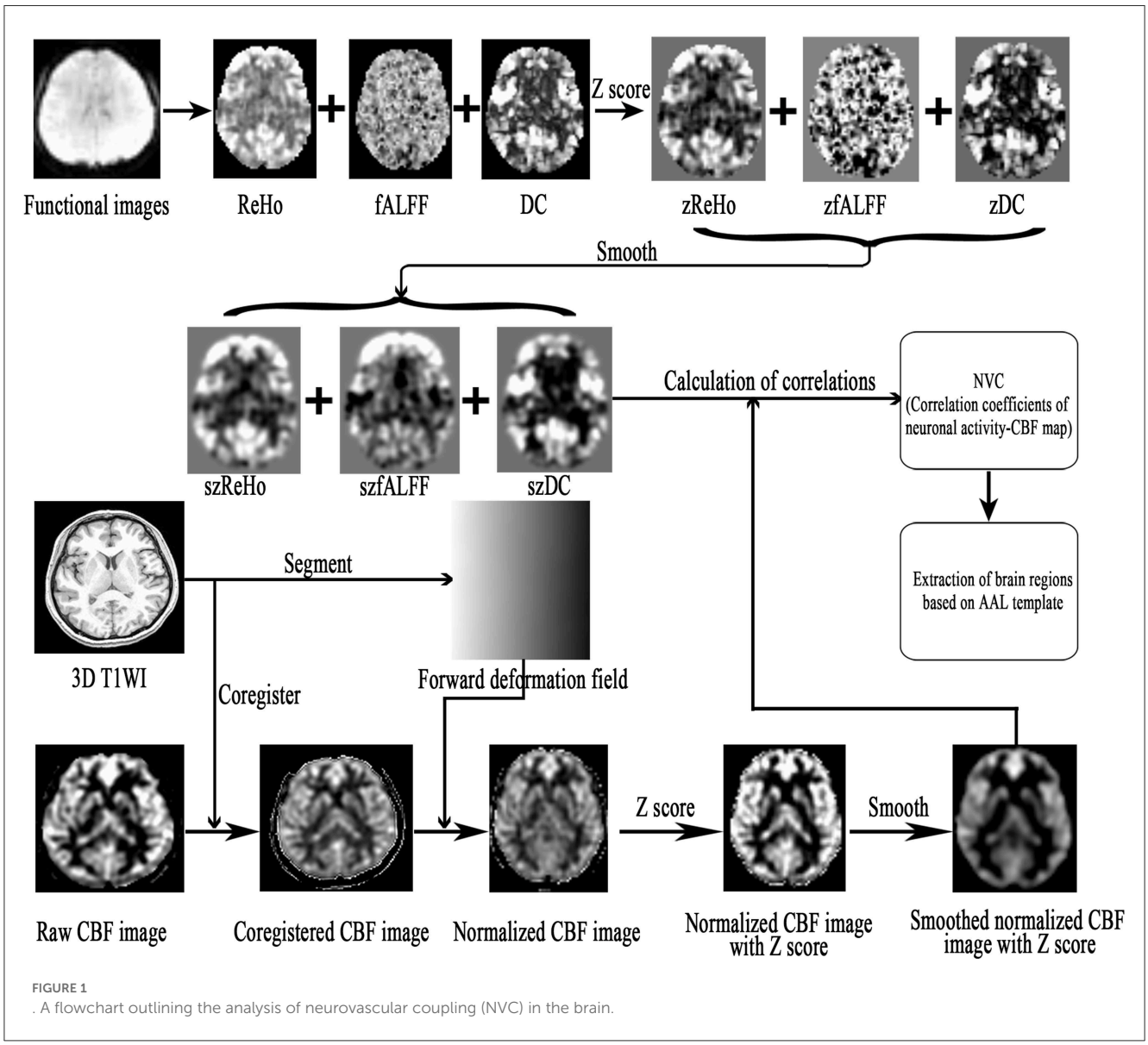

FIGURE 1
. A flowchart outlining the analysis of neurovascular coupling (NVC) in the brain.

slices for each CBF image were automatically generated using Functional Tools (version 9.4.05) after PCASL scanning (Chen et al., 2018).

TABLE 1 Demographic and clinical characteristics of the subjects.

	MOH	NC	*T*-value	*P*-value
Num (F/M)	40 (32/8)	32 (20/12)	2.68 (χ^2)	0.10
Age	41.95 ± 9.82	41.34 ± 10.89	0.25	0.80
HAMA	18.73 ± 8.82	10.19 ± 2.98	5.24	<0.0001
HAMD	19.78 ± 11.94	8.61 ± 4.33	5.48	<0.0001
MMSE	25.35 ± 6.08	25.53 ± 6.24	0.13	0.90
DD (years)	20.00 (3.00, 50.00)	NA		
VAS	8.00 (5.00, 10.00)	NA		
MIDAS	135.00 (0, 260.00)	NA		

MOH, medication-overuse headache; NC, normal control; HAMA, Hamilton Anxiety Scale; HAMD, Hamilton Depression Scale; MMSE, Mini-mental State Examination; DD, disease duration; VAS, Visual Analog Scale; MIDAS, Migraine Disability Assessment questionnaire; NA, not available.

Data processing

Resting-state functional images and CBF images were processed using Statistical Parametric Mapping 12 (SPM12; http://www.fil.ion.ucl.ac.uk/spm) and DPABI (a toolbox for data processing and analysis of brain imaging; V5.1; Chao-Gan and Yu-Feng, 2010), which were run under MATLAB 7.6 (MathWorks, Natick, MA, USA).

The fMRI data preprocessing steps were as follows (Chen et al., 2016; Hu et al., 2019): (1) discarding of the first 10 volumes of each functional time course; (2) slice timing; (3) head motion correction; (4) spatial normalization; (5) calculation of ReHo, DC, and fAlff maps; and (6) Z-score transformation and spatial smoothing.

Cerebral blood flow (CBF) images were obtained using an ASL sequence and processed as follows (Shang et al., 2020): the raw CBF images were coregistered with the raw 3D T1WI (3D T1-FSPGR) and were then normalized to Montreal Neurological Institute (MNI) space using the forward deformation field generated from the segments of 3D T1 images; the normalized CBF images were then Z-scored by subtracting the global mean and dividing by the standard deviation (SD).

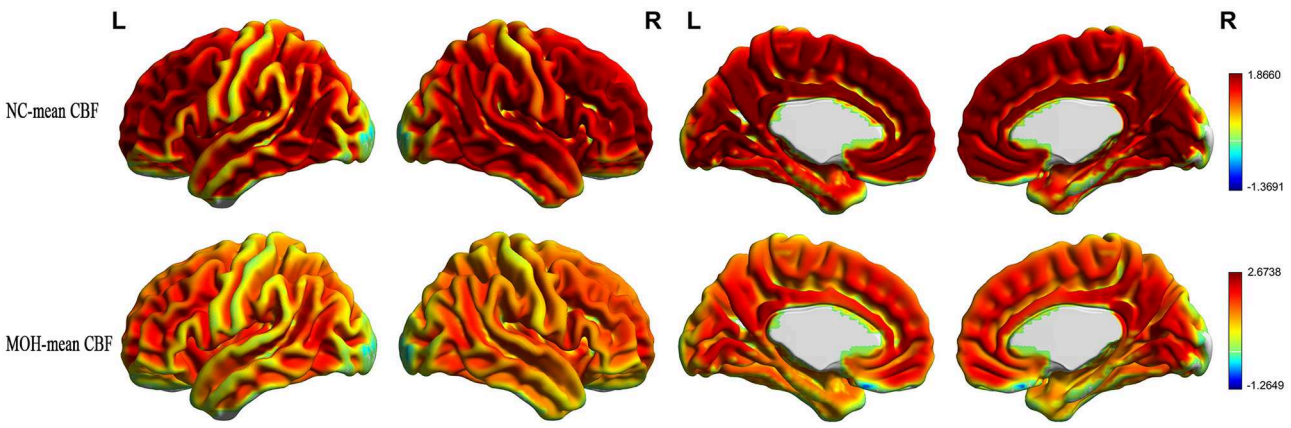

FIGURE 2
Mean CBF maps for the NC and MOH groups, showing no obvious difference in distribution over the entire gray matter level.

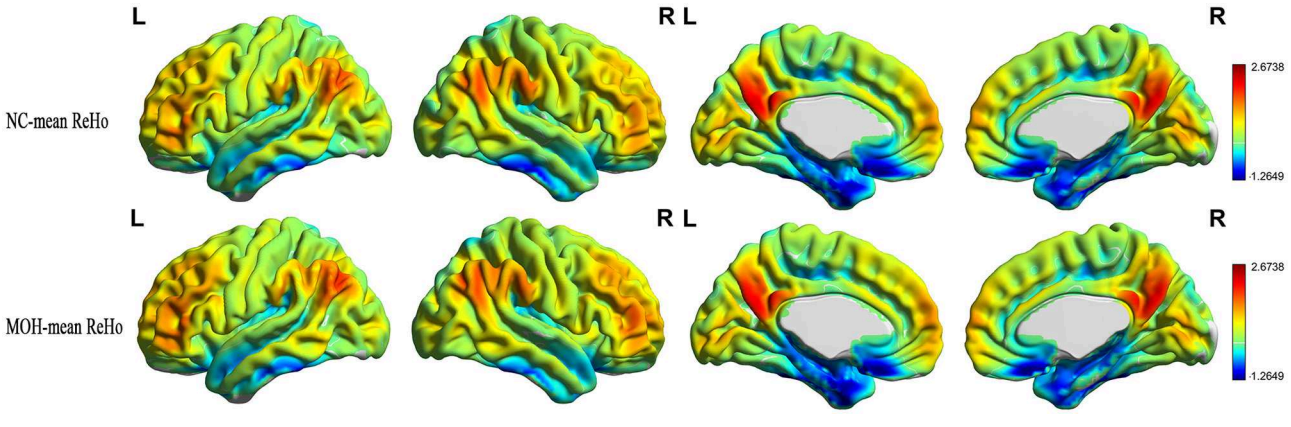

FIGURE 3
Mean ReHo maps for the NC and MOH groups, showing no obvious difference in distribution over the entire gray matter level.

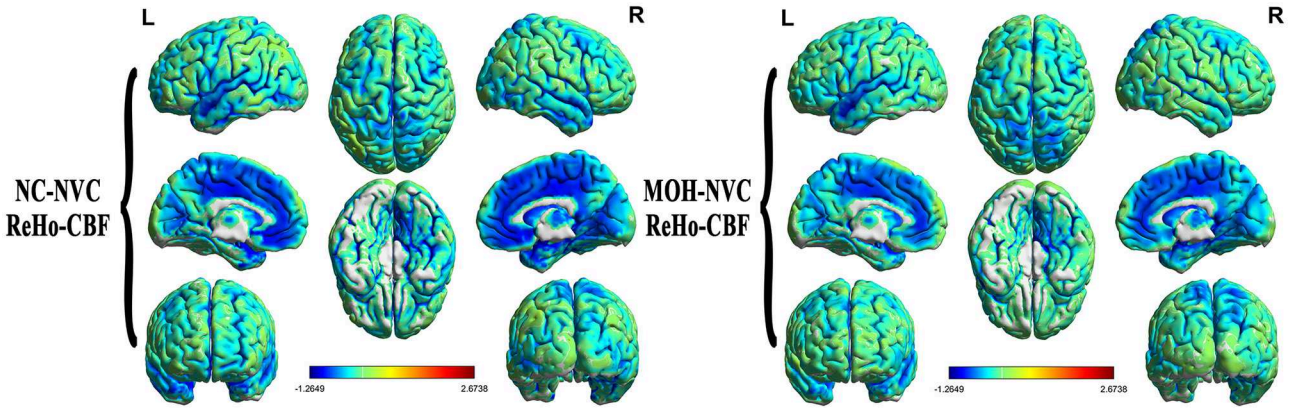

FIGURE 4
Neurovascular coupling (NVC) in normal controls (NCs) and patients with medication-overuse headache (MOH), mainly indicating negative correlation between regional homogeneity (ReHo) and cerebral blood flow (CBF) over the entire gray matter area.

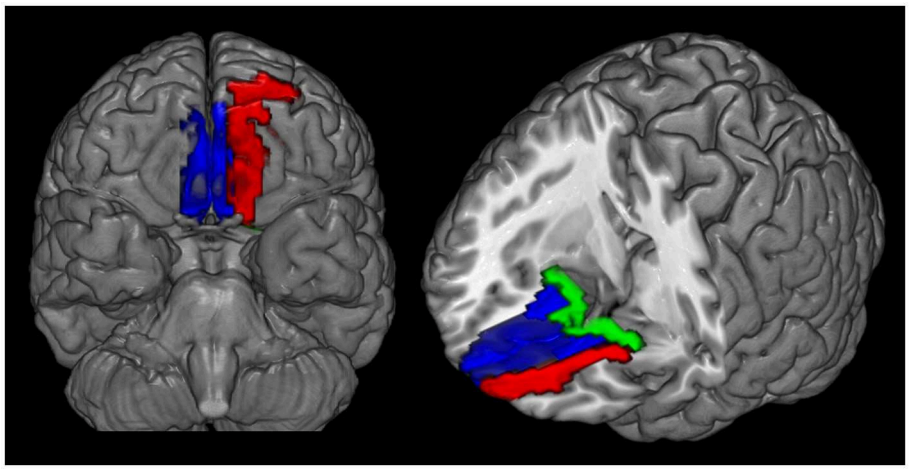

FIGURE 5
Decreased ReHo–CBF connectivity located in the left orbital region of the superior frontal gyrus (red region), the bilateral gyrus rectus (blue region), and the olfactory cortex (green region) in patients with medication-overuse headache (MOH) compared with normal controls (NCs).

The NVC preprocessing steps were as follows (Figure 1). (1) The resting-state fMRI data were processed as described in previous studies, and the zReHo, zfALFF, and zDC (z, z-score) subsequently generated. (2) The CBF images were processed to generate the zCBF. (3) zReHo, zfALFF, zDC, and zCBF were smoothed using a $6 \times 6 \times 6$ mm Gaussian kernel full width at half maximum (FWHM). (4) The NVC maps (ReHo-CBF, fALFF-CBF, and DC-CBF) were calculated by using the Pearson method to compute correlations between maps of neuronal activity (ReHo, fALFF, and DC) and perfusion (CBF) images for the MOH and NC groups. (5) Voxel-wise comparison of NVC was performed using the SPM 12 software, with age and gender as covariates. The minimal number of contiguous voxels was based on the expected cluster size. Significance was set at a P-value of < 0.05 with false discovery rate (FDR) correction. (6) The NVC index (consisting of correlation coefficients between neuronal activity and perfusion maps; Hu et al., 2019) was extracted from the NVC maps using the Automated Anatomical Labeling (AAL) atlas (Rolls et al., 2015).

Statistical analysis

Quantitative data following a normal distribution are presented in the form mean ± SD, and non-normally distributed quantitative data are presented in the form of median (minimum, maximum). Comparisons of quantitative variables were performed with independent-samples t-tests, and comparisons of qualitative variables were performed with the chi-square test. The correlation analysis was performed with the Pearson method for normally distributed data and with the Spearman method for non-normally distributed data. Comparisons of correlation coefficients were performed using the Z-test. These analyses were carried out using

MedCalc (V19.0.4), and a *P*-value of <0.05 was considered to indicate a statistically significant difference.

Results

Demographic and clinical characteristics

Demographic and clinical characteristics of the participants are presented in Table 1. There was no statistically significant difference in Aage, gender, or MMSE scores between the two groups ($P > 0.05$). Patients with MOH had significantly higher HAMA (18.73 ± 8.82) and HAMD (19.78 ± 11.94) scores compared with NCs (HAMA score: 10.19 ± 2.98; HAMD score 8.61 ± 4.33; $P < 0.05$).

Altered ReHo–CBF over all cerebral gray matter regions in MOH

Mean CBF and mean ReHo maps for NCs and patients with MOH are shown in Figures 2, 3, respectively. Figure 4 illustrates the fact that NVC, as indexed by ReHo–CBF, mainly showed a negative correlation over all whole gray matter regions in NCs and patients with MOH. Moreover, there was no significant difference in ReHo–CBF over the entire gray matter level between the MOH ($r = 0.458$) and NC ($r = 0.422$) groups (Z-value = 0.177, $P = 0.860$). However, further regional NVC analysis determined that brain regions with significantly decreased ReHo–CBF connectivity in the MOH group compared with the NC group were located in the left orbital region of the superior frontal gyrus, the bilateral olfactory cortex, and the bilateral gyrus rectus (Figure 5); the corresponding correlation coefficients can be seen in Table 2.

TABLE 2 Brain regions with altered NVC over the whole gray matter in MOH.

NVC	Anatomic region	*r*		*Z*-value	*P*-value
		MOH	NC		
ReHo-CBF	ORBsup.L	−0.298	−0.685	−2.141	0.032
	Olfactory_L	−0.638	−0.903	−2.950	0.003
	Olfactory_R	−0.640	−0.891	−2.702	0.007
	Rectus_L	−0.294	−0.738	−2.295	0.010
	Rectus_R	−0.334	−0.707	−2.155	0.031
fALFF-CBF	ORBsup.L	−0.366	−0.719	−2.102	0.036
	Olfactory_L	−0.630	−0.906	−3.085	0.002
	Olfactory_R	−0.630	−0.881	−2.577	0.010
	Rectus_L	−0.250	−0.726	−2.684	0.007
	Rectus_R	−0.329	−0.706	−2.164	0.030
DC-CBF	ORBsup.L	−0.353	−0.725	−2.214	0.027
	Olfactory_L	−0.506	−0.878	−3.270	0.001
	Olfactory_R	−0.532	−0.872	−3.027	0.003
	Rectus_L	−0.209	−0.725	−0.285	0.004
	Rectus_R	−0.276	−0.704	−2.389	0.017

ReHo, regional homogeneity; fALFF, fractional amplitude of low-frequency fluctuation; DC, degree centrality; CBF, cerebral blood flow; MOH, medication-overuse headache; NC, normal control; NVC, neurovascular coupling; ORBsup.L, left orbit part of superior frontal gyrus; Olfactory, olfactory cortex; Rectus, gyrus rectus; L, left; R, right.

Altered fALFF–CBF over all cerebral gray matter regions in MOH

Mean fALFF in the NC and MOH groups can be seen in Figure 6. The fALFF–CBF measure mainly presented a negative correlation in both NCs and patients with MOH (Figure 7). There was no significant difference in fALFF–CBF connectivity over the entire gray matter level between the MOH ($r = 0.475$) and NC ($r = 0.504$) groups (Z-value = 0.154, $P = 0.878$). However, there was significantly decreased fALFF–CBF connectivity in the MOH group, compared with fALFF–CBF of NCs, in the left orbital region of the superior frontal gyrus, the bilateral olfactory cortex, and the bilateral gyrus rectus (Figure 5; $P < 0.05$).

Altered DC–CBF over all cerebral gray matter regions in MOH

Figure 8 presents the mean DC among NCs and patients with MOH over all gray matter regions. DC–CBF connectivity of NCs and patients with MOH mainly presented a negative correlation over all gray matter (Figure 9). However, mean DC–CBF over all gray matter regions showed no significant difference between the NC ($r = 0.494$) and MOH ($r = 0.492$) groups (Z-value = 0.011, P-value = 0.992). Further comparisons of specific brain regions identified significantly decreased DC–CBF connectivity in the MOH group compared to the NC group in the left orbital region of the superior frontal gyrus, the bilateral olfactory cortex, and the bilateral gyrus rectus (Figure 5; $P < 0.05$).

Correlations of resting-state fMRI variables and NVC in brain regions with altered NVC with clinical characteristics in MOH

As shown in Table 3, the only significant positive correlation with disease duration was that of DC of brain regions with altered NVC ($r = 0.323$, $P = 0.042$; Figure 10). ReHo and fALFF of brain regions with altered NVC did not have any positive significant correlations with any clinical variables in the MOH group ($P > 0.05$).

The DC–CBF value of brain regions with altered NVC presented a significant negative correlation with VAS score ($r = -0.424$, $P = 0.035$; Table 4 and Figure 11). ReHo–CBF and fALFF–CBF of brain regions

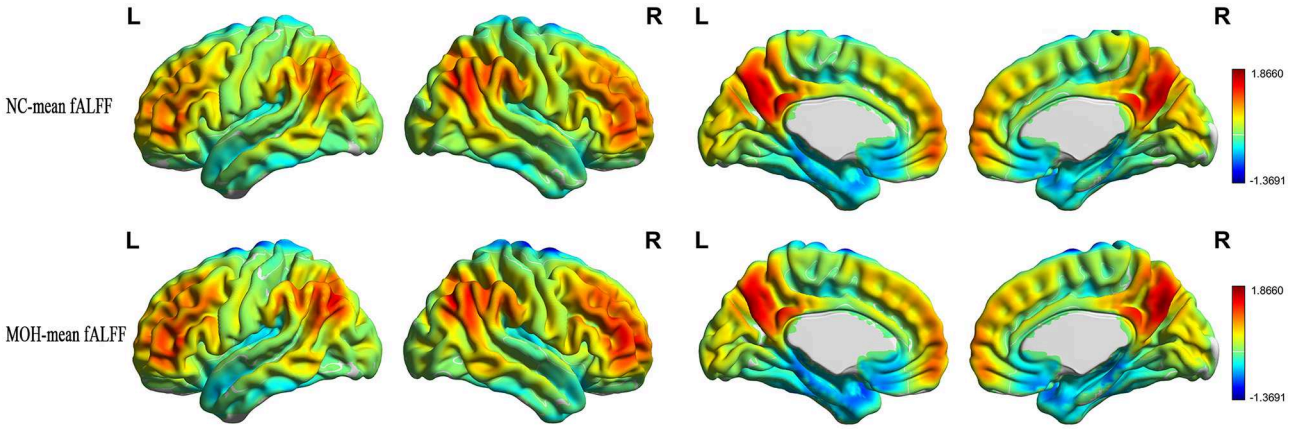

FIGURE 6
Mean fALFF in normal controls (NCs) and patients with medication-overuse headache (MOH).

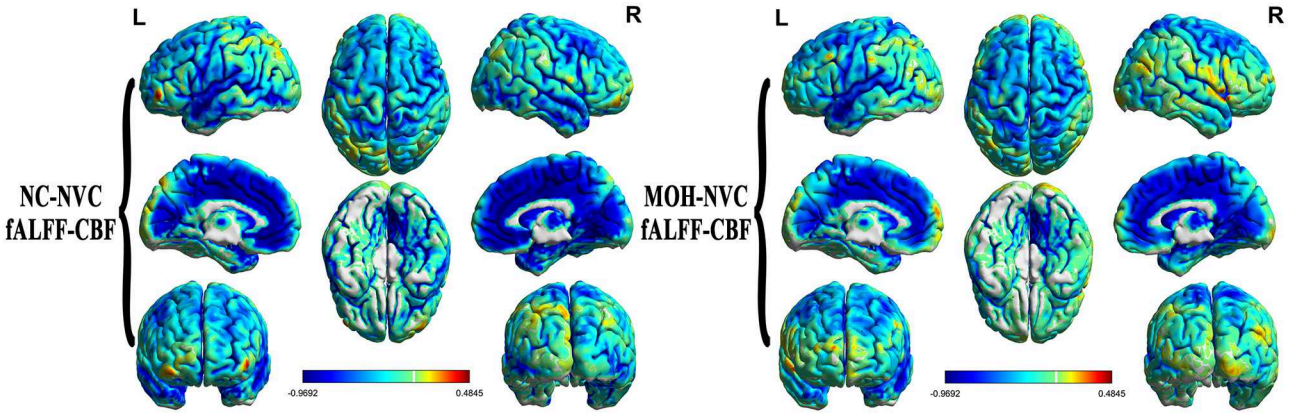

FIGURE 7
fALFF–CBF connectivity, mainly indicating a negative correlation in normal controls (NCs) and patients with medication-overuse headache (MOH), and also showing no significant difference over the entire gray matter level.

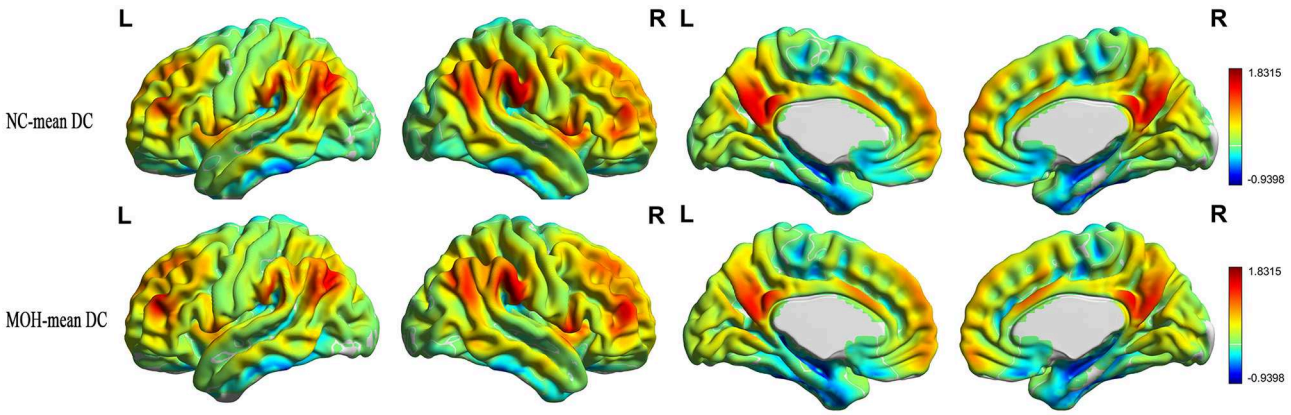

FIGURE 8
Mean DC in normal controls (NCs) and patients with medication-overuse headache (MOH) over the entire gray matter level.

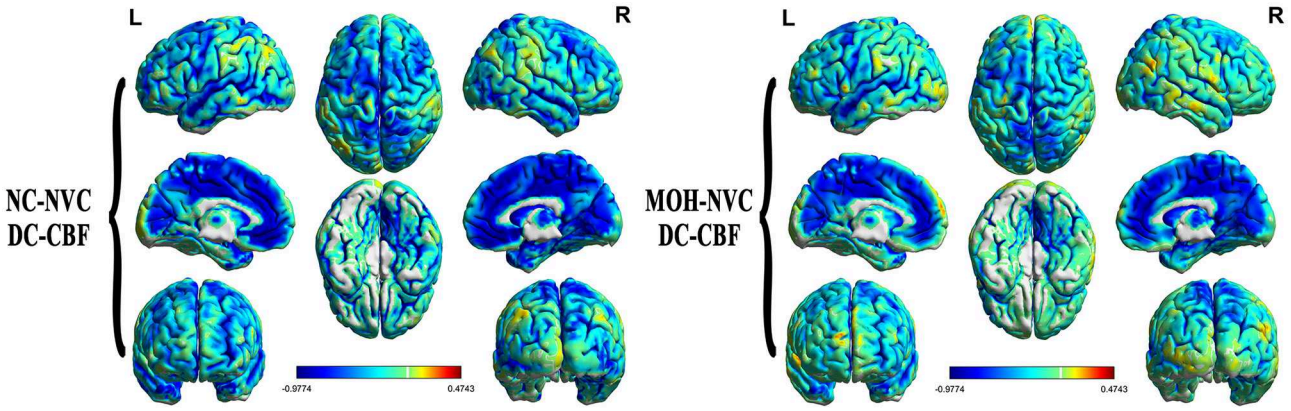

FIGURE 9
DC–CBF connectivity of NCs and patients with MOH, mainly indicating a negative correlation over the entire gray matter level.

TABLE 3 Correlation between the resting-state fMRI variables extracted from the brain regions with altered NVC and the clinical characteristics in MOH.

	ReHo		fALFF		DC		CBF	
	r	*P*	*r*	*P*	*r*	*P*	*r*	*P*
DD	0.121	0.459	0.125	0.443	0.323	0.042	−0.317	0.063
VAS	−0.100	0.557	−0.036	0.827	0.247	0.125	−0.154	0.377
HAMA	0.068	0.678	−0.011	0.947	−0.075	0.646	−0.133	0.447
HAMD	−0.104	0.525	−0.083	0.609	−0.156	0.335	−0.074	0.672
MIDAS	−0.078	0.633	−0.207	0.199	−0.251	0.118	−0.056	0.750
MMSE	0.018	0.911	−0.158	0.331	−0.052	0.750	0.093	0.593

DD, disease duration; VAS, Visual Analog Scale; HAMA, Hamilton Anxiety Scale; HAMD, Hamilton Depression Scale; MIDAS, Migraine Disability Assessment questionnaire; MMSE, Mini-mental State Examination; ReHo, reagional homogeneity; fALFF, fractional amplitude of low-frequency fluctuation; DC, degree centrality; CBF, cerebral blood flow.

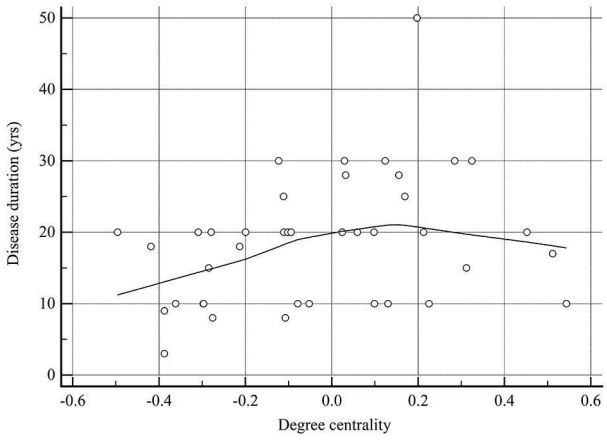

FIGURE 10
There was a significant positive correlation between degree centrality of the brain regions with altered NVC and disease duration in patients with MOH.

with altered NVC showed no significant negative correlations with any clinical variables in the MOH group ($P > 0.05$).

TABLE 4 Correlation between NVC connectivity of the brain regions with altered NVC and the clinical characteristics in MOH.

	ReHo-CBF		fALFF-CBF		DC-CBF	
	r	*P*	*r*	*P*	*r*	*P*
DD	0.023	0.934	0.327	0.137	−0.286	0.166
VAS	−0.054	0.842	0.190	0.397	−0.424	0.035
HAMA	−0.052	0.849	0.236	0.291	−0.291	0.158
HAMD	−0.291	0.274	−0.018	0.936	−0.363	0.074
MIDAS	0.252	0.347	0.311	0.159	−0.237	0.254
MMSE	0.369	0.160	0.081	0.721	0.130	0.534

DD, disease duration; VAS, Visual Analog Scale; HAMA, Hamilton Anxiety Scale; HAMD, Hamilton Depression Scale; MIDAS, Migraine Disability Assessment questionnaire; MMSE, Mini-mental State Examination; ReHo, regional homogeneity; fALFF, fractional amplitude of low-frequency fluctuation; DC, degree centrality; CBF, cerebral blood flow.

Discussion

In the current study, we assessed NVC *via* a combination of rs-fMRI brain maps and CBF maps as measures of neuronal activity and perfusion, respectively. In this article, we have reported a series of NVC findings whose interpretation may help suggest some new hypotheses on the potential neurological pathology of MOH.

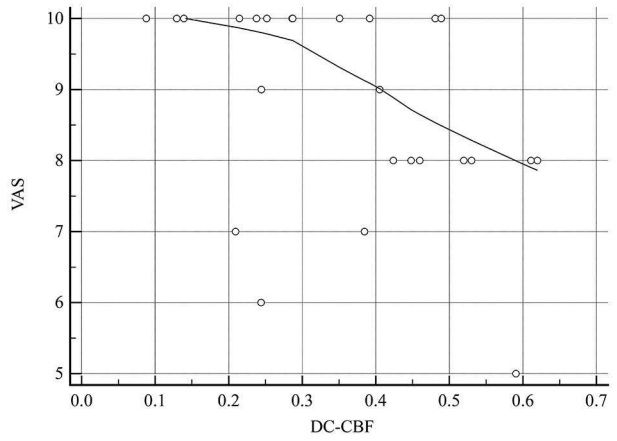

FIGURE 11
There was a significant negative correlation between DC–CBF of the brain regions with altered NVC and VAS score in patients with MOH.

This study revealed that neuronal activity (ReHo, fALFF, and DC) was mainly negatively correlated with brain perfusion (CBF) on the voxel level in patients with MOH. Under physiological conditions, perfusion is tightly coupled with brain metabolism during rest, and functional brain hubs exhibit high CBF, suggesting that highly connected functional hubs are more metabolically active and exhibit higher levels of energy consumption (Liang et al., 2013; Galiano et al., 2020). However, in the present study, neuronal activity mainly showed a negative correlation with brain perfusion in patients with MOH, indicating that the normal physiological condition was disturbed, and the balance between neuronal activity and metabolic supply was probably disrupted from the NVC viewpoint.

In addition, we further explored multiple NVC indices (ReHo–CBF, fALFF–CBF, and DC–CBF), which showed no significant difference between patients with MOH and NCs over the entire cerebral gray matter level. However, regional NVC analysis demonstrated that values of ReHo–CBF, fALFF–CBF, and DC–CBF were lower in the MOH group than that in the NC group in the following brain regions: the left orbital region of the superior frontal gyrus (ORBsup.L), the bilateral olfactory cortex, and the bilateral gyrus rectus. Therefore, regional NVC analysis might be much more sensitive for the evaluation of neuronal vascular activity than overall cerebral NVC assessment in MOH. Meanwhile, changes in NVC could be interpreted in terms of its structural basis, that is, neurovascular units (NVUs), which are mainly composed of neurons, vascular cells, and glial cells (Phillips et al., 2016). Under this view, decreased NVC in patients with MOH implies possible damage to or degeneration of NVUs, which may be a consequence of repeated migraine attacks. Therefore, further NVC evaluation might provide more valuable information to develop an understanding of the neural mechanism of MOH.

In this study, decreased NVC in ORBsup.L was confirmed in patients with MOH; this might be associated with abnormal metabolism in MOH. The majority of rs-fMRI studies have revealed that patients with migraine show functional alterations in the superior frontal gyrus compared with NCs (Tian et al., 2021; Cao et al., 2022; Yang et al., 2022). Furthermore, one 18-FDG-PET study has initially reported hypometabolism in the orbitofrontal cortex, the bilateral thalamus, and other regions. Interestingly, after medication withdrawal, other regional metabolic changes were found to normalize in this study, with the exception of continued hypometabolism in the orbitofrontal region (Fumal et al., 2006), which might be related to the fact that the orbitofrontal cortex plays a role in addictive disorders. Moreover, the results of structural imaging studies have revealed abnormalities, including lower orbitofrontal cortex volume and thickness (Chong, 2019). Therefore, the decreased NVC in ORBsup.L observed in the current study is consistent with the abovementioned previous functional and structural studies, which could be used to explain MOH pathogenesis.

An abnormal condition of the olfactory cortex may be associated with the development of osmophobia, leading to fear, aversion, or psychological hypersensitivity to odors in patients with migraine (Harriott and Schwedt, 2014; Rocha-Filho et al., 2015). Chen et al. reported increased ReHo values in the olfactory cortex of patients with CM, using in measure in which attention was paid only to neural activity, with perfusion changes being ignored (Chen et al., 2019). However, the current study found decreased NVC in the olfactory cortex in patients with MOH; the inconsistency in these results may be due to the consideration of perfusion status and different stages of migraine. In contrast, a "neurolimbic" model has also been proposed, which represents dynamic bidirectional influence of pain and mood (such as anxiety and depression), and the activation of the limbic system, making patients with migraine susceptible to stress and emotional reactions (Maizels et al., 2012). It is well-known that the olfactory cortex is subordinate to the limbic system; this may explain why patients with MOH had significantly higher HAMA and HAMD scores compared with NCs. In addition, dysfunction of the limbic system also plays a role in chronic transformation of migraine (Chen et al., 2019); therefore, the pattern of decreased NVC indicates that the limbic system may play a role in the evolution from CM to MOH. Based on all these factors, the presence of abnormal NVC may bear further investigation in terms of understanding the mechanism of MOH.

The gyrus rectus is situated medially to the olfactory sulcus at the ventromedial edge of the frontal lobe, and is specifically connected to auditory cortex neurons in the convexity of the superior temporal gyrus according to animal research (Müller-Preuss et al., 1980). A PET study demonstrated that the gyrus rectus may be a component of the circuit that mediates certain specific cognitive and emotional functions (Andreasen et al., 1995). The decreased level of NVC in the gyrus rectus implies an abnormal association with auditory cortex neurons, further contributing to a disturbance in the auditory sensory modalities of patients with MOH (Harriott and Schwedt, 2014). A significant decrease in ALFF–CBF has been found in the left gyrus rectus in patients with CM (Hu et al., 2019); however, decreased NVC (including ReHo–CBF, fALFF–CBF, and DC–CBF) of the bilateral gyrus rectus was confirmed in this study. This result indicates, using the NVC approach, that the gyrus rectus may be a conjunctive connection of the brain regions involved in CM and MOH development, but the exact neuromechanism should be investigated more precisely in future.

Finally, correlation analysis revealed that DC in the regions of the brain that were positive for NVC dysfunction was significantly positively correlated with disease duration, and DC–CBF connectivity showed a negative correlation with VAS score. Previous research has demonstrated that nociceptive stimuli may result in NVC dysfunction (Wolf et al., 2011; Uchida et al., 2017); the current study further supports the possibility that the abnormal NVC observed in MOH may be a consequence of the strength and extent of previous migraine attacks. However, in the current study, we did not find significant correlations between ReHo–CBF, or fALFF–CBF values and clinical variables. This is again unsurprising, since DC indexes the number of direct connections for a given voxel in a network, reflecting its functional connectivity within the brain network without requiring *a priori* selection (Gao et al., 2016). Therefore, non-invasive NVC techniques could be considered as an objective strategy for the evaluation of pain status in MOH.

Our study has several limitations. First, this study employed a cross-sectional observational design; a longitudinal study should be performed to observe the evolution of MOH from CM. Second, it would be better to estimate altered NVC in patients with MOH before and after medication withdrawal. Third, this study only examined NVC changes in the interictal stage; future studies should assess different time points (i.e., the interictal and ictal stages) in the migraine cycle to provide more information about patients' NVC status. Fourth, the signal-to-noise ratio (SNR) of rs-fMRI and 3D PCASL is relatively low; therefore, it will be important to improve the resolution of these techniques in future work.

Conclusion

The current study demonstrated that cerebral NVC dysfunction occurs in patients with MOH, and can be detected by multi-modal rs-fMRI combined with a 3D PCASL technique; NVC could function as a new imaging biomarker in future research on headache.

Data availability statement

The raw data supporting the conclusions of this article will be made available by the authors, without undue reservation.

Ethics statement

Institutional Review Board of the Chinese PLA General Hospital approved the research protocol and the procedures conformed to the tenets of the Declaration of Helsinki. Written informed consent for participation was not required for this study in accordance with the national legislation and the institutional requirements.

Author contributions

ZC: conception, design, and revision of the manuscript for intellectual content. ML: acquisition of data. XL: analysis of data. XL, WF, and HX: drafting of the manuscript. All authors read and approved the final manuscript.

Conflict of interest

The authors declare that the research was conducted in the absence of any commercial or financial relationships that could be construed as a potential conflict of interest.

Publisher's note

All claims expressed in this article are solely those of the authors and do not necessarily represent those of their affiliated organizations, or those of the publisher, the editors and the reviewers. Any product that may be evaluated in this article, or claim that may be made by its manufacturer, is not guaranteed or endorsed by the publisher.

References

(2018). Headache classification committee of the international headache society (IHS) the international classification of headache disorders, 3rd edition. *Cephalalgia* 38, 1–211. doi: 10.1177/0333102417738202

Andreasen, N. C., O'leary, D. S., Cizadlo, T., Arndt, S., Rezai, K., Watkins, G. L., et al. (1995). Remembering the past: two facets of episodic memory explored with positron emission tomography. *Am. J. Psychiatry* 152, 1576–1585. doi: 10.1176/ajp.152.11.1576

Bendtsen, L., Munksgaard, S., Tassorelli, C., Nappi, G., Katsarava, Z., Lainez, M., et al. (2014). Disability, anxiety and depression associated with medication-overuse headache can be considerably reduced by detoxification and prophylactic treatment. Results from a multicentre, multinational study (COMOESTAS project). *Cephalalgia* 34, 426–433. doi: 10.1177/0333102413515338

Cao, Z. M., Chen, Y. C., Liu, G. Y., Wang, X., Shi, A. Q., Xu, L. F., et al. (2022). Abnormalities of thalamic functional connectivity in patients with migraine: A resting-state fMRI study. *Pain Ther.* 11, 561–574. doi: 10.1007/s40122-022-00365-1

Chanraud, S., Di Scala, G., Dilharreguy, B., Schoenen, J., Allard, M., and Radat, F. (2014). Brain functional connectivity and morphology changes in medication-overuse headache: Clue for dependence-related processes? *Cephalalgia* 34, 605–615. doi: 10.1177/0333102413519514

Chao-Gan, Y., and Yu-Feng, Z. (2010). DPARSF: A MATLAB toolbox for "pipeline" data analysis of resting-state fMRI. *Front Syst Neurosci* 4, 13. doi: 10.3389/fnsys.2010.00013

Chen, C., Yan, M., Yu, Y., Ke, J., Xu, C., Guo, X., et al. (2019). Alterations in regional homogeneity assessed by fMRI in patients with migraine without aura. *J. Med. Syst.* 43, 298. doi: 10.1007/s10916-019-1425-z

Chen, Z., Chen, X., Liu, M., Liu, M., Ma, L., and Yu, S. (2018). Evaluation of gray matter perfusion in episodic migraine using voxel-wise comparison of 3D pseudo-continuous arterial spin labeling. *J. Headache Pain* 19, 36. doi: 10.1186/s10194-018-0866-y

Chen, Z., Chen, X., Liu, M., Liu, S., Shu, S., Ma, L., et al. (2016). Altered functional connectivity of the marginal division in migraine: A resting-state fMRI study. *J. Headache Pain* 17, 89. doi: 10.1186/s10194-016-0682-1

Chong, C. D. (2019). Brain structural and functional imaging findings in medication-overuse headache. *Front. Neurol.* 10, 1336. doi: 10.3389/fneur.2019.01336

Fabjan, A., Zaletel, M., and Žvan, B. (2015). Is there a persistent dysfunction of neurovascular coupling in migraine? *Biomed. Res. Int.* 2015, 574186. doi: 10.1155/2015/574186

Fumal, A., Laureys, S., Di Clemente, L., Boly, M., Bohotin, V., Vandenheede, M., et al. (2006). Orbitofrontal cortex involvement in chronic analgesic-overuse headache evolving from episodic migraine. *Brain* 129, 543–550. doi: 10.1093/brain/awh691

Galiano, A., Mengual, E., García De Eulate, R., Galdeano, I., Vidorreta, M., Recio, M., et al. (2020). Coupling of cerebral blood flow and functional connectivity is decreased in healthy aging. *Brain Imaging Behav.* 14, 436–450. doi: 10.1007/s11682-019-00157-w

Gao, C., Wenhua, L., Liu, Y., Ruan, X., Chen, X., Liu, L., et al. (2016). Decreased subcortical and increased cortical degree centrality in a nonclinical college student sample with subclinical depressive symptoms: A resting-state fMRI study. *Front. Hum. Neurosci.* 10, 617. doi: 10.3389/fnhum.2016.00617

GBD 2015 Disease and Injury Incidence and Prevalence Collaborators (2016). Global, regional, and national incidence, prevalence, and years lived with disability for 310 diseases and injuries, 1990-2015: A systematic analysis for the Global Burden of Disease Study 2015. *Lancet* 388, 1545–1602. doi: 10.1016/S0140-6736(16)31678-6

Harriott, A. M., and Schwedt, T. J. (2014). Migraine is associated with altered processing of sensory stimuli. *Curr. Pain Headache Rep.* 18, 458. doi: 10.1007/s11916-014-0458-8

Hu, B., Yu, Y., Dai, Y. J., Feng, J. H., and Wang, W. (2019). Multi-modal MRI reveals the neurovascular coupling dysfunction in chronic migraine. *Neuroscience* 419, 22. doi: 10.1016/j.neuroscience.2019.09.022

Lai, T. H., Chou, K. H., Fuh, J. L., Lee, P. L., Kung, Y. C., Lin, C. P., et al. (2016). Gray matter changes related to medication overuse in patients with chronic migraine. *Cephalalgia* 36, 1324–1333. doi: 10.1177/0333102416630593

Liang, X., Zou, Q., He, Y., and Yang, Y. (2013). Coupling of functional connectivity and regional cerebral blood flow reveals a physiological basis for network hubs of the human brain. *Proc. Natl. Acad. Sci. U. S. A.* 110, 1929–1934. doi: 10.1073/pnas.1214900110

Linde, M., Gustavsson, A., Stovner, L. J., Steiner, T. J., Barré, J., Katsarava, Z., et al. (2012). The cost of headache disorders in Europe: The Eurolight project. *Eur. J. Neurol.* 19, 703–711. doi: 10.1111/j.1468-1331.2011.03612.x

Maizels, M., Aurora, S., and Heinricher, M. (2012). Beyond neurovascular: Migraine as a dysfunctional neurolimbic pain network. *Headache* 52, 1553–1565. doi: 10.1111/j.1526-4610.2012.02209.x

Müller-Preuss, P., Newman, J. D., and Jürgens, U. (1980). Anatomical and physiological evidence for a relationship between the "cingular" vocalization area and the auditory cortex in the squirrel monkey. *Brain Res.* 202, 307–315. doi: 10.1016/0006-8993(80)90143-2

Niddam, D. M., Lee, S. H., Su, Y. T., and Chan, R. C. (2017). Brain structural changes in patients with chronic myofascial pain. *Eur. J. Pain* 21, 148–158. doi: 10.1002/ejp.911

Osaki, T., Sivathanu, V., and Kamm, R. D. (2018). Engineered 3D vascular and neuronal networks in a microfluidic platform. *Sci. Rep.* 8, 5168. doi: 10.1038/s41598-018-23512-1

Phillips, A. A., Chan, F. H., Zheng, M. M., Krassioukov, A. V., and Ainslie, P. N. (2016). Neurovascular coupling in humans: Physiology, methodological advances and clinical implications. *J. Cereb. Blood Flow Metab.* 36, 647–664. doi: 10.1177/0271678X15617954

Qiu, H., Li, X., Luo, Q., Li, Y., Zhou, X., Cao, H., et al. (2019). Alterations in patients with major depressive disorder before and after electroconvulsive therapy measured by fractional amplitude of low-frequency fluctuations (fALFF). *J. Affect Disord.* 244, 92–99. doi: 10.1016/j.jad.2018.10.099

Raimondo, L., Oliveira, L., A. F., Heij, J., Priovoulos, N., Kundu, P., et al. (2021). Advances in resting state fMRI acquisitions for functional connectomics. *Neuroimage* 243, 118503. doi: 10.1016/j.neuroimage.2021.118503

Rocha-Filho, P. A., Marques, K. S., Torres, R. C., and Leal, K. N. (2015). Osmophobia and headaches in primary care: prevalence, associated factors, and importance in diagnosing migraine. *Headache* 55, 840–845. doi: 10.1111/head.12577

Rolls, E. T., Joliot, M., and Tzourio-Mazoyer, N. (2015). Implementation of a new parcellation of the orbitofrontal cortex in the automated anatomical labeling atlas. *Neuroimage* 122, 1–5. doi: 10.1016/j.neuroimage.2015.07.075

Rosengarten, B., Deppe, M., Kaps, M., and Klingelhöfer, J. (2012). Methodological aspects of functional transcranial Doppler sonography and recommendations for simultaneous EEG recording. *Ultrasound Med. Biol.* 38, 989–996. doi: 10.1016/j.ultrasmedbio.2012.02.027

Rosengarten, B., and Kaps, M. (2010). A simultaneous EEG and transcranial Doppler technique to investigate the neurovascular coupling in the human visual cortex. *Cerebrovasc. Dis.* 29, 211–216. doi: 10.1159/000267840

Shang, S., Wu, J., Zhang, H., Chen, H., and Yin, X. (2020). Motor asymmetry related cerebral perfusion patterns in Parkinson's disease: An arterial spin labeling study. *Hum. Brain Map.* 2020, 25223. doi: 10.1002/hbm.25223

Shokouhi, M., Clarke, C., Morley-Forster, P., Moulin, D. E., Davis, K. D., and St Lawrence, K. (2018). Structural and functional brain changes at early and late stages of complex regional pain syndrome. *J. Pain* 19, 146–157. doi: 10.1016/j.jpain.2017.09.007

Song, G., Zhang, Y., Qin, B., Zeng, J., Zhang, T., and Xie, P. (2021). Altered neurovascular coupling in patients with chronic myofascial pain. *Pain Physician* 24, E601–E610. doi: 10.36076/ppj.2021.24.E601

Tian, Z., Yin, T., Xiao, Q., Dong, X., Yang, Y., Wang, M., et al. (2021). The altered functional connectivity with pain features integration and interaction in migraine without aura. *Front. Neurosci.* 15, 646538. doi: 10.3389/fnins.2021.646538

Torta, D. M., Costa, T., Luda, E., Barisone, M. G., Palmisano, P., Duca, S., et al. (2016). Nucleus accumbens functional connectivity discriminates medication-overuse headache. *Neuroimage Clin.* 11, 686–693. doi: 10.1016/j.nicl.2016.05.007

Uchida, S., Bois, S., Guillemot, J. P., Leblond, H., and Pich,é, M. (2017). Systemic blood pressure alters cortical blood flow and neurovascular coupling during nociceptive processing in the primary somatosensory cortex of the rat. *Neuroscience* 343, 250–259. doi: 10.1016/j.neuroscience.2016.12.014

Wakerley, B. R. (2019). Medication-overuse headache. *Pract. Neurol.* 19, 399–403. doi: 10.1136/practneurol-2018-002048

Wolf, M. E., Held, V. E., Förster, A., Griebe, M., Szabo, K., Gass, A., et al. (2011). Pearls & oy-sters: dynamics of altered cerebral perfusion and neurovascular coupling in migraine aura. *Neurology* 77, e127–128. doi: 10.1212/WNL.0b013e31823a0ceb

Xie, P., Qin, B., Song, G., Zhang, Y., Cao, S., Yu, J., et al. (2016). Microstructural abnormalities were found in brain gray matter from patients with chronic myofascial pain. *Front. Neuroanat.* 10, 122. doi: 10.3389/fnana.2016.00122

Yang, Y., Wei, K., Zhang, H., Hu, H., Yan, L., Gui, W., et al. (2022). Identifying functional brain abnormalities in migraine and depression comorbidity. *Quant. Imaging Med. Surg.* 12, 2288–2302. doi: 10.21037/qims-21-667

Zang, Y., Jiang, T., Lu, Y., He, Y., and Tian, L. (2004). Regional homogeneity approach to fMRI data analysis. *Neuroimage* 22, 394–400. doi: 10.1016/j.neuroimage.2003.12.030

Zlokovic, B. V. (2011). Neurovascular pathways to neurodegeneration in Alzheimer's disease and other disorders. *Nat. Rev. Neurosci.* 12, 723–738. doi: 10.1038/nrn3114

frontiers | Frontiers in Neuroscience

TYPE Correction
PUBLISHED 13 April 2023
DOI 10.3389/fnins.2023.1195725

OPEN ACCESS

APPROVED BY
Frontiers Editorial Office,
Frontiers Media SA, Switzerland

*CORRESPONDENCE
Zhiye Chen
✉ yyqf@hotmail.com

RECEIVED 28 March 2023
ACCEPTED 30 March 2023
PUBLISHED 13 April 2023

CITATION
Li X, Liu M, Fan W, Xu H and Chen Z (2023) Corrigendum: Altered cerebral neurovascular coupling in medication-overuse headache: a study combining multi-modal resting-state fMRI with 3D PCASL.
Front. Neurosci. 17:1195725.
doi: 10.3389/fnins.2023.1195725

Corrigendum: Altered cerebral neurovascular coupling in medication-overuse headache: a study combining multi-modal resting-state fMRI with 3D PCASL

Xin Li[1,2], Mengqi Liu[1], Wenping Fan[1], Huan Xu[1] and Zhiye Chen[1,2]*

[1]Department of Radiology, Hainan Hospital of PLA General Hospital, Sanya, China, [2]The Second School of Clinical Medicine, Southern Medical University, Guangzhou, China

KEYWORDS

medication-overuse headache, resting-state fMRI, arterial spin labeling, neurovascular coupling, brain, magnetic resonance imaging

A corrigendum on

Altered cerebral neurovascular coupling in medication-overuse headache: a study combining multi-modal resting-state fMRI with 3D PCASL

by Li, X., Liu, M., Fan, W., Xu, H., and Chen, Z. (2023) Front. Neurosci. 17:1139086. doi: 10.3389/fnins.2023.1139086

Incorrect Affiliation

In the published article, there was an error in affiliation(s) 1. Instead of "The Second School of Clinical Medicine, Southern Medical University, Guangzhou, China", it should be "Department of Radiology, Hainan Hospital of PLA General Hospital, Sanya, China".

In the published article, there was an error in affiliation(s) 2. Instead of "Department of Radiology, Hainan Hospital of Chinese PLA General Hospital, Sanya, China", it should be "The Second School of Clinical Medicine, Southern Medical University, Guangzhou, China".

The authors apologize for this error and state that this does not change the scientific conclusions of the article in any way. The original article has been updated.

Additional Affiliation(s)

In the published article, there was an error regarding the affiliation 1 for Xin Li and Zhiye Chen. As well as having affiliation(s) 1, they should also have *The Second School of Clinical Medicine, Southern Medical University, Guangzhou, China*.

The authors apologize for this error and state that this does not change the scientific conclusions of the article in any way. The original article has been updated.

Publisher's note

frontiers | Frontiers in Neuroscience

TYPE Mini Review
PUBLISHED 27 March 2023
DOI 10.3389/fnins.2023.1148400

OPEN ACCESS

EDITED BY
Jing Li,
Beijing Friendship Hospital, Capital Medical University, China

REVIEWED BY
Yan Xue,
Affiliated Hospital of Shandong University of Traditional Chinese Medicine, China
Constantina Aggeli,
National and Kapodistrian University of Athens, Greece

*CORRESPONDENCE
Cuicui Li
✉ cuicuili0649@163.com
Ximing Wang
✉ wxming369@163.com

SPECIALTY SECTION
This article was submitted to Brain Imaging Methods, a section of the journal Frontiers in Neuroscience

RECEIVED 20 January 2023
ACCEPTED 01 March 2023
PUBLISHED 27 March 2023

CITATION
Li T, Bao X, Li L, Qin R, Li C and Wang X (2023) Heart failure and cognitive impairment: A narrative review of neuroimaging mechanism from the perspective of brain MRI. *Front. Neurosci.* 17:1148400. doi: 10.3389/fnins.2023.1148400

Heart failure and cognitive impairment: A narrative review of neuroimaging mechanism from the perspective of brain MRI

Tong Li[1], Xiangyuan Bao[2], Lin Li[1], Rui Qin[1], Cuicui Li[1]* and Ximing Wang[1]*

[1]Department of Radiology, Shandong Provincial Hospital Affiliated to Shandong First Medical University, Jinan, China, [2]School of Radiology, Shandong First Medical University, Taian, China

Both heart failure (HF) and cognitive impairment (CI) have a significant negative impact on the health of the elderly individuals. Magnetic resonance imaging (MRI) can non-invasively detect functional and structural variations in the heart and brain, making it easier to explore the connection between the heart and brain. According to neuroimaging studies, HF patients have a higher chance of developing CI because they have a variety of different types of brain injuries. To examine how HF and CI are influenced by one another, English-language literature was searched in the Web of Science, PubMed EMBASE (OVID), PsycInfo, and Scopus databases. The search terms included "high-frequency," "brain function," "brain injury," "cognition," "cognitive impairment," and "magnetic resonance imaging." Normal brain function is typically impaired by HF in the form of decreased cerebral perfusion pressure, inflammation, oxidative stress, and damage to the BBB, resulting in CI and subsequent HF. Early pathophysiological alterations in patients' brains have been widely detected using a range of novel MRI techniques, opening up new avenues for investigating the connection between HF and CI. This review aims to describe the pathogenesis of HF with CI and the early diagnostic role of MRI in the heart-brain domain.

KEYWORDS

heart failure, cognitive impairment, brain lesions, brain magnetic resonance, MRI

1. Introduction

A common tendency in population growth around the world is aging. Due to their significant incidence in the senior population, heart failure (HF) and cognitive impairment (CI) are receiving increasing amounts of attention. HF is a common clinical disease characterized by a decrease in the blood supply of the heart due to anatomical or functional problems with the heart. In China, studies on the epidemiology of HF have revealed an increase in the prevalence rate among people over 35, from 0.9% in 2000 to 1.3% in 2019 (Hao et al., 2019). CI refers to one or more impairments of cognitive function that affect daily or social abilities for various reasons, such as memory and learning. It covers all stages, from mild CI to dementia. Studies have confirmed that up to 50% of HF patients develop a certain level of CI, and 10% of them have more serious symptoms (Vogels et al., 2008; Almeida et al., 2012).

Ischemic cardiomyopathy and hypertension are considered major causes of HF and are associated with cognitive function (Schmidt et al., 1991). Decreased systolic function of the heart and blood redistribution are symptoms of HF, which is frequently a subsequent condition to myocardial infarction (Roy et al., 2017; Jinawong et al., 2021). The fundamental etiology of brain functional injury is thought to be the decrease in cerebral perfusion pressure brought on by decreased cardiac output and inflammation worsened by oxidative stress (Harkness et al., 2014; Cannon et al., 2017). Although anatomical abnormalities in the brain were linked to biomarkers of myocardial injury and cardiac failure, only older people with poorer cognitive reserves displayed cognitive deficits (Feola et al., 2013; Hjelm et al., 2014). HF and CI patients with poor self-care abilities witness a significantly decreased quality of life and higher rates of readmission and mortality (Yang et al., 2022). Participants in previous studies have not always been categorized according to the subtype of HF. Consequently, the phrase "heart failure" broadly refers to a variety of cardiac failures.

In recent years, an increasing number of studies have verified that CI frequently occurs in patients with HF. Magnetic resonance imaging (MRI) technology and its derivatives can detect spontaneous brain activity and investigate image biomarkers, which offer the foundation for early identification of CI. However, the specific pathogenesis of HF has not yet been clarified, and the correlation between HF and cognitive function needs to be further researched by MRI. Understanding the impact of the heart on the brain in HF patients as well as the function of MRI in early diagnosis in the heart-brain area are the main objectives of this review. Two separate researchers examined the English literature in the PubMed EMBASE, Web of Science, PsycInfo, and Scopus databases after receiving systematic review training. The search terms included "high-frequency," "brain function," "brain injury," "cognition," "cognitive impairment," and "magnetic resonance imaging."

2. Pathogenesis of HF with CI

2.1. Cerebral perfusion pressure decreased

To keep the brain functioning normally, there must be enough oxygen and glucose in the blood—approximately 20 and 25%, respectively, of the body's energy (Sabayan et al., 2016). Endothelial dysfunction in HF patients may result in aberrant cerebrovascular reactivity (the brain's blood vessel response to high amounts of carbon dioxide), decreased automatic brain regulation, and other symptoms (Zuccalà et al., 1997). Cardiovascular illnesses are significantly influenced by hypoperfusion, which is caused by poor cardiac output and low blood pressure. Aging and vascular risk factors both enhance the likelihood of developing Alzheimer's disease and chronic cerebral hypoperfusion (Georgiadis et al., 2000). Patients with HF often have decreased myocardial contractility and cardiac output, which lead to decreased cerebral perfusion pressure. Compared with age-matched healthy controls, HF patients' resting cerebral blood flow (CBF) was 31% lower (Vogels et al., 2008). Patients with mild and moderate HF experienced lower middle cerebral artery blood flow (47.3 and 56.1 cm/s, respectively) (Scherbakov and Doehner, 2018). Other complications, such as sleep apnea, diabetes, hypertension, and depression, are exacerbated by a decrease in CBF (Lorenzi-Filho et al., 2002). There is evidence of reduced CBF in the bilateral hippocampus, parahippocampal gyrus, and right posterior cingulate gyrus cortex in people with HF (Gruhn et al., 2001; Sabayan et al., 2015), which is typically associated with AD. Reduced CBF makes HF patients more susceptible to brain parenchymal injury, particularly gray matter injury (Muller et al., 2011). Various cortical areas linked to executive cognitive performance are affected by reduced gray matter volume (Amanzio et al., 2021). In conclusion, brain tissue loss and dysfunction caused by brain hypoperfusion can speed up CI in people with HF. Further correlation studies are required since the impact of local CBF reduction on molecular cognitive performance has not yet been fully understood.

2.2. Inflammatory response and oxidative stress

Interdependence between the inflammatory response and oxidative stress is common and is linked to brain dysfunction following heart disease (Zhu et al., 2007). Myocardial damage in HF patients usually results in increased inflammation and the immune response (Gill et al., 2010), and low perfusion caused by decreased heart function also results in cerebral inflammation (Akiguchi et al., 1997). In the cortex and hippocampus of HF mouse models, the expression of inflammatory genes such as Toll-like receptor 4 (TLR4), tumor necrosis factor-α (TNF-α), and interleukin-6 (IL-6) increases dramatically (Hong et al., 2013). TNF-α is a key regulator of the brain's proinflammatory response, increasing neurotoxicity through glutamate secretion by neurons and leading to cell damage and death (Perry et al., 2001), affecting synaptic plasticity as well as brain learning and memory function. A brain with decreased cognitive function results from IL-6's increased expression of beta-secretase and aberrant increases in beta-amyloid formation and deposition. These inflammatory cytokines pass through the blood–brain barrier (BBB) and enter the brain, where they trigger an inflammatory reaction that impairs cognition.

2.3. Damage to the blood-brain barrier

The BBB is crucial in preventing metabolic waste and harmful substances from passing into the central nervous system through the blood circulation (Liori et al., 2022). The pathophysiology of CI linked to HF is greatly influenced by aberrant BBB function, which includes pericellular breakdown, endothelial cell activation, and an excessively tight linkage between endothelium and pericellular (Ritz et al., 2013). The primary cell type that make up the blood–brain barrier, endothelial cells, has been demonstrated to be vulnerable to harm from elevated intracellular calcium ion levels (Doyle et al., 2008). BBB dysfunction worsens microvascular damage worse, fosters secondary inflammation, damages vascular tone, leads to stenosis of the cavity, and causes tissue ischemia (Vancheri et al., 2020), which promotes contact between neurotoxic proteins and neurons.

2.4. The neurohumoral axis

The neurohumoral axis of patients with HF plays a role in cognitive and structural changes in the brain. The sympathetic nervous system and the renin-angiotensin-aldosterone system quickly come into action when the output decreases to restore perfusion pressure and stop dehydration and traumatic bleeding (Gruhn et al., 2001). The hormone cortisol, which is linked to stress, has an impact on cognitive function. Temporary high cortisol levels have been linked to impairments in cognitive function. Other studies have shown that persistently elevated cortisol levels may result in atrophy in specific brain areas because of reduced neurogenesis (Chetty et al., 2014). The brain's hypothalamus, hippocampus, and amygdala showed the highest levels of glucocorticoid receptor expression, whereas the hippocampus, amygdala, and prefrontal cortex margin showed the highest amounts of halocorticoid receptor expression (Gallina et al., 2014). Cortisol levels are much higher in HF patients with depression and CI than in HF patients without these symptoms (Huffman et al., 2013), which raises the possibility that cortisol levels in HF may impact how rapidly CI develops.

2.5. Alimentary deficiency

An increasing number of studies have found that there is a close relationship between nutritional deficiency and CI. Researchers have found that nutritional deficiencies can lead to decreased attention, memory, and cognitive function in humans with HF (Stewart et al., 2015). Patients are prone to nutritional deficiency due to increased body consumption and changes in systemic metabolism, and nutritional deficiency will also aggravate the degree of HF (Alosco et al., 2013).

2.6. Depressive disorder

According to research, depression is linked to greater levels of CI, structural alterations in the brain (Sheline et al., 1999), inflammation (Schiepers et al., 2005), and neurohormone biomarkers, which are also present in HF patients. CI performance also improved in patients with depression who received medication (Halvorsen et al., 2012). Further research is necessary to fully understand the function of depression in HF and CI.

3. Advances in brain imaging of HF and CI

3.1. Conventional magnetic resonance imaging

The approach to craniocerebral evaluation most frequently utilized currently for the clinical diagnosis and care of HF patients is conventional MRI scanning. MRI can detect whether there are ischemic lesions, infarction lesions, brain atrophy, and other structural changes in patients' brains. The two main contributing factors to HF are thought to be ischemic heart disease and hypertension (Vogels et al., 2007a). It is believed that overall brain shrinkage and aberrant cerebral vascularization are the root causes of cognitive decline in HF patients (Schmidt et al., 1991). White matter hyperintensity (WMH) was connected to sorrow and anxiety, and atrophy of the medial temporal lobe was connected to cognitive problems such as memory loss and executive dysfunction in HF patients (Vogels et al., 2007a). Reduced hippocampal volume is present in HF patients, which may contribute to depression and short-term memory loss (Woo et al., 2015). According to the studies above, patients with HF and CI will have brain structure changes. Conventional MRI is only applicable to lesions with significant brain structure and cannot fully identify the pathological mechanism. With this limitation, it should be combined with other more effective MRI-derived techniques for observing changes in brain microstructure and function.

3.2. Functional magenetic resonance imaging

Functional magnetic resonance imaging (fMRI) uses computer refinement of multiple images to measure changes in neural signals caused by changes in brain structure and neural activity. fMRI combines the advantages of the high-resolution anatomic imaging capability of conventional MRI with the specificity of blood flow dynamics to directly and accurately observe the large activity processes of the brain during the implementation of cognitive tasks. Lower cardiac function results in decreased task-related brain area efficiency and reduced verbal working memory task performance in older patients with cardiovascular illness (Irani et al., 2009). HF patients showed a reduced neural activation response to Valsalva in a number of autonomic and motor control regions, including the cerebellar cortex and vermis, amygdala, hypothalamus, ACC, left insula, left putamen, and bilateral posterior central gyrus (Ogren et al., 2012; Song et al., 2018). These regions may influence emotional transmission, attention, perception, and long-term memory through structural and functional connections in brain tissues such as the visual cortex. Brain MRI imaging analysis in HF patients has shown that brain dysfunction is connected to cardiac remodeling and results in less gray matter in the primary motor cortex and hippocampus. It might be affected by daily activities and lessen depression symptoms in HF patients (Suzuki et al., 2013). These results support the notion that HF patients experience CI and anatomical alterations to the brain. fMRI has a diverse set of applications in brain cognitive research and neural activities, but much in-depth research is still needed to elucidate the changes in higher brain functions.

3.3. Structural magnetic resonance imaging

In recent years, a variety of image analysis and detection techniques have been applied in structural magnetic resonance imaging (sMRI) research, reducing the influence of subjective manipulation on the experiment, including voxel-based morphometry (VBM) (Frey et al., 2021). VBM is a technique

that involves reflecting subtle changes in gray and white matter volume or density at the unit level to measure brain structure images accurately. Surface-based morphometry (SBM) can extract a variety of anatomical parameters, such as cortical surface area, cortical thickness, and the gyri index, which measures the morphological characteristics of the cerebral cortex more comprehensively (Naegel et al., 2022).

Structural magnetic resonance imaging showed brain atrophy and other static tissue abnormalities in patients with CI. Patients with HF had a greater frequency of medial temporal lobe atrophy than healthy controls (Frey et al., 2021). Many studies have used sMRI to explore the relationship between CI and brain structural changes. The entorhinal cortex and hippocampus of the medial temporal lobe were the first areas of the brain to exhibit cerebral atrophy (Du et al., 2004), and it progressed in line with the Braak stage. Gray matter loss affects the middle temporal gyrus, fusiform gyrus, parahippocampal gyrus, and temporal pole in people with chronic HF. Moderate medial temporal lobe atrophy is where the loss starts, and it progresses to the rest of the temporal lobe (Li et al., 2011). The degree of medial temporal lobe atrophy was assessed using the visual Scheltens score with great sensitivity and specificity (Kilimann et al., 2014). Selective attention impairment, verbal and visual memory deficits, and other cognitive skills are all tightly associated with medial temporal lobe atrophy in HF patients (Frey et al., 2018). CI in HF patients is associated with loss of gray matter density in the lateral, anterior cingulate, and medial frontal cortex. They have been discovered to be connected to psychological functions such as emotion, pain, and cognitive control (Merkler et al., 2019). In fact, both HF and coronary heart disease exhibit the same pattern of brain injury (Mueller et al., 2020). However, investigations have shown that there is gray matter loss in specific areas in patients with HF and that this loss is more widespread than that in patients with coronary heart disease and in unaffected controls. Reduced gray matter density in sizable brain regions such as the hippocampus, prefrontal cortex, and precuneus may enable CI (Vogels et al., 2007b). In addition, the decrease in GMD was correlated with the decrease in left ventricular ejection fraction and the increase in NT-proBNP.

When referring to T2-weighted images or T2 fluid decay inversion recovery sequences, the term "WHM" refers to high signal expression in deep cerebral or periventricular white matter. Small artery disease-induced coronary microvascular dysfunction is a common pathogenic mechanism of WMH and HF (Camici et al., 2020). As a specific variation in CI concomitant with HF, the speed of information processing and executive function have been linked to an increase in WMH (Tan et al., 2022). The severity and duration of HF are associated with decreased cardiac function, which can have a significant impact on the deep white matter of the brain (Vogels et al., 2007a). According to Vogels et al. (2007b) research, individuals with HF who did not also have stroke, dementia, or depression were more likely to have WMH on brain MRI. WMH refers to high signal expression in deep cerebral or periventricular white matter on T2-weighted images or T2 fluid decay inversion recovery sequences. WMH was still substantially more common in HF patients even if IHD, age, and other affecting factors were excluded (Vogels et al., 2007a). These results imply that individuals with HF display localized brain abnormalities on sMRI that are comparable to those in patients with CI, with cognitive function being impacted by gray matter density reduction and white matter microstructure loss. However, most of the studies on brain atrophy have focused on the medial temporal lobe, not other brain regions.

3.4. Cerebral perfusion imaging

Magnetic resonance perfusion imaging is an examination technique that detects microcirculation distribution and hemodynamic changes in brain tissue to assess local tissue and function. It can be used to assess CBF and metabolic status. HF can lead to cerebral hypoperfusion and decreased metabolic activity, resulting in decreased cognitive function. Arterial spin-label perfusion imaging and magnetic resonance perfusion imaging were the imaging methods employed to assess CBF (Chandra et al., 2019). Arterial spin-labeled perfusion imaging is a non-invasive method for measuring arterial blood flow based on nuclear magnetic flow markers. Changes in local cerebral perfusion can be assessed without the use of radiation or contrast agents. In patients with HF, reduced CBF and brain tissue injury were found in many areas, such as the frontal vascular bed, parietal lobe, occipital cortex, hippocampus, thalamus, and cerebellar region (Woo et al., 2003, 2009). In addition, the decrease in CBF was significantly lateralized, with the main decreased areas in the right cortex and diencephalon. According to studies, perfusion imaging can diagnose Alzheimer's disease and moderate CI with 87 and 67% accuracy, respectively (Lacalle-Aurioles et al., 2014). Cerebral perfusion imaging has strong repeatability and can effectively reflect changes in cerebral hemodynamics. However, there are few studies on the use of MRI perfusion imaging in people with HF and CI, and its clinical utility is not frequently used.

4. Conclusion and future directions

There is growing evidence that HF and CI are linked and brought on by HF-induced brain damage. Patients with HF will have apparent CI as well as changes in brain structure, function, and metabolic status due to decreased cerebral perfusion pressure, an inflammatory response, oxidative stress, and BBB breakdown. New MRI techniques such as sMRI, fMRI, and brain perfusion imaging are conducive to further research on the early pathophysiological changes of CI in HF patients. Brain sites with tissue damage in HF patients include the cingulate gyrus, hypothalamus, hippocampus, insula, brainstem, amygdala, and cerebellar regions. Attention deficit hyperactivity disorder, learning disabilities, memory loss, language impairments, and decreased visuospatial performance are all closely associated with HF. It is important to note that neuroimaging studies on HF with CI are still in the beginning stages. Most studies are retrospective, and the application of new techniques needs to be expanded. To better understand the connection between HF and CI, extensive cohort studies on HF, cognitive function, and MRI will be required in the future. Additionally, early magnetic resonance diagnostics play an important role in achieving early detection, diagnosis, and treatment.

Author contributions

TL: writing—original draft. XB: writing—review and editing. LL: conceptualization. RQ: data curation. CL and XW: supervision and writing—review and editing. All authors contributed to the article and approved the submitted version.

Funding

This work was financially supported by the National Natural Science Foundation of China (Grant Nos. 81871354, 81571672, and 81901740), the Taishan Scholars Project of Shandong Province, and the Academic Promotion Program of Shandong First Medical University.

Conflict of interest

The authors declare that the research was conducted in the absence of any commercial or financial relationships that could be construed as a potential conflict of interest.

Publisher's note

References

Akiguchi, I., Tomimoto, H., Suenaga, T., Wakita, H., and Budka, H. (1997). Alterations in glia and axons in the brains of Binswanger's disease patients. *Stroke* 28, 1423–1429. doi: 10.1161/01.str.28.7.1423

Almeida, O., Garrido, G., Beer, C., Lautenschlager, N., Arnolda, L., and Flicker, L. (2012). Cognitive and brain changes associated with ischaemic heart disease and heart failure. *Eur. Heart J.* 33, 1769–1776. doi: 10.1093/eurheartj/ehr467

Alosco, M., Spitznagel, M., Raz, N., Cohen, R., Sweet, L., Colbert, L., et al. (2013). Dietary habits moderate the association between heart failure and cognitive impairment. *J. Nutr. Gerontol. Geriatr.* 32, 106–121. doi: 10.1080/21551197.2013.781408

Amanzio, M., Palermo, S., Stanziano, M., D'Agata, F., Galati, A., Gentile, S., et al. (2021). Investigating neuroimaging correlates of early frailty in patients with behavioral variant frontotemporal dementia: A MRI and FDG-PET Study. *Front. Aging Neurosci.* 13:637796. doi: 10.3389/fnagi.2021.637796

Camici, P., Tschöpe, C., Di Carli, M., Rimoldi, O., and Van Linthout, S. (2020). Coronary microvascular dysfunction in hypertrophy and heart failure. *Cardiovasc. Res.* 116, 806–816. doi: 10.1093/cvr/cvaa023

Cannon, J., Moffitt, P., Perez-Moreno, A., Walters, M., Broomfield, N., McMurray, J., et al. (2017). Cognitive impairment and heart failure: systematic review and meta-analysis. *J. Card Fail* 23, 464–475. doi: 10.1016/j.cardfail.2017.04.007

Chandra, A., Dervenoulas, G., Politis, M., and Alzheimer's Disease Neuroimaging Initiative (2019). Magnetic resonance imaging in Alzheimer's disease and mild cognitive impairment. *J. Neurol.* 266, 1293–1302. doi: 10.1007/s00415-018-9016-3

Chetty, S., Friedman, A., Taravosh-Lahn, K., Kirby, E., Mirescu, C., Guo, F., et al. (2014). Stress and glucocorticoids promote oligodendrogenesis in the adult hippocampus. *Mol. Psychiatry* 19, 1275–1283. doi: 10.1038/mp.2013.190

Doyle, K., Simon, R., and Stenzel-Poore, M. (2008). Mechanisms of ischemic brain damage. *Neuropharmacology* 55, 310–318. doi: 10.1016/j.neuropharm.2008.01.005

Du, A., Schuff, N., Kramer, J., Ganzer, S., Zhu, X., Jagust, W., et al. (2004). Higher atrophy rate of entorhinal cortex than hippocampus in AD. *Neurology* 62, 422–427. doi: 10.1212/01.wnl.0000106462.72282.90

Feola, M., Garnero, S., Vallauri, P., Salvatico, L., Vado, A., Leto, L., et al. (2013). Relationship between cognitive function, depression/anxiety and functional parameters in patients admitted for congestive heart failure. *Open Cardiovasc. Med. J.* 7, 54–60. doi: 10.2174/1874192401307010054

Frey, A., Homola, G., Henneges, C., Mühlbauer, L., Sell, R., Kraft, P., et al. (2021). Temporal changes in total and hippocampal brain volume and cognitive function in patients with chronic heart failure-the COGNITION.MATTERS-HF cohort study. *Eur. Heart J.* 42, 1569–1578. doi: 10.1093/eurheartj/ehab003

Frey, A., Sell, R., Homola, G., Malsch, C., Kraft, P., Gunreben, I., et al. (2018). Cognitive deficits and related brain lesions in patients with chronic heart failure. *JACC Heart Fail* 6, 583–592. doi: 10.1016/j.jchf.2018.03.010

Gallina, D., Zelinka, C., and Fischer, A. (2014). Glucocorticoid receptors in the retina, Müller glia and the formation of Müller glia-derived progenitors. *Development* 141, 3340–3351. doi: 10.1242/dev.109835

Georgiadis, D., Sievert, M., Cencetti, S., Uhlmann, F., Krivokuca, M., Zierz, S., et al. (2000). Cerebrovascular reactivity is impaired in patients with cardiac failure. *Eur. Heart J.* 21, 407–413. doi: 10.1053/euhj.1999.1742

Gill, R., Tsung, A., and Billiar, T. (2010). Linking oxidative stress to inflammation: Toll-like receptors. *Free Radic. Biol. Med.* 48, 1121–1132. doi: 10.1016/j.freeradbiomed.2010.01.006

Gruhn, N., Larsen, F., Boesgaard, S., Knudsen, G., Mortensen, S., Thomsen, G., et al. (2001). Cerebral blood flow in patients with chronic heart failure before and after heart transplantation. *Stroke* 32, 2530–2533. doi: 10.1161/hs1101.098360

Halvorsen, M., Høifødt, R., Myrbakk, I., Wang, C., Sundet, K., Eisemann, M., et al. (2012). Cognitive function in unipolar major depression: a comparison of currently depressed, previously depressed, and never depressed individuals. *J. Clin. Exp. Neuropsychol.* 34, 782–790. doi: 10.1080/13803395.2012.683853

Hao, G., Wang, X., Chen, Z., Zhang, L., Zhang, Y., Wei, B., et al. (2019). Prevalence of heart failure and left ventricular dysfunction in China: The China Hypertension Survey, 2012-2015. *Eur. J. Heart Fail* 21, 1329–1337. doi: 10.1002/ejhf.1629

Harkness, K., Heckman, G., Akhtar-Danesh, N., Demers, C., Gunn, E., and McKelvie, R. (2014). Cognitive function and self-care management in older patients with heart failure. *Eur. J. Cardiovasc. Nurs.* 13, 277–284. doi: 10.1177/1474515113492603

Hjelm, C., Broström, A., Dahl, A., Johansson, B., Fredrikson, M., and Strömberg, A. (2014). Factors associated with increased risk for dementia in individuals age 80 years or older with congestive heart failure. *J. Cardiovasc. Nurs.* 29, 82–90. doi: 10.1097/JCN.0b013e318275543d

Hong, X., Bu, L., Wang, Y., Xu, J., Wu, J., Huang, Y., et al. (2013). Increases in the risk of cognitive impairment and alterations of cerebral β-amyloid metabolism in mouse model of heart failure. *PLoS One* 8:e63829. doi: 10.1371/journal.pone.0063829

Huffman, J., Celano, C., Beach, S., Motiwala, S., and Januzzi, J. (2013). Depression and cardiac disease: Epidemiology, mechanisms, and diagnosis. *Cardiovasc. Psychiatry Neurol.* 2013, 695925. doi: 10.1155/2013/695925

Irani, F., Sweet, L., Haley, A., Gunstad, J., Jerskey, B., Mulligan, R., et al. (2009). A fMRI Study of verbal working memory, cardiac output, and ejection fraction in elderly patients with cardiovascular disease. *Brain Imaging Behav.* 3, 350–357. doi: 10.1007/s11682-009-9077-0

Jinawong, K., Apaijai, N., Chattipakorn, N., and Chattipakorn, S. (2021). Cognitive impairment in myocardial infarction and heart failure. *Acta Physiol.* 232, e13642. doi: 10.1111/apha.13642

Kilimann, I., Grothe, M., Heinsen, H., Alho, E., Grinberg, L., Amaro, E. Jr., et al. (2014). Subregional basal forebrain atrophy in Alzheimer's disease: A multicenter study. *J. Alzheimers Dis.* 40, 687–700. doi: 10.3233/JAD-132345

Lacalle-Aurioles, M., Mateos-Pérez, J., Guzmán-De-Villoria, J., Olazarán, J., Cruz-Orduña, I., Alemán-Gómez, Y., et al. (2014). Cerebral blood flow is an earlier indicator of perfusion abnormalities than cerebral blood volume in Alzheimer's disease. *J. Cereb. Blood Flow Metab.* 34, 654–659. doi: 10.1038/jcbfm.2013.241

Li, X., Coyle, D., Maguire, L., Watson, D., and McGinnity, T. (2011). Gray matter concentration and effective connectivity changes in Alzheimer's disease: A longitudinal structural MRI study. *Neuroradiology* 53, 733–748. doi: 10.1007/s00234-010-0795-1

Liori, S., Arfaras-Melainis, A., Bistola, V., Polyzogopoulou, E., and Parissis, J. (2022). Cognitive impairment in heart failure: Clinical implications, tools of assessment, and therapeutic considerations. *Heart Fail Rev.* 27, 993–999. doi: 10.1007/s10741-021-10118-5

Lorenzi-Filho, G., Azevedo, E., Parker, J., and Bradley, T. (2002). Relationship of carbon dioxide tension in arterial blood to pulmonary wedge pressure in heart failure. *Eur. Respir. J.* 19, 37–40. doi: 10.1183/09031936.02.00214502

Merkler, A., Sigurdsson, S., Eiriksdottir, G., Safford, M., Phillips, C., Iadecola, C., et al. (2019). Association Between Unrecognized Myocardial Infarction and Cerebral Infarction on Magnetic Resonance Imaging. *JAMA Neurol.* 76, 956–961. doi: 10.1001/jamaneurol.2019.1226

Mueller, K., Thiel, F., Beutner, F., Teren, A., Frisch, S., Ballarini, T., et al. (2020). Brain Damage With Heart Failure: Cardiac Biomarker Alterations and Gray Matter Decline. *Circ. Res.* 126, 750–764. doi: 10.1161/CIRCRESAHA.119.315813

Muller, M., van der Graaf, Y., Algra, A., Hendrikse, J., Mali, W., Geerlings, M., et al. (2011). Carotid atherosclerosis and progression of brain atrophy: The SMART-MR study. *Ann. Neurol.* 70, 237–244. doi: 10.1002/ana.22392

Naegel, S., Zeller, J., Hougard, A., Weise, C., Hans-Christoph-Diener, Zuelow, S., et al. (2022). No structural brain alterations in new daily persistent headache - a cross sectional VBM/SBM study. *Cephalalgia* 42, 335–344. doi: 10.1177/03331024211045653

Ogren, J., Macey, P., Kumar, R., Fonarow, G., Hamilton, M., Harper, R., et al. (2012). Impaired cerebellar and limbic responses to the valsalva maneuver in heart failure. *Cerebellum* 11, 931–938. doi: 10.1007/s12311-012-0361-y

Perry, R., Collins, J., Wiener, H., Acton, R., and Go, R. (2001). The role of TNF and its receptors in Alzheimer's disease. *Neurobiol. Aging* 22, 873–883. doi: 10.1016/s0197-4580(01)00291-3

Ritz, K., van Buchem, M., and Daemen, M. (2013). The heart-brain connection: Mechanistic insights and models. *Neth. Heart J.* 21, 55–57. doi: 10.1007/s12471-012-0348-9

Roy, B., Woo, M., Wang, D., Fonarow, G., Harper, R., and Kumar, R. (2017). Reduced regional cerebral blood flow in patients with heart failure. *Eur. J. Heart Fail* 19, 1294–1302. doi: 10.1002/ejhf.874

Sabayan, B., van Buchem, M., Sigurdsson, S., Zhang, Q., Harris, T., Gudnason, V., et al. (2015). Cardiac hemodynamics are linked with structural and functional features of brain aging: The age, gene/environment susceptibility (AGES)-Reykjavik Study. *J. Am. Heart Assoc.* 4, e001294. doi: 10.1161/JAHA.114.001294

Sabayan, B., van Buchem, M., Sigurdsson, S., Zhang, Q., Meirelles, O., Harris, T., et al. (2016). Cardiac and carotid markers link with accelerated brain atrophy: The AGES-Reykjavik Study (Age, Gene/Environment Susceptibility-Reykjavik). *Arterioscler. Thromb. Vasc. Biol.* 36, 2246–2251. doi: 10.1161/ATVBAHA.116.308018

Scherbakov, N., and Doehner, W. (2018). Heart-brain interactions in heart failure. *Card Fail Rev.* 4, 87–91. doi: 10.15420/cfr.2018.14.2

Schiepers, O., Wichers, M., and Maes, M. (2005). Cytokines and major depression. *Prog. Neuropsychopharmacol. Biol. Psychiatry* 29, 201–217. doi: 10.1016/j.pnpbp.2004.11.003

Schmidt, R., Fazekas, F., Offenbacher, H., Dusleag, J., and Lechner, H. (1991). Brain magnetic resonance imaging and neuropsychologic evaluation of patients with idiopathic dilated cardiomyopathy. *Stroke* 22, 195–199. doi: 10.1161/01.str.22.2.195

Sheline, Y., Sanghavi, M., Mintun, M., and Gado, M. (1999). Depression duration but not age predicts hippocampal volume loss in medically healthy women with recurrent major depression. *J. Neurosci.* 19, 5034–5043. doi: 10.1523/JNEUROSCI.19-12-05034.1999

Song, X., Roy, B., Fonarow, G., Woo, M., and Kumar, R. (2018). Brain structural changes associated with aberrant functional responses to the Valsalva maneuver in heart failure. *J. Neurosci. Res.* 96, 1610–1622. doi: 10.1002/jnr.24264

Stewart, M., Traylor, A., and Bratzke, L. (2015). Nutrition and cognition in older adults with heart failure: A systematic review. *J. Gerontol. Nurs.* 41, 50–59. doi: 10.3928/00989134-20151015-06

Suzuki, Y., Matsumoto, H., Ota, Y., Kotozaki, J., Takahashi, K., Ito, Y., et al. (2013). Shimokawa, Interactions between the heart and the brain in heart failure patients assessed by magnetic resonance imaging–interim results from Brain assessment and investigation in Heart Failure Trial (B-HeFT). *Eur. Heart J.* 34:2732. doi: 10.1093/eurheartj/eht309.P2732

Tan, S., Ho, C., Teo, Y., Teo, Y., Chan, M., Lee, C., et al. (2022). Prevalence and incidence of stroke, white matter hyperintensities, and silent brain infarcts in patients with chronic heart failure: A systematic review, meta-analysis, and meta-regression. *Front. Cardiovasc Med.* 9:967197. doi: 10.3389/fcvm.2022.967197

Vancheri, F., Longo, G., Vancheri, S., and Henein, M. (2020). Coronary Microvascular Dysfunction. *J. Clin. Med.* 9, 2880. doi: 10.3390/jcm9092880

Vogels, R., Oosterman, J., Laman, D., Gouw, A., Schroeder-Tanka, J., Scheltens, P., et al. (2008). Transcranial Doppler blood flow assessment in patients with mild heart failure: Correlates with neuroimaging and cognitive performance. *Congest. Heart Fail* 14, 61–65. doi: 10.1111/j.1751-7133.2008.07365.x

Vogels, R., Oosterman, J., van Harten, B., Gouw, A., Schroeder-Tanka, J., Scheltens, P., et al. (2007a). Neuroimaging and correlates of cognitive function among patients with heart failure. *Dement. Geriatr. Cogn. Disord.* 24, 418–423. doi: 10.1159/000109811

Vogels, R., van der Flier, W., van Harten, B., Gouw, A., Scheltens, P., Schroeder-Tanka, J., et al. (2007b). Brain magnetic resonance imaging abnormalities in patients with heart failure. *Eur. J. Heart Fail* 9, 1003–1009. doi: 10.1016/j.ejheart.2007.07.006

Woo, M., Kumar, R., Macey, P., Fonarow, G., and Harper, R. (2009). Brain injury in autonomic, emotional, and cognitive regulatory areas in patients with heart failure. *J. Card Fail* 15, 214–223. doi: 10.1016/j.cardfail.2008.10.020

Woo, M., Macey, P., Fonarow, G., Hamilton, M., and Harper, R. (2003). Regional brain gray matter loss in heart failure. *J. Appl. Physiol.* 95, 677–684. doi: 10.1152/japplphysiol.00101.2003

Woo, M., Ogren, J., Abouzeid, C., Macey, P., Sairafian, K., Saharan, P., et al. (2015). Regional hippocampal damage in heart failure. *Eur. J. Heart Fail* 17, 494–500. doi: 10.1002/ejhf.241

Yang, M., Sun, D., Wang, Y., Yan, M., Zheng, J., and Ren, J. (2022). Cognitive impairment in heart failure: Landscape, challenges, and future directions. *Front. Cardiovasc. Med.* 8:831734. doi: 10.3389/fcvm.2021.831734

Zhu, X., Smith, M., Honda, K., Aliev, G., Moreira, P., Nunomura, A., et al. (2007). Vascular oxidative stress in Alzheimer disease. *J. Neurol. Sci.* 257, 240–246. doi: 10.1016/j.jns.2007.01.039

Zuccalà, G., Cattel, C., Manes-Gravina, E., Di Niro, M., Cocchi, A., and Bernabei, R. (1997). Left ventricular dysfunction: A clue to cognitive impairment in older patients with heart failure. *J. Neurol. Neurosurg. Psychiatry* 63, 509–512. doi: 10.1136/jnnp.63.4.509

frontiers | Frontiers in Aging Neuroscience

TYPE Original Research
PUBLISHED 28 March 2023
DOI 10.3389/fnagi.2023.1148518

OPEN ACCESS

EDITED BY
Jing Li,
Capital Medical University, China

REVIEWED BY
Lv Yasu,
Aerospace Clinical Medical College of Peking University, China
Siqiang Niu,
The First Affiliated Hospital of Chongqing Medical University, China

*CORRESPONDENCE
Tao Chen
✉ ctsci2020@163.com

†These authors have contributed equally to this work and share first authorship

SPECIALTY SECTION
This article was submitted to Neurocognitive Aging and Behavior, a section of the journal Frontiers in Aging Neuroscience

RECEIVED 20 January 2023
ACCEPTED 06 March 2023
PUBLISHED 28 March 2023

CITATION
Wang Y, Guo B, Zhao K, Yang L and Chen T (2023) Correlation between cognitive impairment and serum phosphorylated tau181 protein in patients with preeclampsia. *Front. Aging Neurosci.* 15:1148518. doi: 10.3389/fnagi.2023.1148518

Correlation between cognitive impairment and serum phosphorylated tau181 protein in patients with preeclampsia

Yuanyuan Wang [1†], Bin Guo [2†], Ke Zhao [3], Linfeng Yang [2] and Tao Chen [3*]

[1]Department of Radiology, Binzhou Medical University, Yantai, Shandong, China, [2]Department of Radiology, Jinan Maternity and Child Care Hospital Affiliated to Shandong First Medical University, Jinan, Shandong, China, [3]Department of Clinical Laboratory, Jinan Maternity and Child Care Hospital Affiliated to Shandong First Medical University, Jinan, Shandong, China

Objective: To study the cognitive function status, serum phosphorylated tau181 (P-tau181) protein level, and total tau (T-tau) protein level in patients with preeclampsia (PE), pregnant healthy controls (PHCs), and non-pregnant healthy controls (NPHCs), and to research their feasibility as serum biomarkers for evaluating cognitive functional impairment in PE patients.

Methods: Sixty-eight patients with PE, 48 NPHCs, and 30 PHCs were included. Cognitive functional status was assessed using standardized Symbol Digit Modalities Test (SDMT) and Montreal Cognitive Assessment (MoCA) scales. Enzyme-linked immunosorbent assay (ELISA) was used to detect the level of serum P-tau181 and T-tau protein. The concentration of serum P-tau181 and T-tau protein were compared by one-way analysis of variance in the three groups of subjects. The correlation between P-tau181, T-tau, and SDMT was explore by multiple linear regression analysis. The areas under the receiver operating characteristic (ROC) curves of serum P-tau181 and SDMT were calculated to predict the cognitive level of subjects.

Results: PE patients significantly had lower scores on SDMT (47.97 ± 7.54) and MoCA (28.00 ± 2.00) than normotensive PHCs (30.00 ± 1.25, 54.73 ± 8.55, respectively). The significant difference was found in serum P-tau181 protein levels among the three groups [$H(K)$ = 19.101, $P < 0.001$]. Serum P-tau181 was thicker in PE patients than PHCs or NPHCs (both $P < 0.05$). According to the ROC curve, T-tau had no statistical significance in predicting the ability of cognizance, while P-tau181 and SDMT had. The DeLong test showed that P-tau181 was better than T-tau in predicting the ability of cognizance ($P < 0.05$).

Conclusion: The patients with PE have occurred the decline of cognitive function during pregnancy. The high level of serum P-tau181 can be used as a clinical laboratory indication for non-invasive assessment of cognitive functional impairment in PE patients.

KEYWORDS

preeclampsia, cognitive function, tau protein, serum phosphorylated tau181 protein (P-tau181), Symbol Digit Modalities Test (SDMT)

Introduction

Preeclampsia (PE) is a cumulative multisystem disease, especially of the central nervous system, and defined as hypertension with end-organ dysfunction after 20 weeks of gestation which complicates approximately 4–6% of all pregnancies (Abalos et al., 2013; Chappell et al., 2021). The major causes of severe maternal morbidity and mortality were due to the complications of PE in the brain, including eclampsia, cerebral edema, and stroke (Fishel Bartal and Sibai, 2022). The central nervous system involvement and complications of PE have been recognized for many years, but a good understanding of the long-term consequences of PE, such as cardiovascular and cerebrovascular disease and cognitive impairment, can only be traced back nearly a decade ago (Shawwa et al., 2018).

Brain damage from severe PE is not fully reversible, and PE patients have a higher risk of cognitive impairment, vascular dementia, epilepsy, and stroke than healthy women in the months to years after pregnancy (Nerenberg et al., 2017; Basit et al., 2018). Women with a history of severe PE have poorer learning abilities, more memory problems 3–8 months postpartum, and more working memory problems 6–18 months postpartum (Brussé et al., 2008; Baecke et al., 2009). A recent long-term follow-up study found that women with a history of PE occurred objective cognitive decline after 15 years, more problems with working memory and language learning than previously normotensive women, even clinical depressive symptoms (Adank et al., 2021). In addition, PE can significantly impair the working memory of the patient's offspring (Rätsep et al., 2016). However, there are few studies on cognitive function changes in PE patients.

Serum phosphorylated tau (P-tau) protein and total tau (T-tau) protein are markers of cognitive impairment and are closely related to the cognitive function of individuals. Tau protein is the most abundant neuron microtubule-associated protein, mainly distributed in neuron axons, and its function is to promote the formation of microtubules and maintain the stability of microtubules (Iqbal et al., 2010). The balance between phosphorylation and dephosphorylation of tau protein is a key regulatory process for maintaining microtubule stability. In pathological conditions, hyperphosphorylation of tau protein can reduce the transport efficiency of nerve cell axons, leading to synaptic degeneration of nerve cells and apoptosis or death of nerve cells, eventually leading to cognitive impairment, which is called tauopathy (Guo et al., 2017). Neuronal excitotoxicity induces tau misfolding, leading to altered tau structure and function, and this structural shift leads to more organized aggregation and neurofibrillary tangles, resulting in the degeneration and loss of neurons (Ballatore et al., 2007; Lebouvier et al., 2009). Therefore, there is important clinical significance to explore the changes of concentration of serum phosphorylated tau181 (P-tau181) and T-tau in PE patients, pregnant healthy controls (PHCs), and non-pregnant healthy controls (NPHCs), and their correlation with cognitive impairment.

In this prospective study, the purpose is to assess whether PE patients experience changes in cognitive function during pregnancy, as well as the changes of serum P-tau181 protein and T-tau protein in PE patients, and to determine whether these two proteins can serve as serum biomarkers for estimating altered cognitive function in PE patients.

Materials and methods

Subjects and PE patient assessment

From July 2019 to April 2020, 68 PE patients, 48 NPHCs, and 30 PHCs were included in this study. This study was carried out after the approved by the Ethics Review Committee of Jinan Maternity and Child Care Hospital Affiliated to Shandong First Medical University. All subjects signed written informed consents and clearly understood the experimental procedures. The patients with PE were voluntarily recruited from the inpatients and outpatients in the hospital obstetric department, and none of them had been diagnosed with eclampsia throughout the pregnancy. PHCs were recruited mainly by brochures, online publicity, and placard in the obstetrics and gynecology clinic, and the demographic information of PHCs was matched to the PE patients, such as age, gestational age, etc. PHCs did not include premature infants (<37 weeks) and abnormal weight neonates (reference birth weight ±2 SD for sex and gestational age). The recruitments of the age-appropriate NPHCs was mainly through local community networks. The baseline data of PHCs and NPHCs was collected within 12 h after study enrollment, including underwent blood pressure (BP) measurements, collection of blood and urine sample, neurological examinations, and cognitive function tests within 12 h of study enrollment. Blood pressure values of the right arm were measured after the subjects were placed in a quiet supine position for 15 min. All subjects were right-handed in this experiment and underwent routine blood and urine tests. All NPHC participants had laboratory test results within 7 days.

Preeclampsia patients all meet the diagnostic criteria for PE (American College of Obstetricians and Gynecologists [ACOG], 2019). Diagnostic criteria: when gestational age exceeds 20 weeks, subjects were diagnosed with hypertension [means systolic blood pressure (SBP) >140 mmHg and/or diastolic blood pressure (DBP) >90 mmHg] for the first time and found the evidence of organ damage and/or proteinuria, such as hepatic dysfunction, renal insufficiency, thrombocytopenia, pulmonary edema, or central nervous system symptoms. Singleton pregnancies and the gestational age of NPHCs and PHCs were strictly controlled, ranging from 20 to 41 + 6 weeks. Exclusion criteria: diabetes mellitus (either before or during pregnancy), chronic hypertension, and pre-existing renal disease before pregnancy. Subjects with previous diagnoses of PE and pregnancy-induced hypertension were also ineligible for inclusion criteria in PHCs and NPHCs.

Laboratory test indicators

All subjects received necessary laboratory tests to assist in the diagnosis of PE and to exclude other diseases. All specimens were collected by professional medical technicians, and not receiving the treatment of magnesium sulfate before collection. Five milliliters of fasting venous blood was drawn, and EDTA-K2 anticoagulation and centrifugation were used to

TABLE 1 Clinical characteristics of the pairwise comparison among the three groups.

Features	NPHC (n = 48)	PHC (n = 30)	PE (n = 68)	Statistical value				
				H(K)/F	*P*	*Post-hoc* test		
						a	b	c
Female (n)	48	30	68	NA	NA	NA	NA	NA
Age (years)	33.10 ± 4.78	30.90 ± 6.08	31.00 ± 6.75	4.282[a]	0.118	NA	NA	NA
Gestational age (weeks)	NA	31.31 ± 7.10	33.86 ± 6.36	NA	NA	NA	NA	0.833
Reproductive history (GPL)	NA	G2.00 ± 2.00 P0.00 ± 1.00 L0.00 ± 1.00	G2.00 ± 2.00 P0.00 ± 1.00 L0.00 ± 1.00	NA	NA	NA	NA	NA
Height (cm)	162.50 ± 3.89	161.97 ± 5.24	161.24 ± 5.26	0.977[b]	0.379	NA	NA	NA
Pregnancy weigh (Kg)	NA	63.08 ± 9.11	65.80 ± 15.38	NA	NA	NA	NA	0.132
Weight gain during pregnancy (Kg)	NA	11.38 ± 5.87	13.16 ± 6.21	NA	NA	NA	NA	0.188
Pre-pregnancy BMI (Kg/m^2)	22.09 ± 2.73	24.06 ± 3.36	26.04 ± 4.87	13.898[b]	<0.001	0.036	<0.001	0.025
Systolic pressure (mmHg)	111.35 ± 9.50	118.63 ± 12.49	156.00 ± 19.50	108.932[a]	<0.001	0.005	<0.001	<0.001
Diastolic pressure (mmHg)	70.00 ± 14.00	75.17 ± 9.53	99.69 ± 10.90	100.438[a]	<0.001	0.003	<0.001	<0.001
Mean atrial pressure (mmHg)	82.44 ± 8.65	89.66 ± 9.80	116.84 ± 15.76	108.338 [a]	<0.001	0.001	<0.001	<0.001
Education years	16.00 ± 3.00	15.00 ± 4.00	15.00 ± 3.00	75.519[a]	<0.001	<0.001	<0.001	0.008
Symbol Digit Modalities Test (SDMT)	61.00 ± 7.00	54.73 ± 8.55	47.97 ± 7.54	56.293[a]	<0.001	<0.001	<0.001	<0.001
Montreal Cognitive Assessment (MoCA)	30.00 ± 0.00	30.00 ± 1.25	28.00 ± 2.00	77.019[a]	<0.001	<0.001	<0.001	<0.001
Clinical symptoms								
Headache	NA	1 (3.33%)	9 (13.24%)	NA	NA	NA	NA	NA
Dizziness	NA	2 (6.67%)	5 (7.35%)	NA	NA	NA	NA	NA
Hypogastralgia	NA	7 (23.33%)	NA	NA	NA	NA	NA	NA
Diminution of vision	NA	NA	4 (5.88%)	NA	NA	NA	NA	NA
Pregnancy complicating primary hypertension	NA	2 (6.67%)	25 (36.76%)	NA	NA	NA	NA	NA
Gestational diabetes mellitus	NA	12 (40.00%)	13 (19.12%)	NA	NA	NA	NA	NA
The thyroid disease	NA	8 (26.67%)	4 (5.88%)	NA	NA	NA	NA	NA
Cardiopathy	NA	2 (6.67%)	4 (5.88%)	NA	NA	NA	NA	NA
Fetal distress in uterus	NA	3 (10.00%)	3 (4.41%)	NA	NA	NA	NA	NA
Fetal growth restriction	NA	1 (3.33%)	12 (2.94%)	NA	NA	NA	NA	NA

Data are mean ± SD or median ± inter-quartile range.
Post-hoc test: a, NPHC vs. PHC; b, NPHC vs. PE; c, PHC vs. PE. NPHC, non-pregnant healthy control; PHC, pregnant healthy control; PE, pre-eclampsia.
[a]Kruskal–Wallis test, *H(K)*.
[b]One-way ANOVA, *F*.

separate serum for the detection of relevant laboratory indicators. The measured indicators included, glycosylated hemoglobin, fasting blood glucose, blood lipids, hepatic function, routine blood, and kidney function. Random urine samples (10 ml) were collected from subjects for qualitative detection of urine protein and urinary microalbumin/creatinine ratio. Urinary protein was qualitatively detected by test-paper colorimetry, and the urinary microalbumin/creatinine ratio was detected by immunoscattering turbidimetry. The 24-h urine protein test requires collecting all the urine of the subjects within 24 h and detecting and calculating the total protein in the 24-h urine.

Neurological exams and cognitive tests

The detailed neurological examination was performed on all participants. All subjects underwent the Symbol Digit Modalities Test (SDMT) and Montreal Cognitive Assessment (MoCA) to evaluate the cognitive function status. ① SDMT was used to evaluate attention. The subjects were required to fill in the symbols corresponding to the numbers in sequence as fast as they could within 90 s, and 1 point was awarded for each correctly filled symbol. ② MoCA includes visuospatial structure, executive function, attention, language, memory, calculation, orientation, abstract thinking, and other, multidomain assessments. The total

score is 30 points, and scores <26 points are abnormal. It has higher sensitivity for screening patients with light cognitive function impairment.

Detection of serum P-tau181 and T-tau protein concentrations

In this study, enzyme-linked immunosorbent assay (ELISA) was mainly used to obtain the concentration of serum P-tau181 and T-tau. All specimens were collected and tested by professional medical technicians, and not receiving the treatment of magnesium sulfate before collection. Two milliliters of venous blood was drawn rapidly from each subject, and its serum was separated within 1 h. P-tau181 and T-tau reagents were purchased from Wuhan Saipei Biotechnology Co., Ltd. According to the kit instructions, all procedures of the experiment were carried out seriously. The protein concentration of the experimental samples was the average of three repeated measurements.

Statistical methods

The software we need for statistical analysis in this study included SPSS 26.0, Windows (version 21.0), MedCalc software, and GraphPad Prism 8. First, the basic descriptive analyses was used to perform the variables of the subjects for PE patients, NPHCs, and PHCs. The continuous numerical data was described as the median ± interquartile range or mean ± standard deviation (SD), and the discrete numerical data was expressed as n (%). One-way ANOVA and the two-independent-samples rank sum test were used to compare laboratory test indicators and quantitative clinical data. The ability of P-tau181, T-tau, and SDMT to predict cognitive function was evaluated mainly by the area under the curve (AUC) from the receiver operating characteristic (ROC) curve. The correlation between SDMT and clinical data and laboratory tests indicators was explored by Spearman bivariate correlation analysis. The correlation between P-tau181, T-tau, and SDMT was explored by multiple linear regression analysis.

Results

Clinical data and cognitive test results of each group

This study included 68 patients in the PE group (average age 31.00 ± 6.75), 30 patients in the PHCs group (average age 30.90 ± 6.08), and 48 patients in the NPHCs group (average age 33.10 ± 4.78). The clinical data and its characteristics of the experimental subjects are shown in Table 1. No significant differences were found in age [$H(k)$ = 4.282, P = 0.118] or height (F = 0.977, P = 0.379) among the three groups. No significant differences were found in gestational age (Z = −0.154, P = 0.877) or pre-pregnancy weight (Z = −1.508, P = 0.132) between the PE patients and PHCs. Significant differences were found in SBP/DBP, mean atrial pressure, education years, pre-pregnancy BMI, SDMT, and MoCA among the three groups [$H(k)$ = 108.932, P < 0.001; $H(k)$ = 100.438, P < 0.001; $H(k)$ = 108.338, P < 0.001; $H(k)$ = 75.519, P < 0.001; F = 13.898, P < 0.001; $H(k)$ = 56.293, P < 0.001; $H(k)$ = 77.019, P < 0.001]. The highest values of SBP/DBP, mean atrial pressure, and pre-pregnancy BMI (all P < 0.001) were found in the PE group (Table 1). The SDMT and MoCA results are shown in Figure 1.

Laboratory examinations and P-tau181 and T-tau protein concentrations in each groups

There were significant differences in P-tau181, hemoglobin (Hb), aspartate aminotransferase (AST), and creatinine (Cr) among PE patients, NPHCs, and PHCs groups [$H(K)$ = 19.101, P < 0.001; $H(K)$ = 14.921, P = 0.001; F = 15.118, P = 0.001; F = 17.746, P < 0.001]. No significant differences was found in T-tau, platelets (Plt), blood glucose (Glu), glycosylated hemoglobin (HbA1c), or alanine aminotransferase (ALT) between the three groups [$H(K)$ = 5.937, P = 0.051; F = 1.324, P = 0.269; F = 0.275, P = 0.871; F = 1.649, P = 0.438; F = 3.273, P = 0.195], but a significant difference was found in T-tau between the PHCs and PE groups [$H(K)$ = −2.397, P = 0.017] (Table 2 and Figure 2).

ROC curves to evaluate the ability of cognition-predictive in t-tau, P-tau181, and SDMT

According to the ROC curve, P-tau181 and SDMT can commendably predict the cognitive level of the subjects. The PE group was set as the experimental group, and the NPHC and PHC groups were the control groups. The ROC curves of P-tau181, T-tau, and SDMT are shown in Figure 3. According to the ROC curve, T-tau had no significant ability to predict cognitive ability, while P-tau181 and SDMT had. The DeLong test showed that P-tau181 was better than T-tau in predicting the ability of cognizance (P < 0.05) (Figure 3).

Correlation between P-tau181, T-tau, and SDMT by stepwise multiple linear regression analysis

Spearman bivariate correlation analysis found that P-tau181 and mean arterial pressure were positively correlated with SDMT in NPHCs (r = 0.196, P = 0.183; r = 0.115, P = 0.435); T-tau, BMI, and age were negatively correlated with SDMT in the NPHCs (r = −0.066, P = 0.654; r = −0.201, P = 0.171; r = −0.137, P = 0.352). P-tau181, T-tau, mean arterial pressure, and BMI were all negatively correlated with SDMT by the multiple linear regression analysis of NPHCs and PHCs (r = −0.376, P < 0.001; r = −0.260, P = 0.010; r = −0.397, P < 0.001; r = −0.398, P < 0.001) (Table 3). The correlations between T-tau and SDMT as well as between P-tau181 and SDMT are shown in Figure 4. In the multiple linear

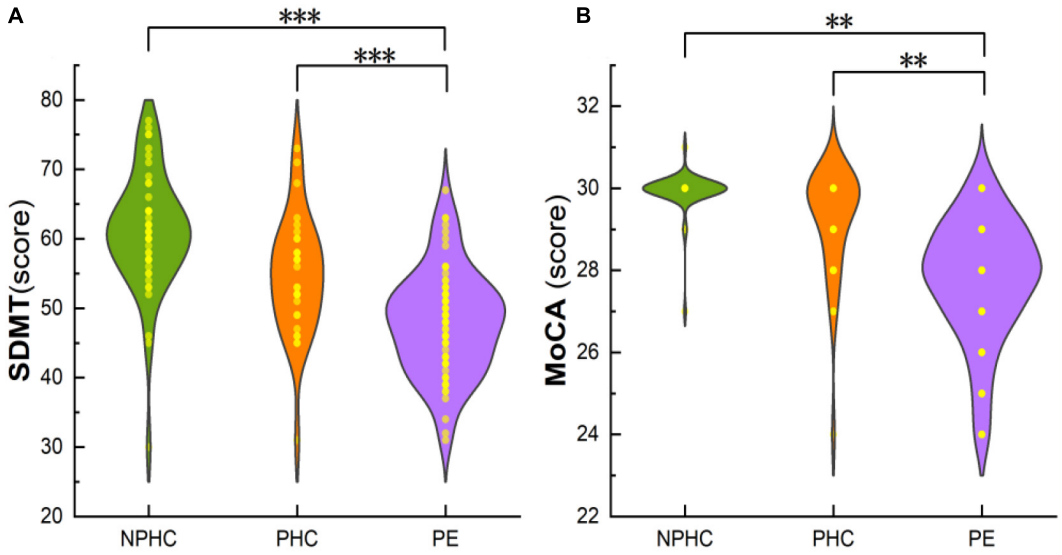

FIGURE 1
The composite plot of the scatter plot and the smoothed violin plot shows the distribution and frequency of SDMT of subjects in the PE, PHCs, and NPHCs groups **(A)**, and MoCA of subjects in the three groups **(B)**. Significant differences were found in SDMT and MoCA between the three groups [$H(K) = 56.293$, $P < 0.051$; $H(K) = 77.019$, $P < 0.001$]. $^{**}P < 0.01$; $^{***}P < 0.001$.

TABLE 2 Laboratory data of the pairwise comparison among the three groups.

Features	NPHC (n = 48)	PHC (n = 30)	PE (n = 68)	Statistical value				
				H(K)/F	*P*	*Post hoc* test		
						a	b	c
P-tau181 (pg/ml)	50.17 ± 44.51	37.03 ± 21.50	68.43 ± 47.55	19.101[a]	< 0.001	0.028	0.030	< 0.001
T-tau (pg/ml)	1, 064.12 ± 614.25	969.87 ± 443.51	1, 245.72 ± 585.93	5.937[a]	0.051	0.083	0.453	0.017
Hemoglobin (Hb) (g/L)	130.50 ± 13.75	118.97 ± 12.04	124.50 ± 10.75	14.921[a]	0.001	0.001	0.016	0.013
Platelet (Plt) ($\times 10^9$/L)	213.15 ± 49.28	209.43 ± 45.47	209.75 ± 67.50	1.324[b]	0.269	0.754	0.439	0.641
Blood glucose (Glu) (mmol/L)	4.64 ± 0.43	4.75 ± 0.67	4.50 ± 1.10	0.275[b]	0.871	0.354	0.749	0.599
Glycated hemoglobin (HbA1c) (%)	5.44 ± 0.29	4.90 ± 1.10	5.00 ± 0.25	1.649[b]	0.438	0.118	0.167	0.398
Alanine transaminase (ALT) (U/L)	12.00 ± 9.00	12.00 ± 6.00	13.00 ± 15.00	3.273[b]	0.195	0.096	0.955	0.103
Aspartate aminotransferase (AST) (U/L)	16.00 ± 9.00	14.90 ± 4.18	19.00 ± 11.25	15.118[b]	0.001	0.077	0.031	< 0.001
Creatinine (Cr) (μmol/L)	47.73 ± 12.04	42.07 ± 9.90	53.00 ± 17.75	17.746[b]	< 0.001	0.034	0.024	< 0.001
24 h-urine protein (mg)	NA	NA	1, 146.00 ± 4, 819.03	NA	NA	NA	NA	NA
Albumin/creatinine ratio	NA	0.03 ± 0.39	0.89 ± 3.31	NA	NA	NA	NA	< 0.001

Data are mean ± SD or median ± inter-quartile range.
Post-hoc test: a, NPHC vs. PHC; b, NPHC vs. PE; c, PHC vs. PE. NPHC, non-pregnant healthy control; PHC, pregnant healthy control; PE, pre-eclampsia.
[a]Kruskal–Wallis test, *H(K)*.
[b]One-way ANOVA, *F*.

regression analysis of NPHCs and PHCs, the independent variables of P-tau181, mean arterial pressure, and BMI were all correlated with SDMT. The analysis of collinear effects was performed by the variance inflation factor (VIF) and tolerance in the multiple linear regression analysis. There was no multicollinearity in the model, since the VIFs of all dependent variables were less than 10 (Table 4). The SDMT value was significantly correlated with P-tau181 in the final multivariate analysis ($r = -0.376$, $P \leq 0.001$) (Figure 4).

Discussion

In this study, serum P-tau181 and T-tau were detected in PE patients, NPHCs, and PHCs, and tests of cognitive function, including SDMT and MoCA, were performed. The results showed that PE patients had a certain degree of cognitive impairment, as the MoCA and SDMT scores of PE patients were lower than those of the PHCs and the NPHCs. At the same time, the concentration of serum P-tau181 and T-tau were thicker in PE patients than those in

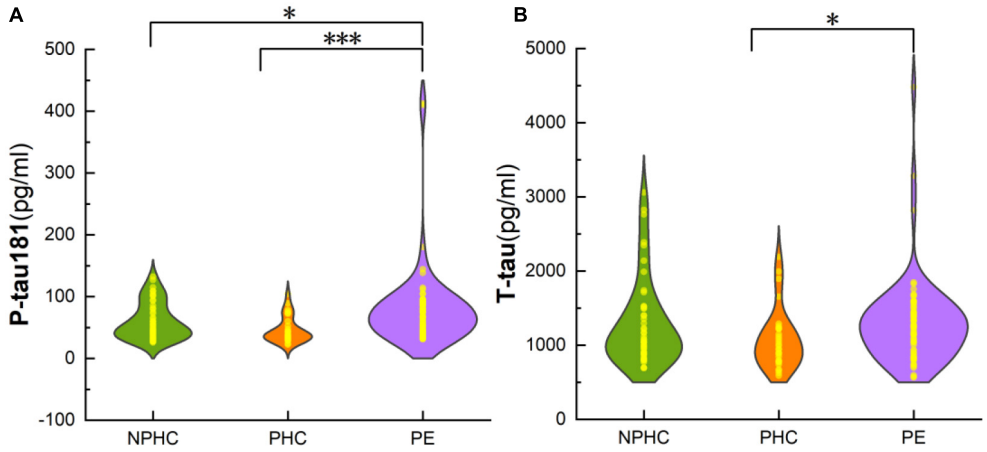

FIGURE 2
The composite plot of the scatter plot and the smoothed violin plot shows the distribution and frequency of P-tau181 of subjects in NPHCs, PHCs, and PE groups **(A)** and T-tau of subjects in the three groups **(B)**. The significant difference was found in P-tau181 and T-tau among the three groups [$H(K) = 19.101$, $P < 0.001$; $Z = -2.397$, $P = 0.017$]. $^{*}P < 0.05$; $^{***}P < 0.001$.

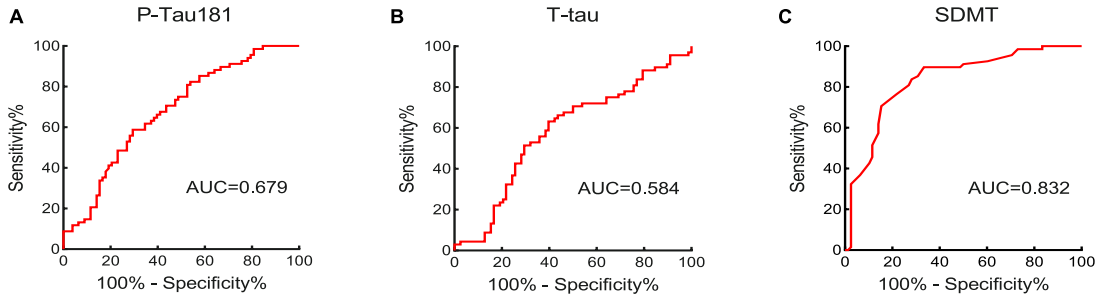

FIGURE 3
The area under the curve (AUC) value was obtained by receiver operator characteristic (ROC) curve to assess the cognition-predictive ability of P-tau181 **(A)**, T-tau **(B)**, and SDMT **(C)**.

TABLE 3 Bivariate correlation analysis between the SDMT and the clinical and laboratory data.

	NPHC		Pregnant women	
	r	*P*	*r*	*P*
P-tau181 – SDMT	0.196[b]	0.183	−0.376[a]	<0.001
T-tau – SDMT	−0.066[b]	0.654	−0.260[a]	0.010
Mean arterial pressure – SDMT	0.115[b]	0.435	−0.397[a]	<0.001
Body mass index – SDMT	−0.201[b]	0.171	−0.398[a]	<0.001
Age – SDMT	−0.137	0.352	−0.093[a]	0.364
Gestational age – SDMT	–	–	−0.076[a]	0.459

NPHC, non-pregnant healthy control; pregnant women, including PHCs and PE patients; SDMT, Symbol Digit Modalities Test.
[a]Spearman bivariate correlation.
[b]Pearson bivariate correlation.

PHCs or NPHCs, and the concentration of serum P-tau181 had a great correlation with SDMT. We speculate that P-tau181 protein may lead to cognitive impairment and subsequent neurological symptoms in PE patients, and may serve as a serum biomarker for the diagnosing cognitive functional impairment of PE. According to our investigation, our study is the first to explore the correlation of serum P-tau181 protein level with cognitive impairment in PE patients, NPHCs, and PHCs.

Previous studies have confirmed that the patients with PE have acute or long-term cognitive functional impairment. It is an extremely serious consequence that PE with pulmonary edema or eclampsia can contribute to acute cognitive functional impairment (Bergman et al., 2021). The neurological negative effects of PE over long periods and its complications can lead to an increased risk of seizures, leukodystrophy, vascular dementia, and stroke at older ages (Nerenberg et al., 2017; Basit et al., 2018), but there are few studies on cognitive function changes in PE patients during pregnancy. In this study, detailed neurological examinations and scaled cognitive function tests were performed on all subjects. The symptoms of headache (13.24%), dizziness (7.35%), and vision loss (5.88%) in PE patients were more frequent than those in PHCs. The PE patients had cognitive function scores (SDMT, 47.97 ± 7.54; MoCA, 28.00 ± 2.00) significantly lower than those of normotensive PHCs (54.73 ± 8.55, 30.00 ± 1.25, respectively), indicating that the cognitive function and information processing speed of PE patients had decreased. Although the MoCA scores in PE patients were all higher than the recommended threshold for cognitive impairment (<26 points), the subjects in this group had indeed experienced a decline in cognitive function, which warrants

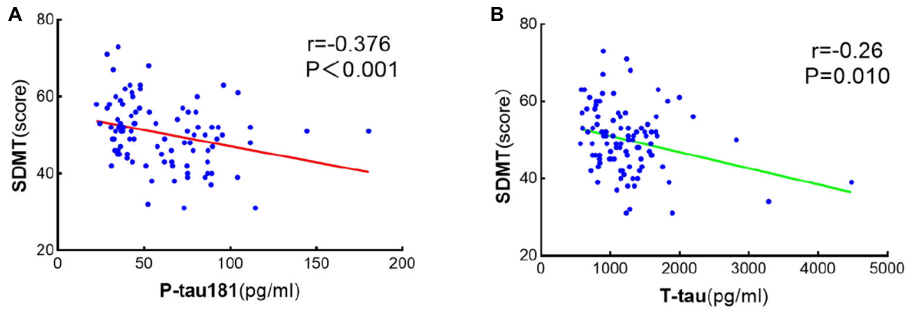

FIGURE 4
Scatter linear regression plot between SDMT and P-tau181 **(A)** and between SDMT and T-tau **(B)**. It was statistically significant that SDMT was negatively correlated with both P-tau181 and T-tau.

TABLE 4 Linear regression analysis regarding SDMT in pregnant women (n = 98).

	Bate	t	P	Collinearity statistics	
				Tolerance	VIF
Constant	–	14.804	<0.001	–	–
P-tau181 (pg/ml)	−0.193	−2.062	0.042	0.911	1.098
Mean arterial pressure (mmHg)	−0.219	−1.990	0.049	0.656	1.524
Body mass index (Kg/m^2)	−0.243	−2.165	0.033	0.633	1.580

Pregnant women, including PHCs and PE patients; VIF, variance inflation factor.

attention from clinicians. Bergman et al. (2021) suggested that PE patients had lower MoCA scores than normotensive pregnant women when they presented with symptoms of eclampsia or pulmonary edema, while they found no difference in MoCA score between PE women without severe features and normotensive women. Our study found that PE patients had already developed cognitive impairment before severe complications.

The mechanism of cognitive impairment in PE has been studied. PE is a multisystem disease that affects multiple organ systems, including the maternal brain. Some hormones secreted through the placenta, such as sex steroids, estradiol, and progesterone, are all markedly elevated during pregnancy and act on neuronal populations through the blood-brain barrier *via* receptors expressed in specific regions (Blennow and Zetterberg, 2018). The impairment of the autoregulation of cerebral circulation in patients with PE leads to the increase of blood–brain barrier permeability and the change of cerebral blood flow (Bergman et al., 2019). Tau protein is one of the main components of neuronal microtubule-associated proteins, and the expression and modification function of tau protein are closely related to cognitive function, and also can reflect the function of neuronal cells. In addition, some scholars have hypothesized that pregnancy may serve as a stress test that can reveal a woman's risk of developing cardiovascular disease in later life, due to PE shares common risk factors with cardiovascular disease and dementia (Williams, 2003).

In this study, we endeavored to explore serum biomarkers that could assess cognitive impairment in PE patients. Many laboratory indicators can be used to diagnose PE, such as placental growth factor (PlGF), soluble endoglin (sEng), and soluble vascular endothelial growth factor receptor 1 (sFlt-1). These indicators can reflect the oxidative stress of the placenta and the functional status of the vascular endothelial cells, and have good predictive value for PE (Zeisler et al., 2016), but cannot reflect the cognitive function status of PE patients. P-tau and T-tau are markers of cognitive impairment and are closely related to the cognitive function of individuals. P-tau181 is phosphorylated at threonine-181, which is an intermediate product produced during the phosphorylation of tau protein. P-tau181 concentration is associated with cognitive decline (Thijssen et al., 2020; Simrén et al., 2021). By measuring the serum T-tau and P-tau181 concentrations of our subjects, we found that they were both significantly higher in PE patients than PHCs or NPHCs. Lederer et al. (2016) found that the concentration of P-tau181 protein in cerebrospinal fluid was significantly associated with PE/HELLP syndrome (P = 0.043: hazard ratio = 1.211). Another report confirmed that the plasma tau protein concentration of women with PE was 2.17 times thicker than that of normotensive women (95% CI, 1.49–3.16). The above results are all in line with the results of our study.

The AUC from the ROC curve analysis have evaluated that P-tau181 had great potential ability of diagnosing cognitive functional impairment in PE patients. Its AUC was 0.679, the cut-off value was 60.95 pg/ml, and P-tau181 performed better than T-tau. Therefore, we believe that the concentration of serum P-tau181 in PE patients is related to cognitive functional impairment and can be used to screen the condition of PE patients. The high level of P-tau181 can be used as a clinical laboratory indication for non-invasive assessment of cognitive functional impairment in PE patients. The P-tau181 cut-off value found in this study must be validated by further studies, which should take into account differences in results caused by different testing methods.

We also studied the correlations between serum P-tau181 and T-tau and the results of cognitive test scales. SDMT can reflect the information processing speed of subjects through attention, visual scanning, and movement speed (Sheridan et al., 2006). In a Parkinson's disease study, the SDMT and MoCA scales were considered appropriate tools for identifying cognitive features regulated by amyloid-β (Aβ) and tau protein phosphorylation in established synucleinopathies (Fiorenzato et al., 2018). Fiorenzato et al. (2018) found that SDMT scores were significantly lower in Aβ-positive Parkinson's patients and were significantly associated with increased amyloid deposition in cortical regions (i.e., frontal,

posterior cingulate, temporal, parietal, and occipital lobes), which is critical for information processing speed. Aβ can directly induce tau hyperphosphorylation and neurodegeneration (Jin et al., 2011). In our subjects, SDMT was negatively correlated with the serum P-tau181 concentration ($r = -0.376$, $P \leq 0.001$) in pregnant women at an average gestational age of 33.86 ± 7.46 weeks. However, there was no significant correlation between the two in the NPHCs. Therefore, we believe that the information processing speed can be well reflected by the measurement of serum P-tau181 in women in the third trimester.

Tau and P-tau can be measured by positron-emission tomography (PET) or cerebrospinal fluid (Schöll et al., 2016; Blennow and Zetterberg, 2018), but these methods are invasive and expensive and require high doses of radiation, so they are not suitable for research in pregnant women. We reviewed the literature and found that serum P-tau181 and T-tau protein concentrations both had good correlations with their cerebrospinal fluid protein concentrations (Barthélemy et al., 2020; Janelidze et al., 2020) and can be used as serum biomarkers of cognitive impairment in PE patients. Studies in Alzheimer's disease confirm the high accuracy of blood P-tau181 assays for identifying individual and combined neurofibrillary tangles and plaque pathology, making it an ideal biomarker for Alzheimer's disease (Jack et al., 2018).

Subjects in this study could only undergo neuropsychological testing and sample collection when they were clinically stable, and patients with severe neurological symptoms could not participate in this study. Many women with PE are treated with magnesium sulfate during hospitalization to protect their nerves. Clinical practice has confirmed that magnesium sulfate has a favorable effect on improving the cognitive function of pregnant women (Rana et al., 2006). Therefore, neuropsychological testing and sample collection of the subjects should be performed before the use of magnesium sulfate to guarantee the accuracy of the results. Our study was a strictly *in vivo* study based on clinical laboratorial data, but absent from the corresponding pathological evidence of PE. This study has the limitation of small sample size, so it is critically urgent to increase the sample volume to further explore the potential mechanism of cognitive dysfunction in PE patients in the future. This was a preliminary study on serum P-tau181 protein concentration in PE patients. In the future, we will conduct long-term follow-up study of the cognitive function, brain functional imaging characteristics, and related serum markers in PE patients, what is more, further explore the changes of neuroimaging characteristics and serum markers in patients with different severity of cognitive dysfunction. The purpose of our research is to commit to further excavate the pathophysiological mechanisms of PE.

Conclusion

The serum P-tau181 protein concentration of the PE patients was significantly thicker than that of the PHCs and NPHCs, and had a great correlation with the SDMT and MoCA scores. The results of this study support the potential value of serum P-tau181 protein concentrations in the diagnosis of cognitive functional impairment in PE patients. Serum P-tau181 protein can serve as a simple, accessible, and scalable marker for the screening and diagnosis of cognitive functional impairment in PE.

Data availability statement

The original contributions presented in this study are included in the article/supplementary material, further inquiries can be directed to the corresponding author.

Ethics statement

The studies involving human participants were reviewed and approved by the Ethical Committee of the Institutional Review Board (IRB) of Jinan Maternal and Child Care Hospital Affiliated to Shandong First Medical University. The patients/participants provided their written informed consent to participate in this study.

Author contributions

LY and TC wrote the main manuscript text. BG and KZ prepared the clinical data. YW did the statistical analysis, prepared the figures, and revised the main manuscript text. All authors reviewed the manuscript.

Funding

This work was supported by grants from the Technology Development Plan of Jinan (202134072 and 202225035), Science and Technology Project of Jinan Municipal Health Commission (2021-2-89 and 2021-2-93), and Special Fund for Scientific and Technological Innovation of Shandong Maternal and Child Health Care Commission (Lu Fu You Xie Fa 2021-19).

Acknowledgments

This manuscript has been edited and proofread by American Journal Experts. We thank all of the volunteers and patients for their participation in our study.

Conflict of interest

The authors declare that the research was conducted in the absence of any commercial or financial relationships that could be construed as a potential conflict of interest.

Publisher's note

References

Abalos, E., Cuesta, C., Grosso, A., Chou, D., and Say, L. (2013). Global and regional estimates of preeclampsia and eclampsia: a systematic review. *Eur. J. Obstet Gynecol. Reprod. Biol.* 170, 1–7. doi: 10.1016/j.ejogrb.2013.05.005

Adank, M. C., Hussainali, R. F., Oosterveer, L. C., Ikram, M. A., Steegers, E. A. P., Miller, E. C., et al. (2021). Hypertensive disorders of pregnancy and cognitive impairment: a prospective cohort study. *Neurology* 96, e709–e718. doi: 10.1212/WNL.0000000000011363

American College of Obstetricians and Gynecologists [ACOG], (2019). ACOG practice bulletin no. 202: gestational hypertension and preeclampsia. *Obstet Gynecol.* 133:1.

Baecke, M., Spaanderman, M. E., and Van Der Werf, S. P. (2009). Cognitive function after pre-eclampsia: an explorative study. *J. Psychosom. Obstet. Gynaecol.* 30, 58–64. doi: 10.1080/01674820802546212

Ballatore, C., Lee, V. M., and Trojanowski, J. Q. (2007). Tau-mediated neurodegeneration in Alzheimer's disease and related disorders. *Nat. Rev. Neurosci.* 8, 663–672. doi: 10.1038/nrn2194

Barthélemy, N. R., Horie, K., Sato, C., and Bateman, R. J. (2020). Blood plasma phosphorylated-tau isoforms track CNS change in Alzheimer's disease. *J. Exp. Med.* 217:e20200861. doi: 10.1084/jem.20200861

Basit, S., Wohlfahrt, J., and Boyd, H. A. (2018). Pre-eclampsia and risk of dementia later in life: nationwide cohort study. *BMJ* 363:k4109. doi: 10.1136/bmj.k4109

Bergman, L., Thorgeirsdottir, L., Elden, H., Hesselman, S., Schell, S., Ahlm, E., et al. (2021). Cognitive impairment in preeclampsia complicated by eclampsia and pulmonary edema after delivery. *Acta Obstet. Gynecol. Scand.* 100, 1280–1287. doi: 10.1111/aogs.14100

Bergman, L., Torres-Vergara, P., Penny, J., Wikström, J., Nelander, M., Leon, J., et al. (2019). Investigating maternal brain alterations in preeclampsia: the need for a multidisciplinary effort. *Curr. Hypertens. Rep.* 21:72. doi: 10.1007/s11906-019-0977-0

Blennow, K., and Zetterberg, H. (2018). Biomarkers for Alzheimer's disease: Current status and prospects for the future. *J. Intern. Med.* 284, 643–663. doi: 10.1111/joim.12816

Brussé, I., Duvekot, J., Jongerling, J., Steegers, E., and De Koning, I. (2008). Impaired maternal cognitive functioning after pregnancies complicated by severe pre-eclampsia: a pilot case-control study. *Acta Obstet. Gynecol. Scand.* 87, 408–412. doi: 10.1080/00016340801915127

Chappell, L., Cluver, C., Kingdom, J., and Tong, S. (2021). Pre-eclampsia. *Lancet* 398, 341–354. doi: 10.1016/S0140-6736(20)32335-7

Fiorenzato, E., Biundo, R., Cecchin, D., Frigo, A. C., Kim, J., Weis, L., et al. (2018). Brain amyloid contribution to cognitive dysfunction in early-stage parkinson's disease: the PPMI dataset. *J. Alzheimers Dis.* 66, 229–237. doi: 10.3233/JAD-180390

Fishel Bartal, M., and Sibai, B. (2022). Eclampsia in the 21st century. *Am. J. Obstet. Gynecol.* 226, S1237–S1253. doi: 10.1016/j.ajog.2020.09.037

Guo, T., Noble, W., and Hanger, D. P. (2017). Roles of tau protein in health and disease. *Acta Neuropathol.* 133, 665–704. doi: 10.1007/s00401-017-1707-9

Iqbal, K., Liu, F., Gong, C., and Grundke-Iqbal, I. (2010). Tau in Alzheimer disease and related tauopathies. *Curr. Alzheimer Res.* 7, 656–664. doi: 10.2174/156720510793611592

Jack, C. R. Jr., Bennett, D. A., Blennow, K., Carrillo, M. C., Dunn, B., Haeberlein, S. B., et al. (2018). NIA-AA research framework: toward a biological definition of Alzheimer's disease. *Alzheimers Dement* 14, 535–562. doi: 10.1016/j.jalz.2018.02.018

Janelidze, S., Mattsson, N., Palmqvist, S., Smith, R., Beach, T. G., Serrano, G. E., et al. (2020). Plasma P-tau181 in Alzheimer's disease: relationship to other biomarkers, differential diagnosis, neuropathology and longitudinal progression to Alzheimer's dementia. *Nat. Med.* 26, 379–386. doi: 10.1038/s41591-020-0755-1

Jin, M., Shepardson, N., Yang, T., Chen, G., Walsh, D., and Selkoe, D. J. (2011). Soluble amyloid beta-protein dimers isolated from Alzheimer cortex directly induce Tau hyperphosphorylation and neuritic degeneration. *Proc. Natl. Acad. Sci. U S A.* 108, 5819–5824. doi: 10.1073/pnas.1017033108

Lebouvier, T., Scales, T. M., Williamson, R., Noble, W., Duyckaerts, C., Hanger, D. P., et al. (2009). The microtubule-associated protein tau is also phosphorylated on tyrosine. *J. Alzheimers Dis.* 18, 1–9. doi: 10.3233/JAD-2009-1116

Lederer, W., Dominguez, C., Popovscaia, M., Putz, G., and Humpel, C. (2016). Cerebrospinal fluid levels of tau and phospho-tau-181 proteins during pregnancy. *Pregnancy Hypertens.* 6, 384–387. doi: 10.1016/j.preghy.2016.08.243

Nerenberg, K. A., Park, A. L., Vigod, S. N., Saposnik, G., Berger, H., Hladunewich, M. A., et al. (2017). Long-term risk of a seizure disorder after eclampsia. *Obstet Gynecol.* 130, 1327–1333. doi: 10.1097/AOG.0000000000002364

Rana, S., Lindheimer, M., Hibbard, J., and Pliskin, N. (2006). Neuropsychological performance in normal pregnancy and preeclampsia. *Am. J. Obstet Gynecol.* 195, 186–191. doi: 10.1016/j.ajog.2005.12.051

Rätsep, M. T., Hickman, A. F., Maser, B., Pudwell, J., Smith, G. N., Brien, D., et al. (2016). Impact of preeclampsia on cognitive function in the offspring. *Behav. Brain Res.* 302, 175–181. doi: 10.1016/j.bbr.2016.01.030

Schöll, M., Lockhart, S. N., Schonhaut, D. R., O'neil, J. P., Janabi, M., Ossenkoppele, R., et al. (2016). PET imaging of tau deposition in the aging human brain. *Neuron* 89, 971–982. doi: 10.1016/j.neuron.2016.01.028

Shawwa, K., McDonnell, N., and Garovic, V. (2018). Pregnancy, preeclampsia, and brain. *Hypertension* 72, 1263–1265. doi: 10.1161/HYPERTENSIONAHA.118.11493

Sheridan, L. K., Fitzgerald, H. E., Adams, K. M., Nigg, J. T., Martel, M. M., Puttler, L. I., et al. (2006). Normative symbol digit modalities test performance in a community-based sample. *Arch Clin. Neuropsychol.* 21, 23–28. doi: 10.1016/j.acn.2005.07.003

Simrén, J., Leuzy, A., Karikari, T. K., Hye, A., Benedet, A. L., Lantero-Rodriguez, J., et al. (2021). The diagnostic and prognostic capabilities of plasma biomarkers in Alzheimer's disease. *Alzheimers Dement.* 17, 1145–1156. doi: 10.1002/alz.12283

Thijssen, E. H., La Joie, R., Wolf, A., Strom, A., Wang, P., Iaccarino, L., et al. (2020). Diagnostic value of plasma phosphorylated tau181 in Alzheimer's disease and frontotemporal lobar degeneration. *Nat. Med.* 26, 387–397. doi: 10.1038/s41591-020-0762-2

Williams, D. (2003). Pregnancy: a stress test for life. *Curr. Opin. Obstet Gynecol.* 15, 465–471. doi: 10.1097/00001703-200312000-00002

Zeisler, H., Llurba, E., Chantraine, F., Vatish, M., Staff, A. C., Sennström, M., et al. (2016). Predictive value of the sFlt-1:PlGF ratio in women with suspected preeclampsia. *N. Engl. J. Med.* 374, 13–22. doi: 10.1056/NEJMoa1414838

frontiers | Frontiers in Neuroscience

TYPE Review
PUBLISHED 31 March 2023
DOI 10.3389/fnins.2023.1144867

OPEN ACCESS

EDITED BY
Han Lv,
Beijing Friendship Hospital, Capital Medical University, China

REVIEWED BY
John John,
Believers Church Medical College Hospital, India
Bin Li,
Beijing Hospital, China

*CORRESPONDENCE
Yue Wang
✉ wy472670862@163.com
Tao Chen
✉ ctsci2020@163.com

†These authors have contributed equally to this work

‡These authors have contributed equally to this work and share first authorship

SPECIALTY SECTION
This article was submitted to Brain Imaging Methods, a section of the journal Frontiers in Neuroscience

RECEIVED 15 January 2023
ACCEPTED 06 March 2023
PUBLISHED 31 March 2023

CITATION
Zhang N, Yang L, Han A, Wang Y, Zhao G, Wang Y and Chen T (2023) Advances in imaging findings of preeclampsia-related reversible posterior leukoencephalopathy syndrome.
Front. Neurosci. 17:1144867.
doi: 10.3389/fnins.2023.1144867

Advances in imaging findings of preeclampsia-related reversible posterior leukoencephalopathy syndrome

Nan Zhang [1‡], Linfeng Yang [2‡], Aiqing Han [3], Yuanyuan Wang [4], Guiwu Zhao [5], Yue Wang [2*†] and Tao Chen [6*†]

[1]Department of Radiology, Shandong Provincial Hospital Affiliated to Shandong First Medical University, Jinan, Shandong, China, [2]Department of Radiology, Jinan Maternity and Child Care Hospital Affiliated to Shandong First Medical University, Jinan, Shandong, China, [3]Department of Obstetrics, Jinan Maternity and Child Care Hospital Affiliated to Shandong First Medical University, Jinan, Shandong, China, [4]Department of Radiology, Binzhou Medical University, Yantai, Shandong, China, [5]Zhucheng Peace Medical Imaging Diagnosis Center, Weifang, Shandong, China, [6]Department of Clinical Laboratory, Jinan Maternity and Child Care Hospital Affiliated to Shandong First Medical University, Jinan, Shandong, China

Preeclampsia (PE)-related reversible posterior leukoencephalopathy syndrome (RPLS) is a common complication of hypertensive disorders of pregnancy. The syndrome usually occurs after 20 weeks of gestation and can lead to brain injury. Severe headache, seizures, disturbance of consciousness, and other neurological symptoms may occur in severe cases. PE-RPLS has high morbidity and mortality rates and seriously damages maternal and fetal health. In recent years, the continuous advancement of medical imaging technology has provided an important imaging basis for the early diagnosis and prognostic evaluation of RPLS. This article mainly details the research status of the etiology and pathogenesis of PE-RPLS and describes its characteristic imaging findings, especially MRI findings, to provide new insights into its early diagnosis, early treatment, and improvement of prognosis.

KEYWORDS

preeclampsia, reversible posterior leukoencephalopathy syndrome (RPLS), neuroimaging, magnetic resonance imaging, multimodal brain MRI

1. Introduction

Hypertensive disorders of pregnancy (HDP) are some of the most common gestational cardiovascular diseases. Worldwide, the incidence rate of HDP is as high as 10%. A number of domestic and foreign guidelines classify HDP into four types, namely, preeclampsia (PE), chronic hypertension, chronic hypertension with PE, and gestational hypertension, according to the onset time of hypertension, the presence or absence of proteinuria, other target organ damage, and clinical manifestations (Wenger et al., 2018). PE is the most common and serious type of HDP. It manifests as elevated blood pressure after 20 weeks of gestation accompanied by different degrees of end-organ damage [such as increased liver alanine transaminase (ALT), decreased platelet count (PLT), and renal insufficiency], with or without proteinuria. PE with seizure is called eclampsia.

With the gradual liberalization of the three-child policy in China, the number of pregnancies at advanced maternal age has increased significantly, and the incidence rate of

PE has increased significantly. PE is one of the pregnancy complications that obstetricians are most worried about (Ananth et al., 2013). This disease has high morbidity and mortality rates and seriously threatens the maternal and fetal life and health. PE usually affects multiple systems throughout the body, especially the central nervous system, and reversible posterior leukoencephalopathy syndrome (RPLS) is the most common complication of the central nervous system of PE.

This article reviews the advances in central nervous system imaging of PE-related RPLS based on the etiology and pathogenesis of the disease, especially the advances in MRI for PE-related RPLS, aiming to provide a theoretical basis for the early detection, early diagnosis, and early treatment of the disease.

2. The etiology and pathogenesis of PE-related RPLS

Reversible posterior leukoencephalopathy syndrome can be caused by a variety of etiologies, including PE, renal insufficiency, elevated blood pressure, component transfusions, autoimmune disease, infection, and shock (Tlemsani et al., 2011; Fa'ak et al., 2021; Virojtriratana et al., 2022). PE is one of the common causes of RPLS, and RPLS is more likely to occur in PE patients with severe headaches, consciousness impairment, visual abnormalities, or other neurological symptoms (Demirtaş et al., 2005; Murali et al., 2020). Eclampsia is an acute cerebrovascular complication considered a clinical manifestation of RPLS (Damak et al., 2022; Fishel Bartal and Sibai, 2022).

No consensus has been reached on the pathophysiological mechanism of PE-related RPLS, but many studies have noted that it may be related to the increase in vascular permeability caused by vascular endothelial injury and the dysfunction of vascular autoregulation caused by excessively high blood pressure. Under normal circumstances, although the cerebral perfusion pressure fluctuates within the range of approximately 50–150 mmHg, the cerebral circulation maintains a constant cerebral blood flow, and the process of maintaining a constant cerebral blood flow through the dilation and contraction of small blood vessels is called cerebral blood flow autoregulation. The blood supply to the back of the brain mainly comes from the vertebral-basilar system. However, since there are almost no sympathetic nerves in the vertebral-basilar system, the system (especially the cerebral blood vessels supplying the occipital lobe and the posterior watershed area) is quite sensitive to blood pressure fluctuations. When blood pressure rises rapidly and exceeds the upper limit of cerebrovascular autoregulation, the area supplied by the posterior cerebral artery is excessively perfused, the blood—brain barrier is destroyed, and a large amount of plasma and macromolecular substances extravasate, resulting in vasogenic cerebral edema (Fugate and Rabinstein, 2015; Virojtriratana et al., 2022). Therefore, the lesions of RPLS are mostly located in the area supplied by the posterior cerebral artery, with a symmetrical distribution, mainly involving the cortex and subcortical white matter areas.

In addition, studies have shown that endothelial cell dysfunction caused by systemic toxic effects is a key step in the occurrence of PE-related RPLS. Cerebral hypoperfusion due to vasoconstriction may be responsible for the development of RPLS, and hypertension may be a response to cerebral hypoperfusion due to endothelial dysfunction caused by systemic toxic effects (Hawkes et al., 2022). Lactate dehydrogenase (LDH) is a marker of endothelial cell damage. Some studies found that PE-related RPLS is closely related to the LDH level. Capillary permeability increases due to vascular endothelial injury, and hypoalbuminemia reduces colloid osmotic pressure and induces the development of RPLS. As the condition improves, the LDH level quickly returns to normal. Some scholars believe that vasogenic cerebral edema in RPLS is caused by the inflow of intravascular fluid into the interstitium due to venous constriction–induced increases in capillary hydrostatic pressure and microvascular permeability (Singhal, 2021). However, this hypothesis does not explain the finding that hypertension often precedes the onset of RPLS symptoms (Rabinstein et al., 2012). Some studies have suggested that the ischemic lesions often caused by vasospasm are mostly located in the cortex or white matter near the cortex (Li et al., 2023). If not treated in time, the lesions will often progress to cytotoxic edema, that is, cerebral infarction. Significant blood pressure fluctuations may be more likely to cause RPLS than increases in absolute blood pressure (Liman et al., 2014), and even septic and hypotensive patients may develop RPLS (Bartynski et al., 2006). The mean baseline blood pressure and the proportion and speed of blood pressure rise may be important factors in the disruption of the blood—brain barrier and the generation of vasogenic edema in RPLS patients.

3. Studies on central nervous system imaging of PE-related RPLS

The concept of RPLS was first proposed by Hinchey et al. (1996). In the past two decades, with the development and application of various imaging techniques, an increasing number of PE-related RPLS cases have been discovered and reported. The most common imaging methods for PE-related RPLS are CT and MRI (**Table 1**).

3.1. Application of CT to PE-related RPLS patients

CT has high-density resolution and unique advantages in diagnosing intracranial hemorrhage. However, there are no specific CT signs for different types of cerebral edema. Most RPLS lesions on CT show symmetrically distributed, patchy hypodensities in the bilateral parietal and occipital parenchyma, which may have a mass effect, but there may be no discernible abnormality on early CT examination. CT involves ionizing radiation, which brings a certain risk of teratogenicity, and has poor soft tissue resolution and poor visualization of small lesions, which limits its wide application in pregnant patients.

3.2. Application of MRI in PE-related RPLS patients

Magnetic resonance imaging has clear soft tissue contrast, high spatial resolution, and no ionizing radiation and so has

TABLE 1 Features on CT and MRI imaging with posterior leukoencephalopathy syndrome (RPLS).

Types	Features on CT and MRI imaging
Regions	Mainly occur in bilateral parieto-occipital lobes;
	Often involve the frontal and temporal lobes;
	The corpus callosum, thalamus, basal ganglia, cerebellum, or brainstem are rarely affected.
Density/Signal intensity	Density: low density.
	T1-weighted images: iso-intense or low signal intensity;
	T2-weighted images and FLAIR: high signal intensity;
	Diffusion-weighted imaging (DWI): isointense or hypointense;
	Apparent diffusion coefficient (ADC): hyperintense.
Contrast enhancement	Not usually seen after injection of a contrast agent.
Characteristics of edema	Almost involving both sides;
	Not completely symmetrical appearance.
Concomitant signs	Intraparenchymal hemorrhage; subarachnoid hemorrhage (SAH).

become the preferred imaging method for diagnosing RPLS (Kastrup et al., 2015). Conventional MRI examinations include T1-weighted imaging (T1WI), T2-weighted imaging (T2WI), and T2-fluid-attenuated inversion recovery (FLAIR) sequences. When brain lesions are found in conventional MRI examinations, diffusion-weighted imaging (DWI) should be performed to identify the lesion types based on DWI and apparent diffusion coefficient (ADC) maps. When necessary, magnetic resonance angiography, magnetic resonance venography, and susceptibility-weighted imaging (SWI) techniques can be used to exclude cranial and cerebrovascular diseases. In addition, some emerging magnetic resonance techniques, including intravoxel incoherent motion (IVIM), quantitative susceptibility mapping (QSM), and magnetic resonance spectroscopy (MRS), have been applied to the study of brain function and metabolism in RPLS patients.

3.2.1. Findings of conventional MRI sequences in patients with RPLS

Brain lesions in patients with RPLS mainly manifest as vasogenic edemas in the posterior white matter region on MRI, which are isointense or hypointense on T1WI images, hyperintense on T2WI images, and hyperintense on T2-FLAIR, and the lesions are often not enhanced much on scans by contrast medium. RPLS lesions mainly occur in bilateral parieto-occipital lobes, often involve the frontal and temporal lobes, but rarely involve the corpus callosum, thalamus, basal ganglia, cerebellum, or brainstem (Fischer and Schmutzhard, 2017; **Figure 1**). Umar et al. (2022) found that when the clinical symptoms of RPLS patients were headache, nausea, and vomiting, their brain imaging examinations had no specific findings, but when RPLS patients had seizures, their RPLS lesions were mainly distributed in the frontal cortex and parietal cortex. Fugate and Rabinstein (2015) believed that a distribution of RPLS lesions mainly in the posterior white matter region may be related to the nearly absence of sympathetic nerve distribution in this region and the susceptibility of this region to rapid blood pressure increases and cerebral hyperperfusion.

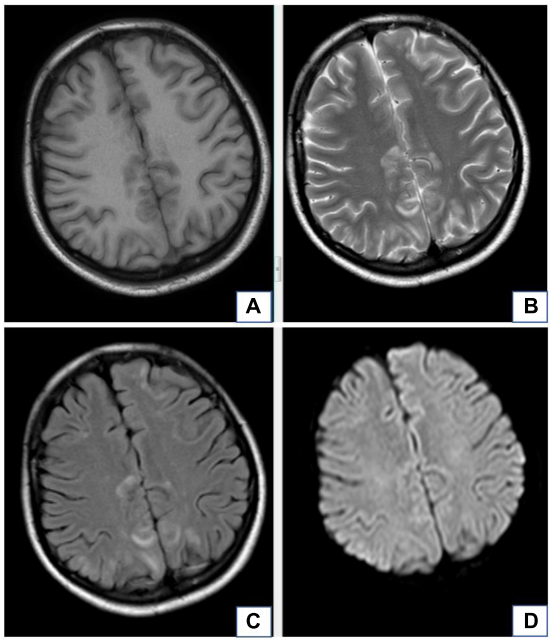

FIGURE 1
A 20-year-old female with diagnosis of preeclampsia-related reversible posterior leukoencephalopathy syndrome. The lesions occur in bilateral parieto-occipital lobes, which are isointense or hypointense on T1WI images **(A)**, hyperintense on T2WI images **(B)**, and hyperintense on T2-FLAIR **(C)**, but there is no obvious hyperintense signal in these lesions on DWI **(D)**.

Compared with the cerebral cortex, the white matter has a looser tissue structure, so the RPLS lesions are mostly located in the subcortical white matter region (the cortex is less likely to be involved).

Reversible posterior leukoencephalopathy syndrome lesions are not completely irreversible. Usually, they will improve spontaneously after early diagnosis and active treatment, and all patients have had improved clinical symptoms and MRI findings. Linear or gyrus-like enhancement was seen in approximately 20% of RPLS patients on contrast-enhanced MR images (Fugate et al., 2010; Gao et al., 2015; Kastrup et al., 2015), which may suggest the important role of endothelial dysfunction in the pathophysiological mechanism of RPLS. The pathophysiological mechanism of RPLS may be related to the endothelial dysfunction and the destruction of the blood–brain barrier caused by cytotoxicity or the inflammatory response.

Delayed treatment or the use of improper treatment methods may affect the condition of RPLS likely due to the increase in mean arterial pressure and the long persistence of pathogenic factors. Factors associated with poor outcomes include severe encephalopathy, a hypertensive cause, hyperglycemia, a neoplastic cause, a longer time to control the causative factor, the presence of multiple comorbidities, elevated C reactive protein, low cerebrospinal fluid glucose, and coagulopathy (Triplett et al., 2022).

Although its nomenclature is well known, many clinical researchers believe that the nomenclature of RPLS is inaccurate because cerebral edema is often not limited to the posterior white matter and is not always reversible. In mild cases, RPLS may only cause some clinical symptoms, such as headache or

seizure activity. For these cases, the results of conventional MRI examinations may only show vasogenic edema in a small area or even no obvious abnormality. In some severe cases, brain MRI findings include acute intracranial hemorrhage and/or extensive edema of the posterior cranial fossa, which result(s) in obstructive hydrocephalus or compression of the brainstem, seriously endangering the mother's life. After timely treatment in the early stage, the clinical symptoms can be significantly improved in most RPLS patients. Without delayed diagnosis and treatment, that may lead to mortality or irreversible neurological deficits (Parasher and Jhamb, 2020).

Sometimes it is necessary to distinguish RPLS from viral encephalitis. The lesions of viral encephalitis occur most commonly in the temporal lobe but can occur in any part of the brain, and most of them are unilateral hypodensities with a mass effect around them. The clinical symptoms of viral encephalitis include fever, headache, nausea, vomiting, and loss of consciousness. Electroencephalography and cerebrospinal fluid laboratory tests can provide a clear diagnosis.

3.2.2. Diagnostic value of DWI for RPLS

Brain lesions in RPLS patients often appear isointense or hypointense on DWI but hyperintense on ADC maps. Some 15–33.3% of RPLS patients have focal restricted diffusion in the brain on DWI images, which is mostly distributed in punctate or patchy areas of angioedema and is related to the severity of edema. Large-area uniform restricted diffusion is rarely seen and is difficult to distinguish from ischemic infarction. Restricted diffusion may be associated with local edema, decreased perfusion, and vasospasm, suggesting irreversible structural damage and incomplete clinical recovery, although complete recovery of restricted diffusion or only mild atrophy after restricted diffusion has been reported in sporadic cases (Covarrubias et al., 2002; Yilmaz et al., 2010; Kastrup et al., 2015). Acute cytotoxic edema does not necessarily evolve into infarction. Up to now, restricted diffusion cannot be used to effectively assess the clinical prognosis of RPLS patients, and its potential value in assessing the clinical prognosis of RPLS patients still needs further research.

The RPLS lesions of some patients are hyperintense on DWI and ADC maps, which means that the foci of hyperintensity on DWI probably reflects that they were affected by the T2 penetration effect. The RPLS lesions of some patients are hyperintense on DWI but hypointense on ADC maps, which indicates cytotoxic edema and poor prognosis (**Figure 2.**). DWI plays a key role in differentiating cytotoxic cerebral edema from vasogenic cerebral edema (Shankar and Banfield, 2017).

A recent study has shown that vascular endothelial injury plays an important role in the pathogenesis of RPLS and that cerebral edema on brain MR images of RPLS patients has a significant correlation with vascular endothelial injury, but no significant relationship with blood pressure fluctuations (Sundin and Johnson, 2018). MR images showed that the brain lesions were gradually disappearing after antispasmodic and antihypertensive treatments, which could also provide a basis for the theory of cerebral edema formation.

3.2.3. The diagnostic value of SWI for RPLS

Susceptibility-weighted imaging is based on the differences in magnetic susceptibility between different tissues of the human body. The technology is highly sensitive to venules, blood components, calcification, and iron deposition and is extremely good at identifying cerebral hemorrhage, especially intracerebral microhemorrhages (with a very high detection rate). Due to the hardened and less elastic vascular wall of PE patients caused by long-term chronic hypertension or the excessive cerebral perfusion caused by a sharp increase in blood pressure, the arteries are easily ruptured, causing hemorrhage. Intracranial hemorrhage is common in patients with RPLS, with an incidence rate of approximately 10–25% (Burnett et al., 2010; Junewar et al., 2014; Karia et al., 2016). Intraparenchymal hemorrhage and subarachnoid hemorrhage (SAH) are the common types of hemorrhage and may occur simultaneously in 18–30% of hemorrhage cases (Sharma et al., 2010). In a retrospective study by Hefzy et al. (2009) of 151 patients, only 3% had SAH, and 8% had lobar hemorrhage. In the retrospective study of Sharma et al. (2010), among 263 RPLS patients, 40 had intracranial hemorrhage, and 5.3% had sulcal SAH. Intracranial hemorrhage may be secondary to anticoagulation therapy and endogenous coagulopathy but is not related to blood pressure. Using SWI-MRI, Mckinney et al. (2012) found that 19.4% of the RPLS patients had intraparenchymal hemorrhage, and 6% had SAH. Even when the lesions in the T2WI sequence completely regressed, tiny hemorrhagic foci were still visible on SWI, so it is necessary to perform follow-up SWI to confirm that the morphological changes are completely resolved.

3.2.4. Diagnostic value of IVIM and MRS for RPLS

Intravoxel incoherent motion is a non-invasive MRI technique for assessing perfusion fraction and edema that can assess blood perfusion at the capillary level without the need for contrast agents. Recent studies have used IVIM to observe that the cerebral blood volume and blood flow indices of PE patients are lower than those of normal pregnant women and non-pregnant women (Yuan et al., 2016; Nelander et al., 2018).

Magnetic resonance spectroscopy can analyze the metabolism of the central nervous system, which is helpful to study the pathogenesis of RPLS at the cellular level (Yuan et al., 2016). MRS can be used to analyze the metabolism of brain lesions in RPLS patients. A prospective observational study of non-pregnant healthy women, healthy pregnant women, and women with PE showed that the *N*-acetylaspartate (NAA)/choline (Cho) ratio gradually increased while the Cho value decreased during healthy pregnancy and that the PE patients had significantly lower NAA/Cho ratios and higher Cho values than healthy pregnant women (Sheikh-Bahaei et al., 2020), which indicated that compared with healthy pregnant women, PE patients had cerebral ischemia. Eichler et al. (2002) found extensive metabolic abnormalities in both brain lesions and adjacent normal brain tissue in patients with RPLS, including increased acetylcholine and creatine levels and mildly decreased NAA levels. A follow-up MRS after 2 months of treatment showed that the metabolic level had returned to normal, confirming the reversibility of RPLS (Eichler et al., 2002).

3.2.5. Related studies of MRI-based oxygen extraction fraction values in RPLS

Magnetic resonance imaging-based OEF mapping uses the phase and amplitude data from QSM-MRI and the amplitude data

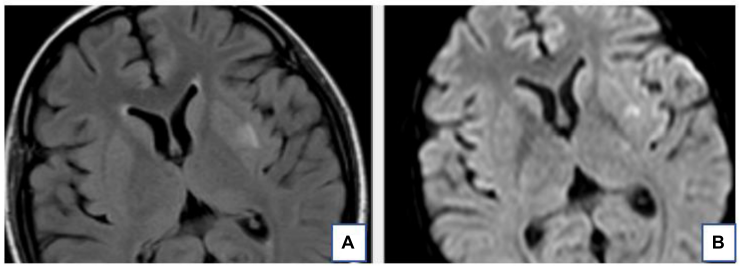

FIGURE 2
The T2-FLAIR **(A)** and DWI **(B)** of the same patient. The hyperintense signal of the Left basal ganglia area on T2-FLAIR is also very obvious on DWI. This suggests local infarction in the left basal ganglia.

in QSM and quantitative blood oxygen level-dependent magnitude to calculate the OEF values. This technology can non-invasively and quantitatively measure the functional status of cerebral oxygen metabolism, which is helpful to explore and evaluate the potential impact of changes in cerebral oxygen metabolism on brain function and cognitive behavior. In a recent study, Yang et al. (2022) used MRI-based OEF values to explore functional imaging indicators of cerebral oxygen metabolism in PE patients and to study the interaction between imaging indicators and central nervous system symptoms. They found that the mean OEF values of the thalamus, caudate nucleus, putamen, globus pallidus, and substantia nigra of PE patients were significantly higher than those of healthy pregnant women and non-pregnant healthy women (Yang et al., 2022), which may be due to a compensatory mechanism to overcome severe hypoxia and maintain cerebral oxygen metabolism. The significant changes in cerebral OEF values of pregnant women can be measured by non-invasive MRI-based OEF mapping to determine their cerebral oxygen metabolic status, which can become an important diagnostic basis for timely clinical intervention, thus providing theoretical support for the effective prevention of RPLS.

Functional magnetic resonance imaging (fMRI) is a class of imaging methods developed to demonstrate regional, time-varying changes in brain metabolism. The popularity of fMRI derives from its widespread availability, non-invasive nature, relatively low cost, and good spatial resolution. Increasingly, fMRI is being used as a biomarker for disease, to monitor therapy, or for studying pharmacologic efficacy. With the rapid development of medical imaging technology, some other functional MRI technologies have gradually emerged, including structural magnetic resonance imaging, diffusion tensor imaging, diffusion kurtosis imaging, resting-state functional connectivity MRI, and neurite orientation dispersion and density imaging. However, fMRI has some limitations, such as, resolution in fMRI is limited primarily by SNR because of the necessity for rapid acquisition of time series information, besides, temporal resolution is also affected by hemodynamic response time (Glover, 2011). In a word, although these emerging technologies have not been widely used in routine imaging examinations of RPLS patients, we believed that they will have increasingly more applications in the imaging diagnosis of RPLS as they become more developed.

In summary, although the pathophysiological mechanism of RPLS is still unclear, it is certain that most RPLS cases are reversible after timely and effective diagnosis and treatment. If the disease is allowed to progress, it can cause irreversible neurological damage and severe sequelae. Therefore, timely brain CT or MRI examinations for RPLS patients is particularly important for the early detection and diagnosis of RPLS lesions. Notably, multimodal brain MRI can facilitate the comprehensive evaluation of the degree of brain damage in RPLS patients, provide a theoretical basis for clinical diagnosis and treatment, and help monitor disease progression, improve prognosis, and protect maternal and fetal health.

Author contributions

NZ and LY wrote the main manuscript text. AH, YW, and GZ collected and organized literatures. TC and YYW revised the manuscript text. All authors reviewed the manuscript and approved the submitted version.

Funding

This work was supported by grants from the Technology Development Plan of Jinan (202134072 and 202225035), the Science and Technology Project of Jinan Municipal Health Commission (2021-2-89 and 2021-2-93), and the Special Fund for Scientific and Technological Innovation of Shandong Maternal and Child Health Care Commission (Lu Fu You Xie Fa 2021-19).

Conflict of interest

The authors declare that the research was conducted in the absence of any commercial or financial relationships that could be construed as a potential conflict of interest.

Publisher's note

References

Ananth, C. V., Keyes, K. M., and Wapner, R. J. (2013). Pre-eclampsia rates in the United States, 1980-2010: Age-period-cohort analysis. *BMJ* 347:f6564. doi: 10.1136/bmj.f6564

Bartynski, W. S., Boardman, J. F., Zeigler, Z. R., Shadduck, R., and Lister, J. (2006). Posterior reversible encephalopathy syndrome in infection, sepsis, and shock. *AJNR Am. J. Neuroradiol.* 27, 2179–2190.

Burnett, M. M., Hess, C. P., Roberts, J. P., Bass, N., Douglas, V., and Josephson, S. (2010). Presentation of reversible posterior leukoencephalopathy syndrome in patients on calcineurin inhibitors. *Clin. Neurol. Neurosurg.* 112, 886–891. doi: 10.1016/j.clineuro.2010.07.023

Covarrubias, D. J., Luetmer, P. H., and Campeau, N. G. (2002). Posterior reversible encephalopathy syndrome: Prognostic utility of quantitative diffusion-weighted MR images. *AJNR Am. J. Neuroradiol.* 23, 1038–1048.

Damak, R., Ketata, S., Derbel, R., Grati, F., Ghorbel, S., Zouche, I., et al. (2022). Posterior reversible encephalopathy syndrome in patients with preeclampsia: Case report. *Pan. Afr. Med. J.* 43:1. doi: 10.11604/pamj.2022.43.1.33548

Demirtaş, O., Gelal, F., Vidinli, B. D., Demirtaş, L., Uluç, E., and Baloğlu, A. (2005). Cranial MR imaging with clinical correlation in preeclampsia and eclampsia. *Diagn. Interv. Radiol.* 11, 189–194.

Eichler, F. S., Wang, P., Wityk, R. J., Beauchamp, N. Jr., and Barker, P. (2002). Diffuse metabolic abnormalities in reversible posterior leukoencephalopathy syndrome. *AJNR Am. J. Neuroradiol.* 23, 833–837.

Fa'ak, F., Al-Bahadili, H., Shah, N., and Julka, K. (2021). Posterior reversible encephalopathy syndrome induced by scleroderma renal crisis in a patient with undiagnosed scleroderma. *J. Clin. Rheumatol.* 27, S825–S826. doi: 10.1097/RHU.0000000000001435

Fischer, M., and Schmutzhard, E. (2017). Posterior reversible encephalopathy syndrome. *J. Neurol.* 264, 1608–1616. doi: 10.1007/s00415-016-8377-8

Fishel Bartal, M., and Sibai, B. (2022). Eclampsia in the 21st century. *Am. J. Obstet. Gynecol.* 226, S1237–S1253. doi: 10.1016/j.ajog.2020.09.037

Fugate, J. E., and Rabinstein, A. A. (2015). Posterior reversible encephalopathy syndrome: Clinical and radiological manifestations, pathophysiology, and outstanding questions. *Lancet Neurol.* 14, 914–925. doi: 10.1016/S1474-4422(15)00111-8

Fugate, J. E., Claassen, D. O., Cloft, H. J., Kallmes, D., Kozak, O., and Rabinstein, A. (2010). Posterior reversible encephalopathy syndrome: Associated clinical and radiologic findings. *Mayo Clin. Proc.* 85, 427–432. doi: 10.4065/mcp.2009.0590

Gao, B., Yu, B. X., Li, R. S., Zhang, G., Xie, H., Liu, F., et al. (2015). Cytotoxic edema in posterior reversible encephalopathy syndrome: Correlation of MRI features with serum albumin levels. *AJNR Am. J. Neuroradiol.* 36, 1884–1889. doi: 10.3174/ajnr.A4379

Glover, G. (2011). Overview of functional magnetic resonance imaging. *Neurosurg. Clin. N. Am.* 22, 133–139. doi: 10.1016/j.nec.2010.11.001

Hawkes, M., Hajeb, M., and Rabinstein, A. (2022). Perfusion deficits in patients with posterior reversible encephalopathy syndrome: A retrospective, two-center study. *Neurocrit. Care* [Epub ahead of print]. doi: 10.1007/s12028-022-01642-9

Hefzy, H. M., Bartynski, W. S., Boardman, J. F., and Lacomis, D. (2009). Hemorrhage in posterior reversible encephalopathy syndrome: Imaging and clinical features. *AJNR Am. J. Neuroradiol.* 30, 1371–9. doi: 10.3174/ajnr.A1588

Hinchey, J., Chaves, C., Appignani, B., Breen, J., Pao, L., Wang, A., et al. (1996). A reversible posterior leukoencephalopathy syndrome. *N. Engl. J. Med.* 334, 494–500. doi: 10.1056/NEJM199602223340803

Junewar, V., Verma, R., Sankhwar, P. L., Garg, R., Singh, M., Malhotra, H., et al. (2014). Neuroimaging features and predictors of outcome in eclamptic encephalopathy: A prospective observational study. *AJNR Am. J. Neuroradiol.* 35, 1728–1734. doi: 10.3174/ajnr.A3923

Karia, S., Rykken, J., McKinney, Z., Zhang, L., and McKinney, A. (2016). Utility and significance of gadolinium-based contrast enhancement in posterior reversible encephalopathy syndrome. *AJNR Am. J. Neuroradiol.* 37, 415–22. doi: 10.3174/ajnr.A4563

Kastrup, O., Schlamann, M., Moenninghoff, C., Forsting, M., and Goericke, S. (2015). Posterior reversible encephalopathy syndrome: The spectrum of MR imaging patterns. *Clin. Neuroradiol.* 25, 161–171. doi: 10.1007/s00062-014-0293-7

Li, Y., Song, J., Huq, A., Timilsina, S., and Gershwin, M. (2023). Posterior reversible encephalopathy syndrome and autoimmunity. *Autoimmun. Rev.* 22:103239. doi: 10.1016/j.autrev.2022.103239

Liman, T. G., Bohner, G., Endres, M., and Siebert, E. (2014). Discharge status and in-hospital mortality in posterior reversible encephalopathy syndrome. *Acta Neurol. Scand.* 130, 34–39. doi: 10.1111/ane.12213

Mckinney, A. M., Sarikaya, B., Gustafson, C., and Truwit, C. (2012). Detection of microhemorrhage in posterior reversible encephalopathy syndrome using susceptibility-weighted imaging. *AJNR Am. J. Neuroradiol.* 33, 896–903. doi: 10.3174/ajnr.A2886

Murali, S., Miller, K., and McDermott, M. (2020). Preeclampsia, eclampsia, and posterior reversible encephalopathy syndrome. *Handb. Clin. Neurol.* 172, 63–77. doi: 10.1016/B978-0-444-64240-0.00004-0

Nelander, M., Hannsberger, D., Sundström-Poromaa, I., Bergman, L., Weis, J., Åkerud, H., et al. (2018). Assessment of cerebral perfusion and edema in preeclampsia with intravoxel incoherent motion MRI. *Acta Obstet. Gynecol. Scand.* 97, 1212–1218. doi: 10.1111/aogs.13383

Parasher, A., and Jhamb, R. (2020). Posterior reversible encephalopathy syndrome (PRES): Presentation, diagnosis and treatment. *Postgrad. Med. J.* 96, 623–628. doi: 10.1136/postgradmedj-2020-137706

Rabinstein, A. A., Mandrekar, J., Merrell, R., Kozak, O., Durosaro, O., and Fugate, J. (2012). Blood pressure fluctuations in posterior reversible encephalopathy syndrome. *J. Stroke Cerebrovasc. Dis.* 21, 254–258. doi: 10.1016/j.jstrokecerebrovasdis.2011.03.011

Shankar, J., and Banfield, J. (2017). Posterior reversible encephalopathy syndrome: A review. *Can. Assoc. Radiol. J.* 68, 147–153. doi: 10.1016/j.carj.2016.08.005

Sharma, A., Whitesell, R. T., and Moran, K. J. (2010). Imaging pattern of intracranial hemorrhage in the setting of posterior reversible encephalopathy syndrome. *Neuroradiology* 52, 855–863. doi: 10.1007/s00234-009-0632-6

Sheikh-Bahaei, N., Acharya, J., Rajamohan, A., and Kim, P. (2020). Advanced imaging techniques in diagnosis of posterior reversible encephalopathy syndrome (PRES). *Front. Neurol.* 11:165. doi: 10.3389/fneur.2020.00165

Singhal, A. (2021). Posterior reversible encephalopathy syndrome and reversible cerebral vasoconstriction syndrome as syndromes of cerebrovascular dysregulation. *Continuum* 27, 1301–1320. doi: 10.1212/CON.0000000000001037

Sundin, C., and Johnson, M. (2018). Posterior reversible encephalopathy syndrome. *MCN Am. J. Matern. Child Nurs.* 43, 77–82. doi: 10.1097/NMC.0000000000000409

Tlemsani, C., Mir, O., Boudou-Rouquette, P., Huillard, O., Maley, K., Ropert, S., et al. (2011). Posterior reversible encephalopathy syndrome induced by anti-VEGF agents. *Target Oncol.* 6, 253–258. doi: 10.1007/s11523-011-0201-x

Triplett, J., Kutlubaev, M., Kermode, A., and Hardy, T. (2022). Posterior reversible encephalopathy syndrome (PRES): Diagnosis and management. *Pract. Neurol.* 22, 183–189. doi: 10.1136/practneurol-2021-003194

Umar, T., Gilani, A., Tasnim, A., Yousaf, M. A., Umar, S., Mehboob, A., et al. (2022). MRI changes among patients of eclampsia and preeclampsia with associated neurological symptom analysis. *J. Ayub Med. Coll. Abbottabad.* 34, 269–272. doi: 10.55519/JAMC-02-8478

Virojtriratana, T., Hongsawong, N., Wiwattanadittakul, N., Katanyuwong, K., Chartapisak, W., and Sanguansermsri, C. (2022). Comparison of clinical manifestations, laboratory, neuroimaging findings, and outcomes in children with posterior reversible encephalopathy syndrome (PRES) in children with and without renal disease. *Pediatr. Neurol.* 134, 37–44. doi: 10.1016/j.pediatrneurol.2022.06.012

Wenger, N. K., Arnold, A., Bairey Merz, C. N., Cooper-DeHoff, R., Ferdinand, K., Fleg, J., et al. (2018). Hypertension across a woman's life cycle. *J. Am. Coll. Cardiol.* 71, 1797–1813. doi: 10.1016/j.jacc.2018.02.033

Yang, L., Cho, J., Chen, T., Gillen, K., Li, J., Zhang, Q., et al. (2022). Oxygen extraction fraction (OEF) assesses cerebral oxygen metabolism of deep gray matter in patients with pre-eclampsia. *Eur. Radiol.* 32, 6058–6069. doi: 10.1007/s00330-022-08713-7

Yilmaz, S., Gokben, S., Arikan, C., Calli, C., and Serdaroglu, G. (2010). Reversibility of cytotoxic edema in tacrolimus leukoencephalopathy. *Pediatr. Neurol.* 43, 359–362. doi: 10.1016/j.pediatrneurol.2010.05.021

Yuan, J., Wang, S., Guo, X., Ding, L., Gu, H., and Hu, W. (2016). Reduction of NAA/Cr ratio in a patient with reversible posterior leukoencephalopathy syndrome using MR spectroscopy. *Arch. Med. Sci. Atheroscler. Dis.* 1, e98–e100. doi: 10.5114/amsad.2016.62376

frontiers | Frontiers in Neuroscience

TYPE Original Research
PUBLISHED 03 May 2023
DOI 10.3389/fnins.2023.1152161

OPEN ACCESS

EDITED BY
Lingfei Guo,
Shandong Provincial Hospital, China

REVIEWED BY
Zan Wang,
Southeast University, China
Ni Shu,
Beijing Normal University, China

*CORRESPONDENCE
Guolin Ma
maguolin1007@qq.com
Hong Tian
tianhong5185@126.com

†These authors share first authorship

SPECIALTY SECTION
This article was submitted to Brain Imaging Methods, a section of the journal Frontiers in Neuroscience

RECEIVED 27 January 2023
ACCEPTED 22 March 2023
PUBLISHED 03 May 2023

CITATION
Yang A, Liu B, Lv K, Luan J, Hu P, Yu H, Shmuel A, Li S, Tian H, Ma G and Zhang B (2023) Altered coupling of resting-state cerebral blood flow and functional connectivity in Meige syndrome. *Front. Neurosci.* 17:1152161. doi: 10.3389/fnins.2023.1152161

Altered coupling of resting-state cerebral blood flow and functional connectivity in Meige syndrome

Aocai Yang[1,2†], Bing Liu[1,2†], Kuan Lv[1,3†], Jixin Luan[1,2], Pianpian Hu[1,3], Hongwei Yu[1], Amir Shmuel[4,5], Shijun Li[6], Hong Tian[7*], Guolin Ma[1,2*] and Bing Zhang[8]

[1]Department of Radiology, China-Japan Friendship Hospital, Beijing, China, [2]Graduate School of Peking Union Medical College, Chinese Academy of Medical Sciences and Peking Union Medical College, Beijing, China, [3]Peking University China-Japan Friendship School of Clinical Medicine, Beijing, China, [4]McConnell Brain Imaging Centre, Montreal Neurological Institute, McGill University, Montreal, QC, Canada, [5]Departments of Neurology and Neurosurgery, Physiology, and Biomedical Engineering, McGill University, Montreal, QC, Canada, [6]Department of Radiology, First Medical Center of Chinese PLA General Hospital, Beijing, China, [7]Department of Neurosurgery, China-Japan Friendship Hospital, Beijing, China, [8]Department of Radiology, The Affiliated Drum Tower Hospital of Nanjing University Medical School, Beijing, China

Introduction: Meige syndrome (MS) is an adult-onset segmental dystonia disease, mainly manifested as blepharospasm and involuntary movement caused by dystonic dysfunction of the oromandibular muscles. The changes of brain activity, perfusion and neurovascular coupling in patients with Meige syndrome are hitherto unknown.

Methods: Twenty-five MS patients and thirty age- and sex-matched healthy controls (HC) were prospectively recruited in this study. All the participants underwent resting-state arterial spin labeling and blood oxygen level-dependent examinations on a 3.0 T MR scanner. The measurement of neurovascular coupling was calculated using cerebral blood flow (CBF)-functional connectivity strength (FCS) correlations across the voxels of whole gray matter. Also, voxel-wised analyses of CBF, FCS, and CBF/FCS ratio images between MS and HC were conducted. Additionally, CBF and FCS values were compared between these two groups in selected motion-related brain regions.

Results: MS patients showed increased whole gray matter CBF-FCS coupling relative to HC (t = 2.262, p = 0.028). In addition, MS patients showed significantly increased CBF value in middle frontal gyrus and bilateral precentral gyrus.

Conclusion: The abnormal elevated neurovascular coupling of MS may indicate a compensated blood perfusion in motor-related brain regions and reorganized the balance between neuronal activity and brain blood supply. Our results provide a new insight into the neural mechanism underlying MS from the perspective of neurovascular coupling and cerebral perfusion.

KEYWORDS

Meige syndrome, arterial spin labeling, cerebral blood flow, functional magnetic resonance imaging, functional connectivity strength

1. Introduction

Meige syndrome (MS), also known as blepharospasm-oromandibular dystonia, was first described and named in 1910 by French neurologist Henry Meige (Juvarra et al., 1981). MS is an idiopathic segmental craniocervical dystonia disease. The age range of the patients is approximately about 30 to 70 years old (Sabesan, 2008). The prevalence rate in males is higher than females and the ratio of males to females is in the range of 1:2 to 1:3 (Pandey and Sharma, 2017). The course of the disease is varied, and eventually manifests as blepharospasm or with oromandibular dystonic motor symptoms (Zalyalova, 2015). To date, the pathogenesis and etiology of MS is not fully understood. Experts opinions are divided, with some suggesting that the basal ganglia is dysfunctional (Tanner et al., 1982), and others suggesting that the lack of inhibition at various levels in the central nervous system results in hyperactivity in patients (Prescott et al., 2013). Such abnormal changes in inhibitory ability can occur in the brain stem, spinal cord, basal ganglia, and cerebral cortex.

Using conventional head magnetic resonance imaging (MRI), it is difficult to detect abnormal brain changes in MS patients; however, advanced MRI technologies such as blood-oxygen-level dependent (BOLD) functional MRI (fMRI) and arterial spin labeling (ASL) MRI may provide important pathophysiological information for understanding the MS. Previous studies of fMRI found that MS patients exhibited altered functional connectivity (FC) at rest in widespread brain regions including basal ganglia, cerebellar, primary/secondary sensorimotor, and visual areas (Baker et al., 2003; Jochim et al., 2018). Cerebral blood flow (CBF) in the resting-state reflects a basic perfusion in the brain. It tightly correlates with the normal function, glucose metabolism and oxygen consumption of the brain, which is a crucially biomarker for indicating cerebral metabolic level. ASL is a non-invasive MR technique that can measure CBF by using endogenous water spins as the tracer without using an exogenous contrast agent (Su et al., 2017). In the normal state, spontaneous brain activity is the cause of the larger part of cerebral energy metabolism. Prior studies combined resting-state BOLD and ASL to explore the relationship between CBF and FC, and found that CBF is tightly associated with FC strength (FCS) in normal state (Liang et al., 2013). Changes in CBF-FCS coupling were found in healthy aging (Galiano et al., 2020). In addition, altered CBF-FCS coupling has been reported in several different diseases, such as generalized anxiety disorder, Wilson's disease primary open angle glaucoma and schizophrenia (Zhu et al., 2017; Hu et al., 2019; Chen et al., 2021; Wang et al., 2021). According to the validated neurovascular coupling theory, hub regions with higher spontaneous brain activity and FCS are associated with greater demand for cerebral perfusion (Kuschinsky, 1991; Venkat et al., 2016). However, to date, using ASL technology to explore changes in CBF in patients with Meige syndrome has not been reported. Therefore, we hypothesized that neurovascular coupling may change in MS and can be indirectly detected by the correlation analysis of CBF-FCS.

Thus, in this study, we firstly investigated the CBF-FCS correlation coefficient across voxels, and conducted the voxel-wise analyses of CBF/FCS ratio, CBF, and FCS in MS patients and healthy control subjects (HC). Additionally, we evaluated the abnormalities of CBF and FCS in motor-related brain regions in MS. We explored a new neuroimaging biomarker of MS and provided some new insights and evidence into the pathogenesis of this disease.

2. Materials and methods

2.1. Subjects

The ethics committee of China-Japan Friendship Hospital has approved this study, and the signed informed consents were obtained from all participants.

Twenty-seven MS patients were prospectively recruited during their inpatient stay in the Department of Neurosurgery at China-Japan Friendship Hospital from September 2020 to January 2022. The inclusion criteria of MS patients were as follows: (a) All patients were diagnosed with primary Meige syndrome by one experienced senior neurosurgeon based on standard clinical criteria (Pakkenberg et al., 1987; Pandey and Sharma, 2017); (b) No abnormal brain changes in conventional MRI examination; (c) No treatment within the past 3 months; (d) Right-handed; and (e) The MRI images are complete and no artifacts. Exclusion criteria of MS patients were as follows: (a) Brain organic diseases; (b) Neuropsychiatric diseases; (c) Severe history of lung, heart, liver and kidney diseases; (d) MRI contraindications; and (e) Other dystonic disorders other than MS. Healthy controls (HC) were recruited from the local communities. The inclusion conditions of HC were as follows: (a) No psychoses and neurological diseases; (b) No abnormal brain lesions in conventional MRI examination; (c) Neurological tests were normal; (d) Right-handed; and (e) The MR images are complete and show no artifacts. All patients with MS underwent Burke-Fahn-Marsden dystonia rating scale-movement (BFMDRS-M) and blepharospasm disability index (BSDI) scale (Jankovic et al., 2009) to assess disease severity. All participants received conventional head MRI, resting-state BOLD and 3D-PCASL MR examinations. Two MS patients were excluded because of image artifacts. Twenty-five MS patients and thirty healthy controls were finally included in this study.

2.2. MRI data acquisition

Magnetic resonance examinations were conducted on a 3.0 T MR scanner (Discovery MR750 scanner; GE Medical Systems, USA) with eight-channel head coils. The scanning protocol included three dimensional pseudo-continuous ASL (3D-PCASL) sequence for perfusion imaging, single-shot gradient recalled echo-planar imaging (GRE-SS-EPI) sequence for resting-state BOLD images, three-dimensional fast spoiled gradient-echo (3D FSPGR) sequence for T1-weighted anatomical images. Acquisition parameters were as follows: (1) 3D-PCASL: repetition time (TR) = 4817 ms, echo time (TE) = 14.6 ms, slice thickness = 4 mm, post-label delay = 1525 ms, field of view (FOV) = 240 mm × 240 mm, bandwidth = 62.5 Hz/pixel; (2) GRE-SS-EPI: TR = 2000 ms, TE = 30 ms, flip angle = 90°, slice thickness = 3.5 mm, slice spacing = 0.7 mm, FOV = 224 mm × 224 mm, matrix = 64 × 64, NEX = 1, scanning time = 8 min, 240 time points; (3) 3D-FSPGR: TE = 2.9 ms, TR = 6.7 ms, flip

angle = 12°, bandwidth = 31.25 Hz/pixel, slice thickness = 1.0 mm, FOV = 256 mm × 256 mm.

During the scanning, all subjects were requested to relax, close their eyes, and remain as still as possible, not to think about anything and not to fall asleep. All raw image data were visually examined to exclude subjects with visible image artifacts.

2.3. Data processing and analysis

2.3.1. CBF processing

The CBF maps were calculated from the ASL data with Functools perfusion software in GE (General Electric Healthcare). In short, the CBF maps were derived from the ASL difference images and the proton density weighted reference images using a single compartment model after the subtraction of the label images from the control images (Buxton et al., 1998; Xu et al., 2010).

Individual CBF images in native space were directly co-registered to the perfusion template in SPM8[1] and spatially normalized to Montreal Neurological Institute (MNI) space. Normalized CBF maps were resampled into isotropic voxel size of 3 mm × 3 mm × 3 mm and the non-brain tissue were removed. Then, CBF maps were further standardized into z-scores (zCBF). Finally, the standardized CBF maps were spatially smoothed with a 6 mm × 6 mm × 6 mm full-width at half maximum (FWHM) Gaussian kernel.

2.3.2. fMRI data processing

The pre-processing of rs-fMRI data was conducted using a standard pipeline in DPABI (Yan et al., 2016). In short, the first ten volumes were removed, and then the remaining volumes were corrected for slice timing and head motion. Participants' data with more than 3°rotation and/or 3 mm translation of head motion were excluded. Then, several nuisance covariates were regressed out, including 24 Friston of head motion parameters, polynomial trend, the average global signal, and signals averaged over the white matter and cerebrospinal fluid. The datasets were bandpass filtered within 0.01−0.08 Hz frequency range. Individual T1-weighted anatomical images were co-registered to the corresponding mean fMRI images, and then segmented and non-linearly normalized into MNI space. Finally, filtered fMRI images were also spatially normalized into the MNI space using the above mentioned transformations and resampled into 3-mm cubic voxels.

We computed the "degree centrality" of each voxel by calculating the Pearson's correlation coefficients between the BOLD time courses of all pairs of voxels within the gray matter mask (Number of voxels = 67451). The threshold of positive FC was set to 0.2 in order to eliminate negative or false correlations from background noise (Liang et al., 2013; Zhu et al., 2017; Chen et al., 2021). The voxel-to-voxel FC lower than 0.2 was set to zero. The FCS maps were calculated by averaging the values of functional connectivity between a given voxel and all other voxels (Liang et al., 2013). Then, the FCS maps were standardized into z-scores (zFCS) and spatially smoothed with a 6-mm FWHM Gaussian kernel.

TABLE 1 Information about motor-related subregions.

ROIs	Anatomical descriptions	lh.MNI coordinates (X, Y, Z)	rh.MNI coordinates (X, Y, Z)
MFG_7_5	Ventrolateral area 8	−33, 23, 45	42, 27, 39
MFG_7_6	Ventrolateral area 6	−32, 4, 55	34, 8, 54
PrG_6_1	Area 4 (head and face region)	−49, −8, 39	55, −2, 33
PrG_6_2	Caudal dorsolateral area 6	−32, −9, 58	33, −7, 57
PrG_6_3	Area 4 (upper limb region)	−26, −25, 63	34, −19, 59
PrG_6_4	Area 4 (trunk region)	−13, −20, 73	15, −22, 71
PrG_6_5	Area 4 (tongue and larynx region)	−52, 0, 8	54, 4, 9
PrG_6_6	Caudal ventrolateral area 6	−49, 5, 30	51, 7, 30

ROIs, regions of interest; MFG, middle frontal gyrus; PrG, precentral gyrus; MNI, Montreal Neurological Institute; lh, left hemisphere; rh, right hemisphere.

2.3.3. CBF-FCS coupling analysis

The relationship between zCBF and zFCS was evaluated through the correlation analyses across voxels in each subject within the whole-cerebrum gray matter (Liang et al., 2013). According to prior studies (Liang et al., 2013; Zhu et al., 2017; Wang et al., 2021), the effective degree of freedom (df_{eff}) of correlation analyses across the voxels was much smaller than the number of voxels in gray matter mask, as each voxel may highly dependent on their neighboring voxels because of true physiological correlation and the previous pre-processing steps like spatial registration and smoothing. The the average spatial smoothness of our CBF and FCS maps was FWHMx × FWHMy × FWHMz = 6.26 mm × 7.63 mm × 8.43 mm estimated by "rp_Smoothest" in REST software,[2] which was much larger than the voxel size (3 mm × 3 mm × 3 mm). Therefore, the spatial correlation would be dominated by the spatial smoothness. Therefore, the df_{eff} of the CBF-FCS correlation coefficient was calculated based on following formulation:

$$df_{eff} = \frac{N}{(\mathrm{FWHMx} \times \mathrm{FWHMy} \times \mathrm{FWHMz})/v} - 2$$

Where v is the voxel size and N is the number of voxels (N = 67451). Then, we corrected the p-value of CBF-FCS correlation coefficient using the df_{eff}. Finally, the CBF-FCS correlation coefficient was obtained from each subject. We evaluated the group differences of CBF-FCS correlation coefficients between the MS patients and HC using Student's t-test. The corrected $p < 0.05$ was considered statistically significant.

2.3.4. Voxel-wise CBF/FCS ratio, CBF, and FCS analyses

The CBF/FCS ratio maps were generated to evaluate the cerebral blood supply per unit of functional connectivity strength

1 http://www.fil.ion.ucl.ac.uk/spm

2 http://www.restfmri.net/

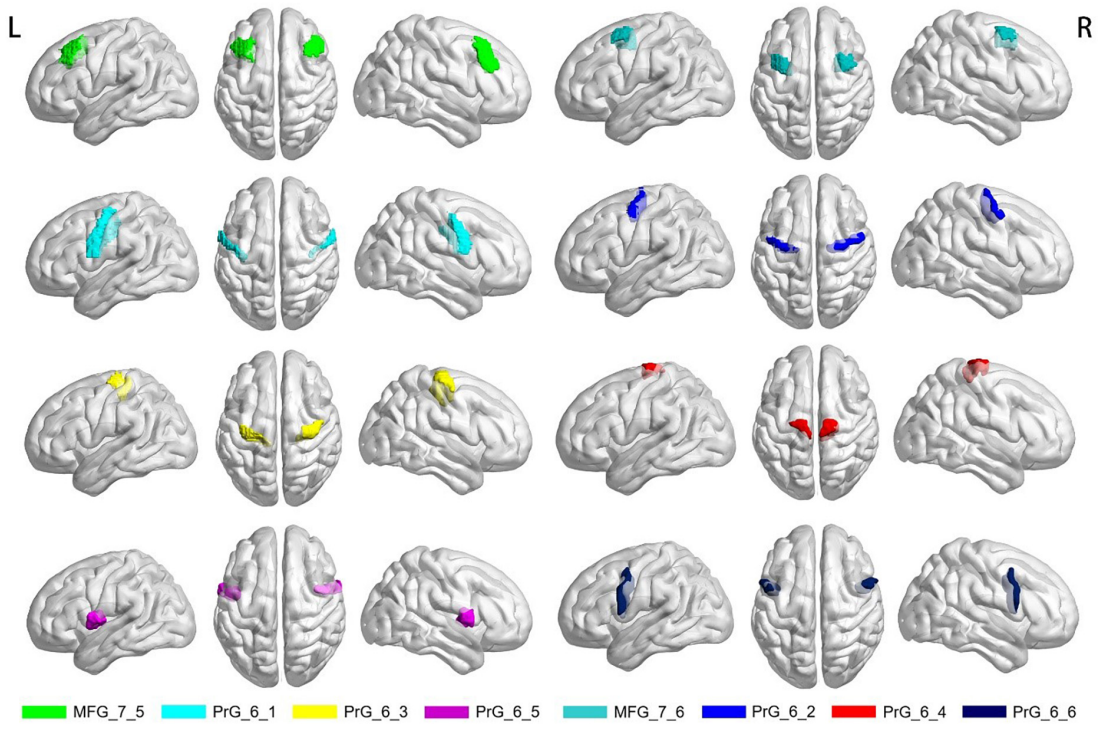

FIGURE 1
Selected motor-related subregions of interest. MFG, middle frontal gyrus; PrG, precentral gyrus; R, right; L, left.

for each voxel. The original CBF (ml/100 g/min) and FCS values were used to calculate CBF/FCS ratio and then transformed into z-scores (zCBF/FCS ratio). A general linear model was constructed for zCBF/FCS ratio in SPM8, with both age and sex were included as covariates. Whole-brain voxel-wised independent *t*-test was used for intergroup comparisons and false discovery rate (FDR) method (voxel level $p < 0.001$ and cluster level $p < 0.05$) was used for multiple comparisons correction. In addition, the differences of zCBF and zFCS between two groups at whole-brain voxel level were also explored using independent *t*-tests controlling for age and sex with FDR correction (voxel level $p < 0.001$ and cluster level $p < 0.05$).

2.3.5. ROI-based analysis of CBF and FCS in motor-related brain regions

Previous studies have found changes in neuronal activity in motor-related brain regions in MS patients. The ventrolateral premotor area (ventrolateral area 6), the ventrolateral frontal eye field (ventrolateral area 8) and the primary motor cortex (precentral gyrus) are the key cortical regions for motor function (Mayka et al., 2006). Based on the human Brainnetome Atlas that consists of 246 brain regions (BNA246),[3] we selected these significant motor-related areas as regions of interest (ROI) to analyze the changes of CBF and FCS in MS patients. The selected motor-related subregions are presented in Table 1 and Figure 1, including bilateral middle frontal gyrus (MFG, MFG_7_5∼6) and bilateral precentral gyrus (PrG, PrG_6_1∼6). As mentioned above, the mean zCBF and zFCS values of each subregion were automatically extracted. The group zCBF- and separately zFCS-values in each subregion were compared, to evaluate differences between MS and HC using Student's *t*-test. The FDR method was applied for multiple comparisons correction. A value of $q < 0.05$ was considered statistically significant.

2.4. Clinical data

Statistical analysis was performed on SPSS software (IBM SPSS 21.0). The Shapiro–Wilk test was used to assess the data normality. Independent *t*-tests were used for intergroup comparisons of age and educational level. Differences between groups of different sex were compared using the Chi-square (χ^2) test. A *p*-value less than 0.05 was considered statistically significant.

TABLE 2 Demographics and clinical characteristics.

	MS group (n = 25)	HC group (n = 30)	*p*-value
Age (years)	57.0 ± 9.5	61.2 ± 7.3	0.064
Gender (M/F)	5/20	10/20	0.269
Education (years)	8.8 ± 4.8	9.0 ± 4.1	0.872
Disease duration (month)	32.1 ± 28.3	NA	NA
BFMDRS-M	7.7 ± 2.7	NA	NA
BSDI	12.9 ± 5.0	NA	NA

Sequential variables are expressed as mean ± standard deviation. MS, Meige syndrome; HC, healthy control; BFMDRS-M, Burke-Fahn-Marsden dystonia rating scale movement; BSDI, blepharospasm disability index; NA, not applicable.

3 http://atlas.brainnetome.org

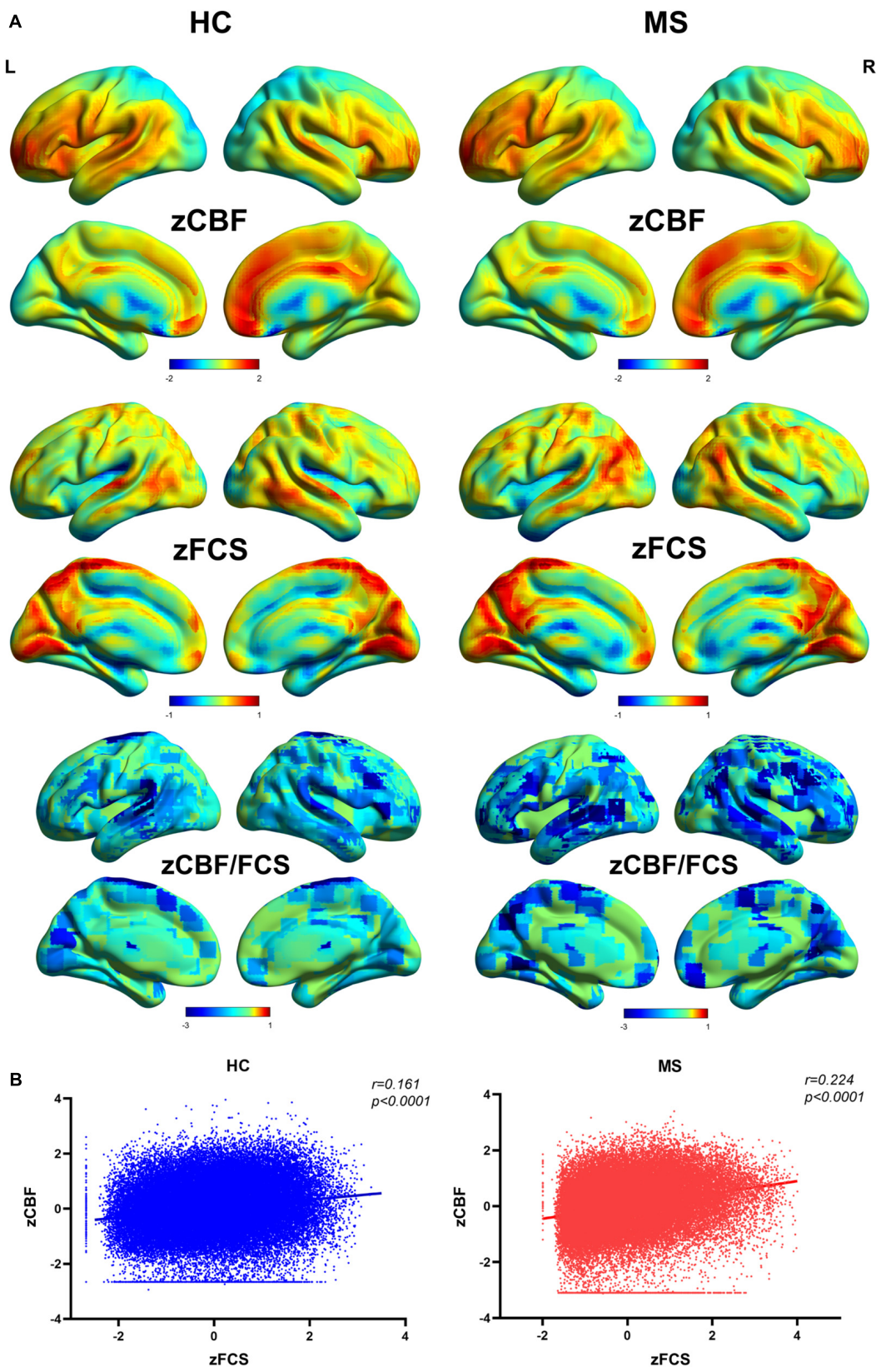

FIGURE 2
Spatial distribution patterns of FCS, CBF, and CBF/FCS ratio in Meige patients and healthy controls. **(A)** Standardized and averaged FCS, CBF and CBF/FCS ratio maps across each group subjects. **(B)** Scatter plots show a significant spatial correlation (computed over all voxels in the gray matter) between FCS and CBF. We represent data from a healthy participant and a Meige syndrome patient. MS, Meige syndrome; HC, healthy control; CBF, cerebral blood flow; FCS, functional connectivity strength; R, right; L, left.

3. Results

3.1. Demographic and clinical characteristics

Data from twenty-five MS patients and thirty age- and sex-matched HC were finally included in the analysis. Demographic characteristics and the scales of disease severity are presented in Table 2. BFMDRS-M scores and BSDI scores were used to assess the severity of dystonia in MS patients. There was no significant difference in sex, age and education between the MS and HC groups (all $P > 0.05$).

3.2. CBF-FCS coupling changes in MS patients

The distributional patterns of zCBF, zFCS, and zCBF/FCS ratio in MS and HC groups are shown in Figure 2A. The spatial distributions of zCBF, zFCS, and zCBF/FCS ratio were visually similar in MS to those in HC. True for both groups, brain regions – most of which within the most of which were within default mode network (DMN) and salience network (SN) – showed higher CBF and FCS values relative to those in other brain regions. These brain regions included the posterior and anterior cingulate gyrus, precuneus, cingulate cortex, medial and lateral frontal cortex, lateral parietal cortex and lateral temporal cortex. The CBF/FCS ratio was relatively higher in the parts of the medial prefrontal cortex, anterior cingulate cortex, sensorimotor cortex, and thalamus.

The MS patients showed a trend of increased global CBF (MS: 45.8 ± 13.4 ml/100 g/min; HC: 43.2 ± 9.6 ml/100 g/min; $t = 0.83$, $p = 0.410$) and global FCS (MS: 0.059 ± 0.021; HC: 0.051 ± 0.013; $t = 1.57$, $p = 0.122$) in comparison to HC. Evaluating the relationship between CBF and FCS across all voxels in the gray matter showed positive correlation in both MS and HC participants (Figure 2B). Compared with HC, the MS patients had a significantly higher CBF-FCS coupling ($t = 2.262$, $p = 0.028$) (Figure 3).

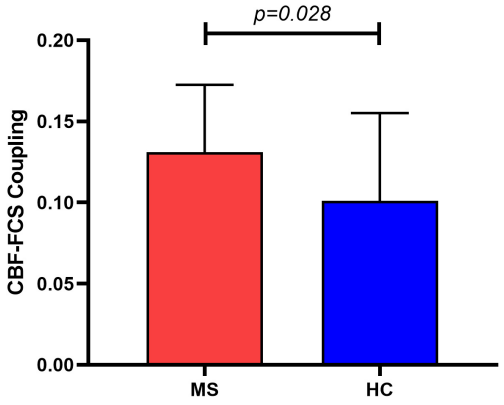

FIGURE 3
Group comparison of CBF-FCS coupling between Meige syndrome patients and healthy controls. MS patients showed increased CBF-FCS coupling relative to healthy controls. Data are shown as the mean ± std. MS, Meige syndrome; HC, healthy control; std, standard deviation.

3.3. Whole gray matter analyses of CBF/FCS ratio, CBF, and FCS in MS patients

Cerebral blood flow /FCS ratio, CBF and FCS maps did not show significant differences between MS and HC groups at voxel level following the FDR corrections.

3.4. CBF of motor-related brain regions changes in MS patients

Compared with HC, MS patients showed increased CBF values in MFG_R_7_5 (MS: 0.49 ± 0.25; HC: 0.33 ± 0.26; $t = 2.367$, $p = 0.022$), MFG_R_7_6 (MS: 0.23 ± 0.26; HC: −0.007 ± 0.28; $t = 3.199$, $p = 0.002$), PrG _6_2 (MS: 0.06 ± 0.24; HC: −0.10 ± 0.21; $t = 2.578$, $p = 0.013$), PrG _6_3 (MS: −0.007 ± 0.30; HC: −0.25 ± 0.22; $t = 3.544$, $p = 0.001$), and PrG _6_4 (MS: −0.12 ± 0.33; HC: −0.36 ± 0.24; $t = 3.126$, $p = 0.003$) following multiple comparisons correction. More detailed information is shown in Figure 4 and Table 3. However, patients with MS exhibited no significant differences in FCS in all selected motor-related ROIs in comparisons to HC.

4. Discussion

In this study, we evaluated the alterations of neurovascular coupling in MS with the combination of resting-state BOLD and ASL techniques. To the best of our knowledge, this is the first study to investigate the relationship between FCS and CBF in MS. Consistent with our hypotheses that neuronal activity or neurovascular coupling may reorganized in MS and CBF may change in motor-related region, our main findings are that: (i) CBF-FCS coupling was higher in MS than that in HC; and (ii) MS patients showed increased CBF value in several motor-related brain regions relative to healthy controls. These findings may provide information to better understand the neural pathophysiological mechanism in Meige syndrome from the perspective of neurovascular coupling.

In agreement with the previous study, we found that CBF and FCS are significantly correlated across the voxels of the gray matter in healthy participants (Liang et al., 2013). We also found significant CBF–FCS correlation in MS patients, however, the coupling strength in MS was higher than that in HC. The normal neurovascular coupling mechanism represents a complete structure of neurons, astrocytes and vascular components (Hawkins and Davis, 2005). According to the neurovascular coupling hypothesis, it can be inferred that changes in CBF are closely related to underlying neuronal activity (Wang et al., 2021). Brain regions with increased neuronal activity have higher metabolic demands and therefore require more perfusion (Venkat et al., 2016). At voxel level, FCS and separately, CBF/FCS ratio demonstrate no significant differences between MS and HC in any local regions. The CBF/FCS ratio depicts the amount of blood supply per

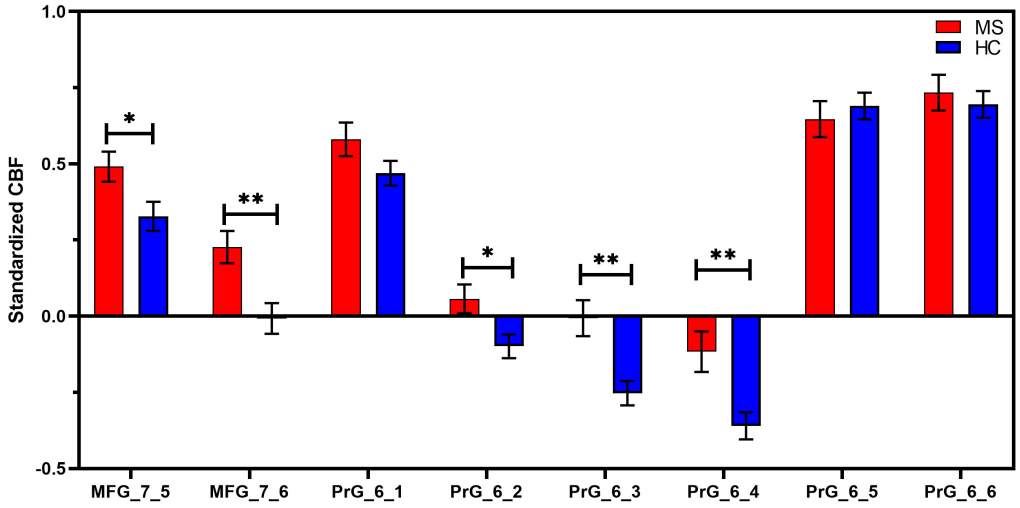

FIGURE 4
ROI-based CBF intergroup comparisons between Meige syndrome patients and healthy controls. In MFG_7_5, MFG_7_6, PrG_6_2, PrG_6_3, and PrG_6_4, standardized CBF values were significantly higher in MS than in HC (false discovery rate correction, $q < 0.05$). Data are shown as the mean ± SEM. *$P < 0.05$ (uncorrected), **$P < 0.01$ (uncorrected). MFG, middle frontal gyrus; PrG, precentral gyrus; MS, Meige syndrome; HC, healthy control; CBF, cerebral blood flow; SEM, standard error of mean.

unit of connectivity strength which reflects a balance between perfusion and neuro functional activity. Our results demonstrated that tighter neurovascular coupling in MS was constructed. Increased neurovascular coupling may attribute to the changes in the level of neurotransmitters such as dopamine, acetylcholine, norepinephrine and γ-aminobutyric acid (GABA) in MS (Hayashi et al., 1998; Yoshimura et al., 2001; Termsarasab et al., 2016), as these compounds may play a role in regulating neuronal metabolism and vascular responses (Cauli et al., 2004; Tayebati et al., 2011).

Patients with MS have increased CBF values in the primary motor cortex, ventrolateral premotor cortex and ventrolateral frontal eye field, which are mainly involved in abnormal motor executive control and sensorimotor guidance. Compared with isolated blepharospasm patients and normal subjects, patients with Meige syndrome showed abnormal activation of the primary motor cortex and ventral premotor cortex in the oral presentation area (Dresel et al., 2006). Several analyses of resting-state FC in MS patients found that reduced connectivity between the cingulate cortex and the primary sensorimotor/premotor and parietal association cortex, between premotor areas and the primary somatosensory cortex, and between the post-central gyrus and temporoparietal and secondary somatosensory regions (Huang et al., 2017; Jochim et al., 2018). A different study reported increased global FC in the right postcentral gyrus/precentral gyrus/paracentral lobule, right superior frontal gyrus, and left paracentral lobule/supplement motor area (Pan et al., 2021). Positron emission tomography of patients with blepharospasm Meige syndrome showed abnormal activation pattern in the auxiliary motor cortex, which indirectly reflected the abnormal sensory processing phenomenon in the auxiliary motor cortex during the performance of vibration and touch stimulation (Feiwell et al., 1999). These demonstrated that altered brain functional activity in MS patients involved a wide range of brain regions including primary/secondary sensorimotor and auxiliary motor areas, which indirectly indicated a tendency for motor inhibition and sensorimotor integration deficits. However, FCS in this study showed no significant differences between MS and HC in motor-related regions or at the whole-brain voxel level. FCS reflected the functional connectivity of each voxel with all other voxels in the gray matter. One possible explanation of our results is that the reorganization of brain function may need a compensatory supplement of blood to provide more energy and keep the normal functional activity, and our MS patients may be at such a compensatory stage. So, the CBF was elevated, but FCS did not massively change. Another possible explanation is that at the early stage of MS, the brain structures including astrocytes and neurons are not damaged significantly, and therefore no alteration of functional activity takes place. However, the microvasculature alterations may regulate CBF in brain motor regions.

TABLE 3 Results of ROI-based analysis of intergroup differences in standardized CBF.

Brian regions	Standardized CBF value		*t*-value	*p*-value
	MS group	HC group		
MFG _7_5	0.49 ± 0.25	0.33 ± 0.26	2.367	**0.022**
MFG _7_6	0.23 ± 0.26	−0.007 ± 0.28	3.199	**0.002**
PrG _6_1	0.58 ± 0.28	0.47 ± 0.22	1.659	0.103
PrG _6_2	0.06 ± 0.24	−0.10 ± 0.21	2.578	**0.013**
PrG _6_3	−0.007 ± 0.30	−0.25 ± 0.22	3.544	**0.001**
PrG _6_4	−0.12 ± 0.33	−0.36 ± 0.24	3.126	**0.003**
PrG _6_5	0.65 ± 0.29	0.69 ± 0.24	−0.596	0.554
PrG _6_6	0.73 ± 0.29	0.70 ± 0.24	0.536	0.594

Data are expressed as mean ± standard deviation. *P*-values in the table represent the original value without correction. False discovery rate corrected *q*-values < 0.05 are presented in bold. MS, Meige syndrome; HC, healthy control; MFG, middle frontal gyrus; PrG, precentral gyrus.

5. Limitations

This study also has several limitations. First, the number of subjects is small sample size, which may reduce the statistical effect of group analysis. In future study, we will enlarge the number of participants to further explore the changes of CBF in MS. Second, this study only collected ASL data for one post-label delay, and we will consider collecting ASL data for multiple PLDs in the future. Third, the CBF–FCS correlation was indirect evaluation of neurovascular coupling, and cannot allow us to uncover an accurate pathophysiological mechanism of our findings. Also, we need to use other functional indexes, like ALFF and ReHo, in future study. Fourth, in this study, only the motion-related brain regions that we consider to be meaningful were selected for research, and thus other unselected motor regions can be explored in future researches. Finally, we used a cross-section study design to reveal the alterations in cerebral blood flow, follow-up of longitudinal studies would help us better understand the underlying neural mechanisms of these changes at different disease stages of Meige syndrome.

6. Conclusion

In conclusion, patients with Meige syndrome showed altered coupling between resting-state CBF and FCS. Moreover, MS is associated with abnormal CBF increase in motor-related brain areas in MS. Our results provide a new insight into neural mechanism in MS from the perspective of neurovascular coupling and cerebral perfusion.

Data availability statement

The original contributions presented in this study are included in the article/supplementary material, further inquiries can be directed to the corresponding authors.

Ethics statement

The studies involving human participants were reviewed and approved by the Ethics Committee of China-Japan Friendship Hospital. The patients/participants provided their written informed consent to participate in this study.

Author contributions

AY, BL, and KL analyzed and explained the data and drafted and revised the manuscript. GM, HT, SL, and BZ designed the study. GM, HT, SL, BZ, and AS critically revised the manuscript. JL, HY, and AY performed the MRI scanning and evaluated the image quality. PH and KL pursued the literature search and review. All authors approved the final manuscript.

Funding

This study was supported by the National Key Research and Development Program of China (Grant No. 2020YFC2003903), the Capital's Funds for Health Improvement and Research (Grant Nos. 2020-2-4061 and 2022-1-2031), the National Natural Science Foundation of China (Grant Nos. 81971585 and 82271953), the STI2030-Major Projects (Grant No. 2022ZD0213300), and Guangzhou Science and Technology Planning Project (Grant No. 202103010001).

Acknowledgments

We thank all participants who were involved in this study. Special thanks to Dr. Zeshan Yao (AnImage Technology Co., Ltd., Beijing, China), who helped to solve MR technical problems and polish the language of the manuscript.

Conflict of interest

The authors declare that the research was conducted in the absence of any commercial or financial relationships that could be construed as a potential conflict of interest.

The reviewer NS declared a past co-authorship with the author GM to the handling editor.

Publisher's note

References

Baker, R. S., Andersen, A. H., Morecraft, R. J., and Smith, C. D. (2003). A functional magnetic resonance imaging study in patients with benign essential blepharospasm. *J. Neuroophthalmol.* 23, 11–15. doi: 10.1097/00041327-200303000-00003

Buxton, R. B., Frank, L. R., Wong, E. C., Siewert, B., Warach, S., and Edelman, R. R. (1998). A general kinetic model for quantitative perfusion imaging with arterial spin labeling. *Magn. Reson. Med.* 40, 383–396. doi: 10.1002/mrm.1910400308

Cauli, B., Tong, X. K., Rancillac, A., Serluca, N., Lambolez, B., Rossier, J., et al. (2004). Cortical GABA interneurons in neurovascular coupling: relays for subcortical vasoactive pathways. *J. Neurosci.* 24, 8940–8949. doi: 10.1523/jneurosci.3065-04.2004

Chen, Y., Cui, Q., Sheng, W., Tang, Q., Lu, F., Pang, Y., et al. (2021). Anomalous neurovascular coupling in patients with generalized anxiety disorder evaluated by combining cerebral blood flow and functional connectivity strength. *Prog. Neuropsychopharmacol. Biol. Psychiatry* 111:110379. doi: 10.1016/j.pnpbp.2021.110379

Dresel, C., Haslinger, B., Castrop, F., Wohlschlaeger, A. M., and Ceballos-Baumann, A. O. (2006). Silent event-related fMRI reveals deficient motor and enhanced somatosensory activation in orofacial dystonia. *Brain* 129(Pt 1), 36–46. doi: 10.1093/brain/awh665

Feiwell, R. J., Black, K. J., McGee-Minnich, L. A., Snyder, A. Z., MacLeod, A. M., and Perlmutter, J. S. (1999). Diminished regional cerebral blood flow response to vibration in patients with blepharospasm. *Neurology* 52, 291–297. doi: 10.1212/wnl.52.2.291

Galiano, A., Mengual, E., García de Eulate, R., Galdeano, I., Vidorreta, M., Recio, M., et al. (2020). Coupling of cerebral blood flow and functional connectivity is decreased in healthy aging. *Brain Imaging Behav.* 14, 436–450. doi: 10.1007/s11682-019-00157-w

Hawkins, B. T., and Davis, T. P. (2005). The blood-brain barrier/neurovascular unit in health and disease. *Pharmacol. Rev.* 57, 173–185. doi: 10.1124/pr.57.2.4

Hayashi, T., Furutani, M., Taniyama, J., Kiyasu, M., Hikasa, S., Horiguchi, J., et al. (1998). Neuroleptic-induced Meige's syndrome following akathisia: pharmacologic characteristics. *Psychiatry Clin. Neurosci.* 52, 445–448. doi: 10.1046/j.1440-1819.1998.00408.x

Hu, S., Wu, H., Xu, C., Wang, A., Wang, Y., Shen, T., et al. (2019). Aberrant Coupling between resting-state cerebral blood flow and functional connectivity in Wilson's disease. *Front. Neural Circ.* 13:25. doi: 10.3389/fncir.2019.00025

Huang, X. F., Zhu, M. R., Shan, P., Pei, C. H., Liang, Z. H., Zhou, H. L., et al. (2017). Multiple neural networks malfunction in primary blepharospasm: an independent components analysis. *Front. Hum. Neurosci.* 11:235. doi: 10.3389/fnhum.2017.00235

Jankovic, J., Kenney, C., Grafe, S., Goertelmeyer, R., and Comes, G. (2009). Relationship between various clinical outcome assessments in patients with blepharospasm. *Mov. Disord.* 24, 407–413. doi: 10.1002/mds.22368

Jochim, A., Li, Y., Gora-Stahlberg, G., Mantel, T., Berndt, M., Castrop, F., et al. (2018). Altered functional connectivity in blepharospasm/orofacial dystonia. *Brain Behav.* 8:e00894. doi: 10.1002/brb3.894

Juvarra, G., Bettoni, L., and Lechi, A. (1981). Meige syndrome: a clinical and EMG study. *Eur. Neurol.* 20, 103–109. doi: 10.1159/000115215

Kuschinsky, W. (1991). Coupling of function, metabolism, and blood flow in the brain. *Neurosurg. Rev.* 14, 163–168. doi: 10.1007/bf00310651

Liang, X., Zou, Q., He, Y., and Yang, Y. (2013). Coupling of functional connectivity and regional cerebral blood flow reveals a physiological basis for network hubs of the human brain. *Proc. Natl. Acad. Sci. U.S.A.* 110, 1929–1934. doi: 10.1073/pnas.1214900110

Mayka, M. A., Corcos, D. M., Leurgans, S. E., and Vaillancourt, D. E. (2006). Three-dimensional locations and boundaries of motor and premotor cortices as defined by functional brain imaging: a meta-analysis. *Neuroimage* 31, 1453–1474. doi: 10.1016/j.neuroimage.2006.02.004

Pakkenberg, B., Bolwig, T. G., and Pakkenberg, H. (1987). Meige's syndrome: a neuropsychiatric disorder. *Compr. Psychiatry* 28, 309–314. doi: 10.1016/0010-440x(87)90066-6

Pan, P., Wei, S., Li, H., Ou, Y., Liu, F., Jiang, W., et al. (2021). Voxel-wise brain-wide functional connectivity abnormalities in patients with primary blepharospasm at rest. *Neural Plast.* 2021:6611703. doi: 10.1155/2021/6611703

Pandey, S., and Sharma, S. (2017). Meige's syndrome: history, epidemiology, clinical features, pathogenesis and treatment. *J. Neurol. Sci.* 372, 162–170. doi: 10.1016/j.jns.2016.11.053

Prescott, I. A., Dostrovsky, J. O., Moro, E., Hodaie, M., Lozano, A. M., and Hutchison, W. D. (2013). Reduced paired pulse depression in the basal ganglia of dystonia patients. *Neurobiol. Dis.* 51, 214–221. doi: 10.1016/j.nbd.2012.11.012

Sabesan, T. (2008). Meige syndrome: a rare form of cranial dystonia that was treated successfully with botulinum toxin. *Br. J. Oral Maxillofac. Surg.* 46, 588–590. doi: 10.1016/j.bjoms.2008.02.002

Su, P., Mao, D., Liu, P., Li, Y., Pinho, M. C., Welch, B. G., et al. (2017). Multiparametric estimation of brain hemodynamics with MR fingerprinting ASL. *Magn. Reson. Med.* 78, 1812–1823. doi: 10.1002/mrm.26587

Tanner, C. M., Glantz, R. H., and Klawans, H. L. (1982). Meige disease: acute and chronic cholinergic effects. *Neurology* 32, 783–785. doi: 10.1212/wnl.32.7.783

Tayebati, S. K., Lokhandwala, M. F., and Amenta, F. (2011). Dopamine and vascular dynamics control: present status and future perspectives. *Curr. Neurovasc. Res.* 8, 246–257. doi: 10.2174/156720211796558032

Termsarasab, P., Thammongkolchai, T., and Frucht, S. J. (2016). Medical treatment of dystonia. *J. Clin. Mov. Disord.* 3:19. doi: 10.1186/s40734-016-0047-6

Venkat, P., Chopp, M., and Chen, J. (2016). New insights into coupling and uncoupling of cerebral blood flow and metabolism in the brain. *Croat. Med. J.* 57, 223–228. doi: 10.3325/cmj.2016.57.223

Wang, Q., Qu, X., Chen, W., Wang, H., Huang, C., Li, T., et al. (2021). Altered coupling of cerebral blood flow and functional connectivity strength in visual and higher order cognitive cortices in primary open angle glaucoma. *J. Cereb. Blood Flow Metab.* 41, 901–913. doi: 10.1177/0271678x20935274

Xu, G., Rowley, H. A., Wu, G., Alsop, D. C., Shankaranarayanan, A., Dowling, M., et al. (2010). Reliability and precision of pseudo-continuous arterial spin labeling perfusion MRI on 3.0 T and comparison with 15O-water PET in elderly subjects at risk for Alzheimer's disease. *NMR Biomed.* 23, 286–293. doi: 10.1002/nbm.1462

Yan, C. G., Wang, X. D., Zuo, X. N., and Zang, Y. F. (2016). DPABI: data processing & analysis for (resting-state) brain imaging. *Neuroinformatics* 14, 339–351. doi: 10.1007/s12021-016-9299-4

Yoshimura, R., Kakihara, S., Soya, A., Ueda, N., Shinkai, K., and Nakamura, J. (2001). Effect of clonazepam treatment on antipsychotic drug-induced Meige syndrome and changes in plasma levels of GABA, HVA, and MHPG during treatment. *Psychiatry Clin. Neurosci.* 55, 543–546. doi: 10.1046/j.1440-1819.2001.00903.x

Zalyalova, Z. A. (2015). [Meige's syndrome or segmental craniocervical dystonia: terminology, history and contemporary view]. *Zh. Nevrol. Psikhiatr. Im. S S Korsakova* 115, 133–136. doi: 10.17116/jnevro2015115112133-136

Zhu, J., Zhuo, C., Xu, L., Liu, F., Qin, W., and Yu, C. (2017). Altered coupling between resting-state cerebral blood flow and functional connectivity in schizophrenia. *Schizophr. Bull.* 43, 1363–1374. doi: 10.1093/schbul/sbx051

frontiers | Frontiers in Neuroscience

TYPE Original Research
PUBLISHED 12 May 2023
DOI 10.3389/fnins.2023.1138952

OPEN ACCESS

EDITED BY
Mark Wagshul,
Albert Einstein College of Medicine,
United States

REVIEWED BY
Takafumi Ushida,
Nagoya University Graduate School
of Medicine, Japan
Chao Zhang,
The Affiliated Hospital of Xuzhou Medical
University, China

*CORRESPONDENCE
Linfeng Yang
✉ ylf19860928@126.com
Lingfei Guo
✉ glfsci@163.com

RECEIVED 06 January 2023
ACCEPTED 17 April 2023
PUBLISHED 12 May 2023

CITATION
Sui C, Wen H, Han J, Chen T, Gao Y, Wang Y, Yang L and Guo L (2023) Decreased gray matter volume in the right middle temporal gyrus associated with cognitive dysfunction in preeclampsia superimposed on chronic hypertension.
Front. Neurosci. 17:1138952.
doi: 10.3389/fnins.2023.1138952

Decreased gray matter volume in the right middle temporal gyrus associated with cognitive dysfunction in preeclampsia superimposed on chronic hypertension

Chaofan Sui[1], Hongwei Wen[2], Jingchao Han[3], Tao Chen[4], Yian Gao[1], Yuanyuan Wang[5], Linfeng Yang[6]* and Lingfei Guo[1]*

[1]Department of Radiology, Shandong Provincial Hospital Affiliated to Shandong First Medical University, Jinan, Shandong, China, [2]Key Laboratory of Cognition and Personality, Ministry of Education, Faculty of Psychology, Southwest University, Chongqing, China, [3]Department of Medical Imaging, Jinan Stomatological Hospital, Jinan, Shandong, China, [4]Department of Clinical Laboratory, Jinan Maternity and Child Care Hospital Affiliated to Shandong First Medical University, Jinan, Shandong, China, [5]Department of Radiology, Binzhou Medical University, Yantai, Shandong, China, [6]Department of Radiology, Jinan Maternity and Child Care Hospital Affiliated to Shandong First Medical University, Jinan, Shandong, China

Introduction: The effects of preeclampsia superimposed on chronic hypertension (CHTN-PE) on the structure and function of the human brain are mostly unknown. The purpose of this study was to examine altered gray matter volume (GMV) and its correlation with cognitive function in pregnant healthy women, healthy non-pregnant individuals, and CHTN-PE patients.

Methods: Twenty-five CHTN-PE patients, thirty-five pregnant healthy controls (PHC) and thirty-five non-pregnant healthy controls (NPHC) were included in this study and underwent cognitive assessment testing. A voxel-based morphometry (VBM) approach was applied to investigate variations in brain GMV among the three groups. Pearson's correlations between mean GMV and the Stroop color-word test (SCWT) scores were calculated.

Results: Compared with the NPHC group, the PHC and CHTN-PE groups showed significantly decreased GMV in a cluster of the right middle temporal gyrus (MTG), and the GMV decrease was more significant in the CHTN-PE group. There were significant differences in the Montreal Cognitive Assessment (MoCA) and Stroop word scores among the three groups. Notably, the mean GMV values in the right MTG cluster were not only significantly negatively correlated with Stroop word and Stroop color scores but also significantly distinguished CHTN-PE patients from the NPHC and PHC groups in receiver operating characteristic curve analysis.

Discussion: Pregnancy may cause a decrease in local GMV in the right MTG, and the GMV decrease is more significant in CHTN-PE patients. The right MTG affects multiple cognitive functions, and combined with the SCWT scores, it may explain the decline in speech motor function and cognitive flexibility in CHTN-PE patients.

KEYWORDS

preeclampsia superimposed, chronic hypertension, voxel-based morphometry, gray matter volume, magnetic resonance imaging

1. Introduction

Hypertensive disorder of pregnancy (HDP), including preeclampsia/eclampsia, gestational hypertension, chronic hypertension, and preeclampsia/eclampsia superimposed on chronic hypertension, continues to be among the major causes of maternal and fetal morbidity and mortality around the world (International Lobour Organization [ILO], 2013; Garovic et al., 2020). HDP affects the mother and fetus during the disease course and is linked to future morbidity and mortality of cardiovascular disease and stroke (Garrido-Gimenez et al., 2020). Chronic hypertension is a dangerous condition for pregnant women and becomes more common as women become pregnant in their later years (Maducolil et al., 2020). In the United States, approximately 26% of women with chronic hypertension have superimposed preeclampsia, a type of HDP (Bramham et al., 2014, 2020). Women who develop superimposed preeclampsia are at an increased risk for preterm delivery, placental abruption (Boriboonhirunsarn et al., 2017), acute renal failure, cardiovascular or coagulation dysfunction, stroke, or even maternal death (Abalos et al., 2014; Bramham et al., 2020). Investigating the pathogenesis of preeclampsia superimposed on chronic hypertension (CHTN-PE) is therefore crucial.

The effects of pregnancy on the structure and function of the human brain are poorly understood. The voxel-based morphometry (VBM) method was utilized in the current investigation, which can fairly and comprehensively evaluate the anatomical differences in gray matter (GM) throughout the entire brain (Ashburner and Friston, 2000). VBM is considered to be a better method than others to compare the relative concentration of GM (that is, the proportion of GM to other tissue types in the region) (Ashburner and Friston, 2000) and to detect brain abnormalities more sensitively at the voxel level (Khan et al., 2015; Goto et al., 2022). A prospective study (before versus after pregnancy) showed that pregnancy is related to significant changes in the human brain structure, and primiparous women have been found to experience a symmetrical pattern of extensive gray matter volume (GMV) reduction throughout pregnancy, particularly in regions subserving social cognition, such as specific regions of the bilateral lateral prefrontal and temporal cortex (Hoekzema et al., 2017). Previous studies have found that older individuals with hypertension is linked to lower regional GMV, which mainly affects the frontal and medial temporal lobes, including the amygdala and hippocampus (Schaare et al., 2019). In addition, a case control study found that women with a history of preeclampsia had lower temporal cortical GMV than women with normotensive pregnancies (Siepmann et al., 2017). These studies have shown that pregnancy, chronic hypertension and preeclampsia may all affect the GMV of the human brain. However, few studies have investigated GMV alterations in CHTN-PE patients.

With the increase in sex hormones during pregnancy, women often show cognitive and subjective emotional changes, as well as a slight decline in cognitive function (Rehbein et al., 2022). Studies have found that women experienced local GMV reduction during pregnancy, and lower GMV is independently related to poor cognitive and locomotive performance (Hoekzema et al., 2017; Beauchet et al., 2019; Rehbein et al., 2022). Therefore, decreased GMV leads to cognitive dysfunction, which may explain why women experience emotional and cognitive changes after pregnancy. The Stroop color-word test (SCWT) is one of the most commonly used measures to evaluate a variety of cognitive functions, including the ability to inhibit cognitive interference, as well as attention, cognitive flexibility, information processing speed, working memory and visual search (Scarpina and Tagini, 2017). At present, few studies have examined the connection between GMV alterations and cognitive function in CHTN-PE patients.

The objectives of this study were, first, to discuss the characteristics of decreased GMV in pregnant healthy women and CHTN-PE patients and, second, to summarize the characterization of GMV reductions associated with cognitive dysfunction.

Abbreviations: CHTN-PE, preeclampsia superimposed on chronic hypertension; PHC, pregnant healthy controls; NPHC; non-pregnant healthy controls; VBM, voxel-based morphometry; SCWT, stroop color-word test; MTG, middle temporal gyrus; MoCA, Montreal Cognitive Assessment; GMV, gray matter volume; GM, gray matter; HDP, hypertensive disorder of pregnancy.

2. Materials and methods

2.1. Subjects

This prospective and cross-sectional study was approved by Jinan Maternity and Child Care Hospital's institutional review board. Twenty-five CHTN-PE patients (age 32.24 ± 5.00 years), thirty-five non-pregnant healthy controls (NPHC) (age 32.29 ± 4.99 years) and thirty-five pregnant healthy controls (PHC) (age 30.34 ± 5.73 years) from July 2020 to April 2021 were enrolled in this cross-sectional study. All participants were clear about the detailed experimental procedures and signed informed consent forms. CHTN-PE patients were recruited from the obstetric ward and had to be clinically stable to complete the MRI examination. No subjects were diagnosed with eclampsia, either before or after participating in the study. All pregnant participants had blood pressure (BP) measured, blood and urine sampling, and MRI examinations within 12 h after study enrollment. BP was measured in the right arm after subjects had been supine for 15 min. Routine blood and urinary tests were performed in all pregnant participants. The CHTN-PE patients included in this study did not demonstrate hypertension crisis after the evaluation of clinicians and could be examined by MRI. MRI examinations and cognitive assessments for all pregnant women were completed after admission, before delivery, and under clinically stable conditions.

The inclusion and exclusion criteria are shown in **Figure 1**. The inclusion criteria of CHTN-PE were as follows: (1) All participants were right-handed, and all CHTN-PE patients met the diagnostic criteria of CHTN-PE: chronic hypertensive pregnant women with new onset proteinuria (0.3 g of protein or more in a 24 h specimen) after 20 weeks gestation and without proteinuria early in pregnancy (less than 20 weeks gestation); had proteinuria before pregnancy with a significant increase in proteinuria after pregnancy or a further increase in blood pressure; or had serious manifestations, such as liver and kidney damage, pulmonary edema, epigastric pain, headache, nervous system abnormalities

or visual impairment (Wilkerson and Ogunbodede, 2019; Kametas et al., 2022). (2) None of the patients were given aspirin or MgSO4 or developed eclampsia, either before or after participation in the study. (3) All patients were clinically stable for transport to the MRI facility. The following were the healthy controls' inclusion criteria: (1) PHC, matched for gestational week and age with the CHTN-PE group, were recruited through informational posters at antenatal outpatient clinics in the Jinan Maternal and Child Care Hospital; (2) NPHC, matched for age, were recruited from the local community. The general exclusion criteria for all subjects were proteinuria during early pregnancy (less than 20 weeks gestation), adiposis, hypothyroidism, previous liver or renal disease, diabetes mellitus, or contraindications for MRI. This analysis eliminated PHC subjects who experienced preeclampsia, delivered an infant prematurely (before 37 weeks), or did not have an infant with normal birthweight (between two standard deviations of the mean birthweight for gestational age and sex).

2.2. Cognitive assessment

All participants underwent detailed neurological examinations by professional neurologists. The Beijing version of the Montreal Cognitive Assessment (MoCA) was used to evaluate cognitive functions (Tian et al., 2020), which is a one-page 30-point test administered in 10 min, including 11 items and it is an assessment tool for rapid screening for mild cognitive impairment (Bergeron et al., 2017). The optimal cut-off for detecting cognitive impairment points was 13/14 for illiterate individuals, 19/20 for individuals with 1–6 years of education, and 24/25 for individuals with 7 or more years of education (Lu et al., 2011). One point is added if the education years is less than 12. The SCWT is one of the most commonly used measures to evaluate a variety of cognitive functions and consists of three parts: Stroop word, Stroop color, and Stroop color-word. The subjects are required to read the names of colors printed in black ink in the first part, and they are also asked to name various color patches in the second part. Conversely, in the last part, each color-word is printed in an inconsistent color ink, and subjects are asked to quickly identify the color of the ink instead of reading the words (Scarpina and Tagini, 2017; Ktaiche et al., 2022). For the SCWT, higher scores were associated with more severe symptoms (Radetz et al., 2021). The implementers of all the above tests had received qualified professional training. The examination was conducted after scanning, and the total examination time shall not exceed 15 min.

2.3. Image acquisition

Magnetic resonance imaging scanning was performed on a 1.5-T MR scanner (Achieva, Philips Healthcare, Best, Netherlands) using a 16-channel head coil for signal reception. A three-dimensional (3D) T1-weighted (T1W) high-resolution sequence with the following parameters was used to generate the structural images [repetition time (TR): 25 ms; echo time (TE): 6.1 ms; inversion time (TI): 900 ms; flip angle: 30°; and isotropic voxel size: 1 mm^3]. Furthermore, T2-weighted (T2W) turbo spin echo, T2W fluid-attenuated inversion recovery (FLAIR) and diffusion-weighted images (DWI) were obtained and used to identify brain abnormalities. The average scanning time of each sequence is about 5 min, and the total imaging time did not exceed 20 min.

2.4. Voxel-based morphometry (VBM)-DARTEL processing

Three-dimensional T1W images were processed using VBM with diffeomorphic anatomical registration through exponentiated lie algebra (DARTEL) (Ashburner, 2007) based on the statistical parametric mapping (SPM8)[1] toolbox after data acquisition (pipeline shown in **Figure 2**). Using a unified tissue-segmentation procedure, the images were segmented into GM, white matter (WM), and cerebrospinal fluid (CSF) after image-intensity non-uniformity correction. The study-specific GM templates were created by the DARTEL algorithm, and all GM images were warped to the template and then normalized to Montreal Neurological Institute (MNI) standard space. Then, the normalized GM images were modulated to correct volume changes, and the generated gray matter volume (GMV) images were smoothed with the isotropic Gaussian kernel of 8 mm full-width at half-maximum.

2.5. Statistical analysis

A two-sample *t*-test was applied to assess differences in gestational weeks between the NPHC and PHC groups, and one-way analysis of variance (ANOVA) and least significant difference (LSD) *post-hoc* tests were used to examine differences in other demographic and clinical parameters among the three groups using the Statistical Package for the Social Sciences (SPSS Inc, v24.0, Chicago, IL, USA). The SPM8 toolbox was used to perform one-way analysis of covariance (ANCOVA) with age and total intracranial volume (TIV) as covariates to compare GMV differences among the three groups, and the family-wise error (FWE) correction (voxel-wise $p < 0.05$, cluster size > 50) based on Random Field Theory (RFT) method was applied to control multiple comparisons (Kilner et al., 2005). Once significant GMV differences among the three groups were identified in any brain clusters, the mean GMV values within the clusters were extracted. Then, the mean GMV value of each significant cluster was analyzed using ANCOVA and LSD post-hoc analyses. SPSS was used to calculate Pearson's correlations between the mean GMV and cognitive parameters in all subjects, and false discovery rate (FDR) corrected p-value < 0.05 was set as the significance threshold.

To verify that GMV can be used as a diagnostic neuroimaging biomarker to distinguish CHTN-PE patients from the PHC and NPHC groups, the mean GMV value of each significant cluster was also used for receiver operating characteristic (ROC) curve analysis using MedCalc Statistical Software.[2] According to the ROC curve, the optimal cut-off point was found based on the Youden index (Hajian-Tilaki, 2013, 2018). Then, sensitivity and specificity were calculated based on the cut-off points.

1 http://www.fil.ion.ucl.ac.uk/spm

2 https://www.medcalc.org

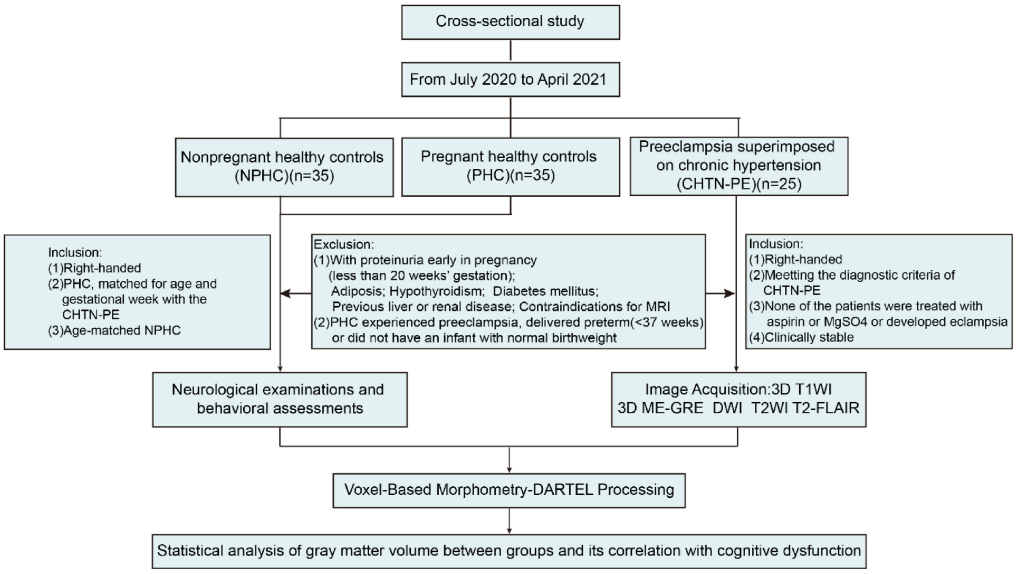

FIGURE 1
Steps for subject selection or study participation and inclusion and exclusion criteria.

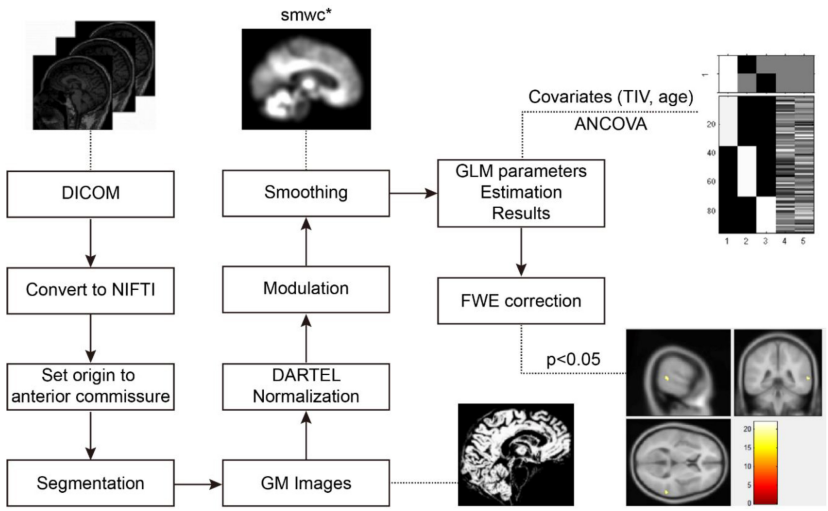

FIGURE 2
The processing pipeline of voxel-based morphometry (VBM)-DARTEL analysis using SPM. DARTEL, diffeomorphic anatomical registration through exponentiated lie algebra; FWE, familywise error; ANCOVA, one-way analysis of covariance; GM, gray matter; SPM, statistical parametric mapping.

3. Results

3.1. Demographic and clinical characteristics

The clinical characteristics of the study participants are summarized in Table 1. Differences in age, body mass index, blood pressure, WM volume, CSF volume, total brain volume, MoCA and SCWT scores were evaluated using ANOVA with LSD *post-hoc* tests, and a two-sample *t*-test was performed to assess differences in gestational week. The mean MoCA and Stroop word scores were significantly different among the three groups. The CHTN-PE group had lower MoCA scores and higher Stroop word scores than the NPHC and PHC groups, and the PHC group had lower MoCA scores and higher Stroop word scores than the NPHC group. No significant differences were found in age, gestational week, Stroop color and Stroop color-word scores among the three groups. No abnormality was found in routine magnetic resonance imaging in three groups (Figure 3).

3.2. GMV differences among groups

Using ANCOVA, we found significant GMV differences in a cluster of the right MTG among the three groups (FWE corrected,

TABLE 1 Clinical characteristics of the participants.

Variables	NPHC $n = 35$	PHC $n = 35$	CHTN-PE $n = 25$	F/t value	*P*-value	*P*-value (*post-hoc*)		
						NPHC vs. CHTN-PE	PHC vs. CHTN-PE	NPHC vs. PHC
Female (n)	35	35	25	–	–	–	–	–
Age (years)	32.29 ± 4.99	30.20 ± 5.38	32.24 ± 5.00	1.787	0.173[a]	–	–	–
Gestational week (week)	–	34.24 ± 4.10	34.92 ± 4.23	0.884	0.380[t]	–	–	–
Body mass index (kg/m^2)	22.00 ± 3.02	27.16 ± 4.44	31.67 ± 4.13	46.045	<0.001[a]	<0.001	<0.001	<0.001
Weight (kg)	57.74 ± 7.41	71.36 ± 11.83	81.94 ± 12.85	38.303	<0.001[a]	<0.001	<0.001	<0.001
Systolic pressure (mmHg)	111.60 ± 11.60	113.57 ± 11.20	162.00 ± 15.07	145.001	<0.001[a]	<0.001	<0.001	0.510
Diastolic pressure (mmHg)	67.97 ± 9.05	73.68 ± 7.96	104.48 ± 9.67	137.139	<0.001[a]	<0.001	<0.001	0.008
Mean atrial pressure (mmHg)	82.51 ± 9.04	86.98 ± 8.13	123.66 ± 10.68	167.303	<0.001[a]	<0.001	<0.001	0.045
WMV	546.82 ± 45.96	542.52 ± 44.85	552.65 ± 47.76	0.353	0.703[a]	0.629	0.697	0.697
CSF volume	172.21 ± 17.19	187.07 ± 19.90	181.59 ± 22.20	5.121	0.008[a]	0.071	0.289	0.002
Total brain volume	1277.60 ± 85.62	1269.31 ± 75.07	1288.04 ± 81.56	0.392	0.677[a]	0.623	0.378	0.669
MoCA	29.74 ± 0.66	29.11 ± 0.90	28.08 ± 1.22	24.153	<0.001[a]	<0.001	<0.001	0.004
Stroop word	18.31 ± 3.62	21.23 ± 4.05	23.56 ± 3.50	14.661	<0.001[a]	<0.001	0.020	0.002
Stroop color	29.17 ± 6.28	32.26 ± 6.83	32.88 ± 6.47	2.963	0.057[a]	–	–	–
Stroop color-word	56.91 ± 11.32	63.03 ± 11.83	59.16 ± 12.51	2.383	0.098[a]	–	–	–

Data are displayed as the mean ± standard deviation.
[a]Analysis of variance (ANOVA) test.
[t]Two-sample *t*-test; NPHC, non-pregnant healthy control; PHC, pregnant healthy control; CHTN-PE, preeclampsia superimposed on chronic hypertension; kg, kilograms; MoCA, Montreal Cognitive Assessment; WMV, white matter volume; CSF, cerebrospinal fluid.

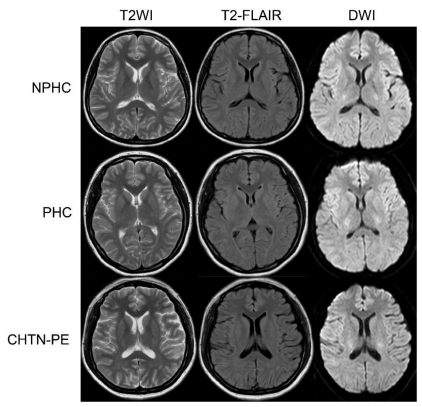

FIGURE 3
Non-pregnant healthy controls, (NPHC) a 35 years old female. Pregnant healthy controls (PHC), a 28 years old female who was pregnant for the first time for 28 weeks. Preeclampsia superimposed on chronic hypertension (CHTN-PE), a 33 years old female who was pregnant for the first time for 38 weeks. No abnormality is found in the routine magnetic resonance imaging in the three groups. T2WI, T2-weighted imaging; T2-FLAIR, T2-fluid-attenuated inversion recovery; DWI, diffusion-weighted imaging.

$p < 0.05$). The mean GMV values within the right MTG cluster were extracted, and follow-up LSD *post-hoc* tests revealed that the CHTN-PE group had significantly lower GMV than the NPHC and PHC groups and that the PHC group had lower GMV than the NPHC group in the right MTG cluster (shown in Table 2 and Figure 4).

3.3. Diagnostic accuracy and performance of GMV

From the ROC curves, the GMV values of the right MTG cluster can distinguish the CHTN-PE group from the NPHC and PHC groups; all AUC values had a significance level of $p < 0.01$. According to the Youden index, the cut-off values for each value in the various ROIs were chosen, and the specifics are shown in Table 3, Figure 5.

3.4. Correlations between neuroimaging and cognitive function

We extracted the mean GMV values within the significantly altered cluster (right MTG) for all subjects. Correlation analysis revealed a significant positive correlation between the mean GMV of the right MTG and MoCA ($r = 0.475$, $p < 0.001$; shown in Figure 6), and a significant negative correlation between the mean GMV of the right MTG and Stroop word and Stroop color scores in all subjects (separately: $r = -0.371$, $p < 0.001$; $r = -0.311$, $p = 0.002$;

TABLE 2 Significantly altered gray matter volume (GMV) among the non-pregnant healthy control (NPHC), pregnant healthy control (PHC), and preeclampsia superimposed on chronic hypertension (CHTN-PE) groups.

Brain regions	Peak MNI (X, Y, Z)		Cluster size	F	Z	*P*		Volume (ml): mean ± SD		
								NPHC	PHC	CHTN-PE
Temporal_Mid_R	61	−42	6	97	15.30	22.01	<0.001	0.64 ± 0.06	0.58 ± 0.04	0.55 ± 0.05

CHTN-PE, preeclampsia superimposed on chronic hypertension; NPHC, non-pregnant healthy controls; PHC, pregnant healthy controls; Temporal_Mid_R, right middle temporal gyrus. Cluster size, the number of voxels in the (identified significant) cluster. The familywise error (FWE) method was used for correction.

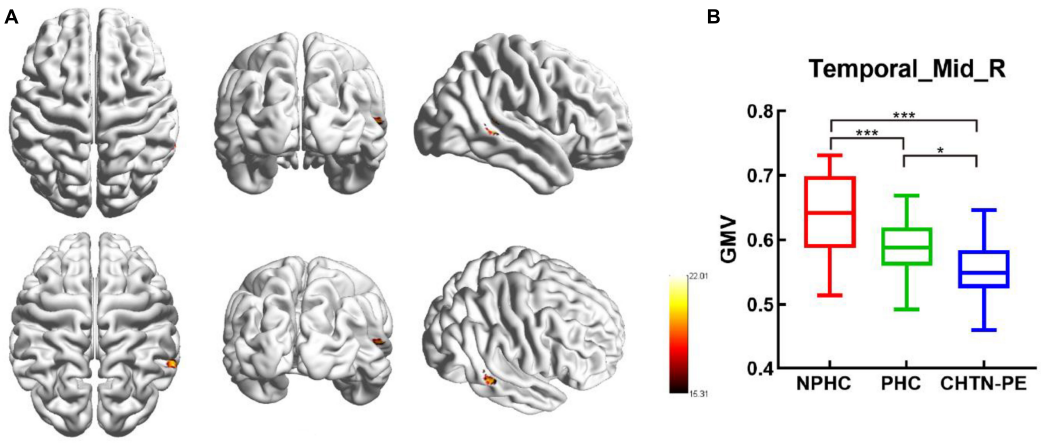

FIGURE 4
Significantly altered gray matter volume (GMV) among groups. **(A)** Clusters with significantly altered GMV among groups [family-wise error (FEW) corrected, $p < 0.05$]. **(B)** Mean GMV values in the cluster of the right middle temporal gyrus among NPHC, PHC, and CHTN-PE patients. CHTN-PE, preeclampsia superimposed on chronic hypertension; NPHC, non-pregnant healthy controls; PHC, pregnant healthy controls; Temporal_Mid_R, right middle temporal gyrus. *$P < 0.05$; ***$P < 0.001$.

TABLE 3 The statistics of receiver operating characteristic (ROC) curve analysis for the cluster of right middle temporal gyrus (MTG) that distinguishes preeclampsia superimposed on chronic hypertension (CHTN-PE) patients from the non-pregnant healthy controls (NPHC) and pregnant healthy controls (PHC) groups.

	AUC (95% CI)	*P*-value	Cut-off value	Sensitivity	Specificity
NPHC vs. CHTN-PE	0.877 (0.766–0.947)	<0.001	0.564	0.680	0.971
PHC vs. CHTN-PE	0.696 (0.564–0.808)	<0.01	0.584	0.800	0.600

CHTN-PE, preeclampsia superimposed on chronic hypertension; NPHC, non-pregnant healthy controls; PHC, pregnant healthy controls; AUC, area under the curve; CI, confidence interval.

FDR corrected). There were no significant correlations between the GMV and Stroop color-word scores in all subjects ($r = -0.105$, $p = 0.316$) (shown in Figure 7).

4. Discussion

The current study applied the VBM approach to explore brain morphological alterations in pregnant women with or without CHTN-PE. In addition to CHTN-PE patients, individuals were recruited to both the PHC and NPHC groups, which is an advantage of our study, as their data can be used to provide a more systematic explanation for the alterations in brain structure of CHTN-PE patients. We found that compared with the NPHC, the PHC and CHTN-PE patients showed significantly decreased GMV in the right MTG cluster, and GMV decreased more significantly in the CHTN-PE patients. We also estimated the correlation between the regions where GMV significantly decreased and cognitive function and found that GMV in the cluster of right MTG was significantly negatively correlated with Stroop word and Stroop color scores and positively correlated with MoCA, suggesting a decline in the ability to inhibit cognitive interference, attention, information processing speed, cognitive flexibility and visual search in CHTN-PE patients. To the best of our knowledge, these data provide the first insight into the profound impact of CHTN-PE on cerebral GMV.

It has been confirmed that pregnancy results in long-lasting alterations of the human brain structure (Hoekzema et al., 2017). However, the effect of CHTN-PE on brain structure is not clear. Previous animal studies have demonstrated that modulation of the renin–angiotensin system (RAS) is the key mechanism in the development of CHTN-PE (Genest et al., 2013), and because renin is species specific for angiotensinogen cleavage, the overexpression of RAS in the uterus and placenta and the release of placental human renin into the circulation trigger preeclampsia-like symptoms in some rodents (Falcao et al., 2009). A previous study showed that cardiovascular disease-related neuronal loss was a similar burden in all women who experienced preeclampsia, which was manifested as GM atrophy (Raman et al., 2017). The occurrence of brain atrophy in chronic hypertension patients is

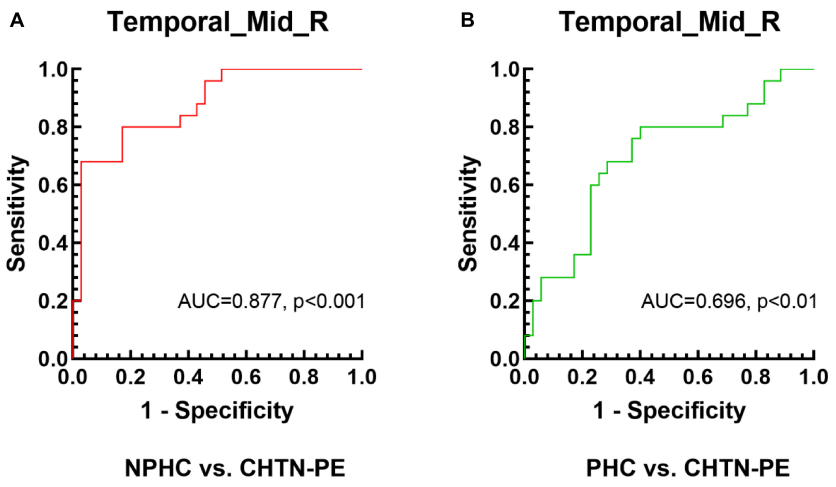

FIGURE 5
Receiver operating characteristic (ROC) curve analysis results. ROC curves for the mean gray matter volume (GMV) values of the right middle temporal gyrus that significantly distinguish the CHTN-PE group from the **(A)** NPHC and **(B)** PHC groups. CHTN-PE, preeclampsia superimposed on chronic hypertension; NPHC, non-pregnant healthy controls; PHC, pregnant healthy controls; Temporal_Mid_R, right middle temporal gyrus.

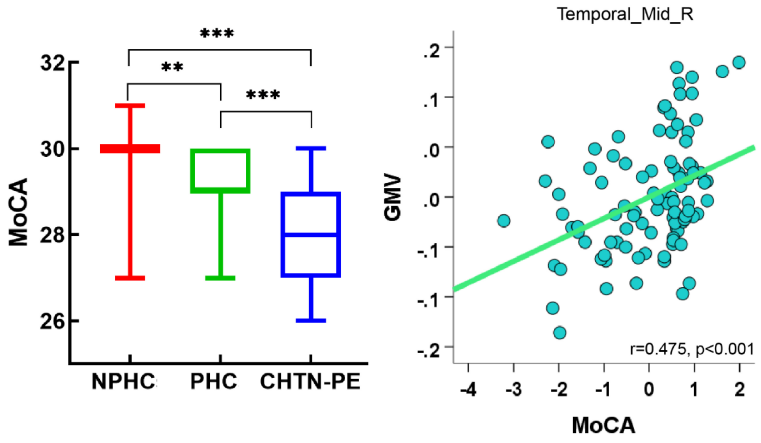

FIGURE 6
Correlations between the mean GMV of the right middle temporal gyrus and Montreal Cognitive Assessment (MoCA) scores in all subjects. Of note, the coordinate values of both the X axis (MoCA scores) and Y axis (GMV) do not reflect the initial values of these variables when considering age and total intracranial volume (TIV) as covariates. Significance was set to $p < 0.05$, false discovery rate (FDR) corrected for multiple comparison. GMV, gray matter volume; Temporal_Mid_R, right middle temporal gyrus; CHTN-PE, preeclampsia superimposed on chronic hypertension; NPHC, non-pregnant healthy controls; PHC, pregnant healthy controls. $^{**}p < 0.01$, $^{***}p < 0.001$.

a long-term and aging process, and young hypertension patients may not necessarily have GMV changes (Strassburger et al., 1997). Previous studies have shown that young chronic hypertension patients (<40 years) are associated with a decrease in GMV in the frontoparietal lobe, and no change in GMV in the temporal lobe has been found (Schaare et al., 2019). The subjects included in this study were young pregnant women (<40 years), therefore, we believe that the likelihood of changes in GMV of the MTG before pregnancy is minimal. We consider that CHTN-PE patients will experience neuronal loss and GM atrophy during pregnancy, resulting in the reduction of GMV in the right MTG. Besides, it was found that there was hemispheric asymmetries of GMV in left and right-handed people (Saenger et al., 2012). In order to eliminate the difference in GMV between left and right-handed people, all the subjects we included are right-handed. Rightward functional asymmetries were observed in the middle frontal and middle/superior temporal gyrus in the right-handed group (Saenger et al., 2012), so the decrease of GMV in CHTN-PE patients may first occur in the right middle frontal gyrus, superior temporal gyrus and middle temporal gyrus. Therefore, our findings that GMV in the cluster of right MTG is significantly decreased in CHTN-PE patients are also reasonable.

It has been found that laboratory indicators such as uric acid, the renin-angiotensin aldosterone system, angiogenic factors and proinflammatory markers of endothelial dysfunction have changed in women with chronic hypertension, but none of these biomarkers have been proved to be useful in the screening and diagnosis of superimposed preeclampsia (Kametas et al., 2022). By using imaging indicators, the early brain structural changes of superimposed preeclampsia can be found sensitively (Raman et al.,

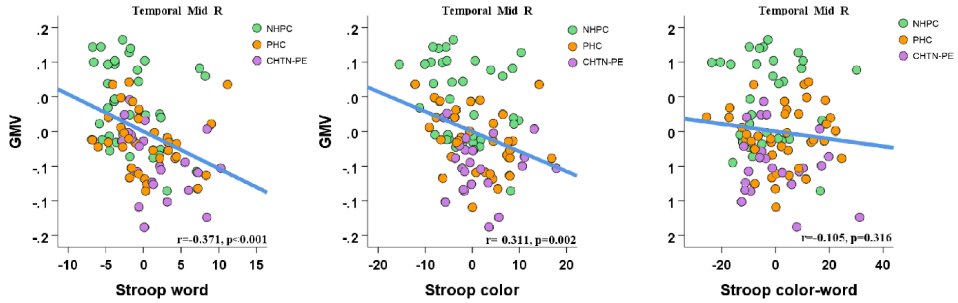

FIGURE 7
Correlations between the mean GMV of the right middle temporal gyrus and Stroop color and word test (SCWT) scores in all subjects. Of note, the coordinate values of both the X axis (SCWT scores) and Y axis (GMV) do not reflect the initial values of these variables when considering age and total intracranial volume (TIV) as covariates. Significance was set to $p < 0.05$, false discovery rate (FDR) corrected for multiple comparison. GMV, gray matter volume; Temporal_Mid_R, right middle temporal gyrus; CHTN-PE, preeclampsia superimposed on chronic hypertension; NPHC, non-pregnant healthy controls; PHC, pregnant healthy controls.

2017), and early identification of CHTN-PE patients from pregnant women would contribute to more intensive surveillance, more aggressive care, and hopefully better maternal and fetal outcomes (August et al., 2004). Therefore, it is also valuable to use imaging indicators to assist in the diagnosis of CHTN-PE. Analysis of the ROC curve in this study revealed that mean GMV values in the right MTG cluster had excellent classification performance for distinguishing CHTN-PE patients from healthy controls, which could be used as a potential diagnostic biomarker. The ROC curve is also used to determine the optimal cut-off value for diagnosing a disease (Nahm, 2022). According to the results of this study and combined with clinical manifestations and laboratory indicators, when GMV in the right MTG is less than 0.584, we should suspect that pregnant women may be at risk of CHTN-PE.

The MTG affects a variety of functions, including language, emotion, memory and social cognition (Xu et al., 2019), and is considered to play an important role in language-related tasks, such as vocabulary comprehension and semantic cognition (Briggs et al., 2021). Therefore, the right MTG is closely related to cognitive and executive functions and it is reasonable for CHTN-PE patients with significantly reduced GMV in the right MTG to have lower MoCA scores and higher SCWT scores. MoCA is more commonly used in the field of dementia and in the diagnosis of mild cognitive impairment, with better sensitivity in this population (Bergeron et al., 2017). SCWT can efficiently evaluate a variety of cognitive functions, including the ability to inhibit cognitive interference, as well as cognitive flexibility, attention, information processing speed, working memory, and visual search (Scarpina and Tagini, 2017). The completion time of SCWT is only 2 or 3 min, fully considering the tolerance of CHTN-PE patients. Therefore, we believe that the SCWT could better reflect the cognitive dysfunction caused by decreased GMV in the right MTG.

Stroop color and word test scores may be affected by the impairment of speech motor function and the decline in cognitive flexibility (Ktaiche et al., 2022). Multiple regression analysis of Stroop word and Stroop color data suggested that Stroop word scores were predicted by the speed of visual search and Stroop color scores were predicted by the speed of visual search and working memory (Periáñez et al., 2021), both of which were related to the speed of visual search, and visual search is closely related to language comprehension (Huettig et al., 2011; Chiu and Spivey, 2014). According to our study, GMV decreases in the right MTG cluster in the PHC and CHTN-PE groups may lead to declines in language and visual comprehension, which could increase Stroop color and Stroop word scores. Hence, it is reasonable that GMV in the right MTG cluster has a significant negative correlation with Stroop word and Stroop color scores. These findings may explain the decline in speech motor function and cognitive flexibility after pregnancy. Moreover, the additional complication of CHTN-PE in pregnant women might have caused a more obvious GMV decrease and might have resulted in more severe related cognitive impairment; this was an important finding of our study.

In the Stroop color-word task, participants were required to perform a task that was less automated (naming ink color) while suppressing interference from a task that was more automated (reading words) (Scarpina and Tagini, 2017). In fact, a previous study found that in the incongruous condition, the subjects also experienced non-pathological slowing down of reading speed even if they understood the task correctly (Scarpina and Tagini, 2017). In other words, the healthy controls may also have non-pathological slow reading speed because of the incongruous condition, resulting in high scores. Although the psychological structures associated with Stroop color-word scores include cognitive control, speech and semantic fluency, interference control, cognitive flexibility or working memory, some studies have found that after controlling visual search and perceptual speed factors, the association between Stroop color-word task and cognitive flexibility disappeared (Periáñez et al., 2021). Besides, the association between Stroop color-word task and verbal fluency may be more related to shared executive control, rather than language skills (Aita et al., 2019; Periáñez et al., 2021). These findings may provide an explanation for our results that there was no difference in Stroop color-word scores among the three groups and no correlation with GMV in the right MTG.

Although VBM is a typical method for measuring GMV, a recent study has shown that the combination of VBM and surface-based morphometry can complement the detection of cortical morphological changes and detect cortical morphological changes more accurately (Goto et al., 2022). Additionally, a brand-new method known as multivariate pattern analysis has been proven to

be more sensitive and accurate in capturing the cerebral cortex's function (Haxby, 2012). Therefore, more detailed brain structure and function analysis of CHTN-PE patients can be carried out by combining more advanced image segmentation methods and artificial intelligence in the future. Second, the study's sample size was small, and only GMV alterations in CHTN-PE patients were studied. Whether there are abnormalities in cerebral blood flow (CBF) and cerebral oxygen metabolic rate ($CMRO_2$) in CHTN-PE patients has not been evaluated. CBF and $CMRO_2$ can be obtained by adding multi-delay arterial spin labeled images (Zhang et al., 2020). Therefore, more imaging methods and larger sample sizes are needed in future studies. We are further expanding the sample size collection and planning to conduct further research on chronic hypertension without superimposed preeclampsia, and conduct longitudinal studies of pregnant women with chronic hypertension.

5. Conclusion

In conclusion, we explored the possible pathogenesis of CHTN-PE by analyzing GMV alterations in CHTN-PE patients. The results showed that GMV in a cognitive-related cerebral regions, the right MTG, was significantly decreased in CHTN-PE patients, and combined with the SCWT scores, it could provide an explanation for related cognitive dysfunction in CHTN-PE patients. These findings might help us better understand the relationship between brain GMV alterations and the pathophysiology of CHTN-PE.

Data availability statement

The raw data supporting the conclusions of this article will be made available by the authors, without undue reservation.

Ethics statement

The studies involving human participants were reviewed and approved by the Ethical Committee of the Institutional Review Board (IRB) of Jinan Maternity and Child Care Hospital (20190618). The patients/participants provided their written informed consent to participate in this study.

Author contributions

CS wrote the main manuscript text. CS and HW performed the statistical analysis. JH, TC, YG, and YW prepared the clinical data and imaging data. LY and LG revised the main manuscript text. All authors reviewed the manuscript.

Funding

This work was supported by grants from the National Natural Science Foundation of China (32100902), the Fundamental Research Funds for the Central Universities (SWU118065), the Natural Science Foundation of Shandong Province (ZR2020MH288), the Technology Development Plan of Jinan (201301049, 201602206, 201907052, 202134072, and 202225035), the Medical and Health Science and Technology Development Project of Shandong Province (2016 WS0529), and the Funding for Study Abroad Program by Shandong Province (201803059).

Acknowledgments

We thank American Journal Experts for edited and proofread the manuscript. We also thank to all of the volunteers and patients for their participation in our study.

Conflict of interest

The authors declare that the research was conducted in the absence of any commercial or financial relationships that could be construed as a potential conflict of interest.

Publisher's note

References

Abalos, E., Cuesta, C., Carroli, G., Qureshi, Z., Widmer, M., Vogel, J. P., et al. (2014). Pre-eclampsia, eclampsia and adverse maternal and perinatal outcomes: a secondary analysis of the World Health Organization multicountry survey on maternal and newborn health. *Bjog* 121(Suppl. 1), 14–24. doi: 10.1111/1471-0528.12629

Aita, S. L., Beach, J. D., Taylor, S. E., Borgogna, N. C., Harrell, M. N., and Hill, B. D. (2019). Executive, language, or both? An examination of the construct validity of verbal fluency measures. *Appl. Neuropsychol. Adult* 26, 441–451. doi: 10.1080/23279095.2018.1439830

Ashburner, J. (2007). A fast diffeomorphic image registration algorithm. *Neuroimage* 38, 95–113. doi: 10.1016/j.neuroimage.2007.07.007

Ashburner, J., and Friston, K. J. (2000). Voxel-based morphometry–the methods. *Neuroimage* 11, 805–821. doi: 10.1006/nimg.2000.0582

August, P., Helseth, G., Cook, E. F., and Sison, C. (2004). A prediction model for superimposed preeclampsia in women with chronic hypertension during pregnancy. *Am. J. Obstet Gynecol.* 191, 1666–1672. doi: 10.1016/j.ajog.2004.03.029

Beauchet, O., Montembeault, M., Barden, J. M., Szturm, T., Bherer, L., Liu-Ambrose, T., et al. (2019). Brain gray matter volume associations with gait speed and related structural covariance networks in cognitively healthy individuals and in patients with mild cognitive impairment: a cross-sectional study. *Exp. Gerontol.* 122, 116–122. doi: 10.1016/j.exger.2019.05.001

Bergeron, D., Flynn, K., Verret, L., Poulin, S., Bouchard, R. W., Bocti, C., et al. (2017). Multicenter validation of an MMSE-MoCA conversion table. *J. Am. Geriatr. Soc.* 65, 1067–1072. doi: 10.1111/jgs.14779

Boriboonhirunsarn, D., Pradyachaipimol, A., and Viriyapak, B. (2017). Incidence of superimposed preeclampsia among pregnant Asian women with chronic hypertension. *Hypertens. Pregnancy* 36, 226–231. doi: 10.1080/10641955.2017.1311340

Bramham, K., Parnell, B., Nelson-Piercy, C., Seed, P. T., Poston, L., and Chappell, L. C. (2014). Chronic hypertension and pregnancy outcomes: systematic review and meta-analysis. *Bmj* 348:g2301. doi: 10.1136/bmj.g2301

Bramham, K., Villa, P. M., Joslin, J. R., Laivuori, H., Hämäläinen, E., Kajantie, E., et al. (2020). Predisposition to superimposed preeclampsia in women with chronic hypertension: endothelial, renal, cardiac, and placental factors in a prospective longitudinal cohort. *Hypertens. Pregnancy* 39, 326–335. doi: 10.1080/10641955.2020.1769643

Briggs, R. G., Tanglay, O., Dadario, N. B., Young, I. M., Fonseka, R. D., Hormovas, J., et al. (2021). The unique fiber anatomy of middle temporal gyrus default mode connectivity. *Oper. Neurosurg.* 21, E8–E14. doi: 10.1093/ons/opab109

Chiu, E. M., and Spivey, M. J. (2014). Timing of speech and display affects the linguistic mediation of visual search. *Perception* 43, 527–548. doi: 10.1068/p7593

Falcao, S., Stoyanova, E., Cloutier, G., Maurice, R. L., Gutkowska, J., and Lavoie, J. L. (2009). Mice overexpressing both human angiotensinogen and human renin as a model of superimposed preeclampsia on chronic hypertension. *Hypertension* 54, 1401–1407. doi: 10.1161/HYPERTENSIONAHA.109.137356

Garovic, V. D., White, W. M., Vaughan, L., Saiki, M., Parashuram, S., Garcia-Valencia, O., et al. (2020). Incidence and long-term outcomes of hypertensive disorders of pregnancy. *J. Am. Coll. Cardiol.* 75, 2323–2334. doi: 10.1016/j.jacc.2020.03.028

Garrido-Gimenez, C., Mendoza, M., Cruz-Lemini, M., Galian-Gay, L., Sanchez-Garcia, O., Granato, C., et al. (2020). Angiogenic factors and long-term cardiovascular risk in women that developed preeclampsia during pregnancy. *Hypertension* 76, 1808–1816. doi: 10.1161/HYPERTENSIONAHA.120.15830

Genest, D. S., Falcao, S., Michel, C., Kajla, S., Germano, M. F., Lacasse, A. A., et al. (2013). Novel role of the renin-angiotensin system in preeclampsia superimposed on chronic hypertension and the effects of exercise in a mouse model. *Hypertension* 62, 1055–1061. doi: 10.1161/HYPERTENSIONAHA.113.01983

Goto, M., Abe, O., Hagiwara, A., Fujita, S., Kamagata, K., Hori, M., et al. (2022). Advantages of using both voxel- and surface-based morphometry in cortical morphology analysis: a review of various applications. *Magn. Reson. Med. Sci.* 21, 41–57. doi: 10.2463/mrms.rev.2021-0096

Hajian-Tilaki, K. (2013). Receiver operating characteristic (ROC) curve analysis for medical diagnostic test evaluation. *Caspian J. Internal Med.* 4, 627–635.

Hajian-Tilaki, K. (2018). The choice of methods in determining the optimal cut-off value for quantitative diagnostic test evaluation. *Stat. Methods Med. Res.* 27, 2374–2383. doi: 10.1177/0962280216680383

Haxby, J. V. (2012). Multivariate pattern analysis of fMRI: the early beginnings. *Neuroimage* 62, 852–855. doi: 10.1016/j.neuroimage.2012.03.016

Hoekzema, E., Barba-Müller, E., Pozzobon, C., Picado, M., Lucco, F., García-García, D., et al. (2017). Pregnancy leads to long-lasting changes in human brain structure. *Nat. Neurosci.* 20, 287–296. doi: 10.1038/nn.4458

Huettig, F., Olivers, C. N., and Hartsuiker, R. J. (2011). Looking, language, and memory: bridging research from the visual world and visual search paradigms. *Acta Psychol.* 137, 138–150. doi: 10.1016/j.actpsy.2010.07.013

International Lobour Organization [ILO] (2013). Hypertension in pregnancy. Report of the American College of obstetricians and gynecologists' task force on hypertension in pregnancy. *Obstet Gynecol.* 122, 1122–1131.

Kametas, N. A., Nzelu, D., and Nicolaides, K. H. (2022). Chronic hypertension and superimposed preeclampsia: screening and diagnosis. *Am. J. Obstet Gynecol.* 226, S1182–S1195. doi: 10.1016/j.ajog.2020.11.029

Khan, A. R., Wang, L., and Beg, M. F. (2015). Unified voxel- and tensor-based morphometry (UVTBM) using registration confidence. *Neurobiol. Aging* 36(Suppl. 1), S60–S68. doi: 10.1016/j.neurobiolaging.2014.04.036

Kilner, J. M., Kiebel, S. J., and Friston, K. J. (2005). Applications of random field theory to electrophysiology. *Neurosci. Lett.* 374, 174–178. doi: 10.1016/j.neulet.2004.10.052

Ktaiche, M., Fares, Y., and Abou-Abbas, L. (2022). Stroop color and word test (SCWT): normative data for the lebanese adult population. *Appl. Neuropsychol. Adult* 29, 1578–1586. doi: 10.1080/23279095.2021.1901101

Lu, J., Li, D., Li, F., Zhou, A., Wang, F., Zuo, X., et al. (2011). Montreal cognitive assessment in detecting cognitive impairment in Chinese elderly individuals: a population-based study. *J. Geriatr. Psychiatry Neurol.* 24, 184–190. doi: 10.1177/0891988711422528

Maducolil, M. K., Al-Obaidly, S., Olukade, T., Salama, H., Alqubaisi, M., and Al Rifai, H. (2020). Maternal characteristics and pregnancy outcomes of women with chronic hypertension: a population-based study. *J. Perinat. Med.* 48, 139–143. doi: 10.1515/jpm-2019-0293

Nahm, F. S. (2022). Receiver operating characteristic curve: overview and practical use for clinicians. *Korean J. Anesthesiol.* 75, 25–36. doi: 10.4097/kja.21209

Periáñez, J. A., Lubrini, G., García-Gutiérrez, A., and Ríos-Lago, M. (2021). Construct validity of the stroop color-word test: influence of speed of visual search, verbal fluency, working memory, cognitive flexibility, and conflict monitoring. *Arch. Clin. Neuropsychol.* 36, 99–111. doi: 10.1093/arclin/acaa034

Radetz, A., Mladenova, K., Ciolac, D., Gonzalez-Escamilla, G., Fleischer, V., Ellwardt, E., et al. (2021). Linking microstructural integrity and motor cortex excitability in multiple sclerosis. *Front. Immunol.* 12:748357. doi: 10.3389/fimmu.2021.748357

Raman, M. R., Tosakulwong, N., Zuk, S. M., Senjem, M. L., White, W. M., Fields, J. A., et al. (2017). Influence of preeclampsia and late-life hypertension on MRI measures of cortical atrophy. *J. Hypertens.* 35, 2479–2485. doi: 10.1097/HJH.0000000000001492

Rehbein, E., Kogler, L., Kotikalapudi, R., Sattler, A., Krylova, M., Kagan, K. O., et al. (2022). Pregnancy and brain architecture: associations with hormones, cognition and affect. *J. Neuroendocrinol.* 34:e13066. doi: 10.1111/jne.13066

Saenger, V. M., Barrios, F. A., Martínez-Gudiño, M. L., and Alcauter, S. (2012). Hemispheric asymmetries of functional connectivity and grey matter volume in the default mode network. *Neuropsychologia* 50, 1308–1315. doi: 10.1016/j.neuropsychologia.2012.02.014

Scarpina, F., and Tagini, S. (2017). The stroop color and word test. *Front. Psychol.* 8:557. doi: 10.3389/fpsyg.2017.00557

Schaare, H. L., Kharabian Masouleh, S., Beyer, F., Kumral, D., Uhlig, M., Reinelt, J. D., et al. (2019). Association of peripheral blood pressure with gray matter volume in 19- to 40-year-old adults. *Neurology* 92, e758–e773. doi: 10.1212/WNL.0000000000006947

Siepmann, T., Boardman, H., Bilderbeck, A., Griffanti, L., Kenworthy, Y., Zwager, C., et al. (2017). Long-term cerebral white and gray matter changes after preeclampsia. *Neurology* 88, 1256–1264. doi: 10.1212/WNL.0000000000003765

Strassburger, T. L., Lee, H. C., Daly, E. M., Szczepanik, J., Krasuski, J. S., Mentis, M. J., et al. (1997). Interactive effects of age and hypertension on volumes of brain structures. *Stroke* 28, 1410–1417. doi: 10.1161/01.STR.28.7.1410

Tian, R., Guo, Y., Ye, P., Zhang, C., and Luo, Y. (2020). The validation of the Beijing version of the montreal cognitive assessment in Chinese patients undergoing hemodialysis. *PLoS One* 15:e0227073. doi: 10.1371/journal.pone.0227073

Wilkerson, R. G., and Ogunbodede, A. C. (2019). Hypertensive disorders of pregnancy. *Emerg. Med. Clin. North Am.* 37, 301–316. doi: 10.1016/j.emc.2019.01.008

Xu, J., Lyu, H., Li, T., Xu, Z., Fu, X., Jia, F., et al. (2019). Delineating functional segregations of the human middle temporal gyrus with resting-state functional connectivity and coactivation patterns. *Hum. Brain Mapp.* 40, 5159–5171. doi: 10.1002/hbm.24763

Zhang, Q., Nguyen, T., Ivanize, J., and Wang, Y. (2020). High resolution water exchange rate mapping using 3D diffusion prepared arterial spin labeled perfusion MRI. ISMRM and SMRT virtual conference and exhibition. Available online at: https://cds.ismrm.org/protected/20MProceedings/PDFfiles/0034.html (accessed August 10, 2020).

frontiers | Frontiers in Neuroscience

TYPE Original Research
PUBLISHED 15 May 2023
DOI 10.3389/fnins.2023.1202374

OPEN ACCESS

EDITED BY
Han Lv,
Capital Medical University, China

REVIEWED BY
Guorong Wu,
Ghent University, Belgium
Guolin Ma,
China-Japan Friendship Hospital, China

*CORRESPONDENCE
Changhu Liang
✉ tigerlch@163.com

RECEIVED 08 April 2023
ACCEPTED 27 April 2023
PUBLISHED 15 May 2023

CITATION
Gao Y, Sui C, Chen B, Xin H, Che Y, Zhang X, Wang N, Wang Y and Liang C (2023) Voxel-based morphometry reveals the correlation between gray matter volume and serum P-tau-181 in type 2 diabetes mellitus patients with different HbA1c levels.
Front. Neurosci. 17:1202374.
doi: 10.3389/fnins.2023.1202374

Voxel-based morphometry reveals the correlation between gray matter volume and serum P-tau-181 in type 2 diabetes mellitus patients with different HbA1c levels

Yian Gao[1], Chaofan Sui[1], Boyao Chen[2], Haotian Xin[3], Yena Che[1], Xinyue Zhang[1], Na Wang[1], Yuanyuan Wang[4] and Changhu Liang[1]*

[1]Department of Radiology, Shandong Provincial Hospital Affiliated to Shandong First Medical University, Jinan, Shandong, China, [2]College of Radiology, Shandong First Medical University (Shandong Academy of Medical Sciences), Tai'an, Shandong, China, [3]Department of Radiology, Shandong Provincial Hospital, Cheeloo College of Medicine, Shandong University, Jinan, Shandong, China, [4]Department of Medical Imaging, Binzhou Medical University, Yantai, Shandong, China

Introduction: Emerging evidence suggested widespread decreased gray matter volume (GMV) and tau hyperphosphorylation were associated with type 2 diabetes mellitus (T2DM). Insulin resistance is one of the mechanisms of neuron degeneration in T2DM; it can decrease the activity of protein kinase B and increase the activity of glycogen synthesis kinase-3β, thus promoting the hyperphosphorylation of tau protein and finally leading to neuronal degeneration. However, the association between GMV and serum tau protein phosphorylated at threonine 181 (P-tau-181) in T2DM patients lacks neuroimaging evidence. We aimed to investigate the difference in brain GMV between T2DM patients with different glycated hemoglobin A1c (HbA1c) levels and healthy control (HC) subjects and the correlation between serum P-tau-181 and GMV in T2DM patients.

Methods: Clinical parameters, biochemical indicators, and MRI data were collected for 41 T2DM patients with high glycosylated hemoglobin level (HGL), 17 T2DM patients with normal glycosylated hemoglobin level (NGL), and 42 HC subjects. Voxel-based morphometry (VBM) method was applied to investigate GMV differences among groups, and multiple regression analysis was used to examine the correlation between serum P-tau-181 and GMV.

Results: Compared with HC subjects, the T2DM patients with HGL or NGL all showed significantly decreased GMV. Briefly, the GMV decreased in T2DM patients with HGL was mainly in the bilateral parahippocampal gyrus (PHG), right middle temporal gyrus (MTG), temporal pole (TPOmid), hippocampus (HIP), and left lingual gyrus. The GMV reduction in T2DM patients with NGL was in the right superior temporal gyrus (STG), and there was no significant difference in GMV between the two diabetic groups. The GMV values of bilateral PHG, right MTG, TPOmid, HIP, and STG can significantly (p<0.0001) distinguish T2DM patients from HC subjects in ROC curve analysis. In addition, we found that serum P-tau-181 levels were positively correlated with GMV in the right superior and middle occipital gyrus and cuneus, and negatively correlated with GMV in the right inferior temporal gyrus in T2DM patients.

Conclusion: Our study shows that GMV atrophy can be used as a potential biological indicator of T2DM and also emphasizes the important role of P-tau-181 in diabetic brain injury, providing new insights into the neuropathological mechanism of diabetic encephalopathy.

KEYWORDS

glycated hemoglobin, type 2 diabetes mellitus, gray matter volume, tau phosphorylated at threonine 181, voxel-based morphometry

1. Introduction

Diabetes mellitus (DM) is a metabolic disease characterized by chronic hyperglycemia caused by insufficient insulin secretion or defective insulin action (Classification and Diagnosis of Diabetes, 2022). Long-term complications of DM include progressive end-organ damage to the central nervous system, cardiovascular system, kidneys, eyes, and peripheral nervous system (Chen et al., 2012; Yazdanpanah et al., 2017; Yao et al., 2021). DM directly affects structural and metabolic alterations in the brain according to earlier research (Seaquist, 2010; García-Casares et al., 2014; Seaquist, 2015). Patients with type 2 diabetes mellitus (T2DM) had less gray matter volume (GMV) in the corticostriatal marginal area according to the structural MRI studies (Brundel et al., 2010; García-Casares et al., 2014). Research has demonstrated that decreased GMV in T2DM patients will result in default mode network dysfunction, which affects working memory and emotional processing and is linked to abnormalities in cognition, anxiety, and depressive regulation (Chen et al., 2016; Yao et al., 2021). It has been confirmed that cognitive function is positively correlated with GMV in patients with T2DM, and the decrease of GMV may lead to cognitive dysfunction (Roy et al., 2020; Yao et al., 2021). Clinical manifestations associated with diabetic brain damage include decreased cognitive, executive, and memory abilities (Brundel et al., 2012; Groeneveld et al., 2018; Hoyos et al., 2022), which increase the risk of vascular dementia and Alzheimer's disease (AD) in patients with T2DM (De la Monte and Tong, 2009; García-Casares et al., 2014; Hoyos et al., 2022). In addition, metabolic disturbances associated with T2DM affect a variety of biochemical pathways, which may also be responsible for neuronal dysfunction and cognitive decline (Yaffe et al., 2011; García-Casares et al., 2014).

The widely used indicator of glycemic management is glycosylated hemoglobin A1c (HbA1c), and it has been recognized as an acceptable indicator of long-term glycemic control by the Federal Drug Association (FDA), American Diabetes Association (ADA), and Canadian Diabetes Association (CDA) (American Diabetes Association, 2011; Yazdanpanah et al., 2017). High HbA1c levels have been linked to harm to brain structure, especially the hippocampus, according to earlier research (Geijselaers et al., 2015; Garfield et al., 2021). Additionally, an increasing number of studies have found that DM damages the integrity of the blood–brain barrier (BBB) structure, increasing its permeability, and causes cerebral hemodynamic impairment. Additionally, it has been demonstrated that tau pathology can cause BBB harm, whereas BBB dysfunction can result in tau hyperphosphorylation (Bogush et al., 2017; Qiao et al., 2020; Oliveira et al., 2021). The BBB is a highly selective semipermeable membrane that separates blood from nerve tissue. Under physiologically normal circumstances, the blood–brain barrier tightly regulates the chemicals that enter and leave the brain tissue, maintains the microenvironment homeostasis of the central nervous system, and guards against immune cells and toxins damaging brain cells (Coucha et al., 2018). Additionally, the blood–brain barrier has several specialized transporters, such as P-glycoprotein (gp), which may remove harmful amyloid β (Aβ) from brain tissue (Deo et al., 2014). The hyperphosphorylation of tau protein leads to the formation of neurofibrillary tangles (NFTs), resulting in the impairment of normal axonal transport, synaptic loss, and neuronal function impairment, which drives neurodegeneration and is closely related to T2DM (Ke et al., 2009; Oliveira et al., 2021). Smaller brain volumes in individuals with DM and white matter lesions have also been observed in neuroimaging studies, and these findings are likely to be connected to BBB degradation (Bogush et al., 2017). We thus proposed the following hypothesis: reduced gray matter volume in diabetes patients results in improper blood–brain barrier function, which, in turn, results in abnormal P-tau-181 metabolism.

At present, due to the lack of reliable and sensitive biomarkers, the definite diagnosis of diabetic brain injury is mainly based on psychological and clinical manifestations. The ability to research diabetic brain changes using brain imaging and image analytic techniques gave us the chance to examine the precise quantitative topological features of the brain structure. With its total automation, standardization, high accuracy, and dependability, voxel-based morphometry (VBM) is a traditional automatic whole-brain analysis approach that allows unbiased research to be performed regarding variations in gray matter between patients and controls (Ashburner and Friston, 2000). The study of the diabetic brain structure has made extensive use of and acceptance of the VBM approach (Chen et al., 2012; García-Casares et al., 2014; Liu et al., 2017; Wu et al., 2017; He et al., 2022). According to recent research, patients with AD dementia have higher serum P-tau-181 levels (Mielke et al., 2018), which correlate with the levels of tau protein in the cerebrospinal fluid and can also predict the progression of the disease in participants with normal cognitive function and in patients with mild cognitive impairment (Janelidze et al., 2020; Thijssen et al., 2020; Karikari et al., 2021). Moreover, a study has shown that plasma p-tau181 can be used in clinical settings as a blood-based predictive biomarker for cognitive deterioration (Clark et al., 2021). However, no studies have investigated the changes in GMV in T2DM patients with different HbA1c levels and the relationship between the changes in GMV and the metabolism of serum P-Tau-181 protein in T2DM patients.

Therefore, in this study, we classified patients with T2DM into two groups according to their HbA1c levels and included healthy controls

(Qaseem et al., 2018; Classification and Diagnosis of Diabetes, 2020). We aimed to compare the significant difference in GMV among the three groups and to analyze the correlation between serum P-tau-181 levels and GMV in T2DM patients, thereby providing a diagnostic biomarker of diabetic brain injury.

2. Materials and methods

2.1. Subjects

The Shandong Provincial Hospital Affiliated to Shandong First Medical University Subcommittee on Human Studies Institutional Review Board examined and approved the study. Before the study began, informed consent was acquired from each participant. All patients met the 1999 World Health Organization T2DM diagnostic criteria. Inclusion criteria for all patients are presented in the Supplementary materials. Current diabetes mellitus management recommendations from the American Diabetes Association (ADA) call for a baseline HbA1c goal of 7.0% for nonpregnant persons with diabetes (Qaseem et al., 2018; Classification and Diagnosis of Diabetes, 2020); therefore, we defined high HbA1c level (HGL) as the HbA1c level above 7.0%. Forty-one T2DM patients with HGL (age: 57.44 ± 9.4 years; 20 females and 21 males) and 17 T2DM patients with normal HbA1c level (NGL) (age: 59.71 ± 9.674 years; 7 females and 10 males) were recruited from outpatient clinics in Shandong Provincial Hospital between January 2022 and December 2022, and 42 healthy control (HC) subjects (age: 54.19 ± 8.194 years; 23 females and 19 males) were also included in our study.

The inclusion criteria for all patients were as follows: (1) an age range from 40 to 70 years; (2) junior high school education or higher; and (3) right-handedness. Patients were excluded from the study if they had (1) left-handedness; (2) neuropathies caused by other reasons; (3) brain trauma, surgery, or brain tumors; (4) acute complications of T2DM and severe hypertension; (5) history of any serious cerebrovascular, neurological, or psychiatric diseases; (6) abuse of alcoholism or drugs; or (7) any contraindications to MRI. The inclusion criteria for the HCs were as follows: (1) age 40–70 years, with junior high school education or above; (2) right-handed; (3) no history of diabetes and glycated hemoglobin (HbA1c) level of between 4 and 6%; (4) no history of any serious medical, psychiatric or neurologic diseases; (5) no history of head trauma, surgery, tumors or loss of consciousness; and (6) absence of alcohol or drug abuse.

2.2. Clinical assessment

All study subjects were evaluated with the Montreal Cognitive Assessment (MoCA) Beijing version[1] by the measurers designated by the research group. To ensure the homogeneity of measurement results, all measurers were trained in the same institution, and the expert group members conducted homogeneous evaluation on the measurers to ensure the homogeneity of measurement results. Plasma samples were obtained from all subjects by venous puncture, and a total of 5 mL of venous blood was drawn with an EDTA tube for anticoagulation and centrifuged at 3000 r/min for 15 min; the separated plasma was stored at −20°C and concentrated at −70°C for detection. Enzyme-linked immunosorbent assay (ELISA) was performed according to the instructions of the Tau (Phospho) [pT 181] Human ELISA Kit provided by Thermo Fisher/Invitrogen, United States. All specimens were tested with the same lot of reagents.

2.3. Image acquisition

All participants were imaged utilizing a 32-channel head coil product on a MAGNETOM Skyra 3.0 T MR scanner (Siemens Healthcare, Erlangen, Germany). The three-dimensional T1-weighted (3DT1W) rapid acquisition gradient-echo sequence with the following settings was used to capture the structural images: TR/TE = 2300/2.32 ms, slice thickness = 0.9 mm, the number of slices = 213, and FOV = 24 × 24 cm^2. To further identify any anomalies in the brain, T2W fluid-attenuated inversion recovery and T2W turbo spin echo were acquired. All participants held motionless during the scan.

2.4. Data preprocessing

Following data acquisition, 3D T1W image processing was carried out using VBM with DARTEL (Diffeomorphic Anatomical Registration Through Exponentiated Lie Algebra) (Ashburner, 2007) method based on the statistical parametric mapping (SPM8,[2]) toolbox. Throughout the iterative unified model, DARTEL's fully deformable registration and normalization method ensures precise intersubject alignment. The anterior commissure (AC), posterior commissure (PC), and mid-sagittal plane were used to manually identify landmarks to match all of the 3D T1W pictures to conventional AC-PC space. The New Segment tool in SPM was then used to segment the aligned images into gray matter (GM), white matter (WM), and cerebrospinal fluid (CSF) in native space with unified segmentation. The next step was to tightly modify each of the segmented GM images to create a set of aligned GM images. The DARTEL algorithm was then applied to the serial images from all the individuals who had been aligned to build the study-specific GM templates. All aligned GM images were distorted to the template during template generation, producing a number of flow fields that parameterized the deformation. After spatial normalization to Montreal Neurological Institute (MNI) space, the GM images were modulated to correct local volume expansion due to the nonlinear component of the spatial transformation. The generated gray matter volume (GMV) images were then smoothed with an isotropic Gaussian kernel of 8 mm full width at half maximum (FWHM).

2.5. Statistical analysis

Statistical analysis of demographic data and clinical parameters was performed using SPSS Version 24.0 (SPSS Inc., Chicago, IL,

1 www.mocatest.org

2 http://www.fil.ion.ucl.ac.uk/spm

United States). Shapiro–Wilk test(S-W test) was used for the normality test, then we used one-way ANOVA to analyze the clinical parameters of the three groups. Nonparametric tests were used for data that did not meet the normality test and sex differences were tested using the Chi-square test (χ^2).

To analyze the differences in GMV images among the three groups, voxel-wise one-way analysis of covariance (ANCOVA) was performed using SPM 8, with age and gender as covariates (we readded education level as covariates in Supplementary materials, the results are shown in Supplementary Table S1), and the analysis was constrained in the binary AAL template as mask (Tzourio-Mazoyer et al., 2002). The significant results were derived after using the cluster-level false discovery rate (FDR) multiple comparisons correction (cluster-wise threshold of $q < 0.05$ based on an uncorrected voxel-wise threshold of $p < 0.001$). For each significantly altered cluster identified by ANCOVA, two-sample t-tests with cluster-level FDR correction (voxel-wise $p < 0.001$, cluster-wise $q < 0.05$) were applied within that cluster to compare differences between two groups. The anatomical positions of clusters were identified using Xjview software[3] and finally visualized by Mricron software.

The voxel-wise correlation between GMV and serum P-tau-181 for all T2DM patients was analyzed using multiple regression in SPM 8, while controlling age and gender as covariates and using the binary AAL template as mask. Multiple comparisons were also corrected using the cluster-level FDR method (voxel-wise $p < 0.001$, cluster-wise $q < 0.05$). In addition, we used both P-tau-181 and HbA1c as independent variables in multiple regression to investigate their combined effects on GMV (the details are presented in the Supplementary materials).

For significantly different clusters between groups, we extracted the mean values within clusters for receiver operating characteristic (ROC) curves to assess each value's potential to serve as a crucial neuroimaging biomarker to distinguish between T2DM with HGL group, T2DM with NGL group, and HC group. The area under the curve (AUC) was then calculated using the MedCalc Statistical Software.[4] We calculated the corresponding optimal cutoff point, the maximum Youden index (Fluss et al., 2005), specificity, sensitivity, and 95% confidence intervals (CIs). Finally, the DeLong test (DeLong et al., 1988) was used to statistically compare the AUC for each mean value.

3. Results

3.1. Demographic and clinical characteristics

The demographic information and clinical data of the three groups are displayed in Table 1. Age, education attainment, or MoCA scores did not significantly differ among the three groups. Additionally, no notable variations were discovered in duration of disease, GMV, P-tau-181, total cholesterol, triglycerides, high-density lipoprotein (HDL), or low-density lipoprotein (LDL) between the T2DM with HGL group and T2DM with NGL group; however, the T2DM with HGL group had significantly higher fasting blood glucose (Glu) and HbA1c.

3.2. Altered gray matter volume among groups

Compared with the HC group, the T2DM with HGL group showed significantly decreased GMV in the bilateral parahippocampal gyrus (PHG), right middle temporal gyrus (MTG), parahippocampal gyrus (PHG), temporal pole (TPOmid), hippocampus (HIP), and left lingual gyrus. The T2DM with NGL group also showed decreased GMV in the right superior temporal gyrus (STG) compared with the HC group. No notable variations were discovered between the T2DM with HGL and T2DM with NGL groups in GMV (Table 2; Figure 1). When age, gender, and education level were used as covariates to recalculate the differences in brain areas among the three groups, we found that the significantly different brain regions were still concentrated in the superior temporal gyrus, middle temporal gyrus, hippocampus, and parahippocampal gyrus. The details are presented in Supplementary Table S1.

3.3. Correlation of gray matter volume with serum P-tau-181 in the diabetes mellitus group

Correlation analysis showed that GMV in many brain regions correlated with P-tau-181 levels in all T2DM patients. There were positive and negative correlations between GMV and serum P-tau-181 values in the T2DM groups ($p < 0.001$). The GMV of the right superior occipital gyrus (SOG), cuneus (CUN), and middle occipital gyrus (MOG) showed significantly positive correlations with serum P-tau-181, and the GMV of the right inferior temporal gyrus (ITG) was significantly negatively correlated with P-tau-181 (Table 3; Figure 2). We also investigated the combined effects of P-tau-181 and HbA1c on GMV using multivariate analysis, and the detailed results are shown in Supplementary Table S2.

3.4. The results of ROC curve analysis

According to the ROC curves, the GMV of the bilateral PHG, right MTG, TPOmid, and HIP can distinguish the T2DM with HGL group from the HC group; all attained a significance level of $p < 0.001$ for AUC. Using a single ROI, the DeLong test showed no significant differences in the AUC values, suggesting that they were equally effective at distinguishing T2DM with HGL and HC groups ($p > 0.05$). Furthermore, the GMV of the right STG could discriminate the T2DM with NGL and HC groups. The cutoff values of each value in the different ROIs were chosen according to the Youden index (Table 4; Figure 3).

3 http://www.alivelearn.net/xjview

4 https://www.medcalc.org

TABLE 1 Demographic and cognitive characteristics of T2DM patients and healthy controls.

Characteristic	HGL	NGL	HC	*p* value (ANOVA/χ^2)	*P* value (post-hoc)		
					HGL vs. HC	HGL vs. NGL	NGL vs. HC
Gender	21 M/20 F	10 M/7 F	19 M/23 F	0.627$^{\chi2}$	-	-	-
Age (y)	57.44 ± 9.4	59.71 ± 9.674	54.19 ± 8.194	0.072^{a}	-	-	-
Education (y)	12.29 ± 3.64	11.82 ± 3.23	13.90 ± 4.11	0.073^{a}	-	-	-
MoCA (score)	24.00 ± 3.33	25.41 ± 2.78	25.28 ± 3.37	0.142^{a}	-	-	-
Duration (y)	11.83 ± 8.41	7.82 ± 8.06	-	0.1^{t}	-	-	-
Smoke, n (%)	11(27)	4(23)	4(9)	0.116$^{\chi2}$	-	-	-
Hypertension, n (%)	23(56)	7(41)	8(19)	0.002$^{\chi2}$	<0.001	N.S	N.S
Glu (mmol/l)	8.9(7.85 ~ 11.21)	6.86(6.36 ~ 7.75)	5.49(4.74 ~ 6.09)	<0.001	<0.001	0.022	0.006
HbA1c (%)	9.40 ± 1.72	6.63 ± 0.22	5.77 ± 0.35	<0.001^{a}	<0.001	<0.001	0.009
BMI (kg/m^2)	26.21 ± 2.83	25.30 ± 2.93	23.93 ± 3.35	0.004	0.001	0.311	0.124
CHOL (mmol/l)	5.02 ± 1.20	4.76 ± 1.06	5.08 ± 1.04	0.554^{a}	-	-	-
TG (mmol/l)	1.80 ± 1.01	1.72 ± 1.23	1.25 ± 0.54	0.017^{a}	0.006	0.766	0.069
HDL (mmol/l)	1.27 ± 0.40	1.36 ± 0.23	1.52 ± 0.34	0.007^{a}	0.002	0.399	0.115
LDL (mmol/l)	3.1 ± 0.91	2.73 ± 0.88	3.02 ± 0.81	0.25^{a}	-	-	-
GMV (mm^3)	528.86 ± 42.46	541.61 ± 26.27	588.00 ± 45.49	<0.001^{a}	<0.001	0.290	<0.001
P-Tau-181	312.02 ± 56.07	301.42 ± 64.53	276.86 ± 56.56	0.022^{a}	0.007	0.544	0.160

HGL, T2DM patients with HGL; NGL, T2DM patients with NGL; HC, healthy controls; GMV, gray matter volume; χ^2, Chi-square test; a, ANOVA test; MoCA, Montreal Cognitive Assessment; *t*, two-sample *t* test; N.S, not significant.

TABLE 2 Brain regions with reduced gray matter volume in the T2DM patients with HGL and T2DM patients with NHL compared with the healthy controls.

Condition	Brain regions	Cluster size	*F* score of the peak voxel	MNI coordinates of the peak voxel (mm)		
				x	*y*	*z*
HGL < HC	Right middle temporal gyrus	756	4.22	54	−31.5	−4.5
	Left parahippocampal gyrus	720	5.14	−15	−24	−15
	Left lingual gyrus	208	4.10	−22.5	−45	−9
	Right temporal pole	1,051	4.49	40.5	21	−34.5
	Right parahippocampal gyrus	284	4.31	21	−25.5	−16.5
	Right hippocampus	474	4.05	16.5	−7.5	−13.5
NGL<HC	Right superior temporal gyrus	362	4.30	48	−37.5	9

HGL, T2DM patients with HGL; NGL, T2DM patients with NGL; HC, healthy controls.

4. Discussion

In the present study, we investigated the differences in GMV between T2DM patients with different levels of HbA1c and healthy controls and further analyzed the correlation between brain GMV and serum P-tau-181 levels in all T2DM patients. The results showed that regardless of how high or low the level of HbA1c was in patients with T2DM, the brain GMV was decreased, and the increase in serum P-tau-181 was significantly correlated with the change in GMV, which suggested that regardless of glycemic control, T2DM patients should be treated as soon as possible to minimize brain damage. In addition, serum P-tau-181 concentrations are increased in T2DM patients, and more studies are needed to clarify the role of serum P-tau-181 as a potential biomarker of diabetic mild cognitive impairment.

There was no significant difference in GMV between the T2DM with HGL and NGL groups, which is similar to a previous study of functional MRI parameters in T2DM with HGL and NGL groups that showed no significant difference in regional homogeneity (ReHo) and amplitude of low-frequency fluctuation (ALFF) indicators between the two groups, indicating that there was no significant difference in the activity level of neurons in brain tissue between the two groups (Zhang et al., 2021). Since most of the GM is made up of the soma and dendrites of neurons, it is reasonable to assume that the structure of the GM in patients with high and normal HbA1c levels is similar.

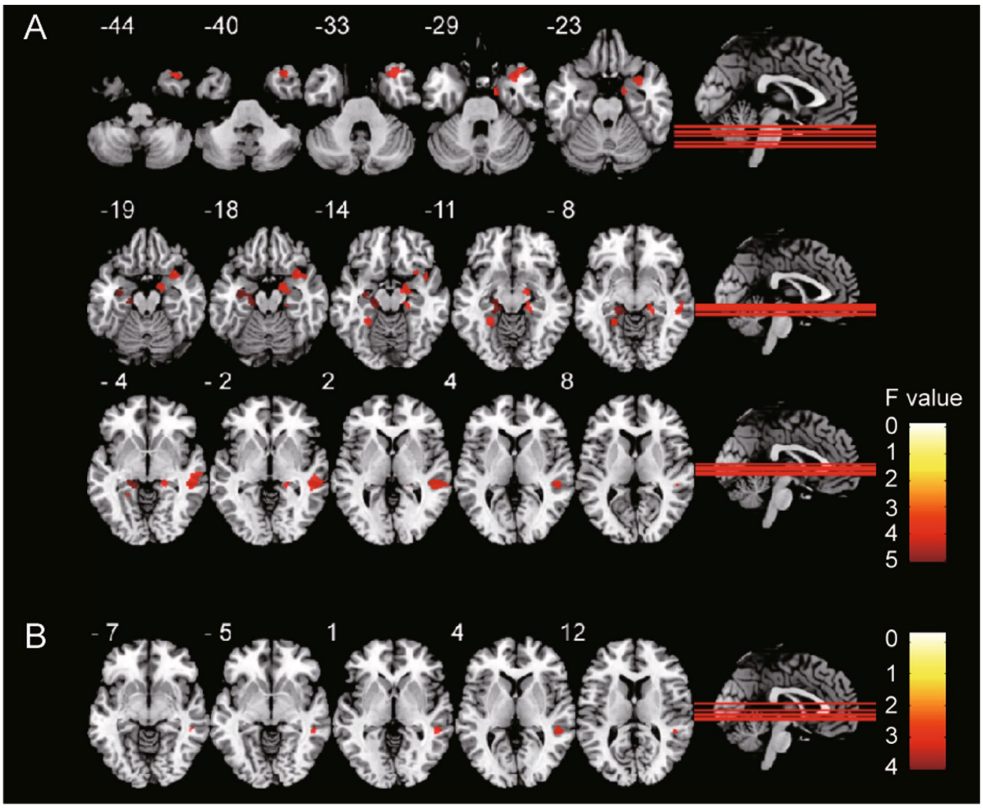

FIGURE 1
GMV differences among groups. The gray matter volume of **(A)** T2DM with HGL group and **(B)** T2DM with NGL group was significantly (cluster-level FDR correction, $p<0.05$) decreased compared with that in the HC group. The color bar shows the range of *F* values.

TABLE 3 Brain regions significantly associated with P-Tau-181 in T2DM patients.

cerebral hemisphere	Brain regions	*T* score of the peak voxel	Cluster size	MNI coordinates of the peak voxel (mm)		
				x	*y*	*z*
Areas of positive correlation between P-Tau-181 and gray matter volume in patients with T2DM						
Right	Superior occipital gyrus	4.3184	173	16.5	−99	15
Right	Cuneus	4.3184	105	16.5	−99	15
Right	Middle occipital gyrus	3.8897	95	28.5	−88.5	16.5
Areas of negative correlation between P-Tau-181 and gray matter volume in patients with T2DM						
Right	Inferior temporal gyrus	3.8733	25	51	−33	−18

The voxel-wise correlation between GMV and serum P-tau-181 for all T2DM patients was analyzed using multiple regression (cluster-level FDR<0.05).

However, GMV was significantly decreased in both T2DM groups compared with the HC group. We further found that the brain GMV of the T2DM with HGL group decreased mainly in the right MTG, PHG, right TPOmid, and right hippocampus; the GMV of right the STG in the T2DM with NGL group was decreased. This is consistent with previous studies showing a decrease in GMV in DM patients. In previous cross-sectional investigations, right temporal cortex and hippocampus volumes in individuals with T2DM have been found to be decreased (Chen et al., 2012; Zhang et al., 2014). Since hyperglycemia may produce a variety of metabolic and molecular changes, including brain cell malfunction or death, it is thought to be the main cause of diabetes-related disturbances in the brain. Consequently, the ensuing neuronal death may be detected on MRI as extensive atrophy (Tomlinson and Gardiner, 2008; Liu et al., 2017; Yao et al., 2021; Cui et al., 2022). The default mode network (DMN), which includes the MTG, has been strongly associated with attention, working memory, language processing, voice production, and related processes (Fox et al., 2006). The shift from normal cognition to moderate cognitive impairment in T2DM patients is accelerated by MTG atrophy, which is linked to the neurodegeneration of the disease and cognitive dysfunction (Zhang et al., 2014; Wu et al., 2017).

The hippocampus is a growth of the cerebral cortex's edge and is in charge of memory and learning (Squire, 1992). The hippocampus is extremely vulnerable to hyperglycemia (Sonneville et al., 2012; Yun et al., 2021) with direct neurotoxic consequences, such as increased polyol pathway flow, oxidative stress, and elevated development of

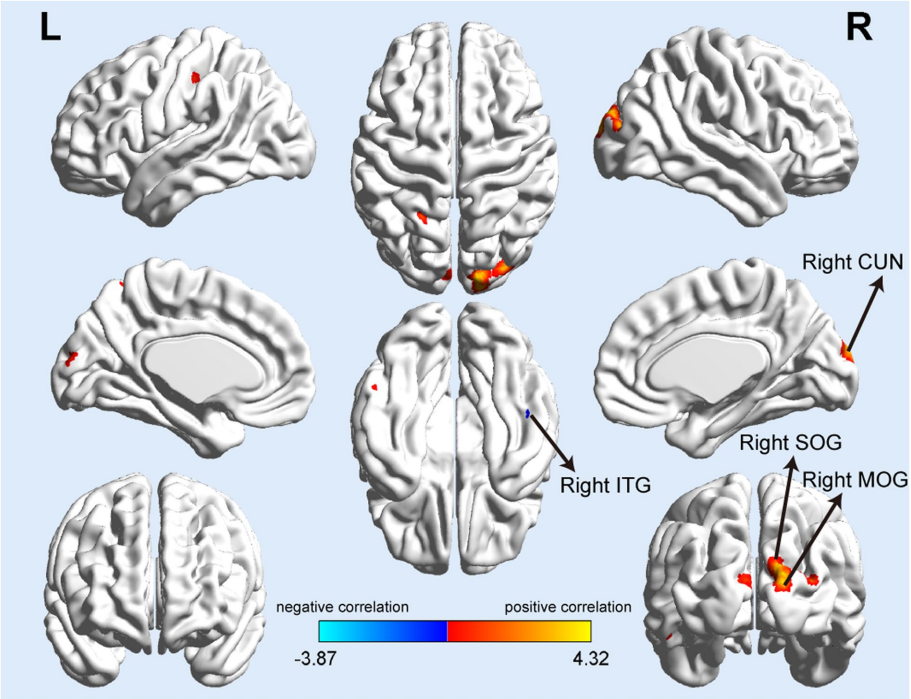

FIGURE 2
Serum P-tau-181 correlated with gray matter volume in T2DM patients. The mean GMV values of the right superior and middle occipital gyrus (SOG and MOG), right cuneus (CUN) showed significantly positive correlations with serum P-tau-181, and the GMV of the right inferior temporal gyrus (ITG) was significantly negatively correlated with serum P-tau-181.

TABLE 4 The statistics of ROC curve analysis for altered brain clusters that distinguish the T2DM patients with HGL from the T2DM patients with NGL and healthy controls.

Clusters	*P* value	Cutoff value	SEN	SPE	AUC	95% CI
HGL vs. HC						
Right middle temporal gyrus	<0.0001	0.524	0.929	0.512	0.763	0.683–0.868
Left parahippocampal gyrus	<0.0001	0.514	0.810	0.707	0.798	0.702–0.894
Right temporal pole	<0.0001	0.630	0.548	0.951	0.772	0.671–0.873
Right parahippocampal gyrus	<0.0001	0.453	0.619	0.854	0.744	0.636–0.851
Right hippocampus	<0.0001	0.658	0.571	0.854	0.748	0.643–0.853
NGL vs. HC						
Right superior temporal gyrus	<0.0001	0.571	0.714	0.882	0.799	0.688–0.910

HGL, T2DM patients with HGL; NGL, T2DM patients with NGL; HC, healthy controls; SEN, sensitivity; SPE, specificity; AUC, The area under the curve; 95% CI, 95% Confidence interval.

advanced glycation end products (AGEs), all of which have been linked to neuronal disease (Gispen and Biessels, 2000). Furthermore, spatial memory and cognition are impaired in diabetic animal models, and hippocampal neuronal death is also promoted (Sadeghi et al., 2016). The development of memories for highly processed sensory information may be greatly influenced by the parahippocampal area in general (Engelien et al., 2000). The PHG is one of the main hubs of the DMN in the medial temporal lobe during the resting state according to previous studies, and injury to the PHG has been proven to cause considerable memory problems (Suzuki et al., 1993; Ward et al., 2014). Past studies have shown that in diabetics, reduced insulin levels lead to a disorder in insulin signaling, excessive deposition of hyperphosphorylated tau, and ultimately atrophy of the hippocampus and parahippocampal region, resulting in a series of clinical symptoms (Adachi et al., 2021). In fact, hippocampal damage occurs throughout the course from impaired fasting glucose levels to diabetes (Convit et al., 2003; Lamport et al., 2009). Long-term hyperglycemia can result in a series of metabolic changes in the body, such as the accumulation of AGEs and the creation of reactive oxygen species, as well as oxidative stress and the production of various inflammatory factors. It can also damage brain neurons and eventually cause gray matter atrophy (Chen et al., 2017). On the other hand, people with T2DM who have persistently high HbA1c levels are more likely to develop vascular problems such retinopathy, atherosclerosis, peripheral artery disease, and cerebrovascular disease. Hypoperfusion of nearby brain tissues will result from damage to cerebral microvessels (Paneni et al.,

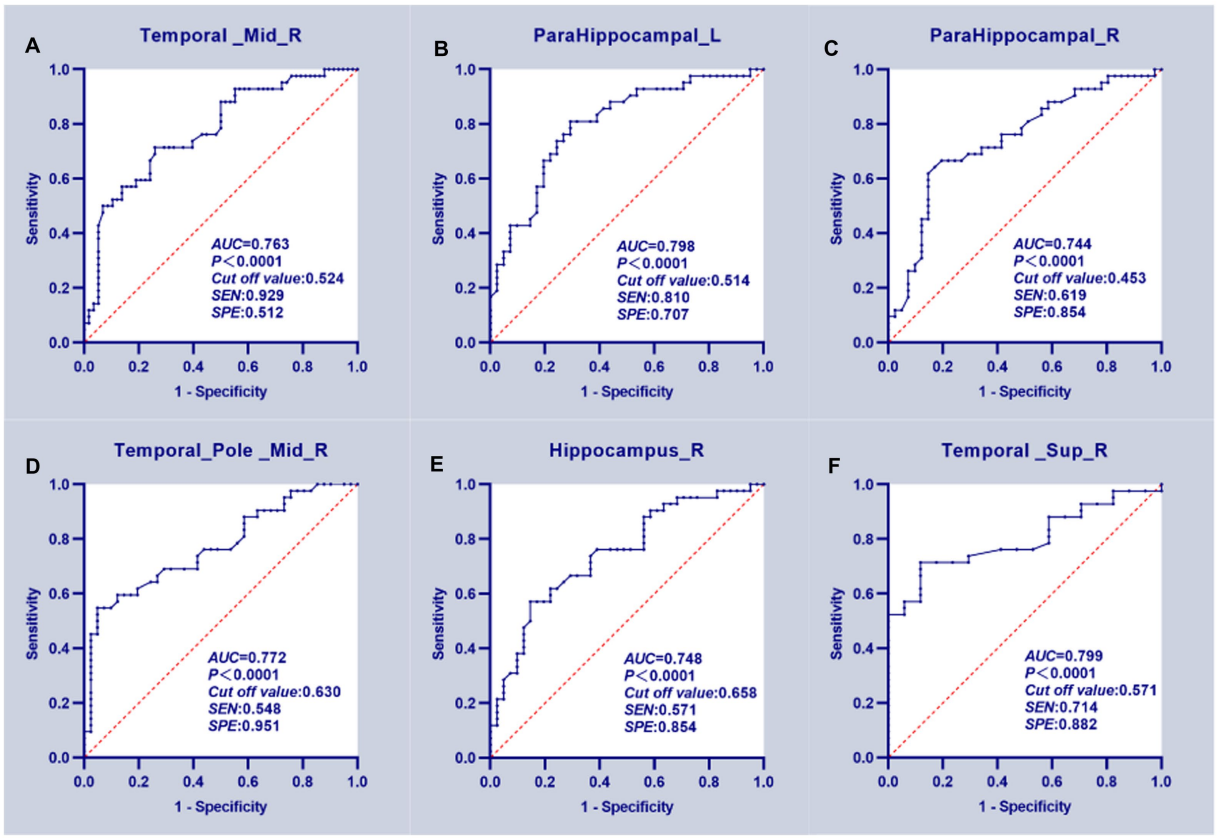

FIGURE 3
ROC curve analysis results. **(A–E)** The mean GMV values of five clusters which can significantly (p<0.0001 for AUC value) distinguish T2DM patients with HGL from the HC group. **(F)** The GMV of the right superior temporal gyrus significantly discriminated T2DM patients in the NGL and HC groups.

2013). In addition, HbA1c levels are consistent with blood glucose levels and diabetes-related complications (Xu et al., 2014). Therefore, the damage to cerebrovascular integrity may be the underlying mechanism of brain atrophy in T2DM patients. In addition, although there was no significant GMV difference between the two T2DM groups, the two groups of diabetic patients showed different volume atrophy of brain regions compared with the healthy group, suggesting that diabetic brain atrophy is specific to hyperglycemia. In a study of factors associated with brain atrophy in normal elderly subjects, HbA1c was identified as a risk factor for a higher incidence of brain atrophy (Enzinger et al., 2005). This confirms our finding that patients in the hyperglycemia group are characterized by more brain atrophy. Additionally, ROC curve research showed that the GMVs of the bilateral PHG, right MTG, TPOmid, HIP, and STG, which may be useful as diagnostic biomarkers, had excellent classification performance for separating T2DM patients from HC subjects.

The deposition of amyloid-protein (Aβ) in the brain parenchyma and phosphorylated tau deposition in NFTs in cerebral neurons are two important features of Alzheimer's disease (AD) (Zou et al., 2020). Tau protein is essential to maintain the stability of microtubules in neurons of the central nervous system (Khan and Bloom, 2016). Instead, hyperphosphorylated tau dissociates and forms insoluble aggregates in neurons called NFTs, leading to loss of synapses and impaired neuronal function, which together with Aβ drive neurodegeneration (Daly et al., 2000; Calvo-Flores Guzman et al., 2020). It has been established that diabetes and AD have a number of shared pathogenic factors (Jash et al., 2020; Sun et al., 2020). These processes might encourage Aβ and phosphorylated tau protein to play an important role in the development of diabetes. An increasing number of studies have shown that the longitudinal increase in serum P-tau-181 is significantly associated with abnormal cerebrospinal fluid biomarker levels, structural imaging atrophy and cognitive deterioration (Nam et al., 2020; Zou et al., 2020; Chen et al., 2021). It has been further demonstrated that plasma P-tau-181 can be used to detect cerebral amyloidosis not only in clinical AD but also in asymptomatic AD patients (De Meyer et al., 2022). Therefore, we collected the serum P-tau-181 of healthy subjects and T2DM patients and tried to reveal the relationship between serum P-tau-181 and diabetic brain damage.

Some studies have found that atrophy of the occipital lobe in T2DM patients is mainly located in the bilateral lateral occipital lobe, lingual gyrus and precuneus (Chen et al., 2017). The lingual gyrus and the middle occipital gyrus are considered to be the brain regions related to the processing of visual information and the encoding of visual memory (Cui et al., 2016). The inferior temporal gyrus also contributes significantly to visual perception (Buckley et al., 1997). These abnormalities in the occipital and inferior temporal lobes may be due to underlying visual impairment, a well-known complication associated with T2DM and diabetic retinopathy. We further found that serum P-tau-181 was positively correlated with the GMV of the right SOG, MOG and CUN but negatively correlated with the GMV of the right ITG for all T2DM patients. In a longitudinal study of

Parkinson's disease (PD) (the average age was 60.89 years), a transient decrease in CSF P-tau was observed in the early stages of the disease (Dolatshahi et al., 2018). It is speculated that this is due to the toxic P-tau in neurons in the early stage of the disease in the form of NFTs, which leads to the compensatory absorption of more functional tau molecules by cells to reverse the function of neuronal transportation; this hypothesis has been verified regarding the ot-syn protein in PD (Førland et al., 2018). In addition, a study on AD demonstrated that serum P-tau-181 was significantly positively correlated with CSF P-tau-181, suggesting that P-tau-181 in plasma should be of brain origin (Tatebe et al., 2017). As a disease with NFTs, the transient decrease in CSF P-tau in PD patients of the same age group may also occur in T2DM patients of the same age group, and the serum P-tau-181 content in T2DM patients may also decrease transiently. If this phenomenon is finally confirmed, the positive correlation between GMV and serum P-tau-181 levels in T2DM patients in this study may also be explained. In addition, a study of nonlinear changes in GMV in AD patients suggests that increased GMV in some brain regions may be due to early neuroinflammation associated with amyloid accumulation, followed by recovery at the onset of neurodegenerative processes associated with tau accumulation (Gispert et al., 2015). DM, which demonstrates the same amyloid accumulation as AD, may also exhibit an increase in GMV associated with neuroinflammation in the early stage of the disease, and when P-tau-181 accumulates excessively, GMV in some brain regions begins to decrease. This also supports the correlation between GMV and serum P-tau levels in DM patients proposed in this study.

The main limitation of this study is that it is a cross-sectional study with a relatively small sample size. In the future, a longitudinal study will be needed to evaluate the relationship between diabetic regional brain atrophy and relevant clinical variables in a larger sample. In addition, due to the pattern of participation, the patients in this study were relatively young, and we could not reject the possibility that the results might only appear in young T2DM patients; at the same time, the imaging and pathological changes must be noted as being possibly characteristic of young patients with T2DM. This study also found bilateral cerebral hemisphere asymmetry in the changes in GM structure in T2DM patients. In the future, we intend to complete our study by performing specific tests on subjects in multiple cognitive domains to analyze a specific cognitive function and further study the white matter structures or the functional metabolic changes related to this asymmetry to better explain correlations with the clinical characteristics of T2DM patients.

5. Conclusion

In summary, we confirmed the differences in GMV between T2DM patients with different HbA1c level and healthy subjects, and suggested that GMV atrophy can be used as a potential biological indicator of T2DM. In addition, we found a significant correlation between serum P-tau-181 and GMV in T2DM patients, indicating the critical role that P-tau-181 plays in diabetic encephalopathy and providing new insights into the neuropathological mechanism of diabetic encephalopathy. This study demonstrates that patients with T2DM, regardless of HbA1c level, should receive active and reasonable intervention as soon as possible to reduce or block further T2DM-related deterioration.

Data availability statement

The original contributions presented in the study are included in the article/Supplementary materials, further inquiries can be directed to the corresponding author.

Ethics statement

The studies involving human participants were reviewed and approved by the Shandong Provincial Hospital Affiliated to Shandong First Medical University Subcommittee on Human Studies Institutional Review Board examined and approved the study.

Author contributions

YG wrote the main manuscript text. CS, BC, HX, YC, XZ, NW, and YW prepared the clinical data and imaging data. CL revised the main manuscript text. All authors contributed to the article and approved the submitted version.

Funding

This work was supported by grants from the Shandong Provincial Natural Science Foundation (ZR2020MH288).

Acknowledgments

The authors thank all of the volunteers and patients for their participation in our study.

Conflict of interest

The authors declare that the research was conducted in the absence of any commercial or financial relationships that could be construed as a potential conflict of interest.

Publisher's note

Supplementary material

The Supplementary material for this article can be found online at: https://www.frontiersin.org/articles/10.3389/fnins.2023.1202374/full#supplementary-material

References

Adachi, Y., Ota, K., Minami, I., Yamada, T., and Watanabe, T. (2021). Lower insulin secretion is associated with hippocampal and parahippocampal gyrus atrophy in elderly patients with type 2 diabetes mellitus. *J. Diabetes Investig.* 12, 1908–1913. doi: 10.1111/jdi.13554

American Diabetes Association (2011). Standards of medical care in diabetes–2011. *Diabetes Care* 34, S11–S61. doi: 10.2337/dc11-S011

Ashburner, J. (2007). A fast diffeomorphic image registration algorithm. *NeuroImage* 38, 95–113. doi: 10.1016/j.neuroimage.2007.07.007

Ashburner, J., and Friston, K. J. (2000). Voxel-based morphometry–the methods. *NeuroImage* 11, 805–821. doi: 10.1006/nimg.2000.0582

Bogush, M., Heldt, N. A., and Persidsky, Y. (2017). Blood brain barrier injury in diabetes: unrecognized effects on brain and cognition. *J. Neuroimmune Pharmacol.* 12, 593–601. doi: 10.1007/s11481-017-9752-7

Brundel, M., Van den Berg, E., Reijmer, Y. D., De Bresser, J., Kappelle, L. J., Biessels, G. J., et al. (2012). Cerebral haemodynamics, cognition and brain volumes in patients with type 2 diabetes. *J. Diabetes Complicat.* 26, 205–209. doi: 10.1016/j.jdiacomp.2012.03.021

Brundel, M., Van den Heuvel, M., De Bresser, J., Kappelle, L. J., and Biessels, G. J.Utrecht Diabetic Encephalopathy Study Group (2010). Cerebral cortical thickness in patients with type 2 diabetes. *J. Neurol. Sci.* 299, 126–130. doi: 10.1016/j.jns.2010.08.048

Buckley, M. J., Gaffan, D., and Murray, E. A. (1997). Functional double dissociation between two inferior temporal cortical areas: perirhinal cortex versus middle temporal gyrus. *J. Neurophysiol.* 77, 587–598. doi: 10.1152/jn.1997.77.2.587

Calvo-Flores Guzman, B., Chaffey, T. E., Palpagama, T. H., Waters, S., Boix, J., Tate, W. P., et al. (2020). The interplay between Beta-amyloid 1-42 (Abeta(1-42))-induced hippocampal inflammatory response, p-tau, vascular pathology, and their synergistic contributions to neuronal death and behavioral deficits. *Front. Mol. Neurosci.* 13:522073. doi: 10.3389/fnmol.2020.552073

Chen, S. D., Huang, Y. Y., Shen, X. N., Guo, Y., Tan, L., Dong, Q., et al. (2021). Longitudinal plasma phosphorylated tau 181 tracks disease progression in Alzheimer's disease. *Transl. Psychiatry* 11:356. doi: 10.1038/s41398-021-01476-7

Chen, Z., Li, L., Sun, J., and Ma, L. (2012). Mapping the brain in type II diabetes: voxel-based morphometry using DARTEL. *Eur. J. Radiol.* 81, 1870–1876. doi: 10.1016/j.ejrad.2011.04.025

Chen, Y., Liu, Z., Wang, A., Zhang, J., Zhang, S., Qi, D., et al. (2016). Dysfunctional organization of default mode network before memory impairments in type 2 diabetes. *Psychoneuroendocrinology* 74, 141–148. doi: 10.1016/j.psyneuen.2016.08.012

Chen, Z., Zang, X., Liu, M., Liu, M., Li, J., Gu, Z., et al. (2017). Abnormal alterations of cortical thickness in 16 patients with type 2 diabetes mellitus: a pilot MRI study. *Chin. Med. Sci. J.* 32, 75–72. doi: 10.24920/J1001-9294.2017.010

Chen, J., Zhang, J., Liu, X., Wang, X., Xu, X., Li, H., et al. (2017). Abnormal subcortical nuclei shapes in patients with type 2 diabetes mellitus. *Eur. Radiol.* 27, 4247–4256. doi: 10.1007/s00330-017-4790-3

Clark, C., Lewczuk, P., Kornhuber, J., Richiardi, J., Maréchal, B., Karikari, T. K., et al. (2021). Plasma neurofilament light and phosphorylated tau 181 as biomarkers of Alzheimer's disease pathology and clinical disease progression. *Alzheimers Res. Ther.* 13:65. doi: 10.1186/s13195-021-00805-8

Classification and Diagnosis of Diabetes (2020). Standards of medical care in diabetes-2020. *Diabetes Care* 43, S14–s31. doi: 10.2337/dc20-S002

Classification and Diagnosis of Diabetes (2022). Standards of medical Care in Diabetes-2022. *Diabetes Care* 45, S17–s38. doi: 10.2337/dc22-S002

Convit, A., Wolf, O. T., Tarshish, C., and De Leon, M. J. (2003). Reduced glucose tolerance is associated with poor memory performance and hippocampal atrophy among normal elderly. *Proc. Natl. Acad. Sci. U. S. A.* 100, 2019–2022. doi: 10.1073/pnas.0336073100

Coucha, M., Abdelsaid, M., Ward, R., Abdul, Y., and Ergul, A. (2018). Impact of metabolic diseases on cerebral circulation: structural and functional consequences. *Compr. Physiol.* 8, 773–799. doi: 10.1002/cphy.c170019

Cui, Y., Li, S. F., Gu, H., Hu, Y. Z., Liang, X., Lu, C. Q., et al. (2016). Disrupted brain connectivity patterns in patients with type 2 diabetes. *AJNR Am. J. Neuroradiol.* 37, 2115–2122. doi: 10.3174/ajnr.A4858

Cui, Y., Tang, T. Y., Lu, C. Q., and Ju, S. (2022). Insulin resistance and cognitive impairment: evidence from neuroimaging. *J. Magn. Reson. Imaging* 56, 1621–1649. doi: 10.1002/jmri.28358

Daly, N. L., Hoffmann, R., Otvos, L., and Craik, D. J. (2000). Role of phosphorylation in the conformation of tau peptides implicated in Alzheimer's disease. *Biochemistry* 39, 9039–9046. doi: 10.1021/bi0004807

De la Monte, S. M., and Tong, M. (2009). Mechanisms of nitrosamine-mediated neurodegeneration: potential relevance to sporadic Alzheimer's disease. *J. Alzheimers Dis.* 17, 817–825. doi: 10.3233/JAD-2009-1098

De Meyer, S., Vanbrabant, J., Schaeverbeke, J. M., Reinartz, M., Luckett, E. S., Dupont, P., et al. (2022). Phospho-specific plasma p-tau181 assay detects clinical as well as asymptomatic Alzheimer's disease. *Ann. Clin. Transl. Neurol.* 9, 734–746. doi: 10.1002/acn3.51553

DeLong, E. R., DeLong, D. M., and Clarke-Pearson, D. L. (1988). Comparing the areas under two or more correlated receiver operating characteristic curves: a nonparametric approach. *Biometrics* 44, 837–845. doi: 10.2307/2531595

Deo, A. K., Borson, S., Link, J. M., Domino, K., Eary, J. F., Ke, B., et al. (2014). Activity of P-glycoprotein, a β-amyloid transporter at the blood-brain barrier, is compromised in patients with mild Alzheimer disease. *J. Nucl. Med.* 55, 1106–1111. doi: 10.2967/jnumed.113.130161

Dolatshahi, M., Pourmirbabaei, S., Kamalian, A., Ashraf-Ganjouei, A., Yaseri, M., and Aarabi, M. H. (2018). Longitudinal alterations of alpha-synuclein, amyloid beta, total, and phosphorylated tau in cerebrospinal fluid and correlations between their changes in Parkinson's disease. *Front. Neurol.* 9:560. doi: 10.3389/fneur.2018.00560

Engelien, A., Stern, E., Isenberg, N., Engelien, W., Frith, C., and Silbersweig, D. (2000). The parahippocampal region and auditory-mnemonic processing. *Ann. N. Y. Acad. Sci.* 911, 477–485. doi: 10.1111/j.1749-6632.2000.tb06750.x

Enzinger, C., Fazekas, F., Matthews, P. M., Ropele, S., Schmidt, H., Smith, S., et al. (2005). Risk factors for progression of brain atrophy in aging: six-year follow-up of normal subjects. *Neurology* 64, 1704–1711. doi: 10.1212/01.WNL.0000161871.83614.BB

Fluss, R., Faraggi, D., and Reiser, B. (2005). Estimation of the Youden index and its associated cutoff point. *Biom. J.* 47, 458–472. doi: 10.1002/bimj.200410135

Førland, M. G., Öhrfelt, A., Dalen, I., Tysnes, O. B., Blennow, K., Zetterberg, H., et al. (2018). Evolution of cerebrospinal fluid total α-synuclein in Parkinson's disease. *Parkinsonism Relat. Disord.* 49, 4–8. doi: 10.1016/j.parkreldis.2018.01.018

Fox, M. D., Corbetta, M., Snyder, A. Z., Vincent, J. L., and Raichle, M. E. (2006). Spontaneous neuronal activity distinguishes human dorsal and ventral attention systems. *Proc. Natl. Acad. Sci. U. S. A.* 103, 10046–10051. doi: 10.1073/pnas.0604187103

García-Casares, N., Berthier, M. L., Jorge, R. E., Gonzalez-Alegre, P., Gutiérrez Cardo, A., Rioja Villodres, J., et al. (2014). Structural and functional brain changes in middle-aged type 2 diabetic patients: a cross-sectional study. *J. Alzheimers Dis.* 40, 375–386. doi: 10.3233/JAD-131736

Garfield, V., Farmaki, A. E., Eastwood, S. V., Mathur, R., Rentsch, C. T., Bhaskaran, K., et al. (2021). HbA1c and brain health across the entire glycaemic spectrum. *Diabetes Obes. Metab.* 23, 1140–1149. doi: 10.1111/dom.14321

Geijselaers, S. L. C., Sep, S. J. S., Stehouwer, C. D. A., and Biessels, G. J. (2015). Glucose regulation, cognition, and brain MRI in type 2 diabetes: a systematic review. *Lancet Diabetes Endocrinol.* 3, 75–89. doi: 10.1016/S2213-8587(14)70148-2

Gispen, W. H., and Biessels, G. J. (2000). Cognition and synaptic plasticity in diabetes mellitus. *Trends Neurosci.* 23, 542–549. doi: 10.1016/S0166-2236(00)01656-8

Gispert, J. D., Rami, L., Sánchez-Benavides, G., Falcon, C., Tucholka, A., Rojas, S., et al. (2015). Nonlinear cerebral atrophy patterns across the Alzheimer's disease continuum: impact of APOE4 genotype. *Neurobiol. Aging* 36, 2687–2701. doi: 10.1016/j.neurobiolaging.2015.06.027

Groeneveld, O., Reijmer, Y., Heinen, R., Kuijf, H., Koekkoek, P., Janssen, J., et al. (2018). Brain imaging correlates of mild cognitive impairment and early dementia in patients with type 2 diabetes mellitus. *Nutr. Metab. Cardiovasc. Dis.* 28, 1253–1260. doi: 10.1016/j.numecd.2018.07.008

He, Y., Li, L., and Liu, J. (2022). The whole-brain voxel-based morphometry study in early stage of T2DM patients. *Brain Behav.* 12:e2497. doi: 10.1002/brb3.2497

Hoyos, C. M., Colagiuri, S., Turner, A., Ireland, C., Naismith, S. L., and Duffy, S. L. (2022). Brain oxidative stress and cognitive function in older adults with diabetes and pre-diabetes who are at risk for dementia. *Diabetes Res. Clin. Pract.* 184:109178. doi: 10.1016/j.diabres.2021.109178

Janelidze, S., Mattsson, N., Palmqvist, S., Smith, R., Beach, T. G., Serrano, G. E., et al. (2020). Plasma P-tau181 in Alzheimer's disease: relationship to other biomarkers, differential diagnosis, neuropathology and longitudinal progression to Alzheimer's dementia. *Nat. Med.* 26, 379–386. doi: 10.1038/s41591-020-0755-1

Jash, K., Gondaliya, P., Kirave, P., Kulkarni, B., Sunkaria, A., and Kalia, K. (2020). Cognitive dysfunction: a growing link between diabetes and Alzheimer's disease. *Drug Dev. Res.* 81, 144–164. doi: 10.1002/ddr.21579

Karikari, T. K., Benedet, A. L., Ashton, N. J., Lantero Rodriguez, J., Snellman, A., Suárez-Calvet, M., et al. (2021). Diagnostic performance and prediction of clinical progression of plasma phospho-tau181 in the Alzheimer's disease neuroimaging initiative. *Mol. Psychiatry* 26, 429–442. doi: 10.1038/s41380-020-00923-z

Ke, Y. D., Delerue, F., Gladbach, A., Götz, J., and Ittner, L. M. (2009). Experimental diabetes mellitus exacerbates tau pathology in a transgenic mouse model of Alzheimer's disease. *PLoS One* 4:e7917. doi: 10.1371/journal.pone.0007917

Khan, S. S., and Bloom, G. S. (2016). Tau: the Center of a Signaling Nexus in Alzheimer's disease. *Front. Neurosci.* 10:31. doi: 10.3389/fnins.2016.00031

Lamport, D. J., Lawton, C. L., Mansfield, M. W., and Dye, L. (2009). Impairments in glucose tolerance can have a negative impact on cognitive function: a systematic research review. *Neurosci. Biobehav. Rev.* 33, 394–413. doi: 10.1016/j.neubiorev.2008.10.008

Liu, J., Liu, T., Wang, W., Ma, L., Ma, X., Shi, S., et al. (2017). Reduced Gray matter volume in patients with type 2 diabetes mellitus. *Front. Aging Neurosci.* 9:161. doi: 10.3389/fnagi.2017.00161

Mielke, M. M., Hagen, C. E., Xu, J., Chai, X., Vemuri, P., Lowe, V. J., et al. (2018). Plasma phospho-tau181 increases with Alzheimer's disease clinical severity and is associated with tau-and amyloid-positron emission tomography. *Alzheimers Dement.* 14, 989–997. doi: 10.1016/j.jalz.2018.02.013

Nam, E., Lee, Y. B., Moon, C., and Chang, K. A. (2020). Serum tau proteins as potential biomarkers for the assessment of Alzheimer's disease progression. *Int. J. Mol. Sci.* 21:5007. doi: 10.3390/ijms21145007

Oliveira, W. H., Braga, C. F., Lós, D. B., Araújo, S. M. R., França, M. R., Duarte-Silva, E., et al. (2021). Metformin prevents p-tau and amyloid plaque deposition and memory impairment in diabetic mice. *Exp. Brain Res.* 239, 2821–2839. doi: 10.1007/s00221-021-06176-8

Paneni, F., Beckman, J. A., Creager, M. A., and Cosentino, F. (2013). Diabetes and vascular disease: pathophysiology, clinical consequences, and medical therapy: part I. *Eur. Heart J.* 34, 2436–2443. doi: 10.1093/eurheartj/eht149

Qaseem, A., Wilt, T. J., Kansagara, D., Horwitch, C., Barry, M. J., Forciea, M. A., et al. (2018). Hemoglobin A1c targets for glycemic control with pharmacologic therapy for nonpregnant adults with type 2 diabetes mellitus: a guidance statement update from the American College of Physicians. *Ann. Intern. Med.* 168, 569–576. doi: 10.7326/M17-0939

Qiao, J., Lawson, C. M., Rentrup, K. F. G., Kulkarni, P., and Ferris, C. F. (2020). Evaluating blood-brain barrier permeability in a rat model of type 2 diabetes. *J. Transl. Med.* 18:256. doi: 10.1186/s12967-020-02428-3

Roy, B., Ehlert, L., Mullur, R., Freeby, M. J., Woo, M. A., Kumar, R., et al. (2020). Regional brain Gray matter changes in patients with type 2 diabetes mellitus. *Sci. Rep.* 10:9925. doi: 10.1038/s41598-020-67022-5

Sadeghi, A., Hami, J., Razavi, S., Esfandiary, E., and Hejazi, Z. (2016). The effect of diabetes mellitus on apoptosis in hippocampus: cellular and molecular aspects. *Int. J. Prev. Med.* 7:57. doi: 10.4103/2008-7802.178531

Seaquist, E. R. (2010). The final frontier: how does diabetes affect the brain? *Diabetes* 59, 4–5. doi: 10.2337/db09-1600

Seaquist, E. R. (2015). The impact of diabetes on cerebral structure and function. *Psychosom. Med.* 77, 616–621. doi: 10.1097/PSY.0000000000000207

Sonneville, R., den Hertog, H. M., Güiza, F., Gunst, J., Derese, I., Wouters, P. J., et al. (2012). Impact of hyperglycemia on neuropathological alterations during critical illness. *J. Clin. Endocrinol. Metab.* 97, 2113–2123. doi: 10.1210/jc.2011-2971

Squire, L. R. (1992). Memory and the hippocampus: a synthesis from findings with rats, monkeys, and humans. *Psychol. Rev.* 99, 195–231. doi: 10.1037/0033-295X.99.2.195

Sun, Y., Ma, C., Sun, H., Wang, H., Peng, W., Zhou, Z., et al. (2020). Metabolism: a novel shared Link between diabetes mellitus and Alzheimer's disease. *J. Diabetes Res.* 2020:4981814. doi: 10.1155/2020/4981814

Suzuki, W. A., Zola-Morgan, S., Squire, L. R., and Amaral, D. G. (1993). Lesions of the perirhinal and parahippocampal cortices in the monkey produce long-lasting memory impairment in the visual and tactual modalities. *J. Neurosci.* 13, 2430–2451. doi: 10.1523/JNEUROSCI.13-06-02430.1993

Tatebe, H., Kasai, T., Ohmichi, T., Kishi, Y., Kakeya, T., Waragai, M., et al. (2017). Quantification of plasma phosphorylated tau to use as a biomarker for brain Alzheimer pathology: pilot case-control studies including patients with Alzheimer's disease and down syndrome. *Mol. Neurodegener.* 12:63. doi: 10.1186/s13024-017-0206-8

Thijssen, E. H., La Joie, R., Wolf, A., Strom, A., Wang, P., Iaccarino, L., et al. (2020). Diagnostic value of plasma phosphorylated tau181 in Alzheimer's disease and frontotemporal lobar degeneration. *Nat. Med.* 26, 387–397. doi: 10.1038/s41591-020-0762-2

Tomlinson, D. R., and Gardiner, N. J. (2008). Glucose neurotoxicity. *Nat. Rev. Neurosci.* 9, 36–45. doi: 10.1038/nrn2294

Tzourio-Mazoyer, N., Landeau, B., Papathanassiou, D., Crivello, F., Etard, O., Delcroix, N., et al. (2002). Automated anatomical labeling of activations in SPM using a macroscopic anatomical parcellation of the MNI MRI single-subject brain. *NeuroImage* 15, 273–289. doi: 10.1006/nimg.2001.0978

Ward, A. M., Schultz, A. P., Huijbers, W., van Dijk, K. R. A., Hedden, T., and Sperling, R. A. (2014). The parahippocampal gyrus links the default-mode cortical network with the medial temporal lobe memory system. *Hum. Brain Mapp.* 35, 1061–1073. doi: 10.1002/hbm.22234

Wu, G., Lin, L., Zhang, Q., and Wu, J. (2017). Brain gray matter changes in type 2 diabetes mellitus: a meta-analysis of whole-brain voxel-based morphometry study. *J. Diabetes Complicat.* 31, 1698–1703. doi: 10.1016/j.jdiacomp.2017.09.001

Xu, N., Wu, H., Li, D., and Wang, J. (2014). Diagnostic accuracy of glycated hemoglobin compared with oral glucose tolerance test for diagnosing diabetes mellitus in Chinese adults: a meta-analysis. *Diabetes Res. Clin. Pract.* 106, 11–18. doi: 10.1016/j.diabres.2014.04.010

Yaffe, K., Lindquist, K., Schwartz, A. V., Vitartas, C., Vittinghoff, E., Satterfield, S., et al. (2011). Advanced glycation end product level, diabetes, and accelerated cognitive aging. *Neurology* 77, 1351–1356. doi: 10.1212/WNL.0b013e3182315a56

Yao, L., Yang, C., Zhang, W., Li, S., Li, Q., Chen, L., et al. (2021). A multimodal meta-analysis of regional structural and functional brain alterations in type 2 diabetes. *Front. Neuroendocrinol.* 62:100915. doi: 10.1016/j.yfrne.2021.100915

Yazdanpanah, S., Rabiee, M., Tahriri, M., Abdolrahim, M., Rajab, A., Jazayeri, H. E., et al. (2017). Evaluation of glycated albumin (GA) and GA/HbA1c ratio for diagnosis of diabetes and glycemic control: a comprehensive review. *Crit. Rev. Clin. Lab. Sci.* 54, 219–232. doi: 10.1080/10408363.2017.1299684

Yun, J. H., Lee, D. H., Jeong, H. S., Kim, H. S., Ye, S. K., and Cho, C. H. (2021). STAT3 activation in microglia exacerbates hippocampal neuronal apoptosis in diabetic brains. *J. Cell. Physiol.* 236, 7058–7070. doi: 10.1002/jcp.30373

Zhang, X., Yu, Y., Shi, Z. S., Xu, K., Feng, J. H., Li, Z. Y., et al. (2021). Increased resting state functional irregularity of T2DM brains with high HbA1c: sign for impaired verbal memory function? *Brain Imaging Behav.* 15, 772–781. doi: 10.1007/s11682-020-00285-8

Zhang, Y., Zhang, X., Zhang, J., Liu, C., Yuan, Q., Yin, X., et al. (2014). Gray matter volume abnormalities in type 2 diabetes mellitus with and without mild cognitive impairment. *Neurosci. Lett.* 562, 1–6. doi: 10.1016/j.neulet.2014.01.006

Zou, K., Abdullah, M., and Michikawa, M. (2020). Current biomarkers for Alzheimer's disease: from CSF to blood. *J. Pers. Med.* 10:85. doi: 10.3390/jpm10030085

frontiers | Frontiers in Neuroscience

TYPE Mini Review
PUBLISHED 06 June 2023
DOI 10.3389/fnins.2023.1163274

OPEN ACCESS

EDITED BY
Delia Cabrera DeBuc,
University of Miami, United States

REVIEWED BY
Xiaofei Hu,
Army Medical University, China

*CORRESPONDENCE
Hongwei Wen
✉ wenhongwei@swu.edu.cn
Lingfei Guo
✉ glfsci@163.com

†These authors have contributed equally to this work and share first authorship

RECEIVED 10 February 2023
ACCEPTED 15 May 2023
PUBLISHED 06 June 2023

CITATION
Wang N, Liang C, Zhang X, Sui C, Gao Y, Guo L and Wen H (2023) Brain structure–function coupling associated with cognitive impairment in cerebral small vessel disease.
Front. Neurosci. 17:1163274.
doi: 10.3389/fnins.2023.1163274

Brain structure–function coupling associated with cognitive impairment in cerebral small vessel disease

Na Wang [1†], Changhu Liang [1†], Xinyue Zhang [1], Chaofan Sui [1], Yian Gao [1], Lingfei Guo [1*] and Hongwei Wen [2*]

[1]Department of Radiology, Shandong Provincial Hospital Affiliated to Shandong First Medical University, Jinan, Shandong, China, [2]Key Laboratory of Cognition and Personality (Ministry of Education), Faculty of Psychology, Southwest University, Chongqing, China

Cerebral small vessel disease (CSVD) is a common chronic and progressive disease that can lead to mental and cognitive impairment. Damage to brain structure and function may play an important role in the neuropsychiatric disorders of patients with CSVD. Increasing evidence suggests that functional changes are accompanied by structural changes in corresponding brain regions. Thus, normal structure–function coupling is essential for optimal brain performance, and disrupted structure–function coupling can be found in many neurological and psychiatric disorders. To date, most studies on patients with CSVD have focused on separate structures or functions, including reductions in white matter volume and blood flow, which lead to cognitive dysfunction. However, there are few studies on brain structure–function coupling in patients with CSVD. In recent years, with the rapid development of multilevel (voxel-wise, neurovascular, regional level, and network level) brain structure–functional coupling analysis methods based on multimodal magnetic resonance imaging (MRI), new evidence has been provided to reveal the correlation between brain function and structural abnormalities and cognitive impairment. Therefore, studying brain structure–function coupling has a potential significance in the exploration and elucidation of the neurobiological mechanism of cognitive impairment in patients with CSVD. This article mainly describes the currently popular brain structure–function coupling analysis technology based on multimodal MRI and the important research progress of these coupling technologies on CSVD and cognitive impairment to provide a perspective for the study of the pathogenesis and early diagnosis of CSVD.

KEYWORDS

cerebral small vessel disease, cognitive impairment, structure–function coupling, neurovascular coupling, multimodal magnetic resonance imaging

1. Introduction

Cerebral small vessel disease (CSVD) is a general term for intracranial vascular (including arteriolar, arteriolar, capillary, and venular) diseases based on a variety of pathological and neurological processes and refers to syndromes with different clinical manifestations and neuroimaging features caused by structural changes in blood vessels and brain parenchyma (Cuadrado-Godia et al., 2018; Li et al., 2018). CSVD is one of the

major diseases affecting cognitive function and extremity function. According to previous studies, the main clinical manifestations of CSVD include cognitive decline, stroke, mental disorders, dementia, urinary incontinence, and abnormal gait (Li et al., 2018; Chojdak-Lukasiewicz et al., 2021). Researchers have shown that CSVD has become the main cause of stroke, depression, cognitive impairment, dementia, and gait disturbance in elderly individuals (Rost and Etherton, 2020). The use of advanced magnetic resonance imaging (MRI) technology can detect cerebrovascular abnormalities before the disease appears (Zabetian-Targhi et al., 2019). Brain imaging biomarkers for CSVD include white matter hyperintensities, cerebral microbleeds, recent small subcortical infarcts, lacunae, brain atrophy, and enlarged perivascular spaces (Cuadrado-Godia et al., 2018; Li et al., 2018).

MRI can detect brain structure and function. It is well known that brain structure and function are closely related. The coupling of structural imaging and functional imaging has become an increasingly important research topic in modern neuroimaging. The brain structure can provide the skeleton for functional mechanisms, and the integration of functional and structural information can help us better understand communication in the brain. Thus, changes in brain function may lead to changes in the gray or white matter and vice versa. However, most studies have only examined functional or anatomical changes in isolation. In recent years, with the rapid development of multimodal MRI technology, researchers have carried out a large number of neuroimaging studies on the structural and functional damage to the brain caused by CSVD (Liu et al., 2019; Meng et al., 2022). Studies have shown that changes in brain function are often accompanied by changes in the structure of the corresponding brain regions. For example, the persistence, intensity, and spatial statistics of brain activities in the resting state are usually limited by the anatomical structure of the brain (Honey et al., 2009). Thus, normal structure–function coupling is essential for the brain, and disruptions in structure–function coupling can be found in many neurological and psychiatric disorders (Zhang X. et al., 2022). Therefore, the exploration of brain structure–function coupling is more significant for elucidating the neurobiological mechanisms of cognitive and mental impairment in CSVD.

Brain structure–function coupling exists at various levels, including voxel, neurovascular, regional, and network levels. Neurovascular coupling (NVC) is a tight regional and temporal coupling in the brain, which means that brain regions with stronger connectivity tend to have more frequent neuronal activity and more energy expenditure, resulting in increased cerebral blood flow (CBF) (Li P. et al., 2021). The dysfunction of structure–function coupling of NVC may have great significance in the neuropathological mechanism of CSVD. As an important mechanism to achieve autonomic regulation of CBF, NVC can ensure appropriate blood supply to maintain basic physiological activities such as respiration, blood pressure, and endocrine function and carry out a series of advanced cognitive functions such as memory, learning, and emotion. NVC is a complex process that involves the coordination and feedback loops of multiple cells. The basic structure for the realization of NVC function is the neurovascular unit, which is composed of neurons, astrocytes, vascular smooth muscle cells/pericytes, and Virchow–Robin space (Kaplan et al., 2020). In the field of neuroimaging, NVC is the physiological basis of functional MRI (Whittaker et al., 2015). In terms of pathophysiology, disruption of its function is one of the important pathogeneses of a variety of ischemic nervous system diseases, including CSVD (Sutherland et al., 2017). However, numerous current NVC studies mainly focus on temporal and regional associations between neural activity and CBF responses but ignore major structural factors related to NVC, including the anatomical structure of cerebral vasculature and organ structure regulating CBF (Phillips et al., 2016). In addition to functional neuroimaging, future research should consider further introducing structural neuroimaging features to assess the NVC and highlight the related alterations in the NVC underlying CSVD.

To date, most studies on patients with CSVD have focused on separate structural or functional abnormalities but have ignored the important relationship between them, which may be highly related to cognitive dysfunction. Although structure–function coupling information from neuroimaging techniques is essential for understanding abnormal changes in brain diseases, there are few studies on brain structure–function coupling in patients with CSVD. Defining the significance of coexisting structural and functional deficits can provide specific insights into the changes that occur in the brains of CSVD patients.

The aim of this review is to describe a series of useful structure–function coupling analysis methods based on multimodal MRI and the research progress of brain structure–function coupling related to cognitive impairment and to provide a new perspective for the study of CSVD.

2. Voxel-wise structure–function coupling

There are two commonly used voxel-wise structure–function coupling approaches: one is the coupling of resting-state functional MRI (rs-fMRI) parameters and gray matter (GM) morphological parameters, and the other is the coupling of rs-fMRI parameters and diffusion tensor imaging (DTI)-based white matter (WM) microstructural parameters.

In the first approach, Kang et al. (2022) combined regional homogeneity (ReHo) and voxel-based morphometry (VBM) features and calculated the ratio of ReHo to GM volume (GMV) to detect altered voxel-wise structure–function coupling and its importance in predicting radiation encephalopathy (RE) in patients with nasopharyngeal carcinoma (NPC). They found that compared with the preradiotherapy group, patients in the postradiotherapy group showed lower ReHo/VBM coupling values in the bilateral medial temporal lobes, indicating that ReHo/VBM may be a novel effective neuroimaging metric that reflects the neural mechanism underlying cognitive impairment caused by RE in patients with NPC. Gray et al. (2020) performed a coordinator-based meta-analysis including VBM studies and resting-state voxel-based pathophysiology (VBP) studies (including glucose metabolism, cerebral blood flow (CBF), ReHo, amplitude of low-frequency fluctuation (ALFF), and fractional ALFF) to investigate spatially convergent structural and functional abnormalities in major depressive disorder (MDD) patients and identified that the regions of significant convergence include the right middle occipital gyrus, inferior temporal gyrus, amygdala/putamen and left hippocampus,

subgenual cingulate cortex, and retrosplenial cortex, which may contribute to the cognitive and recall memory deficits often seen in MDD patients. A study on schizophrenia showed that the ALFF value in the hippocampus of schizophrenia patients was significantly different from the GMV measurements, and this difference may be due to cognitive and emotional dysfunction caused by hippocampal damage, which is related to the production of hallucinations in schizophrenia patients (Zhao et al., 2017). These studies suggest that the brain structural defect and functional defect are related to each other, and the differences in this correlation indicated that the structure and function relationships of the brain regions have changed.

In the second approach, Tan et al. combined DTI and rs-fMRI and found that patients with classical trigeminal neuralgia had high fractional anisotropy (FA) and low ReHo in the right hippocampus, and the ReHo and FA values were positively correlated with the Montreal Cognitive Assessment scale score. This indicated that there is a clear correlation between cognitive dysfunction and hippocampal functional and structural dysfunction in classical trigeminal neuralgia patients. Strong evidence has been provided showing that pain depends on the activation of mechanisms in higher brain centers that control emotions and generate emotional recognition (Tan et al., 2022). In addition, some researchers have used fMRI and DTI techniques to propose a skeleton-based method for WM functional analysis, which achieves voxel-based function–structure coupling by projecting fMRI signals onto the skeleton in WM. The researchers' study showed that local WM regions (frontotemporal tracts including the right anterior corona radiata, the orbitofrontal region, the hippocampus, the anterior limb of internal capsule, and the genu of corpus callosum) in patients with schizophrenia demonstrated increased amplitude of low-frequency fluctuations (SWALFF) and decreased FA. The correlation between FA changes and SWALFF changes was negative in schizophrenia patients but positive in healthy controls (Jiang et al., 2021). Thus, hard evidence was provided to support the hypothesis that structure–function associations may be one of the underlying mechanisms of impaired connectivity in schizophrenia patients.

Recently, to further develop the voxel-wise coupling analysis method, Hu et al. proposed a new coupling method called principal-component-based intermodal coupling (pIMCo) (Hu et al., 2022). The method uses local covariance decomposition to define a symmetric, voxel-wise coupling coefficient that holds for two or more modal parameters. Hu et al. used this approach to investigate the coupling among CBF, ALFF, and ReHo, demonstrating that coupling is spatially heterogeneous, varies with age and sex in neural development, and reveals patterns that are absent in individual patterns. This new approach provides a new perspective for summarizing the overall covariance structure between more than two modalities.

3. Brain network structural-functional connectivity coupling

The graph theory of brain networks conceptualizes the brain as a network that achieves functional performance through the interaction among various brain regions through structural connectivity (SC) or functional connectivity (FC) (Shah et al., 2018). The brain network can be assessed by structural and functional neuroimaging data. CSVD can affect SC and FC by damaging the integrity of the nodes in the network and the connections between them, thus disrupting the effective communication of the whole-brain network and leading to different degrees of cognitive impairment. It has been shown that the coupling of SC and FC based on multimodal MRI allows the detection of brain network disruption, which is more sensitive than any single modality (Kong et al., 2021). However, the changes in SC-FC coupling of brain networks at the system level in CSVD patients are still unclear and need further investigation.

Studies have shown significantly altered SC and FC between hippocampal cognitive and emotional subregions and cortical areas in patients with cognitive impairment, which is manifested as an increase in the early stage of the disease, possibly due to compensatory mechanisms (Liang et al., 2020; Xu et al., 2021). Filippi et al. found that hippocampal SC changes were greater than FC changes in patients with Alzheimer's disease and amnestic mild cognitive impairment (MCI), indicating that reduced SC may precede FC changes (Filippi et al., 2020). Other studies have found that subcortical vascular MCI has significant SC and FC reductions in the brain, especially in the brain regions connected to the hippocampus, which may be related to cognitive impairment in patients with this disease, while the FC of hippocampal subregions and the posterior cingulate cortex is enhanced. Since the functional interaction between the hippocampus and the posterior cingulate cortex is related to episodic memory, this interaction can be interpreted as a compensatory mechanism for memory impairment; the increased structural association between the inferior colliculus of the hippocampus and the pole part of the superior temporal gyrus in amnestic MCI may be related to depressive symptoms, such as difficulties in processing facial emotions in patients (Xu et al., 2021). These findings suggest that different brain regions may have specific relationships with depressive symptoms and/or cognitive impairment. In addition, another study found that the Papez circuit, including the amygdala, ipsilateral hippocampus, caudal anterior cingulate gyrus, and thalamus, had significant GM atrophy, and the directional functional connection between the cingulate gyrus and the bilateral hippocampus within the Papez circuit was also altered in stroke patients. These alterations in effective connectivity have been associated with cognitive function after cerebrovascular events (Yan et al., 2022). A previous study also found selectively abnormal SC-FC coupling in subcortical vascular MCI, that is, SC-FC coupling is preserved at the whole-brain level but is increased in the dorsal attention module and reduced in the ventral attention module (Ma et al., 2021). These findings motivate us to obtain a better understanding of the underlying mechanisms of vascular cognitive impairment and to explore novel therapeutic targets that could reduce the cognitive burden.

4. Structural and functional neurovascular coupling

The tight coupling between neuronal activity and CBF is called NVC (Li L. et al., 2021). As an important mechanism regulating CBF, NVC can deliver oxygen and nutrients to regions in a timely

manner according to the requirements of brain activity to maintain the homeostasis of the brain environment. Cerebral small vessels play a critical role in the automatic regulation of the brain, which mainly depends on the normal operation of the NVC. Impairment of the NVC mechanism can lead to ischemia and hypoxia of small vessels located at the end of cerebral microcirculation, resulting in the failure of the local brain to respond to neuronal signal transduction, thus causing or aggravating small vessel diseases and even cognitive dysfunction and dementia. In recent years, NVC has been widely studied for its key role in the automatic regulation of CBF in the brain. Therefore, understanding the regulatory mechanism of NVC in CSVD is of great significance for preventing the further development of CSVD and improving cerebral ischemia and cognitive dysfunction.

There is increasing evidence that impaired NVC is present in many patients with CSVD. Increased microvascular damage and a decrease in the number of microvessels in the hippocampus and neocortex can cause a decrease in vasodilator reserve, leading to impaired NVC function, which is associated with cognitive decline (Phillips et al., 2016; Kirschen et al., 2018), and the decline in cognitive function can cause a decrease in CBF. Previous animal experiments demonstrated reduced blood flow, oxygenation, and NVC in the hippocampus of mice with cerebrovascular dysfunction (Li P. et al., 2021). At the same time, the hippocampus was more susceptible to hypoxic damage under pathological conditions that led to impaired NVC (Zhang H. et al., 2022). Studies have shown that structural and functional changes in neurovascular aspects may underlie cognitive decline in numerous pathological states (Segarra et al., 2019). Some researchers have used mathematical dynamic multivariate and autoregressive models, in which the changes in critical closing pressure and the resistance area product are considered to provide selective indicators of metabolic and myogenic cerebrovascular regulation, respectively, in the hope of providing insights into the mechanisms of NVC from a structural

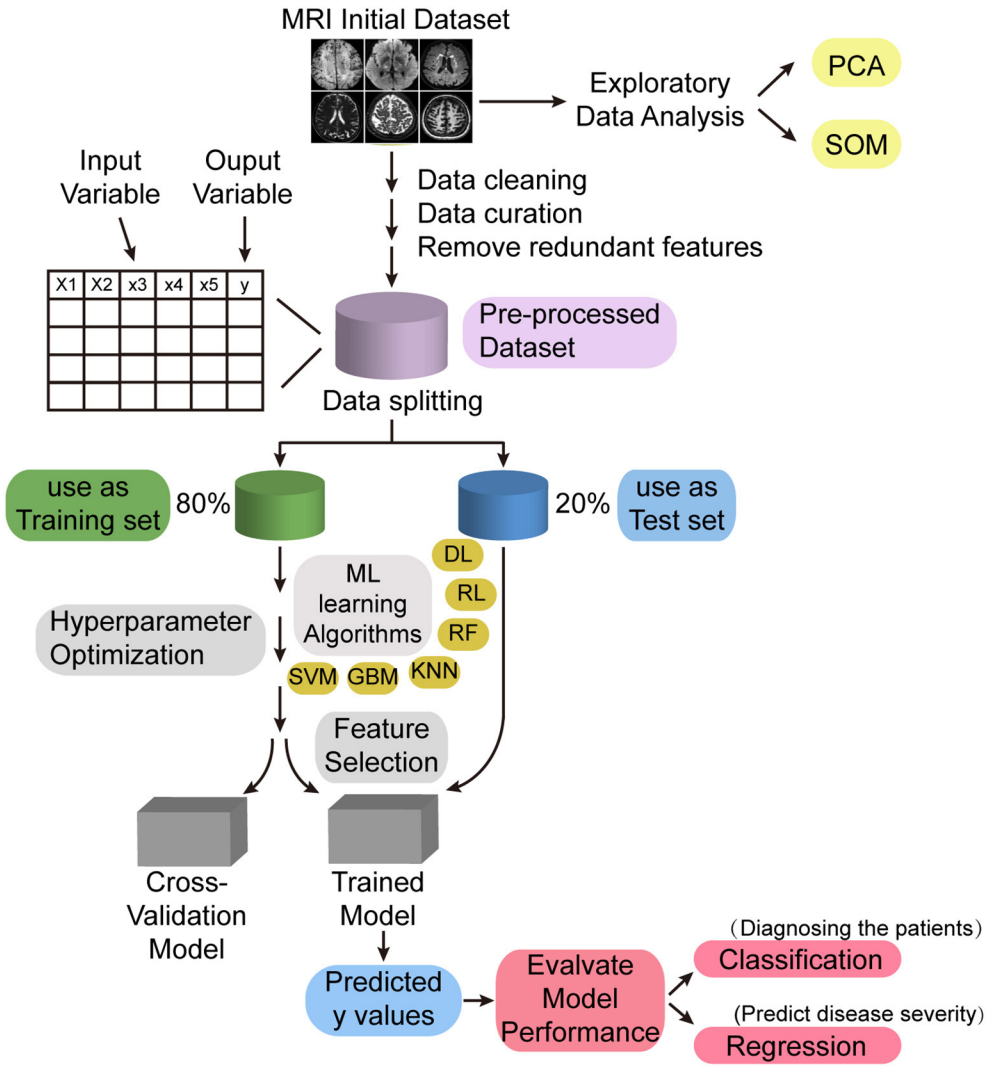

FIGURE 1
Machine learning model for intelligent diagnosis of diseases. PCA, principal component analysis; SOM, self-organizing map; ML, machine learning; DL, deep learning; RL, reinforcement learning; RF, random forest; KNN, K-nearest neighbor; GBM, gradient boosting machine; SVM, support vector machine.

perspective (Phillips et al., 2016). Previous studies of NVC have mainly focused on the coupling of the functional indicators ALFF and CBF and have not involved the content of the structural NVC. Therefore, further studies are needed to clarify the specific role of structure–function NVC in CSVD.

5. Hippocampal structure–function coupling

As an important anatomical structure, the hippocampus is of great significance in the pathogenesis of neuropsychiatric diseases. Neuropsychiatric disorders caused by CSVD can lead to structural and functional damage to the hippocampus in many ways. Indeed, hippocampal neuronal loss and atrophy, regional cerebral blood volume reduction, and hippocampal microinfarction have been observed in patients with CSVD (Perosa et al., 2020). Correspondingly, when the structure and function of the hippocampus are damaged (especially if both exist at the same time), the cognitive, emotional, and motor abilities of the patient are greatly affected (van Norden et al., 2012; Wu et al., 2022). Therefore, the study of structure–function coupling specifically targeting the hippocampus may be more meaningful for CSVD.

At present, structure–function coupling analysis methods and research specific to the hippocampal region are developing continuously. Recently, Bayrak et al. isolated the hippocampus and investigated its structure–function coupling using the twin setup of the Human Connectome Project with multimodal neuroimaging (Bayrak et al., 2022). To measure structure–function coupling, they assessed the degree of spatial overlap between hippocampal microstructure intensity covariance and FC measures at the vertices of each subfield. In addition, they examined the shared organization of hippocampal function and structure to characterize the spatial covariation in structure–function associations along the genetic hippocampal organization axis. They used the connectivity gradient method rather than the network decomposition method because the connectivity gradient method positions brain regions in a continuous manner according to their functional connectome patterns, whereas network decomposition draws sharp boundaries for brain regions (Krienen and Sherwood, 2016). The coupling between structure and function was found to be highest in the medial/posterior part of the hippocampal subfields but not in the anterior part. In addition, hippocampal structure–function coupling showed covariation with intrinsic structural and functional axes, with the posterior regions having major structural and functional connections to unimodal cortical regions, whereas anterior regions are linked to the transmodal cortex. The study by Bayrak et al. provided an important step toward a better understanding of how the anatomy of the hippocampus supports its versatile and unique functions.

6. Conclusion and outlook

In summary, the above structure–function coupling methods, including voxel-wise structure–function coupling, SC-FC coupling, and NVC, are of great significance for CSVD, but the current research is not perfect, and most of them only focus on independent structural or functional aspects. In addition, although multimodal MRI has been widely used in studies of CSVD, some issues remain. For instance, the mechanisms leading to cognitive impairment are complex and may be the result of a combination of factors other than CSVD alone (Lawrence et al., 2013). Second, since each CSVD patient usually has a different combination of MRI markers and severity, each single MRI marker may be difficult to use to predict individual clinical outcome (Lee et al., 2021). Disruptions in the brain structure and function have been widely recognized to be associated with cognitive decline in CSVD, but the neural mechanisms remain unclear (Xu et al., 2021). Different MRI examination methods have their own advantages and disadvantages; however, if the structural imaging and functional imaging of the brain are coupled and the anatomical information and functional information are integrated, it will be helpful for the early diagnosis and prediction of CSVD progression.

In addition, advances in machine learning have led to the development of artificial intelligence algorithms that can aid in the diagnosis of diseases based on MRI for detection at the preclinical stage. Using machine learning techniques, Uysal and Ozturk, successfully differentiated patients with cognitive impairment, patients with Alzheimer's disease, and normal subjects by hippocampal volume information (Uysal and Ozturk, 2020); Sarwar et al. also demonstrated through machine learning that the structure–function coupling in the human brain is very tight (Sarwar et al., 2021). Therefore, as a novel neuroimaging feature, brain structure–function coupling can be combined with machine learning technology to establish a computer-aided diagnostic system based on multimodal MRI data (Figure 1), and the structure–function coupling features highly correlated with CSVD and cognitive impairment can be mined through machine learning methods, which can help clinicians diagnose patients with CSVD and predict the severity of this disease.

Therefore, with the continuous development of multimodal MRI fusion analysis technology, brain structure–function coupling will become a hot spot in the study of CSVD in the future.

Author contributions

NW and CL wrote the main manuscript text. XZ, CS, and YG prepared the imaging data. LG and HW revised the main manuscript text. All authors reviewed the manuscript. All authors contributed to the article and approved the submitted version.

Funding

This work was supported by grants from the National Natural Science Foundation of China (32100902), the Fundamental Research Funds for the Central Universities (SWU118065), the Natural Science Foundation of Shandong Province (ZR2020MH288), the Technology Development Plan of Jinan (201301049, 201602206, 201907052, 202134072, and 202225035), the Medical and Health Science and Technology Development

Project of Shandong Province (2016 WS0529), and the Funding for Study Abroad Program by Shandong Province (201803059).

Conflict of interest

The authors declare that the research was conducted in the absence of any commercial or financial relationships that could be construed as a potential conflict of interest.

Publisher's note

All claims expressed in this article are solely those of the authors and do not necessarily represent those of their affiliated organizations, or those of the publisher, the editors and the reviewers. Any product that may be evaluated in this article, or claim that may be made by its manufacturer, is not guaranteed or endorsed by the publisher.

References

Bayrak, S., de Wael, R. V., Schaare, H. L., Hettwer, M. D., Caldairou, B., Bernasconi, A., et al. (2022). Heritability of hippocampal functional and microstructural organisation. *Neuroimage.* 264, 119656. doi: 10.1016/j.neuroimage.2022.119656

Chojdak-Lukasiewicz, J., Dziadkowiak, E., Zimny, A., and Paradowski, B. (2021). Cerebral small vessel disease: a review. *Adv Clin Exp Med.* 30, 349–356. doi: 10.17219/acem/131216

Cuadrado-Godia, E., Dwivedi, P., Sharma, S., Ois Santiago, A., Roquer Gonzalez, J., Balcells, M., et al. (2018). Cerebral small vessel disease: a review focusing on pathophysiology, biomarkers, and machine learning strategies. *J Stroke.* 20, 302–320. doi: 10.5853/jos.2017.02922

Filippi, M., Basaia, S., Canu, E., Imperiale, F., Magnani, G., Falautano, M., et al. (2020). Changes in functional and structural brain connectome along the Alzheimer's disease continuum. *Mol Psychiatry.* 25, 230–239. doi: 10.1038/s41380-018-0067-8

Gray, J. P., Muller, V. I., Eickhoff, S. B., and Fox, P. T. (2020). Multimodal abnormalities of brain structure and function in major depressive disorder: a meta-analysis of neuroimaging studies. *Am J Psychiatry.* 177, 422–434. doi: 10.1176/appi.ajp.2019.19050560

Honey, C. J., Sporns, O., Cammoun, L., Gigandet, X., Thiran, J. P., Meuli, R., et al. (2009). Predicting human resting-state functional connectivity from structural connectivity. *Proc Natl Acad Sci U S A.* 106, 2035–2040. doi: 10.1073/pnas.0811168106

Hu, F., Weinstein, S. M., Baller, E. B., Valcarcel, A. M., Adebimpe, A., Raznahan, A., et al. (2022). Voxel-wise intermodal coupling analysis of two or more modalities using local covariance decomposition. *Hum Brain Mapp.* 43, 4650–4663. doi: 10.1002/hbm.25980

Jiang, Y., Duan, M., Li, X., Huang, H., Zhao, G., Li, X., et al. (2021). Function-structure coupling: white matter functional magnetic resonance imaging hyper-activation associates with structural integrity reductions in schizophrenia. *Hum Brain Mapp.* 42, 4022–4034. doi: 10.1002/hbm.25536

Kang, Y. f., Chen, R., Ding, H., Li, L., Gao, J.-., Liu, L., et al. (2022). Structure–function decoupling: a novel perspective for understanding the radiation-induced brain injury in patients with nasopharyngeal carcinoma. *Front. Neurosci.* (2022). 16, 915164. doi: 10.3389/fnins.2022.915164

Kaplan, L., Chow, B. W., and Gu, C. (2020). Neuronal regulation of the blood-brain barrier and neurovascular coupling. *Nat Rev Neurosci.* 21, 416–432. doi: 10.1038/s41583-020-0322-2

Kirschen, G. W., Kery, R., and Ge, S. (2018). The hippocampal neuro-glio-vascular network: metabolic vulnerability and potential neurogenic regeneration in disease. *Brain Plast.* 3, 129–144. doi: 10.3233/BPL-170055

Kong, L. Y., Huang, Y. Y., Lei, B. Y., Ke, P. F. L., and i,. H. H., Zhou, J., et al. (2021). Divergent alterations of structural-functional connectivity couplings in first-episode and chronic schizophrenia patients. *Neuroscience.* 460, 1–12. doi: 10.1016/j.neuroscience.02, 008.

Krienen, F. M., and Sherwood, C. C. (2016). Gradients of connectivity in the cerebral cortex. *Trends Cogn Sci. (2017)* 21:61–63. doi: 10.1016/j.tics.12, 002.

Lawrence, A. J., Patel, B., Morris, R. G., MacKinnon, A. D., Rich, P. M., Barrick, T. R., et al. (2013). Mechanisms of cognitive impairment in cerebral small vessel disease: multimodal MRI results from the St George's cognition and neuroimaging in stroke (SCANS) study. *PLoS ONE.* 8, e61014. doi: 10.1371/annotation/bbde462e-c699-4c4d-9b61-050c7e6e5ce3

Lee, W. J., Chou, K. H., Lee, P. L., Peng, L. N., Wang, P. N., Lin, C. P., et al. (2021). Cerebral small vessel disease phenotype and 5-year mortality in asymptomatic middle-to-old aged individuals. *Sci Rep.* 11, 23149. doi: 10.1038/s41598-021-02656-7

Li, L., Tong, X. K., Hosseini Kahnouei, M., Vallerand, D., Hamel, E., Girouard, H., et al. (2021). Impaired hippocampal neurovascular coupling in a mouse model of Alzheimer's disease. *Front Physiol.* 12, 715446. doi: 10.3389/fphys.2021.715446

Li, P., Mu, J., Ma, X., Ding, D., Ma, S., Zhang, H., et al. (2021). Neurovascular coupling dysfunction in end-stage renal disease patients related to cognitive impairment. *J Cereb Blood Flow Metab.* 41, 2593–2606. doi: 10.1177/0271678X211007960

Li, Q., Yang, Y., Reis, C., Tao, T., Li, W., Li, X., et al. (2018). Cerebral small vessel disease. *Cell Transplant.* 27, 1711–1722. doi: 10.1177/0963689718795148

Liang, L., Zhao, L., Wei, Y., Mai, W., Duan, G., Su, J., et al. (2020). Structural and functional hippocampal changes in subjective cognitive decline from the community. *Front Aging Neurosci.* 12, 64. doi: 10.3389/fnagi.2020.00064

Liu, D., Li, K., Ma, X., Li, Y., Bu, Q., Pan, Z., et al. (2019). Correlations between the microstructural changes of the medial temporal cortex and mild cognitive impairment in patients with cerebral small vascular disease (cSVD): a diffusion kurtosis imaging study. *Front Neurol.* 10, 1378. doi: 10.3389/fneur.2019.01378

Ma, J., Liu, F., Yang, B., Xue, K., Wang, P., Zhou, J., et al. (2021). Selective aberrant functional-structural coupling of multiscale brain networks in subcortical vascular mild cognitive impairment. *Neurosci Bull.* 37, 287–297. doi: 10.1007/s12264-020-00580-w

Meng, F., Yang, Y., and Jin, G. (2022). Research progress on MRI for white matter hyperintensity of presumed vascular origin and cognitive impairment. *Front Neurol.* 13, 865920. doi: 10.3389/fneur.2022.865920

Perosa, V., Priester, A., Ziegler, G., Cardenas-Blanco, A., Dobisch, L., Spallazzi, M., et al. (2020). Hippocampal vascular reserve associated with cognitive performance and hippocampal volume. *Brain.* 143, 622–634. doi: 10.1093/brain/awz383

Phillips, A. A., Chan, F. H., Zheng, M. M., Krassioukov, A. V., and Ainslie, P. N. (2016). Neurovascular coupling in humans: physiology, methodological advances and clinical implications. *J Cereb Blood Flow Metab.* 36, 647–664. doi: 10.1177/0271678X15617954

Rost, N. S., and Etherton, M. (2020). Cerebral small vessel disease. *Continuum (Minneap Minn).* 26, 332–352. doi: 10.1212/CON.0000000000000841

Sarwar, T., Tian, Y., Yeo, B. T. T., Ramamohanarao, K., and Zalesky, A. (2021). Structure-function coupling in the human connectome: a machine learning approach. *Neuroimage.* 226, 117609. doi: 10.1016/j.neuroimage.2020.117609

Segarra, M., Aburto, M. R., Hefendehl, J., and Acker-Palmer, A. (2019). Neurovascular interactions in the nervous system. *Annu Rev Cell Dev Biol.* 35, 615–635. doi: 10.1146/annurev-cellbio-100818-125142

Shah, P., Bassett, D. S., Wisse, L. E. M., Detre, J. A., Stein, J. M., Yushkevich, P. A., et al. (2018). Mapping the structural and functional network architecture of the medial temporal lobe using 7T MRI. *Hum Brain Mapp.* 39, 851–865. doi: 10.1002/hbm.23887

Sutherland, B. A., Fordsmann, J. C., Martin, C., Neuhaus, A. A., Witgen, B. M., Piilgaard, H., et al. (2017). Multi-modal assessment of neurovascular coupling during cerebral ischaemia and reperfusion using remote middle cerebral artery occlusion. *J Cereb Blood Flow Metab.* 37, 2494–2508. doi: 10.1177/0271678X16669512

Tan, Y., Zhou, C., and He, L. (2022). Altered structural and functional abnormalities of hippocampus in classical trigeminal neuralgia: a combination of DTI and fMRI study. *J Healthc Eng.* 2022, 8538700. doi: 10.1155/2022/8538700

Uysal, G., and Ozturk, M. (2020). Hippocampal atrophy based Alzheimer's disease diagnosis via machine learning methods. *J Neurosci Methods.* 337, 108669. doi: 10.1016/j.jneumeth.2020.108669

van Norden, A. G., de Laat, K. F., Fick, I., van Uden, I. W., van Oudheusden, L. J., Gons, R. A., et al. (2012). Diffusion tensor imaging of the hippocampus and verbal memory performance: the RUN DMC study. *Hum Brain Mapp.* 33, 542–551. doi: 10.1002/hbm.21231

Whittaker, J. R., Driver, I. D., Bright, M. G., and Murphy, K. (2015). The absolute CBF response to activation is preserved during elevated perfusion: implications for neurovascular coupling measures. *Neuroimage.* 125, 198–207. doi: 10.1016/j.neuroimage.10, 023.

Wu, M., Schweitzer, N., Iordanova, B. E., Halligan-Eddy, E., Tudorascu, D. L., Mathis, C. A., et al. (2022). In pre-clinical AD small vessel disease is associated with altered hippocampal connectivity and atrophy. *Am J Geriatr Psychiatry.* (2022). doi: 10.1016/j.jagp.09, 011.

Xu, J., Wang, J., Lyu, H., Pu, X., Xu, Z., Hu, Y., et al. (2021). Different patterns of functional and structural alterations of hippocampal sub-regions in subcortical vascular mild cognitive impairment with and without depression symptoms. *Brain Imaging Behav.* 15, 1211–1221. doi: 10.1007/s11682-020-00321-7

Yan, S., Li, Y., Lu, J., Tian, T., Zhang, G., Zhou, Y., et al. (2022). Structural and functional alterations within the Papez circuit in subacute stroke patients. *Brain Imaging Behav.* 16, 2681–2689. doi: 10.1007/s11682-022-00727-5

Zabetian-Targhi, F., Srikanth, V. K., Smith, K. J., Oddy, W. H., Beare, R., Moran, C., et al. (2019). Dietary patterns are not associated with brain atrophy or cerebral small vessel disease in older adults with and without type 2 diabetes. *J Nutr.* 149, 1805–1811. doi: 10.1093/jn/nxz139

Zhang, H., Roman, R. J., and Fan, F. (2022). Hippocampus is more susceptible to hypoxic injury: has the Rosetta Stone of regional variation in neurovascular coupling been deciphered? *Geroscience.* 44, 127–130. doi: 10.1007/s11357-021-00449-4

Zhang, X., Suo, X., Yang, X., Lai, H., Pan, N., He, M., et al. (2022). Structural and functional deficits and couplings in the cortico-striato-thalamo-cerebellar circuitry in social anxiety disorder. *Transl Psychiatry.* 12, 26. doi: 10.1038/s41398-022-01791-7

Zhao, C., Zhu, J., Liu, X., Pu, C., Lai, Y., Chen, L., et al. (2017). Structural and functional brain abnormalities in schizophrenia: a cross-sectional study at different stages of the disease. *Prog Neuropsychopharmacol Biol Psychiatry.* 83, 27–32. doi: 10.1016/j.pnpbp.12, 017.

frontiers | Frontiers in Aging Neuroscience

TYPE Original Research
PUBLISHED 21 June 2023
DOI 10.3389/fnagi.2023.1224525

OPEN ACCESS

EDITED BY
Han Lv,
Capital Medical University, China

REVIEWED BY
Jiajia Zhu,
The First Affiliated Hospital of Anhui Medical University, China
Peng Li,
First Affiliated Hospital of Xi'an Jiaotong University, China

*CORRESPONDENCE
Haibo Xu
✉ xuhaibo1120@hotmail.com
Lei Gao
✉ ncu6096@126.com

†These authors share first authorship

RECEIVED 17 May 2023
ACCEPTED 08 June 2023
PUBLISHED 21 June 2023

CITATION
Ruan Z, Sun D, Zhou X, Yu M, Li S, Sun W, Li Y, Gao L and Xu H (2023) Altered neurovascular coupling in patients with vascular cognitive impairment: a combined ASL-fMRI analysis. *Front. Aging Neurosci.* 15:1224525. doi: 10.3389/fnagi.2023.1224525

Altered neurovascular coupling in patients with vascular cognitive impairment: a combined ASL-fMRI analysis

Zhao Ruan[1†], Dong Sun[2†], Xiaoli Zhou[1], Minhua Yu[1], Sirui Li[1], Wenbo Sun[1], Yidan Li[1], Lei Gao[1*] and Haibo Xu[1*]

[1]Department of Radiology, Zhongnan Hospital of Wuhan University, Wuhan, Hubei, China, [2]Department of Neurology, Zhongnan Hospital of Wuhan University, Wuhan, Hubei, China

Background and objective: This study aims to examine the role of neurovascular coupling (NVC) in vascular cognitive impairment (VCI) by investigating the relationship between white matter lesion (WML) burden, NVC, and cognitive deficits. Additionally, we aim to explore the potential of NVC as a tool for understanding the neural mechanisms underlying VCI.

Methods: This study included thirty-eight small vessel disease cognitive impairment (SVCI) patients, 34 post-stroke cognitive impairment (PSCI) patients, and 43 healthy controls (HC). Comprehensive assessments, including neuroimaging and neuropsychological testing, were conducted to evaluate cognitive function. WML burden was measured and correlated with NVC coefficients to examine the relationship between white matter pathology and NVC. Mediation analysis was employed to explore the link relationship between NVC, WML burden, and cognitive function.

Results: The present study showed that NVC was significantly reduced in the SVCI and PSCI groups compared with HCs at both whole-brain and brain region level. The analysis revealed notable findings regarding NVC in relation to WML burden and cognitive function in VCI patients. Specifically, reduced NVC coefficients were observed within higher order brain systems responsible for cognitive control and emotion regulation. Mediation analysis demonstrated that NVC played a mediating role in the relationship between WML burden and cognitive impairment.

Conclusion: This study reveals the mediating role of NVC in the relationship between WML burden and cognitive function in VCI patients. The results demonstrate the potential of the NVC as an accurate measure of cognitive impairment and its ability to identify specific neural circuits affected by WML burden.

KEYWORDS

vascular cognitive impairment, cerebral small vessel disease, post-stroke cognitive impairment, neurovascular coupling, white matter lesion

Introduction

With increased human longevity, dementia has emerged as a prominent health issue among the elderly. Cerebrovascular disease represents the second leading cause of dementia (Toledo et al., 2013). The prevalence of vascular cognitive impairment (VCI) ranges 15–40% in individuals over the age of 65 (van der Flier et al., 2018). VCI encompasses a wide range of cognitive impairment, from mild vascular cognitive impairment to vascular dementia (VaD) (van der Flier et al., 2018). The most common cause of VCI is cerebral small vessel disease (CSVD) (Iadecola et al., 2019), while stroke also contributes significantly to VCI (Lo et al., 2019). Both CSVD and stroke impact cerebral blood flow (CBF) regulation, metabolic demand, and neuronal activity (Wallin et al., 2018). However, the neural mechanisms underlying VCI remain incompletely understood.

Neurovascular coupling (NVC) is the temporal coordination between CBF and neural activity. This concept has a long history, originating from the work of Dutch psychologist Donders (Phillips et al., 2016). NVC is essential for maintaining normal brain function, with the neurovascular unit playing a key role in regulating blood supply and cellular processes to maintain homeostasis between neurons, glial cells, and vascular cells (Attwell et al., 2010). In cerebrovascular diseases, including CSVD, disruption of the neurovascular unit is often referred to as "neurovascular decoupling" (Iadecola, 2013; Shabir et al., 2018). Numerous studies have shown a strong correlation between neurovascular decoupling and cognitive impairment (Tarantini et al., 2019), although most of these studies have been conducted in animal experiments (Tucsek et al., 2014; Toth et al., 2017).

Non-invasive imaging techniques are urgently needed to investigate NVC. Liang et al. (2013) established a link between CBF and intrinsic brain activity measured by resting-state functional magnetic resonance imaging (rs-fMRI), suggesting that this correlation reflects NVC. Studies integrating neurophysiology and rs-fMRI have demonstrated a close relationship between the amplitude of low-frequency fluctuations (ALFF) in blood oxygen level-dependent (BOLD) signals (Zang et al., 2007) and spontaneous neuronal activity (Logothetis et al., 2001; Nir et al., 2007). Arterial spin labeling (ASL), a technique utilizing endogenous water molecules as diffusion markers, provides valuable insights into CBF and disease pathogenesis. Reduced CBF, associated with the extent of cognitive impairment, has been observed in VCI (Sun et al., 2016). The integration of ASL-derived cerebral perfusion information and rs-fMRI-derived cerebral neural function, along with their coupling analysis, has gradually gained traction in the field of cognitive impairment research. This approach has been utilized in several neurological disorders such as end-stage renal disease (Li et al., 2021), chronic migraine (Hu et al., 2019), and schizophrenia (Zhu et al., 2017), as well as cerebrovascular diseases such as hypertension and ischemic stroke, demonstrating associations with NVC dysfunction and cognitive impairment (Rousseaux et al., 2010; Bloch et al., 2015). These findings suggest that NVC may serve as a physiological basis for cognitive function and can be studied in VCI patients using this approach.

Neurovascular coupling has been chosen as the focus of this study due to its unique advantages in VCI researches. It serves as a bridge between vascular pathology and cognitive decline by capturing the dynamic relationship between neuronal activity and CBF (Sanford et al., 2022). Unlike other measures, NVC detects early changes in cerebral perfusion and neural activity, providing a non-invasive assessment of neurovascular regulation. Impaired NVC in VCI leads to a mismatch between metabolic demand and blood supply, resulting in cognitive impairment (Yabluchanskiy et al., 2020). NVC also integrates functional and physiological aspects of brain function, simultaneously assesses CBF and spontaneous neural activity. This holistic approach goes beyond cognitive assessments alone, which may miss physiological changes (Hu et al., 2019). Moreover, NVC is highly sensitive to subtle alterations in cerebral perfusion and neuronal activity (Claassen et al., 2021), enabling early diagnosis and monitoring in the heterogeneous and subtle changes seen in VCI.

Several studies have investigated NVC in VCI using various neuroimaging techniques. For instance, Liu et al. (2021) demonstrated disrupted NVC in patients with subcortical ischemic vascular disease, showing a mismatch between regional cerebral blood flow and neuronal activity. Similarly, Shabir et al. (2018) reported impaired NVC in patients with small vessel disease, highlighting the association between reduced NVC and cognitive decline. These studies collectively emphasize the significance of NVC dysfunction in VCI pathogenesis. Accumulating evidence highlights the role of the NVC in influencing an individual's cognitive abilities. However, it is important to note that previous research in this field has primarily focused on studying specific subtypes of VCI, thereby overlooking the diverse subtypes that VCI encompasses. Furthermore, an important factor that has been relatively neglected in these studies is the presence of white matter lesions (WML), which has intricate connections with both NVC and VCI. WML represent a prevalent manifestation of cerebral small vessel lesions observed in neuroimaging, capable of eliciting cognitive impairment and other associated symptoms (Sarbu et al., 2016). However, recent studies have demonstrated incongruent effects of WML volume and location on cognitive impairment in patients (Kim et al., 2015; Veselý and Rektor, 2016). Moreover, WML shows a strong association with NVC (Sorond et al., 2013). Therefore, the interactions between WML, NVC, and VCI are worth studying.

To investigate whether NVC dysfunction is a potential mechanism leading to VCI, to identify new imaging markers of VCI and to investigate the interaction of WML, NVC, and VCI, this study performed a broad series of multimodal neuroimaging analyses to test three hypotheses. First, we hypothesized that

Abbreviations: AAL, automatic anatomical labeling; AD, Alzheimer's disease; ALFF, amplitude of low frequency fluctuations; ANOVA, analysis of variance; ASL, arterial spin labeling; BOLD, blood oxygen level dependent; CBF, cerebral blood flow; CSVD, cerebral small vessel disease; DMN, default-mode network; FC, functional connectivity; FLAIR, fluid attenuated inversion recovery; FWE, family wise error; FWHM, full width at half maximum; GMV, gray matter; HCs, healthy controls; MCI, mild cognitive impairment; MMSE, mini-mental state examination; MoCA, Montreal cognitive assessment; NVC, neurovascular coupling; PCASL, pseudo-continuous arterial spin labeling; PET, positron emission tomography; PSCI, post-stroke cognitive impairment; PSD, post-stroke dementia; ReHo, regional homogeneity; ROI, region of interest; rs-fMRI, resting-state functional magnetic resonance imaging; SVCI, small vessel disease cognitive impairment; TMS, transcranial magnetic stimulation; VCI, vascular cognitive impairment; VMCI, vascular mild cognitive impairment; VaD, vascular dementia; VOI, volume of interest; WMH, white matter hyperintensity; WML, white matter lesions.

patients with VCI would have impaired NVC. Second, we hypothesized that NVC dysfunction would be associated with cognitive decline. Finally, we hypothesized that NVC dysfunction would act as a mediator in the relationship between clinical features of VCI and cognitive impairment. To test these hypotheses, the main objectives of this study were to determine changes in regional ALFF and CBF in patients with VCI, to assess the extent of NVC changes, and to examine the mediating role of NVC in the relationship between WML burden and cognitive performance. NVC coefficients calculated from regional ALFF and CBF measures were used in a mediation model to examine the role of NVC in the relationship between WML burden and global cognition in patients with VCI.

Subjects and methods

Participants

This study received approval from the Ethical Medicine Society of Zhongnan Hospital of Wuhan University, and all participants provided informed consent by signing a consent form. Given that small vessel cognitive impairment (SVCI) and post-stroke cognitive impairment (PSCI) constitute the majority of VCI (Skrobot et al., 2018; Iadecola et al., 2019), the inclusion of SVCI and PSCI patients ensures adequate representation. A total of 72 VCI patients (38 SVCI and 34 PSCI) were recruited from outpatient and inpatient settings between December 2019 and October 2021. Additionally, 43 demographically matched healthy controls (HCs) were enrolled during the same period. Detailed inclusion and exclusion criteria are as follows.

Inclusion and exclusion criteria

Inclusion criteria: (1) SVCI: at least one acute ischemic cerebrovascular disease has been onset for more than 3 months; PSCI: the onset time of stroke patients is within 6 months; confirm that the stroke through medical history and medical imaging and rule out hemorrhagic stroke; and neuroimaging findings of these two subtypes meeting the VICCS-2 neuroimaging criteria (Skrobot et al., 2018); (2) age 40–70 years; (3) meet the diagnostic criteria for VCI (Skrobot et al., 2018); (4) able to cooperate in completing various instrumental examinations and neuropsychological scale tests; and (5) voluntary signing of informed consent.

Exclusion criteria: (1) with severe heart, brain, lung, and kidney diseases; (2) with vision and hearing impairment that significantly affect cognitive testing; (3) With a history of psychoactive substance abuse; (4) other severe physical diseases that affect cognitive testing, such as coma, epilepsy, hypothyroidism, hypoxemia, etc.; (5) with a history of mental illness; and (6) with contraindication to MRI, and is unwilling to participate research and unconditional follow-up.

Neuropsychological assessment

All participants underwent the following neuropsychological assessments: (1) neuropsychiatric inventory (NPI), and (2) global cognition: the mini-mental state examination (MMSE) (Tombaugh and McIntyre, 1992) and the Montreal Cognitive Assessment (MoCA) (Nasreddine et al., 2005).

MRI data acquisition

One hour following the completion of the neuropsychological assessment, imaging data were acquired using a 3.0 T MR scanner (Discovery 750 w, GE Healthcare, Waukesha, WI, USA) equipped with a 32-channel head coil. The imaging protocol encompassed high-resolution T1 and T2-FLAIR scans (176 sagittal slices, 1-mm in-plane resolution), rs-fMRI (TR/TE = 2000/30 ms, voxel size 3.75 mm × 3.75 mm × 3.75 mm, 40 slices) with a duration of 8 min and 10 s, consisting of 185 functional volumes, and a background-suppressed three-dimensional pseudo-continuous arterial spin labeling (PCASL) sequence (TR/TE = 10.5/4.9 ms, flip angle 111°, 50 slices, slice thickness 4 mm without gap, field of view (FOV) 240 mm × 240 mm, matrix size 128 × 128, labeling duration 1500 ms, post-labeling delay 2025 ms).

BOLD signals processing

Data were pre-processed using SPM8[1] and the Data Processing Assistant for Resting-State fMRI toolbox33 (DPARSF)[2] (Chao-Gan and Yu-Feng, 2010). The first 10 volumes of functional images were discarded, and the remaining images were then corrected for temporal shifts caused by head motion (using 24 motion-related regressions) and slice acquisition (using a least-squares approach). The realigned images were then spatially normalized to the MNI template. The resulting normalized functional images were z-transformed and smoothed with a Gaussian kernel (FWHM = 8 mm). Finally, a band-pass filter was applied to retain frequencies between 0.01 and 0.1 Hz to preserve low-frequency fluctuations. The ALFF was calculated for the filtered images using the RESTplus toolkit (V1.24)[3] (Jia et al., 2019). The main steps involved transforming the pre-processed time series into the frequency domain using Fast Fourier Transform to compute the square root of the power spectrum for each frequency. A temporal band-pass filter (0.01–0.1 Hz) was then applied to remove low-frequency drift and physiological high-frequency noise. Finally, the individual ALFF maps were normalized using the Fisher Z-transformation. Based on previous literature and our group's experience, ALFF shows better retest reliability and stability compared to fALFF; therefore, only ALFF calculations were performed, excluding fALFF.

PCASL images processing

Individual raw CBF images were generated automatically using the GE workstation. The raw images underwent a visual screening process to exclude those with incomplete whole-brain coverage, significant head motion artifacts, or other conditions that did not

1 http://www.fil.ion.ucl.ac.uk/spm
2 http://www.restfmri.net/forum/DPARSF
3 http://www.restfmri.net/forum/RESTplus

meet the inclusion criteria. The excluded raw CBF images were processed using SPM12, ASLtbx,[4] and MATLAB with the following key steps: (1) format conversion to NII; (2) alignment to the corresponding high-resolution T1-3D image of each individual to correct for partial volume effects; (3) spatial standardization to the MNI standard space; (4) whole-brain normalization using Fisher Z-transformation to correct for variance of individual CBF maps; and (5) spatial smoothing using a 6-mm FWHM smoothing kernel suitable for subsequent statistical analysis.

NVC analysis

The NVC was calculated using the Multimodal Image Coupling Analysis (MICA) toolkit.[5] Globally, the NVC was determined by calculating the correlations between vicarious neuronal activity images (ALFF maps) and regional CBF maps across the entire gray matter mask for each subject, as outlined in Hu et al. (2021). Regionally, NVC was computed by calculating the correlations between ALFF maps and regional CBF maps within each voxel of the automatic anatomical labeling 2 (AAL2) atlas region (Rolls et al., 2015), The AAL2 atlas divides the human brain into 116 regions, each with a unique label and identifier number. This analysis resulted in 116 ALFF-CBF coefficients representing the NVC within the given sub-regions.

White matter lesions mapping

White matter lesion burden can be assessed using a conventional T2-weighted fluid-attenuated inversion recovery (T2-FLAIR) sequence. The white matter of the brain is typically divided into two regions: (1) periventricular and (2) deep subcortical white matter. Baseline WML refers to a hyperintense lesion on T2-FLAIR within the white matter. Various white matter abnormalities were assessed, including (1) total WML volume, which is the sum of individual lesion volumes, (2) WML in the right and left hemispheres, and (3) subcortical WML. WML lesions were delineated on 3D anatomical T1 and T2 FLAIR images using ITK-Snap software (version 3.8).[6] ITK-Snap's regional competition preprocessing function was then applied using 5 tissue clusters, 0.5 regional competition, and 0.5 smoothing force. The initial lesion segmentation was manually refined based on lesion characteristics and 3D visualization. Consensus was reached among three experts blinded to the radiologic diagnosis. In cases of disagreement, a senior neuroradiologist with more than 10 years of experience in neuroimaging was consulted for final consensus. In addition, the Fazekas score was used in this study for graded assessment of WML (Fazekas et al., 1987).

Association analysis

Neurobehavioral associations between NVC, WML burden, and global cognition (MoCA scores) were evaluated through *Pearson's* linear correlations, with a significance level of $p < 0.05$, *Bonferroni's* corrected.

Mediation analysis

Mediation analysis is a statistical approach used to examine the indirect effects of an independent variable on a dependent variable through a third variable, known as the mediator variable.

4 https://www.cfn.upenn.edu/zewang/ASLtbx.php

5 https://github.com/hubolll/MICA_v1

6 http://www.itksnap.org

TABLE 1 Demographic and clinical characteristics of the subjects.

	SVCI (n = 38)	PSCI (n = 34)	HCs (n = 43)	$F/X^2/t(p)$
Gender (male/female)	30/8	27/7	33/10	0.226 (0.798)
Age (years)	60.81 ± 8.42	60.88 ± 8.68	58.23 ± 4.38	1.741 (0.180)
Education (years)	9.83 ± 2.08	9.64 ± 1.73	10.41 ± 2.30	0.156 (0.856)
Hypertension	20 (52%)	17 (50%)	16 (37%)	2.229 (0.328)
Diabetes	15 (39%)	13 (38%)	11 (25%)	2.14 (0.343)
Hyperlipidemia	13 (34%)	11 (32%)	12 (27%)	0.397 (0.819)
Smoke	22 (57%)	20 (58%)	23 (53%)	0.263 (0.876)
Alcohol	16 (42%)	17 (50%)	19 (44%)	0.909 (0.634)
MMSE	24.18 ± 2.27	21.94 ± 2.42	27.38 ± 1.21	31.36 (<0.01**)
MoCA	23.10 ± 2.34	20.88 ± 2.39	25.07 ± 2.23	49.12 (<0.001**)
WML load, ml ± SD	5.25 ± 1.65	6.32 ± 2.21	0.45 ± 0.71	−6.76 (< 0.01**)
Periventricular WML load, ml ± SD	2.88 ± 1.32	3.47 ± 2.34	0.24 ± 0.47	−7.35 (< 0.01**)
Subcortical WML load, ml ± SD	0.84 ± 1.21	2.04 ± 2.65	–	−3.48 (0.01**)
Fazekas score [median (range)]	1 (0–3)	2 (0–3)	1 (0–2)	−4.52 (0.04*)

Data are presented as mean ± SD. SVCI, small vessel disease cognitive impairment; PSCI, post-stroke cognitive impairment, HC, healthy controls; MMSE, Mini-Mental state examination; MoCA, Montreal cognitive assessment; WML, white matter lesion; a, p-value was obtained using the two-tailed Chi-squared test; Lesion burden corrected (corrected by total cranial volume). **$p < 0.01$; *$p < 0.05$.

In this study, the independent variable is WML burden, the dependent variable is global cognition, and the mediator variable is NVC in specific brain regions. We conducted mediation analyses using model 4 in Hayes' SPSS macro-PROCESS (ver3.4), controlling for covariates of no interest such as TIV, age, gender, and education.

In this model, NVC within the significant regions (identified by AAL labels) served as a mediator (M), and WML burden (X) influenced the outcome of global cognition (Y). There were three pathways: (1) a direct pathway represented by c', and two indirect pathways denoted by (2) a and (3) b. We used a bootstrapping method with 10,000 samples and a 95% confidence interval (CI) to assess the significance of the indirect effects. A 95% CI that does not include zero indicates a significant indirect effect.

Statistical analyses

Demographic and clinical data and global NVC were analyzed using SPSS software (SPSS 22.0, Inc., Chicago, IL, USA). One-way analysis of variance (ANOVA) and Mann-Whitney *U*-tests were used to compare differences between SVCI, PSCI, and HCs for continuous variables, adjusting for data distribution and homogeneity of variance. Chi-squared tests were used for categorical variables. The threshold for statistical significance was set at $p < 0.05$.

For ALFF, CBF, and GM volume images, voxel-wise statistical analyses were performed using SPM12. These analyses were restricted to the gray matter mask, controlling for age and sex as mixed regression variables. Cluster-level family wise error (FWE) correction was applied to these imaging measures (voxel $p < 0.001$ and cluster $p < 0.05$). Surviving brain regions were visualized on cortical surfaces using BrainNetViewer software[7].

Two-tailed, two-sample Student's *t*-tests were performed for regional NVC. The resulting *p*-values were corrected using a false discovery rate (FDR) strategy with a threshold of $p < 0.05$.

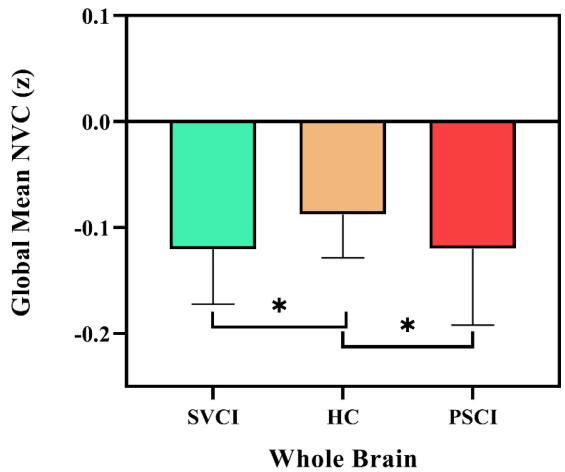

FIGURE 1
Global neurovascular coupling. Reduced global ALFF-CBF coupling in SVCI and PSCI patients, compared to HCs. At the group level, the mean of global ALFF-CBF coupling is, respectively, significantly lower ($p = 0.009$) in patients with SVCI ($p = 0.002$) and PSCI ($p = 0.022$) than in healthy controls. Error bars represent the standard error; SVCI, small vessel disease cognitive impairment; PSCI, post-stroke cognitive impairment, HC, healthy controls; NVC, neurovascular coupling. *$p < 0.05$.

Results

Demographics and neuropsychological assessment

Demographic characteristics, neuropsychological test results, and WML burden for each group are shown in Table 1. There were no significant differences between the three groups in terms of age, gender, education, hypertension, diabetes, hyperlipidemia, smoking, or alcohol consumption ($p > 0.05$). However, both PSCI and SVCI patients exhibited lower global cognitive scores on MoCA and MMSE, as well as a higher WML burden compared to the HCs group ($p < 0.05$) (Table 1).

Between-group comparison of CBF and ALFF

Supplementary Figure 1 displays the average spatial patterns of CBF for each group. Both PSCI and SVCI patient exhibit modified regional CBF in the somatomotor and default mode network (DMN) regions. Specifically, compared to the subjects in the HCs group, those with PSCI display increased perfusion in the right ventral posterolateral thalamus and decreased perfusion in the left inferior parietal, left inferior frontal, and left middle frontal gyri. Conversely, the SVCI group shows increased perfusion in the right hippocampus and vermis, along with decreased perfusion in the right middle frontal and superior temporal gyri. Moreover, the SVCI group demonstrates higher regional CBF in the left middle cingulate and posterior gyrus (refer to Supplementary Table 1). Supplementary Figure 2 illustrates the average spatial distributions of ALFF for each group. PSCI and SVCI patient exhibit altered regional ALFF in the language network and DMN regions.

Between-group comparisons on NVC

We first delineated the global NVC patterns of the entire brain using the gray matter mask, as shown in Figure 1. Notably, both the PSCI and SVCI cohorts showed significantly reduced global NVC, with the PSCI group being among the lowest.

We then quantified cross-voxel NVC within each region defined by the AAL 116 atlas, as shown in Figure 2. Significantly divergent regions of interest (ROIs) included the left superior frontal gyrus, bilateral inferior frontal gyrus, left rolandic operculum, left insula, right paracentral lobule, middle temporal gyrus, crus II of the cerebellar hemisphere, lobule III VI VIII of the cerebellum, and lobule III VII of the vermis ($p < 0.01$, FDR corrected) (Table 2).

7 http://www.nitrc.org/projects/bnv

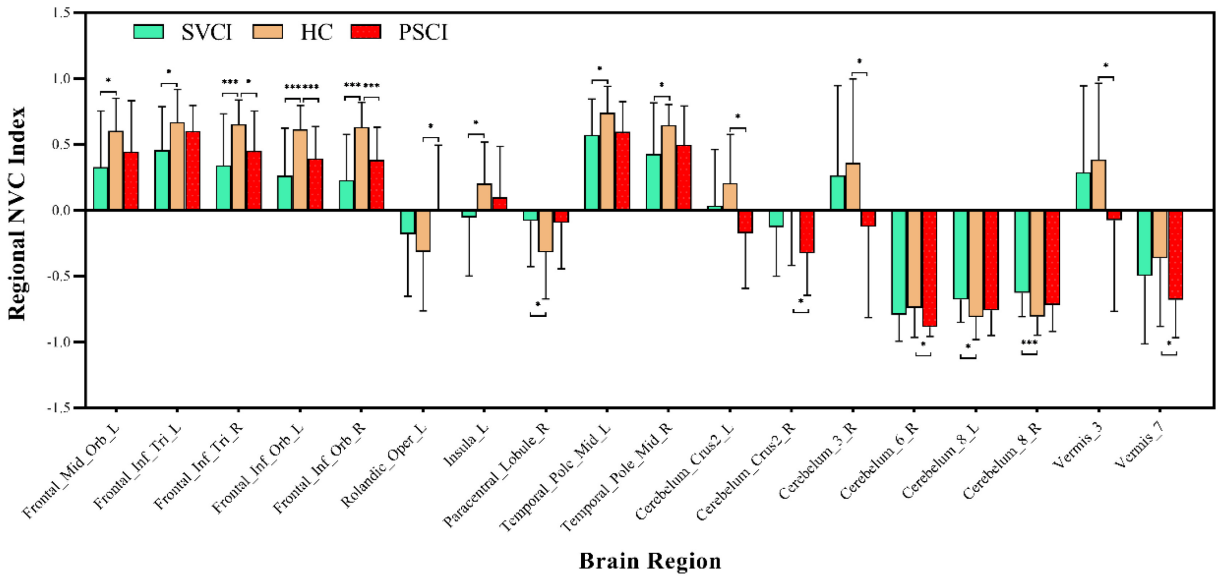

FIGURE 2
Regional neurovascular coupling. ALFF-CBF coupling differences between every two groups of SVCI, PSCI, and HCs ($p < 0.05$, FWE corrected). Compared to HCs, the SVCI patients had decreased NVC coefficient in the left middle frontal gyrus, left inferior frontal gyrus, left insula, **(middle)** temporal gyrus, and cerebellum; increased NVC coefficient in the **(right)** paracentral lobule and cerebellum while PSCI patients had decreased NVC coefficient in the right middle frontal gyrus, left inferior frontal gyrus (orbital part), **(left)** rolandic operculum, cerebellum, and vermis; SVCI, small vessel disease cognitive impairment; PSCI, post-stroke cognitive impairment, HC, healthy controls; NVC, neurovascular coupling. *$p < 0.05$; ***$p < 0.001$.

Association analyses

White matter lesion burden (ml) were negatively correlated with MoCA scores (SVCI patients, $R^2 = 0.3869$, $r = -0.622$, $p < 0.001$; PSCI patients, $R^2 = 0.383$, $r = -0.619$, $p < 0.001$) and regional NVC (SVCI patients, $R^2 = 0.523$, $r = -0.723$, $p < 0.001$; PSCI patients, $R^2 = 0.523$, $r = -0.723$, $p < 0.001$) in both the SVCI and PSCI groups (Figure 3).

Furthermore, regional NVC were positively correlated with MoCA scores in both the SVCI ($R^2 = 0.438$, $r = 0.611$, $p < 0.001$) and PSCI groups ($R^2 = 0.261$, $r = 0.540$, $p < 0.001$) (Figure 3).

Mediation analysis

Mediation analyses revealed that regional NVC in the left middle frontal gyrus and left inferior frontal gyrus served as partial mediators in the association between WML burden and global cognition in SVCI ($c' = -0.307$, $p < 0.001$) and PSCI patients ($c' = -0.323$, $p < 0.001$) (Figure 4).

Discussion

Main findings

This study aimed to investigate the utility of NVC as a reliable measure of cognitive decline in SVCI and PSCI patients, and its association with cognitive function and WML burden. The main findings confirmed our initial hypotheses and revealed significant correlations between NVC, cognitive test scores, and WML burden. These results support the effectiveness of NVC in examining cognitive decline in SVCI and PSCI patients. Furthermore, the study identified specific brain regions where NVC acted as a partial mediator in the relationship between WML burden and global cognition, which may indicate potential targets for interventions to improve cognitive function in these patient populations. By using multiple neuroimaging techniques, such as perfusion and functional imaging, this study provided a comprehensive understanding of the neural mechanisms underlying cognitive impairment in SVCI and PSCI patients.

Potential physiological correlates

Neurons, including astrocytes and blood vessels, form the intricate neurovascular unit in the human brain. The integrity of this unit is critical for proper NVC (Kozberg and Hillman, 2016; Phillips et al., 2016). The connections between its components are highly complex, and damage to any element can disrupt brain structure and function, resulting in impaired NVC.

Amplitude of low frequency fluctuations represents the total power of low frequency fluctuations (0.01∼0.1 Hz), while fALFF represents the relative contribution of specific low frequency fluctuations to the total frequency range. Both ALFF and fALFF derived from BOLD signals effectively capture neuronal oxygen uptake capacity. Therefore, ALFF-CBF and fALFF-CBF analyses reveal the coordination between oxygen demand and blood supply, reflecting the functionality of the neurovascular unit (Kisler et al., 2017). In this study, 3D ASL technology provided information on CBF while rs-fMRI provided information on cerebral neural function (ALFF). The combined analysis of these two measures allowed us to investigate the impact of the disease on the

TABLE 2 Comparisons of NVC at regional level.

Brain region	PSCI	SVCI	HCs	SVCI vs. HCs *t(P)*	PSCI vs. HCs *t(P)*
Frontal_Mid_Orb_L	0.440 ± 0.389	0.326 ± 0.427	0.601 ± 0.246	−3.453 (0.019*)	—
Frontal_Inf_Tri_L	0.601 ± 0.194	0.455 ± 0.330	0.667 ± 0.249	−3.162 (0.031*)	—
Frontal_Inf_Tri_R	0.450 ± 0.302	0.338 ± 0.391	0.651 ± 0.185	−4.450 (0.001**)	−3.391 (0.016*)
Frontal_Inf_Orb_L	0.392 ± 0.242	0.261 ± 0.360	0.612 ± 0.182	−5.638 (0.001**)	−4.370 (0.001**)
Frontal_Inf_Orb_R	0.382 ± 0.246	0.228 ± 0.346	0.629 ± 0.189	−6.283 (0.001**)	−4.793 (0.001**)
Rolandic_Oper_L	0.005 ± 0.488	−0.181 ± 0.470	−0.318 ± 0.446	—	2.962 (0.046*)
Insula_L	0.098 ± 0.385	−0.056 ± 0.442	0.202 ± 0.315	−2.947 (0.043*)	—
Paracentral_Lobule_R	−0.095 ± 0.349	−0.081 ± 0.345	0.368 ± 0.355	2.968 (0.043*)	—
Temporal_Pole_Mid_L	0.594 ± 0.229	0.569 ± 0.274	0.739 ± 0.200	−3.102 (0.033*)	—
Temporal_Pole_Mid_R	0.494 ± 0.296	0.427 ± 0.388	0.645 ± 0.157	−3.221 (0.028*)	—
Cerebelum_Crus2_L	−0.175 ± 0.418	0.031 ± 0.428	0.204 ± 0.370	—	−4.119 (0.003**)
Cerebelum_Crus2_R	−0.326 ± 0.319	−0.129 ± 0.372	−0.004 ± 0.415	—	−3.764 (0.010*)
Cerebelum_3_R	−0.125 ± 0.689	0.263 ± 0.682	0.358 ± 0.637	—	−3.120 (0.036*)
Cerebelum_6_R	−0.887 ± 0.070	−0.793 ± 0.200	−0.743 ± 0.221	—	−3.842 (0.010*)
Cerebelum_8_L	−0.760 ± 0.191	−0.678 ± 0.171	−0.746 ± 0.171	3.373 (0.022*)	—
Cerebelum_8_R	−0.720 ± 0.200	−0.627 ± 0.180	−0.807 ± 0.141	4.803 (0.001**)	—
Vermis_3	−0.075 ± 0.692	0.286 ± 0.656	0.382 ± 0.582	—	−3.057 (0.037*)
Vermis_7	−0.680 ± 0.287	−0.499 ± 0.516	−0.364 ± 0.517	—	−3.294 (0.033*)

Data were reported as mean ± SD, and significant differences were labeled with asterisks; SVCI, small vessel disease cognitive impairment; PSCI, post-stroke cognitive impairment, HCs, healthy controls. $^{**}p < 0.01$; $^{*}p < 0.05$.

neurovascular unit. This technique has been increasingly used in neuropsychiatric research (Roquet et al., 2016; Leeuwis et al., 2017). Our results indicated impaired neurovascular autonomic regulation in SVCI and PSCI patients. Notably, previous studies by Zhu et al. (2017) and Sheng et al. (2018) demonstrated reduced coupling strength in patients with schizophrenia and major depressive disorder compared with healthy subjects. Inspired by their research, the present study examined the correlation of ALFF with CBF, providing a unique perspective on this phenomenon. In addition, our study is the first to simultaneously analyze NVC in patients with both SVCI and PSCI subtypes. The observed decline in NVC in patients with PSCI and SVCI may have some impact on the treatment of cognitive impairment, as previous studies have demonstrated the efficacy of various drugs in improving NVC in animal experiments (Toth et al., 2014).

From a mechanistic perspective, the increased and decreased regions of ALFF-CBF between groups reflect different characteristics of NVC function in VCI. The comprehensive literature review highlights that NVC plays a critical role in maintaining cognitive function and that its dysfunction is associated with cognitive impairment in VCI. Specifically, the increased regions of ALFF-CBF indicate enhanced NVC, suggesting a robust coupling between neural activity and blood flow regulation. This enhancement may result from upregulated neurotransmitter release, increased vascular reactivity and improved endothelial function, facilitating efficient oxygen and nutrient delivery to active brain regions. This suggests increased neural metabolic demand and effective NVC mechanisms supporting enhanced cognitive processes. On the other hand, the decreased regions of ALFF-CBF indicate impaired NVC, where the coordination between neural activity and blood flow is compromised. This dysfunction may result from reduced neurotransmitter release, impaired vascular reactivity or endothelial dysfunction, leading to inadequate blood supply to the affected brain regions. As a result, neuronal activity may be dampened and metabolic support may be inadequate, resulting in reduced spontaneous neuronal activity and impaired cognitive function. The altered ALFF-CBF patterns in these regions provide valuable insights into the complex relationship between neural activity and vascular responses. Understanding the underlying mechanisms driving these changes is critical to unraveling the neurophysiological basis of cognitive impairment. Further investigations could explore factors such as vascular remodeling, alterations in neurovascular signaling pathways or disturbances in the neurovascular unit that may contribute to the observed changes in NVC.

In line with previous research, both cohorts of VCI patients in our study exhibited a notable increase in WML burden, particularly around the ventricles. Moreover, PSCI patients displayed additional cortical and subcortical damage. The distribution of these injuries aligned with findings from previous studies involving similar subject populations (Meyer et al., 2016; Altermatt et al., 2019). However, our primary focus was to examine changes in the intrinsic activity of the brain at rest, specifically the ALFF and local CBF. These alterations primarily affected the default mode, somatosensory/motor, dorsal attention, and language networks, which diverged to some extent from previous research findings (Cai et al., 2018; Nasios et al., 2019).

Relationship between the NVC, WML burden, and cognitive impairment

Consistent with our hypothesis, both SVCI and PSCI patients exhibit a similar NVC pattern across the entire brain, but with an overall lower level of coupling compared to HCs. This reduction in coupling supports the findings of Liu et al. (2021) and animal studies (Tarantini et al., 2017), suggesting a disrupted interaction between spontaneous neural activity and cerebral blood flow at the global level.

In PSCI and SVCI patients, mediation analysis results show that NVC in the left middle frontal gyrus and left inferior frontal gyrus partially mediate the relationship between WML load and global cognition. This suggests that NVC in these regions may contribute significantly to the cognitive deficits observed in PSCI and SVCI patients. These findings are consistent with previous research highlighting the vulnerability of the frontal lobes to the effects of WML burden and its association with cognitive impairment in individuals with cerebrovascular disease (McAleese et al., 2021).

The left middle frontal gyrus and left inferior frontal gyrus are components of the prefrontal cortex and are located within the famous Broca's area, which is known to be involved in several cognitive processes, including attention, working memory, and executive function. Broca's area, a classic motor language region, plays a critical role in integrating the broader neural network and is located at the top of the cortical hierarchy. The prefrontal cortex also shows strong correlations with other brain regions and plays a role in regulating cognitive control and coordination across the brain (Ray and Zald, 2012). In this study, NVC in Broca's area showed a significant association with WML lesions and global cognition. Mediation analysis revealed that NVC in Broca's area partially mediated the relationship between WML burden and global cognitive impairment.

The results of this study suggest that WML burden may influence prefrontal regulation of cognitive function in patients with PSCI and SVCI, and that this effect is mediated by NVC. NVC, which reflects the interplay between resting cerebral blood flow and spontaneous neural activity, provides a more direct assessment of brain dysfunction and has greater specificity than WML burden alone (Huang et al., 2021). Identifying specific brain regions, such as the left middle frontal gyrus and the left inferior frontal gyrus, that mediate the relationship between WML burden and cognitive function is critical for developing targeted interventions to improve cognitive function in PSCI and SVCI patients. Based on the results, interventions targeting the left middle frontal gyrus and the left inferior frontal gyrus hold promise for improving cognitive function in these patient populations. Potential interventions may include cognitive training programs, brain stimulation techniques such as transcranial magnetic stimulation, or pharmacological approaches aimed at enhancing neural function and plasticity in these regions.

In conclusion, employing mediation analysis to explore the involvement of NVC in mediating the correlation between WML burden and global cognition introduces a novel methodology for comprehending the neural mechanisms associated with cognitive impairment in patients diagnosed with PSCI and SVCI. Understanding the disrupted NVC mechanisms in relation to WML burden may guide the development of interventions that specifically target these neural circuits. For example, interventions focused on enhancing NVC and improving blood flow regulation in affected brain regions may help mitigate cognitive impairment in VCI patients. The identification of specific brain regions that facilitate this correlation provides valuable insight into potential targets for interventions aimed at improving cognitive function in these patient cohorts. Further investigation is warranted to validate these findings and to develop and evaluate interventions tailored to these specific brain regions.

Brain regions and future considerations

The default mode network (DMN), which includes the posterior cingulate cortex/precuneus, medial and dorsal prefrontal cortex, temporoparietal junction, temporal lobe, and posterior inferior parietal lobe, is the most extensively studied resting-state network system (Raichle, 2015). In this study, numerous brain regions with altered CBF and ALFF were found to be located within the DMN, suggesting that it may be the primary network affected in VCI patients. In particular, the NVC coefficient showed a significant reduction in the left precentral gyrus of VCI patients. It is noteworthy that the precentral gyrus serves as a central brain region in the sensorimotor network and is actively involved in cognitive control and motor functions (Park and Friston, 2013). This finding is consistent with previous research highlighting the vulnerability of the precentral gyrus to cerebrovascular disease, which can lead to cognitive impairment (Vipin et al., 2018; Caruso et al., 2019). In addition, reduced NVC was observed in the insula, inferior parietal lobule, and middle temporal gyrus, areas associated with specific cognitive domains. For instance, the insula has been implicated in language processing (Gogolla, 2017), and hypoperfusion in this region has been linked to the severity of cognitive decline (Sun et al., 2016).

Parietal and medial temporal regions have been implicated in visuospatial attention and working memory processes (Wang et al., 2015; Lim et al., 2020), The observed decline in cognitive function in VCI patients in this study suggests that abnormal reductions in NVC within these brain regions may contribute to deficits in specific cognitive domains. Furthermore, recent studies in both humans and rodents have revealed that cerebellar regions, in addition to their role in balance and eye movements, are associated with various aspects of cognitive function, including cognitive flexibility, spatial navigation, working memory, and certain types of discriminative learning during aging and disease states (Shipman and Green, 2019; Liang and Carlson, 2020). Specifically, reduced anatomical connectivity, ALFF, and CBF have been observed in cerebellar regions of VCI patients (Yoon et al., 2013; Diciotti et al., 2017; Li et al., 2020). Consistently, the present study also observed reduced NVC in the cerebellum, further emphasizing its importance in cognitive processes.

Moreover, when analyzing brain regions, VCI patients and HCs exhibited no significant group differences in CBF and ALFF for several brain regions. However, significant differences in NVC correlation coefficients were observed. In this context, NVC correlation coefficients serve as valuable tools for identifying abnormal regions in VCI that may not be detected by single-modality analyses of CBF or ALFF using the same statistical

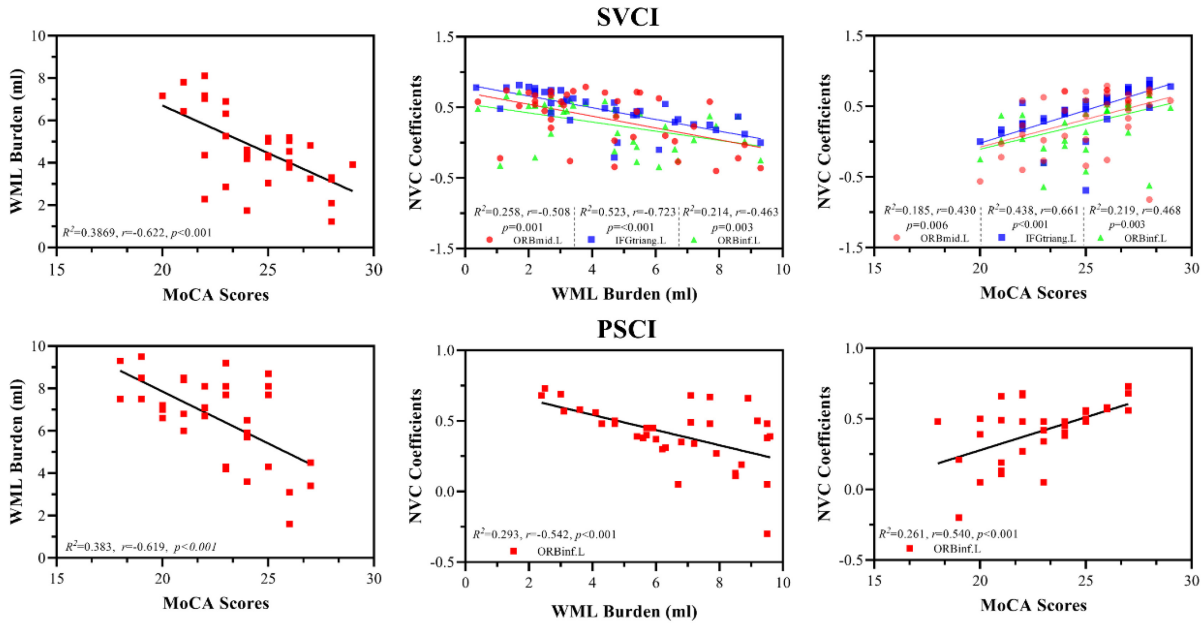

FIGURE 3
Association analyses between WML lesion, MoCA scores, and NVC; WML burden (ml) were negatively correlated with MoCA scores (SVCI patients, R^2 = 0.3869, r = −0.622, p < 0.001; PSCI patients, R^2 = 0.383, r = −0.619, p < 0.001) and regional NVC (SVCI patients, R^2 = 0.523, r = −0.723, p < 0.001; PSCI patients, R^2 = 0.523, r = −0.723, p < 0.001) in both the SVCI and PSCI groups. Furthermore, regional NVC were positively correlated with MoCA scores in both the SVCI (R^2 = 0.438, r = 0.611, p < 0.001) and PSCI groups (R^2 = 0.261, r = 0.540, p < 0.001) MoCA, Montréal cognitive assessment; SVCI, small vessel disease cognitive impairment; PSCI, post-stroke cognitive impairment, HC, healthy controls; NVC, neurovascular coupling; WML, white matter lesion; ORBmid.L, left middle orbital gyrus; ORBinf.L, left inferior orbital gyrus; IFGtriang.L, left triangular part of the inferior frontal gyrus.

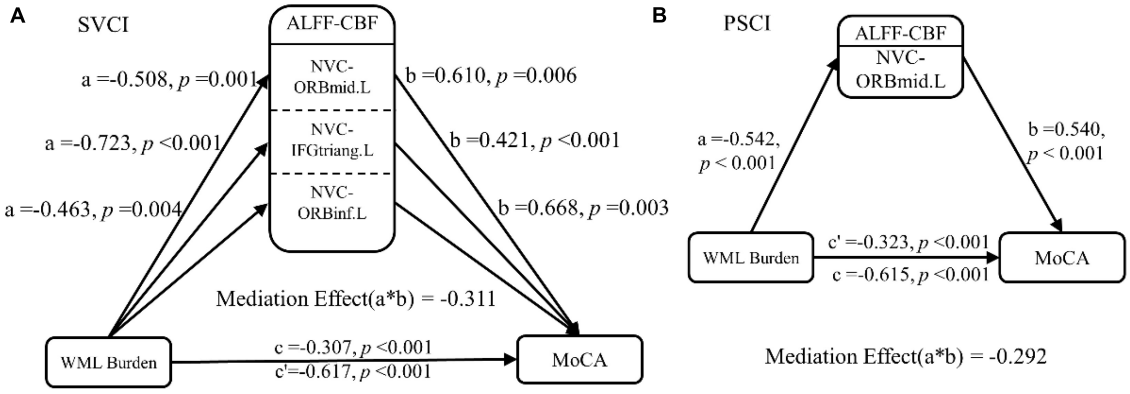

FIGURE 4
Mediation analysis. In the mediation analysis, the independent factor was the WML burden and the dependent variable was the cognitive function indicator. These were reflected by the MoCA scores, while the ALFF-CBF coefficient in the **(A)** SVCI and **(B)** PSCI patients served as the proposed mediator. The result of the mediation analysis indicated that NVC dysfunction (lower ALFF-CBF coefficient) in SVCI and PSCI patients partially mediated the effect of WML burden on global cognitive function decline. ALFF, amplitude of low frequency fluctuations; CBF, cerebral blood flow; SVCI, small vessel disease cognitive impairment; PSCI, post-stroke cognitive impairment, HC, healthy controls; NVC, neurovascular coupling; WML, white matter lesion; ORBmid.L, left middle orbital gyrus; ORBinf.L, left inferior orbital gyrus; IFGtriang.L, left triangular part of the inferior frontal gyrus.

threshold. Conversely, the NVC correlation coefficient did not show differences between the two groups in certain brain regions with significant group differences in CBF, ALFF, or both. Taken together, NVC correlation coefficients may provide complementary information for detecting pathological changes in VCI when used in conjunction with CBF and ALFF analyses. Patients with VCI exhibit reduced NVC levels in the dorsolateral prefrontal cortex and insula, regions primarily involved in cognitive control and emotion regulation processes (Richter-Levin, 2004; Opitz, 2014; Fama and Sullivan, 2015). Within these brain regions, the dorsolateral prefrontal cortex and insula have normal CBF but reduced ALFF, suggesting that the reduced CBF-ALFF correlation in these regions is mainly due to reduced ALFF. This abnormality may partially explain the cognitive and behavioral deficits associated with

these regions in VCI patients. Structural imaging studies have consistently shown reduced hippocampal volume in VCI patients, which correlates with cognitive performance (Bartsch and Wulff, 2015; Li et al., 2016). Moreover, a recent functional imaging study revealed a negative correlation between resting-state hippocampal activity and cognition in VCI patients (Zhuang et al., 2020). Based on these findings, it can be hypothesized that neurovascular decoupling impairs hippocampal function, leading to cognitive decline.

In summary, the current study identified decreased NVC coefficients within higher-order brain networks involved in cognitive control and emotion regulation, while NVC coefficients within lower-order brain networks involved in sensory processing and motor regulation remained largely unchanged. These observations provide additional support for the hypothesis that neurovascular decoupling within the brain may serve as a plausible pathological mechanism underlying VCI.

Limitations

Firstly, while a comprehensive set of imaging and neuropsychological assessments were employed to enhance specificity, it is worth mentioning that pathological confirmation was not obtained for any of the subjects, thereby making it impossible to completely exclude concurrent neurodegenerative conditions, including AD. It is important to acknowledge that the findings may not apply universally to all individuals with VCI and that further studies incorporating pathological confirmation are needed to validate and extend the current findings. Future research should include a wider range of VCI subgroups, taking into account different etiologies and lesion locations, to provide a more comprehensive understanding of NVC alterations in different VCI populations. Secondly, this study solely focused on evaluating global cognitive function and did not encompass an assessment of other specific cognitive domains, which may limit the ability to establish associations with a broader range of brain regions displaying intergroup disparities. Lastly, it is important to acknowledge that this study only represents a cross-sectional analysis, and future longitudinal investigations are warranted to gain a more comprehensive understanding of the dynamic changes in NVC, WML burden, and cognitive impairment over time.

Conclusion

To summarize, NVC plays an important role in mediating the association between WML burden and cognitive function in VCI patients, thus serving as a crucial neural foundation for VCI. This study provides objective neuroimaging evidence that expands our understanding of the neural mechanisms underlying VCI, with a particular focus on NVC. In essence, this research highlights the importance of using innovative approaches, such as NVC, to study cognitive decline in VCI. By providing a more accurate and reliable assessment of cognitive impairment and identifying the specific neural circuits affected by WML burden, NVC has the potential to guide the development of targeted interventions aimed at improving cognitive function in this patient population.

Data availability statement

The original contributions presented in the study are included in the article/**Supplementary material**, further inquiries can be directed to the corresponding authors.

Ethics statement

The studies involving human participants were reviewed and approved by the Ethical Medicine Society of Zhongnan Hospital of Wuhan University. The patients/participants provided their written informed consent to participate in this study. Written informed consent was obtained from the individual(s) for the publication of any potentially identifiable images or data included in this article.

Author contributions

ZR and DS collected data, designed the experiment, analyzed data, and drafted the manuscript. LG analyzed data and revised the manuscript. HX revised the manuscript and interpreted the data. XZ and YL collected data. SL, WS, and MY provided intellectual content of critical importance to the work described. All authors also approved the version to be published.

Acknowledgments

We thank Vivian Liu and Zhuang Yin for their assistance in performing MRI scans and data analysis.

Conflict of interest

The authors declare that the research was conducted in the absence of any commercial or financial relationships that could be construed as a potential conflict of interest.

Publisher's note

Supplementary material

The Supplementary Material for this article can be found online at: https://www.frontiersin.org/articles/10.3389/fnagi.2023.1224525/full#supplementary-material

References

Altermatt, A., Gaetano, L., Magon, S., Bauer, L., Feurer, R., Gnahn, H., et al. (2019). Clinical associations of t2-weighted lesion load and lesion location in small vessel disease: insights from a large prospective cohort study. *Neuroimage* 189, 727–733. doi: 10.1016/j.neuroimage.2019.01.052

Attwell, D., Buchan, A. M., Charpak, S., Lauritzen, M., Macvicar, B., and Newman, E. (2010). Glial and neuronal control of brain blood flow. *Nature* 468, 232–243.

Bartsch, T., and Wulff, P. (2015). The hippocampus in aging and disease: from plasticity to vulnerability. *Neuroscience* 309, 1–16. doi: 10.1016/j.neuroscience.2015.07.084

Bloch, S., Obari, D., and Girouard, H. (2015). Angiotensin and neurovascular coupling: beyond hypertension. *Microcirculation* 22, 159–167. doi: 10.1111/micc.12193

Cai, Y., Zhang, D., Liang, B., Wang, Z., Li, J., and Gao, M. (2018). Relation of visual creative imagery manipulation to resting-state brain oscillations. *Brain Imaging Behav.* 12, 258–273. doi: 10.1007/s11682-017-9689-8

Caruso, P., Signori, R., and Moretti, R. (2019). Small vessel disease to subcortical dementia: a dynamic model, which interfaces aging, cholinergic dysregulation and the neurovascular unit. *Vasc. Health Risk Manag.* 15, 259–281. doi: 10.2147/VHRM.S190470

Chao-Gan, Y., and Yu-Feng, Z. (2010). Dparsf: a matlab toolbox for "pipeline" data analysis of resting-state fmri. *Front. Syst. Neurosci.* 4:13. doi: 10.3389/fnsys.2010.00013

Claassen, J. A., Thijssen, D. H., Panerai, R. B., and Faraci, F. M. (2021). Regulation of cerebral blood flow in humans: physiology and clinical implications of autoregulation. *Physiol. Rev.* 101, 1487–1559.

Diciotti, S., Orsolini, S., Salvadori, E., Giorgio, A., Toschi, N., and Ciulli, S. (2017). Resting state fmri regional homogeneity correlates with cognition measures in subcortical vascular cognitive impairment. *J. Neurol. Sci.* 373, 1–6. doi: 10.1016/j.jns.2016.12.003

Fama, R., and Sullivan, E. V. (2015). Thalamic structures and associated cognitive functions: relations with age and aging. *Neurosci. Biobehav. Rev.* 54, 29–37. doi: 10.1016/j.neubiorev.2015.03.008

Fazekas, F., Chawluk, J. B., Alavi, A., Hurtig, H. I., and Zimmerman, R. A. (1987). Mr signal abnormalities at 1.5 t in alzheimer's dementia and normal aging. *Am. J. Roentgenol.* 149, 351–356. doi: 10.2214/ajr.149.2.351

Gogolla, N. (2017). The insular cortex. *Curr. Biol.* 27, R580–R586. doi: 10.1016/j.cub.2017.05.010

Hu, B., Yu, Y., Dai, Y., Feng, J., Yan, L., and Sun, Q. (2019). Multi-modal mri reveals the neurovascular coupling dysfunction in chronic migraine. *Neuroscience* 419, 72–82. doi: 10.1016/j.neuroscience.2019.09.022

Hu, B., Yu, Y., Wang, W., and Cui, G. B. (2021). Mica: a toolkit for multimodal image coupling analysis. *J. Neurosci. Methods* 347:108962. doi: 10.1016/j.jneumeth.2020.108962

Huang, H., Zhao, K., Zhu, W., Li, H., and Zhu, W. (2021). Abnormal cerebral blood flow and functional connectivity strength in subjects with white matter hyperintensities. *Front. Neurol.* 12:752762. doi: 10.3389/fneur.2021.752762

Iadecola, C. (2013). The pathobiology of vascular dementia. *Neuron* 80, 844–866. doi: 10.1016/j.neuron.2013.10.008

Iadecola, C., Duering, M., Hachinski, V., Joutel, A., Pendlebury, S. T., and Schneider, J. A. (2019). Vascular cognitive impairment and dementia: jacc scientific expert panel. *J. Am. Coll. Cardiol.* 73, 3326–3344. doi: 10.1016/j.jacc.2019.04.034

Jia, X. Z., Wang, J., Sun, H. Y., Zhang, H., Liao, W., and Wang, Z. (2019). Restplus: an improved toolkit for resting-state functional magnetic resonance imaging data processing. *Sci. Bull.* 64, 953–954. doi: 10.1016/j.scib.2019.05.008

Kim, S., Choi, S. H., Lee, Y. M., Kim, M. J., Kim, Y. D., and Kim, J. (2015). Periventricular white matter hyperintensities and the risk of dementia: a credos study. *Int. Psychogeriatr.* 27, 2069–2077. doi: 10.1017/S1041610215001076

Kisler, K., Nelson, A. R., Rege, S. V., Ramanathan, A., Wang, Y., and Ahuja, A. (2017). Pericyte degeneration leads to neurovascular uncoupling and limits oxygen supply to brain. *Nat. Neurosci.* 20, 406–416. doi: 10.1038/nn.4489

Kozberg, M., and Hillman, E. (2016). Neurovascular coupling and energy metabolism in the developing brain. *Prog. Brain Res.* 225, 213–242.

Leeuwis, A. E., Benedictus, M. R., Kuijer, J. P., Binnewijzend, M. A., Hooghiemstra, A. M., and Verfaillie, S. J. (2017). Lower cerebral blood flow is associated with impairment in multiple cognitive domains in alzheimer's disease. *Alzheimer's Dement.* 13, 531–540. doi: 10.1016/j.jalz.2016.08.013

Li, F., Lu, L., Shang, S., Chen, H., and Wang, P. (2020). Cerebral blood flow and its connectivity deficits in mild traumatic brain injury at the acute stage. *Neural Plast.* 2020:2174371. doi: 10.1155/2020/2174371

Li, P., Mu, J., Ma, X., Ding, D., Ma, S., and Zhang, H. (2021). Neurovascular coupling dysfunction in end-stage renal disease patients related to cognitive impairment. *J. Cereb. Blood Flow Metab.* 41, 2593–2606. doi: 10.1177/0271678X211007960

Li, X., Li, D., Li, Q., Li, Y., Li, K., and Li, S. (2016). Hippocampal subfield volumetry in patients with subcortical vascular mild cognitive impairment. *Sci. Rep.* 6:20873. doi: 10.1038/srep20873

Liang, K. J., and Carlson, E. S. (2020). Resistance, vulnerability and resilience: a review of the cognitive cerebellum in aging and neurodegenerative diseases. *Neurobiol. Learn. Mem.* 170:106981. doi: 10.1016/j.nlm.2019.01.004

Liang, X., Zou, Q., He, Y., and Yang, Y. (2013). Coupling of functional connectivity and regional cerebral blood flow reveals a physiological basis for network hubs of the human brain. *Proc. Natl. Acad. Sci. U.S.A.* 110, 1929–1934. doi: 10.1073/pnas.1214900110

Lim, J. S., Kwon, H. M., and Lee, Y. S. (2020). Effect of cholinergic pathway disruption on cortical and subcortical volumes in subcortical vascular cognitive impairment. *Eur. J. Neurol.* 27, 210–212. doi: 10.1111/ene.14073

Liu, X., Cheng, R., Chen, L., Gong, J., Luo, T., and Lv, F. (2021). Altered neurovascular coupling in subcortical ischemic vascular disease. *Front. Aging Neurosci.* 13:598365. doi: 10.3389/fnagi.2021.598365

Lo, J. W., Crawford, J. D., Desmond, D. W., Godefroy, O., Jokinen, H., and Mahinrad, S. (2019). Profile of and risk factors for poststroke cognitive impairment in diverse ethnoregional groups. *Neurology* 93, e2257–e2271. doi: 10.1212/WNL.0000000000008612

Logothetis, N. K., Pauls, J., Augath, M., Trinath, T., and Oeltermann, A. (2001). Neurophysiological investigation of the basis of the fmri signal. *Nature* 412, 150–157. doi: 10.1038/35084005

McAleese, K. E., Miah, M., Graham, S., Hadfield, G. M., Walker, L., and Johnson, M. (2021). Frontal white matter lesions in alzheimer's disease are associated with both small vessel disease and ad-associated cortical pathology. *Acta Neuropathol.* 142, 937–950.

Meyer, S., Kessner, S. S., Cheng, B., Bönstrup, M., Schulz, R., and Hummel, F. (2016). Voxel-based lesion-symptom mapping of stroke lesions underlying somatosensory deficits. *Neuroimage Clin.* 10, 257–266. doi: 10.1016/j.nicl.2015.12.005

Nasios, G., Dardiotis, E., and Messinis, L. (2019). From broca and wernicke to the neuromodulation era: insights of brain language networks for neurorehabilitation. *Behav. Neurol.* 2019:9894571. doi: 10.1155/2019/9894571

Nasreddine, Z. S., Phillips, N. A., Bédirian, V., Charbonneau, S., and Whitehead, V. (2005). The montreal cognitive assessment, moca: a brief screening tool for mild cognitive impairment. *J. Am. Geriatr. Soc.* 53, 695–699. doi: 10.1111/j.1532-5415.2005.53221.x

Nir, Y., Fisch, L., Mukamel, R., Gelbard-Sagiv, H., Arieli, A., and Fried, I. (2007). Coupling between neuronal firing rate, gamma lfp, and bold fmri is related to interneuronal correlations. *Curr. Biol.* 17, 1275–1285. doi: 10.1016/j.cub.2007.06.066

Opitz, B. (2014). Memory function and the hippocampus. *Front. Neurol. Neurosci.* 34:356422. doi: 10.1159/000356422

Park, H. J., and Friston, K. (2013). Structural and functional brain networks: from connections to cognition. *Science* 342:1238411. doi: 10.1126/science.1238411

Phillips, A. A., Chan, F. H., Zheng, M. M., Krassioukov, A. V., and Ainslie, P. N. (2016). Neurovascular coupling in humans: physiology, methodological advances and clinical implications. *J. Cereb. Blood Flow. Metab.* 36, 647–664. doi: 10.1177/0271678X15617954

Raichle, M. E. (2015). The brain's default mode network. *Annu. Rev. Neurosci.* 38, 433–447. doi: 10.1146/annurev-neuro-071013-014030

Ray, R. D., and Zald, D. H. (2012). Anatomical insights into the interaction of emotion and cognition in the prefrontal cortex. *Neurosci. Biobehav. Rev.* 36, 479–501. doi: 10.1016/j.neubiorev.2011.08.005

Richter-Levin, G. (2004). The amygdala, the hippocampus, and emotional modulation of memory. *Neuroscientist* 10, 31–39. doi: 10.1177/1073858403259955

Rolls, E. T., Joliot, M., and Tzourio-Mazoyer, N. (2015). Implementation of a new parcellation of the orbitofrontal cortex in the automated anatomical labeling atlas. *Neuroimage* 122, 1–5. doi: 10.1016/j.neuroimage.2015.07.075

Roquet, D., Sourty, M., Botzung, A., Armspach, J., and Blanc, F. (2016). Brain perfusion in dementia with lewy bodies and alzheimer's disease: an arterial spin labeling mri study on prodromal and mild dementia stages. *Alzheimer's Res. Ther.* 8, 1–13. doi: 10.1186/s13195-016-0196-8

Rousseaux, M., Daveluy, W., and Kozlowski, O. (2010). Communication in conversation in stroke patients. *J. Neurol.* 257, 1099–1107.

Sanford, M., Negri, S., and Tarantini, S. (2022). New developments in understanding brain and cerebromicrovascular aging: toward prevention of vascular cognitive impairment and Alzheimer's disease. *Front. Aging Neurosci.* 14:1020271. doi: 10.3389/fnagi.2022.1020271

Sarbu, N., Shih, R. Y., Jones, R. V., Horkayne-Szakaly, I., Oleaga, L., and Smirniotopoulos, S. (2016). White matter diseases with radiologic-pathologic correlation. *Radiographics* 36, 1426–1447. doi: 10.1148/rg.2016160031

Shabir, O., Berwick, J., and Francis, S. E. (2018). Neurovascular dysfunction in vascular dementia, alzheimer's and atherosclerosis. *BMC Neurosci.* 19:62. doi: 10.1186/s12868-018-0465-5

Sheng, J., Shen, Y., Qin, Y., Zhang, L., Jiang, B., and Li, J. (2018). Spatiotemporal, metabolic, and therapeutic characterization of altered functional connectivity in major depressive disorder. *Hum. Brain Mapp.* 39, 1957–1971. doi: 10.1002/hbm.23976

Shipman, M. L., and Green, J. T. (2019). Cerebellum and cognition: does the rodent cerebellum participate in cognitive functions? *Neurobiol. Learn. Mem.* 13:106996. doi: 10.1016/j.nlm.2019.02.006

Skrobot, O. A., Black, S. E., Chen, C., DeCarli, C., Erkinjuntti, T., and Ford, G. (2018). Progress toward standardized diagnosis of vascular cognitive impairment: guidelines from the vascular impairment of cognition classification consensus study. *Alzheimers Dement.* 14, 280–292. doi: 10.1016/j.jalz.2017.09.007

Sorond, F. A., Hurwitz, S., Salat, D. H., Greve, D. N., and Fisher, N. D. (2013). Neurovascular coupling, cerebral white matter integrity, and response to cocoa in older people. *Neurology* 81, 904–909. doi: 10.1212/WNL.0b013e3182a351aa

Sun, Y., Cao, W., Ding, W., Wang, Y., Han, X., and Zhou, X. (2016). Cerebral blood flow alterations as assessed by 3d asl in cognitive impairment in patients with subcortical vascular cognitive impairment: a marker for disease severity. *Front. Aging Neurosci.* 8:211. doi: 10.3389/fnagi.2016.00211

Tarantini, S., Fulop, G. A., Kiss, T., Farkas, E., Zölei-Szénási, D., and Galvan, V. (2017). Demonstration of impaired neurovascular coupling responses in tg2576 mouse model of Alzheimer's disease using functional laser speckle contrast imaging. *Geroscience* 39, 465–473. doi: 10.1007/s11357-017-9980-z

Tarantini, S., Yabluchanskiy, A., Csipo, T., Fulop, G., Kiss, T., and Balasubramanian, P. (2019). Treatment with the poly (adp-ribose) polymerase inhibitor pj-34 improves cerebromicrovascular endothelial function, neurovascular coupling responses and cognitive performance in aged mice, supporting the nad+ depletion hypothesis of neurovascular aging. *Geroscience* 41, 533–542. doi: 10.1007/s11357-019-00101-2

Toledo, J. B., Arnold, S. E., Raible, K., Brettschneider, J., Xie, S. X., and Grossman, X. (2013). Contribution of cerebrovascular disease in autopsy confirmed neurodegenerative disease cases in the national alzheimer's coordinating centre. *Brain* 136, 2697–2706. doi: 10.1093/brain/awt188

Tombaugh, T. N., and McIntyre, N. J. (1992). The mini-mental state examination: a comprehensive review. *J. Am. Geriatr. Soc.* 40, 922–935. doi: 10.1111/j.1532-5415.1992.tb01992.x

Toth, P., Tarantini, S., Csiszar, A., and Ungvari, Z. (2017). Functional vascular contributions to cognitive impairment and dementia: mechanisms and consequences of cerebral autoregulatory dysfunction, endothelial impairment, and neurovascular uncoupling in aging. *Am. J. Physiol. Heart Circ. Physiol.* 312, H1–H20. doi: 10.1152/ajpheart.00581.2016

Toth, P., Tarantini, S., Tucsek, Z., Ashpole, N. M., Sosnowska, D., and Gautam, T. (2014). Resveratrol treatment rescues neurovascular coupling in aged mice: role of improved cerebromicrovascular endothelial function and downregulation of nadph oxidase. *Am. J. Physio. Heart Circ. Physiol.* 306, H299–H308. doi: 10.1152/ajpheart.00744.2013

Tucsek, Z., Toth, P., Tarantini, S., Sosnowska, D., Gautam, T., and Warrington, J. (2014). Aging exacerbates obesity-induced cerebromicrovascular rarefaction, neurovascular uncoupling, and cognitive decline in mice. *J. Gerontol.* 69, 1339–1352. doi: 10.1093/gerona/glu080

van der Flier, W. M., Skoog, I., Schneider, J. A., Pantoni, L., Mok, V., and Chen, C. (2018). Vascular cognitive impairment. *Nat. Rev. Dis. Primers* 4, 573–591. doi: 10.1038/nrdp.2018.3

Veselý, B., and Rektor, I. (2016). The contribution of white matter lesions (wml) to parkinson's disease cognitive impairment symptoms: a critical review of the literature. *Parkinsonism Relat. Dis.* 22, S166–S170. doi: 10.1016/j.parkreldis.2015.09.019

Vipin, A., Foo, H., Lim, J., Chander, R. J., Yong, T. T., and Ng, A. (2018). Regional white matter hyperintensity influences grey matter atrophy in mild cognitive impairment. *J. Alzheimers Dis.* 66, 533–549. doi: 10.3233/JAD-180280

Wallin, A., Román, G. C., Esiri, M., Kettunen, P., Svensson, J., and Paraskevas, G. (2018). Update on vascular cognitive impairment associated with subcortical small-vessel disease. *J. Alzheimer's Dis.* 62, 1417–1441.

Wang, J., Yang, Y., Fan, L., Xu, J., Li, C., and Fox, P. (2015). Convergent functional architecture of the superior parietal lobule unraveled with multimodal neuroimaging approaches. *Hum. Brain Mapp.* 36, 238–257. doi: 10.1002/hbm.22626

Yabluchanskiy, A., Balasubramanian, P., and Tarantini, S. (2020). *Cerebrovascular rejuvenation: novel strategies for prevention of vascular cognitive impairment*. Larchmont, NY: Mary Ann Liebert, Inc.

Yoon, C. W., Seo, S. W., Park, J. S., Kwak, K. C., Yoon, U., and Suh, M. (2013). Cerebellar atrophy in patients with subcortical-type vascular cognitive impairment. *Cerebellum* 12, 35–42. doi: 10.1007/s12311-012-0388-0

Zang, Y. F., He, Y., Zhu, C. Z., Cao, Q. J., Sui, M. Q., and Liang, M. (2007). Altered baseline brain activity in children with adhd revealed by resting-state functional mri. *Brain Dev.* 29, 83–91. doi: 10.1016/j.braindev.2006.07.002

Zhu, J., Zhuo, C., Xu, L., Liu, F., Qin, W., and Yu, C. (2017). Altered coupling between resting-state cerebral blood flow and functional connectivity in schizophrenia. *Schizophr. Bull.* 43, 1363–1374. doi: 10.1093/schbul/sbx051

Zhuang, L., Ni, H., Wang, J., Liu, X., Lin, Y., and Su, Y. (2020). Aggregation of vascular risk factors modulates the amplitude of low-frequency fluctuation in mild cognitive impairment patients. *Front. Aging Neurosci.* 12:604246. doi: 10.3389/fnagi.2020.604246

frontiers | Frontiers in Neuroscience

TYPE Original Research
PUBLISHED 22 June 2023
DOI 10.3389/fnins.2023.1158928

OPEN ACCESS

EDITED BY
Jennifer L. Robinson,
Auburn University, United States

REVIEWED BY
Ping Liu,
Guangdong Second Provincial General Hospital, China
Xiaofei Hu,
Army Medical University, China

*CORRESPONDENCE
Huihui Wang
✉ wanghh07001@sina.com
Zhenchang Wang
✉ cjr.wzhch@vip.163.com

†These authors have contributed equally to this work and share first authorship

RECEIVED 04 February 2023
ACCEPTED 06 June 2023
PUBLISHED 22 June 2023

CITATION
Wang H, Wen H, Li J, Chen Q, Li S and Wang Z (2023) Disrupted topological organization of white matter structural networks in high myopia patients revealed by diffusion kurtosis imaging and tractography. *Front. Neurosci.* 17:1158928. doi: 10.3389/fnins.2023.1158928

Disrupted topological organization of white matter structural networks in high myopia patients revealed by diffusion kurtosis imaging and tractography

Huihui Wang[1,2*†], Hongwei Wen[3†], Jing Li[2], Qian Chen[2], Shanshan Li[4] and Zhenchang Wang[2*]

[1]Department of Radiology, Beijing Chaoyang Hospital, Capital Medical University, Beijing, China, [2]Department of Radiology, Beijing Friendship Hospital, Capital Medical University, Beijing, China, [3]Key Laboratory of Cognition and Personality (Ministry of Education), Faculty of Psychology, Southwest University, Chongqing, China, [4]Department of Ophthalmology, Beijing Friendship Hospital, Capital Medical University, Beijing, China

Introduction: High myopia (HM) is a public health issue that can lead to severe visual impairment. Previous studies have exhibited widespread white matter (WM) integrity damage in HM patients. However, how these WM damages are topologically related, and the network-level structural disruptions underlying HM has not been fully defined. We aimed to assess the alterations of brain WM structural networks in HM patients using diffusion kurtosis imaging (DKI) and tractography in the present study.

Methods: Individual whole-brain and ROI-level WM networks were constructed using DKI tractography in 30 HM patients and 33 healthy controls. Graph theory analysis was then applied to explore the altered global and regional network topological properties. Pearson correlations between regional properties and disease duration in the HM group were also assessed.

Results: For global topology, although both groups showed a small-world network organization, HM patients exhibited significant decreased local efficiency and clustering coefficient compared with controls. For regional topology, HM patients and controls showed highly similar hub distributions, except for three additional hub regions in HM patients including left insula, anterior cingulate and paracingulate gyri (ACG), and median cingulate and paracingulate gyri (DCG). In addition, HM patients showed significantly altered nodal betweenness centrality (BC) mainly in the bilateral inferior occipital gyrus (IOG), left superior occipital gyrus (SOG), caudate nucleus, rolandic operculum and right putamen, pallidum, and gyrus rectus compared with controls. Intriguingly, the nodal BC of left IOG was negatively correlated with disease duration in HM patients.

Discussion: Our findings suggest that HM exhibited alterations in WM structural networks as indicated by decreased local specialization. This study may advance the current understanding of the pathophysiological mechanisms underlying HM.

KEYWORDS

high myopia, diffusion kurtosis imaging, white matter, structural network, graph theory analysis

Introduction

High myopia (HM) is a serious health issue worldwide, characterized by visual impairment. The prevalence of HM is 2.9% globally, and up to 10–20% among young adults in East and Southeast Asia (Holden et al., 2015; Morgan et al., 2018). It is defined as the ocular refractive diopter lower than-6.00 diopters (D) or the axial length larger than 26 mm. HM is also named "pathological myopia" and "degenerative myopia," reflecting the extensive progressive trend of pathological and degenerative changes of the neurosensory retina and choroid and may extend to the brain structure (Morgan et al., 2012; Hsu et al., 2014). Therefore, exploring the high myopia-related brain structural alterations will enhance our understanding of the pathophysiological mechanisms underlying HM.

Some previous neuroimaging studies have demonstrated changes in brain volume and white matter (WM) in HM (Huang et al., 2018; Wang et al., 2021). Besides, recent studies also demonstrated that high myopia was accompanied by neural activity changes (Ptito and Kupers, 2005) and may trigger neural plasticity (Wang et al., 2020). These studies showed the truth that HM was not merely a disease that involved the fundus structure but also closely related to the structure and function of the brain. These previous studies, however, only put the focus on the individual structural alterations and neural activities of the brain, ignoring the structural and functional communication of separated structures anatomically, which may play a crucial role in information transference and processing of the brain (van den Heuvel and Hulshoff Pol, 2010).

The diffusional kurtosis imaging (DKI) technique is a noninvasive and promising imaging modality for evaluating the microstructural characteristics of WM (Cao et al., 2013). Additionally, DKI tractography reveals the brain's structural connectivity vividly by reconstructing the major WM tracts (Basser et al., 2000). Graph theory analysis regards the brain as a graph, in which brain regions are regarded as nodes and functional or structural connections between nodes are regarded as the edges. Through the graph theoretical analysis of the brain network, we can discover the brain characteristics at both local and global levels (Wang et al., 2016). Graph theory analysis has been increasingly prevalent in the field of neuroimaging in recent years, which provides an advanced tool for investigating the topological organization of brain networks (Wen et al., 2018). Combining the DKI technique and the graph theory analysis method allows the small-world, hub properties, and modularity in the complex brain structural network to be discovered (Fang et al., 2017).

In the present research, we constructed DKI networks to study potential abnormal mechanisms underlying brain dysfunction in HM. Briefly, we first used DKI tractography to construct individual whole-brain WM networks. Three weighted networks featured by kurtosis fractional anisotropy (KFA), fractional anisotropy (FA), and fiber number (FN) were analyzed by the graph theory method to explore the potentially altered regional and global topological properties in HM patients and if these topology alterations would correlate with the disease duration significantly. The results of our research may facilitate further recognition of the underlying neurophysiological mechanisms of HM individuals.

Materials and methods

Subjects

Our prospective study was approved by the medical research ethics committee of Beijing Friendship Hospital, and written informed consent was acquired from all subjects according to the Declaration of Helsinki prior to enrollment. From January 2017 to December 2019, HM patients and normal controls were recruited from outpatient clinics at our institute. Patients with the following diseases or conditions were excluded: (1) other ocular diseases, such as glaucoma, strabismus, and amblyopia; (2) unilateral high myopia; (3) psychiatric or neurological disorders; (4) brain tumor or obvious cerebral infarction; (5) any systemic diseases that may affect the brain structure, such as hypertension and diabetes; (6) MRI contraindications; (7) MR images with visible artifacts. According to the exclusion criteria, five HM patients and two NCs were excluded. A total of 30 HM patients and 33 age-and gender-matched normal controls (NCs) were enrolled in the study eventually; the uncorrected visual acuity (VA) of NCs was larger than 1.0.

Image acquisition

MR imaging was acquired using a 3.0 T GE Discovery MR750 scanner (GE Healthcare Systems, Milwaukee, WI, United States) equipped with an eight-channel, phased-array head coil. Images are acquired using slice-interleaved encoding. DKI images were obtained using a single-shot, echo planar imaging sequence, with an encoding scheme of two b-values (b = 1,000 and 2000 s/mm^2) along 25 diffusion-encoding directions, respectively, and b value of 0 s/mm^2 along five non-diffusion-weighted images. The sequence parameters of DKI images were as follows: TR/TE = 9000/96 ms; voxel size = 1 mm × 1 mm; matrix = 256 × 256; slice thickness/spacing = 3.0/0 mm; flip angle = 90; field of view = 256 × 256 mm; frequency/phase resolution = 128 × 128; 44 axial slices. For anatomical reference and image segmentation, T1-weighted fast-spin-echo images were obtained with the following parameters: TR/TE = 8.2/3.2 ms; voxel size = 0.46875 mm × 0.46875 mm; matrix = 512 × 512; slice thickness = 1.0 mm; flip angle = 12; FOV = 240 mm × 240 mm; frequency/phase resolution = 256 × 256; 200 axial slices. Regular T2-weighted fast-spin-echo images were obtained before acquiring diffusion kurtosis images. Images with visible artifacts, obvious WM hyperintensities, cerebral infarction lesions, and brain tumors were excluded from our study.

DKI data processing

First, we created brain masks from the b0 image to delete nonbrain tissues using the Brain Extraction Tool (BET) in FSL (v5.0, http://www.fmrib.ox.ac.uk/fsl). Second, using the eddy tool in FSL, we corrected motion artifacts and eddy current distortions of DKI images by applying an affine alignment of each diffusion-weighted image to the b0 image. Then, the Diffusional Kurtosis Estimator toolbox (v2.6, http://www.nitrc.org/projects/dke) was applied to calculate the diffusion tensor (DT) and kurtosis tensor (KT) parameters using the constrained linear least squares-quadratic

programming (CLLS-QP) algorithm (Tabesh et al., 2011). The DKI model was parameterized by the DT and KT from which several rotationally invariant scalar measures were extracted. We mainly calculated the DT-derived measure including FA and the KT-derived measure including KFA.

Network construction

We defined the network nodes (details shown in Supplementary Table S1) as our previous study (Wen et al., 2017). Each individual high-resolution structural image (T1WI image) was first coregistered to the b_0 image in the diffusion space using a linear transformation. Then, the transformed T1 images were nonlinearly transformed to the ICBM152 T1 template in the MNI space. The resulting inverse transformations were used to warp the automated anatomical labeling (AAL) atlas (Tzourio-Mazoyer et al., 2002) from the MNI space to the individual native space, and the nearest-neighbor interpolation method was used to preserve discrete labeling values. We manually checked the quality of all registered images to remove subjects with poor registration results, and all images passed the quality check and were retained. Using this procedure, we segmented the entire cerebrum into 90 cortical and subcortical regions (45 for each hemisphere), each representing a network node.

To define the network connections, we performed diffusion tractography using a fiber tracking (FT) module embedded in DKE. The FT module uses the diffusion and kurtosis tensors from DKE for the DKI approximation of the diffusion orientation distribution function (dODF), and this module uses the closed-form solution of the kurtosis dODF derived in Jensen et al., 2014 along with the image processing algorithms developed in Glenn et al. (2015). We set the ODF optimization and tractography parameters (details shown in Supplementary materials) to perform FT using the scripts provided by the FT Module, utilizing the Euler method. Each network connection represents the connecting fiber that links two brain nodes. The weight of network connection is defined as three types: FN, FA, and KFA. Thus, for each subject, three 90×90 symmetric weighted networks were constructed. To remove spurious connections, each network was thresholded over a wide range of sparsity (6 to 20%, interval of 1%). The flowchart of DKI preprocessing and network construction is shown in Supplementary Figure S1.

Network topological analysis

Graph theoretical quantitative parameters were assessed at each sparsity threshold to characterize the WM structural network topology, using a graph theoretical network analysis toolbox (*GRETNA v2.0*, http://www.nitrc.org/projects/gretna/; Wang et al., 2015). As in our previous studies (Wen et al., 2017, 2018), seven global topological measures were calculated (general descriptions for the network properties are shown in Table 1): shortest path length (L_p), global efficiency (E_{glob}), local efficiency (E_{loc}), clustering coefficient (C_p), normalized L_p (λ), normalized C_p (γ), and small-worldness (σ). For nodal measures, we considered the nodal betweenness centrality (BC) that plays a vital role in identifying hub nodes of structural networks, defined as follows:

TABLE 1 Global and local topological properties used in the study.

	General descriptions
Global properties	
Shortest path length L_p	L_p is defined as the average length of the shortest path between every two nodes in network G that quantifies the ability for information to be propagated in parallel, which is computed as follows: $Lp(G)=\frac{1}{N(N-1)}\sum_{i\neq j\in G} L_{ij}$
Global Efficiency E_{glob}	E_{glob} is defined as the mean value of all regions' global efficiency, which is computed as follows: $E_{glob}(G)=\frac{1}{N(N-1)}\sum_{i\neq j\in G}\frac{1}{L_{ij}}$
Local Efficiency E_{loc}	E_{loc} is defined as the mean value of all regions' local efficiency, which is computed as follows: $E_{loc}(G)=\frac{1}{N}\sum_{i\in G} E_{glob}(G_i)$ where G_i denotes the subgraph composed of the nearest neighbors of node i.
Clustering coefficient C_p	C_p is the average clustering coefficient over all nodes that indicates the extent of local interconnectivity or cliquishness in a network, which is computed as follows: $C_i \frac{2}{k_i(k_i-1)}\sum_{j,k}(\bar{w}_{ij}\bar{w}_{jk}\bar{w}_{ki})^{1/3}$ where k_i is the degree of node i, and $\bar{w}$ is the weight, which is scaled by the mean of all weights to control each subject's cost at the same level.
Normalized L_p (λ)	$\lambda = L_p^{real}/L_p^{rand}$ and L_p^{rand} are the mean shortest path lengths of 100 matched random networks.
Normalized C_p (γ)	$\gamma = C_p^{real}/C_p^{rand}$ and C_p^{rand} are the mean clustering coefficients of 100 matched random networks.
Small-worldness σ	$\sigma = \lambda/\gamma$, A real network would be considered a small world if $\gamma > 1$ and $\lambda \approx 1$.
Nodal properties	
Nodal Betweenness Centrality $B_{nodal}(i)$	$B_{nodal}(i)$ is defined as the fraction of all shortest paths in the network G that pass through a given node i.

$$B_{nodal}(i) = \sum_{s\neq i\neq t\in G}\frac{e_{st}(i)}{e_{st}} \quad (1)$$

where $e_{st}(i)$ denotes the number of shortest paths in the network G between node s and node t, which pass through node i, while e_{st} denotes the total number of shortest paths in the network G between node s and node t. Node *i* was considered a brain hub if $B_{nodal}(i)$ was at least one standard deviation (SD) greater than the average nodal BC of the network (i.e., $B_{nodal}(i) > \text{mean} + \text{SD}$). Notably, we calculated the average value of each topological metric under all sparsity thresholds to provide a summarized scalar independent of single threshold selection (Zhang et al., 2015). The computer specifications and Operating System for performing image processing and analysis were a CentOS 7.1 Linux system on a Huawei high-performance cluster computing platform with 12 computing nodes, 240 processor cores, and 250-TB storage capacity.

Between-group statistical comparison and correlation analysis

A two-sample *t*-test was used to analyze the differences in the network measurements (global and nodal properties) between the two groups. Of note, the average values of nodal BC across thresholds were used to investigate brain hubs and significantly altered nodes. We also calculated the Pearson correlation between significantly altered nodal BC and disease duration in patient groups using SPSS v21.0.

Results

Clinical characteristics and demographic of the subjects

Thirty HM patients (age: 35.13 ± 13.73 years, range: 22–65, 19 women/11 men) and thirty-three NCs (age: 38.55 ± 18.00 years, range: 24–65 years, 19 women/14 men) were recruited in our study eventually. The baseline data of recruited subjects were well-balanced between the two groups (Table 2). No significant differences in age ($p = 0.315$, two-sample *t*-test) and gender ($p = 0.641$, chi-square test) were found between the HM and NCs.

Alterations in the global properties of WM networks in HM

For KFA-weighted networks, both HM patients and NCs presented with a small-world property of WM networks characterized by $\gamma > 1, \lambda \approx 1$ and $\sigma = \gamma/\lambda > 1$ (Cao et al., 2013; Wen et al., 2018; Figure 1). Besides, patients with HM showed significantly ($p < 0.05$) decreased C_p, λ, γ, E_{loc}, and σ over a wide range of thresholds compared with NCs. Moreover, HM subjects showed significantly decreased average values of C_p, λ, and E_{loc} across thresholds (Table 3). Significant *p*-values were obtained after false discovery rate (FDR) correction (Benjamini and Hochberg, 1995). Nevertheless, no significant difference was found between groups in all global properties in the FA-weighted and FN-weighted networks though both groups also showed a small-world organization at each sparsity threshold (details shown in Supplementary Table S2).

TABLE 2 Demographic and clinical characteristics of high myopia patients and healthy controls.

Characteristic	High myopia patients	Normal controls	*p*-value
Number of subjects	30	33	
Age (years)	35.13 ± 13.73	38.55 ± 18.00	0.315[t]
Gender (female/male)	19/11	19/14	0.641[c]
Duration of illness (years)	23.8 ± 11.8	NA	
Refractive diopter_R (D)	−8.4 ± 4	NA	
Refractive diopter_L (D)	−8.5 ± 4	NA	
Axial length_R	28.0 ± 1.7	NA	
Axial length_L	27.9 ± 2.2	NA	

NA, not applicable; D, diopter; *t*, two-sample *t*-test; c, chi-square test.

Alterations in the regional properties of WM networks in HM

Since significant differences between HM and NCs were only found in KFA-weighted networks, we focused on the KFA-weighted network and identified the brain structural hubs of each group based on it. A node is considered the hub region if its nodal BC is at least one SD larger than the average BC of the network (Wen et al., 2018).

Patients with HM and NCs showed highly similar hub distributions, with core regions mainly in the bilateral caudate nucleus, putamen, insula, median cingulate and paracingulate gyri (DCG), left anterior cingulate and paracingulate gyri (ACG), right precuneus, thalamus, and hippocampus. Only three additional hub regions in the HM group were identified, including the left insula, ACG, and DCG (Table 4; Figures 2A,B).

We also assessed the nodal betweenness centrality (average value across thresholds) in the two groups. Compared with NCs, patients with HM showed significantly altered nodal betweenness centrality mainly in the bilateral inferior occipital gyrus (IOG), left superior occipital gyrus (SOG), caudate nucleus, rolandic operculum and right putamen, pallidum, and gyrus rectus (Table 5; Figure 2C), involving vision, default-mode network (DMN), sensorimotor, and subcortical functional modules (Yong et al., 2009). Noteworthy, among these above-altered regions, the left caudate nucleus and the right putamen were hub regions for both groups. Pearson correlation analysis revealed a negative correlation between nodal betweenness centrality of the left inferior occipital gyrus and disease duration ($r = -0.541$, $p = 0.002$, FDR corrected for multiple comparisons; Figure 3).

Discussion

In this study, we reconstructed the individual whole-brain, ROI-level WM networks and then performed graph theory analysis to explore the regional and global network topological properties in HM subjects and normal controls. The major findings of our study were as follows: (1) Both HM and NCs presented with an efficient small-world organization in all types of weight networks, (2) Characterized by KFA-weighted networks, HM patients showed significantly decreased Eloc and C_p in comparison to NCs, (3) Despite nine common hub distributions in both groups, three more hubs (left insula, ACG, and DCG) appeared in the HM patients compared with NCs, (4) HM patients showed widespread regional topological changes characterized by nodal BC, mainly involving brain regions within vision, DMN, sensorimotor, and subcortical functional modules, and (5) Significantly negative correlations between the BC values of the left inferior occipital gyrus with disease duration in HM were found.

Topological property comparison in different networks

In this study, three types of networks (FN, FA, and KFA-weighted network) were constructed. However, topological attribute alterations between the patients with HM and NCs were only found in KFA-weighted networks rather than FN or FA-weighted network. It was suggested that the KFA-weighted network dried from the DKI model was more sensitive in reflecting the topological attributes in WM structural network than the

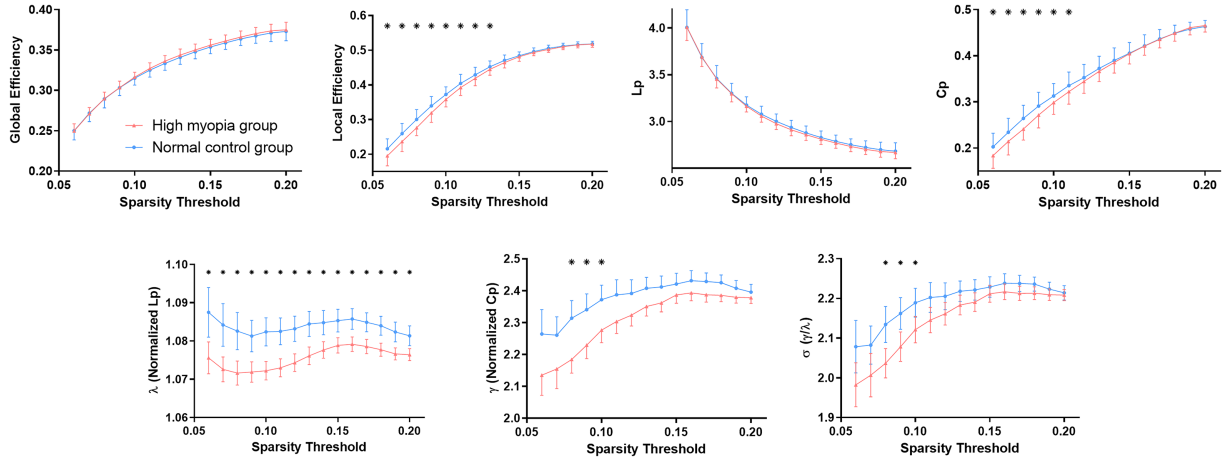

FIGURE 1
Differences in global topological properties of KFA-weighted networks between high myopia patients and controls. Data points marked with a star indicate a significant (p<0.05, FDR corrected for multiple comparisons) difference between groups in the global network metric under a corresponding threshold. FDR, False discovery rate; KFA, kurtosis fractional anisotropy.

TABLE 3 Group comparisons of average values of global topological metrics under all thresholds.

KFA-weighted Network	E_{glob}	E_{loc}	L_p	C_p	λ	γ	σ
NC	0.331 ± 0.009	**0.419 ± 0.013**	3.066 ± 0.087	**0.361 ± 0.018**	**1.084 ± 0.019**	2.377 ± 0.202	2.192 ± 0.156
HM	0.333 ± 0.007	**0.408 ± 0.014**	3.052 ± 0.064	**0.351 ± 0.018**	**1.075 ± 0.012**	2.308 ± 0.162	2.145 ± 0.133
p value	0.372	**0.005***	0.469	**0.039***	**0.046***	0.152	0.222

HM: high myopia; NC: normal control.
The symbol "*" represents there have statistical differences between the two groups and the value of p smaller than 0.05. The bold values represent the ranges of the corresponding values.

FA network dried from the DTI model. The DTI model is based on the hypothesis that water molecules were in Gaussian distribution in the biological tissue (Veraart et al., 2011). However, the displacement distribution of water molecules often manifests as non-Gaussian distribution. As the extension of the DTI, DKI well reflected the non-Gaussian diffusion pattern of water molecules in the tissue by evaluating the excess kurtosis of the displacement distribution (Veraart et al., 2011; Zhu et al., 2015). Conclusively, as verified in our study, DKI had a better sensitivity and practicality in identifying the pathological and developmental changes in the brain as compared to DTI.

Small-world topology of the WM networks alterations in HM

Brain networks with small-worldness properties were found in both HM and NCs. Small-worldness network has efficient information transmission and processing capabilities (Wang et al., 2016), which has been proven by various modal images, such as MRI, magnetoencephalography, and electroencephalography (Stam, 2004; Zhu et al., 2017; Yang et al., 2019). Small-world property enables the brain network's shortest path lengths and high clustering coefficients and thus achieves the best balance between global integration and local specialization (Shu et al., 2009). Our results agreed with previous research and support the view that a small-worldness network can accommodate developmental alteration and disease conditions (Cao et al., 2013).

Despite the common small-world topological properties, HM subjects showed decreased E_{loc} and C_p. However, it should be noted that no significant difference in the glob efficiency and shortest path was identified between the two groups. The E_{loc} and E_{glob} represent the information transmission efficiency of the local and glob brain network, respectively. The C_p reflects the degree of clustering between nodes and the modularity of the network. The shortest path was the most efficient path for the information transmission between nodes in the network, with maximum efficiency and the least energy consumption (Jiang et al., 2021). These results in our present study showed that the destruction of the brain network in HM mainly involved the efficiency of local information transmission. The overall information transmission efficiency of the brain and the shortest path for information transmission were not affected. In the previous study on DKI, the tract-based spatial statistics method was used to analyze brain microstructural abnormalities in HM (Wang et al., 2021), and it was found that HM subjects presented microstructural damage in motor conduction and vision-related brain regions. We assumed that the reduction of the ability to handle local information in HM may be attributable to the microstructural damage in WM.

One diffusion tensor tractography study analyzed the global topological properties in blind people and reported that the adolescent-blind and late-blind had significantly reduced C_p and E_{loc}, but comparable E_{glob} and L_p to that of the sighted controls (Li et al., 2013). Besides, decreased E_{glob} was observed in the congenitally blind and early blind compared with the sighted controls (Li et al., 2013). It suggested that late

TABLE 4 Hub regions of KFA-weighted networks in control and HM groups.

NC			HM		
Hub regions	Module	mean B_{nodal}	Hub regions	Module	mean B_{nodal}
INS.R	sensory/motor	23.07	INS.R	sensory/motor	21.68
DCG.R	Subcortical	21.29	DCG.R	Subcortical	25.65
HIP.R	Subcortical	21.93	HIP.R	Subcortical	28.31
PCUN.R	DMN	20.03	PCUN.R	DMN	22.68
CAU.L	Subcortical	31.21	CAU.L	Subcortical	23.19
CAU.R	Subcortical	39.80	CAU.R	Subcortical	34.66
PUT.L	Subcortical	55.30	PUT.L	Subcortical	54.93
PUT.R	Subcortical	58.06	PUT.R	Subcortical	40.59
THA.R	Subcortical	29.72	THA.R	Subcortical	33.22
			INS.L	sensory/motor	20.08
			ACG.L	DMN	18.58
			DCG.L	Subcortical	18.30

Bnodal represents the average value of the nodal betweenness centrality across thresholds.

visual defects after the completion of neurodevelopment may only result in a reduction in local efficiency but cannot affect global efficiency. For the onset ages of HM patients in our study, after establishing an intact and efficient anatomical network in the human brain, our results were consistent with this previous study. Given the fact that the small-worldness property represents the best balance between local specialization and global integration (Cao et al., 2013), our findings may be a reminder that the brain always keeps in a dynamic process of development, plasticity, and disuse to reach an optimal balance in a certain period.

Hub-distributing reorganization and regional topology changes in HM

Hub regions of the WM networks for each group based on KFA-weighted networks were identified. We found the hub distributions in both groups showed high similarity. The common core regions were mainly in the bilateral caudate nucleus, putamen, insula, median cingulate and DCG, left ACG, right precuneus, thalamus, and hippocampus. However, there were three additional hub regions including the left insula, ACG, and DCG in HM. Insula is a part of the multisensory integration center for spatial orientation and eye movement (Yin et al., 2021). The cingulate gyrus belongs to the limbic system and is involved in multiple functions, such as memory, attention, and cognitive function. Additionally, ACG has been shown to be associated with cognitive-related visual functions, participating in the recognition and classification of visual objects (Zhang et al., 2021). The neural activity alterations of the insula (Chen et al., 2019) and cingulate gyrus (Samanchi et al., 2021) have been reported in other visual-related diseases. The three more hubs in HM subjects suggested that long-term myopia is accompanied by hub-distributing reorganization, with the function of information transference and processing of the vision, memory, and cognitive and attention enhancement. The three core nodes were all located on the left side, and we speculated that it may be related to the dominant hemisphere.

The regional topology alterations between the two groups were also analyzed, and we observed that the HM group had widespread altered nodal BC, involving areas within vision-related (left SOG and bilateral IOG), subcortical (left caudate nucleus, right putamen, and right pallidus), sensorimotor (left rolandic operculum), and default mode network (right gyrus rectus) functional modules. It should be noted that the caudate and putamen were core nodes, which manifested BC value decreased in HM compared to NCs. The Caudate and putamen are parts of the dorsal striatum and are vital to eye movement (Yin et al., 2021) and visually-guided decision-making (Moss et al., 2021). Structural alterations in the caudate and putamen were reported in other ophthalmic diseases (Shu et al., 2009; Zikou et al., 2012). Although no study has demonstrated structural changes in the dorsal striatum in myopia subjects, we speculated patients with HM might have functional weakness of the eye movement combined with impaired visually guided decision-making based on our results, and long-term visual deficit may incorporate structural plasticity and hub distributing reorganization of the brain in HM.

Correlations between nodal betweenness centrality and disease duration

The relationships between the nodal BC values and the disease duration in HM were analyzed. It was demonstrated that the BC value of left IOG negatively correlated with disease durations. The occipital lobe is mainly responsible for visual information processing, and the IOG plays a crucial role in face processing (Sato et al., 2017). The hypofunction of the left IOG and its negative correlation with disease duration reflected the visual function gradually damaging and weakening in our study. Consistently, Li et al. (2013) found a significant correlation between the ages of blindness onset and the topological properties of anatomical networks in blind individuals. These findings suggested that abnormal visual information input can cause abnormality in the brain structure and induce neural reorganization in the brain.

Conclusion

In summary, our preliminary results demonstrated that HM incorporates structural plasticity and reorganization of the brain,

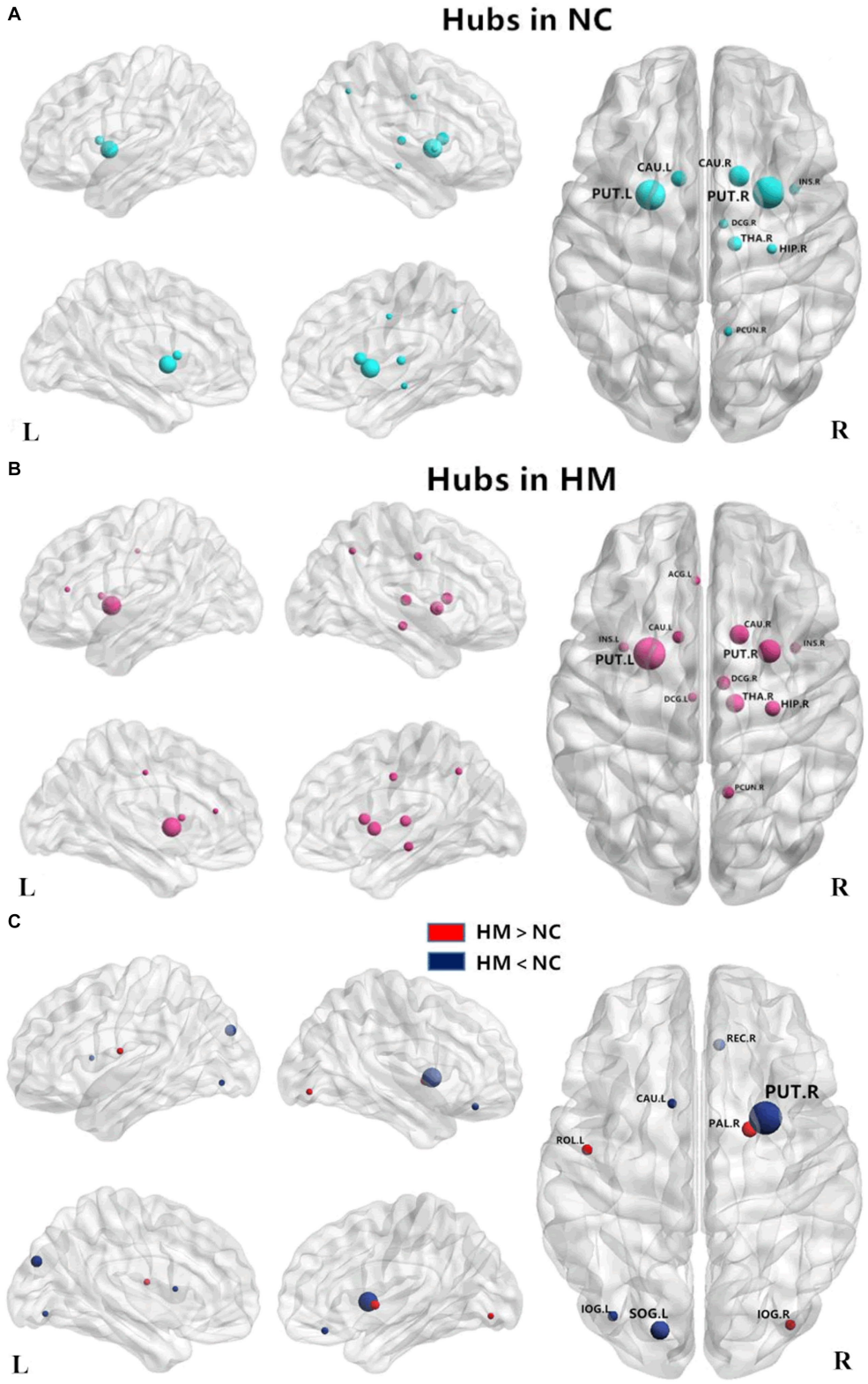

FIGURE 2
Distribution of hub regions in the WM structural networks of both groups and altered nodes in HM patients. **(A,B)** Three-dimensional representations of the hub distributions in the NC and HM groups, respectively. The hub nodes are shown in blue and red with node sizes indicating their nodal betweenness centrality values. **(C)** The disrupted nodes with significantly decreased or increased nodal betweenness centrality in the HM group are shown in blue or red, and the node sizes indicate the t values in the t-test. The brain graphs were visualized by using BrainNet Viewer software (http://www.nitrc.org/projects/bnv/). For the abbreviations of nodes, see Table 1. WM, white matter; HM, high myopia; NC, normal controls.

TABLE 5 Brain regions showing significantly altered nodal betweenness centrality in the high myopia group for KFA-weighted networks.

		B_{nodal}			
Module	Region	NC	HM	*t* value	*p* value
sensory/ motor	ROL.L	2.74 ± 2.92	5.17 ± 4.70	−2.094	0.042
DMN	REC.R	5.40 ± 4.93	2.91 ± 4.00	2.182	0.031
vision	SOG.L	13.13 ± 12.31	5.97 ± 6.83	2.570	0.031
vision	IOG.L	3.67 ± 4.19	1.83 ± 2.59	2.064	0.043
vision	IOG.R	0.82 ± 1.14	1.94 ± 2.72	−2.085	0.044
Subcortical	CAU.L	31.36 ± 17.92	23.19 ± 13.66	2.017	0.048
Subcortical	PUT.R	58.06 ± 25.56	40.59 ± 13.84	3.413	0.001
Subcortical	PAL.R	5.43 ± 4.54	9.06 ± 7.26	−2.395	0.020

Bnodal represents the average values (mean ± SD) of the nodal betweenness centrality of each group.

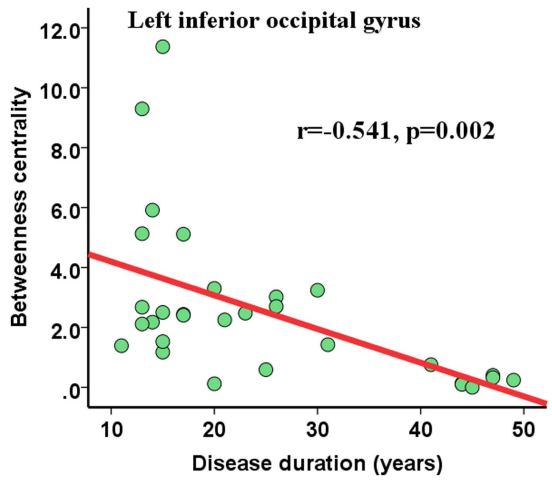

FIGURE 3
Pearson correlations between nodal topological properties and disease duration. The nodal betweenness centrality of the left inferior occipital gyrus showed significant (FDR-corrected) negative correlations with disease duration. Abbreviations: FDR, False discovery rate.

mainly manifesting as local specialization decrease in WM structural networks. DKI based on the graph theoretical analysis is a promising and novel approach for detecting topological properties of brain networks in HM, which provides new perspectives on the understanding of the brain's re-organization and pathophysiological mechanisms in the specific population with high myopia.

Data availability statement

The data analyzed in this study is subject to the following licenses/ restrictions: The datasets generated for this study are available on request to the corresponding author. Requests to access these datasets should be directed to cjr.wzhch@vip.163.com.

Ethics statement

The studies involving human participants were reviewed and approved by The medical research ethics committee of Beijing Friendship hospital. The patients/participants provided their written informed consent to participate in this study.

Author contributions

HHW: conceptualization, data curation, investigation, methodology, formal analysis, resources, and writing - original draft. HWW: data curation, investigation, methodology, formal analysis, and software. JL: conceptualization and data curation. QC: formal analysis and software. SSL: data curation and supervision. ZCW: writing - review and editing, supervision, validation, project administration, and funding acquisition. All authors contributed to the article and approved the submitted version.

Funding

This work was supported by the National Natural Science Foundation of China (grant numbers: 61527807, 32100902, 81800840, 62171297, 81701644, and 61801311), the Beijing Scholars Program [grant number: (2015) 160], the Beijing Municipal Administration of Hospitals (grant numbers: SML20150101, PX2018001, YYZZ2017A14, and YYZZ2017B01), the Beijing Chao-Yang Hospital Golden Seeds Foundation (CYJZ202156), and the Fundamental Research Funds for the Central Universities (SWU118065).

Acknowledgments

The authors thank the patients and volunteers for participating in this study.

Conflict of interest

The authors declare that the research was conducted in the absence of any commercial or financial relationships that could be construed as a potential conflict of interest.

Publisher's note

Supplementary material

The Supplementary material for this article can be found online at: https://www.frontiersin.org/articles/10.3389/fnins.2023.1158928/full#supplementary-material

References

Basser, P. J., Pajevic, S., Pierpaoli, C., Duda, J., and Aldroubi, A. (2000). In vivo fiber tractography using DT-MRI data. *Magn. Reson. Med.* 44, 625–632. doi: 10.1002/1522-2594(200010)44:4<625::Aid-Mrm17>3.0.Co;2-O

Benjamini, Y., and Hochberg, Y. (1995). Controlling the false discovery rate - a practical and powerful approach to multiple testing. *J. R. Stat. Soc.* 57, 289–300. doi: 10.1111/j.2517-6161.1995.tb02031.x

Cao, Q., Shu, N., An, L., Wang, P., Sun, L., Xia, M. R., et al. (2013). Probabilistic diffusion tractography and graph theory analysis reveal abnormal white matter structural connectivity networks in drug-naive boys with attention deficit/hyperactivity disorder. *J. Neurosci.* 33, 10676–10687. doi: 10.1523/JNEUROSCI.4793-12.2013

Chen, L. L., Li, S. H., Cai, F. Q., Wu, L., Gong, H. H., Pei, C. G., et al. (2019). Altered functional connectivity density in primary angle-closure glaucoma patients at resting-state. *Quant. Imaging Med. Surg.* 9, 603–614. doi: 10.21037/qims.2019.04.13

Fang, J. P., Chen, H. M., Cao, Z. T., Jiang, Y., Ma, L. Y., Ma, H. Z., et al. (2017). Impaired brain network architecture in newly diagnosed Parkinson's disease based on graph theoretical analysis. *Neurosci. Lett.* 657, 151–158. doi: 10.1016/j.neulet.2017.08.002

Glenn, G. R., Helpern, J. A., Tabesh, A., and Jensen, J. H. (2015). Optimization of white matter fiber tractography with diffusional kurtosis imaging. *NMR Biomed.* 28, 1245–1256. doi: 10.1002/nbm.3374

Holden, B. A., Wilson, D. A., Jong, M., Sankaridurg, P., Fricke, T. R., Smith, E. L. III, et al. (2015). Myopia: a growing global problem with sight-threatening complications. *Community Eye Health* 28:35.

Hsu, C. C., Chen, S. J., Li, A. F., and Lee, F. L. (2014). Systolic blood pressure, choroidal thickness, and axial length in patients with myopic maculopathy. *J. Chin. Med. Assoc.* 77, 487–491. doi: 10.1016/j.jcma.2014.06.009

Huang, X., Hu, Y., Zhou, F., Xu, X., Wu, Y., Jay, R., et al. (2018). Altered whole-brain gray matter volume in high myopia patients: a voxel-based morphometry study. *Neuroreport* 29, 760–767. doi: 10.1097/WNR.0000000000001028

Jensen, J. H., Helpern, J. A., and Tabesh, A. (2014). Leading non-Gaussian corrections for diffusion orientation distribution function. *NMR Biomed.* 27, 202–211. doi: 10.1002/nbm.3053

Jiang, W., Zhao, Z., Wu, Q., Wang, L., Zhou, L., Li, D., et al. (2021). Study on brain structure network of patients with delayed encephalopathy after carbon monoxide poisoning: based on diffusion tensor imaging. *Radiol. Med.* 126, 133–141. doi: 10.1007/s11547-020-01222-x

Li, J. J., Liu, Y., Qin, W., Jiang, J. F., Qiu, Z. X., Xu, J. C., et al. (2013). Age of onset of blindness affects brain anatomical networks constructed using diffusion tensor Tractography. *Cereb. Cortex* 23, 542–551. doi: 10.1093/cercor/bhs034

Morgan, I. G., French, A. N., Ashby, R. S., Guo, X. X., Ding, X. H., He, M. G., et al. (2018). The epidemics of myopia: Aetiology and prevention. *Prog. Retin. Eye Res.* 62, 134–149. doi: 10.1016/j.preteyeres.2017.09.004

Morgan, I. G., Ohno-Matsui, K., and Saw, S. M. (2012). Myopia. *Lancet* 379, 1739–1748. doi: 10.1016/S0140-6736(12)60272-4

Moss, M. M., Zatka-Haas, P., Harris, K. D., Carandini, M., and Lak, A. (2021). Dopamine axons in dorsal striatum encode contralateral visual stimuli and choices. *J. Neurosci.* 41, 7197–7205. doi: 10.1523/JNEUROSCI.0490-21.2021

Ptito, M., and Kupers, R. (2005). Cross-modal plasticity in early blindness. *J. Integr. Neurosci.* 4, 479–488. doi: 10.1142/s0219635205000951

Samanchi, R., Prakash Muthukrishnan, S., Dada, T., Sihota, R., Kaur, S., and Sharma, R. (2021). Altered spontaneous cortical activity in mild glaucoma: a quantitative EEG study. *Neurosci. Lett.* 759:136036. doi: 10.1016/j.neulet.2021.136036

Sato, W., Kochiyama, T., Uono, S., Matsuda, K., Usui, K., Usui, N., et al. (2017). Bidirectional electric communication between the inferior occipital Gyrus and the amygdala during face processing. *Hum. Brain Mapp.* 38, 4511–4524. doi: 10.1002/hbm.23678

Shu, N., Liu, Y., Li, J., Li, Y., Yu, C., and Jiang, T. (2009). Altered anatomical network in early blindness revealed by diffusion tensor tractography. *PLoS One* 4:e7228. doi: 10.1371/journal.pone.0007228

Stam, C. J. (2004). Functional connectivity patterns of human magnetoencephalographic recordings: a 'small-world' network? *Neurosci. Lett.* 355, 25–28. doi: 10.1016/j.neulet.2003.10.063

Tabesh, A., Jensen, J. H., Ardekani, B. A., and Helpern, J. A. (2011). Estimation of tensors and tensor-derived measures in diffusional kurtosis imaging. *Magn. Reson. Med.* 65, 823–836. doi: 10.1002/mm.22655

Tzourio-Mazoyer, N., Landeau, B., Papathanassiou, D., Crivello, F., Etard, O., Delcroix, N., et al. (2002). Automated anatomical labeling of activations in SPM using a macroscopic anatomical Parcellation of the MNI MRI single-subject brain. *NeuroImage* 15, 273–289. doi: 10.1006/nimg.2001.0978

van den Heuvel, M. P., and Hulshoff Pol, H. E. (2010). Exploring the brain network: a review on resting-state fMRI functional connectivity. *Eur. Neuropsychopharmacol.* 20, 519–534. doi: 10.1016/j.euroneuro.2010.03.008

Veraart, J., Poot, D. H., Van Hecke, W., Blockx, I., Van der Linden, A., Verhoye, M., et al. (2011). More accurate estimation of diffusion tensor parameters using diffusion kurtosis imaging. *Magn. Reson. Med.* 65, 138–145. doi: 10.1002/mrm.22603

Wang, H., Li, S., Chen, X., Wang, Y., Li, J., and Wang, Z. (2020). Cerebral blood flow alterations in high myopia: An arterial spin labeling study. *Neural Plast.* 2020, 6090262–6090267. doi: 10.1155/2020/6090262

Wang, J., Li, T., Wang, N., Xian, J., and He, H. (2016). Graph theoretical analysis reveals the reorganization of the brain network pattern in primary open angle glaucoma patients. *Eur. Radiol.* 26, 3957–3967. doi: 10.1007/s00330-016-4221-x

Wang, J., Wang, X., Xia, M., Liao, X., Evans, A., and He, Y. (2015). GRETNA: a graph theoretical network analysis toolbox for imaging connectomics. *Front. Hum. Neurosci.* 9:386. doi: 10.3389/fnhum.2015.00386

Wang, H., Wen, H., Li, J., Chen, Q., Li, S., Wang, Y., et al. (2021). Characterization of brain microstructural abnormalities in high myopia patients: a preliminary diffusion kurtosis imaging study. *Korean J. Radiol.* 22, 1142–1151. doi: 10.3348/kjr.2020.0178

Wen, H. W., Liu, Y., Rekik, I., Wang, S. P., Chen, Z. Q., Zhang, J. S., et al. (2018). Combining disrupted and discriminative topological properties of functional connectivity networks as neuroimaging biomarkers for accurate diagnosis of early Tourette syndrome children. *Mol. Neurobiol.* 55, 3251–3269. doi: 10.1007/s12035-017-0519-1

Wen, H. W., Liu, Y., Rekik, I., Wang, S. P., Zhang, J. S., Zhang, Y., et al. (2017). Disrupted topological organization of structural networks revealed by probabilistic diffusion tractography in Tourette syndrome children. *Hum. Brain Mapp.* 38, 3988–4008. doi: 10.1002/hbm.23643

Yang, C., Zhang, Y., Lu, M., Ren, J., and Li, Z. (2019). White matter structural brain connectivity of young healthy individuals with high trait anxiety. *Front. Neurol.* 10:1421. doi: 10.3389/fneur.2019.01421

Yin, X., Chen, L., Ma, M., Zhang, H., Gao, M., Wu, X., et al. (2021). Altered brain structure and spontaneous functional activity in children with concomitant strabismus. *Front. Hum. Neurosci.* 15:777762. doi: 10.3389/fnhum.2021.777762

Yong, H., Jinhui, W., Liang, W., Chen, Z. J., Chaogan, Y., Hong, Y., et al. (2009). Uncovering intrinsic modular Organization of Spontaneous Brain Activity in humans. *PLoS One* 4:e5226. doi: 10.1371/journal.pone.0005226

Zhang, D., Liu, X., Chen, J., Liu, B., and Wang, J. (2015). Widespread increase of functional connectivity in Parkinson's disease with tremor: a resting-state FMRI study. *Front. Aging Neurosci.* 7:6. doi: 10.3389/fnagi.2015.00006

Zhang, Y. Q., Peng, M. Y., Wu, S. N., Yu, C. Y., Chen, S. Y., Tan, S. W., et al. (2021). Fractional amplitude of low-frequency fluctuation in patients with neovascular glaucoma: a resting-state functional magnetic resonance imaging study. *Quant. Imaging Med. Surg.* 11, 2138–2150. doi: 10.21037/qims-20-855

Zhu, H., Qiu, C., Meng, Y., Yuan, M., Zhang, Y., Ren, Z., et al. (2017). Altered topological properties of brain networks in social anxiety disorder: a resting-state functional MRI study. *Sci. Rep.* 7:43089. doi: 10.1038/srep43089

Zhu, J., Zhuo, C., Qin, W., Wang, D., Ma, X., Zhou, Y., et al. (2015). Performances of diffusion kurtosis imaging and diffusion tensor imaging in detecting white matter abnormality in schizophrenia. *Neuroimage Clin* 7, 170–176. doi: 10.1016/j.nicl.2014.12.008

Zikou, A. K., Kitsos, G., Tzarouchi, L. C., Astrakas, L., Alexiou, G. A., and Argyropoulou, M. I. (2012). Voxel-based morphometry and diffusion tensor imaging of the optic pathway in primary open-angle glaucoma: a preliminary study. *AJNR Am. J. Neuroradiol.* 33, 128–134. doi: 10.3174/ajnr.A2714

frontiers | Frontiers in Aging Neuroscience

TYPE Original Research
PUBLISHED 30 June 2023
DOI 10.3389/fnagi.2023.1148738

OPEN ACCESS

EDITED BY
Peter Edward Wais,
University of California, San Francisco,
United States

REVIEWED BY
Xiaofei Hu,
Army Medical University, China
Kai Liu,
960th Hospital of the PLA, China

*CORRESPONDENCE
Hongwei Wen
✉ wenhongwei@swu.edu.cn
Lingfei Guo
✉ glfsci@163.com

†These authors have contributed equally to this work and share first authorship

RECEIVED 20 January 2023
ACCEPTED 13 June 2023
PUBLISHED 30 June 2023

CITATION
Zhang X, Liang C, Wang N, Wang Y, Gao Y, Sui C, Xin H, Feng M, Guo L and Wen H (2023) Abnormal whole-brain voxelwise structure-function coupling and its association with cognitive dysfunction in patients with different cerebral small vessel disease burdens.
Front. Aging Neurosci. 15:1148738.
doi: 10.3389/fnagi.2023.1148738

Abnormal whole-brain voxelwise structure-function coupling and its association with cognitive dysfunction in patients with different cerebral small vessel disease burdens

Xinyue Zhang [1†], Changhu Liang [1†], Na Wang [1], Yuanyuan Wang [2], Yian Gao [1], Chaofan Sui [1], Haotian Xin [3], Mengmeng Feng [3], Lingfei Guo [1*] and Hongwei Wen [4*]

[1]Key Laboratory of Endocrine Glucose and Lipids Metabolism and Brain Aging, Ministry of Education, Department of Radiology, Shandong Provincial Hospital Affiliated to Shandong First Medical University, Jinan, Shandong, China, [2]Department of Medical Imaging, Binzhou Medical University, Yantai, Shandong, China, [3]Department of Radiology, Shandong Provincial Hospital, Cheeloo College of Medicine, Shandong University, Jinan, Shandong, China, [4]Key Laboratory of Cognition and Personality (Ministry of Education), Faculty of Psychology, Southwest University, Chongqing, China

Cerebral small vessel disease (CSVD) is a universal neurological disorder in older adults that occurs in connection with cognitive dysfunction and is a chief risk factor for dementia and stroke. While whole-brain voxelwise structural and functional abnormalities in CSVD have been heavily explored, the degree of structure-function coupling abnormality possible in patients with different CSVD burdens remains largely unknown. This study included 53 patients with severe CSVD burden (CSVD-s), 108 patients with mild CSVD burden (CSVD-m) and 76 healthy controls. A voxelwise coupling metric of low frequency fluctuations (ALFF) and voxel-based morphometry (VBM) was used to research the important differences in whole-brain structure-function coupling among groups. The correlations between ALFF/VBM decoupling and cognitive parameters in CSVD patients were then investigated. We found that compared with healthy controls, CSVD-s patients presented notably decreased ALFF/VBM coupling in the bilateral caudate nuclei and increased coupling in the right inferior temporal gyrus (ITG). In addition, compared with the CSVD-m group, the CSVD-s group demonstrated significantly decreased coupling in the bilateral caudate nuclei, right putamen and inferior frontal gyrus (IFG) and increased coupling in the left middle frontal gyrus and medial superior frontal gyrus. Notably, the ALFF/VBM decoupling values in the caudate, IFG and ITG not only showed significant correlations with attention and executive functions in CSVD patients but also prominently distinguished CSVD-s patients from CSVD-m patients and healthy controls in receiver operating characteristic curve research. Our discoveries demonstrated that decreased ALFF/VBM coupling in the basal ganglia and increased coupling in the frontotemporal lobes were connected with more severe burden and worse cognitive decline in CSVD patients. ALFF/VBM coupling might serve as

a novel effective neuroimaging biomarker of CSVD burden and provide new insights into the pathophysiological mechanisms of the clinical development of CSVD.

KEYWORDS

cerebral small vessel disease, low frequency fluctuations, voxel-based morphometry, structure-function coupling, cognitive dysfunction, burden

1. Introduction

Cerebral small vessel disease (CSVD) represents a cluster of vascular diseases involving a variety of cerebral vessels, including arterioles, venules, and capillaries; it is believed to be a major factor in dementia, cognitive decline, mood disorders, gait impairment and stroke (Litak et al., 2020). Common imaging markers of CSVD include cerebral microbleeds (CMBs), white matter magnetic resonance hyperintensities (WMHs) of presumed vascular origin, lacunes of presumed vascular origin, enlarged perivascular spaces (PVSs), brain atrophy and recent small subcortical infarcts (Wardlaw et al., 2013). Previous studies have proposed combining the above imaging markers to score the severity of CSVD, namely, the burden of CSVD, which can be used to predict the risk of dementia (Amin Al Olama et al., 2020) and is related to cognition and blood pressure in lacunar stroke patients (Staals et al., 2014). It has been shown that higher total CSVD burden was associated with overall cognitive ability in middle-aged and older Chinese people (Li X. et al., 2021) and can be a long-term strong predictor of cognitive decline and dysfunction (Jokinen et al., 2020). CSVD burden provides a better estimate of the overall effect of CSVD on the brain than a single imaging marker. Furthermore, previous studies have shown that the concept of a total score for small vessel disease in cerebral amyloid angiopathy is valid and can be used in prospective clinical studies (Charidimou et al., 2016). Therefore, stratification based on burden risk for other clinical studies of CSVD is reliable. However, in only a few studies have participants been grouped according to CSVD severity scores.

Currently, multimodal magnetic resonance imaging (MRI) techniques are widely applied to reveal the functional and structural alterations underlying CSVD pathology. For functional changes in CSVD, based on resting-state functional MRI (rs-fMRI), the amplitude of low frequency fluctuations (ALFF) metric, which can reliably and reproducibly reflect the level of regional functional neural activity (Yu-Feng et al., 2007), was used to reveal that CSVD patients with CMBs demonstrated higher ALFF values in the putamen, left precuneus and right insula (Feng et al., 2021). In addition, substantially increased fractional ALFF in the right inferior frontal gyrus and the left caudate were revealed in CSVD patients with gait disturbances (Zhou et al., 2020). Regarding structural changes in CSVD, voxel-based morphometry (VBM) research was used to reveal that CSVD patients showed substantially decreased gray matter (GM) and white matter (WM) volumes in the right inferior frontal gyrus and left medial superior frontal gyrus (Li et al., 2022). Furthermore, CSVD patients frequently experience brain functional changes accompanied by structural abnormalities (Telgte et al., 2018). At present, few studies have coupled ALFF and VBM to analyze neurological and psychiatric diseases, and it is a relatively blank field of current research to use coupling indicators to analyze CSVD. Some scholars (Li H. et al., 2021) combined ALFF and VBM analysis to find that patients with vascular mild cognitive impairment presented GM atrophy in the right precentral gyrus and inferior temporal gyrus and decreased ALFF in structures of the default mode network (DMN), which may be a calculable biomarker of cognitive impairment. Since the impacted brain areas are not consistently revealed by structural and functional MRI studies, it is more beneficial to directly study the association between structural and functional alterations in CSVD patients, which may help to elucidate the underlying neurobiological mechanisms of CSVD.

Emerging evidence indicates that the coupling of multimodal structural and functional imaging can be used to analyze a variety of neuropsychiatric diseases as it demonstrates additional messages and promotes the sensitivity of diagnosis compared to a single imaging modality (Wen et al., 2017). The present study showed that structural-functional deficits have been observed in patients with social anxiety disorder (Zhang et al., 2022), and the integration of structural and functional MRI contributes to identifying mild cognitive impairment (MCI), improving its diagnostic efficacy (Kim and Lee, 2013). Among the current numerous multimodal fusion analysis methods, structure-function coupling is a novel measure that describes the structural support for functional interaction, and increased structure–function coupling in the frontal association cortex may support functional specialization in connection with cognition (Baum et al., 2019). Importantly, previous studies (Zhao et al., 2015; Li H. et al., 2021) revealed that GM volume (GMV) alterations obtained by VBM analysis are highly related to ALFF deficits in CSVD patients with cognitive impairment. Therefore, ALFF/VBM coupling may be a reliable structure-function coupling metric that can reflect the neural mechanism underlying CSVD with cognitive impairment. Notably, Kang et al. (2022) recently developed a voxelwise coupling analysis of rs-fMRI and VBM parameters to assess structure–function decoupling and its importance in evaluating patients with nasopharyngeal carcinoma (NPC). They found that after radiotherapy, NPC patients showed increased rs-fMRI/VBM coupling parameters in the putamen, thalamus, and substantia nigra (SN) and decreased coupling parameters mainly in the medial temporal and prefrontal gyrus. However, despite these advances, structure-function decoupling in CSVD patients, especially those with different CSVD burdens, has not been explored.

In this study, we aimed to first compute ALFF and VBM maps and then establish an ALFF/VBM coupling metric to assess structure–function decoupling in CSVD patients with

different burdens. Notably, in VBM research, the brain can be segmented into gray matter, white matter and cerebrospinal fluid (Nyatega et al., 2022). Therefore, ALFF can be coupled with WMV and GMV to explore alterations in different brain regions. Furthermore, we analyzed the correlation between ALFF/VBM coupling metrics and cognitive parameters in CSVD patients. Finally, it was hypothesized that ALFF/VBM would be a reliable and valid neuroimaging parameter that indicated structure–function decoupling under different CSVD burdens and that structure–function decoupling may be distinctly related to cognitive impairment.

2. Materials and methods

2.1. Participants

This cross-sectional study was approved for implementation by Shandong Provincial Hospital Affiliated with Shandong First Medical University's institutional review board. Between December 2018 and January 2022, 53 patients with severe CSVD burden (CSVD-s age: 63.90 ± 6.23 years; 19 females) and 108 patients with mild CSVD burden (CSVD-m; age: 61.45 ± 7.79 years; 51 females) were recruited. We also included 76 age-, sex- and education-matched healthy controls (age: 60.55 ± 9.29 years; 42 females) in our study. All participants voluntarily signed an informed consent form before the research began.

According to current MRI consensus standards (Wardlaw et al., 2013), the criteria for inclusion were as follows: CMBs, WMHs of presumed vascular origin, lacunes of presumed vascular origin, enlarged PVSs, brain atrophy and recent small subcortical infarcts. The "total SVD burden" (Klarenbeek et al., 2013) was used to evaluate the seriousness of the CSVD, and a pragmatic ordinal scale of 0–4 was applied, reflecting the four mentioned MRI symbols of CSVD. One point was given if ≥1 CMB was observed; one point if an early syncretic deep WMH [Fazekas score (Fazekas et al., 1987) 2 or 3] or anomalous periventricular WMH progressing to the deep white matter (Fazekas score 3) was observed; one point if ≥1 lacune was observed; and one point if moderate to severe (grade 2–3) enlargement of a PVS in the basal ganglia was observed. Participants with scores of 0–1 were classified in the CSVD-m group, and those with scores of 2–4 were classified in the CSVD-s group.

The following conditions were criteria for exclusion: (1) a medical history of stroke, epilepsy, brain trauma, or tumor; (2) a medical history of alcohol or drug abuse; (3) a medical history of thrombolysis; (4) an occurrence of liver, heart, or kidney injury; (5) severe hypertension or acute complications of type 2 diabetes mellitus; and (6) a medical history of serious psychiatric or neurological illnesses.

2.2. MRI obtainment

A 3.0-Tesla MR system (Siemens Healthcare, Erlangen, Germany) equipped with a 32-channel head coil for signal reception was used to acquire MRI images. High-resolution 3D T1-weighted structural images were obtained by a magnetization-prepared rapid gradient echo (MPRAGE) sequence on the basis of the following settings: repetition time (TR)/echo time (TE) = 7.3/2.4 ms; flip angle = 9°; field of view (FOV) = 240 mm^2 × 240 mm^2; matrix size = 256 × 256; slice thickness = 1 mm; 192 slices; and slice thickness = 0.9 mm with no gap. The rs-fMRI images were obtained using a gradient echo-echo-planar imaging (GE-EPI) sequence with the following index: TR/TE = 1,500/30 ms; FOV = 240 mm^2 × 240 mm^2; matrix size = 64 × 64; slice thickness = 3 mm; slice gap = 1 mm; 50 axial slices; 200 volumes and 50 axial slices.

2.3. Cognitive assessments

The Montreal Cognitive Assessment (MoCA) Beijing version[1] was given to all participants (Bergeron et al., 2017). The optimal threshold for identifying cognitive dysfunction was 13/14 points for illiteracy, 19/20 for those with 1–6 years of schooling and 24/25 for those with 7 or more years of schooling (Lu et al., 2011). Additionally, other executive abilities were tested, including adaptability, working memory, and inhibiting ability. In brief, these tests included the symbol digit modalities test (SDMT) to gauge information processing speed and attention (Benedict et al., 2017), the trail-making test (TMT), which measures information processing speed, visual search, attention and motor coordination (Wei et al., 2018), the Rey auditory verbal learning test (AVLT) to evaluate verbal memory skills (Putcha et al., 2019), and the Stroop color-word test (SCWT) (Scarpina and Tagini, 2017). The test administrator had professional training and appropriate credentials and knew nothing about the subject grouping in advance.

2.4. Data preprocessing and function-structure coupling analysis

We adopted the standard procedure for the preprocessing of rs-fMRI data following our previous studies (Wen et al., 2018; Feng et al., 2021) and used the Data Processing and Analysis for Brain Imaging toolbox (DPABI v6.0[2]). Briefly, the main procedures were as follows: (1) the removal of the first ten time points; (2) slice timing correction; (3) head motion correction, for which the exclusion criteria were a maximum head motion of 3.0 degree and 3.0 mm, with mean framewise displacement (FD) >0.2 mm (Jenkinson et al., 2002); (4) the regression of nuisance covariates, which included signals from WM and cerebrospinal fluid (CSF), and 24 rigid body motion parameters; (5) normalization to the MNI standard space at 3 mm isotropic voxel resolution by DARTEL (Ashburner, 2007); (6) spatial smoothing with an isotropic Gaussian kernel of 4 mm full width at half maximum (FWHM); and (7) the calculation of ALFF by transforming the smoothed time series of each voxel into frequency domain data by a fast Fourier transform (FFT). The square root of the power spectrum was calculated and

1 www.mocatest.org
2 http://rfmri.org/dpabi

averaged over a predetermined frequency range (0.01–0.08 Hz) at each voxel (Yu-Feng et al., 2007). Finally, the ALFF per voxel was separated by the global ALFF (mean ALFF of all voxels) to generate the standardized ALFF metric for further coupling analysis.

The T1W images were preprocessed and analyzed using VBM-DARTEL analysis as described in our recent studies (Wen et al., 2017; Li et al., 2022) based on the SPM8[3] toolbox. Briefly, every T1W image was manually readjusted by placing the origin at the anterior commissure. Afterward, using SPM's New Segment tool, the aligned images were separated into GM, WM, and CSF in the original space using unitive segmentation. Afterward, to create a variety of aligned GM and WM images, all of the segmented GM and WM images were highly modified. The DARTEL algorithm was used to construct the study-specific GM templates, and every aligned GM image was then warped to the template, producing numerous flow fields that specified distortion. The GM/WM images were modified to correct volume alterations after being spatially adjusted to the MNI standard space. GMV and WM volume (WMV) maps were smoothed with a Gaussian kernel of 4 mm FWHM.

Subsequently, we combined rs-fMRI and VBM metrics for structure-function coupling analysis. Since both the ALFF maps and the regulated VBM maps (GMV/WMV) for each subject were normalized to the same MNI standard space, based on a previous study (Kang et al., 2022), voxelwise ALFF/VBM coupling research was executed by determining the ratio of the ALFF value to the GMV/WMV value per voxel at the same coordinate.

2.5. Between-group statistical comparisons and correlation analysis

One-way analysis of variance (ANOVA) and least significant difference (LSD) post-hoc tests were applied to assess differences in age, education, head motion and cognitive parameters among the three groups, and a chi-square test was performed to probe the difference in sex.

For the voxelwise ALFF/VBM coupling metric, one-way analysis of covariance (ANCOVA) was used to assess differences among the three groups while controlling age, sex, education and head motion as covariates. Then, LSD post-hoc tests were used, and the corrected p-values for comparison between each pair of groups were calculated. After the corrected p-value maps were converted to z value maps, Gaussian random field (GRF) correction (voxel level $p < 0.001$, cluster level $p < 0.05$) was performed on the z value maps using DPABI utilities (Yan et al., 2016; Bansal and Peterson, 2018). The peak voxel coordinates of clusters were expounded in MNI space, and the AAL atlas (Tzourio-Mazoyer et al., 2002) was used for anatomical definition. We further extracted the mean ALFF/VBM coupling values from the identified altered clusters and calculated the Pearson correlation coefficients between the coupling metrics and cognitive test scores for the CSVD-s and CSVD-n groups using SPSS v24.0 software.

2.6. Receiver operating characteristic curve analysis

The results of our recent studies (Feng et al., 2021; Li et al., 2022) suggest that ALFF and VBM changes may be reliable imaging metrics to discriminate CSVD patients from healthy controls. The mean ALFF/VBM coupling values of markedly altered clusters in ANCOVA were extracted for receiver operating characteristic (ROC) curve analysis using MedCalc Statistical Software[4] to confirm the performance of these biomarkers for discriminating CSVD patients from healthy controls. We calculated the greatest Youden index (specificity + sensitivity–1) (Fluss et al., 2005), as well as the corresponding specificity, sensitivity, and 95% confidence intervals (CIs) for all clusters, to provide a summary of the tests' overall diagnostic efficacy.

3. Results

3.1. Demographic and cognitive parameters of the participants

The demographic and cognitive parameters in every group are summarized in **Table 1**. The CSVD-s group exhibited obviously decreased SDMT, AVLT, and MoCA scores and distinctly increased TMT and SCWT scores compared with the CSVD-m and control groups, apart from there being no visible distinction in MoCA scores between the CSVD-s and CSVD-m groups. In addition, the patients in the CSVD-m group showed distinctly lower SDMT scores and higher SCWT scores than those in the control group. No apparent differences were found in age, sex, education or head motion (mean FD) among groups.

3.2. Abnormal ALFF/VBM coupling among groups

Adopting the voxelwise structure-function coupling metric, we found multiple disrupted regions among the three groups. Specifically, compared with patients in the control group, the patients in the CSVD-s group showed significantly decreased ALFF/GMV and ALFF/WMV coupling values in the bilateral caudate clusters and increased ALFF/GMV coupling in the right inferior temporal gyrus (**Figure 1** and **Table 2**). In addition, compared with patients in the CSVD-m group, patients in the CSVD-s group revealed obviously decreased ALFF/GMV coupling in the bilateral caudate and right putamen clusters, decreased ALFF/WMV coupling in the right inferior frontal gyrus (IFG) and increased ALFF/GMV coupling in the left middle frontal gyrus (MFG) and medial superior frontal gyrus (SFGmed) (**Figure 2** and **Table 3**). No significant ALFF/VBM coupling distinction was found between the CSVD-m and control groups.

3 http://www.fil.ion.ucl.ac.uk/spm

4 https://www.medcalc.org

TABLE 1 Demographic and clinical characteristics of CSVD patients and healthy controls.

Characteristic	CSVD-s	CSVD-m	HC	*P*-value (ANOVA/χ^2)	*P*-value (*post-hoc*)		
					CSVD-s vs. HC	CSVD-s vs. CSVD-m	CSVD-m vs. HC
Gender	34 M/19 F	57 M/51 F	34 M/42 F	0.094χ^2	–	–	–
Age (y)	63.90 ± 6.23	61.45 ± 7.79	60.55 ± 9.29	0.060[a]	–	–	–
Education (y)	11.26 ± 3.22	12.07 ± 3.14	12.67 ± 3.35	0.053[a]	–	–	–
MoCA	24.47 ± 2.91	25.38 ± 3.57	26.39 ± 3.57	0.009[a]	0.002	0.121	0.052
AVLT	54.66 ± 13.5	61.05 ± 12.19	64.6 ± 11.94	<0.001[a]	<0.001	0.003	0.059
SDMT	26.56 ± 11.94	32.16 ± 12.23	40.57 ± 13.53	<0.001[a]	<0.001	0.010	<0.001
SCWT	178.68 ± 59.41	145.47 ± 44.98	131.78 ± 31.08	<0.001[a]	<0.001	<0.001	0.045
TMT (B-A)	161.8 ± 91.09	125.59 ± 106.34	104.84 ± 80.08	0.005[a]	0.001	0.028	0.152
FD_Jenkinson	0.13 ± 0.04	0.12 ± 0.04	0.11 ± 0.04	0.135[a]	–	–	–
Lacunes	22 (41.5%)	2 (1.9%)	–	<0.001χ^2			
WMHs	52 (98.1%)	105 (97.2%)	–	<0.001χ^2			
PVSs	47 (88.7%)	34 (31.5%)	–	<0.001χ^2			
CMBs	34 (64.2%)	13 (12.0%)	–	<0.001χ^2			

χ^2: chi-square test.
[a]ANOVA test. MoCA, montreal cognitive assessment; AVLT, sum of Rey auditory verbal learning test (N1-7); SDMT, symbol digit modalities test; SCWT, sum of Stroop color-word test (stroop1–3); TMT, the trail-making test; TMT (B-A), the difference between TMT-B and TMT-A; CSVD-s, severe CSVD burden (score ≥2) group; CSVD-m, mild CSVD burden (score ≤1) group; HC, healthy controls; FD Jenkinson, framewise displacement (Jenkinson et al., 2002); Lacunes, one of the imaging markers of CSVD; WMHs, white matter magnetic resonance hyperintensities; PVSs, enlarged perivascular spaces; CMBs, cerebral microbleeds.

3.3. ROC curve analysis results

For discriminating CSVD-s patients from healthy controls, the mean ALFF/GMV coupling value of the left caudate achieved the best performance, and for discriminating CSVD-s patients from CSVD-m patients, the mean ALFF/GMV coupling value of the right caudate achieved the best performance in view of the Youden index, region under the ROC curve (AUC) and 95% CIs. Each changed brain cluster met the $p < 0.001$ AUC significance threshold, indicating that the discoveries are meaningful and that these parameters have potential as diagnostic neuroimaging biomarkers (Figure 3 and Table 4).

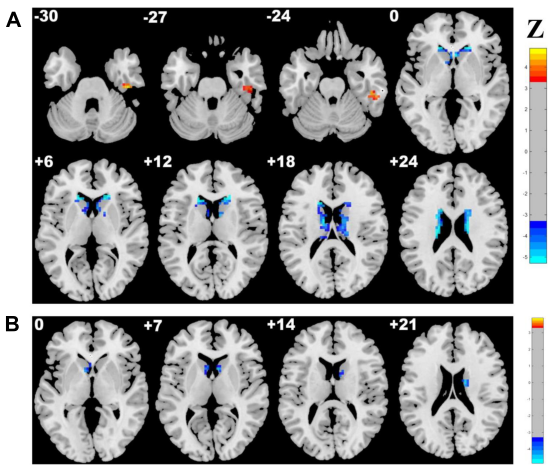

FIGURE 1
Brain clusters revealing distinctly abnormal ALFF/VBM coupling in the CSVD-s group compared with the control group. Clusters with significantly changed **(A)** ALFF/GMV and **(B)** ALFF/WMV coupling identified by ANCOVA and LSD *post-hoc* test with GRF correction (voxel level $p < 0.001$, cluster level $p < 0.05$). The red–yellow and blue–light blue color bars represent the level of significance for ALFF/VBM coupling increases and decreases in the CSVD-s group, respectively.

3.4. Associations between ALFF/VBM coupling and cognitive parameters

Pearson's correlation analysis was performed to estimate the relevance between the mean coupling values of aberrant clusters and cognitive scores in CSVD-s and CSVD-m patients. In CSVD-s patients, the mean ALFF/GMV value of the bilateral caudate ($r = -0.307$, $p = 0.025$ and $r = -0.357$, $p = 0.009$) and the mean ALFF/WMV value of the right caudate ($r = -0.274$, $p = 0.047$) showed significant negative correlations with TMT scores (Figure 4A). In CSVD-m patients, the mean ALFF/GMV value of the left caudate ($r = -0.223$, $p = 0.020$) and right ITG ($r = -0.236$, $p = 0.014$) and the mean ALFF/WMV value of the right IFG ($r = -0.269$, $p = 0.005$) showed obvious negative correlations with SDMT scores, while the mean ALFF/GMV value of the left caudate ($r = 0.257$, $p = 0.007$) and the mean ALFF/WMV value of the right IFG ($r = 0.209$, $p = 0.031$) showed evident positive correlations with TMT scores (Figure 4B).

4. Discussion

As far as we know, this study designed to detect structure-function decoupling in patients with different CSVD burdens by

TABLE 2 Clusters with significantly altered ALFF/VBM coupling in the CSVD-s group compared with the control group.

Metrics and condition	Brain regions	Cluster size	z score of peak voxel	MNI coordinates of peak voxel		
				x	y	z
ALFF/GMV	Right caudate	173	5.295	15	27	0
CSVD-s < control	Left caudate	159	5.295	−18	27	6
ALFF/GMV CSVD-s > control	Right inferior temporal gyrus	31	4.901	45	−21	−30
ALFF/WMV	Right caudate	39	4.586	15	−6	21
CSVD-s < control	Left caudate	25	4.271	−9	9	0

ANCOVA and LSD *post-hoc* tests were applied to identify the altered ALFF/VBM coupling among groups with Gaussian random field (GRF) multiple comparison corrections (voxel level $p < 0.001$, cluster level $p < 0.05$). CSVD-s, severe CSVD burden (score ≥2) group.

coupling analysis of rs-fMRI and VBM metrics is novel. In our research, an ALFF/VBM metric was applied to reflect the coupling between spontaneous brain activity and GM/WM volume. For each participant, the voxelwise ALFF/VBM ratio characterizes the quantity of regional neuronal activity requirement per unit of regional GM/WM morphological alterations, which could measure the structure–function coupling for a concrete region or voxel. Compared with the patients in the CSVD-m and control groups, ALFF/VBM coupling was significantly altered in CSVD-s patients and was prominently associated with TMT scores. Specifically, decreased ALFF/GMV and ALFF/WMV coupling values in the CSVD-s group were observed mainly in the basal ganglia and right IFG, and increased coupling mainly occurred in the frontal and temporal cortical areas. The increase and decrease of coupling values in different regions are both involved in the structural and functional decoupling, which indicated that the structure and function of the brain in CSVD patients were dysregulated; that is, the duration and intensity of the activity were altered along with the structural damage of corresponding brain regions. Overall, our findings highlighted the importance of multimodal MRI fusion and provided insights promoting a better comprehension of the correlation between structure–function decoupling and cognitive deficits in patients with different CSVD burdens.

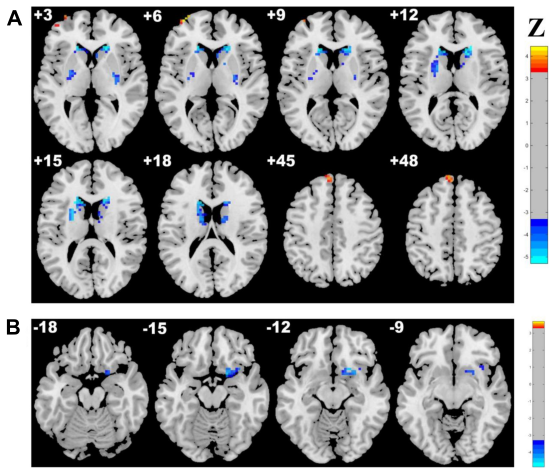

FIGURE 2
Brain clusters revealing distinctly abnormal ALFF/VBM coupling in the CSVD-s group compared with the CSVD-m group. Clusters with significantly changed **(A)** ALFF/GMV and **(B)** ALFF/WMV coupling are shown in red–yellow and blue–light blue colors, representing the level of significance for ALFF/VBM coupling increases and decreases in the CSVD-s group, respectively.

Notably, the disturbed basal ganglia regions mainly contain the caudate and putamen. The caudate and putamen make up the dorsal striatum, which is the pathway to the basal ganglia. Furthermore, the plasticity of the striatum may be a crucial neuronal matrix for motor control and procedural memory (Kreitzer and Malenka, 2008). Thus, gait disturbance may result from decreased structure-function coupling in this area. Recent research has demonstrated that CSVD-induced microscopic brain structural changes impact motor ability in the upper and lower limbs (Su et al., 2017), and slower gait speed is related to weaker basal ganglia connectivity in the resting state (Karim et al., 2020), supporting this viewpoint. Furthermore, gait abnormalities predict declines in overall cognitive, memory, and language abilities (Blumen et al., 2023). On the other hand, decoupling also occurs in the temporal and frontal lobes. It was shown that cognitive decline associated with cerebrovascular disease (including CSVD) affects frontal executive function (Dichgans and Leys, 2017), particularly episodic memory. The gradual decline in cognitive function has been related to frontal and parietal hypometabolism and inferior temporal cortical thinning (Halawa et al., 2019). The frontal lobes play a prominent role in human cognitive functions and socioemotional function, and several neurodegenerative illnesses have an impact on frontal lobe function (Butler and Chiong, 2019). It can be inferred that the disruption of structural and functional coupling found in the frontotemporal lobe is associated with cognitive impairment and that the burden of CSVD lesions corresponds with disruption in brain morphology and activity, which also promotes cognitive decline. Thus, the different trends of coupling values may be due to the different functional characteristics and damage degree of basal ganglia and frontotemporal lobe.

Furthermore, we found that the above key abnormal areas were more affected in the CSVD-s group than in the other two groups, while there was no apparent difference between the CSVD-m and control groups; this discordance was due to more severe pathological changes, correspondingly more varied MRI features, and more obvious disruption of brain topology in the CSVD-s group. It was proven that the classification of severe and mild groups based on the burden score is reliable, which is beneficial to the analysis of abnormal imaging indicators (e.g., structure the burden coupling) and the interpretation of

TABLE 3 Clusters with significantly altered ALFF/VBM coupling in the CSVD-s group compared with the CSVD-m group.

Metrics and condition	Brain regions	Cluster size	z score of peak voxel	MNI coordinates of peak voxel		
				x	y	z
ALFF/GMV CSVD-s < CSVD-m	Left caudate	181	5.295	−18	27	6
	Right caudate	137	5.295	15	21	15
	Right putamen	23	4.360	27	−9	3
ALFF/GMV CSVD-s > CSVD-m	Left middle frontal gyrus	11	4.388	−36	60	6
	Left medial superior frontal gyrus	14	4.046	−6	51	48
ALFF/WMV CSVD-s < CSVD-m	Right inferior frontal gyrus	42	4.427	18	9	−15

ANCOVA and LSD *post-hoc* tests were applied to identify the altered ALFF/VBM coupling among groups with Gaussian random field (GRF) multiple comparison corrections (voxel level $p < 0.001$, cluster level $p < 0.05$). CSVD-s, severe CSVD burden (score ≥2) group; CSVD-m, mild CSVD burden (score ≤1) group.

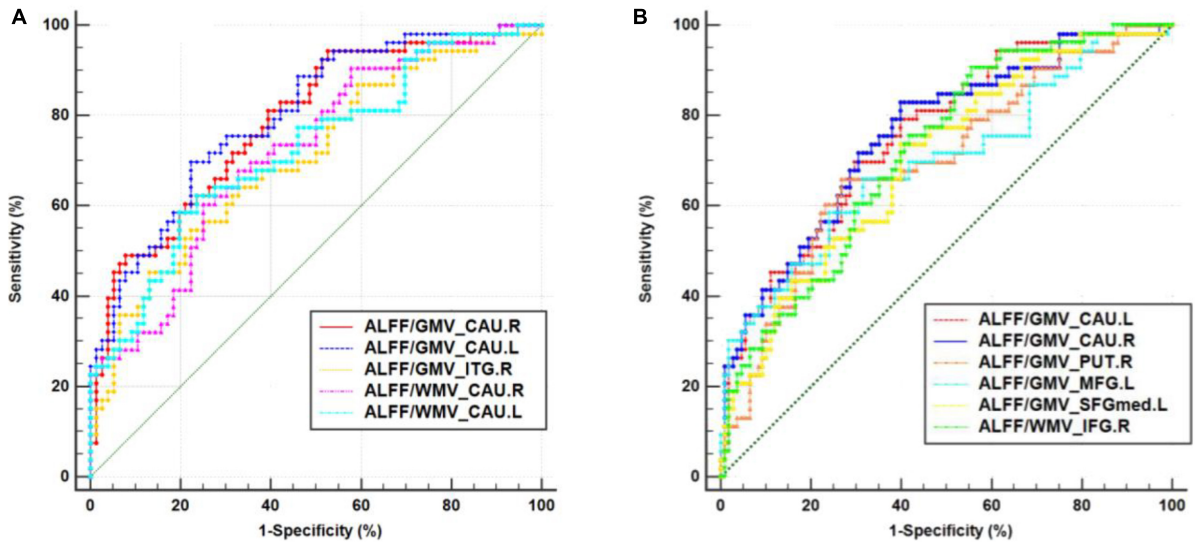

FIGURE 3
Receiver operating characteristic (ROC) curve analysis results. ROC curves for brain clusters that discriminate **(A)** CSVD-s patients from healthy controls and discriminate. **(B)** CSVD-s patients from CSVD-m patients. CAU, caudate; ITG, inferior temporal gyrus; MFG, middle frontal gyrus; SFGmed, medial superior frontal gyrus; IFG, inferior frontal gyrus.

pathophysiological processes in CSVD. In our previous study, we divided CSVD patients into groups according to whether they had CMBs and demonstrated alterations in ALFF and fALFF values, GMV and WMV in different brain regions in different groups (Feng et al., 2021; Li et al., 2022). To further explore CSVD, we need to conduct coupling analysis of ALFF with WMV and GMV to search for the deeper effects of diseases on the brain. To further explore CSVD, we need to conduct coupling analysis of ALFF with WMV and GMV to search for the deeper effects of diseases on the brain. Specifically, ALFF/VBM decoupling may be attributed to the asynchronism of disruptive brain activity and morphological structure or diminished correlations between functional interactions and underlying anatomy. The inconsistent direction of coupling values in various regions and the uneven change in ALFF and VBM indexes are likely related. The function of relevant regions is impacted by the structural changes caused by CSVD, and the primary functional abnormity may lead to secondary volume changes. One explanation for this phenomenon might be the compensatory effects of structure and function (Shang et al., 2019) in disease development. Namely, the intensive structure-function coupling in the frontotemporal region makes up for the reduced motor function and control arising from structure-function decoupling in the dorsal striatum. Therefore, ALFF/VBM decoupling can provide new explanations for the interaction of structure and function and the underlying pathophysiological mechanism of CSVD in patients.

Intriguingly, the mean ALFF/VBM values of all disrupted brain clusters achieved the significance level in ROC curve analysis. Among them, the mean ALFF/VBM value in the bilateral caudate nucleus performed the best, which indicated that structure–function coupling abnormalities in the caudate nucleus make a difference in discriminating CSVD patients from healthy controls. The caudate nucleus is a crucial component of brain executive functions, such as cognitive control, working memory and certain aspects of attention, such as the separation of attention (Aumont et al., 2019), and controls body movement. The caudate nucleus can

TABLE 4 The statistics of ROC curve analysis for altered brain clusters that discriminate CSVD-c patients from healthy controls.

Clusters	SEN	SPE	AUC	95% CIs
Task: Distinguish between CSVD-s and control groups				
ALFF/GMV_Right caudate	94.34%	47.37%	0.786*	0.705–0.853
ALFF/GMV_Left caudate	69.81%	77.63%	0.799*	0.720–0.865
ALFF/GMV_Right ITG	54.72%	77.63%	0.707*	0.620–0.784
ALFF/WMV_Right caudate	60.38%	75.00%	0.722*	0.636–0.797
ALFF/WMV_Left caudate	58.49%	80.26%	0.723*	0.638–0.799
Task: Distinguish between CSVD-s and CSVD-m groups				
ALFF/GMV_Left caudate	69.81%	70.37%	0.757*	0.683–0.821
ALFF/GMV_Right caudate	83.02%	60.19%	0.759*	0.685–0.823
ALFF/GMV_Right putamen	66.04%	73.15%	0.698*	0.621–0.768
ALFF/GMV_Left MFG	66.04%	68.52%	0.696*	0.619–0.766
ALFF/GMV_Left SFGmed	73.58%	60.19%	0.702*	0.625–0.771
ALFF/WMV_Right IFG	90.57%	44.44%	0.719*	0.643–0.787

SEN/SPE, sensitivity/specificity corresponding to maximum Youden index; AUC, area under the ROC curve; *$p < 0.001$; CIs, confidence intervals; ITG, inferior temporal gyrus; MFG, middle frontal gyrus; SFGmed, medial superior frontal gyrus; IFG, inferior frontal gyrus.

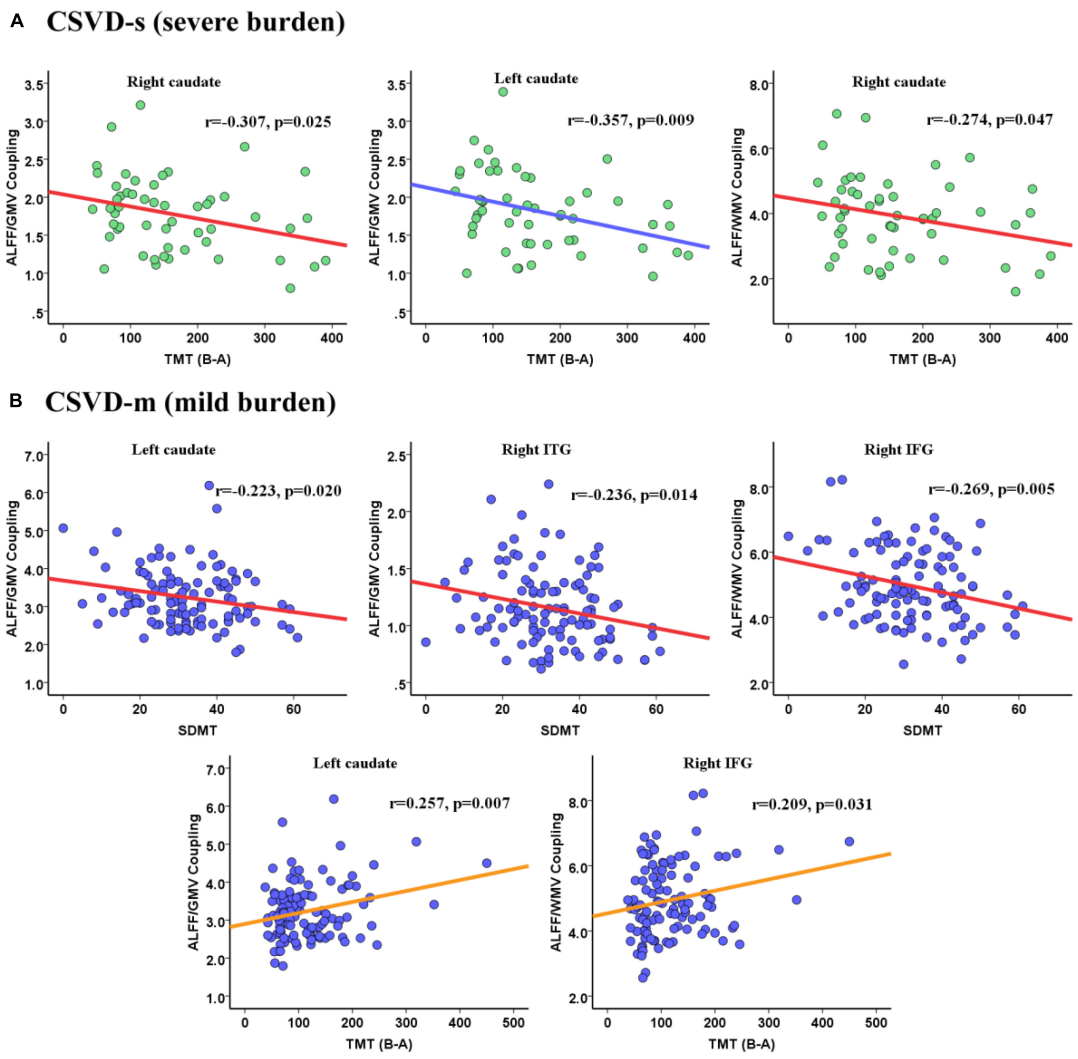

FIGURE 4
Pearson correlations between the ALFF/VBM coupling values and cognitive scores for the **(A)** CSVD-s group and **(B)** CSVD-m group.

be segmented into ventral and dorsal according to its connectivity and function, where the dorsal caudate nucleus is extraordinarily joined to the dorsolateral prefrontal cortex (DLPFC) and the latter is associated with executive function and working memory. The ventral caudate nucleus is more closely related to the limbic system and is related to emotional functions (Huang et al., 2017). CSVD-s patients are more prone to acquiring dementia, apathy, and vascular Parkinson's disease as their disease worsens. In contrast, Parkinson's disease and apathy are likely linked by structural abnormalities in the caudate nucleus (Gez et al., 2022). Therefore, the performance of ALFF-VBM coupling in the caudate nucleus was more impressive for distinguishing the CSVD-s group from the CSVD-m and control groups, suggesting that more attention should be given to changes in the function and/or structure of the caudate nucleus in CSVD patients in future studies.

Notably, CSVD burden is an important predictor of cognitive impairment in patients (Chen et al., 2019). Our recent studies demonstrated that alterations in brain structure (Sui et al., 2023) and function (Feng et al., 2021; Xin et al., 2022) were significantly correlated with cognitive dysfunction in CSVD patients. However, whether structure-function coupling plays a mediating role in the correlation between CSVD burden and cognitive parameters has not been explored. Our study may answer the above question. The main significant correlations observed were between the bilateral caudate nuclei and scores on the TMT, which are used to assess motor coordination executive functioning, and information processing speed (Wei et al., 2018). Our discoveries confirm the viewpoint that CSVD is the most universal mechanism leading to vascular cognitive impairment (Zanon Zotin et al., 2021) and that cognitive ability gradually declines with the gradual increase in the severity of CSVD burden. Cognitive impairment in the CSVD-s group with the most severe pathological changes may be closely related to abnormalities in the caudate nucleus, which can directly regulate motor control and indirectly affect executive function. Furthermore, our findings also showed that the correlation pattern between ALFF/VBM coupling and cognitive function was not consistent between CSVD-s and CSVD-m patients, especially in the inferior frontotemporal lobe. We speculate that the autoregulatory mechanisms of the brain may be able to respond, resulting in less pronounced ALFF/VBM decoupling and less consistent relevance between decoupling and cognitive function in CSVD-m patients. However, the regulating mechanism fails when the burden reaches a certain level. The inferior frontal gyrus is known to be closely connected with the dorsal caudate nucleus, forming a frontal-subcortical circuit mainly responsible for executive function (Raimo et al., 2019), and the hypometabolism and volume atrophy of the inferior frontotemporal gyrus are gradually aggravated with a worsening of CSVD burden. These results highlight the importance of investigating the correlation between structure-function coupling and cognitive function in patients with different CSVD burdens, suggesting that early screening, diagnosis, detection and treatment of CSVD in patients could prevent or delay cognitive decline.

Several limitations of this study need to be pointed out. Firstly, our study was cross-sectional, which limited us in terms of cause-and-effect analysis. A longitudinal design should be explored in future research to monitor individual neuroimaging and neuropsychological changes. Secondly, structural destruction of the lesion area could not be confirmed by histopathology due to our noninvasive analysis *in vitro*, which is another limitation. Thirdly, our prediction of dementia based on coupling abnormalities in different brain regions with different burdens of CSVD needs to be verified by further study of brain networks. Finally, the number of subjects in the CSVD-s group is relatively small compared to the other two groups. In the future, we will strengthen our recruitment efforts for more accurate and in-depth research.

5. Conclusion

In summary, significantly decreased ALFF/VBM coupling in the CSVD-s group was observed in the bilateral caudate nuclei, putamen and right IFG, and increased coupling was found in the right ITG, left MFG and SFGmed compared with the CSVD-m and control groups. In addition, ALFF/VBM decoupling in the caudate, IFG and ITG was significantly correlated with executive and attention functions in CSVD patients. Structure–function decoupling in the bilateral caudate nuclei is excellent at identifying patients with severe CSVD burden. These findings imply that ALFF/VBM coupling might be a powerful and innovative neuroimaging metric to track changes in CSVD burden and cognitive impairment and would be useful for the early diagnosis and prediction of CSVD progression. Early intervention plays a vital role in slowing cognitive decline and improving the quality of life of patients. In addition, this research offers new perspectives regarding the pathophysiological mechanisms involved in the clinical development of CSVD.

Data availability statement

The original contributions presented in the study are included in the article/supplementary material, further inquiries can be directed to the corresponding authors.

Ethics statement

The studies involving human participants were reviewed and approved by the Shandong Provincial Hospital Affiliated with Shandong First Medical University's Institutional review board. The patients/participants provided their written informed consent to participate in this study.

Author contributions

XZ and CL wrote the main manuscript text. NW, YW, YG, CS, MF, and HX prepared the clinical data and imaging data. HW and LG revised the main manuscript text. All authors reviewed the manuscript and contributed to the article and approved the submitted version.

Funding

This work was supported by grants from the National Natural Science Foundation of China (32100902), the Fundamental Research Funds for the Central Universities (SWU118065), the Funding for Study Abroad Program by Shandong Province (201803059), and the Shandong Provincial Natural Science Foundation (ZR2020MH288).

Acknowledgments

The authors are grateful to all of the volunteers and patients for their participation in our study.

Conflict of interest

The authors declare that the research was conducted in the absence of any commercial or financial relationships that could be construed as a potential conflict of interest.

Publisher's note

All claims expressed in this article are solely those of the authors and do not necessarily represent those of their affiliated organizations, or those of the publisher, the editors and the reviewers. Any product that may be evaluated in this article, or claim that may be made by its manufacturer, is not guaranteed or endorsed by the publisher.

References

Amin Al Olama, A., Wason, J., Tuladhar, A., van Leijsen, E., Koini, M., Hofer, E., et al. (2020). Simple MRI score aids prediction of dementia in cerebral small vessel disease. *Neurology* 94, e1294–e1302.

Ashburner, J. (2007). A fast diffeomorphic image registration algorithm. *Neuroimage* 38, 95–113.

Aumont, E., Arguin, M., Bohbot, V., and West, G. (2019). Increased flanker task and forward digit span performance in caudate-nucleus-dependent response strategies. *Brain Cogn.* 135:103576. doi: 10.1016/j.bandc.2019.05.014

Bansal, R., and Peterson, B. (2018). Cluster-level statistical inference in fMRI datasets: The unexpected behavior of random fields in high dimensions. *Magn. Reson. Imaging* 49, 101–115.

Baum, G., Cui, Z., Roalf, D., Ciric, R., Betzel, R., Larsen, B., et al. (2019). Development of structure–function coupling in human brain networks during youth. *Proc. Natl. Acad. Sci. U. S. A.* 117, 771–778.

Benedict, R., DeLuca, J., Phillips, G., LaRocca, N., Hudson, L., and Rudick, R. (2017). Validity of the symbol digit modalities test as a cognition performance outcome measure for multiple sclerosis. *Multiple Sclerosis* 23, 721–733.

Bergeron, D., Flynn, K., Verret, L., Poulin, S., Bouchard, R., Bocti, C., et al. (2017). Multicenter validation of an MMSE-MoCA conversion table. *J. Am. Geriatr. Soc.* 65, 1067–1072.

Blumen, H., Jayakody, O., and Verghese, J. (2023). Gait in cerebral small vessel disease, pre-dementia, and dementia: A systematic review. *Int. J. Stroke* 18, 53–61. doi: 10.1177/17474930221114562

Butler, P., and Chiong, W. (2019). Neurodegenerative disorders of the human frontal lobes. *Handb. Clin. Neurol.* 163, 391–410.

Charidimou, A., Martinez-Ramirez, S., Reijmer, Y., Oliveira-Filho, J., Lauer, A., Roongpiboonsopit, D., et al. (2016). Total magnetic resonance imaging burden of small vessel disease in cerebral amyloid angiopathy: An imaging-pathologic study of concept validation. *JAMA Neurol.* 73, 994–1001. doi: 10.1001/jamaneurol.2016.0832

Chen, X., Wang, J., Shan, Y., Cai, W., Liu, S., Hu, M., et al. (2019). Cerebral small vessel disease: Neuroimaging markers and clinical implication. *J. Neurol.* 266, 2347–2362.

Dichgans, M., and Leys, D. (2017). Vascular cognitive impairment. *Circ. Res.* 120, 573–591.

Fazekas, F., Chawluk, J., Alavi, A., Hurtig, H., and Zimmerman, R. (1987). MR signal abnormalities at 1.5 T in Alzheimer's dementia and normal aging. *AJR* 149, 351–356.

Feng, M., Wen, H., Xin, H., Zhang, N., Liang, C., and Guo, L. (2021). Altered spontaneous brain activity related to neurologic dysfunction in patients with cerebral small vessel disease. *Front. Aging Neurosci.* 13:731585. doi: 10.3389/fnagi.2021.731585

Fluss, R., Faraggi, D., and Reiser, B. (2005). Estimation of the Youden Index and its associated cutoff point. *Biometr. J.* 47, 458–472.

Gez, S., İnce, B., Tütüncü, M., Kızıltan, G., Bakar, M., Tanriverdi, U., et al. (2022). Prevalence of clinical manifestations and neuroimaging features in cerebral small vessel disease. *Clin. Neurol. Neurosurg.* 217:107244.

Halawa, O., Gatchel, J., Amariglio, R., Rentz, D., Sperling, R., Johnson, K., et al. (2019). Inferior and medial temporal tau and cortical amyloid are associated with daily functional impairment in Alzheimer's disease. *Alzheimers Res. Ther.* 11:14. doi: 10.1186/s13195-019-0471-6

Huang, H., Nguyen, P., Schwab, N., Tanner, J., Price, C., and Ding, M. (2017). Mapping dorsal and ventral caudate in older adults: Method and validation. *Front. Aging Neurosci.* 9:91. doi: 10.3389/fnagi.2017.00091

Jenkinson, M., Bannister, P., Brady, M., and Smith, S. (2002). Improved optimization for the robust and accurate linear registration and motion correction of brain images. *Neuroimage* 17, 825–841. doi: 10.1016/s1053-8119(02)91132-8

Jokinen, H., Koikkalainen, J., Laakso, H., Melkas, S., Nieminen, T., Brander, A., et al. (2020). Global burden of small vessel disease-related brain changes on mri predicts cognitive and functional decline. *Stroke* 51, 170–178. doi: 10.1161/STROKEAHA.119.026170

Kang, Y., Chen, R., Ding, H., Li, L., Gao, J., Liu, L., et al. (2022). Structure–function decoupling: A novel perspective for understanding the radiation-induced brain injury in patients with nasopharyngeal carcinoma. *Front. Neurosci.* 16:915164. doi: 10.3389/fnins.2022.915164

Karim, H., Rosso, A., Aizenstein, H., Bohnen, N., Studenski, S., and Rosano, C. (2020). Resting state connectivity within the basal ganglia and gait speed in older adults with cerebral small vessel disease and locomotor risk factors. *Neuroimage Clin.* 28:102401. doi: 10.1016/j.nicl.2020.102401

Kim, J., and Lee, J. (2013). Integration of structural and functional magnetic resonance imaging improves mild cognitive impairment detection. *Magn. Reson. Imaging* 31, 718–732.

Klarenbeek, P., van Oostenbrugge, R., Rouhl, R., Knottnerus, I., and Staals, J. (2013). Ambulatory blood pressure in patients with lacunar stroke: Association with total MRI burden of cerebral small vessel disease. *Stroke* 44, 2995–2999.

Kreitzer, A., and Malenka, R. (2008). Striatal plasticity and basal ganglia circuit function. *Neuron* 60, 543–554.

Li, H., Jia, X., Li, Y., Jia, X., and Yang, Q. (2021). Aberrant Amplitude of Low-Frequency Fluctuation and Degree Centrality within the Default Mode Network in Patients with Vascular Mild Cognitive Impairment. *Brain Sci.* 11:1534. doi: 10.3390/brainsci11111534

Li, J., Wen, H., Wang, S., Che, Y., Zhang, N., and Guo, L. (2022). Altered brain morphometry in cerebral small vessel disease with cerebral microbleeds: An investigation combining univariate and multivariate pattern analyses. *Front. Neurol.* 13:819055. doi: 10.3389/fneur.2022.819055

Li, X., Yuan, J., Qin, W., Yang, L., Yang, S., Li, Y., et al. (2021). Higher total cerebral small vessel disease burden was associated with mild cognitive impairment and overall cognitive dysfunction: A propensity score-matched case-control study. *Front. Aging Neurosci.* 13:695732. doi: 10.3389/fnagi.2021.695732

Litak, J., Mazurek, M., Kulesza, B., Szmygin, P., Litak, J., Kamieniak, P., et al. (2020). Cerebral small vessel disease. *Int. J. Mol. Sci.* 21, 1711–1722.

Lu, J., Li, D., Li, F., Zhou, A., Wang, F., Zuo, X., et al. (2011). Montreal cognitive assessment in detecting cognitive impairment in Chinese elderly individuals: A population-based study. *J. Geriatr. Psychiatry Neurol.* 24, 184–190.

Nyatega, C., Qiang, L., Adamu, M., and Kawuwa, H. (2022). Gray matter, white matter and cerebrospinal fluid abnormalities in Parkinson's disease: A voxel-based morphometry study. *Front. Psychiatry* 13:1027907. doi: 10.3389/fpsyt.2022.1027907

Putcha, D., Brickhouse, M., Wolk, D., and Dickerson, B. (2019). Fractionating the rey auditory verbal learning test: Distinct roles of large-scale cortical networks in prodromal Alzheimer's disease. *Neuropsychologia* 129, 83–92. doi: 10.1016/j.neuropsychologia.2019.03.015

Raimo, S., Santangelo, G., D'Iorio, A., Trojano, L., and Grossi, D. (2019). Neural correlates of apathy in patients with neurodegenerative disorders: An activation likelihood estimation (ALE) meta-analysis. *Brain Imaging Behav.* 13, 1815–1834. doi: 10.1007/s11682-018-9959-0

Scarpina, F., and Tagini, S. (2017). The stroop color and word test. *Front. Psychol.* 8:557. doi: 10.3389/fpsyg.2017.00557

Shang, J., Fisher, P., Bäuml, J., Daamen, M., Baumann, N., Zimmer, C., et al. (2019). A machine learning investigation of volumetric and functional MRI abnormalities in adults born preterm. *Hum. Brain Mapp.* 40, 4239–4252. doi: 10.1002/hbm.24698

Staals, J., Makin, S., Doubal, F., Dennis, M., and Wardlaw, J. (2014). Stroke subtype, vascular risk factors, and total MRI brain small-vessel disease burden. *Neurology* 83, 1228–1234.

Su, N., Zhai, F., Zhou, L., Ni, J., Yao, M., Li, M., et al. (2017). Cerebral small vessel disease burden is associated with motor performance of lower and upper extremities in community-dwelling populations. *Front. Aging Neurosci.* 9:313. doi: 10.3389/fnagi.2017.00313

Sui, C., Wen, H., Wang, S., Feng, M., Xin, H., Gao, Y., et al. (2023). Characterization of white matter microstructural abnormalities associated with cognitive dysfunction in cerebral small vessel disease with cerebral microbleeds. *J. Affect. Disord.* 324, 259–269. doi: 10.1016/j.jad.2022.12.070

Telgte, A., Leijsen, E., Wiegertjes, K., Klijn, C., Tuladhar, A., and Leeuw, F. (2018). Cerebral small vessel disease: From a focal to a global perspective. *Nat. Rev. Neurol.* 14, 387–398.

Tzourio-Mazoyer, N., Landeau, B., Papathanassiou, D., Crivello, F., Etard, O., Delcroix, N., et al. (2002). Automated anatomical labeling of activations in SPM using a macroscopic anatomical parcellation of the MNI MRI single-subject brain. *Neuroimage* 15, 273–289.

Wardlaw, J., Smith, E., Biessels, G., Cordonnier, C., Fazekas, F., Frayne, R., et al. (2013). Neuroimaging standards for research into small vessel disease and its contribution to ageing and neurodegeneration. *Lancet Neurol.* 12, 822–838.

Wei, M., Shi, J., Li, T., Ni, J., Zhang, X., Li, Y., et al. (2018). Diagnostic accuracy of the Chinese version of the trail-making test for screening cognitive impairment. *J. Am. Geriatr. Soc.* 66, 92–99. doi: 10.1111/jgs.15135

Wen, H., Liu, Y., Rekik, I., Wang, S., Chen, Z., Zhang, J., et al. (2017). Multi-modal multiple kernel learning for accurate identification of Tourette syndrome children. *Pattern Recogn.* 63, 601–611.

Wen, H., Liu, Y., Rekik, I., Wang, S., Chen, Z., Zhang, J., et al. (2018). Combining disrupted and discriminative topological properties of functional connectivity networks as neuroimaging biomarkers for accurate diagnosis of early tourette syndrome children. *Mol. Neurobiol.* 55, 3251–3269. doi: 10.1007/s12035-017-0519-1

Xin, H., Wen, H., Feng, M., Gao, Y., Sui, C., Zhang, N., et al. (2022). Disrupted topological organization of resting-state functional brain networks in cerebral small vessel disease. *Hum. Brain Mapp.* 43, 2607–2620. doi: 10.1002/hbm.25808

Yan, C., Wang, X., Zuo, X., and Zang, Y. (2016). DPABI: Data Processing & Analysis for (Resting-State) Brain Imaging. *Neuroinformatics* 14, 339–351.

Yu-Feng, Z., Yong, H., Chao-Zhe, Z., Qing-Jiu, C., Man-Qiu, S., Meng, L., et al. (2007). Altered baseline brain activity in children with ADHD revealed by resting-state functional MRI. *Brain Dev.* 29, 83–91.

Zanon Zotin, M., Sveikata, L., Viswanathan, A., and Yilmaz, P. (2021). Cerebral small vessel disease and vascular cognitive impairment: From diagnosis to management. *Curr. Opin. Neurol.* 34, 246–257.

Zhang, X., Suo, X., Yang, X., Lai, H., Pan, N., He, M., et al. (2022). Structural and functional deficits and couplings in the cortico-striato-thalamo-cerebellar circuitry in social anxiety disorder. *Transl. Psychiatry* 12:26. doi: 10.1038/s41398-022-01791-7

Zhao, Z., Fan, F., Lu, J., Li, H., Jia, L., Han, Y., et al. (2015). Changes of gray matter volume and amplitude of low-frequency oscillations in amnestic MCI: An integrative multi-modal MRI study. *Acta Radiol.* 56, 614–621. doi: 10.1177/0284185114533329

Zhou, X., Zhang, C., Li, L., Zhang, Y., Zhang, W., Yin, W., et al. (2020). Altered brain function in cerebral small vessel disease patients with gait disorders: A resting-state functional mri study. *Front. Aging Neurosci.* 12:234. doi: 10.3389/fnagi.2020.00234

frontiers | Frontiers in Aging Neuroscience

TYPE Original Research
PUBLISHED 14 July 2023
DOI 10.3389/fnagi.2023.1163349

OPEN ACCESS

EDITED BY
Han Lv,
Capital Medical University, China

REVIEWED BY
De-Sheng Zhu,
Shanghai Jiao Tong University, China
Zezhi Li,
Guangzhou Medical University, China
Ali M. Pourbagher-Shahri,
Mashhad University of Medical Sciences, Iran

*CORRESPONDENCE
Lun-Lin Mao
✉ maolunlin2018@163.com
Wen-Ya Chen
✉ chenwenyajs@163.com

RECEIVED 10 February 2023
ACCEPTED 26 June 2023
PUBLISHED 14 July 2023

CITATION
Hua M, Ma A-J, Liu Z-Q, Ji L-L, Zhang J, Xu Y-F, Chen W-Y and Mao L-L (2023) Arteriolosclerosis CSVD: a common cause of dementia and stroke and its association with cognitive function and total MRI burden. *Front. Aging Neurosci.* 15:1163349. doi: 10.3389/fnagi.2023.1163349

Arteriolosclerosis CSVD: a common cause of dementia and stroke and its association with cognitive function and total MRI burden

Min Hua, Ai-Jin Ma, Zhi-Qing Liu, Li-Li Ji, Jin Zhang, Yuan-Feng Xu, Wen-Ya Chen* and Lun-Lin Mao*

Department of Neurology, Wujin Hospital Affiliated to Jiangsu University, The Wujin Clinical College of Xuzhou Medical University, Changzhou, Jiangsu, China

Objective: Arteriolosclerosis cerebral small vessel disease (CSVD) is a common type of CSVD. This study aimed to explore the factors associated with cognitive function and total MRI burden related to the disease.

Methods: The demographic characteristics, clinical manifestations, cognitive function score, Barthel Index (BI), blood test index, and follow-up results of arteriolosclerosis CSVD patients treated for the first time in our hospital from January 2014 to August 2022 were collected. White matter hyperintensity (WMH) Fazekas score, total MRI burden, and cerebral atrophy grade were evaluated according to brain MRI findings. Factors associated with CSVD cognitive function were analyzed by binary logistic regression. The correlative factors related to the total MRI burden of CSVD were analyzed by ordered multiple logistic regression.

Results: A total of 146 patients were included in this study, of which 132 cases (90.4%) had hypertension. There were 108 patients (74.0%) with cognitive dysfunction, 97 patients (66.4%) with balance and gait disorders, and 83 patients (56.8%) with moderate-to-severe dependence in daily life (BI $\leq$ 60 points). Of 146 patients, 79 (54.1%) completed clinical and imaging follow-ups for a median of 3 years. The number of patients with cognitive impairment and BI $\leq$ 60 points after follow-up significantly increased compared with the first admission ($P < 0.001$). There were also significant differences in total MRI burden ($P = 0.001$), WMH Fazekas score, and cerebral atrophy grade ($P < 0.001$). Mean age ($P = 0.012$), median deep WMH Fazekas score ($P = 0.028$), and median deep ($P < 0.001$) and superficial ($P = 0.002$) cerebral atrophy grade of patients with cognitive impairment at first admission were all higher than those with non-cognitive impairment. Multivariate analysis showed that deep cerebral atrophy was independently and significantly associated with cognitive impairment of CSVD ($P = 0.024$), and hypertension was significantly and independently associated with total MRI burden ($P = 0.001$).

Conclusion: The disease course of arteriolosclerosis CSVD may be related to cognitive function and total MRI burden. Deep cerebral atrophy was an independent risk factor for cognitive dysfunction in arteriolosclerosis CSVD, and hypertension was an independent risk factor for total MRI burden.

KEYWORDS

cerebral small vessel disease, white matter hyperintensities, lacunar infarcts, cerebral microbleed, cerebral atrophy, cognitive impairment

Introduction

Cerebral small-vessel disease (CSVD) refers to a series of clinical, imaging, and pathological syndromes caused by various etiologies affecting cerebral arterioles and their distal branches, arterioles, capillaries, capillary vein, and venules. The common etiological types of CSVD include arteriolosclerosis, sporadic or inherited cerebral amyloid angiopathy (CAA), other inherited cerebral small vascular lesions, inflammation, immune-mediated small vascular disease, venous collagen disease, and other small vascular diseases (Pantoni, 2010). The two most common pathologies underlying CSVD are arteriolosclerosis caused by aging, hypertension, and other conventional vascular risk factors, and CAA caused by vascular deposition of β-amyloid.

CSVD is a common cause of dementia and stroke. According to stroke classification, CSVD caused by small artery occlusion accounts for about 30% of the causes of ischemic stroke in China (Wu et al., 2019). The clinical manifestations of CSVD are heterogeneous and can be categorized into acute ischemic CSVD and chronic clinical syndrome with occult onset. Acute ischemic CSVD presents as a specific lacunar syndrome, while chronic CSVD may be asymptomatic and can be diagnosed by imaging. As the burden of CSVD increases gradually, patients may develop symptoms, such as mild cognitive dysfunction, dementia, mood disorders, motor and gait dysfunction, and urinary incontinence. CSVD is diagnosed on the basis of brain imaging biomarkers, including recent small subcortical infarct (RSSI), also known as lacunar infarct, lacune of vascular origin, white matter hyperintensity (WMH) of vascular origin, perivascular space (PVS), cerebral microbleed (CMB), and cerebral atrophy (Wardlaw et al., 2013b). Other imaging features include intracerebral hemorrhage due to single perforator artery lesions, iron deposition on the cortical surface, and cortical microinfarction. Four closely related features on brain MRI, including lacunar, WMH, CMB, and enlarged PVS, are markers of CSVD (Pantoni, 2010; Wardlaw et al., 2013a). Cerebral atrophy may also be associated with CSVD (Appelman et al., 2009; Nitkunan et al., 2011; Aribisala et al., 2013). Individual CSVD features are also associated with vascular risk factors (Ovbiagele and Saver, 2006; Vermeer et al., 2007; Greenberg et al., 2009; Doubal et al., 2010).

CSVD usually has both clinical and imaging manifestations, while CSVD imaging markers may not be accompanied by clinical manifestations. Even in the presence of objective clinical features, these radiological features of CSVD are important, being strong predictors of both stroke and dementia risk. Currently, most studies pay more attention to non-acute with cognitive and gait disorders as clinical manifestations and non-acute CSVD imaging markers without obvious clinical manifestations. Few studies have focused solely on arteriolosclerosis CSVD in combination with these features of CSVD. Therefore, we collected clinical information, imaging data, and follow-up results of previously diagnosed CSVD and used the "CSVD imaging total MRI burden score" to evaluate global brain injury (Klarenbeek et al., 2013; Staals et al., 2014) and the predefined visual standards from the Cardiovascular Health Study to assess cerebral atrophy (Manolio et al., 1994; Yue et al., 1997), to analyze risk factors, clinical features, and imaging features of arteriolosclerosis CSVD, and to explore the correlative aspects of cognitive function and total MRI burden in arteriolosclerosis CSVD.

Recent studies have shown that intensive blood pressure lowering to a systolic of 120 mmHg was associated with both reduced WHM progression (SPRINT MIND Investigators for the SPRINT Research Group et al., 2019a) and a reduction in the combined endpoint of mild cognitive impairment and dementia (SPRINT MIND Investigators for the SPRINT Research Group et al., 2019b). However, this study is a single-center retrospective study on the case data of arteriolosclerosis CSVD, and no further analysis was made on the control of conventional vascular risk factors. Therefore, as in other areas of stroke research, large international collaborative ventures are vital to take the field forward, and the need for large-scale prospective randomized controlled trials of arteriolosclerosis CSVD to demonstrate whether control of other risk factors reduces total MRI burden and delays the onset of cognitive impairment.

Methods

Subjects

This was a retrospective study. From January 2014 to August 2022, 146 patients with arteriolosclerosis CSVD were first hospitalized in Wujin Hospital affiliated to Jiangsu University, and were included in this study. Inclusion criteria included brain MRI indicating at least one of the following manifestations: (1) RSSI: neuroimaging evidence of recent infarction in the territory of one perforating arteriole, with imaging features or clinical symptoms consistent with a lesion occurring in the previous few weeks, the maximum diameter of lesion <20 mm in the axial plane. (2) Lacune of vascular origin: a round or ovoid, subcortical, fluid-filled cavity (signal similar to CSF) of between 3 mm and about 15 mm in diameter, consistent with a previous acute small subcortical infarct or hemorrhage in the territory of one perforating arteriole. (3) WMH of vascular origin: signal abnormality of variable size in the white matter that shows hyperintensity on T2-weighted images such as fluid-attenuated inversion recovery, without cavitation (signal different from CSF). Lesions in the subcortical gray matter or brainstem are not included in this category. (4) CMB: small (generally 2–5 mm in diameter, but sometimes up to 10 mm) areas of the signal void with associated blooming seen on T2*-weighted MRI or other sequences that are sensitive to susceptibility effects. (5) PVS: fluid-filled spaces that follow the typical course of a vessel as it goes through gray or white matter. The spaces have a signal intensity similar to CSF on all sequences. Because they follow the course of penetrating vessels, they appear linear when imaged parallel to the course of the vessel, and round or ovoid, with a diameter generally smaller than 3 mm, when imaged perpendicular to the course of the vessel. (6) Cerebral atrophy: a lower brain volume that is not related to a specific macroscopic focal injury such as trauma or infarction. Exclusion criteria included the following: (1) symptomatic intracranial or extracranial large artery (diameter > 2 mm) stenosis and occlusions, asymptomatic extracranial carotid artery stenosis ≥ 70%; (2) non-lacunar infarction (infarct lesion with maximum diameter > 20 mm) caused by large vascular lesions (intracranial or extracranial large artery stenosis and

occlusions) or cardiogenic embolism, cerebral amyloid vascular disease, aneurysms or arteriovenous malformations, and other cerebral bleeds; (3) special causes of white matter lesions (multiple sclerosis, sarcoidosis, radiotherapy); (4) brain lesions (such as from Alzheimer's disease, dementia with Lewy bodies, frontotemporal dementia, Parkinson's disease, tumors, hydrocephalus, trauma, syphilis, acquired immune deficiency syndrome, and Creutzfeldt–Jakob disease); (5) severe mental illness, epilepsy, alcohol or drug abuse, intoxication, and metabolic abnormalities; and (6) inflammation- or immune-mediated small cerebral vascular disease, venous collagen disease, or hereditary CSVD.

All patients had well-documented medical histories, complete laboratory examinations (routine blood tests and biochemical indicators), and brain MRI, CT angiography, or magnetic resonance angiography examinations. In this study, all personal identifiers were removed or anonymized during data collection and analysis to protect the privacy of the participants. The study was conducted under the Declaration of Helsinki, and all participants provided informed consent.

General patient characteristics

General characteristics of all patients were collected based on medical records, including age, sex, education, body mass index (BMI), smoking, hypertension, diabetes, hypercholesterolemia, hyperhomocysteinemia, stroke, transient ischemic attack, ischemic heart disease, and history of atrial fibrillation. Hypertension was defined as blood pressure $\geq$ 140/90 mmHg, diabetes as fasting blood glucose $\geq$ 7.0 mmol/L, hypercholesterolemia as total cholesterol $\geq$ 5.18 mmol/L or LDL cholesterol $>$ 3.12 mmol/L, hyperhomocysteinemia as homocysteine (Hcy) $>$ 15 μmol/L, ischemic heart disease as myocardial infarction, angina, or evidence of myocardial ischemia on the electrocardiogram (ECG), atrial fibrillation as previously diagnosed or found on the ECG, and smoking as currently smoking. At the same time, the main clinical manifestations (core symptoms) of all patients were recorded, and laboratory tests were performed within 7 days after admission, including routine blood tests, liver and kidney function, fasting blood glucose, blood lipid, folic acid, vitamin B12, and homocysteine. Cerebrovascular status was assessed by carotid Doppler ultrasound, CTA, or MRA. Asymptomatic extracranial carotid stenosis $<$ 70% of the patients were still enrolled in the study. The Barthel Index (BI) scale was used to evaluate the activities of daily living (ADL), with a score ranging from 0 to 100 and a higher score indicating greater independence (Pistoia et al., 2016). Self-care ability was divided into four levels: severe dependence, moderate dependence, mild dependence, and no dependence. A BI score $\leq$ 40 indicated severe dependence, 41–60 indicated moderate dependence, 61–99 indicated mild dependence, and 100 indicated no dependence. The Mini-Mental State Examination (MMSE) was used to evaluate cognitive function, and the MMSE points for cognitive impairment screening were 17 for illiterate, 20 for individuals with 1–6 years of education, and 24 for individuals with 7 or more years of education (Li et al., 2016).

Brain MRI analysis

All patients completed a brain MRI examination (1.5T, Siemens, Germany), including axial diffusion-weighted imaging (DWI) scan, with a pulse repetition time (TR), 3,000 milliseconds; echo time (TE), 79.5 milliseconds; thickness, 5 mm; gap, 1.5 mm; and matrix, 210 × 256; axial T1-weighted imaging (T1WI) scan, with TR, 451 milliseconds; TE, 12.5 milliseconds; thickness, 5 mm; gap, 1.5 mm; and matrix, 214 × 352; axial T2-weighted imaging (T2WI) scan, with TR, 4,500 milliseconds; TE, 82.9 milliseconds; thickness, 5 mm; gap, 1.5 mm; and matrix, 233 × 384; axial fluid-attenuated inversion recovery (FLAIR) scan, with TR, 8,000 milliseconds; TE, 75.9 milliseconds; thickness, 5 mm; gap, 1.5 mm; and matrix, 155 × 256; and axial susceptibility weighted imaging (SWI) scan, with TR, 50.1 milliseconds; TE, 40 milliseconds; thickness, 4 mm; gap, 2 mm; and matrix, 194 × 320. All axial scan planes were parallel to the anterior commissure–posterior commissure (AC/PC) line.

All MRI images were assessed blinded to clinical information by one experienced neuroradiologist and one neurologist for the presence, location, and size of the recent symptomatic infarct and any other vascular lesions. (1) RSSI: the imaging features were round or ovoid lesions located in the area of perforating arteries, with low signal on the T1WI sequence, with a hyperintense area on DWI, T2WI, and FLAIR. The diameter of the lesions was 3–20 mm. The lesions were mainly distributed in the basal ganglia, internal capsule, centrum semiovale, or brainstem. (2) Lacune: a round or ovoid, in the basal ganglia, internal capsule, centrum semiovale, or brainstem, a fluid-filled cavity of between 3 mm and about 15 mm in diameter, with a CSF signal intensity on T1WI, T2WI, and FLAIR, generally with a hyperintense rim on FLAIR and no increased signal on DWI. (3) WMH: in the early stage, it was a small cap lesion in the frontal lobe and the occipital horn. The progression of the lesion may extend to the subcortical white matter area and fuse, showing abnormal signals of varying sizes in the white matter area of the brain. It offers a high signal on T2WI and FLAIR and an equal or low signal on T1WI. (4) CMB: with the paramagnetic properties of hemosiderin-containing blood breakdown products. Small round or ovoid lesion, well-defined, and homogenous signal loss foci were seen on SWI in the cerebellum, brainstem, basal ganglia, white matter, or cortico-subcortical junction. However, it was not visible on FLAIR, T1WI, and T2WI. The diameter ranges from 2 to 5 mm, with a maximum of 10 mm, differentiated from vessel flow voids and mineral depositions in the globi pallidi. (5) PVS: they appeared round in the axial section and linear if in longitudinal sections and were smaller than 3 mm wide. They were of high signal on T2WI and low signal on T1WI and FLAIR sequences. They were distinguished from lacunes by the latter's large size (more than 3 mm and spheroid shape). PVS mainly occurred in the basal ganglia, subcortical, and brain stem, but rarely in the cerebellum. (6) Cerebral atrophy: it was classified as both deep (enlargement of the ventricles) and superficial (enlargement of the sulci), and MRI showed that the brain volume was reduced, the ventricle was enlarged, and the sulci and gyrus were widened.

Total MRI burden score of CSVD

A score scale proposed by Staals et al. (2014) was used to comprehensively evaluate the total MRI burden of CSVD, including the lacune, WMH, CMB, and PVS, the four most typical CSVD imaging findings. Deep and periventricular WMH were coded according to the Fazekas scale from 0 to 3 (Fazekas et al., 1987). Periventricular WMH scoring was 0 = no lesions; 1 = cap or pencil thin-layer lesions; 2 = the lesion showed a smooth halo; and 3 = irregular periventricular WMH extending into the deep white matter. Deep WMH scoring was 0 = no lesions; 1 = spotty lesions; 2 = the lesions were beginning to fuse; and 3 = large area fusion of lesions. PVS in both the basal ganglia and centrum semiovale were coded with the following scale applied to standard axial images (Doubal et al., 2010): 0 = no PVS; 1 = <10 PVS; 2 = 11–20 PVS; 3 = 21–40 PVS; and 4 = >40 PVS. The numbers refer to PVS on one side of the brain; the higher score was used if there was an asymmetry between the sides, and PVS was counted in the slice with the highest number. The total MRI burden of CSVD on an ordinal scale from 0 to 4 by measuring the presence of each of the four MRI features of CSVD. A point was awarded for each of the following: the presence of lacunes and CMB, defined as the presence of one or more lacunes (1 point if present) or any CMB (1 point if present). The presence of PVS was counted if there were moderate-to-severe (grade 2–4) PVS in the basal ganglia (1 point if present). The presence of WMH was defined as either (early) confluent deep WMH (Fazekas score 2 or 3) or irregular periventricular WMH extending into the deep white matter (Fazekas score 3, 1 point if present).

Cerebral atrophy assessment

Cerebral atrophy is characterized by reduced brain volume and is not associated with local volume reduction caused by brain trauma and cerebral infarction. Cerebral atrophy was classified as either deep (enlargement of the ventricles) or superficial (enlargement of the sulci). Reduced brain volume, enlarged ventricles, and widened sulci were seen on brain MRI. The sulcal prominence and ventricular size in each individual were assessed on a semiquantitative 10-point scale (grades of 0–9) using predefined visual standards from the Cardiovascular Health Study (Manolio et al., 1994; Yue et al., 1997). According to the T1-weighted images for grading ventricular and sulcal size, the atrophy grade is determined by visual comparison with templates indicating normal to atrophied brains obtained in Cardiovascular Health Study, sulcal widening and a ventricular size ranging from small and presumably normal (grade 1) to severe enlargement (grade 8). Studies considered having sulci or ventricles smaller than those in grade 1 received a grade of 0, and those worse than grade 8 received a grade of 9.

Statistical analysis

Continuous variables were described as means ± standard deviations or medians (interquartile ranges, IQR) based on whether data were normally distributed or not. Categorical variables were presented as frequencies and percentages. Two independent sample *t*-test, the Wilcoxon rank sum test and the chi-square test, were used to compare the differences between patients with cognitive impairment and non-cognitive impairment at the first admission. Paired-samples *t*-test, Wilcoxon rank sum test and chi-square test were used to compare the differences in clinical and imaging characteristics between the first admission and follow-up. The binary logistic regression analysis was subsequently performed to identify the independent risk factors for CSVD cognitive impairment, of which those variables with $P < 0.05$ in the univariate analysis and clinical parameters that may be closely related to CSVD cognitive impairment in light of clinical experience and previous research were included, such as age, sex, history of TIA or stroke, WMH, total MRI burden, cerebral atrophy, and risk factors that are frequently associated with individual features of arteriolosclerosis CSVD, i.e., hypertension, diabetes mellitus, and hyperhomocysteinemia. Finally, we performed univariate and multivariable ordinal logistic regression analyses related to the total MRI burden with age, sex, smoking, history of TIA or stroke, cerebral atrophy, hypertension, diabetes mellitus, hyperhomocysteinemia, and hypercholesterolemia, and the results were expressed as odds ratio (OR) and 95% confidence interval (CI). Analyses were performed with SPSS version 21.0, and statistical significance was set at $P < 0.05$.

Results

Patients' characteristics

A total of 146 patients with arteriolosclerosis CSVD were enrolled in this study from January 2014 to August 2022. The mean age of the patients was 75.13 ± 8.93 years old (age range: 46–100 years old), 88 cases (60.3%) were male, 132 cases (90.4%) were complicated with hypertension, 40 patients (27.4%) presented with diabetes mellitus, 27 cases (18.5%) presented with hypercholesterolemia, 71 cases (48.6%) presented with hyperhomocysteinemia, and 57 patients (39.0%) were overweight. There were 17 cases (11.6%) with asymptomatic extracranial carotid artery stenosis on the first admission. There were 123 cases (84.2%) of transient ischemic attack (TIA) or stroke in previous or first diagnosis (Table 1), including 100 cases (68.5%) of TIA or cerebral infarction, eight cases (5.5%) of cerebral hemorrhage, and 15 cases (10.3%) of cerebral infarction and cerebral hemorrhage. The median NIHSS score for patients with cerebral infarction admitted for the first time was 3 (IQR 2–4).

Clinical manifestation

At the first admission of all patients, 97 patients (66.4%) had balance and gait disorders, 69 patients (47.3%) had limb weakness, 65 patients (44.5%) had speech disorders, and 25 patients (17.1%) had dizziness or headache. Additionally, 12 patients (8.2%) had emotional and behavioral abnormalities, and 11 patients (7.5%) had dysphagia. According to the ADL assessment, 83 patients

TABLE 1 Clinical and imaging characteristics of all patients at first admission.

Characteristics	All patients ($n = 146$)	Cognitive impairment patients ($n = 108$)	Non-cognitive impairment patients ($n = 38$)	*P*
Age, y	75.13 ± 8.93	76.22 ± 8.32	72.03 ± 9.95	0.012
Male sex	88 (60.3)	64 (59.3)	24 (63.2)	0.673
BMI (overweight)	57 (39.0)	42 (38.9)	15 (39.5)	0.949
BI ≤ 60 points	83 (56.8)	73 (67.6)	10 (26.3)	0.000
Ischemic heart disease	6 (4.1)	6 (5.6)	0 (0.0)	0.313
Diabetes mellitus	40 (27.4)	27 (25.0)	13 (34.2)	0.274
Hypertension	132 (90.4)	98 (90.7)	34 (89.5)	1.000
Atrial fibrillation	7 (4.8)	7 (6.5)	0 (0.0)	0.243
Smoking	32 (21.9)	23 (21.3)	9 (23.7)	0.760
Hyperhomocysteinemia	71 (48.6)	54 (50.0)	17 (44.7)	0.577
Hypercholesterolemia	27 (18.5)	22 (20.4)	5 (13.2)	0.325
Hyperuricemia	27 (18.5)	18 (16.7)	9 (23.7)	0.338
Chronic renal insufficiency	27 (18.5)	22 (20.4)	5 (13.2)	0.325
Folate deficiency	21 (14.4)	18 (16.7)	3 (7.9)	0.185
Vitamin B12 deficiency	19 (13.0)	16 (14.8)	3 (7.9)	0.418
Asymptomatic extracranial carotid artery stenosis (<70%)	17 (11.6)	12 (11.1)	5 (13.2)	0.965
Anemia	19 (13.0)	17 (15.7)	2 (5.3)	0.170
History of TIA or stroke	123 (84.2)	91 (84.3)	32 (84.2)	0.994
MRI feature				
Lacune	144 (98.6)	108 (100.0)	36 (94.7)	0.066
CMB	136 (93.2)	100 (92.6)	36 (94.7)	0.939
PVS (grade 2–4)	73 (50.0)	53 (49.1)	20 (52.6)	0.706
Periventricular WMH Fazekas score	3 (3–3)	3 (3–3)	3 (2–3)	0.150
Deep WMH Fazekas score	2 (1–2)	2 (1–2)	1 (1–2)	0.028
Total MRI burden score	3 (3–4)	3 (3–4)	3 (3–4)	0.226
Superficial cerebral atrophy grade	4 (3–5)	4 (3–5)	2 (2–4)	0.002
Deep cerebral atrophy grade	5 (4–6)	5 (4–6)	4 (3–5)	0.000

BMI, body mass index; BI, Barthel index; hsCRP, high-sensitivity C-reactive protein; TIA, transient ischemic attack; MRI, magnetic resonance imaging; CMB, cerebral microbleed; PVS, perivascular space; WMH, white matter hyperintensity. Data presented as mean ± SD or number (%) or median (interquartile range).

(56.8%) had moderate-to-severe dependence in daily life (BI ≤ 60). MMSE assessment indicated that 108 patients (74.0%) had cognitive impairment (Table 2).

Brain MRI manifestations and total MRI burden

A brain MRI analysis of all patients at the first admission revealed that 73 cases (50.0%) had RSSI, six cases (4.1%) had a cerebral hemorrhage, 144 cases (98.6%) had lacune, and 136 cases (93.2%) had CMB. Meanwhile, 73 patients (50.0%) had PVS (grade 2–4), 145 cases (99.3%) had WMH, the total WMH Fazekas score median was 5 (IQR 4–5), and the periventricular WMH Fazekas score median was 3 (IQR 3–3). The median deep WMH Fazekas score was 2 (IQR 1–2). The median score of total MRI burden was 3 (IQR 3–4) points, including 53 cases (36.3%) with four points, 80 patients (54.8%) with three points, and 13 cases with two points (8.9%). Furthermore, 146 cases (100.0%) all had different degrees of cerebral atrophy according to the visual standards from the Cardiovascular Health Study, with a median superficial cerebral atrophy grade of 4 (IQR 3–5) and a median deep cerebral atrophy grade of 5 (IQR 4–6) (Table 1).

10.3389/fnagi.2023.1163349

TABLE 2 Clinical manifestation of all patients at first admission.

Characteristics	All patients ($n = 146$)
Core symptoms	
Cognition impairment	108 (74.0)
Balance and gait disorder	97 (66.4)
Limb weakness	69 (47.3)
Speech disorder	65 (44.5)
Dizziness or headache	25 (17.1)
Emotional and behavioral abnormalities	12 (8.2)
Dysphagia	11 (7.5)
Sensory disorder	7 (4.8)
Disturbance of consciousness or seizures	5 (3.4)
Bowel and urination disorders	4 (2.7)
Visual impairment	2 (1.4)
BI	
100 points	14 (9.6)
61–69 points	49 (33.6)
41–60 points	42 (28.8)
≤40 points	41 (28.1)

BI, Barthel index.

Comparison of clinical and imaging characteristics of patients at first admission and follow-up

There were 79 (54.1%) patients who completed clinical and imaging follow-up for more than 6 months, of which 75 patients had hypertension. The median clinical and imaging follow-up was 3 (IQR 2–5) years, with 48 patients followed up for more than 3 years and 28 patients followed up for more than 5 years. During the follow-up period, 32 cases (32/79, 40.5%) had an average of one to three TIA or stroke events, of which one case had TIA, 29 patients had a new small infarction with a median NIHSS score of 4 (IQR 2–4), and two cases had a cerebral hemorrhage. After a median follow-up of 3 years, the average age of patients increased significantly and the number of patients with cognitive impairment was significantly higher than at the time of initial admission (70/79 vs. 54/79, $P < 0.001$). There was also a significant increase in the number of people with moderate-to-severe dependence on daily living requirements compared with the first admission (64/79 vs. 41/79, $P < 0.001$). During follow-up, the WMH range and the degree of cerebral atrophy progressed with the prolongation of the disease course (Figure 1). At follow-up, although the periventricular and deep WMH Fazekas scores and median total MRI burden scores were the same as those at first admission, the overall distribution of the total MRI burden ($P = 0.001$) and the WMH Fazekas score ($P < 0.001$) were significantly different. The median of deep and superficial cerebral atrophy grades was significantly higher than that at the first admission ($P < 0.001$) (Table 3).

TABLE 3 Comparison of clinical and imaging characteristics of patients at the first admission and follow-up.

Characteristics	First admission patients ($n = 79$)	Follow-up patients ($n = 79$)	*P*
Age	71.75 ± 8.94	75.55 ± 9.86	0.000
Cognition impairment	54 (68.4)	70 (88.6)	0.000
BI ≤ 60 points	41 (51.9)	64 (81.0)	0.000
Lacune	79 (100.0)	79 (100.0)	–
WMH	79 (100.0)	79 (100.0)	–
CMB	75 (94.9)	75 (94.9)	1.000
PVS (grade 2–4)	38 (48.1)	39 (49.4)	1.000
Periventricular WMH Fazekas score	3 (2–3)	3 (3–3)	0.000
Deep WMH Fazekas score	2 (1–2)	2 (2–3)	0.000
Total MRI burden score	3 (3–4)	3 (3–4)	0.001
4 points	25 (31.6)	34 (43.0)	0.004
≤3 points	54 (68.4)	45 (57.0)	
Superficial cerebral atrophy grade	3 (3–4)	5 (4–5)	0.000
Deep cerebral atrophy grade	5 (4–6)	6 (5–7)	0.000

BI, Barthel index; CMB, cerebral microbleed; WMH, white matter hyperintensity; PVS, perivascular space; MRI, magnetic resonance imaging.
Data presented as mean ± SD or number (%) or median (interquartile range).

Comparison of clinical characteristics between patients with cognitive impairment and non-cognitive impairment at the first admission

The mean age of the patients with cognitive impairment at first admission was 76.22 ± 8.32 years, which was higher than those with non-cognitive impairment (72.03 ± 9.95 years, $P = 0.012$). The proportion of severely dependent patients (BI ≤ 60) with cognitive impairment was significantly higher than those with non-cognitive impairment ($P < 0.001$). There were no significant differences in total MRI burden scores between the two groups ($P = 0.226$), but the median deep WMH Fazekas score ($P = 0.028$), deep ($P < 0.001$), and superficial ($P = 0.002$) cerebral atrophy grades of patients with cognitive impairment at first admission were all higher than those with non-cognitive impairment. There were no significant differences in other clinical characteristics (Table 1). In multivariate analysis, deep cerebral atrophy was independently and significantly associated with cognitive impairment after correction for important confounders, including vascular risk factors, age, WMH, and total MRI burden ($P = 0.024$) (Table 4).

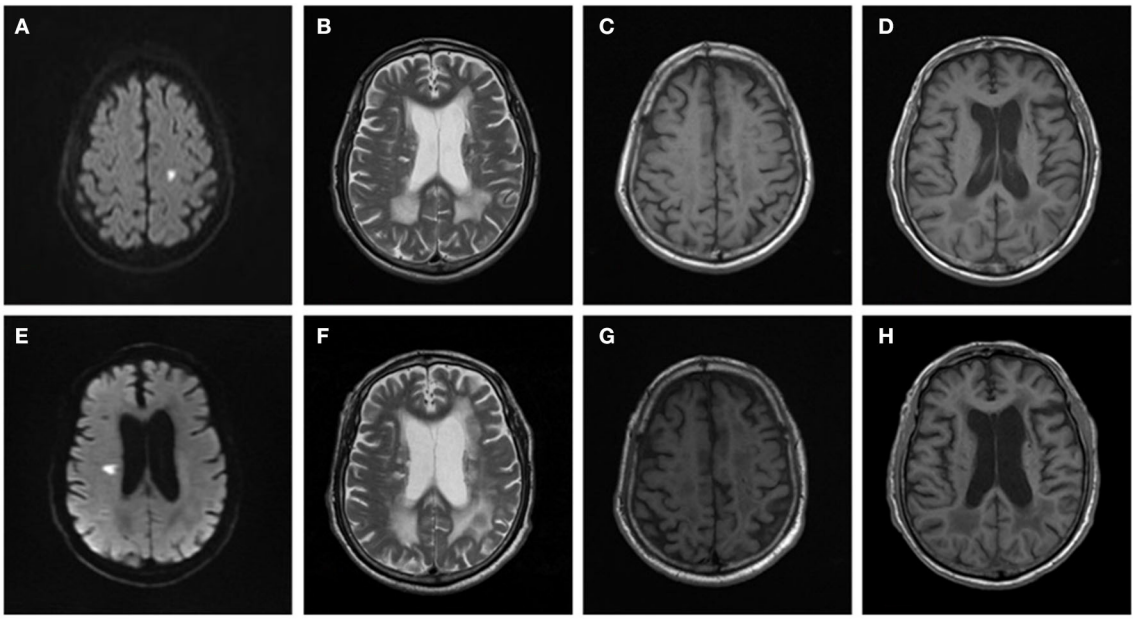

FIGURE 1
Brain MRI changes in a patient with arteriolosclerosis CSVD. Male, 66 years old, was admitted to the hospital due to right limb weakness for 2 days in 2014. Brain MRI: **(A)** DWI showed a small flake of high signal in the left centrum semiovale. **(B)** T2WI showed irregular hyperintensity near the ventricle. **(C, D)** T1WI showed enlargement of the sulci and slight enlargement of the ventricles. In 2018, the patient was readmitted to the hospital due to dysarthria and left limb weakness for 1 day. Brain MRI: **(E)** DWI showed a small flake of high signal near the right lateral ventricle. **(F)** T2WI, the range of irregular hyperintensity near the ventricle was enlarged and extended to deep white matter with large area fusion. **(G, H)** T1WI showed enlargement of the sulci and enlargement of the ventricles, which made progress compared with 2014.

TABLE 4 Multivariate analysis of cognitive impairment associated with CSVD.

Factors	*P*	OR (95% CI)
Age	0.735	1.175 (0.462–2.983)
Male sex	0.416	1.022 (0.969–1.078)
Hypertension	0.588	1.532 (0.328–7.166)
Diabetes mellitus	0.251	0.599 (0.250–1.435)
Hyperhomocysteinemia	0.870	1.073 (0.462–2.494)
Periventricular WMH	0.581	0.757 (0.281–2.037)
Deep WMH	0.271	1.437 (0.754–2.738)
Total MRI burden	0.484	1.303 (0.621–2.730)
Superficial cerebral atrophy	0.068	1.481 (0.971–2.260)
Deep cerebral atrophy	0.024	1.491 (1.054–2.109)
History of TIA or stroke	0.557	0.707 (0.223–2.245)

CSVD, cerebral small vessel disease; CI, confidence interval; OR, odds ratio; WMH, white matter hyperintensity; MRI, magnetic resonance imaging; TIA, transient ischemic attack. Multivariable analysis with correction for all variables in the table.

Univariate and multivariate analyses of the total MRI burden

In univariate analysis, the total MRI burden of CSVD was associated with smoking (OR 2.192, 95% CI 1.010–4.754, $P = 0.047$) and hypertension (OR 4.904, 95% CI 1.547–15.549, $P = 0.007$). However, there was no significant association with sex, age, diabetes, hypercholesterolemia, hyperhomocysteinemia, TIA or stroke history, or cerebral atrophy. In multivariable analysis, after correction for important confounders, including vascular risk factors, age, smoking, and cerebral atrophy, hypertension was significantly and independently associated with total MRI burden in arteriolosclerosis CSVD (OR 7.338, 95% CI 2.175–24.730, $P = 0.001$) and the association for hypertension becoming stronger in multivariable than in univariate testing (Table 5).

Discussion

Small cerebral vascular disease is an age-related disease, with its prevalence increasing with age. It affects about 5% of people aged 50 to almost 100% of people over 90 years old. Additionally, 25% of strokes and 45% of dementia are caused by CSVD (Cannistraro et al., 2019). Arteriolosclerosis CSVD is the most common type of CSVD. It is well-known that hypertension is a major risk factor for CSVD (Veglio et al., 2009; Meissner, 2016). This study summarized the clinical characteristics of patients with arteriolosclerosis CSVD, whose average age was over 75 years old, and found that hypertension was the main intervention risk factor. In addition, 84.2% of patients had a history of TIA or stroke, mainly in the form of subcortical infarction. This suggests a higher risk of TIA or stroke events in arteriolosclerosis CSVD. Most patients with CSVD have occult onset and various clinical manifestations, including asymptomatic CSVD, lacunar syndrome, and cognitive impairment. The presence and severity of the patient's symptoms depend on the location, extent, and number of

TABLE 5 Univariate and multivariate analysis of the total MRI burden.

Factors	Univariate		Multivariate	
	P	OR (95% CI)	*P*	OR (95% CI)
Male sex	0.058	1.898(0.979–3.677)	0.119	1.921(0.845–4.371)
Age	0.724	1.006(0.971–1.043)	0.481	1.016(0.971–1.063)
Smoking	0.047	2.192(1.010–4.754)	0.160	1.923(0.773–4.787)
Hypertension	0.007	4.904(1.547–15.549)	0.001	7.338(2.175–24.730)
Diabetes mellitus	0.891	0.951(0.467–1.937)	0.735	0.880(0.418–1.850)
Hypercholesterolemia	0.933	0.966 (0.427–2.184)	0.778	1.145(0.447–2.930)
Hyperhomocysteinemia	0.354	1.351(0.715–2.552)	0.555	1.230(0.618–2.447)
History of TIA or stroke	0.995	1.003(0.420–2.392)	0.476	0.705(0.270–1.842)
Superficial cerebral atrophy	0.194	1.202(0.911–1.584)	0.208	1.220(0.895–1.664)
Deep cerebral atrophy	0.177	1.165(0.933–1.456)	0.397	1.116(0.865–1.441)

CSVD, cerebral small vessel disease; CI, confidence interval; OR, odds ratio; TIA, transient ischemic attack.
Multivariable analysis with correction for all variables in the table.

lesions. In this study, cognitive impairment was the primary clinical manifestation of CSVD, followed by balance and gait disorder, and with the prolongation of the disease, patients' ADL gradually decreased. Studies have shown that CSVD cognitive dysfunction can present a characteristic pattern of cognitive decline; that is, it has a characteristic early involvement in the areas of attention, processing speed, and executive function, and memory function is relatively intact, which can progress to mild cognitive impairment and vascular dementia (Sachdev et al., 2014). Therefore, attention should be paid to patients with cognitive and gait disorders in clinical practice to identify CSVD as early as possible.

The recurrence rate of stroke caused by CSVD is slightly lower than that caused by atherosclerosis of large vessels. The 1-year recurrence rate of stroke caused by CSVD with hypertension is 14%, while the recurrence rate of stroke caused by CSVD without hypertension is 9.3% (Wang et al., 2013). A total of 79 patients in this study completed clinical and imaging follow-up for more than 6 months, of which 75 patients had hypertension. The median clinical and imaging follow-up was 3 (IQR 2–5) years, and during the follow-up period, 32 cases (40.5%) had an average of one to three TIA or stroke events, which also indicated that arteriolosclerosis CSVD with hypertension had a high risk of stroke. In addition, as the disease course progressed, the incidence of cognitive impairment and reduced ability to schedule life also increased gradually. The total MRI burden, WMH Fazekas score, and cerebral atrophy grade also showed significant changes. Therefore, we speculate that the course of arteriolosclerosis CSVD may be related to cognitive function and total MRI burden.

In this study, the mean age, the deep WMH Fazekas score, and the deep and superficial cerebral atrophy grades of patients with cognitive dysfunction were significantly higher than those without cognitive dysfunction. At the same time, the degree of life dependence of patients with cognitive dysfunction was significantly higher than that of patients with non-cognitive dysfunction. After adjusting for age and other factors, deep cerebral atrophy was independently associated with cognitive dysfunction. Several different grading scales are used for the assessment of cerebral atrophy, including medial temporal atrophy (Scheltens et al., 1992), posterior cerebral atrophy (Koedam et al., 2011), and global cortical atrophy (Pasquier et al., 1996). Because arteriolosclerosis CSVD affects the entire brain, not just part of it, the CHS scale was used in this study to assess the entire superficial cortex and deep cerebral atrophy. While many studies have reported cerebral atrophy associated with CSVD, it is not specific to CSVD and occurs in many other conditions, including normal aging. However, several studies have suggested that cerebral atrophy is a marker of CSVD and modulates the effect of vascular disease on cognition (Levy-Cooperman et al., 2008; Carmichael et al., 2010; Wardlaw et al., 2013b). Other studies reported cerebral atrophy caused by CSVD is a predictor of cognitive dysfunction in CSVD patients (Viswanathan et al., 2010). This study also indicated that cerebral atrophy was closely related to cognitive dysfunction in CSVD patients. However, a visual analog scale was used to evaluate cerebral atrophy, and quantitative brain volume measurements may be required to explore this issue further.

For CSVD, the diagnostic specificity of any single imaging marker is low, and the high MRI burden score may better reflect the overall effect of CSVD on the brain than considering one or two features alone. For example, WMH usually occurs in white matter, while lacune occurs in deep gray matter. Therefore, the total MRI burden score was also used in this study to improve the specificity of CSVD diagnosis. Total MRI burden score was positively correlated with the severity of CSVD, and a study has shown that a higher total MRI CSVD burden was associated with overall cognitive impairment. It was shown that the total MRI CSVD burden score was negatively correlated with the overall MMSE and Montreal Cognitive Assessment Scale (Li et al., 2021). However, there was also a study indicating that no association was found between total MRI burden score and cognitive declines (Hu et al., 2022). Similarly, in this study, there was no significant difference in the total MRI CSVD burden score between the cognitive impairment group and the non-cognitive impairment group. Maybe it will also require a larger sample size research to further explore the correlation between total MRI burden and cognitive impairment.

When analyzing factors associated with total MRI burden in arteriolosclerosis CSVD, hypertension was determined to be an independent risk factor. Yang et al. (2018) found that 24-h day and night systolic blood pressure (SBP) levels and SBP variability were positively related to CSVD burden. Higher SBP levels and SBP variability were independent risk factors for CSVD. Recent studies have also shown that blood pressure variability was associated with a high MRI burden of CSVD imaging markers, especially WMH (Ma et al., 2020). However, the underlying pathophysiological mechanisms between blood pressure levels and the MRI burden of CSVD are complicated and still not fully understood. Studies have confirmed that increased permeability of small vascular walls and the blood–brain barrier contributes to the development of CSVD, and reports have associated CSVD with microvascular endothelial cells and tight junction damage (Pantoni, 2010; Wardlaw et al., 2013a). Higher blood pressure and ambulate blood pressure variability (ABPV) can lead to increased mechanical stress on the vessel wall, resulting in endothelial damage and atherosclerosis (Schillaci et al., 2012; Diaz et al., 2013). Therefore, it has been suggested that higher blood pressure and ABPV promote the development of CSVD through endothelial cell damage (Yang et al., 2018). This study also found that hypertension was independent of the total MRI burden of CSVD, but failed to explore the influence of blood pressure and ABPV on CSVD, which still needs to be investigated by prospective clinical studies and animal experiments with a larger sample size.

In this study, multivariate analysis showed that the effect of hypertension on the total MRI burden was greater than that in univariate analysis, which may be related to the inclusion of variables with protective factors, thereby increasing the OR value of hypertension. Therefore, there are some limitations to our study. First, our study subjects were chosen from hospitalized patients at a single center; thus, cases may not be representative of the general population. Second, this was a retrospective study with limited data and small sample size, which is prone to selection bias and recall bias. So a randomized controlled prospective study with larger samples is needed to explore further the factors affecting cognitive function and total MRI burden of arteriolosclerosis CSVD and to determine whether there is a causal relationship between cognitive function and deep cerebral atrophy, hypertension, and total MRI burden in arteriolosclerosis CSVD patients.

Currently, CSVD has an enormous global impact; uncertainties regarding pathogenesis have delayed the development of effective treatment. The most widely accepted approach to treatment is to intensively control well-established vascular risk factors, of which hypertension is the most important, and intensive blood pressure lowering reduces WMH progression (SPRINT MIND Investigators for the SPRINT Research Group et al., 2019a) and delays the onset of cognitive impairment (SPRINT MIND Investigators for the SPRINT Research Group et al., 2019b), but these studies did not evaluate the efficacy of intensive antihypertensive therapy on RSSI, CMB, or PVS. Therefore, further research is needed to explore the preventive and therapeutic effects of intensive antihypertensive therapy on CSVD in future. Our study will provide important information on the progression of arteriolosclerosis CSVD to cognitive impairment and factors that influence cognitive function and the total MRI burden, and this is a piece of valuable clinical information for clinicians. However, large-scale studies to explore the pathophysiological mechanisms of arteriolosclerosis CSVD and develop novel therapeutic approaches are essential if we take the field forward. With a better understanding of pathogenesis, specific therapies may emerge.

Conclusion

This study analyzed the clinical features and imaging data of 146 patients with arteriolosclerosis CSVD. Based on our results, it can be speculated that the disease course of arteriolosclerosis CSVD may be related to cognitive function and total MRI burden. Deep cerebral atrophy was an independent risk factor for cognitive impairment in CSVD, and hypertension was an independent risk factor for total MRI burden. Therefore, in clinical practice, we should pay attention to the characteristic MRI features of CSVD, and early identification of brain MRI imaging characteristics of CSVD will provide an opportunity to forestall progression before the emergence of symptoms. Attention should be paid to the common clinical manifestations of CSVD, such as lacunar syndrome and cognitive impairment. Pay attention to the follow-up of arteriolosclerosis CSVD, screening, and intervention of vascular risk factors. Attention should be paid to the evaluation of cognitive function in patients with deep cerebral atrophy and take individualized secondary prevention of stroke for arteriolosclerosis CSVD with hypertension, which may help to delay the progression of arteriolosclerosis CSVD and reduce the risk of disability and dementia in CSVD patients.

Data availability statement

The original contributions presented in the study are included in the article/supplementary material, further inquiries can be directed to the corresponding authors.

Ethics statement

The studies involving human participants were reviewed and approved by the Institutional Ethics Committee at Wujin Hospital, Affiliated with Jiangsu University. The patients/participants provided their written informed consent to participate in this study. Written informed consent was obtained from the individual(s) for the publication of any potentially identifiable images or data included in this article.

Author contributions

L-LM and W-YC were responsible for the conception and design of the study. MH, A-JM, Z-QL, L-LJ, JZ, and Y-FX collected the clinical data, discussed the results, and contributed to the final version of the manuscript. All authors read and approved the final manuscript, contributed toward data analysis, drafting, revising the manuscript, and agreed to be accountable for all aspects of the study.

Funding

This study was supported by the Changzhou Science and Technology Program (No. CJ20210011), the Science and Technology Project (Social Development) of Wujin District (Nos. WS202019 and WS202112), and the Science and Technology Development Foundation of the affiliate hospitals of Xuzhou Medical University (No. XYFY2020042).

Acknowledgments

The authors thank all patients and their relatives who participated in this study.

Conflict of interest

The authors declare that the research was conducted in the absence of any commercial or financial relationships that could be construed as a potential conflict of interest.

Publisher's note

All claims expressed in this article are solely those of the authors and do not necessarily represent those of their affiliated organizations, or those of the publisher, the editors and the reviewers. Any product that may be evaluated in this article, or claim that may be made by its manufacturer, is not guaranteed or endorsed by the publisher.

References

Appelman, A. P., Exalto, L. G., van der Graaf, Y., Biessels, G. J., Mali, W. P., Geerlings, M. I., et al. (2009). White matter lesions and brain atrophy: more than shared risk factors? A systematic review. *Cerebrovasc Dis.* 28, 227–242. doi: 10.1159/000226774

Aribisala, B. S., Valdés Hernández, M. C., Royle, N. A., Morris, Z., Muñoz Maniega, S., Bastin, M. E., et al. (2013). Brain atrophy associations with white matter lesions in the ageing brain: the Lothian Birth Cohort 1936. *Eur. Radiol.* 23, 1084–1092. doi: 10.1007/s00330-012-2677-x

Cannistraro, R. J., Badi, M., Eidelman, B. H., Dickson, D. W., Middlebrooks, E. H., Meschia, J. F., et al. (2019). CNS small vessel disease: a clinical review. *Neurology* 92, 1146–1156. doi: 10.1212/WNL.0000000000007654

Carmichael, O., Schwarz, C., Drucker, D., Fletcher, E., and Harvey, D., Beckett, L., et al. (2010). Longitudinal changes in white matter disease and cognition in the first year of the Alzheimer disease neuroimaging initiative. *Arch. Neurol.* 67, 1370–1378. doi: 10.1001/archneurol.2010.284

Diaz, K. M., Veerabhadrappa, P., Kashem, M. A., Thakkar, S. R., Feairheller, D. L., Sturgeon, K. M., et al. (2013). Visit-to-visit and 24-h blood pressure variability: association with endothelial and smooth muscle function in African Americans. *J. Hum. Hypertens.* 27, 671–677. doi: 10.1038/jhh.2013.33

Doubal, F. N., MacLullich, A. M., Ferguson, K. J., Dennis, M. S., and Wardlaw, J. M. (2010). Enlarged perivascular spaces on MRI are a feature of cerebral small vessel disease. *Stroke* 41, 450–454. doi: 10.1161/STROKEAHA.109.564914

Fazekas, F., Chawluk, J. B., Alavi, A., Hurtig, H. I., and Zimmerman, R. A. (1987). signal abnormalities at 1.5 T in Alzheimer's dementia and normal aging. *Am. J. Roentgenol.* 149, 351–356. doi: 10.2214/ajr.149.2.351

Greenberg, S. M., Vernooij, M. W., Cordonnier, C., Viswanathan, A., Al-Shahi Salman, R., Warach, S., et al. (2009). Cerebral microbleeds: a guide to detection and interpretation. *Lancet Neurol.* 8, 165–174. doi: 10.1016/S1474-4422(09)70013-4

Hu, Z., Zeng, Q., Zhang, R., Luo, X., Li, K., Xu, X., et al. (2022). White matter free water outperforms cerebral small vessel disease total score in predicting cognitive decline in persons with mild cognitive impairment. *J. Alzheimers Dis.* 86, 741–751. doi: 10.3233/JAD-215541

Klarenbeek, P., van Oostenbrugge, R. J., Rouhl, R. P., Knottnerus, I. L., and Staals, J. (2013). Ambulatory blood pressure in patients with lacunar stroke: association with total MRI burden of cerebral small vessel disease. *Stroke* 44, 2995–2999. doi: 10.1161/STROKEAHA.113.002545

Koedam, E. L., Lehmann, M., van der Flier, W. M., Scheltens, P., Pijnenburg, Y. A., Fox, N., et al. (2011). Visual assessment of posterior atrophy development of a MRI rating scale. *Eur. Radiol.* 21, 2618–2625. doi: 10.1007/s00330-011-2205-4

Levy-Cooperman, N., Ramirez, J., Lobaugh, N. J., and Black, S. E. (2008). Misclassified tissue volumes in Alzheimer disease patients with white matter hyperintensities: importance of lesion segmentation procedures for volumetric analysis. *Stroke* 39, 1134–1141. doi: 10.1161/STROKEAHA.107.498196

Li, H., Jia, J., and Yang, Z. (2016). Mini-mental state examination in elderly chinese: a population-based normative study. *J. Alzheimers Dis.* 53, 487–496. doi: 10.3233/JAD-160119

Li, X., Yuan, J., Qin, W., Yang, L., Yang, S., Li, Y., et al. (2021). Higher total cerebral small vessel disease burden was associated with mild cognitive impairment and overall cognitive dysfunction: a propensity score-matched case-control study. *Front. Aging Neurosci.* 13, 695732. doi: 10.3389/fnagi.2021.695732

Ma, Y., Song, A., Viswanathan, A., Blacker, D., Vernooij, M. W., Hofman, A., et al. (2020). Blood pressure variability and cerebral small vessel disease: a systematic review and meta-analysis of population-based cohorts. *Stroke* 51, 82–89. doi: 10.1161/STROKEAHA.119.026739

Manolio, T. A., Kronmal, R. A., Burke, G. L., Poirier, V., O'Leary, D. H., Gardin, J. M., et al. (1994). Magnetic resonance abnormalities and cardiovascular disease in older adults. The Cardiovascular Health Study. *Stroke* 25, 318–327. doi: 10.1161/01.STR.25.2.318

Meissner, A. (2016). Hypertension and the brain: a risk factor for more than heart disease. *Cerebrovasc. Dis.* 42, 255–262. doi: 10.1159/000446082

Nitkunan, A., Lanfranconi, S., Charlton, R. A., Barrick, T. R., and Markus, H. S. (2011). Brain atrophy and cerebral small vessel disease: a prospective follow-up study. *Stroke* 42, 133–138. doi: 10.1161/STROKEAHA.110.594267

Ovbiagele, B., and Saver, J. L. (2006). Cerebral white matter hyperintensities on MRI: current concepts and therapeutic implications. *Cerebrovasc. Dis.* 22, 83–90. doi: 10.1159/000093235

Pantoni, L. (2010). Cerebral small vessel disease: from pathogenesis and clinical characteristics to therapeutic challenges. *Lancet Neurol.* 9, 689–701. doi: 10.1016/S1474-4422(10)70104-6

Pasquier, F., Leys, D., Weerts, J. G., Mounier-Vehier, F., Barkhof, F., Scheltens, P., et al. (1996). Inter- and intraobserver reproducibility of cerebral atrophy assessment on MRI scans with hemispheric infarcts. *Eur. Neurol.* 36, 268–272. doi: 10.1159/000117270

Pistoia, F., Sacco, S., Ornello, R., Degan, D., Tiseo, C., Carolei, A., et al. (2016). Composite scores and other outcome measures in stroke trials. *Front. Neurol. Neurosci.* 39, 60–70. doi: 10.1159/000445413

Sachdev, P., Kalaria, R., O'Brien, J., Skoog, I., Alladi, S., Black, S. E., et al. (2014). Diagnostic criteria for vascular cognitive disorders: a VASCOG statement. *Alzheimer Dis. Assoc. Disord.* 28, 206–218. doi: 10.1097/WAD.0000000000000034

Scheltens, P., Leys, D., Barkhof, F., Huglo, D., Weinstein, H. C., Vermersch, P., et al. (1992). Atrophy of medial temporal lobes on MRI in "probable" Alzheimer's disease and normal ageing: diagnostic value and neuropsychological correlates. *J. Neurol. Neurosurg. Psychiatr.* 55, 967–972. doi: 10.1136/jnnp.55.10.967

Schillaci, G., Bilo, G., Pucci, G., Laurent, S., Macquin-Mavier, I., Boutouyrie, P., et al. (2012). Relationship between short-term blood pressure variability and large-artery stiffness in human hypertension: findings from 2 large databases. *Hypertension* 60, 369–377. doi: 10.1161/HYPERTENSIONAHA.112.197491

SPRINT MIND Investigators for the SPRINT Research Group, Nasrallah, I. M., Pajewski, N. M., Auchus, A. P., Chelune, G., Cheung, A. K., et al. (2019a). Association of intensive vs standard blood pressure control with cerebral white matter lesions. *JAMA* 322, 524–534. doi: 10.1001/jama.2019.10551

SPRINT MIND Investigators for the SPRINT Research Group, Williamson, J. D., Pajewski, N. M., Auchus, A. P., Bryan, R. N., Chelune, G., et al. (2019b). Effect of intensive vs standard blood pressure control on probable dementia: a randomized clinical trial. *JAMA* 321, 553–561. doi: 10.1001/jama.2018.21442

Staals, J., Makin, S. D., Doubal, F. N., Dennis, M. S., and Wardlaw, J. M. (2014). Stroke subtype, vascular risk factors, and total MRI brain small-vessel disease burden. *Neurology* 83, 1228–1234. doi: 10.1212/WNL.0000000000000837

Veglio, F., Paglieri, C., Rabbia, F., Bisbocci, D., Bergui, M., Cerrato, P., et al. (2009). Hypertension and cerebrovascular damage. *Atherosclerosis* 205, 331–341. doi: 10.1016/j.atherosclerosis.2008.10.028

Vermeer, S. E., and Longstreth, W. T. Jr., Koudstaal, P. J. (2007). Silent brain infarcts: a systematic review. *Lancet Neurol.* 6, 611–619. doi: 10.1016/S1474-4422(07)70170-9

Viswanathan, A., Godin, O., Jouvent, E., O'Sullivan, M., Gschwendtner, A., Peters, N., et al. (2010). Impact of MRI markers in subcortical vascular dementia: a multi-modal analysis in CADASIL. *Neurobiol. Aging.* 31, 1629–1636. doi: 10.1016/j.neurobiolaging.2008.09.001

Wang, Y., Xu, J., Zhao, X., Wang, D., Wang, C., Liu, L., et al. (2013). Association of hypertension with stroke recurrence depends on ischemic stroke subtype. *Stroke* 44, 1232–1237. doi: 10.1161/STROKEAHA.111.000302

Wardlaw, J. M., Smith, C., and Dichgans, M. (2013a). Mechanisms of sporadic cerebral small vessel disease: insights from neuroimaging. *Lancet Neurol.* 12, 483–497. doi: 10.1016/S1474-4422(13)70060-7

Wardlaw, J. M., Smith, E. E., Biessels, G. J., Cordonnier, C., Fazekas, F., Frayne, R., et al. (2013b). Neuroimaging standards for research into small vessel disease and its contribution to ageing and neurodegeneration. *Lancet Neurol.* 12, 822–838. doi: 10.1016/S1474-4422(13)70124-8

Wu, S., Wu, B., Liu, M., Chen, Z., Wang, W., Anderson, C. S., et al. (2019). Stroke in China: advances and challenges in epidemiology, prevention, and management. *Lancet Neurol.* 18, 394–405. doi: 10.1016/S1474-4422(18)30500-3

Yang, S., Yuan, J., Qin, W., Yang, L., Fan, H., Li, Y., et al. (2018). Twenty-four-hour ambulatory blood pressure variability is associated with total magnetic resonance imaging burden of cerebral small-vessel disease. *Clin. Interv. Aging* 13, 1419–1427. doi: 10.2147/CIA.S171261

Yue, N. C., Arnold, A. M., and Longstreth, W. T. Jr., Elster, A. D., Jungreis, C. A., O'Leary, D. H., et al. (1997). Sulcal, ventricular, and white matter changes at MR imaging in the aging brain: data from the cardiovascular health study. *Radiology* 202, 33–39. doi: 10.1148/radiology.202.1.8988189

Frontiers in Neuroscience

Provides a holistic understanding of brain function from genes to behavior

Part of the most cited neuroscience journal series which explores the brain - from the new eras of causation and anatomical neurosciences to neuroeconomics and neuroenergetics.

Discover the latest Research Topics

See more →

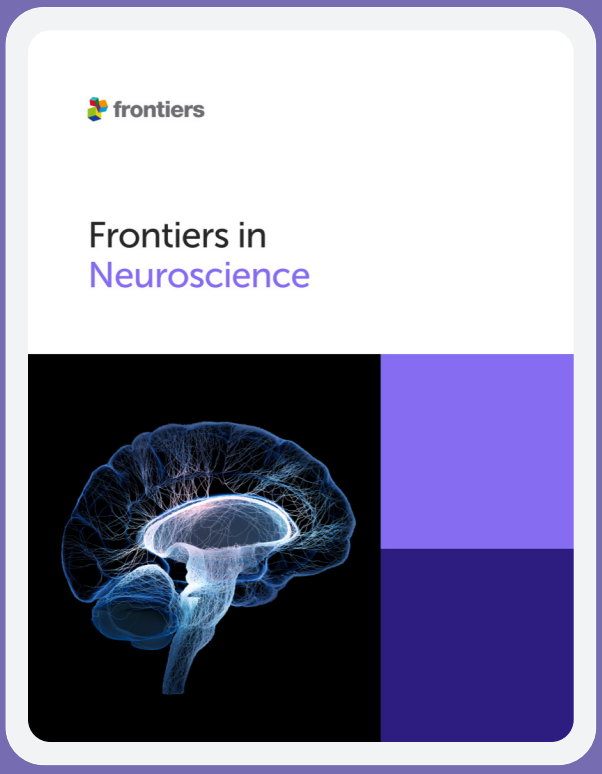

Frontiers

Avenue du Tribunal-Fédéral 34
1005 Lausanne, Switzerland
frontiersin.org

Contact us

+41 (0)21 510 17 00
frontiersin.org/about/contact